FLOW PATTERNS ON DISTILLATION TRAYS

A THESIS SUBMITTED

BY

KEVIN STUART FENWICK B.Eng. (Hons.)

A candidate for the degree of

Doctor of Philosophy

DEPARTMENT OF CHEMICAL ENGINEERING

AND

APPLIED CHEMISTRY

UNIVERSITY OF ASTON IN BIRMINGHAM

JANUARY 1996

CERTIFICATE

The University of Aston in Birmingham

FLOW PATTERNS ON DISTILLATION TRAYS

A Thesis submitted by

Kevin Stuart Fenwick B.Eng. (Hons.)

A candidate for the degree of Doctor of Philosophy

January 1996.

THESIS SUMMARY

Studies into the two-phase flow patterns produced on a sieve tray were carried out using an air-water simulator of 2.44 m in diameter. The flow patterns were investigated by a number of methods, direct observation using directional flow pointers; by water-cooling to simulate mass transfer; and by measurement of the height of clear liquid across the tray with manometers. The flow rates used were designed to show how the flow pattern changed with the change in the gas and liquid rates.

The results from water-only studies on an un-perforated tray were compared with those produced on a sieve tray with holes of 12.7 mm diameter. The presence of regions on the sides of the tray where the liquid was circulating was noted from the water-only experiments. The presence and magnitude of the circulations was reduced when the air was passed through the liquid. These were similar to the findings of Hine (1990) and Chambers (1993). When circulation occurred, the flow separated at the ends of the inlet downcomer and circulations of up to 30% of the tray area were observed.

Water-cooling and the manometer measurements were used to show the effect of the flow pattern on the tray efficiency and the height of clear liquid respectively. The efficiency was severely reduced by the presence of circulations. The height of clear liquid tended to rise in these areas.

A comparison of data collected on trays with different hole diameters showed that the larger hole diameter inhibited the on-set of separation to a greater extent than small hole diameters. The tray efficiency was affected by a combination of the better mixing on smaller hole trays and the detrimental effect of greater circulation on these trays.

Work on a rectangular tray geometry was carried out to assess the effect of hole size on the height of clear liquid. It was found that the gradient on the outlet half of the tray was very small and that the highest clear liquid height was given by the highest hole size.

Overall, the experiments helped to clarify the effect that the flow pattern had on the operation of the tray. It is hoped that the work can be of use in the development of models to predict the flow pattern and hence the tray efficiency.

Keywords: SIEVE TRAYS, TRAY EFFICIENCY, HOLE SIZE, MASS TRANSFER, LIQUID HEAD

ACKNOWLEDGEMENTS

I would like to express my thanks to the following:

Professor K.E. Porter for his stimulating ideas and help throughout this research programme.

The workshop technicians, Ian Murkett, Roger Wheeler, Maurizio Santoro, Bill Curtis and Pete Green for their practical help with modifications to the distillation simulator.

The technicians and secretarial staff of the Chemical Engineering and Applied Chemistry Department for their help throughout the period of this research.

Mr. J.T. Lavin and Dr. C.J. Hine for their advice and expertise in the field of distillation design.

BOC Process Plants for their sponsorship of this work.

The Engineering and Physical Science Research Council (ESPRC) for their funding of the CASE award.

Dr. J.P.Fletcher for his advice during the writing of this thesis.

To all my friends who have made my time at university so enjoyable and especially Paula who helped me so much in the finishing of this thesis.

Finally to my family who have always been there for me.

TABLE OF CONTENTS

LIST OF FIGURES

LIST OF TABLES

CHAPTER 1

INTRODUCTION

Distillation has been in use for many centuries. It is thought to have been discovered by the Chinese and thereafter used in the production of distilled liquors. It is still used in the production of alcoholic beverages today but it has also taken on a much greater role, to the extent that it is now the dominant separation process in industry.

Distillation works by using energy to boil the material and a recent survey by Legg (1986) stated that distillation accounted for 13% of the U.K. chemical industries total energy consumption. This comparatively high use of energy is at the heart of research into distillation. To keep the process competitive, improvements need to be made in the capital and operating costs of the columns. These can be achieved by making the contacting devices more efficient, which will decrease the capital cost, and integrating the column more fully into the process, which will reduce the operating cost. The wide-scale use of distillation means that even small-scale improvements can have a significant effect. Zuiderweg (1973) estimated that between 1950 and 1970, two billion dollars in column investment costs were saved by research and development. Obviously, the industry has changed since this quote but it gives an indication of the scale of savings that can be made by improved design.

Alternatives to distillation are available but they often have higher investment costs, which out-weigh the extra energy cost of the less energy efficient distillation. This was found by Rush (1979), who demonstrated that for most cases distillation was still the most economically viable process despite its energy usage. He went on to outline the fact that if distillation was the chosen method, then the greatest saving would be

found by running the distillation equipment more efficiently. Indeed, he suggested that the columns should be run "leaner and harder".

If this last statement is to be implemented it would mean designing columns to run at lower reflux ratios, close to the system's pinch point. This leaves less scope for error with the consequence being that the column would be more likely to fail. As columns are designed from past experience a great deal of uncertainty is involved in using designs from similar, but not identical, columns. To overcome uncertainties caused by this and the lack of knowledge of the various systems to be distilled, empirical factors are included. These factors basically cover the lack of knowledge by over-designing the column. If the knowledge of the design process could be improved so that these factors could be reduced or eliminated, then this would lead to more certainty that a particular design will work and allow the reflux ratio to be reduced.

Clearly, a better, more scientific understanding of what is happening in the column is required. The starting point for this must be in the choice of contacting device to be used. This comes down to a choice of trays or packings. Packings have certain advantages over trays, namely that the pressure drop over the column is about one-fifth that of a similar trayed column. This has an effect on the column temperatures and may be very important where a low pressure drop is required such as in vacuum distillation. With the case of trays, more is known about their behaviour. There are established design techniques already employed and the way that the two phases move through a trayed column is fairly well understood. Trays also have the advantage of being cheaper than packings, suitable for fouling services and flexible in where any feed points are located. Also the even distribution of the gas and liquid over the diameter is more difficult with large diameter packed columns than with those fitted with trays. Advances in the design of packings are being made all the time but trays still hold the edge for most services. Until problems such as cost, fouling service and scale-up problems caused by poor distribution of the phases are overcome, then trays will continue to be employed. In 1984, Krummrich estimated that 90% of installed distillation columns contained trays. This number is likely to have dropped in the intervening years but trays are still employed in the large majority of cases.

One problem with large diameter tray columns is that the liquid on the tray is not completely mixed. The liquid enters at one point on the tray and leaves at another. To understand the performance of large distillation trays requires a thorough understanding of the liquid flow patterns. Therefore, to help predict these flow patterns, development of the appropriate two-phase flow theory needs to take place. This allows the flow pattern to be predicted for any combination of fluid system and tray design. To allow this to happen, knowledge of how the bi-phase crosses the tray is required. A major objective of this work is to carry out an experimental analysis of how this occurs and to identify the main variables that influence it, in conjunction with others workers who are developing theoretical models.

The importance of the flow patterns on distillation trays has been recognised since the 1930s and many attempts have been made to relate it to the tray efficiency. Theoretical models have been proposed by many workers who include Kirschbaum (1934), Lewis (1936), Gautreaux and O'Connell (1955), Gerster et al. (1958), Porter et al. (1972), Bell and Solari (1974), Sohlo and Kouri (1982) and Yu et al. (1990, 1991). These models are either based on the concept of mixed pools or the plug flow of liquid. The mixed pool models have liquid flow between them and the models of plug flow of liquid are generally enhanced by backmixing, which is described in terms of diffusion theory. The differences between the model are generally between models that work in only one direction, two directions or, very rarely, in three directions. The more modern models use at least two directions after it was discovered that this was necessary to predict trays of large diameter. In the main, the models have assumed a flow pattern and used it to solve the model's equations. The success of the model relies on the accuracy of the flow pattern assumed.

A scientific investigation of the flow on a tray was started by Hine (1990) and continued by Chambers (1993). Their work has helped to identify variables that affect the flow pattern on the tray. The next step is to extend the database to contain data on more tray types. Also the development of a model to predict the flow pattern is needed. To help with this objective the science of open-channel two-phase flow

needs to advanced. To this end the number of variables needs to be reduced still further and work on a rectangular column has been undertaken. This allows data to be assessed as two-dimensional. The removal of the side segments of the tray allows the transverse direction to be ignored.

A literature survey is included in the next chapter to help place this thesis in the whole of the research into distillation. It contains evidence for the presence of the flow patterns and its effect on the tray efficiency. Also included are ways in which designers have tried to overcome the adverse effects of the flow pattern by trying to correct it. A brief description of the approach to the problem is then included and followed by two chapters describing the experimental apparatus and how it is used. The experimental results are reported in the next chapters before the whole programme is summarised in the last two chapters.

CHAPTER 2

LITERATURE SURVEY

2.1 Introduction

Distillation has been used for many centuries but it is only over the last seventy-five years that it has enjoyed scientific development. This corresponds with the establishment of a petrochemical industry that relies heavily on the separation of organic chemicals. The main problem with the development of tray technology was the difficulty in testing full scale operating units. This meant that very little plant data were published over the first six decades of column development.

In the beginning, research was aimed at finding conditions where the column would operate safely. Mainly these experiments were carried out on small-scale columns and mathematical models were formulated to correlate existing experience with the experimental data. In essence these models were empirical and allowed columns to be designed using rules of thumb that had been tried and tested. For the majority of designs this approach worked but it hindered the further development of 'better' designs.

Porter and Jenkins (1979) reviewed this approach to distillation design and concluded that the background of many of these empirical correlations was incorrect. The way forward for distillation research was discussed and the question was raised as to whether a better understanding of the basic phenomena on the tray would lead to enhanced tray performance.

Since the 1970s there has been an increase in data collected on commercial scale trays. This has led to a new generation of theoretical models that have given a better understanding of the two-phase nature of the flow on trays. This approach is still in its infancy in terms of the scientific basis of the fluid flow and prediction of the flow patterns produced.

This literature survey puts the experiments presented in this thesis into context with the previous work. It explains why the research was carried out by identifying areas where a better understanding is required. This can be achieved in the following sections:

i. A description of the current method for designing a tray,

ii. A summary of the flow regimes that can be encountered on trays,

iii. A discussion of the tray models that have been developed to predict tray efficiency,

iv. The techniques used for the investigation of the flow patterns on trays.

2.2 Tray Design

The design of a distillation column is a balance between two requirements. Perhaps the most important aspect of the design is that it actually achieves the separation it has been designed for. The second major requirement is that the column is economically viable. This in itself is a combination of a number of factors, but it is imperative to a profitably operated process that the column design is not over-extravagant in terms of cost, whether capital or operating.

The cost of the column is heavily dependent on the diameter of the tray. Thus the main objective of a tray design is to calculate the bubbling area, downcomer area and the number of passes in order to find the minimum column diameter for a given separation. This is mainly achieved by a combination of empirical methods and factors that have

been known to work. Usually this leads to a sieve tray designed for 80% of total flooding. Flooding in this case is usually caused by the liquid in the downcomer reaching the tray above, but may be caused by excessive entrainment. This design point should also ensure that the flows are kept well above the weeping limit of the tray and that the maximum throughput flows through the smallest possible column.

To start the design it is necessary to have the gas and liquid mass flow rates, and the density ratio between the two phases. This is important, as Porter and Jenkins (1979) showed that the other properties of the system can be approximately correlated against each other in terms of the density ratio (i.e. the flow parameter $L/V(\rho_V/\rho_L)^{0.5}$).

Empirical factors are present in most designs to hide ignorance of what is occurring on the tray. Two examples of this are the derating factor, S, and the majority of single-pass sieve tray designs using a weir length of 0.6 times the diameter. The first example is usually used when a design for a certain system of chemicals has been known to fail. This may be due to foaming causing an increase in the froth height. The derating factor decreases the flood factor to make flooding less likely. The second example is taken from past experience and is thought to minimise the channelling of the liquid from downcomer to downcomer. These examples are given to highlight the empirical nature of some sections of tray design.

2.2.1 An Outline of the Tray Design Procedure

A typical design for sieve trays is set out below, based on Lockett (1986):

a) The number of passes, tray spacing and hole diameter should be fixed from previous experience in similar applications. If previous experience is negligible, use may be made of the total flows chart of Porter and Jenkins (1979) to give the number of passes. The chart makes use of total volumetric vapour and liquid flow rates:

$$\overline{V} = Q_G\left(\frac{\rho_v}{\rho_L - \rho_v}\right)^{0.5} \qquad Q_L = \frac{W_L}{\rho_L} \tag{2.1}$$

An initial tray spacing of 0.61 m should be chosen. The hole size should be 4.8-6.4 mm unless fouling or corrosion is likely to be excessive.

b) The turndown required should be fixed at this point. Turndown is expensive to provide for and thought should be given to the amount incorporated into the design. Typical values of turndown for a sieve tray are 60-70% of full loadings. Greater turndown can be designed, but this is at the cost of pressure drop and tray spacing may need to be increased.

c) The exit weir height should be set. If no past experience is available for weir height then typically 50 mm is chosen. Increasing the weir height increases the efficiency at the expense of pressure drop. Therefore, vacuum distillation weir heights would be lower at between 0-25 mm.

d) The downcomer and bubbling areas can be calculated from capacity correlations. The downcomer area is calculated by relation to the downcomer velocity. The area is related to the velocity by:

$$A_D = \frac{Q_L}{U_{DF}.F} \tag{2.2}$$

(F is the flood factor.)

A number of empirical relationships are available for the downcomer velocity and are shown below:

$$U_{DF} = 0.17 ms^{-1} \qquad : \qquad U_{DF} = 0.007(\rho_L - \rho_v)^{0.5} ms^{-1}$$

$$U_{DF} = 0.008\left[T.S.(\rho_L - \rho_v)\right]^{0.5} ms^{-1} \tag{2.3}$$

The bubbling area is calculated by finding the diameter of the column from correlations such as those produced by Fair (1961) or Porter and Jenkins (1979). These correlate the flow parameter $[(L/G).(\rho_G/\rho_L)^{0.5}]$ against a capacity factor. From the capacity factor the area of the column can be found and the diameter from this. The bubbling area is then found by subtracting two downcomer areas from the column area.

e) For the agreed turndown conditions the fractional free area of the tray should be calculated to ensure that the tray is stable and weeping is minimised. This is an iterative procedure due to weeping correlations involving the clear liquid height, which itself involves the fractional free area.

f) The next step is to check various points and alter the design if necessary:
   - If the maximum load over the weir is exceeded then the number of passes must be increased.
   - If the pressure drop is excessive then this can be corrected by increasing the bubbling area or the free area of the tray can be increased. As a last resort the weir height can be reduced but this will greatly affect the efficiency.
   - If the downcomer back-up is excessive then this can be fixed by either increasing the tray spacing, reducing the tray's dry pressure drop or reducing the weir height.
   - The flow regime should be checked. If the regime is found to be unacceptable to the designer then this can be altered by altering the number of passes or altering the clear liquid height to hole diameter ratio.
   - If entrainment is a problem then the tray spacing can be increased to reduce its affect.

g) The tray efficiency should now be estimated and if this is unacceptably low then alterations to the design can be made. The weir height can be increased but this is at the expense of the pressure drop, downcomer back-up and turndown. Alternatively the bubbling area can be increased. This has the effect of increasing the gas-liquid contact time.

h) The design of the tray is a trade-off and as such the above steps should be repeated for different initial tray spacings. This will allow a minimum cost design to be achieved.

This method will produce a tray design and is typical of the empirical nature of this work. It is worth noting that the method relies on estimating an efficiency for the tray. It is usually difficult to predict an efficiency at the design stage and this is an important part of the programme of research of which this thesis forms a part. The development of predictive methods to calculate efficiencies from first principles would be a very useful tool.

2.3 Flow Regimes on Sieve Trays

As with two-phase flow in a closed channel, the flow on a sieve tray can be characterised by recourse to the amount of each phase in the dispersion and how they flow past each other. With distillation, there are three main areas of operation. The limiting cases occur where one of the phases dominates the other to such an extent that it can be considered single-phase flow. Operating distillation flow rates will be well inside any such limiting case.

At one end of the scale is the case where the gas momentum is dominant. The liquid is projected from the surface of the tray and carried as small droplets. This is known as the spray regime. At the other end of the scale is a regime where the liquid is dominant. The gas is carried along by the liquid in the form of small bubbles. This is generally referred to as the emulsion flow regime. In between these two is a region where there is a high proportion of liquid near the tray floor and liquid droplets are projected from the surface by the gas. This type of flow is termed mixed froth.

Other flow regimes are possible with open channel two-phase flow but are rarely met in operating columns. Two such examples are the free bubbling regime and the foaming regime. Free bubbling only occurs at very low liquid loads that are well below industrial

flow rates and foaming is deliberately avoided by designers due to its adverse affects on the flooding of the column.

It has been found that designing the tray to operate in a particular regime can be beneficial and may improve the tray efficiency (Porter et al., 1977; Raper et al., 1984). With this in mind it is important to have an understanding of the regime that the tray operates under, as ignorance could lead to the column underperforming.

2.3.1 The Spray Regime

The spray regime is gas dominated and the liquid is carried as fine droplets projected into the inter-tray spacing by the gas. It is favoured by high gas velocities, low clear liquid heights and large hole sizes. The first two conditions are commonly found in vacuum distillation.

The regime was first observed by De Goederen (1965) using an air-water system and further work was carried out by Porter and Wong (1969) to confirm its presence. It was thought to behave like a fluidised bed and the first attempts to model it used this basis (Porter and Wong 1969 and Ho et al., 1969). Later this idea was rejected and a free trajectory model was introduced (Hofhuis and Zuiderweg, 1979 and Raper et al., 1979). This type of model proposed a small layer of liquid close to the tray surface, termed a droplet formation zone, with droplets thrown out of it with a projection velocity of between the hole velocity and the superficial gas velocity. The droplets then follow a trajectory that returned the larger droplets back to the tray while the smaller droplets are entrained in the gas and carried to the tray above. Some success was gained by using this model but the scope of its use was hindered by the need to know the total amount of liquid in the dispersion.

The transition from the spray regime to the froth regime has been extensively studied (Porter and Wong, 1969; Muller and Prince, 1972; Loon et al., 1973; Jeronimo and Sawistowski, 1973; Pinczewski et al., 1973; Payne and Prince, 1975 & 1977;

Pinczewski and Fell, 1977; Raper et al., 1979 and Lockett, 1981). A wide variety of techniques have been used to study the transition, but the problem remains in identifying the actual transition point. Porter and Wong (1969) used a method that made use of light beam attenuation at a point above the tray. The transition is dependent on the positioning of this light beam. Similarly Jeronimo and Sawistowski (1973) suggested that the transition took place when 50% of the holes were jetting, i.e. the gas penetrated the froth in one continuous flow of gas. Later workers (Pinczewski et al., 1973 and Raper et al., 1979) suggested that the transition was closer to 95%+ of the holes jetting. The discussion is largely academic due to the difficulty of measuring the number of holes jetting at any one point. Due to this, Lockett (1981) suggested that no model was completely satisfactory and therefore little would be lost by resorting to empiricism. He proposed a transition based on a comparison of published data.

It may be noted that Porter and Jenkins (1979) associated the spray to bubbling transistion with minimum entrainment, and therefore maximum capacity. This was largely based on an examination of the data of Sakata and Yanagi (1979).

The large majority of the equations proposed to model the transition are of the following nature:

$$\frac{h_{cl}}{d_h} = f(u_G) \tag{2.4}$$

These agree with the observations mentioned above, that the spray regime is favoured by the large hole diameters, low clear liquid height and large gas velocities.

2.3.2 The Mixed-Froth Regime

In this regime the liquid is the continuous phase with the gas being transported through it in either jets or bubbles. Above the main bulk of the liquid there is a proportion of droplets carried out of it by the gas jets. Neither the liquid nor the vapour momentum is

dominating in this regime and these conditions are commonly found when atmospheric distillation is carried out.

This regime is considered as a transition between the emulsion and the spray regimes, but it can be wide given the right conditions. Little information is available about this regime but Hofhuis and Zuiderweg (1979) covered it in a paper on the various regimes encountered on a tray. What little experimental work that has been carried out to assess this region has been undertaken on small-scale apparatus and wall effects come into play. The general theory is that at a certain gas rate the bubbles are prevented from freely leaving the froth by the presence of other bubbles. At some point the bubbles coalesce and then this moves on to jetting as the gas velocity is increased. As the jetting reaches an extreme the tray has passed into the spray regime.

2.3.3 The Emulsion Flow Regime

As mentioned above, Hofhuis and Zuiderweg (1979) produced a paper that split the froth regime into two, the above mentioned mixed-froth regime and the emulsion regime. The latter regime is liquid continuous with the liquid momentum dominating the gas momentum and is characterised by small gas bubbles mixed, or emulsified, in the liquid stream. It is thought that the bubbles remain small due to being sheared off by the high liquid momentum before they are fully formed.

It was noted that when a certain value of the flow parameter (0.1) was exceeded then the form of the liquid being carried over the outlet weir changed. The change was from the bulk of the liquid being carried over by splashes and slugs, to being continuous. This led to further work into this area (Zuiderweg et al., 1984) to assess the effect that this regime has on the efficiency, the clear liquid height and the downcomer (due to greater entrainment of gas).

2.3.4 The Effect of the Flow Regime on the Liquid Flow Pattern

In 1975, Lockett et al. attempted to explain their earlier findings of liquid channelling associated with circulating flow by suggesting that where this occurred the froth was flowing in a similar fashion to liquid only. This was caused by a high liquid momentum and the circulation can to some degree be caused by the liquid deflecting from the outlet weir. Bell and Solari (1974) found that the liquid channelling occurred at very low gas velocities but receded at "commercial vapour flow rates". Lockett et al. (1975) attempted to explain this as a result of the tray being operated in the spray regime. In this case the liquid is randomly dispersed by the high gas flow rate through it and channelling is prevented. This approach led to spray being thought of as a diffusion process (Porter et al., 1977) in which the height of clear liquid was analogous to the drop concentration in molecular diffusion. Measurements of the eddy diffusivity, a measure of the liquid mixing, suggest that there is a limit to the way liquid flows in this manner. This leads to the question of how the liquid flows in this regime and it currently needs an answer.

To conclude, it has been noted that channelling tends not to occur in the spray regime and that it will only occur when the froth is flowing in the manner of liquid only. This leads to almost plug flow of the liquid in the spray regime, with the possibility of circulations in the other regimes.

2.4 Tray Models

Due to the limited knowledge of the flow across sieve trays at the time and the savings that can be made by improved designs, models to predict the conditions on the tray have existed for many decades. As mentioned above, the tray efficiency is very important to the cost of the column and because of this it has been the subject of many predictive models. A large number of models have been proposed over the years and this literature survey gives an overview of the major ones that have had an effect on the thinking of the time.

2.4.1 Efficiency Models

The design of a distillation column involves using vapour-liquid equilibrium data. By using this we are assuming that the column consists of a number of stages that are in equilibrium, e.g. the vapour leaving the tray is in perfect equilibrium with the liquid leaving the tray. In reality this is not the case and the flows are usually not in equilibrium. To compensate for this we use a term called the efficiency to relate the ideal, equilibrium case, to the real case. With the design we will have a number of equilibrium stages and the real column will contain more trays, or contacting devices, than the ideal case due to equilibrium not being reached on each tray. At this stage it is useful to have a definition of the efficiency used in this thesis.

Definition of Tray and Point Efficiency

A number of methods have been proposed for the calculation of tray efficiency (e.g. Murphree, 1925; Hausen, 1953; Standart, 1965 and Holland, 1963). By far the most widely used is the Murphree tray efficiency, even though it is not the most rigorous in its derivation. This efficiency is used throughout this thesis and it is this that is defined below.

At any point on the tray the mass transfer that is actually taking place can be related to the equilibrium conditions. This is achieved by comparing the change in the composition of the liquid or vapour that is attained by passing through the point, with that which would occur if equilibrium was reached. For the vapour phase this is given by:

$$E_{OG} = \frac{y_n - y_{n-1}}{y_n^* - y_{n-1}} \tag{2.5}$$

y_{n-1} and y_n are the compositions of the vapour entering and leaving the point on the n^{th} tray which is under consideration. y^*_n is the composition of the vapour in equilibrium with the liquid at the point, x_n. This efficiency, E_{OG}, is known as the point efficiency.

For the Murphree tray efficiency we assume that for a single ideal tray the vapour exiting the froth is in equilibrium with the exiting liquid. To define the tray efficiency we use the ratio of the actual change to the change that would occur for a tray where equilibrium is assumed. For the vapour phase this is given by:

$$E_{MV} = \frac{\bar{y}_n - \bar{y}_{n-1}}{y^*_n - \bar{y}_{n-1}} \tag{2.6}$$

$\bar{y}_n$ and $\bar{y}_{n-1}$ are average compositions exiting and entering the tray respectively. y^*_n is the composition of the vapour in equilibrium with the liquid actually leaving the tray, x_n.

For the liquid phase the efficiencies can be rewritten to leave the liquid tray efficiency as:

$$E_{ML} = \frac{\bar{x}_n - \bar{x}_{n+1}}{x^*_n - \bar{x}_{n+1}} \tag{2.7}$$

$\bar{x}_{n+1}$ and $\bar{x}_n$ are the average composition for the liquid entering and exiting the tray. x^*_n is the composition of the liquid that would be in equilibrium with the average composition of the vapour exiting the froth, y_n.

We can now make use of the relationships that tie the liquid and vapour concentrations together, namely the equations of the equilibrium lines. Assuming that the operating line is constant and that for the composition range the equilibrium line can be approximated by a straight line, then we can relate the liquid tray efficiency to the vapour tray efficiency thus:

$$y^*_n = mx_n + b \qquad \text{and} \qquad y_n = mx^*_n + b \tag{2.8}$$

We can combine equations 2.6, 2.7 and 2.8 to give:

$$E_{MV} = \frac{E_{ML}}{E_{ML} + \lambda(1 - E_{ML})} \tag{2.9}$$

Equation 2.9 shows the relation between the two tray efficiencies where λ is the ratio of the slope of the operating line to the slope of the equilibrium line. This relation shows one of the weaknesses of the Murphree efficiencies, mainly that the two phases give different values.

Types of Model

Over the years different models have been developed to account for the calculation of the tray efficiency. Generally they have assumed a way in which the froth flows across the tray and in which it is mixed. As more was found about the flow on the tray, better models have been developed but they still rely on knowing the flow pattern on the tray. Present development of models will hopefully enable the prediction of the flow patterns on the tray and allow the use of appropriate equations to calculate the efficiency.

Generally, two different types of model have been proposed. The first type is based on assuming that the tray is made up of a number of completely mixed pools with liquid being allowed to flow between them. Mathematical solutions to this type of model are fairly easy to compute but they are only a simple approximation to the process taking place on the tray. The other problem with such a model is setting the number of pools that are necessary to model the tray. Ashley and Haselden (1970) overcame this problem by relating the number of mixed pools to be used to the Peclet number.

The second main type of model is based on the back-mixing of liquid. It is analogous to molecular transfer in that it estimates the eddy diffusivity of the process. The eddy diffusivity is a measure of the amount of liquid that is mixed on the tray and provides a

more accurate picture of what is occurring. The diffusivity can be estimated by using tracers and measuring the way they are 'spread' by the mixing on the tray.

The major advances of both type of model have been through the calculation in different directions. The first models worked only in one direction, that of the liquid flow path. Later models developed to take into account the flow in the transverse direction. Very little has been developed to model the flow in the vertical direction and most workers assume the froth to be well mixed in this direction.

The Completely Mixed Tray

In the beginning of the development of distillation, it was thought that the froth on the tray was completely mixed by the vapour passing through it. If this were the case then liquid composition on the tray would be exactly the same as that crossing the outlet weir. The vapour entering the tray was also thought to be completely mixed and therefore the vapour exiting the froth would all have the same composition. These conditions lead to the point efficiency being equal to the tray efficiency.

Kirschbaum (1934) found that even for small diameters there was a concentration gradient across the tray. This led to his development of the first mixed pool model. The idea coming from the assumption of the tray being split into smaller areas that themselves were completely mixed. The model was fairly flexible but it has found little application due to its complex nature.

The Plug Flow Model

The approach of Lewis (1936) was different to that of Kirschbaum and led to the first development of the second type of model, although no back-mixing was included. The assumption was made that the froth on the tray travels in plug flow. Further assumptions were made:

i. There was no mixing of liquid across the tray,

ii. The flow path was rectangular,

iii. There was a constant point efficiency and

iv. The liquid and vapour flow rates were constant.

Lewis's model applied to a tray within a section of trays and he identified three alternative cases:

Case1. The vapour is completely mixed between the trays. The direction of the liquid flow on successive trays is irrelevant.

Case2. The vapour is unmixed between the trays. The liquid flows in the same direction on successive trays.

Case3. The vapour is unmixed between the trays. The liquid on successive trays is in the opposite direction.

The equations that were developed were as follows:

Case 1:
$$E_{MV} = \frac{[\exp(\lambda E_{OG}) - 1]}{\lambda} \tag{2.10}$$

Case 2:
$$E_{MV} = \frac{\alpha - 1}{\lambda - 1} \tag{2.11}$$

$$\lambda = \left[\frac{1}{E_{OG}} + \frac{1}{\alpha - 1}\right] \ln \alpha \tag{2.12}$$

α is the concentration similarity ratio and is calculated from equation 2.12.

Case 3: Equation 2.11 is also applicable for this case but should be used with the following equations:

For $\alpha<1$ use:

$$\lambda = \sqrt{\left[\frac{\alpha^2 - (1-E_{\infty})^2}{E_{\infty}^2(1-\alpha^2)}\right]}\cos^{-1}\left[1 - \frac{(1-\alpha)(\alpha - 1 + E_{\infty})}{\alpha(2-E_{\infty})}\right] \tag{2.13}$$

or when $\alpha>1$ use:

$$\lambda = \sqrt{\left[\frac{\alpha^2 - (1-E_{\infty})^2}{E_{\infty}^2(\alpha^2-1)}\right]}\cosh^{-1}\left[1 + \frac{(\alpha - 1)(\alpha - 1 + E_{\infty})}{\alpha(2-E_{\infty})}\right] \tag{2.14}$$

Lewis's model showed the difference between co-current liquid flow and con-current liquid flow on successive trays. Case 2 gave the highest tray efficiency with case 3 giving the lowest. With vapour mixing, the efficiency of case 2 is reduced and that of case 3 is improved until they both approach case 1. Lewis admitted that the enhancement of the tray efficiency over the point efficiency on an actual tray will be less than predicted due to mixing of both the liquid and the vapour.

Mixed Pool Models

As mentioned, models were also developed by using mixed pools. Kirschbaum (1948) developed his earlier theories using mixed pools in series, with the composition of the liquid changing as it passed between pools. Gautreaux and O'Connell (1955) extended this approach by making use of Lewis's case 1 but with liquid mixing. They developed the method to include an equation for tray efficiency.

By the 1970s attempts were being made to relate the principles of the eddy diffusion and the mixing pools models so that the advantages of each could be utilised. As mentioned above Ashley and Haselden (1970) identified a relationship between the Peclet number and the number of mixed pools. It was noted that they were both attempts to measure the same phenomena, namely the extent of mixing. They identified a method of determining the number of mixed pools by a tracer experiment. Bruin and Freije (1974) extended this modelling approach to introduce side mixing pools in an attempt to model the stagnant zones. The results obtained were almost identical to those of Porter et al. (1972) using a diffusion model.

Kafarov et al. (1979) proposed a combination model that comprised both diffusion and mixing pools. The model was effective but seemed to be too complicated for practical use. Yu et al. (1983) produced a mixed pools model as part of a two-part paper, with an eddy diffusion model as the first part. The model makes use of two-dimensions and allows complex flows to be simulated by altering the flows in the two directions. The inclusion of back-mixing fixes the number of pools and makes it possible to solve the model by matrix computation. This model can be reduced to other models by altering the number of pools in each direction.

This has been a short overview of the models produced by using mixed pools. Their use generally leads to simpler equations than those produced by eddy diffusion models, but mixed pools are only a concept and the eddy diffusion process is probably closer to the true picture. The advantages of the pools approach is reduced thanks to the increased computing power now available. This allows more complex models, such as those produced from eddy diffusion models to be solved quicker. Thus the main advantage of ease of solution is lost. This has led to the increase in the development of more realistic models at the cost of the mixed pool approach.

Plug Flow with Backmixing

In the U.S.A., the research of distillation in the fifties was directed by the AIChE. A series of reports was produced over the decade to detail the progress made. Gerster et al. (1955 and 1958) worked within this programme and produced the first model to use eddy diffusion to describe the liquid mixing on the tray. The model assumed that the rate of mixing was proportional to the local concentration gradient. The model was incorporated into the method produced by the AIChE (1958) to estimate the tray efficiency. This method involves the mass transfer being calculated on a two-film theory basis, liquid and vapour phase. To use the method the tray design needs to be fixed and then the operating and system variables calculated. The method was

developed for use with bubble-cap plates but has been modified for use with sieve trays (Smith, 1963).

The method takes into account the major factors that are known to affect the tray efficiency, namely:

i. Mass transfer characteristics of the liquid and vapour phases,
ii. Design parameters of the tray,
iii. Degree of mixing on the tray and
iv. Vapour and liquid flow rates.

The equations involved in the method are given below along with a very brief explanation. For further information the AIChE (1958) manual should be consulted.

The resistances to mass transfer are expressed in terms of the number of transfer units, N_G and N_L. The point efficiency is related to them by the following equation:

$$\frac{1}{\ln(1-E_{OG})} = -\left[\frac{1}{N_G} + \frac{mV}{L} \times \frac{1}{N_L}\right] \tag{2.15}$$

The number of transfer units for each phase are given by equations 2.16 and 2.17 below. For a description of the symbols used, reference should be made to the nomenclature.

$$N_G = \frac{\left(0.776 + 4.57 \times 10^{-3} h_w - 0.24 F_v + 105 L_p\right)}{\sqrt{\left(\mu_v / \rho_v D_v\right)}} \tag{2.16}$$

$$N_L = (4.13 \times 10^8 D_L)^{0.5} (0.21 F_V + 0.15) t_L \tag{2.17}$$

t_L is the liquid contact time and is given by:

$$t_L = \frac{Z_c Z_L}{L_p} \tag{2.18}$$

where Z_L is the length of the liquid path and Z_C is the liquid hold-up on the tray. Z_C is different for each type of tray. The original work was done on bubble-cap trays where the liquid hold-up is given by:

$$Z_c = 0.042 + 0.19 \times 10^{-3} h_w + 0.014 F_v + 2.5 L_p \tag{2.19}$$

Smith (1963) has proposed the following equation for use with sieve trays:

$$Z_c = 0.006 + 0.73 \times 10^{-3} h_w - 0.24 \times 10^{-3} F_v h_w + 1.22 L_p \tag{2.20}$$

As has been mentioned above, the point and tray efficiencies are only equal if the tray is perfectly mixed. To estimate the tray efficiency from the point efficiency, the degree of mixing on the tray needs to be determined. Use is made of the Peclet number which characterises the mixing in a system. For a tray the Peclet number is:

$$Pe = \frac{Z_L^2}{D_e t_L} \tag{2.21}$$

The eddy diffusivity, D_e, for both bubble-caps and sieve trays can be estimated from the following equation:

$$D_e = \left(0.0038 + 0.017 u_a + 3.86 L_p + 0.18 \times 10^{-3} h_w\right)^2 \tag{2.22}$$

A Peclet number of zero indicates that the tray is perfectly mixed and a value of ∞ indicates plug flow. The Peclet number is then used to find the tray efficiency by using graphs contained in the manual. E_{MV}/E_{OG} is plotted against $(mVE_{OG})/L$ and lines are drawn that correspond to different Peclet numbers. At this stage we will have calculated the Peclet number and point efficiency and therefore be able to find the tray efficiency from the ordinate value obtained.

To use the above method, estimates of the physical properties of the system are needed. The AIChE manual recommends equations to calculate liquid diffusivity and the gas diffusivity. The significance of the weir height should be noted. The weir height was found to be the tray parameter with the most effect on the tray efficiency. The correlation for mixing on the tray was not tested on large diameter trays and Smith (1963) states that the correlation should not be used for these trays. In practice a large tray can be split into smaller sections and each section calculated separately. The method does not account for the circular nature of the tray as only the liquid path length is used.

The Model of Chan and Fair (1984)

This particular model is included here as it is used in a future chapter to compare the experimental data. It fits in after the AIChE model as it is a hybrid of it, lying somewhere between it and the model proposed by Zuiderweg (1982). The Chan and Fair (1984) correlation is based on an extensive data bank collected on trays with diameters from 0.46 m to 1.22 m and hole sizes ranging from 2.5 mm to 12.7 mm in diameter. Point efficiencies were obtained from distillation data and equation 2.23 was used to calculate a value for the overall number of binary vapour phase transfer units, N_{OG}.

$$E_{oG} = 1 - \exp(-N_{oG}) \tag{2.23}$$

The AIChE correlation was used to obtain the liquid phase resistance, N_L and values of N_G were calculated as below:

$$\frac{1}{N_{oG}} = \frac{1}{N_G} + \frac{\lambda}{N_L} \tag{2.24}$$

This calculation is open to the same criticism as the AIChE model in that it tends to underestimate the percentage liquid phase resistance. However, the redeeming feature

of this model is that it is based on actual data obtained from distillation experiments. The correlation that is finally obtained is:

$$N_L = 1.97 \times 10^4 (D_L)^{0.5} (0.40 F_s + 0.17) t_L \tag{2.25}$$

$$t_L = \frac{h_{cl} Z W}{Q_L} \tag{2.26}$$

$$N_G = \frac{1000 (D_G)^{0.5} (10.3(FF) - 8.67(FF)^2 t_G}{h_{cl}^{0.5}} \tag{2.27}$$

$$t_G = \frac{(1-\alpha_e) h_{cl}}{(\alpha_e u_s)} \tag{2.28}$$

In the above equations, FF is the fractional approach to flooding and is given by $FF=u_s/(u_s \text{ at flooding})$, and h_{cl} and α_e are given by the equations below:

$$h_{cl} = \alpha_e \left[h_w + C \left(\frac{Q_L}{W \alpha_e} \right)^{0.67} \right] \tag{2.29}$$

$$\alpha_e = \exp\left[-12.55 \left(u_s \left(\frac{\rho_G}{\rho_L - \rho_G} \right)^{0.5} \right)^{0.91} \right] \tag{2.30}$$

where C is given by:

$$C = 0.50 + 0.438 \exp(-137.8 h_w) \tag{2.31}$$

Equations 2.29 to 2.31 are given by Bennett et al. (1983).

The correlation predicts almost exactly the same liquid phase resistance as the AIChE model, but this is not surprising as the same correlation for N_L is used in both cases.

The method tends to predict high values of point efficiency and the inclusion of the fractional approach to flooding implies that the efficiency depends on the tray spacing for fixed vapour and liquid loads. This does not seem reasonable and reminds us of the empirical nature of the correlations developed.

Tray Models with Multi-Regions and Backmixing

Other models have been developed using the eddy diffusional view of the flow on trays to predict efficiency (Porter et al., 1972; Bell and Solari, 1974; Biddulph, 1975; Sohlo and Kouri, 1982 and Yu et al., 1983 and 1990). Some of these models allow for diffusion in two directions and as such they attempt to model the circular tray. The main basis of these models is a material balance over an element of froth and the differences that occur can be attributed to the different boundary conditions used or assumptions made.

To illustrate the development of the models, the example of the Porter et al. (1972) model is given below. As mentioned above, the various models follow a similar development. The model makes a number of assumptions:

1. a constant point efficiency over the tray,
2. liquid will channel between the two downcomers and at the sides it is stagnant,
3. the entering streams are perfectly mixed,
4. the equilibrium line is linear over the concentration range,
5. liquid is perfectly mixed over the depth of the froth,
6. the eddy diffusivity is equal in all directions and
7. the bulk liquid flow occurs in the z-direction.

The co-ordinates for the model are shown in figure 2.1. The direction with the flow path length is denoted the z-direction and the transverse direction is denoted as w. The tray is symmetrical about the centre-line in the z-direction and therefore the calculations are based on one half of the tray. As the model assumes stagnant zones,

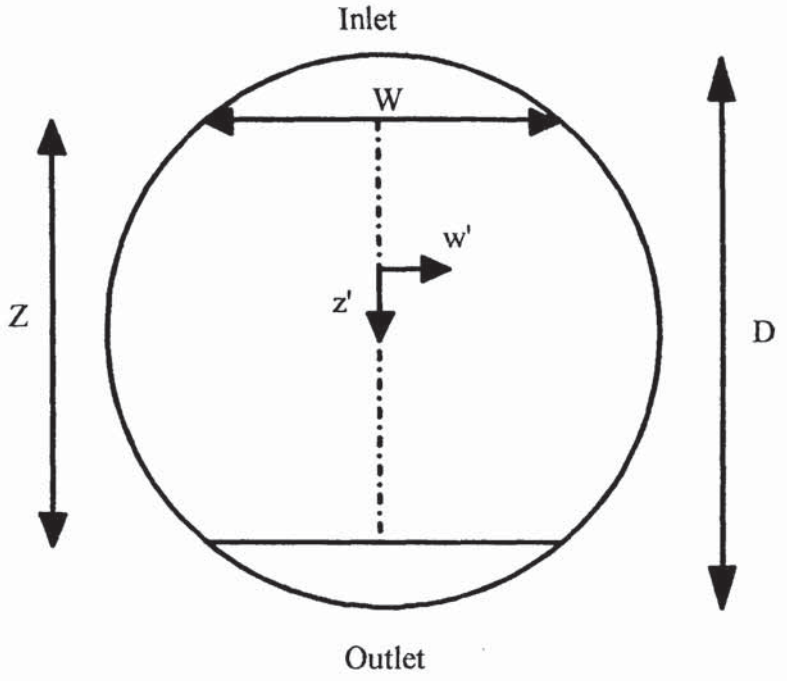

Figure 2.1 Co-ordinate system used for the Porter et al. (1972) model

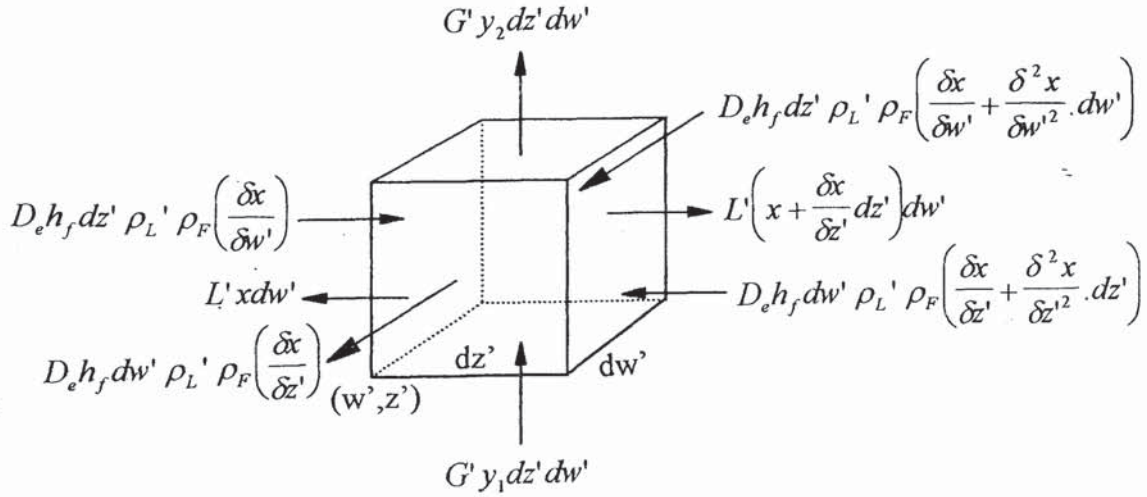

Figure 2.2 Flows through an element of froth

i.e. no flow, in the segments of the tray, the half tray is defined so that $0 \leq w \leq (W/2)$.

The equations that govern this model are based on figure 2.2, which shows the flows through the element of froth. The model further assumes that material is transferred into and out of the froth by the following mechanisms:

a) Mass transfer from the liquid to the vapour,
b) Bulk movement of the liquid across the tray in the z-direction only and
c) Liquid backmixing as a result of the gas passage.

If we now consider the material balance over the element, we can derive the equation below for the main flow region, termed region I by the authors.

$$D_e\left\{\frac{\partial^2 x}{\partial w'^2}+\frac{\partial^2 x}{\partial z'^2}\right\}-\frac{L'}{h_f.\rho_L'.\rho_F}.\frac{\partial x}{\partial z'}+(y_1-y_2)\frac{G'}{h_f.\rho_L'.\rho_F}=0 \qquad (2.32)$$

In the stagnant zones the material balance can be written as below. The authors term this section of the tray region II and there is no liquid flow in this area. Therefore the liquid flow term is zero.

$$D_e\left\{\frac{\partial^2 x}{\partial w'^2}+\frac{\partial^2 x}{\partial z'^2}\right\}+(y_1-y_2)\frac{G'}{h_f.\rho_L'.\rho_F}=0 \qquad (2.33)$$

If we use the following definitions and dimensionless quantities:

$$E_{OG}=\frac{(y_2-y_1)}{(y^*-y_1)}=\frac{(y_2-y_1)}{m(x-x_e^*)} \qquad (2.34)$$

$$Pe=\frac{LD}{W.h_f.\rho_L'.\rho_F.D_e} \qquad (2.35)$$

$$\lambda = \frac{mG}{L} \tag{2.36}$$

$$z = \frac{z'}{D}, \qquad w = \frac{w'}{D} \qquad \text{and} \qquad X = \frac{\left(x - x_e^*\right)}{\left(x_1 - x_e^*\right)} \tag{2.37}$$

Equations 2.32 and 2.33 can be changed into dimensionless equations:

$$\frac{1}{Pe}\left\{\frac{\partial^2 X}{\partial w^2} + \frac{\partial^2 X}{\partial z^2}\right\} - \frac{\partial X}{\partial z} - E_{OG}\lambda\left\{\frac{WD}{A}\right\}X = 0 \tag{2.38}$$

$$\frac{1}{Pe}\left\{\frac{\partial^2 X}{\partial w^2} + \frac{\partial^2 X}{\partial z^2}\right\} - E_{OG}\lambda\left\{\frac{WD}{A}\right\}X = 0 \tag{2.39}$$

The boundary conditions to solve the model are given below:

a) By symmetry along the z-direction centre line:

at w=0 for $0 \le z \le Z/D$, $\frac{\partial X}{\partial w} = 0$ (2.40)

b) At the liquid inlet (Danckwerts, 1953 and Wehner and Wilhelm, 1956):

at z=0 for $0 \le w \le W/2D$, $X_+ = 1 + \frac{1}{Pe}.\left\{\frac{\partial X}{\partial z}\right\}$ (2.41)

c) At the liquid outlet:

at z=z/D for $0 \le w \le W/2D$, $\frac{\partial X}{\partial z} = 0$ (2.42)

d) At the impermeable column wall:

$$\frac{\partial X}{\partial n} = 0 \tag{2.43}$$

To solve the equations they are transformed into their finite difference form and then solved numerically. The solution is a function of the dimensionless groups, λ, E_{OG}, Pe and DW/A. The first three groups appear in the simple back-mixing theory and the fourth group is a measure of region II, the stagnant zone, relative to region I.

A consequence of this model was the mixing zone concept. The authors calculated that volatile material could be replenished in the stagnant zones by mixing caused by the vapour. They estimated that the width of these mixing zones was approximately 0.3 m to 0.5 m. This allowed columns with diameters of up to 1.5 m to have the liquid in their stagnant zones replenished. Trays over this diameter would suffer due to no replenishment of the volatile material and thus suffer a reduction in efficiency.

Comments on the Other Diffusional Models

The model of Bell and Solari (1974) predicted a tray with no diffusion due to the range of Peclet numbers that they encountered. They stated that little would be lost by assuming plug flow due to Peclet numbers of between 20 and 35 being sufficiently high to set it to infinity. The model was then solved for three velocity distributions, inverted parabolic, linear and parabolic. Each distribution is given as a function of its transverse position and a slip velocity at the wall was allowed for. Kouri and Sohlo (1985) solved their equations for a similar inverted parabolic velocity distribution but diffusion was included by use of the Peclet number.

Sohlo and Kouri (1982) developed a model that was similar to that of Porter et al. (1972), but it allowed for movement of material in the transverse and longitudinal directions by other than eddy diffusion. To solve the equations developed, it was assumed that the eddy diffusion was the same in all directions. Also, from measurements taken by Bell (1972) and Sohlo and Kinnunen (1977), a simple non-uniform velocity profile was assumed. Three profiles were also assumed, severe channelling, parabolic and turbulent. The main conclusion of this work was that the adverse effects caused by the non-uniform velocity profile could best be over come by an improvement in the velocity profile, as opposed to other methods.

Yu et al. (1983) developed the model of Porter et al. (1972) by reconsidering the stagnant regions. It was noted that in this region the liquid was split into slowly forward

flow and backward flow, with a completely mixed region close to the inlet. A new velocity distribution function was proposed to take account of the non-uniformity present on large trays.

Fluid Mechanical Models

Yu et al. (c. 1991) proposed a model based on fluid dynamic principles. The model made use of the Navier-Stokes equations to model the flow of the froth. In essence, the model is liquid only but the effect of the gas is incorporated into the equations in the form of an added resistance. Assumptions are made about the momentum that is transferred to the gas from the liquid. The gas is assumed to be accelerated from a case of no horizontal velocity, i.e. it enters the froth vertically, to having a horizontal velocity equal to the velocity of the local liquid. The second effect of the gas is to cause turbulence in the liquid and Yu dealt with this by introducing an eddy viscosity term. It was argued that this viscosity was equal to the eddy diffusivity.

A number of assumptions are made in the solving of the equations developed by this model. A boundary layer close to the tray floor is assumed which has yet to be proved by experiment. Resistances are added, which forms the main difference from the Navier-Stokes equations and therefore the equations are very similar to those produced for single-phase flow. Also, if the instantaneous values of velocities are used, it is assumed that laminar flow equations can be used. This treatment has been applied before and it is felt that it is valid in this case.

The validity of some of the assumptions used in this model may be questionable, but it does show close agreement with the salt tracer experiments determined by Yu. The approach also provides a good starting point for models of this nature. The model also predicts its own flow pattern and will be useful in the determining of tray and point efficiencies from first principles.

The method has been further developed in recent years by collaborative work between the research groups of Yu and Porter. This has resulted in a model being published in the open literature (Porter et al., 1992) based on computational fluid dynamics (CFD). Once again it is based on two-dimensional Navier-Stokes equations for turbulent flow, with the effect of the gas being modelled as a resistance to the liquid flow. The paper compares predicted flow patterns with those produced on a 2.44 m diameter tray and finds that the model can predict reverse flow on the tray.

Very recently the method has been further extended by the use of CFD to allow the solving of more complex equations (Porter et al., 1995 and Walton, 1995). These methods have seen the prediction of point and tray efficiencies from a similar model to that of Yu. The values have also been compared with those obtained from water-cooling experiments on a 2.44 m diameter tray. It was found that the efficiencies were predicted fairly accurately and that the model could also be used to gain an insight into flow features that promote liquid mixing. In this way it is hoped to be able to find ways in which to prevent the stagnant regions suggested by Porter et al. (1972) from appearing. The accuracy of the model could be further improved by experimental work to improve correlations for the liquid hold-up, eddy diffusivity and to assess the resistance term.

Conclusions on Tray Models

Over the years models to predict the tray efficiency have come a long way from simple models devised by use of small, laboratory scale, columns to models to predict the non-uniformity of flow on a large-scale column. With the increase in computing power available nowadays, much more complex equations can be solved in a reasonable time scale. This has led to different methods of solving problems caused by the complexity of the two-phase flow. We have passed through the early one-dimensional models and progressed to three-dimensional models. Many of these assumed a flow pattern. We have now come to a new generation of models that can predict the flow pattern. We have had seventy years of modelling, but the experimental work on large-scale trays has

lagged behind. We are now at the stage where techniques have been invented to measure the flow on trays of a large scale. The imbalance between theoretical and experimental work must now be dealt with. Experimental work to determine the flow patterns on trays would be highly advantageous to the development and accuracy of future models.

2.5 Hypothetical Flow Patterns on Trays

Due to the experimental work that has been carried out into how the liquid flows across a circular tray, several hypothetical flow patterns have been proposed. These have been used as the basis of the efficiency models produced. It is useful now to give a brief description of these flow pattern models. There are three main models that have been proposed and these will be described below:

The Stagnant Regions Model

This model was proposed by Porter et al. (1972) and suggested that the flow on the tray was from downcomer to downcomer with stagnant flow in the segments of the tray. This flow pattern came about by the observation of water flowing across a 1.2 m diameter test section in a water flume. The water flowed onto the section and then straight across it with a uniform bulk velocity. The water in the side regions of the tray was separated from that in the centre and was found to be either slowly circulating or stagnant. The flow pattern was observed by watching the motion of table tennis balls on the water surface and was found to be independent of the water flow rate and the weir height.

Retrograde Flow Model

This was proposed by Bell (1972a) and was based on the findings of an experimental technique using fibre optics, as described below. The experiments were carried out on a

tray of 2.44 m in diameter. The data, when extrapolated to the column wall, identified closed lines of constant residence time. The presence of these lines was explained by reverse or retrograde flow occurring in these areas, with flow down the centre of the tray between the two weirs. The confirmation of this flow pattern was sought by an injection of dye along the transverse centre line of the tray. Dye was discovered near the inlet at the sides of the tray, confirming the presence of the retrograde flow.

Composite Model

This is the most complex of the flow pattern models described here. It was proposed by Yu et al. (1982, 1986) and is based upon their experimental observations on 2 and 2.44 m diameter trays. Three regions are found over the tray. The main flow is between the inlet and outlet weirs, with a non-uniform velocity distribution. The side regions of the tray are separated into two smaller regions. A slowly forward flow region exists on the outlet side of the section and a backwards flow region is found towards the inlet.

Conclusions on the Flow Pattern Models

The proposed flow patterns are in agreement that there is some form of channelling down the centre of the tray. However there is disagreement about how the side segments of the tray should be treated. The liquid in these regions is thought to be either stagnant, slowly circulating or slowly flowing forward. It is felt that how the liquid behaves in these regions is very much a symptom of the design of the tray and the flow rates. This could explain the variations in the flow patterns proposed.

It is felt that with the improvement of computers and the predictive models it is now possible to predict the flow pattern from first principles and that future models will do this. This will do away with the need for a hypothetical flow pattern to be proposed before the model can be solved. Experimental work will be required to determine the

conditions that each flow pattern occurs under and to test the predictive powers of the proposed models.

2.6 Measurement Techniques

Over the years, many techniques have been employed to investigate the flow on trays. These have usually employed adding something to the liquid to give an indication of the residence time. More recent techniques have involved direct measurement of some property, either temperature, concentration or froth velocity.

2.6.1 Coloured Dye with Camera

This technique involves adding dye to the froth, usually at the inlet or along the transverse centre line, and recording how it flows across the tray using a video camera. The technique has proved popular and has been used by many researchers (Weiler et al., 1971, 1973; Aleksandrov and Vybronov, 1971; Porter et al., 1972; Solari et al., 1982; Ani, 1988 and Hine, 1990) to obtain raw data that can be transformed into residence time distributions. The technique can be split into two variations.

1. Dye is continuously injected onto the tray until the froth is completely coloured. Once this has occurred the injection is stopped and the dye begins to be removed by the clear liquid entering the tray. This is recorded by the camera and areas where the dye remains longest are an indication of increased residence time. This method highlights the presence of non-uniform flow over the tray but it consumes large quantities of water that must then be discharged.

2. A pulse of dye is injected into the froth in a line perpendicular to the flow path length (transverse) and the movement of it is recorded using the camera. This method uses less water and is used to obtain data from which the residence time distribution can be calculated. As mentioned above, the dye can be injected either at

the inlet (Weiler et al., 1971, 1973; Ani, 1988 and Hine, 1990) or along the transverse centre line (Porter et al., 1972 and Solari et al., 1982).

The main difficulty with calculation of residence time distributions from this type of experiment is that the band of dye spreads out as it is mixed by the gas passage through the liquid. Weiler et al. (1971, 1973) proposed that the mid-point of the band was a measure of the bulk liquid flow and the widening of the band was an indication of the mixing at the point on the tray. Once again the problem lies with defining where the mid-point lies due to the continuous fall off in the intensity of the dye, making it difficult to determine the edges of the band.

Aleksandrov and Vybronov (1971) modified the technique slightly to try to overcome this problem. A known concentration of dye was injected at the inlet and then samples were extracted from three evenly spaced points close to the outlet, at discreet time intervals. The samples were then mixed and a photocolorimeter was used to measure the dye concentration. The results were then used to produce residence time distribution response curves for the whole tray.

2.6.2 Floating Balls with Camera

This technique has been utilised for studying the flow of water only across an open channel water flume (Porter et al., 1972), set up to model the shape of a tray. Table tennis balls were half submerged on the liquid surface and the way that they passed across the flume was observed. The results showed that the water rapidly flowed from the inlet to the outlet with stagnant or recirculating liquid in the side sections of the tray. The results from these experiments were used by the researchers to produce a number of theoretical models for different situations (Porter et al., 1972; Lim et al., 1974 and Lockett et al., 1976).

Sohlo and Kinnunen (1977) used cork balls on a sieve tray in an attempt to measure the froth velocity. This was a crude method involving the timing of the balls between set points on a 0.5 m tray.

2.6.3 The Use of Fibre Optics

A system was developed by Bell (1972 a and b) that made use of a fluorescent tracer injected into an n-hexane/toluene binary system. The tracer had a very rapid activation and decay time that allows its passage across the 2.44 m diameter tray to be observed by a system of 'double' probes. The probes are split into two parts, the first transmits light into the liquid which activates the tracer. The second part of the probe detects the fluorescence of the tracer and transmits it to a photomultiplier tube.

The collection of the data was carried out by an on-line computer and was processed by finding the mean residence time of the tracer as it passed the probes. This in turn led to the residence time distribution over the tray. The variance of the residence time of the tracer at the probe was taken as a measure of the localised mixing. Further studies of trays by this method were carried out by Solari and Bell (1986) on 1.22 m trays. This assessed twenty-five points in approximately thirty seconds and led to measurements of the residence time distribution on the trays. The earlier studies where combined with a flow visualisation technique on a water-only system which showed circulation of the liquid. However, the tests on the 1.22 m trays only showed the presence of stagnant zones with a degree of backmixing. The earlier studies were incorporated into a model for the tray efficiency on a square tray with recirculation (Bell and Solari, 1974).

This method is very useful in that it allows the assessment of real columns where the hazard is great and the disruption to the operation is small.

2.6.4 Salt Tracer and Electrode Detectors

Yu et al. (1982, 1986 and 1990) used an array of conductivity probes on a movable truss to measure the concentration of a salt tracer across the tray. The sodium chloride tracer was added along the length of the inlet downcomer and allowed to cross the tray. The change in the conductivity of the liquid around the probe indicated the movement of the tracer past it. The data were collected by a personal computer and the sampling time of each probe was 0.033 seconds. The measurements were then taken to be simultaneous. Mean values for the residence time were recorded by duplicating runs and calculating the mean value. These values were then used to plot residence time distributions for the whole tray and used to assess the accuracy of mathematical models being developed.

2.6.5 The Water-Cooling Technique

This technique makes use of the analogy between heat and mass transfer. Hot water is passed onto the tray and is cooled by the passage of rising air through it. The temperature of the water is measured by an array of temperature measuring devices and isolines are constructed. Isolines are lines that join together points with the same value, in this case temperatures (isotherms). A lower temperature indicates that the liquid on that section of the tray has a higher residence time.

Stichlmair et al. (1973, 1985 and 1987) were the first to make use of this technique to assess the effect of tray levelness and alterations to the inlet and outlet downcomers. The constant temperature lines which were generated were at first interpreted as lines of constant residence time. This was replaced by using thermographic images of the froth where the colour is related to the temperature.

The method was developed by Porter et al. (1982) to allow the calculation of Murphree efficiencies from the temperature profiles produced. This was repeated by Porter's co-

workers in the succeeding years (Enjugu, 1986; Porter et al., 1987; Ani, 1988; Hine, 1990 and Chambers, 1993).

2.6.6 Measurement of the Froth Velocity

Biddulph and Bultitude (1990) developed a technique to measure the velocity of the froth. It involves the induction of a strain on a titanium probe inserted into the froth. The magnitude of the strain is related to the momentum of the froth and can be measured by strain gauges attached to the probe. These gauges convert the strain into an electrical signal that is passed to a data logger. By using calibrations the signal can be converted into the froth velocity. The only drawback with this method, and indeed with many others, is that the probe may alter the very property it is trying to measure.

2.6.7 Flow Pointers and Camera

Flow pointers similar to weather vanes were used by Hine (1990) to provide a simple method for the visualisation of the flow of the bi-phase across the tray. The pointers were made of thin, lightweight aluminium and consisted of a vertical sheet topped with an arrowhead. The flag was attached to a rod and allowed to freely rotate about it. This led to the flags lining up with the local flow and indicating the direction. Residence time distributions could not be made from this method due to the flags only showing direction and giving no indication of the local velocity. The position of the flags was recorded using an overhead camera and indicated that circulation of the bi-phase was possible with certain conditions.

2.7 Conclusions on the Literature Survey

There is evidence from the experiments that have been carried out that the flow pattern has a significant effect on the tray efficiency, and hence column efficiency. Indeed the effect of a detrimental flow pattern on a series of trays can have a disastrous effect on

the column or section efficiency (Locket et al., 1973). Typically a non-uniform flow of liquid is in evidence on an operating distillation tray and this affects the efficiency. Little work has been carried out to assess the causes of this non-uniformity and it is only recently that experimental programmes have been put in place to research this area. A full understanding of the conditions that cause non-uniformity is essential to allow future models to develop.

Although work has been carried out at Aston University (Enjugu, 1986; Ani, 1988; Hine, 1990 and Chambers, 1993) into the conditions for various flow patterns, the earlier work was on a 1.22 m column. If we take note of Porter et al.'s (1972) finding that the mixing zone can mask the effect of stagnant zones up to column diameters of 1.5 m, then obviously a larger diameter is required. The later work was carried out on a 2.44 m diameter tray and therefore the effect of channelling and circulation will be more marked. Little work has been carried out to assess the effect of the hole size on the flow pattern and this is the subject of a future chapter.

The models of Yu et al. (1992) include resistance terms that need to be assessed by experiment. A start is made to help determine this by using experiments on a rectangular tray. The effect of hole size can be further assessed by this work and its effect on the resistances determined. It is felt that the way forward in modelling is by the techniques derived by Yu and using CFD techniques to gain further models of the flow. However, the use of these models and their basis in theory should also be tested by reference to experimentally determined data.

CHAPTER 3

APPROACH TO THE PROBLEM

The study of bi-phase flows on distillation trays has, in the main, been restricted to small scale test rigs. Problems have occurred when these data have been scaled up, with effects such as column failure or a reduction in efficiency. The work presented in this thesis was carried out on a 2.44 m diameter test rig using an air-water system. The diameter was chosen because it is large enough to highlight problems of uneven flow and it is also representative of industrial columns. Typically industrial columns vary between 1.0 and 10 meters in diameter with a mean of between 2 to 3 m (Porter & Jenkins, 1979).

Work has already been carried out on this test rig to test 1 mm (Hine, 1990) and 6.35 mm hole diameter trays (Chambers, 1993). These trays are typical of those used in air separation and the petrochemical industry respectively. This work has extended the previous work to cover trays with 12.7 mm diameter holes, such trays are commonly used in the chemical and petrochemical industries, especially where fouling or corrosion are a problem. The effect of forcing gas through the liquid on the tray is analysed by comparing studies of the perforated tray with data collected on an unperforated tray.

A number of techniques were used to assess the performance of a tray:

1) Direct observation of the bi-phase was carried out using flow pointers which were semi-submerged in the froth or spray. These work in a similar way to weather vanes, with the pointers showing the local direction of flow. The position of the pointers was recorded on video to create a permanent record.

2) The efficiency of the tray was assessed by making use of the water-cooling technique. This uses the analogy between heat and mass transfer. Hot water was fed onto the tray and cooled by interaction with cool air. The water temperature is analogous to the liquid concentration and the air enthalpy is analogous to the concentration of the most volatile component in the vapour. The temperature of the bi-phase was measured using platinum resistance thermometers (PRTs) evenly spaced over the test tray. The data produced were used to create computer generated diagrams that showed lines of constant temperature.

3) The height of clear liquid across the tray was measured using a regularly spaced grid of manometers attached to pressure tappings on the tray floor. By using these measurements it was possible to make 3D computer generated images of the variation of liquid head across the tray.

The techniques outlined above were used to carry out a number of experiments:

a) An investigation into separated and non-separated flow on a 12.7 mm hole diameter test tray was carried out. The techniques were used to show which type of flow was occurring and the effect that it had on the efficiency and the liquid head.

b) The test rig was altered to contain a rectangular test tray and three different hole diameters (1 mm, 6.35 mm and 12.7 mm) were tested. The manometer technique was used on these trays to measure the liquid head profile on a tray section where there was no change in width. Water-cooling was used to produce efficiency data which could be compared to that generated by the Chan and Fair (1984) model. Direct observation was only carried out on a selection of flow rates to show that the flow was in the forward direction only.

The experiments and techniques outlined here are given fuller description in the chapters that follow, along with the results obtained from them.

CHAPTER 4

EXPERIMENTAL APPARATUS

4.1 Introduction

This chapter gives a detailed description of the test facilities used during the experiments reported in this thesis. This mainly involves the air-water simulator column along with its ancillary services. The services include the air supply, water supply and heating system. Also described below is the system for ensuring that both the water and air enter the tray in a way representative of that encountered on a normal distillation tray in an operating column. The chapter concludes with the alterations to the simulator to allow investigation of flow across a rectangular column.

4.2 The Test Facility Flowsheet

Figure 4.1 is a schematic diagram of the air-water simulator on which the experiments were carried out. The air enters the rig through the air fan and passes into the base of the column via a tangential inlet. Any swirl in the air is eliminated by the baffle system in the base of the column. From there the air is passed into the tray test section.

Water is stored in two sump tanks at ground level. From there it is pumped to the top of the column via a heat exchanger. The heat exchanger is in two sections, the first contains hot water from the gas-fired burners and the second contains condensing steam. The water then passes into the column through a sparge pipe and is distributed into the downcomer by random packings.

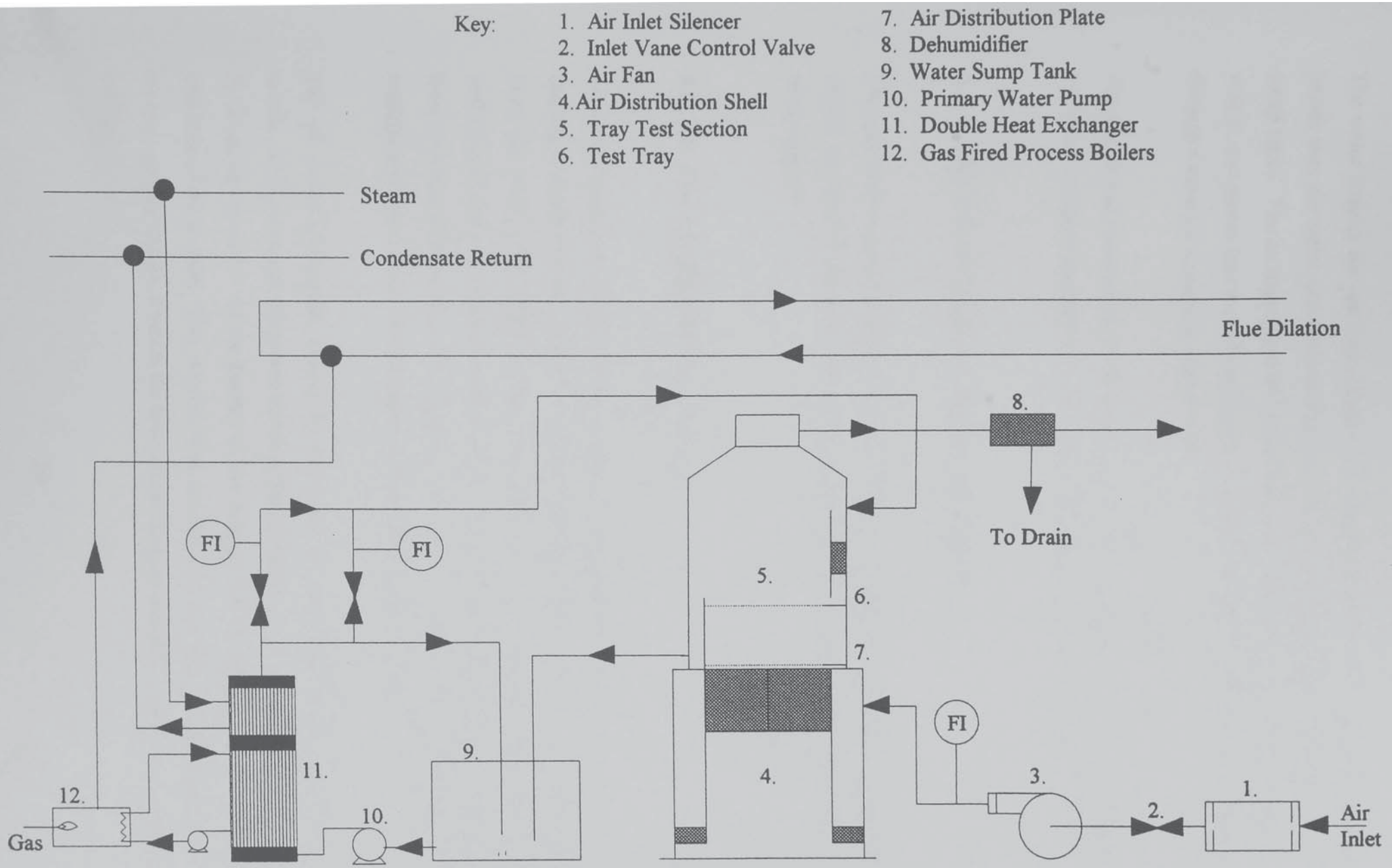

Figure 4.1 Schematic diagram of the air-water simulator

The water crosses the test tray where it is contacted, and mixed, by the air. It then passes over the outlet weir and into the outlet downcomer, from where it returns to the sump tanks. The air disengages from the bulk of the water, carrying a certain amount with it, and passes into the exhaust system. Before exiting to the outside, the air passes through a demister to remove excess water.

The design and construction of the test facility is described by Hine (1990), but a fuller and more technical description of the various ancillary systems now follows.

4.2.1 The 2.44 m Diameter Simulator Column

The simulator column comprises three sections, an air inlet and distribution system, a middle test section and an air exhaust system. Figure 4.2 shows a schematic diagram of the column.

4.2.1.1 The Air Distribution System

An air fan introduces the air into the column via a section of rectangular ducting. The ducting is attached to the column at a tangent to it and hence some swirl is introduced. From the work of Ali (1984), it was shown that a system of internal cross and radial baffles in an internal cylinder could be used to minimise any high velocity swirling and large pressure differentials. This would produce a more uniform distribution with a negligible pressure drop. Such a system was installed in the column.

The air enters an annulus, created by the inner and outer walls of the distribution section, which contains thirty-two radial baffles to eliminate the swirl in the flow, and is forced downwards. At the bottom of the annulus the air passes into the internal chamber of the section. This is cylindrical and contains four large cross baffles. The air rises up this section, towards the test section, and any residual swirl is cut out by the baffles.

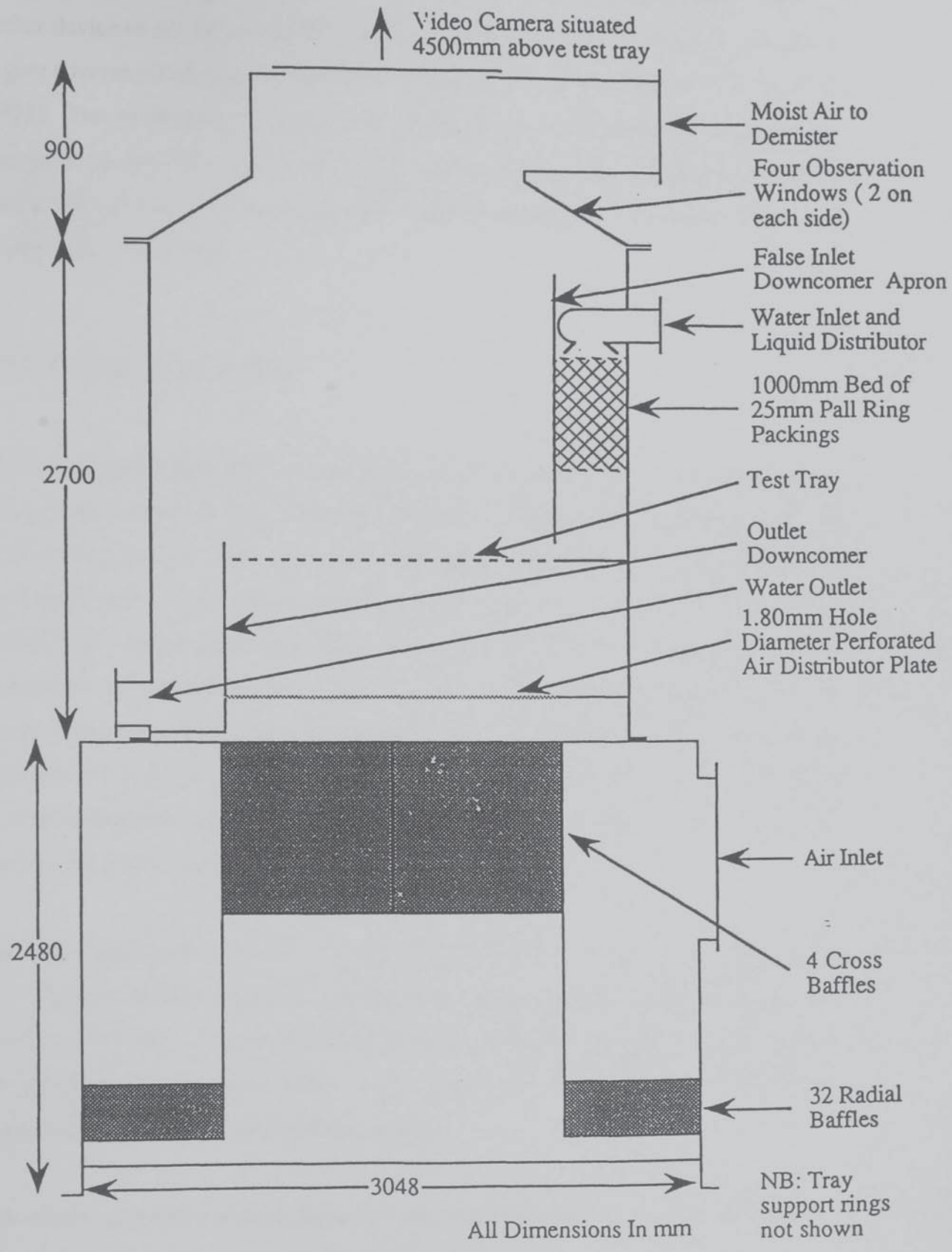

Figure 4.2 Schematic diagram of the simulator column

Above the baffle system there is a 1.80 mm hole diameter perforated plate. This is a further device to aid the air distribution. The old system of a chimney tray was found to give adverse effects and was replaced after experimental investigation by Chambers (1993). The air entering the test section ideally should not contact any water that has weeped from the tray above (hence the original design with a chimney tray). To combat this problem four drain pipes have been installed in the distribution tray to aid the drainage of any water.

4.2.1.2 Tray Test Section

The test section houses the test tray and the measurement devices. The tray sits on a lattice beam framework that is 850 mm above the distributor plate and water is fed to it via a downcomer. The water enters the downcomer from a sparge pipe and is discharged onto a 1 m deep packed bed, which consists of 25 mm Pall rings. The packed bed is contained between the downcomer wall and a sieve plate positioned 600 mm above the downflow plate. This system was developed by Enjugu (1986) to ensure a uniform distribution of water across the weir length. At the bottom of the downcomer the gap to allow the liquid on to the tray can be altered. This is achieved by a moveable plate that can be set at heights of between 10 and 50 mm by the use of spacers, the plate is then secured and the spacers removed.

The water enters under the inlet gap and crosses the tray, where it is contacted by the gas. The gas becomes saturated and enters the exhaust ducting, while the water flows over the outlet weir. The height of the weir can be altered between 0 and 50 mm by the use of angled aluminium strips. Once over the weir, the water enters the outlet downcomer from where it enters the exit pipe.

This whole test section is housed in a 6.35 mm thick aluminium shell that contains observation windows and manways to allow access.

4.2.1.3 Test Trays

The test tray used during experiments on a circular tray contained perforations of 12.7 mm diameter on a triangular pitch and the holes were sharp edged, which is consistent with industrial applications. The tray consisted of four quadrants that were fixed to the support framework by way of steel strips and screws.

For the rectangular experiments the trays used were circular in nature with sections blocked off to make the rectangular test section (see section 4.4). They were fixed to the framework in a similar manner to the circular tray but three different hole diameters were used, 1 mm, 6.35 mm and 12.7 mm.

A summary of the design specifications of the test trays is contained in table 4.1 below.

4.2.1.4 Air Exhaust System

Above the test section the column has a truncated cone shape to allow connection to the exhaust ducting. The ducting is rectangular and leaves the column perpendicular to its centre-line. The saturated air passes through a demister before venting to the outside atmosphere. This section also contains windows where the flow patterns can be viewed from above. A perspex cone is fitted above the air exhaust ducting offtake to facilitate video recording of the flow patterns. This is carried out from a platform 4.5 m above the test tray, from where the whole tray is visible to the camera lens.

Test Tray Design Specifications		
Tray	Tray Material	Aluminium
	Total Tray Diameter (mm)	2430
	Weir Length (mm)	1500
	W/D ratio	0.615
	Dimensions of Support Ring (mm)	50 x 50 x 6
	Flow Path Length (mm)	1925
Tray Perforations	Hole Diameters (mm)	1, 6.35 and 12.7
	Tray Thickness (mm)	2.00
	Edge of Hole	Sharp
	Hole Pitch	Triangular
Areas	Downcomer Area (mm^2)	2.43×10^5
	Active Area (mm^2)	4.189×10^6
	Free Area (mm^2)	4.189×10^5
	Fractional Free Area (%)	10.0

Table 4.1 Tray design specifications

4.2.2 The Water Circuit

The water is stored in two 2.7 m^3 tanks that are linked in series. A PVC pipe network is used to connect the storage tanks to the column via a pump and heat exchanger. The pipework will withstand a temperature of 75°C, which is well above that used for the heat transfer experiments.

For experiments where heat transfer is not required, the water is taken from the tanks by the 15 kW pump and fed through the heat exchanger. From there it is returned to the tanks via a by-pass pipe. Once the column is running and the air is passing through the test tray the water can be passed to it. This is done via one of two flow meters.

One flow meter is of the rotameter variety and is used for low liquid flow rates. A second electromagnetic flowmeter works by measuring the current produced by the fluid acting as a moving conducter in a magnetic field and is used for the higher flowrates. The desired flow rate can then be set and the water is passed to the tray via the sparge pipe and packing arrangement described above. The water passes over the tray, where it is contacted by the air, and then flows over the outlet weir into the outlet downcomer. This downcomer is connected by a pipe to the storage tanks.

When heat transfer is required for water-cooling experiments the water is introduced to the column in the same manner as described above, the main difference being that the heat transfer streams are turned on. The water is circulated around the by-pass loop and is heated. The lower part of the heat exchanger is supplied with hot water from the gas-fired burners and the upper section is heated by condensing steam from the departmental generator. When the water is hot enough for the experiments (assessed by taking the water temperature in the tanks) it is passed through the flow meters and onto the tray in the normal way.

In order to replace any water lost with the air, a fresh water supply has been fitted to the storage tanks. The water that is lost also causes environmental problems because of the heating. The column acts in the same way as a cooling tower and the constantly circulated and reheated water is at the right conditions for the *legionella* bacteria to thrive. The water that is vented with the air is suspended in a mist and can easily be breathed in by the public. With this in mind, a bromine dosing system was fitted to stop the bacteria developing.

4.2.3 The Air Circuit

The air circuit is a very simple arrangement where unsaturated air is drawn from outside through a protective grill and passed into a silencer to reduce excess noise. The air then enters a vane system that is used to control the flow rate and on into the fan itself. The fan has a rotary impeller blade driven by a 150 hp electric motor via a

fan belt. From the fan the air enters a short section of ducting where it passes an array of fifteen pitot tubes. The pitot tubes are connected to a manometer that is used to set the pressure drop across the section and thus the flow rate. On entering the column the air passes through the aforementioned distribution system and then through the test tray. The saturated air leaves the column via the exhaust ducting at a height of approximately 8 m from the ground and is passed through a demister, to remove excess water, before being vented to the atmosphere.

4.2.4 Heat Sources

When water-cooling experiments are taking place, heat is lost from the system by contact with the water, as well as the usual radiation losses. To achieve steady state it is necessary to replace this heat. Since the experiments use a range of throughputs, the heat required is not constant and therefore the heat source must be flexible. From the work of Ani (1988) and Hine (1990) it has been shown that for a given air flow rate the heat removed was greatest at high weir loads. It was also calculated that at the maximum weir load, the heat capacity was 1.2 MW for the 2.44 m diameter column. With this capacity in mind, the facility was designed with two 0.50 MW gas fired boilers, with a top-up supply of steam. This also gave the flexibility required.

4.2.4.1 The Double Heat Exchanger

The heat exchanger is in two parts, the bottom section is a water-water heat exchanger and the top section is a steam condenser. The process water is pumped into the water-water heat exchanger and is heated by a counter-current flow of hot water from the gas-fired boilers. The heating water from the boilers is in a closed loop system and returns to the boilers to be reheated. This section of the exchanger has the greatest area as it is where the main heat transfer takes place.

The process water leaves the bottom exchanger and immediately enters the steam condenser. Further heating takes place inside the condenser, with the condensate returning to the boiler. The process water leaves the heat exchanger at temperatures up to 55°C and travels on to the test section via the flow meters.

4.2.4.2 The Gas Fired Boilers

The gas-fired boilers are used as the primary source of heat to the process water. The two boilers can be operated separately, or together, to supply hot water to the bottom of the heat exchanger, in a closed loop system. The water in the boilers is kept topped up by a header tank supplied through a ballcock arrangement. The flue gas is diluted with ambient air that is drawn from outside the pilot plant by the extractor fan system before being discharged at a height of 8 m above ground level.

4.2.4.3 The Steam Supply

The steam supplied to the top section of the heat exchanger is at a pressure of 80 psig. It arrives at the exchanger from the departmental generator via a 100 mm inside diameter lagged steam line and the condensate is returned to the generator through a condensate line for recycle. The steam is used to provide a top-up heat source to allow fine-tuning of the water temperature. The steam entering the exchanger is controlled using a spring valve of perforated copper tube with a length of 0.5 m and a diameter of 25.4×10^{-3} m.

4.3 Measurement of Variables

The variables to be measured on the rig can be split into two categories. The main components are the air and water flow rates, which are set, and can be classified as operating variables. The air enthalpy, air humidity and water temperatures are determined by the operating variables and can be classified as system variables. The

other physical properties of the air-water system are assumed to be constant over the range of experiments.

4.3.1 Specification of the Air and Water Flow Rates

To specify the maximum and minimum water and air flow rates, use is made of a tray loading diagram. The diagram shows a capacity factor, which is based on the superficial air velocity, plotted against the weir load. The jet flooding curve and the weeping limit are generally shown and provide the maximum and minimum flow rate combinations. It is usual to design the maximum flow rates of the tray at 80% of actual flooding and this line is sometimes shown on the loading diagram. Such a loading diagram was used by Hine (1990) to specify the equipment to be purchased for the simulator and a summary of this work is included below.

The loading diagram used is shown in figure 4.3 and was for a sieve tray with 12.7 mm hole diameter, an 8% free area and a 0.6 m tray spacing. While tray spacing is not a factor with the one test tray arrangement it defines the backup height in the downcomer and has a great significance to entrainment. The capacity factor used is defined by :

$$CF = \frac{Q_G}{A_b}\sqrt{\frac{\rho_V}{\rho_L - \rho_V}} \qquad (4.1)$$

The maximum vapour load factor value for 80% of flooding can be obtained from the diagram and is 0.12 m/s. Given that A_b = 4.189 m^2, ρ_L = 1000 kg/m^3 and ρ_V = 1.22 kg/m^3 we can substitute the values into equation 4.1 to obtain the maximum air flow rate of 14.38 m^3/s.

Similarly, the maximum value of water flow rate can be found by using the maximum weir load value of 0.03 $m^3/m.s$ and substituting into equation 4.2, where the weir length, W, is 1.50 m.

$$Q_L = \left[\frac{Q_L}{W}\right] W \tag{4.2}$$

This yields a value of optimum water flow rate of 0.045 m^3/s.

The specification of pumps or fans does not just depend on the flow rate to be delivered, but also on the resistance to the delivery. For the water pump the specification was for a delivery of 5.5 x 10^{-2} m^3/s against a head of 12.75 m of H_2O. The head value takes into account the vertical height the water has to rise to as well as friction caused by expansions, contractions and fittings, and head lost due to the double heat exchanger.

The resistance to the delivery of the air fan was slightly more involved. Terms for the resistance due to the inlet silencer, air flow meter, air distributor and loses due to expansions and contractions had to be taken into account. But by far the greatest resistance was that due to the air passing through the test tray. The wet tray pressure drop is the resistance expressed in mm of H_2O and is made up of three components, thus:

$$h_{WT} = h_{DT} + h_{cl} + h_R \tag{4.3}$$

h_{DT} is the dry tray pressure drop and is the pressure resistance caused by the air passing through the perforated tray. It is usually represented by an orifice type equation and has been calculated to be a maximum of 0.19 m of H_2O.

h_{cl} is the height of clear liquid and is the resistance caused by the height of froth on the tray. The clear liquid height is the height that the froth would collapse to if the air was turned off and the liquid could be measured immediately. Many equations have been published to calculate the height of clear liquid and from the equations of Bennett et al. (1983) it has been calculated that for an outlet weir of 0.075 m, the clear liquid height is 0.17 m of H_2O.

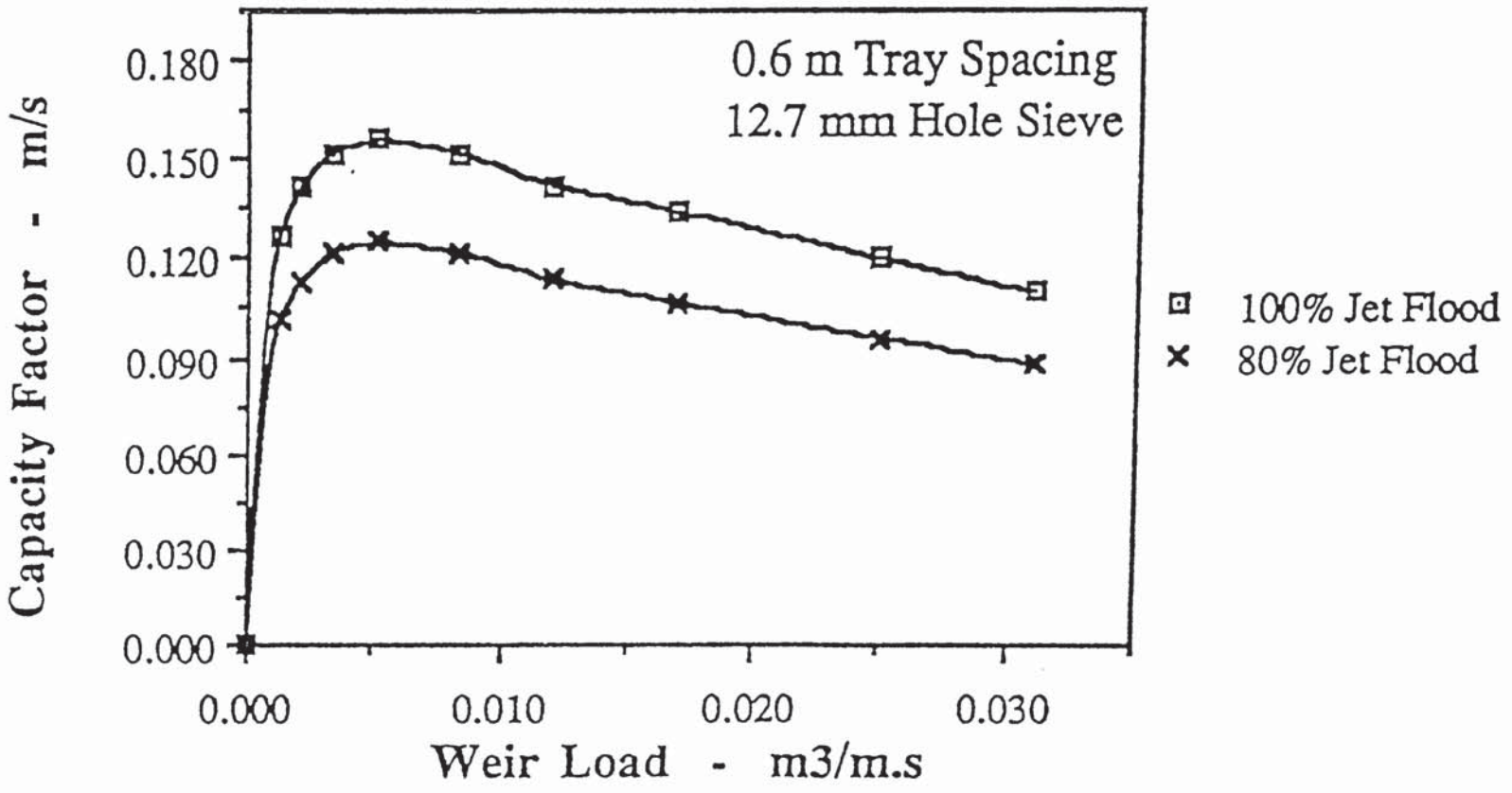

Figure 4.3 Tray flooding curve
(Taken from Hine, 1990, and based on data of Sakata and Yanagi)

h_R is the residual pressure drop and is caused by the gas-liquid momentum transfer processes. The effect is expected to be small compared to the values of h_{DT} and h_{cl} and a value of 0.03 m of H_2O has been assigned to h_R.

The specification of the air fan was to deliver 14.38 m^3/s against a resistance of 0.51 m of H_2O. The resistance includes the various components of the wet tray pressure drop and the terms mentioned above.

4.3.2 Specification of Instruments

To determine the specification of the instruments it was necessary to carry out an error analysis. This was done by Hine (1990) and is outlined below. The principle involved is that every experimental reading has an associated error due to practical scales not providing infinite resolution, i.e. a reading has to be to some 'nearest value'. A low error is desirable so that greater confidence can be expressed in any results published. This leads to a high cost for instrumentation. Conversely, a high error specification would lead to low instrumentation costs, but with a lowering of the confidence in the results. Clearly a trade off is necessary to achieve the best combination of cost and accuracy. It is necessary to obtain the dependency that a property has on specific measurements and to do this an error analysis was carried out on the Murphree tray efficiency.

To obtain the Murphree tray efficiency it was necessary to calculate the air enthalpy driving forces from the temperature measurements made during water-cooling experiments. The accuracy of the efficiency calculated was determined by the error range that had been allowed by the instruments used to measure the system and operating variables. To this end the error ranges of the instruments could be calculated by assuming an acceptable error in the tray efficiency and working back to acceptable errors in the readings used to calculate it. This was possible by using the "Principle of Superposition of Errors", in that the error in a calculated quantity is subject to a combination of the individual errors of the measured quantities. In this case the

measured quantities are the water and air flow rates and the temperatures. The effect of the accuracy of the flow rate measurements on the efficiency was shown to be equal and opposite. The effect of errors in the temperature measurements were more varied. The greatest effect was with errors in T_{out}, followed by T_{in}, then T_{wb} and finally T_{db}. The error analysis is summarised in table 4.2. As expected, the error in the tray efficiency decreased with an increase in accuracy of the measured variables, and vice versa.

Measured Variable	Error	Error	Error	Error
Water Flow rate	4.0%	2.0%	1.0%	0.5%
Air Flow rate	4.0%	2.0%	1.0%	1.0%
Inlet and Outlet Water Temperatures	0.1°C	0.05°C	0.02°C	0.02°C
Inlet Air Wet and Dry Bulb Temperatures	1.0°C	1.0°C	0.5°C	0.5°C
Murphree Tray Efficiency - 0.867	± 0.0573 Or ± 6.6%	± 0.0328 Or ± 3.8%	± 0.0161 Or ± 1.9%	± 0.0142 Or ± 1.6%

Table 4.2 Accuracy of Murphree Tray Efficiency for Given Variable Errors (Hine, 1990)

The final specification of the instruments from the error analysis was as follows:

Air Flow rate	2.0%
Liquid Flow rate	0.5%
Water Temperatures	0.02°C
Air Temperatures	0.5°C

This specification yielded an accuracy of 2.1% in the Murphree tray efficiency. This seems an acceptable allowance. The calculations of the errors quoted above assume steady state operation and any change of the measured variables with time must be taken into account in any final error analysis.

4.3.2.1 Air Flow Meter

Problems occur with where to site the air flow meter. There is limited straight ducting either before or after the air fan and what there is has a large effective diameter. This limits the number of effective diameters, before any measuring device, to one and a half. Together with the specification of a 2% accuracy for the flow meter, this makes it a considerable challenge to design.

A suitable flow meter was purchased from Tekflo Ltd. The meter consisted of a grid of fifteen impact and static pitot sensors which developed a differential pressure across it according to classic Bernouli theory. Each of the sensors occupied an equal area and any irregularities are reduced by the use of shrouds around the sensors, as well as an array of honeycomb flow straighteners up stream from the measurement. All of the sensors are interconnected to produce a representative average differential pressure which is proportional to the air velocity. The superficial air velocity range designed, of between 0.70 and 3.00 ms^{-1}, produces a differential pressure range of 3.19 to 57.92 mm of manometric fluid. This differential pressure is measured using an inclined micromanometer from Perflow Instruments. The principle behind this micromanometer is described in a paper by Bradshaw (1965). The instrument has an accuracy of ± 0.005 mm of manometric fluid and combined with the certificate of calibration for the flow meter, gives a system that conforms to the error specification.

4.3.2.2 Water Flow Meter

With the wide range of flow rates and the limited space available for piping, the water flow meter selection was another challenging design. A suitable position was found near the top of the rig that gave approximately 5 m of uninterrupted flow before the measurement position. The problem caused by the range of flow rates was solved by the decision to use two flow meters. For low flows an orifice plate rotameter was used. This meter was used for less than 5% of experiments and as such had an error specification of approximately 2.0%, slightly higher than the error analysis

specification, but justified by the low level of use. The rotameter had a range of flows of up to 32.4 m^3/h.

For higher flows a more accurate meter was required. Such a meter was purchased from Combustion Engineering, along with a calibration certificate to meet the required accuracy of less than 0.5%. The meter was of the electromagnetic flow type that did not disturb the flow. Use is made of Faraday's law of electromagnetic induction, in that the water flows through a magnetic field and induces a current that is proportional to the average flow rate. The current is displayed in milliamps on a digital display and calibrated against a flow table. The range of flows that can be measured is 32.4 to 324 m^3/h, the lower rate is determine by the minimum flow necessary to produce a measurable current.

4.3.2.3 Temperature Measurement

Humidity Sensor

The hygrometer selected contains a moisture sensitive silicon chip. If the water vapour pressure in the air surrounding the chip alters, a corresponding change in the number of water molecules held in the pores of the chip is registered. The change is converted into an analogue signal, which is translated into the wet bulb temperature by means of the calibration chart supplied by the manufacturers. The meter requires a minimum flow rate of 0.5 l/min of air to operate correctly and gives a wet bulb temperature with an error of 0.5°C.

Temperature Probes

The method chosen to obtain temperatures was through platinum resistance thermometers. The thermometer contains a strip of platinum whose resistance alters with temperature. This causes a change in the voltage required to pass a steady current

across the strip. This change can be picked up by the use of a computer, interfaced to a data logger. The technique used and a much fuller description of the probes is contained in the following chapter.

4.4 Modification of the Test Tray to a Rectangular Section

To perform the experiments based on a rectangular section of the tray it was necessary to alter the test section of the simulator. Also to ensure that the gas distribution was even and vertical, the space under the test tray was modified.

4.4.1 Selection of Method

The choice of the size of the section was determined by practical considerations, such as how the dividing walls would be supported. It was decided that the existing support framework would be used to support the side walls of the rectangular section and with this consideration, the lateral beams either side of the centre line would be used. The walls themselves were designed to minimise the splashing of water over them into the side sections and were 0.6 m in height. The section covered the whole length of the tray, so the walls were 1.925 m in length and were attached to the support beams by a number of screws along the length of the wall. Further support of the walls was made by attaching them to the inlet downcomer and the existing bolting bars at the outlet. The section width was constrained to be 1.26 m about the centre line of the tray.

The simulator was designed to test circular trays and the distribution system was manufactured to give an even spread of gas over the circular section. Obviously the distribution section would need to be altered for a rectangular section.

A number of methods for achieving an even gas distribution were suggested:

1. Allow water to flow on and off the side sections as normal, but the centre flow is kept separate by the dividing walls.

2. Water is allowed to flow onto the side sections but not off them. The water flow to the sides can be interrupted while experiments take place.

3. Water is not allowed to flow onto the side sections.

Problems occur with each of the methods. With method one it is not certain how much water is flowing down the centre test section of the tray and with methods two and three the gas distribution is uncertain. Method one was rejected due to the problems with the uncertain weir load, leaving the methods with gas flow problems to be solved. On first observation the second method gives a better gas distribution, but like method one this is uncertain. With method three, the gas would tend to channel through the sections with no water on them. This problem could be overcome by blanking the sections to the gas, but at the cost of the convergence of the gas flow.

Taking into account all the factors, it was decided to proceed with method three because of the certainty of the flows, i.e. it is known what flows into the section under test. This left some problems to be solved, which are discussed below.

4.4.2 The Distribution of the Water

The width of the rectangular test section is slightly smaller than the weir length of the round tray. This causes problems with the convergence of the flow under the inlet gap, which could cause eddies at the inlet. To overcome this, it was decided to alter the base of the downcomer. The small sides of the inlet gap were completely blocked leaving a downcomer length of 1.26 m, the same size as the test section width. To eliminate any convergence effects caused by the downcomer chamber being longer than the inlet, it was necessary to alter the chamber itself. To do this, aluminium strips were attached to the inside of the downcomer to blank the ends of the chamber. These

strips were 0.3 m in height and fitted vertically inside the downcomer to give in effect a downcomer of 1.26 m in width. This solution eliminated the contraction at the inlet which may have caused eddies.

4.4.3 The Distribution of the Air

The air distribution was a major problem to be overcome. The flow was known to be vertical for a circular tray (Chambers, 1993) but when a contraction in the effective flow area was introduced, the streamlines of the gas would converge. This had been confirmed during earlier work by the author and Chambers, using a system where the tray segments were blanked. It was felt that if the contraction in the area occurred earlier, then the flow would be able to correct itself to the vertical again. It was decided to run a test case through the PHOENICS[1] computerised fluid dynamics package to test this assumption before any work was carried out. The test case was run and it showed that if the contraction occurred at the gas distribution plate, then the flow would correct itself in the gap before the test tray. It was then decided to carry out the modifications.

Both the test tray and the gas distribution tray segments were blanked using aluminium sections, which were fixed to the support framework of the relevant tray. This created the same active area on the two trays. The gap between the distribution tray and the test tray was then required to be made into a rectangular section. This was done using aluminium sheeting which was attached to the framework of the tray above and to the sheeting covering the segments of the distribution tray. In effect this gave the air a rectangular duct in which to flow from the gas distribution section into the test section.

[1] CHAM Ltd, Bakery House, 40 High Street, Wimbledon, London, SW19 5AU

4.5 Discussion

This chapter has covered the test facilities used to carry out the experiments described in this thesis. The way that the data are obtained and are processed is discussed in the next chapter. In subsequent chapters the data are analysed and the trends are presented.

CHAPTER 5

DATA COLLECTION AND PROCESSING METHODS

5.1 Introduction

The air-water test facility has incorporated into it a number of experimental techniques. These involve the study of the bi-phase by direct observation, mass transfer and measurement of the liquid head. This chapter describes each technique in detail, along with the way in which they should be interpreted. The results obtained from these procedures will form the basis of the data analysis carried out in the following chapters.

The chapter concludes with a summary of procedures for the safe operation of the test facility. This includes the safe start-up, normal operation and shut-down of the simulator.

5.2 Direct Observation Experiments

The direct observation of the dispersion is carried out by the use of flow pointers. They were first developed by Hine (1990) and were placed over the tray in order to gain information regarding the local flow of the dispersion. Before this, coloured dye had been used to indicate the flow direction but the dye suffered from localised mixing. This is manageable with water-only studies, but once the air is added the mixing can become considerable. Another disadvantage is that the water is used in a

loop and the dye tends to accumulate in the tanks, necessitating periodic water changes. This problem is overcome by the use of pointers.

5.2.1 Description of a Flow Pointer

The device has two parts, namely a spindle that is attached to the tray and a flag to show the flow direction. The flag is made of aluminium to minimise weight and is allowed to freely rotate on the spindle by means of a spacer, which keeps it clear of the tray floor. The top of the flag is made into a double-winged arrow shape to indicate the direction. Figure 5.1 shows a diagram of a flow pointer.

The flow pointer sits in the dispersion and acts like a weather vane to show the direction of flow. The flow pointers are observed from above and their position is recorded by hand and by video, once steady state has been achieved. The pointer shows the direction of the froth in its vicinity and is highly sensitive due to the narrow width between the spindle and the edge of the flag.

The double-winged arrow on the top of the flag is used so that the effect of the air leaving the dispersion is the same on both sides of the flag. An earlier version had a half arrow, formed by bending over the top of the flag. The effect of this is to introduce an imbalance in the resistance to the flow of the gas on either side of the flag. As a result the gas would impart a rotational force on the flag. This is overcome by making the resistance to the gas the same on both sides by use of the double-wing.

Two sets of flow pointers were used in the direct observation experiments, the only difference being the height of the flag and spindle. The horizontal dimensions remained the same. The reason for the use of the two sets was the wide range of flow rates used. On the 12.7 mm tray, when high air velocities are used, the spray regime is encountered. Before this is reached the tray goes through the mixed flow regime, where there is a large quantity of spray above the main liquid dominant froth. Both these large dispersion heights made the normal short pointers difficult to see and

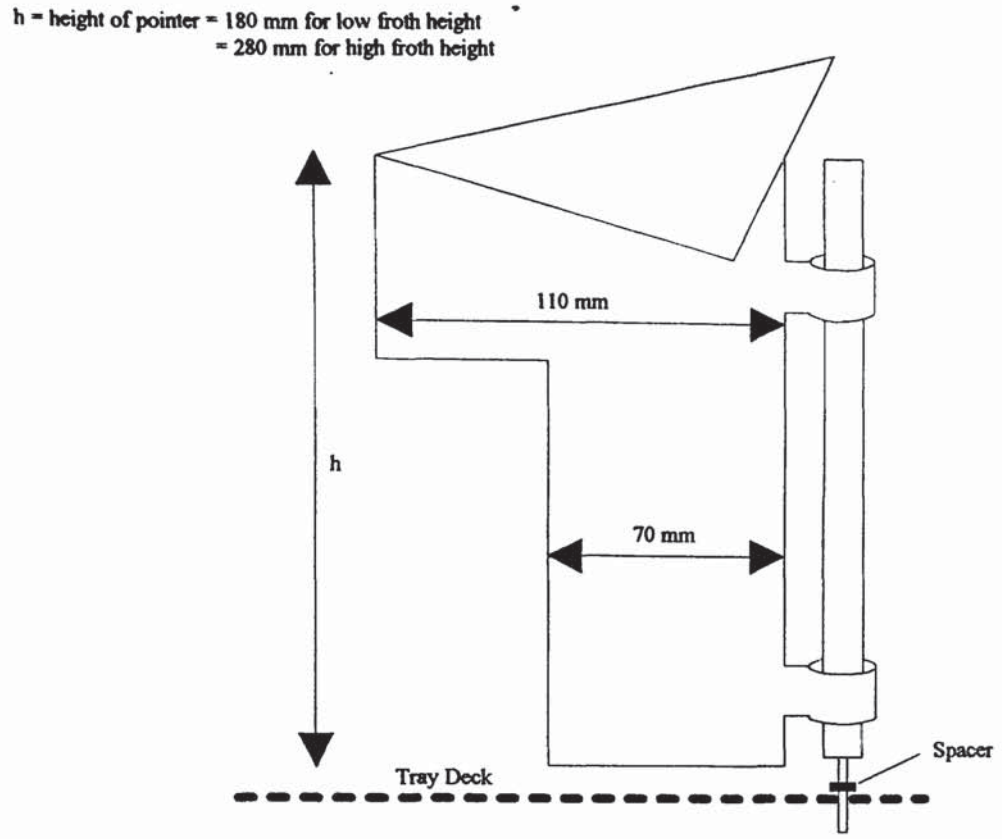

Figure 5.1 Schematic diagram of a flow pointer

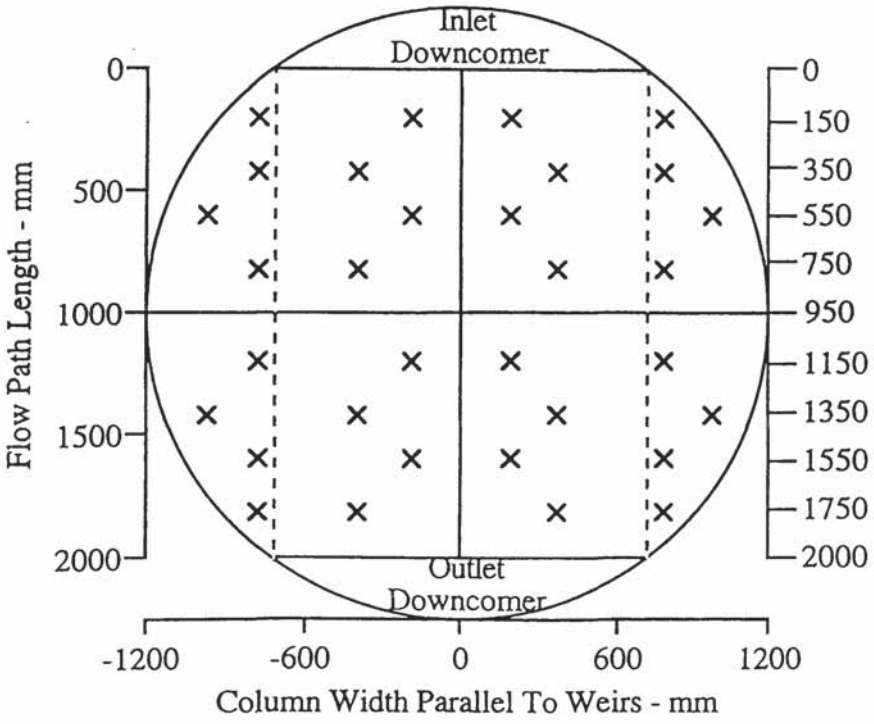

Figure 5.2 Positions of the flow pointers on the tray

hence the use of taller pointers. The short flow pointers were still used at the low dispersion heights.

To ensure that a representative flow pattern can be recorded the flow pointers are spread evenly over the tray in thirty-two positions. These are shown in figure 5.2 and are evenly distributed between the downcomers and on the segments at the sides of the tray.

As mentioned above the pointers are recorded using video equipment. A camera is positioned 4.5 m above the test tray. This height permits the whole of the tray to be viewed. The video of the dispersion can be overlaid with the flow rates and the set-up of the inlet gap and the outlet weir by means of a character generator attached to the camera. In addition to the video recording, the positions of the pointers are recorded on paper by observing their position through viewing windows in the top of the column. This visual record compliments the video recording and can be of great use if the video is obscured by excessive spray.

The flow pointers provide information on the direction that the dispersion is moving but not its velocity. However they provide a method for viewing the circulation that can occur on the tray under certain conditions. With this in mind it is useful to note that flow from inlet to outlet is termed forward flow and flow in the opposite direction is termed reverse flow.

5.2.2 Interpretation of the Flow Pointer Results

It has been discovered that under certain conditions the dispersion on the tray can circulate in the segments of the tray. This can be recorded by the flow pointers, but a method of expressing these results is needed. This can be done by considering the area of the tray that is covered by the circulations.

At low liquid rates the water on the tray spreads out to cover the whole tray and flows towards the outlet downcomer. All of the liquid on the tray is flowing in the forward

direction and under these circumstances there is no circulation of the dispersion. Hence, there is no area of the tray covered by circulations and therefore this would be deemed 0% circulation. At the other extreme, usually at high liquid rates and low inlet gaps, the liquid enters the tray and the majority of it channels down the section between the downcomers. At the sides of the tray the dispersion has separated from this main body of flow and is circulating. The circulation covered the whole of the segments at the side of the tray. With a tray where the weir length is 0.6 times the diameter, the area of the segments is approximately 30% of the tray area, and this type of flow pattern is termed 30% circulation. Circulations covering smaller areas are termed according to the area that they cover.

Lastly, the area where circulations occur may be important. Usually the circulation starts in the area of the segments close to the inlet and grows to cover the whole of the segments. This is termed inlet circulation. It has been found that circulation can start at the outlet and this would be termed outlet circulation accordingly. This type of circulation is usually gas driven and indicates problems with the gas distribution.

5.3 Height of Clear Liquid Measurements

The traditional view of froth depth has been of a gradient existing from the inlet of the tray to the outlet, with the greatest depth at the inlet. The gradient is generally assumed to exist to overcome resistance effects such as friction and the passage of the gas. However, in many cases the bi-phase flow over the tray is non-uniform and it is reasonable to assume that this is also true of the froth height. With this in mind, an existing method involving the use of manometers was used to measure the froth height across the tray to give a representation of any irregularities that occurred.

5.3.1 The Use of Manometers to Measure the Height of Clear Liquid

The measurement of the actual froth height is difficult due to the continuous movement of the froth surface. Methods such as light beam attenuation have been

used on small diameter columns but can not be used on the large scale. The method that was implemented makes use of the proportionality between pressure drop and the froth height. Pressure tappings were fixed to the tray floor and attached to manometer tubes outside the simulator by pipework. The manometers measure the pressure drop between the tray floor and the space above the froth. This pressure drop gives a measure of the height of clear liquid. The definition of the height of clear liquid states that it is the depth the dispersion would collapse to if the gas and liquid flows were instantaneously cut off and the weeping of liquid could be prevented. Figure 5.3 shows how the equipment is set up.

The effect of capillary rise and the gas momentum were taken into account by relating the raw data readings to a datum level. The datum levels were taken by operating the simulator at various gas flow rates without the presence of liquid. The manometer readings were recorded and then subtracted from the raw data. The datum readings effectively give the manometer height for a zero height of clear liquid.

5.3.2 Experimental Procedure

Thirty-two manometers are used to collect measurements of the height of clear liquid. The tappings for these manometers are spread evenly across the tray and are shown in figure 5.4. The tappings are connected to glass tubes outside the simulator by PVC tubing. The tubing is filled with water that is applied under pressure to remove any air bubbles that may form while filling. After the air and water flow rates have been set, a period of approximately ten minutes is set aside for steady state to be achieved. The readings of the clear liquid are taken from a scale set next to the glass tubes, which in turn are situated at the correct height for the range of the liquid on the tray. The readings are then corrected by subtracting the datum readings to give the height of clear liquid at the given point.

The results are treated in two ways. Firstly the data are entered into a spreadsheet and the calculation of the height of clear liquid at the measurement points is carried out. This allows manipulation of the data to produce the average clear liquid height.

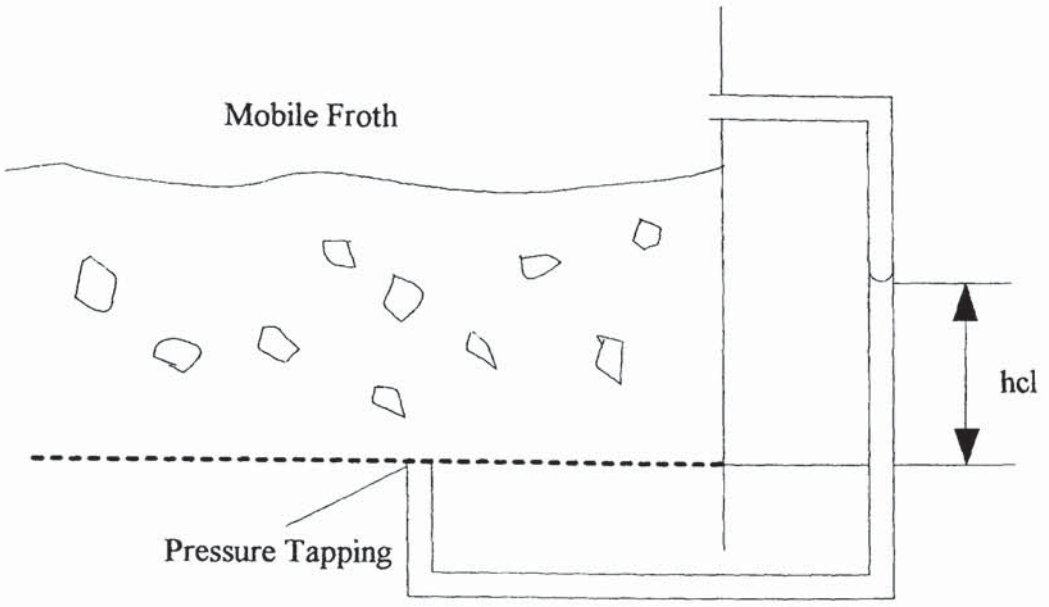

Figure 5.3 Manometer set-up to measure the height of clear liquid

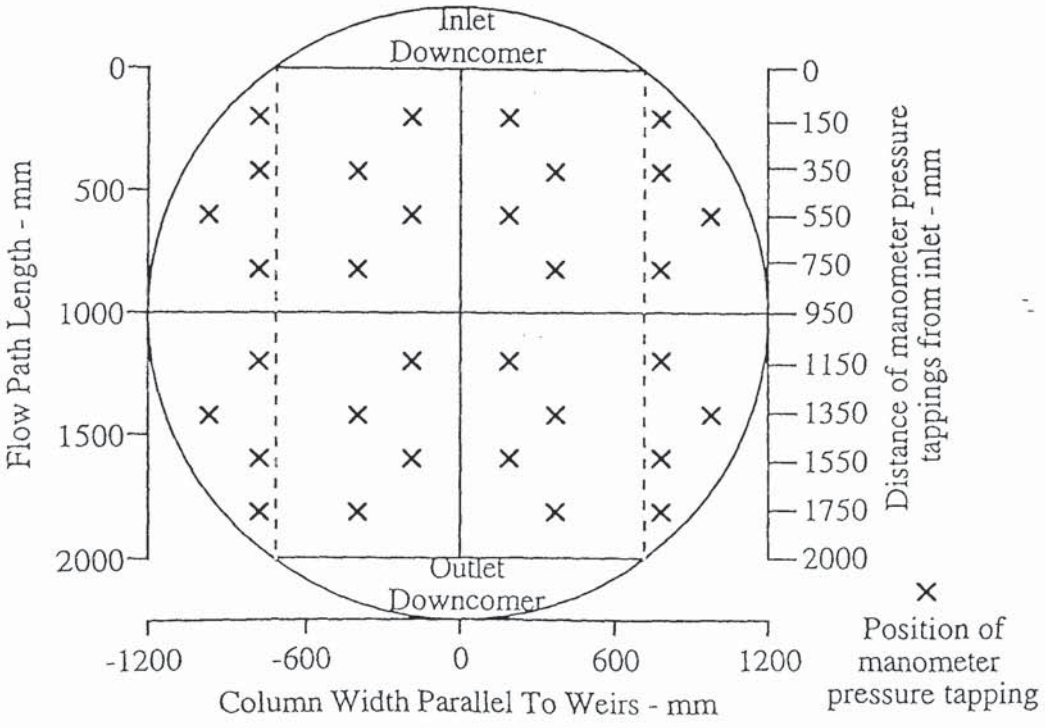

Figure 5.4 Position of the manometer tappings on the tray

Secondly, the data are fed into a FORTRAN program as a series of data files. This also calculates the height of clear liquid at the measurement points as well as plotting it as a three-dimensional surface profile. The program makes use of the UNIRAS plotting subroutines to enable this graphical representation of the clear liquid height.

The measurement of the total pressure drop across the tray is also recorded. This is carried out by attaching pressure tappings to the wall of the simulator. The tappings are positioned below the test tray and in the space above the dispersion. A U-tube manometer is attached to the tappings by PVC tubing so that the pressure difference can be measured.

5.3.3 Manipulation and Interpretation of Results

As mentioned above, each experimental run produces data for the measurement of the height of clear liquid, along with the datum readings. These data are firstly entered into a spreadsheet where the necessary calculations are carried out to turn the raw height of clear liquid measurements into the actual measurements, corrected for capillary rise and gas momentum effects. The data can then be easily manipulated to produce average height of clear liquids as well as the standard deviation of the data.

The second method of processing the data involves creating files that can be processed by a FORTRAN program. The program first calculates the height of clear liquid and then uses these point values to plot a three dimensional surface of the clear liquid. These surface plots can be of several different types. The surface may be flat at low weir loads and air velocities. The unevenness of the surface increases with the increase in the weir load and the air velocity. This unevenness can occur at the inlet or the outlet of the tray as well as all over the tray. This gives us four different classifications for the interpretation of the surface plots.

Examples of an uneven surface at the inlet to the tray would be where jetting is occurring. This is prevalent at low inlet gaps with a high weir load. An uneven

surface plot may be found with flow rates that produce a high level of turbulence over the tray. These are more likely at high gas velocities.

5.4 Heat Transfer Experiments Using the Water-Cooling Technique

It has been stated previously that heat transfer experiments which make use of water-cooling can be used to simulate distillation. The experiments involve the cooling of hot water flowing across the tray by air passing through it. The success of the technique relies on the analogy between mass and heat transfer. This makes it possible to relate concentration profiles produced in practical distillation to temperature profiles. The temperature profiles are produced by taking temperature measurements across the tray. By using these measurements and calculated enthalpy driving forces, it is possible to calculate thermal point and tray efficiencies.

The water-cooling technique involves measuring the temperature at a number of positions on the tray. The more measuring positions used means the greater the accuracy of the generated profiles, due to interpolation over a smaller distance. Over one hundred different temperature values are measured during the experiment. To give the best picture of the flow it would be advantageous to take all the measurements instantaneously. However this is not possible, but an approach to instantaneous measurement can be achieved. A data-logging device allowed all of the temperatures to be read in less than two seconds. If steady state has been achieved then they can be treated as if they were all taken at the same time.

This section describes the measuring devices used and also how the data was processed to produce meaningful results.

5.4.1 Temperature Measuring Devices

As has been described in the previous chapter the choice of measuring device was largely due to the required accuracy. The error analysis determined that an accuracy

of 0.02°C was required and this led to the technique of resistance thermometry being chosen. The main advantages of using this technique are that the calibration of the instrument is absolute and therefore does not require correction techniques such as referring to the cold junction. The resistance thermometer is free from the drift associated with thermocouples and does not require frequent recalibration. Lastly the accuracy and stability of the probe is higher than that associated with thermocouples.

Resistance thermometry uses the principle that the resistance to electrical current of the metal strip used varies with the temperature. The high accuracy of the technique means that the resistance of the connections to the measurement strip must be taken into account. The probes used minimise this effect by using four lead wires in a current\voltage measuring mode. The set-up is shown in figure 5.5. The errors are further minimised by using a very high input impedance amplifier. The whole device was housed in the tip of a probe of 300 mm in length and 3 mm diameter. The lead wires were six meters long and individually sheathed before being cased in a PVC coating.

The probes used contain a platinum strip with a resistance that is temperature dependent. As such they are often referred to as Platinum Resistance Thermometers or PRTs. The voltage to drive a given current through the PRT can be measured and the value used to calculate a corresponding temperature.

5.4.2 Mounting the Probes

To obtain an even coverage 108 PRTs are spread over the area of the tray. The probes are fitted into the tray from below and the lead wires are spread out to minimise any effect that they may have on the gas flow. A rubber grommet was fixed into a hole drilled in the tray and the probe could be mounted through this. A shroud was fitted around the tip of the probe to protect it from measuring the temperature of the air passing through the froth. Water was allowed to pass through the shroud and circulate the probe tip so that a measurement of the water temperature could be made. The whole set-up is shown in figure 5.6.

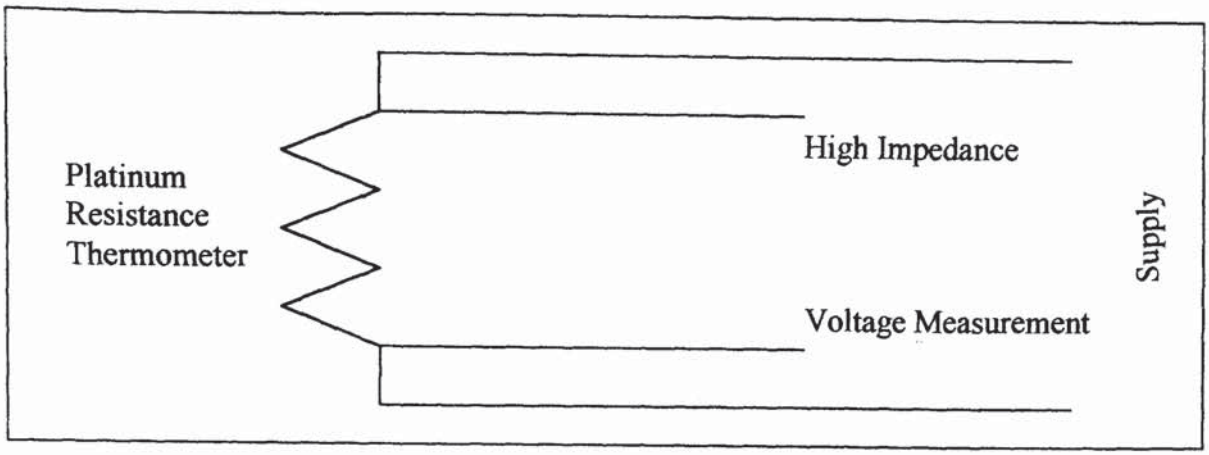

Figure 5.5 The four lead connections to the platinum resistance strip

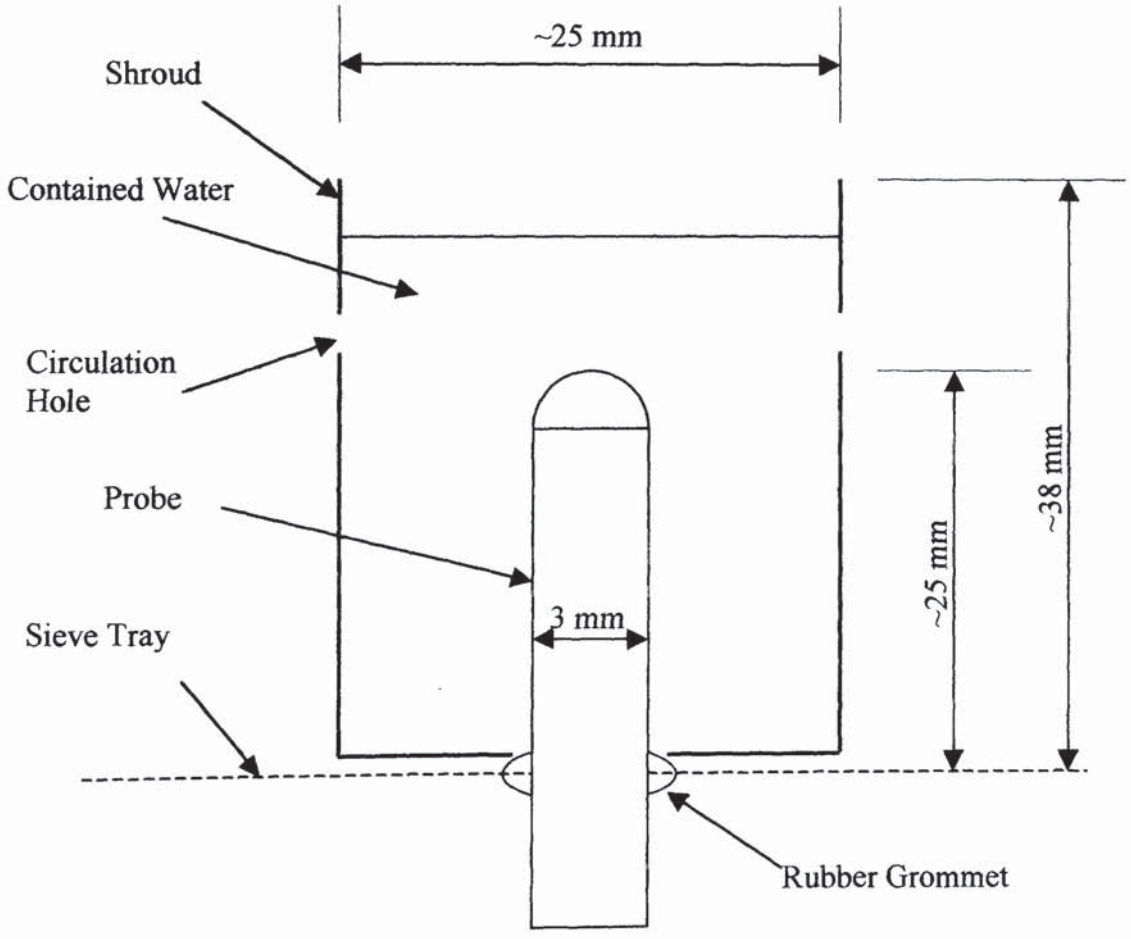

Figure 5.6 The probe mounting on the tray

5.4.3 The Data Logging

A MICROLINK data-logging interface was used to collect the temperatures. This was connected to a personal computer by use of an IEEE-488 bus and used to control the data logger. The temperatures were collected at steady state conditions. This was assessed by monitoring the temperature during a collection period to determine if the conditions were met. This is described in a subsequent section.

The data logger consists of a main unit with eighteen slots for different modules. These modules consist of a high speed clock, an Analogue to Digital converter and sixteen RTD8H modules. The RTD8H modules are analogue input devices that can take eight, four wire PRTs. Each RTD8H can be set to measure temperature over either a wide range, -200°C to 900°C or a reduced range of -10°C to 55°C. The latter range was used for the experiments undertaken and gave an accuracy of better than the 0.02°C required.

The high speed clock allowed the data collection to be both rapid and equally spaced between the channels. As the ideal was to collect the data instantaneously then the clock enabled the smallest delay between the channels. This was set at one milli-second, as this was slightly longer than the settling time of the current in each PRT. If the measurement was taken earlier then erroneous readings would occur. With 120 channels available the total time to scan them all is 1.2 seconds. This seemed reasonably close to instantaneous measurement and taking into account that the readings are taken at steady state it was thought that this system was adequate.

The analogue to digital converter has a size of twelve bits and converted the temperature into the digital signal that is received by the computer. Each measurement has a resolution of 2^{-12} of the full scale range and is sent to the computer via the IEEE-488 bus.

5.4.4 Calibrating the Platinum Resistance Thermometers

To allow for slight variations in the measured temperature due to small differences in the length of the leads or the resistance wires, a calibration was required. An insulated water bath was used to set the temperature that was to be measured and the probe tips were immersed in the centre of the bath with liquid flowing around them by use of a submerged pump. A platinum standard thermometer was used to set the water temperature at 0°C, 15°C, 25°C, 35°C and 50°C where the standardisation of the probes was to take place. At each temperature, steady state was achieved and the readings of the thermometers were recorded to provide a calibration point. Linear interpolation is used to determine the actual temperatures from the measured temperatures.

5.4.5 Collecting the Temperature Data

A computer program was written in the FORTRAN language to drive the data logger. The program sets up the data logger to accept the temperature measurements and uses some subroutines supplied by the manufacturer to achieve this. Once steady state has been achieved, the program is run and it scans the temperatures twenty times. The values are corrected by reference to the calibration point. To ascertain if steady state was achieved, one inlet temperature and the outlet downcomer temperature were monitored during the collection period. If either varied more than 0.1°C then it was considered the tray was not under steady state conditions and the data were not saved. If the data were to be saved then they were averaged and information on the conditions and set-up of the tray was included.

The temperature was measured at 108 positions on the tray and the coverage is shown in figure 5.7. A square pitch of 200 mm spacing is used for the main section of the tray with a slight alteration to take account of the side sections. The inlet water temperature was measured by five PRTs positioned across the bottom of the downcomer and 50 mm to the rear of the gap. The outlet temperature is measured by

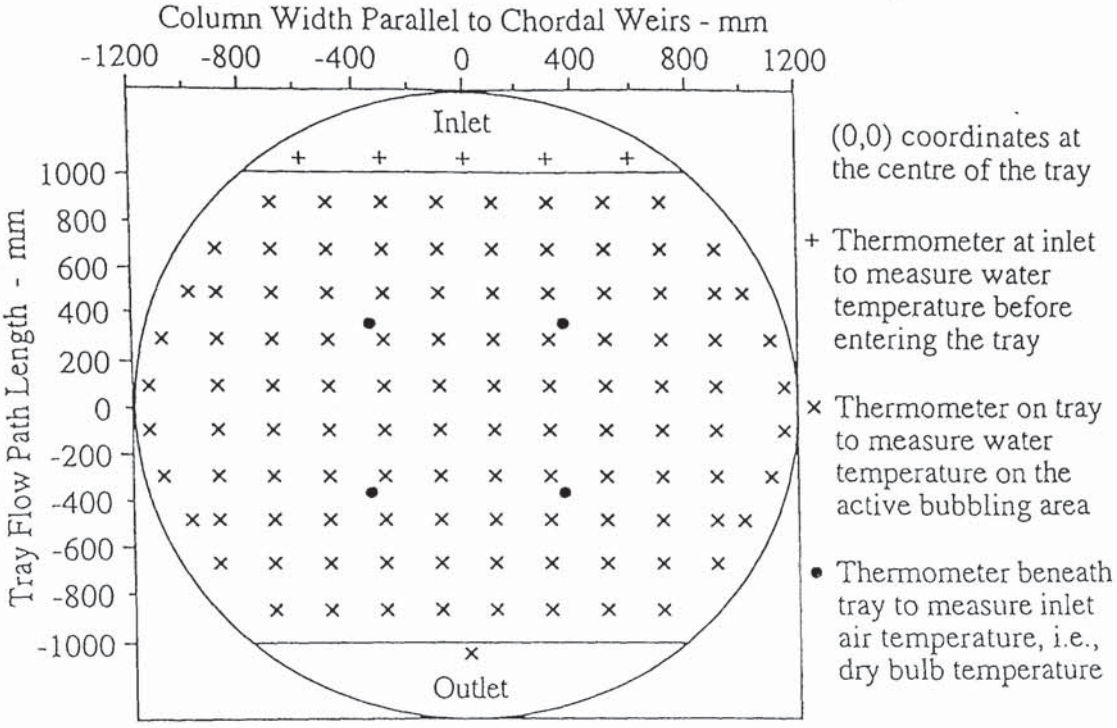

Figure 5.7 The position of the PRTs on the tray

AIR VELOCITY (m/s) 1.250
WEIR LOAD (cm3/cm.s) 50.0
DEW POINT (deg c) 7.5

COLUMN DIAMETER (m) 2.440
WEIR LENGTH (m) 1.500
FREE AREA (%) 10.0
OUTLET WEIR HEIGHT (m) .020
INLET GAP (m) .020
HOLE DIAMETER (m) .012

				49.70	50.54	49.65	50.09	49.85			
		52.63	99.99	46.79	46.10	48.65	48.16	50.02	37.31		
	38.13	46.01	45.79	45.81	45.21	46.79	99.99	45.31	38.40	29.53	
34.01	36.78	40.04	44.18	44.18	43.27	44.38	44.68	43.80	38.38	31.15	29.53
31.46	35.92	37.53	41.42	40.85	42.18	42.09	41.56	41.77	38.10	32.38	26.66
28.41	16.74	38.76	37.80	38.64	38.81	99.99	40.84	40.49	40.28	29.20	25.28
28.26	33.39	35.52	37.40	37.13	99.99	38.56	37.54	37.80	35.63	99.99	25.27
28.57	32.05	34.37	35.66	35.90	36.76	38.12	99.99	36.16	34.12	29.40	24.25
28.22	29.85	32.43	33.82	33.81	35.25	37.12	36.13	34.13	33.37	27.82	25.72
	27.87	28.75	31.71	32.30	35.08	35.19	34.52	34.04	31.16	26.84	
		28.11	30.06	31.52	33.40	33.99	33.28	32.08	28.24		
					32.18						
	11.83	12.66	11.69	11.74							

Figure 5.8 Average temperature data file

5.4.7 Temperature Contour Processing

A method was required to present the large amount of data produced from the experiments. The method used was to present temperature isotherms. As the temperatures are measured at discreet intervals it is necessary to find a way of interpolating between values. The UNIRAS suite of routines was chosen to carry this out and also to display the temperatures as a series of two-dimensional isotherms.

The system used for the display of the temperatures used a grid system to carry out the plotting. It makes use of this by taking the data it is fed and calculating weighted averages to find a value on its set grid. The surface slope is computed by quadratic interpolation between the values on the grid and then final smoothing takes place by using distance weighting. A full description of this process is given by Hine (1990) and for further information on the calculation procedure involved, reference should be made to this or the UNIRAS instruction manuals.

The graphical representation of the temperature data is displayed alongside details of the condition of the tray and the flows. Examples of the profiles produced are displayed in Appendix 5. Three-dimensional display of the temperature data is possible but it is felt that little is gained by this. The calculation procedure is identical for both cases.

5.4.8 Calculation of Thermal Efficiencies

Tray and point efficiencies can be calculated from the temperature data by recourse to a heat balance across an element of froth. The tray efficiency can be obtained from the following equation:

$$E_{MV} = \frac{\overline{H}_2 - H_1}{H^*_{Tout} - H_1} \tag{5.1}$$

$\overline{H}_2$ is the average enthalpy of the almost saturated air leaving the froth and H_1 is the enthalpy of the entering air. H^*_{Tout} is the enthalpy of the saturated air in equilibrium with the average temperature of the water leaving the tray. Similarly, the point efficiency at a position i on the tray can be given by:

$$E_{OG} = \frac{H_{2i} - H_1}{H^*_{Ti} - H_1} \tag{5.2}$$

T_i is the local temperature at the point i on the tray and H^*_{Ti} is the enthalpy of the air in equilibrium with T_i. H_1, H^*_{Tout} and H^*_{Ti} are found from psychrometric data tables. The actual calculation is carried out in the form of a FORTRAN program. The coding of this program is contained in Appendix 3.

5.5 Operating the Air-Water Simulator

The procedures for the safe start-up, normal operation and shut-down of the simulator are set out below. All of the equipment is used during a water-cooling run and therefore this is what is presented. For a run without heat transfer, steps 2, 4, 5, 6, 9 and 12 can be eliminated and there is obviously no need to wait for a water temperature to be reached.

5.5.1 Start-Up Procedure

1. The main electricity isolator is located on the fuse box and should be switched to on. The manual gas valves on the gas feed line to the process boilers should then be opened.

2. The water circulation pump in the primary heating circuit and the flue dilation fan should then be started from the wall mounted switch box.

3. The main water pump is located in the water supply line from the two storage tanks. It should be operated at this stage to send the water through the double heat exchanger and back to the storage tanks via the bypass network.

4. Switch on the electricity supply to the gas shut-off valve. The boilers will not operate without this safety device activated.

5. The primary heating source to the water comes from the gas fired boilers. Depending on the heat required, one or both should be started up using the procedure outlined in their operating manual.

6. The secondary heating source is provided by the steam and is used as a top-up supply. The steam valve should be opened at this stage and the spring valve associated with it is used to fine tune the water temperature prior to it entering the test tray.

7. The temperature of the water in the sump tanks should be checked regularly and as it approaches 40°C the air fan should be started using the wall mounted switch. The air flow rate required can then be set using the vane controlled inlet to the simulator and the micromanometer. The inlet should be closed before start-up to avoid blowing the air fan fuse.

8. Once the temperature reaches 45°C, the valve that is being used to control the flow of the water on to the tray should be opened/adjusted. The required flow rate should be set using either the manometer or the electromagnetic flow meter. Any small adjustments in the air flow rate should then be made.

9. The flow rates from the gas fired boilers and the steam rate should be manually adjusted to provide a steady water temperature.

10. After ten minutes of steady-state operation has been achieved then data can be collected. In this case the temperature data collection program is initiated. Equally, height of clear liquid or direct observation readings are taken at this point.

5.5.2 Normal Operation

11. Under normal operation a set of experiments will be carried out. To facilitate this, any new air and water flow rates should be set and then return to instruction number 8.

5.5.3 Shut-Down Procedure

12. After the last of a set of runs is completed then the simulator can be shut-down. First the heating sources are removed by closing the steam valve and switching off the gas fired boilers.

13. All the electrical equipment except the water pump in the primary heating circuit, the water delivery pump and the air fan, can be switched off. The manual gas valves should also be closed.

14. The simulator should be left running until the water in the sump tanks has cooled to 20°C and both sections of the double heat exchanger are cool. When this stage has been reached, both water pumps can be stopped.

15. The air fan is left running to clear any water that is left on the tray. Once the water has been removed from the tray it is safe to switch the air fan off. The time it takes to remove the water depends on the tray and the air flow rate used.

The procedure above should be followed for safe operation of the simulator. As mentioned earlier in this section, for direct observation and height of clear liquid experiments it is not necessary to heat the water before it enters the tray.

This chapter and those that preceded it have covered the equipment used to obtain the distillation data. The results of the experiments undertaken will now be discussed in the next chapters.

CHAPTER 6

THE EFFECT OF GAS FLOW ON THE SEPARATION OF LIQUID FLOW ON A 12.7 MM HOLE TRAY

6.1 Introduction

This chapter is concerned with the identification of two phase flow patterns on a distillation tray with 12.7 mm diameter perforations. The effect on the flow pattern of forcing the gas through the tray is compared with the situation where there is no gas flow, i.e. an unperforated tray. Separation of the liquid flow is analysed and the effect it has on the temperature profile during water-cooling experiments is assessed. The variation of head is also investigated by measurement of the clear liquid height across the tray.

6.2 A Definition of Separated and Non-Separated Flow

It is necessary now to define the terms that will be used throughout this chapter, namely what is meant by separated and non-separated flow.

As fluid flows through a conduit, the fluid close to the wall is continually being slowed down. This occurs due to the shear stress at the wall being balanced by a decrease in the momentum of the fluid. With this in mind, the question arises of whether the fluid closest to the wall will ever be brought to rest. To answer this we must consider the pressure gradient, dp/dx (where p is the pressure and x is the distance along the flow path).

If the pressure decreases in the direction of flow, then the pressure gradient is said to be favourable and if it increases in the direction of flow, it is said to be adverse. It can be shown that for pressure gradients that are favourable, or zero, then the reduction in momentum is not sufficient to cause the fluid close to the wall to come to rest. Therefore, although there is a velocity distribution profile, all of the fluid is flowing forward. This is non-separated flow.

However, if an adverse pressure gradient is encountered, then the fluid close to the wall can be brought to rest. Thus neighbouring particles are forced to avoid these particles and are deflected away from the wall. This is called the point of separation. A separated region builds up behind this point and the low energy fluid in this region is forced back upstream by the increased pressure downstream. This causes fluid in the separated region to flow in the opposite direction to the main fluid. This is termed reverse flow. This does not mean that reverse flow will always occur with an adverse pressure gradient, but that it is a necessary condition for separated flow.

In the context of distillation trays, both separated and non-separated flow can occur. The tray can be viewed as first an expanding and then a contracting conduit. The physical flow boundary is constantly changing and the fluid close to the wall in the expanding section is slowed due to the pressure gradient and the increased flow path length. This can bring the fluid at the wall to rest and result in separation. The main fluid flow will now be bounded by the separated streamlines and fluid in the separated region may reverse.

6.3 Studies in Liquid Flow Separation

To assess the effect of gas flow on the liquid flow pattern it was necessary to be able to compare two-phase experiments with single, liquid phase experiments. With this in mind a review of the single phase experiments of Hine (1990) was performed. These

experiments were carried out on the 2.44 m diameter column with an unperforated tray.

In both water-only and air-water experiments the direction of flow is observed at many points. Flow from the inlet downcomer to the outlet weir is termed *forward flow* and flow in the opposite direction is *reverse flow*.

6.3.1 Water Only Experiments

With an unperforated tray it was shown that liquid would start to circulate in the side segments at low weir loads of between 50 and 80 $cm^3/cm.s$. As the weir load increased, the area occupied by the circulation rapidly increased up to a maximum of 30% of the tray area. This corresponds to the area of the side segments of a 60% weir to diameter ratio tray, i.e. the circulations completely occupied the segments. Increasing the weir load did not affect the area of the tray in circulation, but it did enhance the velocity of the rotations and increased the definition of the separation streamlines. The inlet gap and the outlet weir had very little effect on the flow patterns. Figure 6.1 shows a summary of the results obtained from the water-only experiments.

6.3.2 Experimental Programme

A wide range of air flow rates and water weir loads were used to test the tray, along with combinations of inlet gap and outlet weir. A summary of the various flow rates is given in table 6.1.

The experiments were in three stages :

1. The flow of the bi-phase across the tray was observed by use of flow pointers. The air flow rate was held constant for several values of water weir load and the

position of the pointers were recorded. This was repeated for different air velocities and different combinations of inlet gap and outlet weir e.g. 10 mm, 10 mm; 20 mm, 20 mm and 50 mm, 50 mm. The change of the bi-phase from non-separated to separated flow was observed and recorded. An estimate of the percentage of the tray covered by reverse or circulating flow was also made.

2. The variation of liquid head across the tray was measured by means of thirty-two evenly spaced manometers, connected to pressure tappings on the tray floor. The effect of separated and non-separated flow was assessed by computer generated surface profiles of the height of clear liquid.

3. The water-cooling technique was used to assess the effect of non-separated and separated flow on mass transfer. The water temperature was measured using an evenly spaced array of 108 platinum resistance thermometers which were interfaced to a data logger and computer processed to provide temperature profiles. The temperature profiles are analogous to the concentration profiles produced during distillation. Thermal point and tray efficiencies can be calculated by using the analogy between heat and mass transfer.

Air Velocity $m.s^{-1}$	Weir Load $x\ 10^4\ m^3/m.s$	Inlet Gap mm	Outlet Weir mm
1.00	25.0		
1.25	50.0	10	10
1.50	100.0	20	20
2.00	150.0	50	50
2.50	200.0		
	250.0		

Table 6.1 Summary of flow rates and inlet and outlet settings used in air-water experiments.

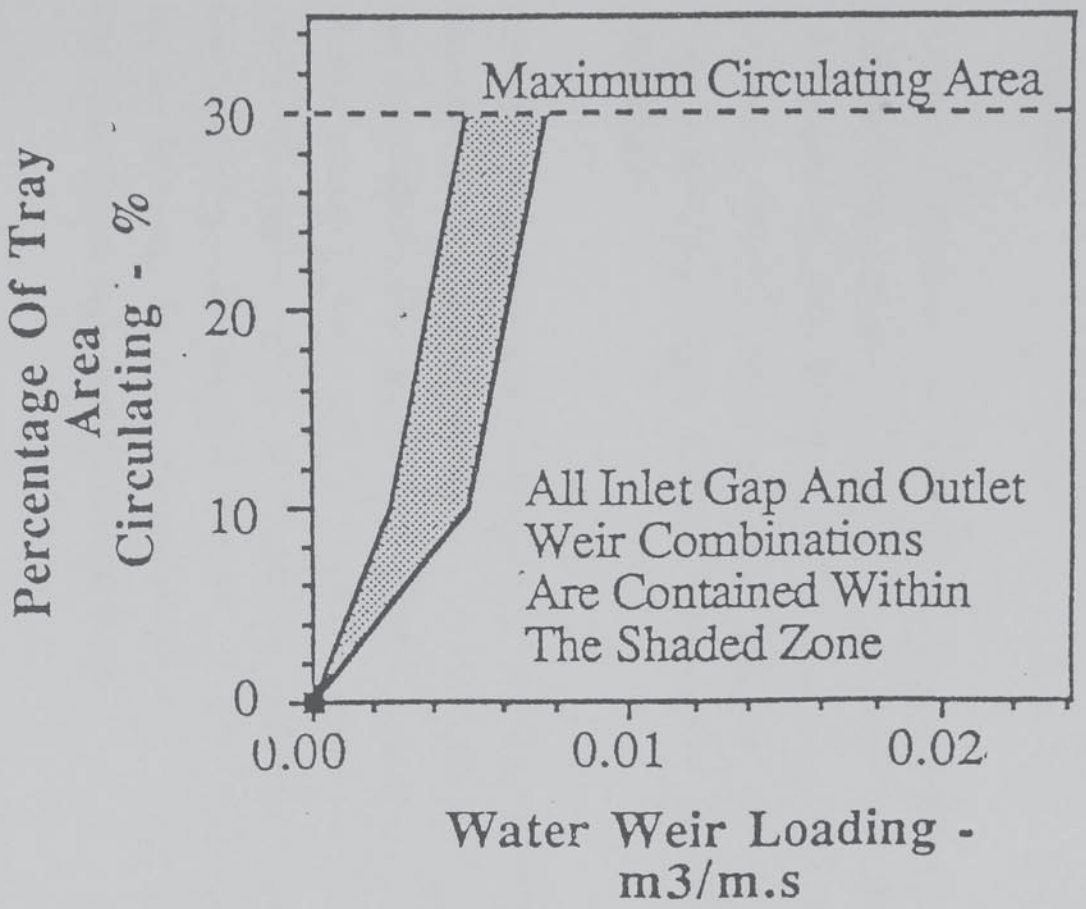

Fig. 6.1 Summary of the water-only circulation experiments

6.3.3 Direct Observation

When the water entered the tray, in all experiments, it spread out to cover the whole of the tray area. The liquid was completely aerated by the action of the gas passing through it and formed a two-phase froth. The bubbling action of the gas is very chaotic and tends to randomise the froth motion, especially when the froth has a low momentum.

The direct observation of the flow patterns produced during the gas-liquid contacting experiments was undertaken by the use of directional flow pointers and an overhead video camera. The flow pointers are partially submerged in the froth or spray on the tray and act in a similar manner to weather vanes. The vanes are evenly spread over the tray in thirty-two positions and the localised bi-phase direction is recorded by the video camera.

Minor drawbacks to using the flow pointers occur with the low momentum systems mentioned above. The pointers tend to show the localised movement by the gas rather than any overall trend in the liquid flow. This can be seen in the asymmetric nature of the flow pointers in some experiments, especially when the gas passes a support beam. Another drawback is that the pointers must have a position. Even when there is no flow the pointers show a direction. There will be a limit to the use of pointers at very, very low flow rates, due to the momentum required to turn them. Thankfully this is well below the flow rates used in these experiments.

6.3.3.1 Results of Direct Observation

From previous work, it has been shown that passing the air through the water on the tray inhibits the onset of separation. When the results presented below were compared to those for water only, a similar effect was encountered. In the following sections the

work is presented along with the factors influencing separation and the formation of circulating regions.

Small Froth Heights

Low froth heights were produced by using the equal inlet gap and outlet weir pairings of 10 and 20 mm. The low outlet weir heights produce the low froth heights, but the froth velocities are relatively high due to the low inlet gaps. Non-separated flow was produced at weir loadings of up to 100 $cm^3/cm.s$ for the inlet gap, outlet weir combination of 20 mm for all air velocities. Similarly for the 10 mm combination, non-separated flow was produced at all weir loads up to 50 $cm^3/cm.s$ as well as the majority of air velocities at this weir load. Indeed it was not until the air velocity dropped to 1.00 m/s that a degree of circulation was detected. Forward flow was produced on most points of the tray during these experiments and the flow pointers were, in the main, pointing towards the outlet weir. The flow pointers at these water weir loads can show asymmetry for a number of reasons. The pointers around the perimeter of the tray can point towards the column walls. This may be due to either the froth expanding onto the unperforated section caused by the support ring, or by the froth being diverted by the gas as it contracts and then expands around the support ring. The pointers in the centre section may be deflected because of the presence of a velocity distribution profile in the froth or by a slight deflection caused by the gas passage around them. The latter effect would be very slight and only have an effect when the water momentum is low.

The effect of the gas flow through the water on the tray is to delay the onset of separation. This can be seen by reference to figures 6.2 and 6.3. These show that no separation occurs at weir loads that produced circulations covering between 10 and 30% of the tray area during water-only experiments. At weir loads of greater than 50 $cm^3/cm.s$ the flow separates at the ends of the inlet downcomer and circulations were produced in the tray segments. As the weir load increased, the velocity of the forward flow increased and the pointers in the central section straightened up so that they were

pointing perpendicular to the weirs. The faster flow in the central section was accompanied by larger circulations in the segments. The area of the tray occupied by these circulations increased up to a maximum of 30%, which was only produced at the higher weir loads. The area of the tray in circulation was estimated by observation of the number of pointers affected by the circulation. Evidence that the pointer was in a circulating area included the pointer indicating reverse flow i.e. pointing back towards the inlet downcomer, or the rarer occurrence of the pointer continually circulating.

The maximum area covered by circulation was 30%, which, as stated above, is the area of the segments of the tray. When this value was reached there was no increase in the area of the circulations, but the velocity of the rotation appeared to increase. This maximum circulation was reached at 200 $cm^3/cm.s$ for the 10 mm inlet gap and at 250 $cm^3/cm.s$ for the 20 mm set-up. The water entering the tray beneath the lower inlet gap has a higher velocity and therefore it is easier for it to reach the conditions necessary for separation.

To summarise the information on figures 6.2 and 6.3, for a fixed air velocity, increasing the weir load increased the likelihood of separation. Once separation occurred, the increase in the weir load increased the area of the tray affected by circulations, up to a maximum of 30%. Once this was reached, no more area was taken up, but the velocity of the circulations increased. On increasing the air velocity, for a fixed weir load, the area of the tray affected by the circulations was reduced slightly. The increase in the gas flow also tended to decrease the rotational velocity.

The figures also show flow regimes suggested by Sagata and Yanagi (1979). These are for rough orientation but do show some interesting trends. Circulation does not tend to occur in the spray regime. This is probably due the relatively low liquid momentum in this regime. The froth regime shows some circulation, but the majority occurs in the emulsion regime. Again, this is probably due to the relatively large liquid momentum in this regime.

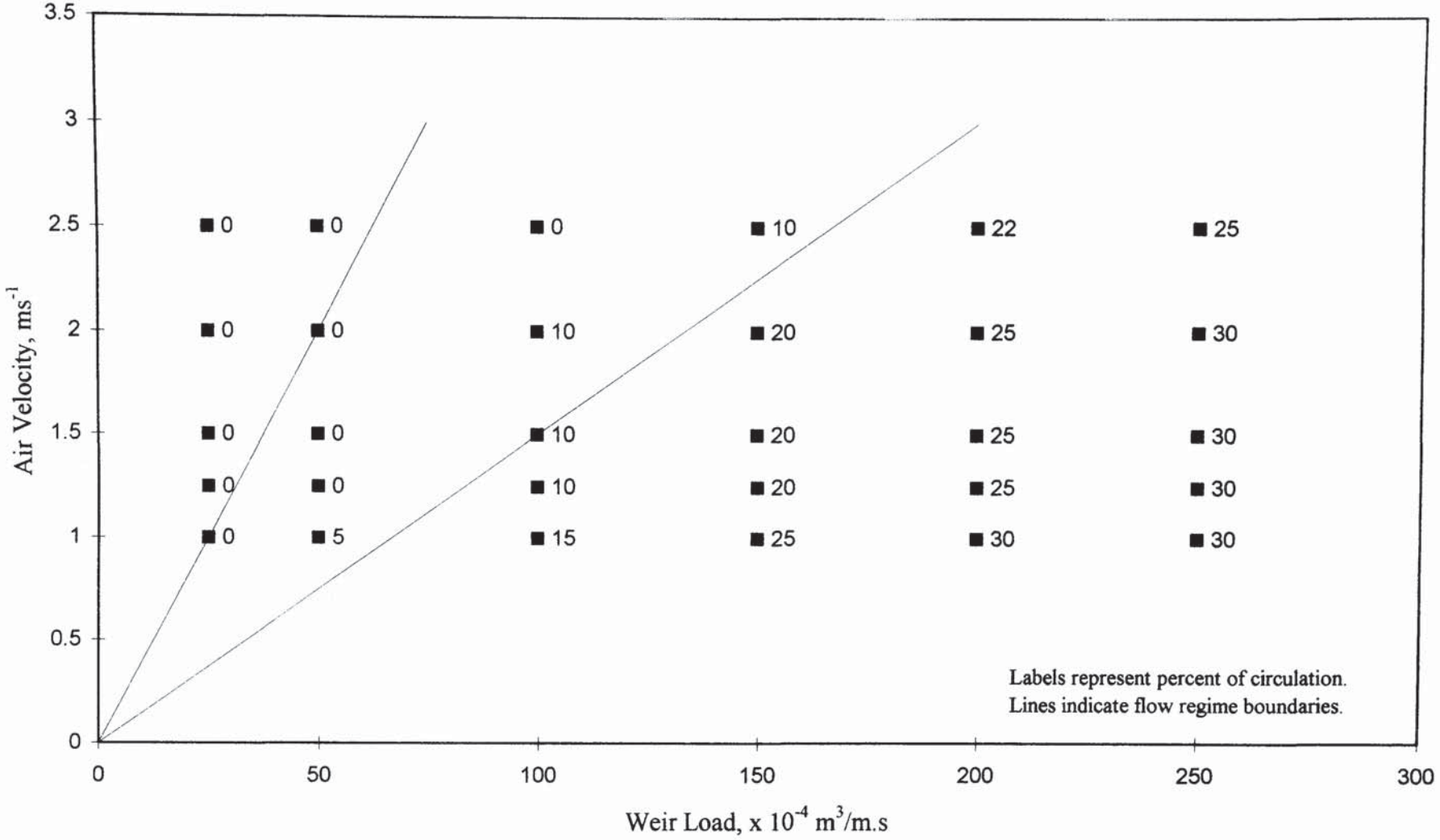

Figure 6.2 Summary of flow pattern results on a weir load versus air velocity diagram. Inlet gap and outlet weir are both 10 mm.

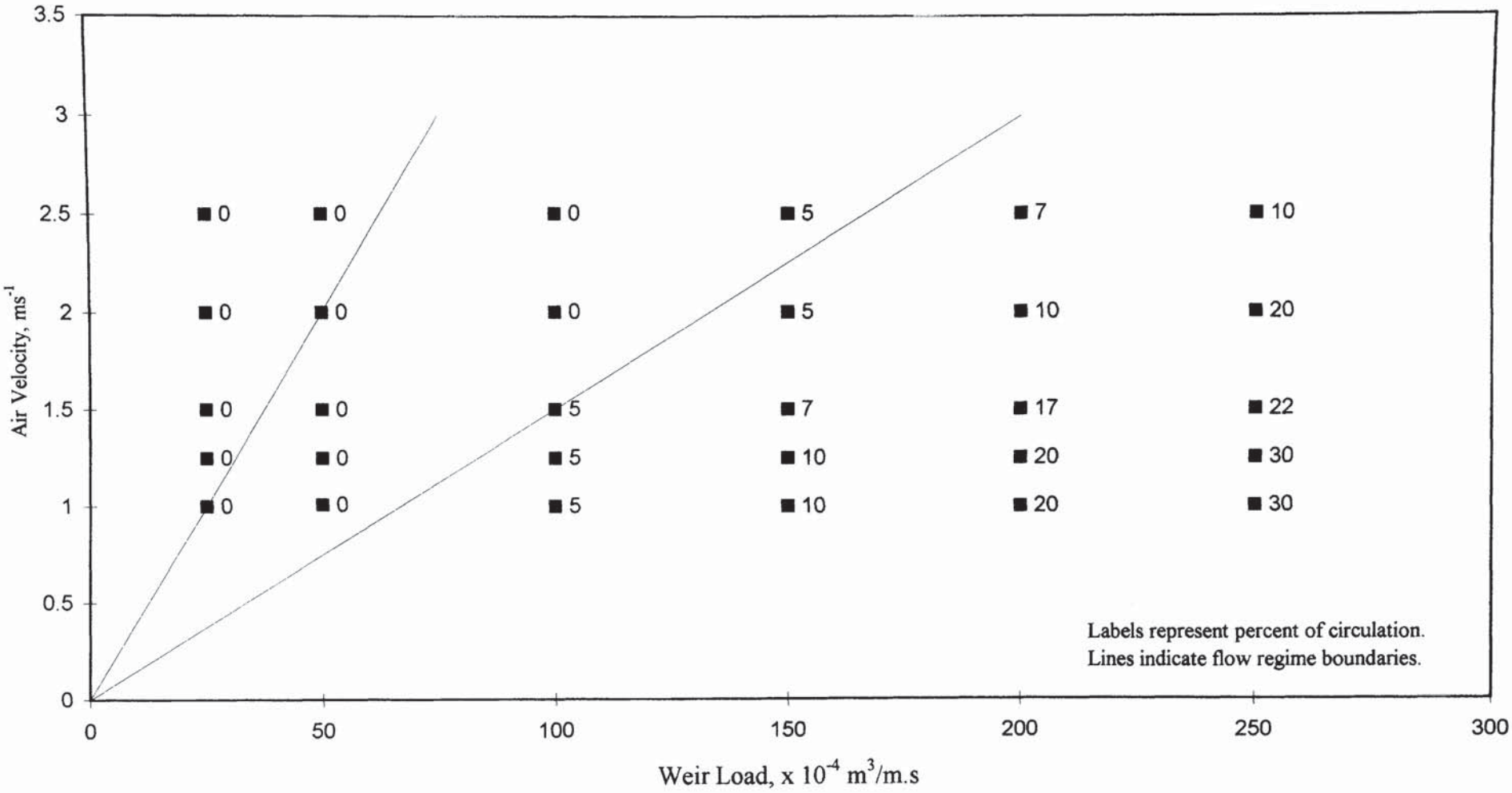

Figure 6.3 Summary of flow pattern results on a weir load versus air velocity diagram. Inlet gap and outlet weir are both 20 mm.

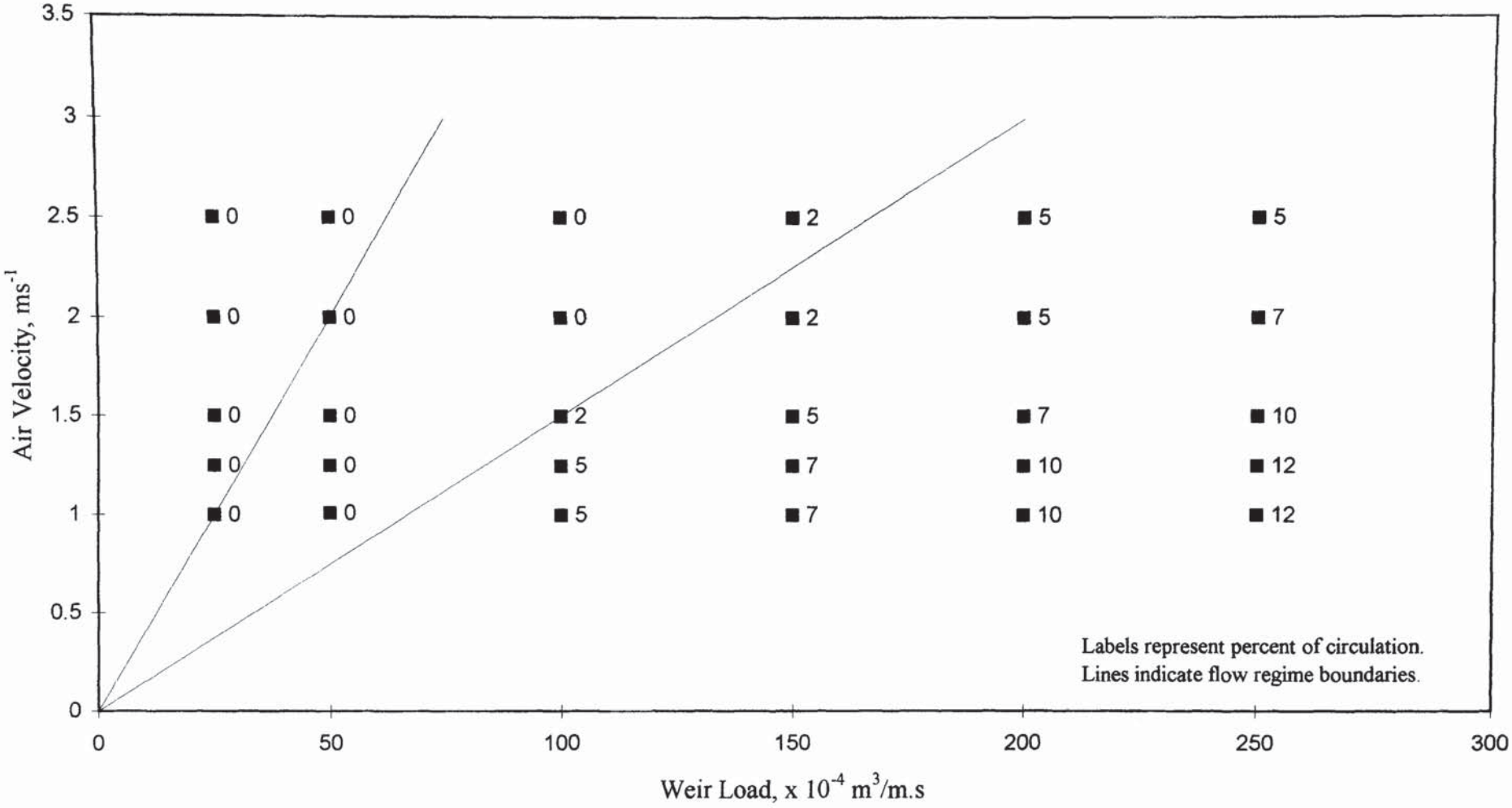

Figure 6.4 Summary of flow pattern results on a weir load versus air velocity diagram. Inlet gap and outlet weir are both 50 mm.

Large Froth Heights

The large froth heights were produced by using the combination of a 50 mm outlet weir and a 50 mm inlet gap. The entrance velocity of the liquid on to the tray was relatively slow due to the large gap. This meant that the velocity of the forward flow of liquid on the tray was much less than that produced during the lower froth height experiments. Another factor affecting the flow patterns produced was the longer contact time of the gas with the liquid. This is due to the larger froth height which increased the residence time of the gas in the liquid. As a result the dispersion tended to be more chaotic than that produced at low froth heights.

The onset of separation was increased to a weir load of 100 $cm^3/cm.s$ and the maximum area of circulation was only 12% of the tray area at 250 $cm^3/cm.s$. This was caused by the slower velocity of the froth and the gas resistance combining to prevent the maximum possible circulation of 30%. The results of the direct observation experiments on large froth heights are summarised in figure 6.4. Once again regime boundaries are shown. These illustrate that spray is caused by a low liquid momentum and hence no circulation occurs in this region. It is not until the higher momentum of the emulsion regime that any circulation occurs.

6.3.3.2 Discussion

The passage of air through the liquid on the tray has a significant effect on the flow patterns developed. With water-only flowing across the tray the liquid was found to separate at the ends of the inlet downcomer with all but the very lowest flow rates. In the majority of cases this resulted in regions where the water was circulating. The effect of forcing the gas through the liquid was to delay the onset of flow separation. Separation only occurred at much higher weir loads and inlet velocities, caused by low inlet gaps. The rate at which the circulating flow increased in area was also reduced when the air was introduced.

The increase in area of the circulating flow showed a strong relation to the entrance velocity i.e. the maximum area of circulation was reached far quicker when operating with an inlet gap of 10 mm than when the gap is 20 mm. For a gap of 50 mm the maximum area of circulation is not reached. Figure 6.5 is a summary of the circulation area against the weir load and can be compared with figure 6.1 for water-only studies.

To sum up, the effect of increasing the weir height and the contact time of the phases is to reduce the liquid circulation. Reducing the circulation also has the added effect of reducing the channelling of the liquid along the centre of the tray.

6.3.3.3 Conclusion

Forcing gas through water on a tray has the effect of reducing the risk of separation. Separation only occurred at much higher weir loads than with water-only studies and higher water entrance velocities were needed to cause the separation. Separation was a necessary condition for circulation but the presence of separated flow did not necessarily mean circulation would occur.

6.3.4 Liquid Head Measurements

The effect of separation on the froth height on the tray was determined by using manometers to measure the pressure drop between the tray floor and the space above the froth. Thirty-two manometers were spread evenly over the tray and point values of the pressure drop were recorded. The pressure drop is related to the height of clear liquid on the tray and the results were computer processed to yield a three-dimensional graph of the head profile. The flow rates used for these experiments were the same as those used for the direct observation experiments and are presented in table 6.1.

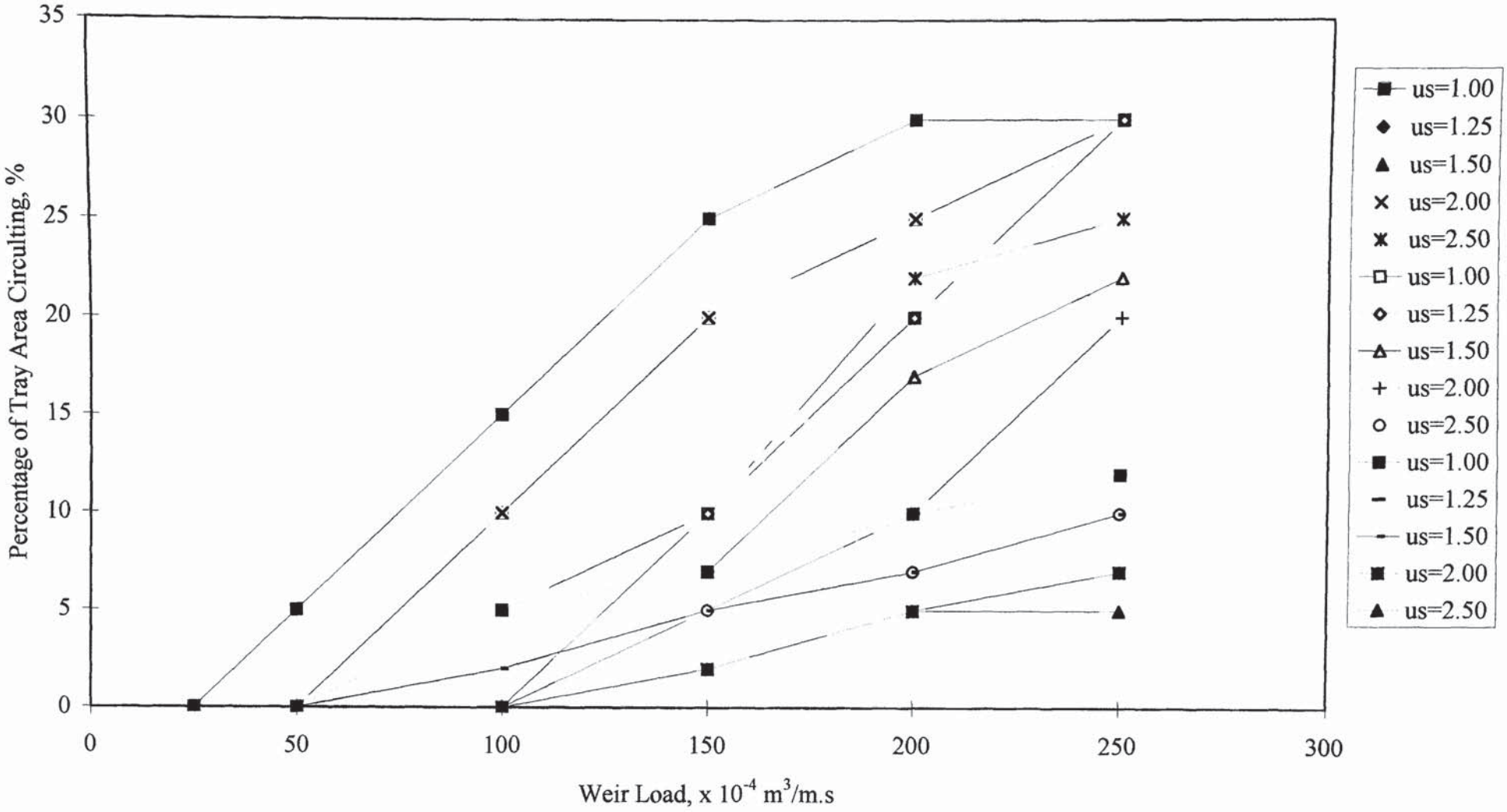

Figure 6.5 A summary of the area of circulations found on a tray with 12.7 mm diameter holes. (Some lines coincide)

6.3.4.1 Height of Clear Liquid Results

The measurements of the height of clear liquid on the tray indicated that there was a significant variation on the tray. This is visible in the surface profiles produced from the computer processing of the results and presented in Appendix 6. Values of mean liquid hold-up are presented in tables 6.2, 6.3 and 6.4, along with the standard deviation of the data. From this data it can be seen that the trend is for the mean liquid hold-up to increase with the water flow rate and to decrease with an increase in air flow rate. This trend is also predicted by previous workers (Hofhuis and Zuiderweg 1979, Stichlmair 1978, Bennett et al. 1983, Hine 1990 and Chambers 1993). The standard deviation of the data gives a measure of the variation in the height of clear liquid on the tray. This could be as a gradual slope, e.g. from the inlet to the outlet, or a measure of the build up of liquid on certain parts of the tray, e.g. larger clear liquid heights on the segments during circulation.

In the majority of cases, the standard deviation increases with increased weir load. This is possibly due to a greater head gradient across the tray but could also be explained by larger clear liquid heights on the segments. The standard deviation of the data also decreases with air velocity, up to 1.50 m/s, but this effect is very slight. At air velocities of 2.00 and 2.50 m/s the standard deviations were very large. A look at the surface profiles for these flow rates shows large peaks and troughs. The interesting point is that these irregularities occur in the same place for all the weir loads. This suggests an error with the datum readings taken at these air velocities when there was no water present. This is possibly due to a venturi effect caused by the contraction and expansion of the gas as it goes through the reduced area of the tray holes. This effect can either force liquid down into the pressure tappings or extract it. Either effect would give erroneous readings as the effect is unlikely to be as significant when the water is introduced to the tray.

Air Superficial Velocity (m/s)	Water Loading ($cm^3/cm.s$)	Mean Liquid Hold-up (mm)	Standard Deviation (mm)
1.00	25.0	15.7	3.1
	50.0	20.0	3.0
	100.0	22.4	3.8
	150.0	28.2	3.5
	200.0	26.7	8.3
	250.0	22.8	13.6
1.25	25.0	17.3	3.7
	50.0	20.6	3.8
	100.0	24.8	4.3
	150.0	23.6	4.7
	200.0	23.8	8.4
	250.0	24.4	10.9
1.50	25.0	16.0	3.7
	50.0	18.3	3.4
	100.0	22.9	3.9
	150.0	22.5	5.4
	200.0	23.5	8.0
	250.0	25.8	9.0
2.00	25.0	17.2	14.8
	50.0	21.5	12.2
	100.0	26.3	12.8
	150.0	32.8	16.7
	200.0	30.7	19.8
	250.0	30.6	21.0
2.50	25.0	15.8	18.8
	50.0	22.1	19.3
	100.0	23.0	13.7
	150.0	29.0	17.9
	200.0	24.4	16.9
	250.0	24.1	18.4

Table 6.2 Mean height of clear liquid for an inlet gap and outlet weir of 10 mm.

Air Superficial Velocity (m/s)	Water Loading ($cm^3/cm.s$)	Mean Liquid Hold-up (mm)	Standard Deviation (mm)
1.00	25.0	24.7	3.1
	50.0	25.3	3.3
	100.0	27.2	3.5
	150.0	29.0	4.3
	200.0	33.0	7.5
	250.0	30.2	8.6
1.25	25.0	24.8	2.5
	50.0	21.3	3.1
	100.0	25.2	3.0
	150.0	23.3	4.4
	200.0	26.2	6.6
	250.0	27.2	7.6
1.50	25.0	16.3	3.4
	50.0	22.1	3.2
	100.0	23.9	3.5
	150.0	27.5	4.7
	200.0	27.3	5.9
	250.0	28.8	6.9
2.00	25.0	11.9	11.9
	50.0	14.3	13.1
	100.0	20.4	13.6
	150.0	21.8	16.5
	200.0	22.5	14.7
	250.0	22.3	18.2
2.50	25.0	12.3	15.1
	50.0	19.4	16.0
	100.0	16.7	10.4
	150.0	24.2	12.8
	200.0	27.2	11.5
	250.0	25.3	13.9

Table 6.3 Mean height of clear liquid for an inlet gap and outlet weir of 20 mm.

Air Superficial Velocity (m/s)	Water Loading ($cm^3/cm.s$)	Mean Liquid Hold-up (mm)	Standard Deviation (mm)
1.00	25.0	31.1	5.4
	50.0	33.6	5.4
	100.0	36.5	5.9
	150.0	38.9	6.0
	200.0	41.2	6.3
	250.0	43.9	6.3
1.25	25.0	23.6	4.0
	50.0	27.7	3.5
	100.0	31.3	4.0
	150.0	30.3	4.8
	200.0	38.5	5.2
	250.0	39.9	5.8
1.50	25.0	30.1	3.5
	50.0	30.0	3.6
	100.0	32.7	4.0
	150.0	39.3	4.4
	200.0	33.2	4.8
	250.0	36.6	5.0
2.00	25.0	21.0	13.3
	50.0	24.3	9.8
	100.0	24.1	10.4
	150.0	15.8	12.2
	200.0	21.8	14.4
	250.0	21.3	14.8
2.50	25.0	17.2	17.6
	50.0	13.0	14.9
	100.0	27.4	14.4
	150.0	22.3	13.8
	200.0	21.7	14.0
	250.0	22.6	12.2

Table 6.4 Mean height of clear liquid for an inlet gap and outlet weir of 50 mm.

From the 3D head profiles it can be seen that the clear liquid hold-up decreases with distance from the inlet gap until the liquid starts to jet from beneath the gap. The first evidence of this occurring is at a weir load of 150 $cm^3/cm.s$ irrespective of the height of the inlet gap. The effect is greater with a gap of 10 mm than a gap of 20 mm and so on. With a gap of 10 mm the liquid can jet up to a distance of approximately 600 mm onto the tray before it expands. The worst case is found at this gap height with a weir

load of 250 $cm^3/cm.s$ and an air velocity of 1 m/s. The effect is reduced with an increase of gas velocity with the gas jetting to only 200 mm when it is raised to 1.5 m/s. For the inlet gaps of 20 mm and 50 mm the worst case is at the same combination of flow rates and the distances of jetting are approximately 200 mm and 100 mm respectively.

Flat surface profiles were produced at low weir loads and as the weir load was increased the surface at the inlet of the tray became disturbed. The disturbance was in two ways, the previously mentioned jetting on to the tray and the liquid height on the segments at the sides of the tray becoming greater than that on the inlet. The latter is possibly caused by circulation of liquid into this area or the liquid slowing down due to an adverse pressure gradient. Either mechanism will increase the liquid height.

An increase in air superficial velocity caused the bubbling on the tray to become more turbulent and viewing the froth from above made it clear that the surface was not flat. There was a series of eruptions over the whole surface as the gas broke through as large jets. This mechanism is more noticeable at the high froth heights as the gas tends to carry a higher proportion of liquid with it. At lower froth heights the jets break the surface earlier and there is less liquid to force out of the path. This is revealed by the data due to the prevalence of uneven surface profiles at the higher air velocities. A tentative link can be drawn with the higher standard deviations at the high velocities of 2.00 and 2.50 m/s.

6.3.4.2 Predictive Models of Height of Clear Liquid

The experimental data for the height of clear liquids was compared to heights predicted by models. The models used were those proposed by Bennett et al. (1983), Colwell (1979) and Stichlmair (1978). The average height of clear liquid from the models is quoted in tables 6.5, 6.6 and 6.7.

The correlations used are based on Francis's (1883) equation for flow over a weir. A derivation of which can be found in many standard fluid mechanics text-books with the final equation being:

$$h_{OW} = \frac{1.04}{C_d^{0.67} g^{0.33}} \left(\frac{Q_L}{(1-\varepsilon_W)W} \right)^{0.67} \tag{6.1}$$

This equation can be transformed to give the height of clear liquid by making use of the following equation:

$$h_{cl} = (1-\varepsilon)h_f = (1-\varepsilon)(h_W + h_{OW}) \tag{6.2}$$

The one difficulty with this approach is that ε_W is unknown. It is expected from liquid hold-up profiles that it will be larger than the gas hold-up averaged over the total dispersion height, ε. It is convenient to put $\varepsilon_W = \varepsilon$, but this will lead to an underestimation of the clear liquid height.

Colwell (1979) put $\varepsilon_W = \varepsilon$ and developed the following equation:

$$h_{cl} = (1-\varepsilon)\left[h_W + \frac{0.49k}{C_d^{0.67}} \left(\frac{Q_L}{(1-\varepsilon)W} \right)^{0.67} \right] \tag{6.3}$$

The above equation was verified for the froth regime, where k was set equal to 1.49, using data from a wide variety of systems. The coefficient for the weir was taken from single phase flow:

$$C_d = 0.61 + 0.08\frac{h_{OW}}{h_W} \qquad \text{when } (h_{OW}/h_W) \leq 8.14 \tag{6.4}$$

and

$$C_d = 1.06\left(1 + \frac{h_W}{h_{OW}}\right)^{1.5} \qquad \text{when } (h_{OW}/h_W) > 8.14 \tag{6.5}$$

where

$$h_{OW} = \frac{h_{cl}}{1-\varepsilon} - h_W \tag{6.6}$$

The calculation procedure is iterative as correlations for ε involve h_{cl}. Colwell developed his correlation for the froth regime and as such it tends to under predict h_{cl} values not in this regime. However, the restriction is quoted as $u_S < 2.0$ m/s and therefore its use is valid. The change in h_{cl} in the different regimes is due to drops being projected over the weir by the gas. The k value incorporates this effect in the Colwell model, but Stichlmair (1978) adopted a different approach. The projected droplets were accounted for by an additional term. The equations derived are as below:

$$h_{cl} = (1-\varepsilon)\left[h_W + \frac{0.49}{C_d^{0.67}}\left(\frac{Q_L}{(1-\varepsilon)W}\right)^{0.67} + \frac{125\left(u_S - u_b\right)^2 \rho_G}{g\left(\rho_L - \rho_G\right)\varepsilon^2} \right] \tag{6.7}$$

$$u_b = 1.55\left(\frac{\sigma\left(\rho_L - \rho_G\right)g}{\rho_L^2}\right)^{0.25} \cdot \left(\frac{\rho_G}{\rho_L}\right)^{1/24} \tag{6.8}$$

and C_d=0.61.

Stichlmair suggested that only gas velocities in excess of the rise velocity for single bubbles are significant in causing drops to be projected over the weir. The model of Bennett et al. (1983) is once again based on the Francis weir equation and is given by:

$$h_{cl} = \alpha_e\left[h_W + C\left(\frac{Q_L}{W\alpha_e}\right)^{0.67} \right] \tag{6.9}$$

$$\alpha_e = \exp\left[-12.55\left(u_S\left(\frac{\rho_G}{\rho_L - \rho_G}\right)^{0.5}\right)^{0.91} \right] \tag{6.10}$$

where C is given by:

$$C = 0.50 + 0.438\exp(-137.8h_w) \tag{6.11}$$

The values obtained show an upward trend in the height of clear liquid with an increase in weir load. This is as expected on an elementary analysis of the flow on the tray but it is not matched by the experimentally determined average height of clear liquids. At the low inlet gap of 10 mm, the average height of clear liquid starts to dip under that of the predictive models at a relatively early stage. For the higher gap heights the tail-off is not as dramatic, with the data still predicting higher clear liquid heights with the increase in the weir load. The reason for this is that the models do not take into account the entrance velocity of the liquid, as they are not concerned with the inlet gap height. This ignores the mechanism of the liquid jetting onto the tray at high weir loads, and hence higher entrance velocities. The effect is enhanced by low inlet gap heights and is therefore worse at the 10 mm gap than at the higher gaps. The values quoted in tables 6.2, 6.3 and 6.4 are average heights. As such the average value is reduced by the presence of this area of low liquid height on the tray.

The standard deviation of the models is presented alongside the average values and gives an indication of the variation between the predicted values. The values predicted for the clear liquid are in relative agreement at low gas velocities, but as it increases the difference in the height predicted by each model becomes fairly large. The effect is also felt between high liquid heights and low liquid heights. The standard deviations are higher at the large froth heights created by the larger weir than those for the smaller froth heights.

At low weir loads the experimental values usually fall within one standard deviation of the predicted average and can be said to be in a rough agreement with the predicted heights. As discussed above, the experimental values drop well below the predicted heights at higher weir loads and hence are well outside statistical agreement with the models.

Air Superficial Velocity	Water Loading ($cm^3/cm.s$)	Mean Liquid Hold-up (mm)	Standard Deviation (mm)
1.00	25.0	13.9	2.7
	50.0	19.1	2.8
	100.0	26.9	3.7
	150.0	33.4	4.7
	200.0	39.8	4.8
	250.0	45.8	5.0
1.25	25.0	13.7	3.4
	50.0	18.6	3.8
	100.0	26.0	4.8
	150.0	32.6	5.4
	200.0	38.9	5.6
	250.0	44.6	5.8
1.50	25.0	13.6	4.3
	50.0	18.3	4.7
	100.0	25.4	5.9
	150.0	32.0	6.3
	200.0	38.0	6.6
	250.0	43.6	6.9
2.00	25.0	13.5	5.9
	50.0	17.8	6.7
	100.0	24.8	7.8
	150.0	31.0	8.5
	200.0	36.6	9.1
	250.0	41.8	9.6
2.50	25.0	13.4	7.9
	50.0	17.3	9.0
	100.0	24.2	10.3
	150.0	30.0	11.3
	200.0	35.2	12.2
	250.0	40.1	13.1

Table 6.5 Mean heights of clear liquid predicted from a selection of models for an inlet gap and outlet weir of 10 mm.

Air Superficial Velocity	Water Loading ($cm^3/cm.s$)	Mean Liquid Hold-up (mm)	Standard Deviation (mm)
1.00	25.0	17.7	2.5
	50.0	23.2	2.0
	100.0	31.5	1.9
	150.0	38.2	2.3
	200.0	44.1	3.1
	250.0	49.5	3.9
1.25	25.0	17.0	3.1
	50.0	22.2	2.9
	100.0	30.1	3.2
	150.0	36.6	3.9
	200.0	42.2	4.8
	250.0	47.3	5.7
1.50	25.0	16.5	3.9
	50.0	21.5	3.9
	100.0	29.1	4.6
	150.0	35.2	5.5
	200.0	40.6	6.5
	250.0	45.5	7.5
2.00	25.0	15.9	5.6
	50.0	20.4	6.2
	100.0	27.4	7.4
	150.0	33.0	8.7
	200.0	38.0	10.0
	250.0	42.6	11.0
2.50	25.0	15.3	7.9
	50.0	19.5	8.8
	100.0	25.9	10.6
	150.0	31.1	12.2
	200.0	35.9	13.4
	250.0	40.5	14.5

Table 6.6 Mean heights of clear liquid predicted from a selection of models for an inlet gap and outlet weir of 20 mm.

Air Superficial Velocity	Water Loading ($cm^3/cm.s$)	Mean Liquid Hold-up (mm)	Standard Deviation (mm)
1.00	25.0	29.3	4.0
	50.0	35.3	2.9
	100.0	44.5	1.6
	150.0	52.1	1.7
	200.0	58.7	2.5
	250.0	64.7	3.3
1.25	25.0	27.2	3.8
	50.0	32.9	2.8
	100.0	41.7	2.0
	150.0	49.0	2.3
	200.0	55.3	3.2
	250.0	61.0	4.2
1.50	25.0	25.6	4.1
	50.0	31.0	3.5
	100.0	39.5	3.4
	150.0	46.4	4.0
	200.0	52.4	4.9
	250.0	57.9	5.8
2.00	25.0	23.1	5.9
	50.0	28.1	6.0
	100.0	35.9	6.9
	150.0	42.2	8.0
	200.0	47.7	9.1
	250.0	52.8	10.1
2.50	25.0	21.2	8.7
	50.0	25.8	9.5
	100.0	32.9	11.0
	150.0	38.7	12.4
	200.0	43.8	13.9
	250.0	48.4	15.2

Table 6.7 Mean heights of clear liquid predicted from a selection of models for an inlet gap and outlet weir of 50 mm.

6.3.4.3 Conclusions

The experiments to determine the height of clear liquid highlight the way that the variables affect the surface profile. As expected, the higher the outlet weir, the greater

the depth of clear liquid on the tray. The affect that the gap under the downcomer has is to make the liquid jet on to the tray at low gaps and high weir loads. This can be predicted due to the liquid entrance velocity increasing with the reducing gap height, for a fixed weir load.

The increase of the weir load causes the jetting of the liquid onto the tray, as mentioned above, and also the onset of separation. The technique of measuring the height of clear liquid does not distinguish between the direction of flow of the liquid or its velocity, but it did show that the liquid on the segments of the tray was larger than that in the middle of the tray when separation occurred. This can be attributed to the higher residence time of the liquid on these parts of the tray.

It has been shown that an increase in the air velocity reduces the average clear liquid height on the tray but increases the uneven nature of the froth surface. Gas jets can break the surface of the froth and cause a considerable amount of splashing. This could affect the efficiency of the tray as the liquid may become more mixed at these higher gas velocities. On the whole, non-uniform head profiles could have a significant effect on the functioning of a tray. An adverse effect could be seen on the point efficiency and subsequently on the tray efficiency. Other effects may be that the gas would preferentially flow through the regions of the tray with the least resistance, i.e. those with lower clear liquid heights. This would have a two-fold effect on weeping from the tray. The larger liquid height would make the region of the tray more susceptible to weeping and this would be compounded by the reduced flow of gas through the area. Therefore it would benefit the operation of the tray if the clear liquid profile could be kept uniform.

The predictive models of clear liquid height do not take into account jetting from below an inlet gap. As such, with increase in weir load, the predictions become increasingly higher than those obtained by experiment.

6.3.5 Water-Cooling

The technique of water-cooling was used to generate isothermal contour maps and to calculate thermal efficiencies by use of the enthalpy driving forces. The method involved measuring the water temperature at evenly spaced points on the tray, in the inlet and outlet downcomers. The air temperature was also measured under the tray, along with the humidity of the entering air. The method is described in the previous chapter along with a description of the calculation involved to produce the thermal efficiencies. The flow rates involved in the studies are the same as those involved for the direct observation experiments and are presented in table 6.1.

6.3.5.1 Two-Dimensional Isotherm Results

To compare the results obtained from the water-cooling experiments, reduced temperatures were used. This was necessary because in the time allocated for the experiments it was impossible to set the inlet temperature the same for all the runs. The use of reduced temperatures allows the profiles to be compared on a like basis. By definition the water entering the tray is at a reduced temperature of 1.0 and any point on the tray is at a reduced temperature of between 1.0 and 0.0.

Temperature Profile Results at Low Froth Heights

At low weir loads the reduced temperature isotherms were, in the main, straight and parallel to the downcomers. As shown by direct observation experiments, this is the region where there is no separation of the flow, and the liquid momentum is low. Previous research (Hofhuis and Zuiderweg, 1979 and Raper et al., 1979) into the spray regime, where the majority of the parallel isotherms lie, has shown that parallel lines of constant concentration are expected within this regime. This is explained by the high degree of mixing caused by the gas. The isotherms spread over the whole tray and indicate that the liquid at the sides of the tray has the same reduced temperature as

that in the middle. As the time the liquid spends on the tray is related to its reduced temperature, then the parallel isotherms indicate that the liquid at the tray sides has a similar residence time to that at the middle. This is despite the flow path length being greater across the segments. Again this could be explained by the theory that a tray in the spray regime is very well mixed.

As the weir load was increased the isotherms became slightly U-shaped. This can be explained due to the longer flow path travelled by the liquid at the sides of the tray. The liquid takes longer to cross the tray and hence its residence time is greater. With the residence time being linked to the reduced temperature, these side sections appear colder, i.e. the liquid on them has been reduced closer to the equilibrium, or wet bulb, temperature.

On further increase of the weir load, separation of the froth occurred. This showed up in the isotherms as an increase in the severity of the U-shape. The velocity distribution across the tray showed up as a U-shape across the whole tray with the liquid at the sides being very much colder than that at the centre of the tray. As circulation occurred, the U-shape ceased to cross the whole tray and consisted of a section of parallel isotherms coupled with swept back lines to the inlet downcomer. The section of parallel isotherms had a width of between 1300 mm and 1400 mm, just less than the width of the downcomer. This suggested that plug flow between the downcomers was occurring. In the segments of the tray the isotherms were bounded by the swept back sides of the central isotherms and the column wall. In this area the isotherms were approximately perpendicular to the downcomer and reduced down to the wall, or formed closed loops. The severity of the temperature reduction in this area was indicative of circulation, i.e. if the liquid is circulating over the full segment then the liquid in this section will approach equilibrium.

At the maximum circulating area of 30%, the reduction of temperature in the circulating area was very severe and the lowest reduced temperature lines are contained in the circulating region. The temperature is less than that crossing the

outlet weir, with the effect that the driving force for mass transfer is reduced and hence the tray efficiency is also reduced.

The effect of increasing the gas flow rate on the isotherms was generally to flatten them. At the highest weir load, for a 10 mm inlet gap and outlet weir, the effect of increasing the air velocity was to change the isotherms from severe U-shapes to parallel. The liquid circulation and its associated channelling had a great effect on the isotherms produced on the tray. This has a 'knock-on' effect on the tray efficiency, which will be discussed later.

Temperature Profile Results at High Froth Heights

The major difference between the results obtained at low froth heights and those obtained at a larger froth height are due to the increased contact time of the gas and the liquid. The isotherms produced with a larger froth height are similar to those at the lower height but there is more confusion. The patterns of the isotherms are more difficult to categorise due to the increase in random mixing. With the spray regime the mixing is still across the whole tray but at the higher weir loads the mixing can become more localised causing the effect of confused, or mixed, isotherms.

The U-shapes produced on the tray tended to be of a more severe nature than those produced by the lower froth heights. The pattern was more V-shaped with the point of the V being on or about the centre-line of the tray. This suggested that there was a prominent velocity distribution, even across the centre section, with the fastest moving liquid down the centre of the tray.

The reduction in temperature in the area of circulated flow revealed itself via the concentration of isotherms on the segments. The temperature reduction was not as severe, in the main, as those produced at the lower froth heights, e.g. it did not contain as many isotherms. The lines tended to be packed close to the inlet downcomer which is the domain associated with an area of circulation of 15% or less. In many cases the

lines in this area indicated that the liquid was colder than that crossing the downcomer. As mentioned above, this led to a reduction in the driving force for heat transfer.

Once again the effect of increasing the gas velocity was to flatten out the isotherm profiles. The effect on the isotherms of the flow patterns appeared to be less, but this could be masked by the fact that there was less circulation on the tray when a high froth height was employed. Indeed, the highest area of circulation encountered during the experiments was only 12%. The mechanism for this was suggested to be the time of contact between the gas and the liquid. This also had the effect on the isotherms of making them more confused, with localised abnormalities appearing.

Discussion

A small value of reduced temperature was produced by liquid that was approaching the wet bulb temperature. For this to occur the liquid residence time had to be high. With this in mind, it is possible to draw conclusions about the residence time of the liquid from the temperature isotherms, e.g. the coldest liquid has spent the longest time on the tray. From the experiments undertaken, the shortest residence time was of the liquid along the centre of the tray and the longest was of that on the tray segments. The relatively long residence time of the liquid on the segments was due to three factors:

1. The longer flow path of the liquid,
2. Liquid moving slower across the segment due to an adverse pressure gradient, and
3. The liquid circulating on the segment.

Either one, or a combination, of these factors was at play in the production of the longer residence time.

Parallel isotherms were produced in the spray regime by the high level of mixing associated with this regime. In the other regimes, the parallel isotherms tended to tail-off close to the wall, due to the higher residence time of the liquid in this region.

When flow separation occurred the temperature isotherms became U-shaped. The temperature of the liquid in the segments of the tray was reduced due to its greater residence time. This was caused by the slow movement of the liquid or circulation. In many cases this was shown up by a plug-flow of liquid down the centre of the tray and an area of closed isotherms in the segments. The segmental isotherms were mainly bounded by the wall on one side, but in some cases completely closed isotherms were obtained. In these cases the liquid was often colder than that passing over the outlet weir and led to a reduction in the driving force. These regions quickly approach equilibrium with the air temperature, with the result that little change in water temperature occurs, combined with a very small change in the enthalpy of the air passing through these sections. The net result of this is a reduction of the tray efficiency.

6.3.5.2 Thermal Efficiency Results

The temperature profile results in the previous section were used to calculate thermal efficiencies by making use of the enthalpy of the air and the water temperature (as described elsewhere). The values of the point efficiency, E_{OG}, tray efficiency, E_{MV} and the enhancement ratio, E_{MV}/E_{OG} are presented in tables 6.8, 6.9 and 6.10.

The efficiency results tables are supplemented by three figures showing a graphical analysis of the data. The water weir load has a major effect on the separation of the flow and therefore the figures are intended to shed light on how this variable affects the efficiency results. Consequently, the values of point efficiency, tray efficiency and the enhancement ratio are plotted against the weir load. The values of the efficiencies were averaged for a particular weir load. Due to excess weeping at the low air velocities of 1.00 and 1.25 m/s during the experiments with an inlet gap and outlet weir of 50 mm, the efficiency values are erroneous and have not been quoted here.

The point efficiency results are presented in figure 6.6 and show a rapid increase at low flow rates, from a low of 41% at 25 $cm^3/cm.s$ to 77% at 100 $cm^3/cm.s$. The rate

I.G., O.W. -mm	10, 10									
Superficial Air Velocity - ms^{-1}	1.00		1.25		1.50		2.00		2.50	
Weir Load x 10^4 - $m^3/m.s$	Efficiency - %		Efficiency - %		Efficiency - %		Efficiency - %		Efficiency - %	
25.0	E_{OG}	49	E_{OG}	52	E_{OG}	43	E_{OG}	41	E_{OG}	45
	E_{MV}	77	E_{MV}	94	E_{MV}	75	E_{MV}	83	E_{MV}	102
	E_{MV}/E_{OG}	1.57	E_{MV}/E_{OG}	1.81	E_{MV}/E_{OG}	1.76	E_{MV}/E_{OG}	1.99	E_{MV}/E_{OG}	2.24
50.0	E_{OG}	74	E_{OG}	70	E_{OG}	72	E_{OG}	67	E_{OG}	67
	E_{MV}	100	E_{MV}	104	E_{MV}	114	E_{MV}	109	E_{MV}	129
	E_{MV}/E_{OG}	1.35	E_{MV}/E_{OG}	1.49	E_{MV}/E_{OG}	1.59	E_{MV}/E_{OG}	1.62	E_{MV}/E_{OG}	1.91
100.0	E_{OG}	82	E_{OG}	80	E_{OG}	71	E_{OG}	77	E_{OG}	74
	E_{MV}	92	E_{MV}	99	E_{MV}	88	E_{MV}	107	E_{MV}	105
	E_{MV}/E_{OG}	1.12	E_{MV}/E_{OG}	1.24	E_{MV}/E_{OG}	1.25	E_{MV}/E_{OG}	1.38	E_{MV}/E_{OG}	1.42
150.0	E_{OG}	86	E_{OG}	82	E_{OG}	74	E_{OG}	74	E_{OG}	78
	E_{MV}	80	E_{MV}	96	E_{MV}	87	E_{MV}	90	E_{MV}	98
	E_{MV}/E_{OG}	0.93	E_{MV}/E_{OG}	1.18	E_{MV}/E_{OG}	1.19	E_{MV}/E_{OG}	1.22	E_{MV}/E_{OG}	1.26
200.0	E_{OG}	83	E_{OG}	77	E_{OG}	76	E_{OG}	79	E_{OG}	78
	E_{MV}	77	E_{MV}	84	E_{MV}	85	E_{MV}	91	E_{MV}	91
	E_{MV}/E_{OG}	0.93	E_{MV}/E_{OG}	1.08	E_{MV}/E_{OG}	1.11	E_{MV}/E_{OG}	1.15	E_{MV}/E_{OG}	1.16
250.0	E_{OG}	83	E_{OG}	76	E_{OG}	85	E_{OG}	84	E_{OG}	80
	E_{MV}	88	E_{MV}	80	E_{MV}	92	E_{MV}	93	E_{MV}	89
	E_{MV}/E_{OG}	1.05	E_{MV}/E_{OG}	1.04	E_{MV}/E_{OG}	1.08	E_{MV}/E_{OG}	1.10	E_{MV}/E_{OG}	1.11

Table 6.8 Summary of measured point and tray efficiencies on a 12.7 mm hole diameter tray. Inlet gap and outlet weir are both set at 10 mm.

I.G., O.W. -mm	20, 20									
Superficial Air Velocity - ms^{-1}	1.00		1.25		1.50		2.00		2.50	
Weir Load x 10^4 - $m^3/m.s$	Efficiency - %		Efficiency - %		Efficiency - %		Efficiency - %		Efficiency - %	
25.0	E_{OG}	40	E_{OG}	47	E_{OG}	47	E_{OG}	48	E_{OG}	49
	E_{MV}	53	E_{MV}	68	E_{MV}	71	E_{MV}	97	E_{MV}	93
	E_{MV}/E_{OG}	1.34	E_{MV}/E_{OG}	1.46	E_{MV}/E_{OG}	1.51	E_{MV}/E_{OG}	2.03	E_{MV}/E_{OG}	1.89
50.0	E_{OG}	69	E_{OG}	67	E_{OG}	65	E_{OG}	73	E_{OG}	69
	E_{MV}	88	E_{MV}	93	E_{MV}	91	E_{MV}	130	E_{MV}	116
	E_{MV}/E_{OG}	1.26	E_{MV}/E_{OG}	1.37	E_{MV}/E_{OG}	1.41	E_{MV}/E_{OG}	1.78	E_{MV}/E_{OG}	1.68
100.0	E_{OG}	86	E_{OG}	78	E_{OG}	75	E_{OG}	77	E_{OG}	74
	E_{MV}	96	E_{MV}	88	E_{MV}	85	E_{MV}	106	E_{MV}	102
	E_{MV}/E_{OG}	1.12	E_{MV}/E_{OG}	1.13	E_{MV}/E_{OG}	1.15	E_{MV}/E_{OG}	1.37	E_{MV}/E_{OG}	1.38
150.0	E_{OG}	86	E_{OG}	74	E_{OG}	77	E_{OG}	82	E_{OG}	78
	E_{MV}	84	E_{MV}	73	E_{MV}	78	E_{MV}	95	E_{MV}	94
	E_{MV}/E_{OG}	0.98	E_{MV}/E_{OG}	0.99	E_{MV}/E_{OG}	1.01	E_{MV}/E_{OG}	1.16	E_{MV}/E_{OG}	1.21
200.0	E_{OG}	86	E_{OG}	78	E_{OG}	74	E_{OG}	85	E_{OG}	78
	E_{MV}	82	E_{MV}	77	E_{MV}	71	E_{MV}	91	E_{MV}	87
	E_{MV}/E_{OG}	0.96	E_{MV}/E_{OG}	0.98	E_{MV}/E_{OG}	0.96	E_{MV}/E_{OG}	1.07	E_{MV}/E_{OG}	1.10
250.0	E_{OG}	83	E_{OG}	85	E_{OG}	81	E_{OG}	90	E_{OG}	89
	E_{MV}	74	E_{MV}	79	E_{MV}	78	E_{MV}	94	E_{MV}	96
	E_{MV}/E_{OG}	0.90	E_{MV}/E_{OG}	0.93	E_{MV}/E_{OG}	0.96	E_{MV}/E_{OG}	1.04	E_{MV}/E_{OG}	1.09

Table 6.9 Summary of measured point and tray efficiencies on a 12.7 mm hole diameter tray. Inlet gap and outlet weir are both set at 20 mm.

I.G., O.W. -mm	50, 50					
Superficial Air Velocity - ms^{-1}	1.50		2.00		2.50	
Weir Load x 10^4 - $m^3/m.s$	Efficiency - %		Efficiency - %		Efficiency - %	
25.0	E_{OG}	49	E_{OG}	45	E_{OG}	45
	E_{MV}	74	E_{MV}	79	E_{MV}	83
	E_{MV}/E_{OG}	1.51	E_{MV}/E_{OG}	1.79	E_{MV}/E_{OG}	1.85
50.0	E_{OG}	78	E_{OG}	67	E_{OG}	68
	E_{MV}	112	E_{MV}	107	E_{MV}	116
	E_{MV}/E_{OG}	1.44	E_{MV}/E_{OG}	1.60	E_{MV}/E_{OG}	1.71
100.0	E_{OG}	91	E_{OG}	81	E_{OG}	73
	E_{MV}	105	E_{MV}	113	E_{MV}	92
	E_{MV}/E_{OG}	1.15	E_{MV}/E_{OG}	1.40	E_{MV}/E_{OG}	1.27
150.0	E_{OG}	96	E_{OG}	84	E_{OG}	77
	E_{MV}	99	E_{MV}	93	E_{MV}	91
	E_{MV}/E_{OG}	1.03	E_{MV}/E_{OG}	1.11	E_{MV}/E_{OG}	1.18
200.0	E_{OG}	94	E_{OG}	84	E_{OG}	79
	E_{MV}	90	E_{MV}	87	E_{MV}	85
	E_{MV}/E_{OG}	0.96	E_{MV}/E_{OG}	1.03	E_{MV}/E_{OG}	1.07
250.0	E_{OG}	93	E_{OG}	89	E_{OG}	80
	E_{MV}	86	E_{MV}	88	E_{MV}	82
	E_{MV}/E_{OG}	0.93	E_{MV}/E_{OG}	0.99	E_{MV}/E_{OG}	1.02

Table 6.10 Summary of measured point and tray efficiencies on a 12.7 mm hole diameter tray. Inlet gap and outlet weir are both set at 50 mm.

of increase in the point efficiency then levels off with further rises in the weir load. The point efficiency is calculated independent of the flow pattern on the tray and therefore it is possible that the trend is down to variations in the height of clear liquid on the tray. These variations were greatest for high weir load experiments, especially where the flow had separated. Under these circumstances the liquid on the segments can be greater than that down the middle of the tray. This would reduce the residence time of the gas in the middle of the tray relative to that in the segments and may cause the gas to channel through the path of least resistance. This, combined with the liquid on the segments approaching the equilibrium temperature, would cause a reduction in the average point efficiency.

The point efficiency for the inlet gap and outlet weir of 50 mm is higher than that for the lower combinations for all weir loads. For the two lower combinations there is little to choose between their point efficiencies for the majority of the weir loads. At the lowest weir load of 25 $cm^3/cm.s$, the point efficiency of the inlet gap and outlet weir of 20 mm is slightly lower than that for the 10 mm combination. They are then almost concurrent until the point efficiency of the 20 mm combination edges above that of the 10 mm combination at the higher weir loads.

Figure 6.7 shows how the tray efficiency varies with the weir load. The tray efficiency starts at a minimum of 68% at the lowest weir load of 25 $cm^3/cm.s$ and rises rapidly to a peak of 112% at a weir load of 50 $cm^3/cm.s$, from where it steadily falls off with increasing weir load. There is little to choose between the inlet gap and outlet weir combination of 10 mm and that of 50 mm. The 20 mm combination however is the lowest for all the weir loads investigated.

The peak in the tray efficiency is at a relatively low weir loading for each of the fixed air velocities. A possible explanation for this is that it corresponds to non-separated flow and provides the most favourable conditions for the gas and liquid to contact each other. The decline in the tray efficiency is possibly down to the build up of circulating flow. As has been mentioned above, this type of flow is associated with an uneven liquid profile and corresponding gas problems.

From figure 6.8 it can be seen that the 10 mm combination produces the greatest enhancement of the point efficiency. This is predictable due to the fact that the point efficiency for this combination is the lowest and the tray efficiency is comparable with that of the 50 mm combination. This obviously leads to a high enhancement ratio. However there is little to choose between the different combinations. The ratio is highest at the low weir loads even though they produce the lowest tray efficiencies. This occurs because they are also combined with a low point efficiency and the result is an enhancement ratio of 1.87. The enhancement ratio falls off with an increase in the weir load due to the point efficiency increasing at a faster rate than the tray

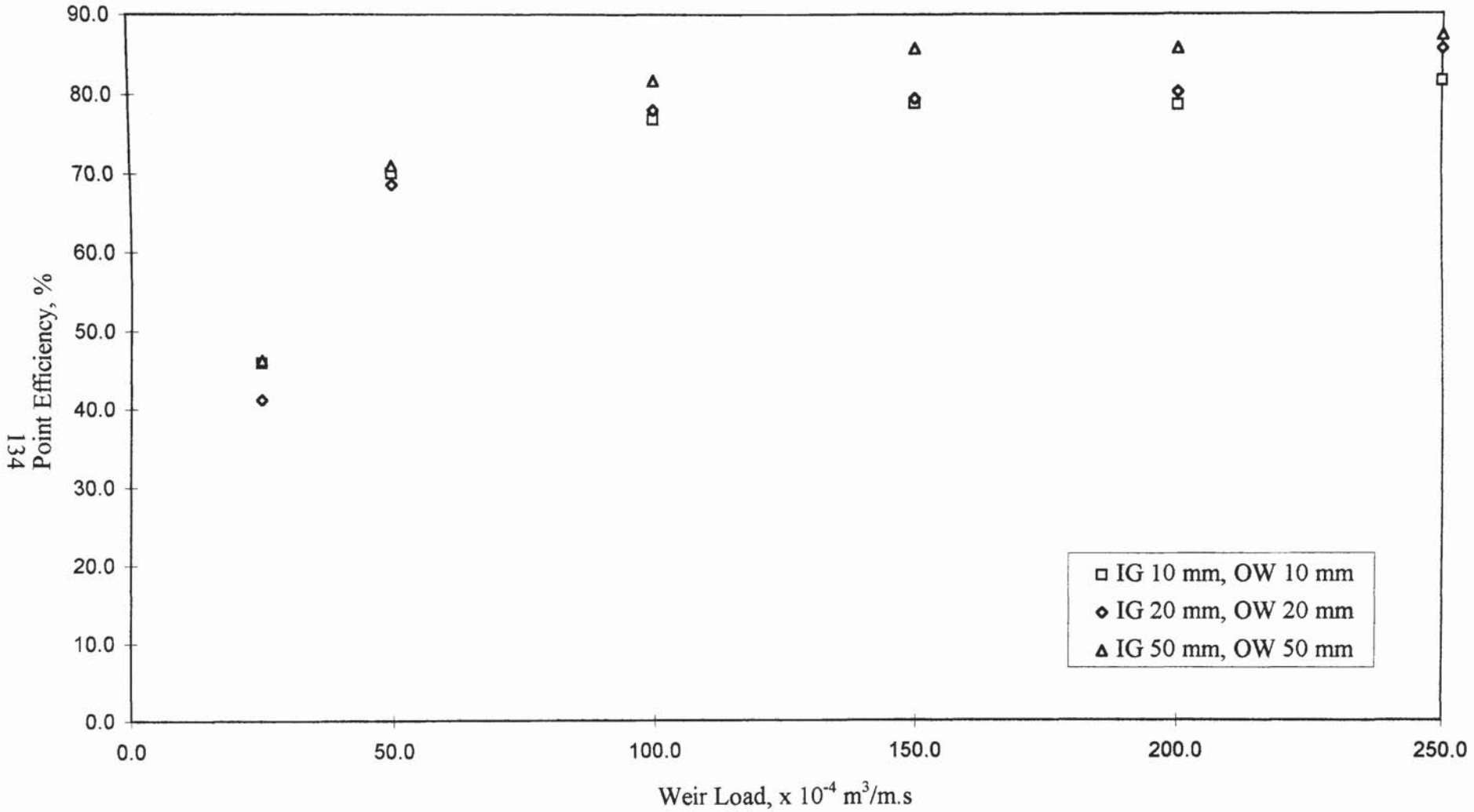

Figure 6.6 Graph of point efficiency versus weir load.

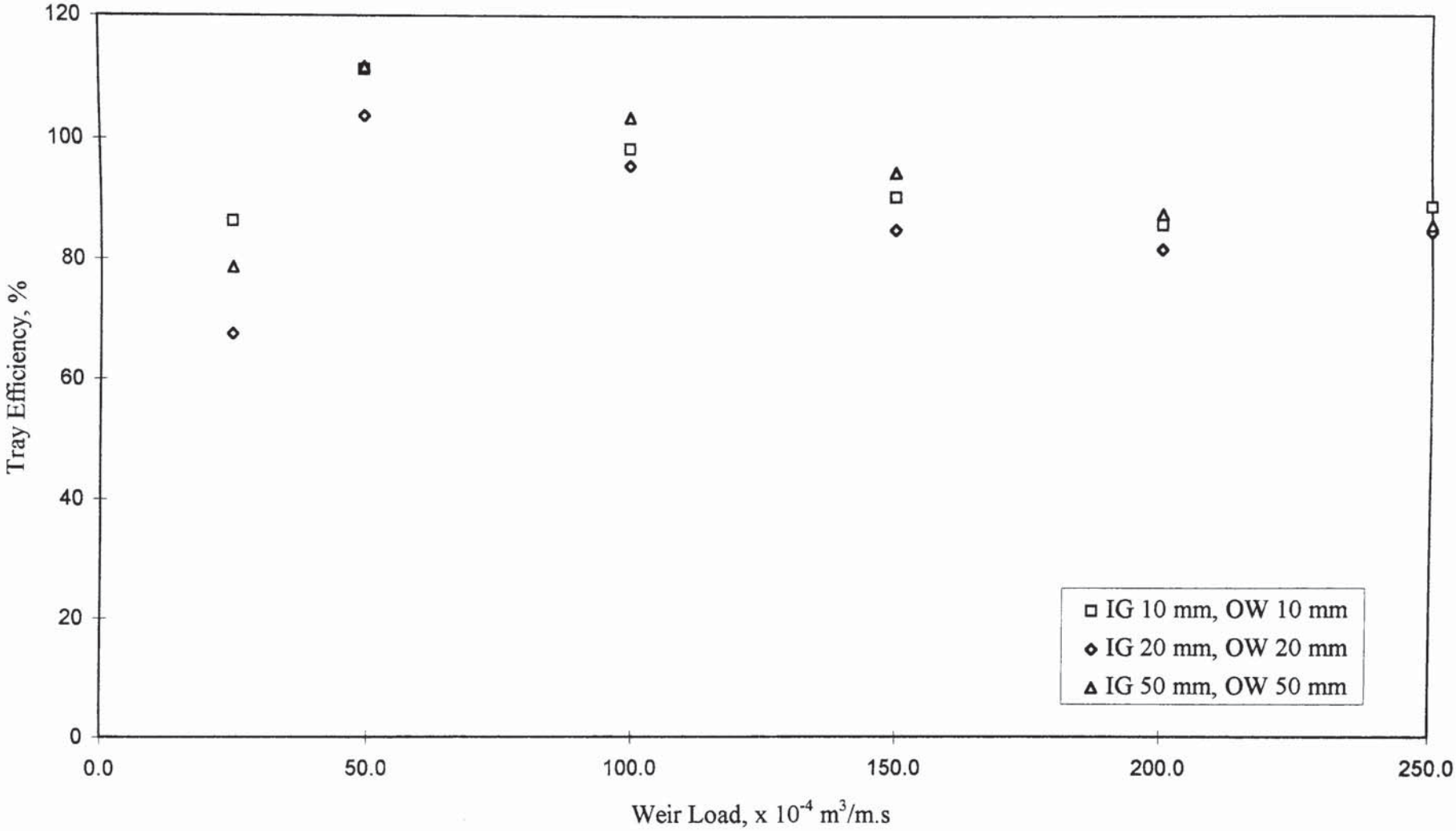

Figure 6.7 Graph of tray efficiency versus weir load.

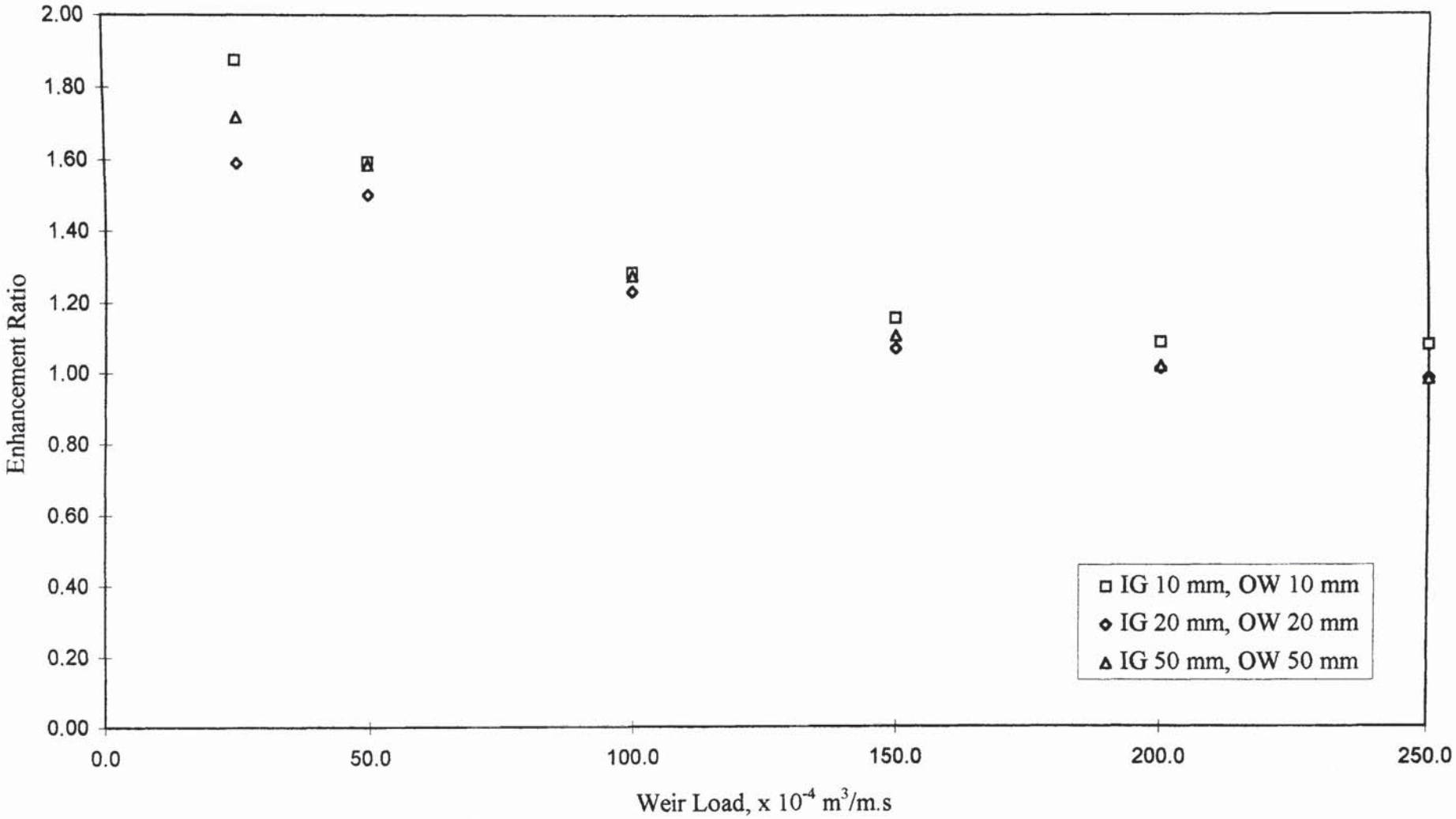

Figure 6.8 Graph of enhancement ratio versus weir load.

efficiency and then staying relatively steady while the tray efficiency drops off. Once again the 20 mm combination gives the lowest figures.

In simple tray efficiency models where plug flow with back-mixing of the liquid is assumed, the enhancement of the point efficiency is related to λ, the ratio of the equilibrium line to the operating line. For most practical distillation purposes, λ is in the range 0.7 to 1.3 and is defined by equation 6.12.

$$\lambda = \frac{mG}{L} \tag{6.12}$$

Using the water-cooling technique it is impossible to separate the value of λ from the air and water flow rates and thus values outside the norm can be produced. Therefore, high water flow rates can give values of λ as low as approximately 0.5 and low water flow rates can give values as high as 12.0. The actual values depend on the temperature drop across the tray, which determines the value of m. If a small temperature drop across the tray is used (approximately 10°C for the experiments undertaken here) then the gradient of the saturation line (the equivalent of the equilibrium line in mass transfer) can be assumed to be constant for the range. Changes in the value of λ are therefore solely due to the change in ratio of G/L.

With a high value of λ the tray efficiency is low and as the λ value decreases with the increase in the weir load, then the tray efficiency also increases. This only occurs up to a weir load of 50 $cm^3/cm.s$ and it is believed that the flow up to this point is non-separated. After this weir load the detrimental effects of separated flow are beginning to be felt and they have begun to overtake the enhancement effect of the reduction in λ.

In some cases the adverse effects of liquid channelling and circulating zones reduced the tray efficiency to less than the point efficiency. This can be explained by the circulating zones being large in area and rapidly approaching equilibrium with the

incoming air. There will be little change in the air and water temperatures in this region. This will subsequently cause a tailing off of tray efficiency.

The results here have been obtained by using one test tray only. It is worth considering the effect the circulating regions would have on the section efficiency in a column if they are stacked directly above each other, as is the case with counter- and co-current single pass trays. Assuming that there is no mixing of the vapour between the trays, the vapour would in effect pass from one circulating region to another with little change in its concentration\temperature. A paper by Lockett, Lim and Porter (1973) assessed this system and found that the above mentioned set-up caused a greater reduction in both the efficiency of the trays and the section efficiency. They predicted that the reduction in the tray efficiency for a single tray was only enough to restrict the tray efficiency to a value close to the point efficiency. With a section of ten trays or more above each other, they predicted that the section and the tray efficiency would be reduced to much less than the point efficiency.

6.3.6 Conclusions

The results have shown that the flow pattern can have a significant effect on the efficiency of a tray. A uniform flow pattern with relatively straight isotherms leads to a high tray efficiency and conversely, circulation and its related U-shaped isotherms bring lower efficiencies. The results show similar trends to the data collected on 1 mm and 6.35 mm hole diameter sieve trays by Hine (1990) and Chambers (1993). This will be discussed more fully in the next chapter.

6.4 Overall Conclusions

- The work presented in this chapter has shown that passing the gas through the liquid on a sieve tray has a significant effect on the flow pattern. The gas delays the onset of separation of the liquid, which occurs at much higher weir loads than

that of single phase flow. High liquid entrance velocities are necessary to achieve the maximum circulating area of 30%.

- When separation occurs on a tray it has a significant effect on the height of clear liquid surface profiles and the temperature profiles. The liquid tends to have a longer residence time on the tray segments, either through the occurrence of circulation, a longer flow path length or the slowing of the liquid due to an adverse pressure gradient. This causes a greater hold-up of liquid in these tray areas and the liquid becomes colder than that in the centre of the tray. This reduces the driving force in these areas and in the most severe cases the liquid on the segments was colder than that leaving the tray over the outlet weir. This caused a significant fall in tray efficiency.

- The results obtained in the course of these studies provides a database with which to test future and existing models of tray efficiency. These experiments were carried out on a purely fluid mechanical basis and as such the back-up of liquid in the downcomer has, in some cases, been greater than would be allowed in practice.

The effect of the hole size used in the experiments has yet to be addressed and this will be the subject of the next chapter.

CHAPTER 7

THE EFFECT OF HOLE SIZE ON THE OPERATION OF A SIEVE TRAY

7.1 Introduction

With the completion of experiments on a sieve tray with 12.7 mm diameter holes, it is now possible to compare data to assess the effect of the hole size on trays of this nature. Hine (1990) and Chambers (1993) carried out work on sieve trays with hole diameters of 1 mm and 6.35 mm respectively. The data were collected on trays with an identical geometry, save hole size, to that used to produce the data presented in Chapter 6. This chapter assesses differences in the three trays that can be attributable to the increase in hole diameter.

7.2 Comparison of the Various Experiments

The data to be compared were collected from experiments on the 2.44 m diameter air-water simulator at Aston University. The geometry of the trays used and the configuration of the weirs and gaps were identical in each case. The methods used to collect the data were the same as presented in Chapter 6, namely:

1. Direct observation with the use of flow pointers,
2. Measurement of the pressure drop to obtain the height of clear liquid on the tray,
3. Water-cooling to determine thermal efficiencies.

Table 7.1 is a summary of the flow rates and configurations used for the various experiments.

Air Flow Rates, m/s	Weir Loads, $x10^{-4}$ m^3/m.s	Inlet Gaps and Outlet Weirs, mm	Hole Diameters, mm
0.7	25	10	1.00
0.9	35	20	6.35
1.0	55	50	12.70
1.2	75		
1.25	100		
1.5	110		
2.0	150		
2.5	200		
	250		

Table 7.1 Summary of the flow rates and configurations used to test the three different hole sizes

7.3 The Spray-Froth Transition

Perhaps the best point to start a comparison of different trays is to determine the flow regime that each experiment is operating under. This can best be achieved by plotting each individual data point on a graph showing the spray-froth transition line. To be able to plot this line we must first discuss where it should be positioned.

The transition from froth to spray occurs when a substantial proportion of the gas penetrates the dispersion as jets. The proportion of holes carrying jets at this transition is open to dispute, but the issue is purely academic as it is very difficult to measure. Thus the transition must be characterised by a change in some other property. Attempts to classify the transition line have been made by many workers using a variety of techniques. The techniques used are:

1. Light beam attenuation,
2. Entrainment rate,
3. Hole pulsation frequency,
4. Residual pressure drop,
5. Visual observation,
6. Change in shape of dispersion density profile,
7. Change in sound made by the gas.

Correlations have been proposed based on data collected in these ways. The majority of the equations take the form of the height of clear liquid divided by the hole diameter correlated against the hole velocity. None of the models produced are completely satisfactory and therefore little is lost by resorting to empiricism. Lockett (1981) suggests the use of the equation 7.1.

$$\frac{h_{cl}}{d_h} = 2.78.u_h\left(\frac{\rho_G}{\rho_L}\right)^{0.5} \qquad (7.1)$$

This equation was produced from comparison with experimental data from various workers (Porter and Wong, 1969, Wong, 1967, Pinczewski and Fell, 1972, Payne and Prince, 1977, Prince et al., 1979 and Fane and Sawistowski, 1969).

Figures 7.1 to 7.4 show the transition line plotted alongside data obtained from trays with 1 mm (Hine 1990), 6.35 mm (Chambers 1993) and 12.7 mm diameter holes. Figure 7.1 shows data for a combination of a 10 mm inlet gap and a 10 mm outlet weir. Height of clear liquid data are available for all three hole sizes with this combination. It is clear that with the small hole diameter of 1 mm as the denominator the ordinate value is relatively high and as a consequence the bi-phase is well into the froth regime. Figure 7.2 eliminates the 1 mm data to allow an expansion of the area around the transition line. This shows that the 6.35 mm tray operates in the froth regime for this combination and only the 12.7 mm tray enters the spray regime at the higher gas velocities.

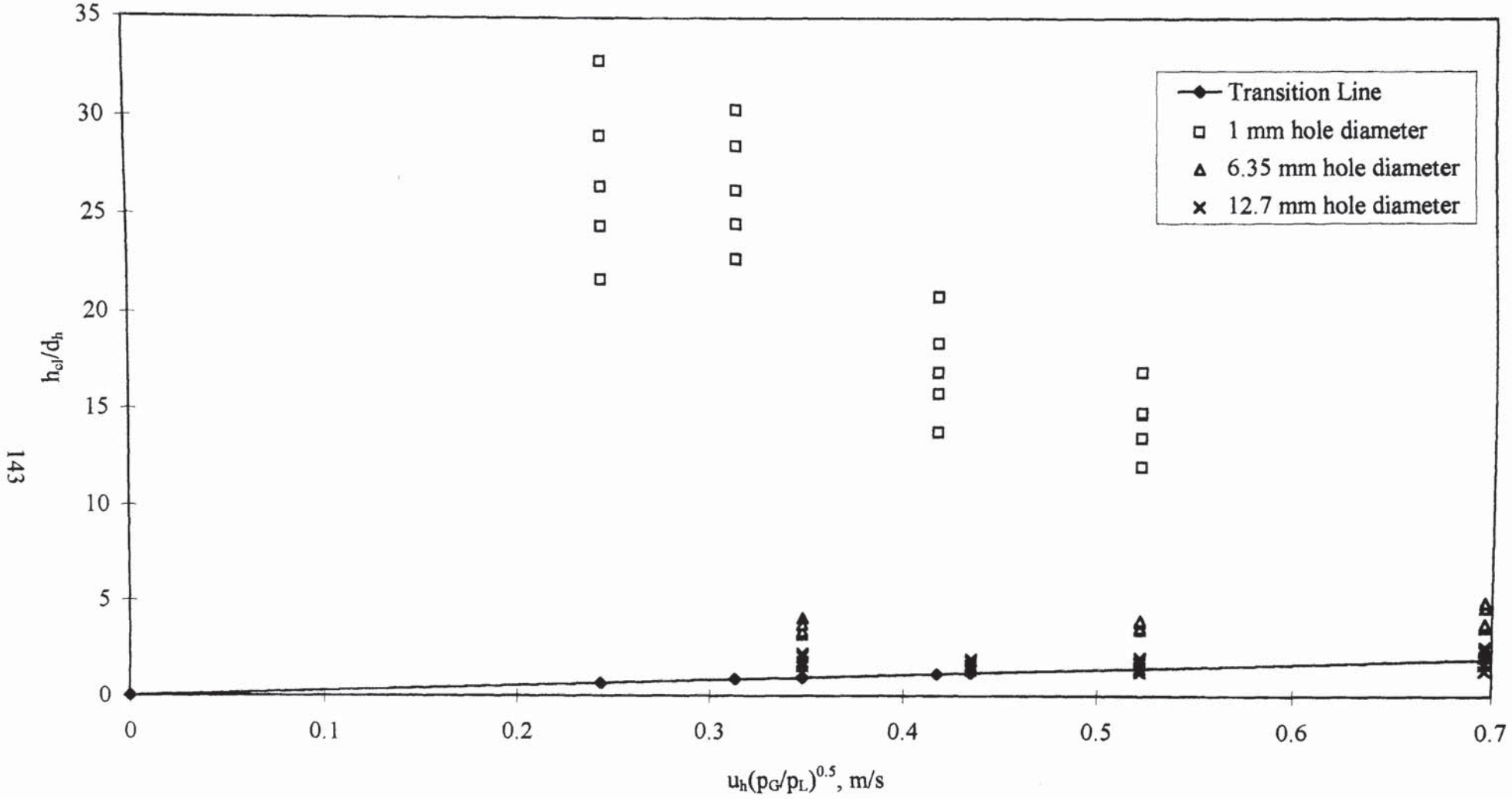

Figure 7.1 Spray-froth transition for an inlet gap and outlet weir of 10 mm.

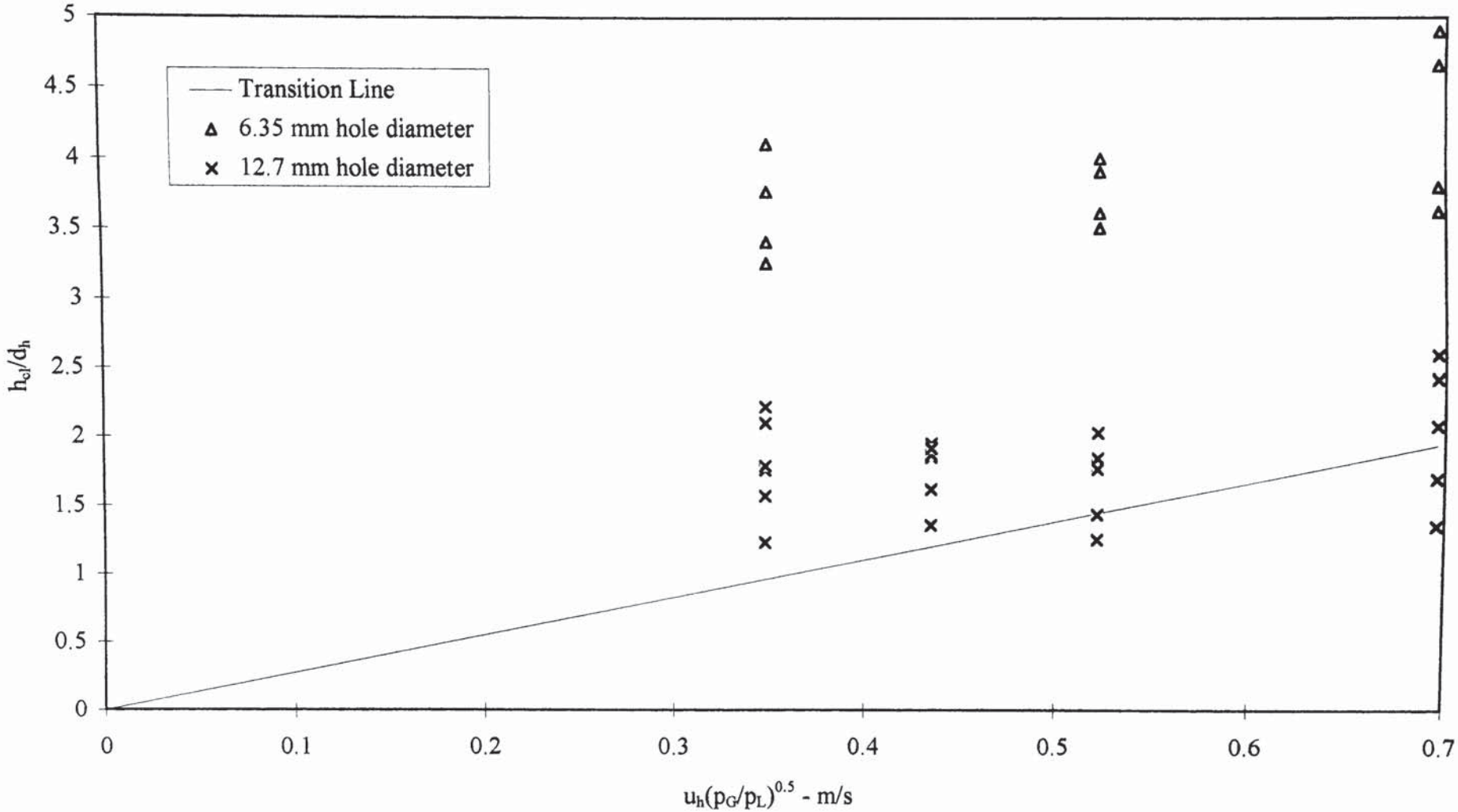

Figure 7.2 Expansion of the spray-froth transition for an inlet gap and outlet weir of 10 mm

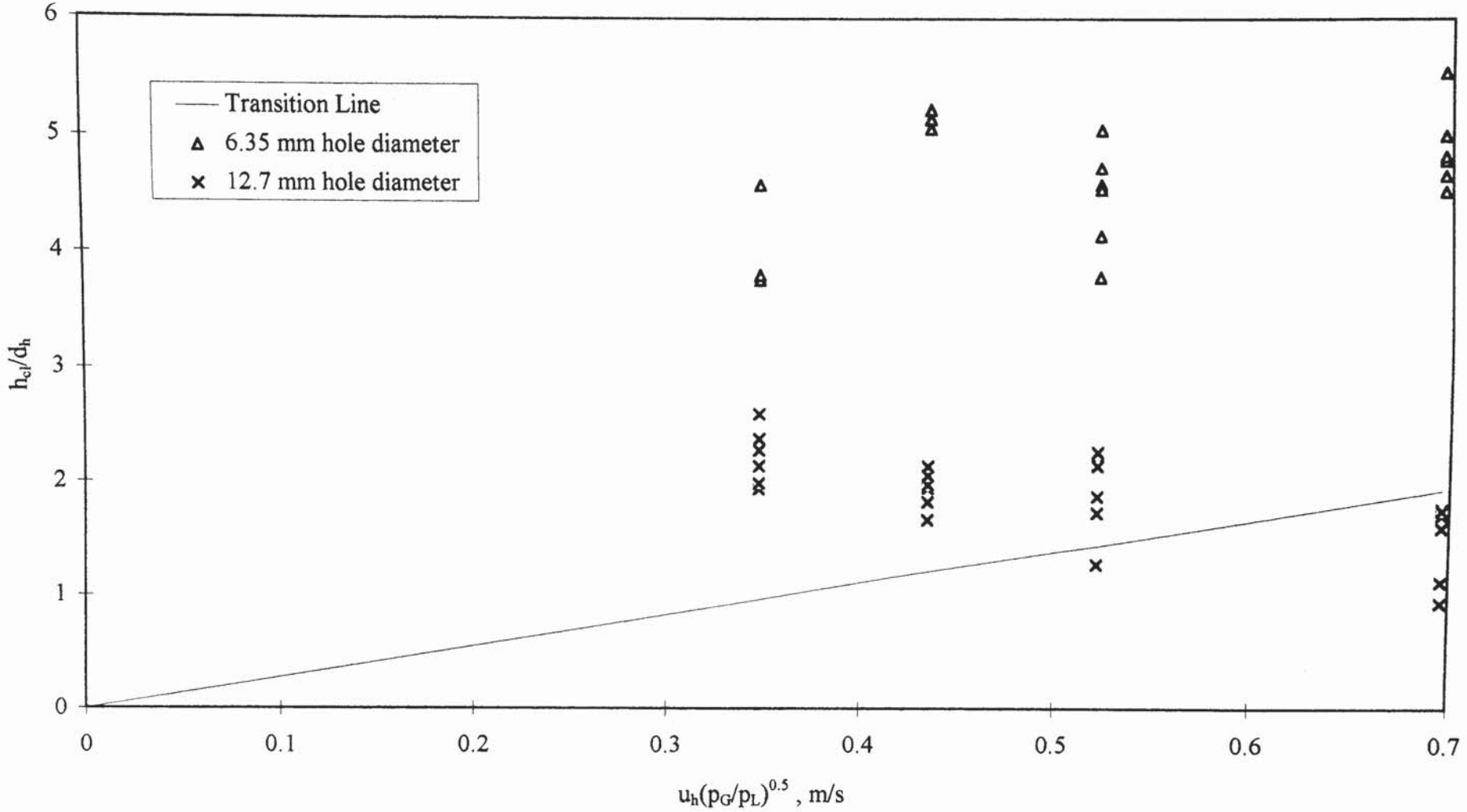

Figure 7.3 Spray-froth transition for an inlet gap and outlet weir of 20 mm

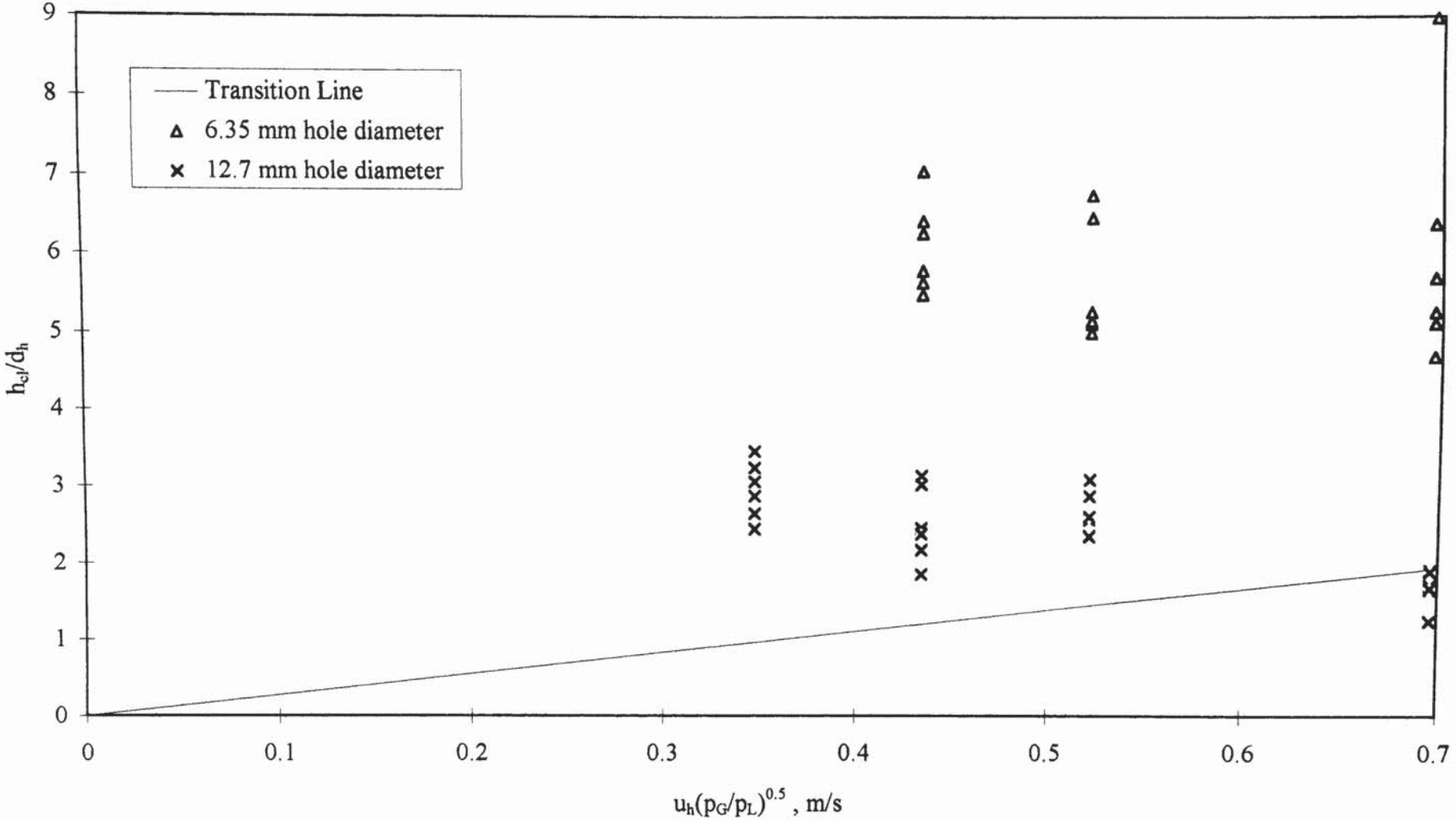

Figure 7.4 Spray-froth transition for an inlet gap and outlet weir of 50 mm

Data are not available for the height of clear liquid on the 1 mm tray at the equal inlet gap and outlet weir heights of 20 and 50 mm. It is safe to assume that the tray will be operating in the froth regime as the clear liquid height tends to increase with the outlet weir height, while the hole diameter is constant. Figures 7.3 and 7.4 tell a similar story to the lower 10 mm combination, in that the 12.7 mm tray is the only tray to operate in the spray regime and then only at high gas velocities.

We have now identified the regimes under which the trays are operating for each data point. This is an important step for analysis of the data from the different trays as it allows us a background picture of the bi-phase on the tray. It should be stressed that the change from one regime to the other is a continuous process and a sudden phase inversion does not occur. Indeed, a theory proposed for the transition involves the percentage of holes producing jets that penetrate the froth. This quantity obviously increases with the increase in the gas velocity until all holes carry such jets. It is open to conjecture what regime the tray is operating under in between no jetting and complete jetting. It is worth keeping this in mind when analysing the data.

7.4 The Effect on Separated Flow

A good starting point for the evaluation of the effect of hole size on the degree of separation on a tray is to look at the no hole, or 0 mm hole diameter, case. This has already been reviewed in Chapter 6. If we treat the case of a tray with no holes as a tray with a hole diameter of 0 mm, then we have a set of trays with an increasing hole size from 0 to 12.7 mm in diameter.

The work on the single phase tray, i.e. that with no holes, showed that the liquid separated at very low flow rates. The area of the tray that contained circulations quickly increased to a maximum of 30% of the tray area, pertaining to the tray segments. The effect of forcing the gas through the liquid on the tray has been found to delay the onset of separation. This is the case with all hole sizes studied. Indeed,

the presence of the gas can reduce the area covered by circulating froth so that the maximum area of 30% is not reached with the flow rates tested.

7.4.1 Results

The results obtained from the experiments with the various hole sizes are summarised in Figures 7.5 to 7.8. These show the area of the tray found to contain circulating bi-phase against the weir load. The weir load is chosen as it has been shown that this variable, along with the inlet gap, has a significant effect on the area of circulating flow. The effect of other variables, such as air velocity and outlet weir, has been found to be much less.

Figure 7.5 is a reproduction of that presented by Hine and shows the circulation associated with water-only studies. It can be seen that circulation occurs at a relatively low weir load and that the maximum circulating area of 30% is rapidly reached. The second chart, figure 7.6, is also from Hine and shows the circulation on a tray with 1 mm hole diameters. This shows that at the lowest weir load of 25 x 10^{-4} m^3/m.s, no circulation was observed for any setting of the inlet gap. Above this weir load circulation is present at the sides of the tray. The degree of circulation is dependant on the inlet gap, with the 10 mm gap generating the largest degree of circulation and the 50 mm gap generating the smallest degree of circulation, for a fixed weir load. The rate of increase of the circulation area against the weir load was also greater for the 10 mm gap than for the 50 mm gap. Once again the maximum area of circulation was 30% and once this was reached further increases in the weir load only strengthened the rotational velocity of the circulations.

The results of Chambers were on a sieve tray with 6.35 mm diameter holes and the circulation results are summarised in figure 7.7. From this chart it can be seen that circulation did not occur until a weir load of 50 x 10^{-4} m^3/m.s was reached. Once again the maximum circulation encountered is 30% of the tray area, with the inlet gap of 10 mm generating the largest degree of circulation and the 50 mm gap the smallest, for a

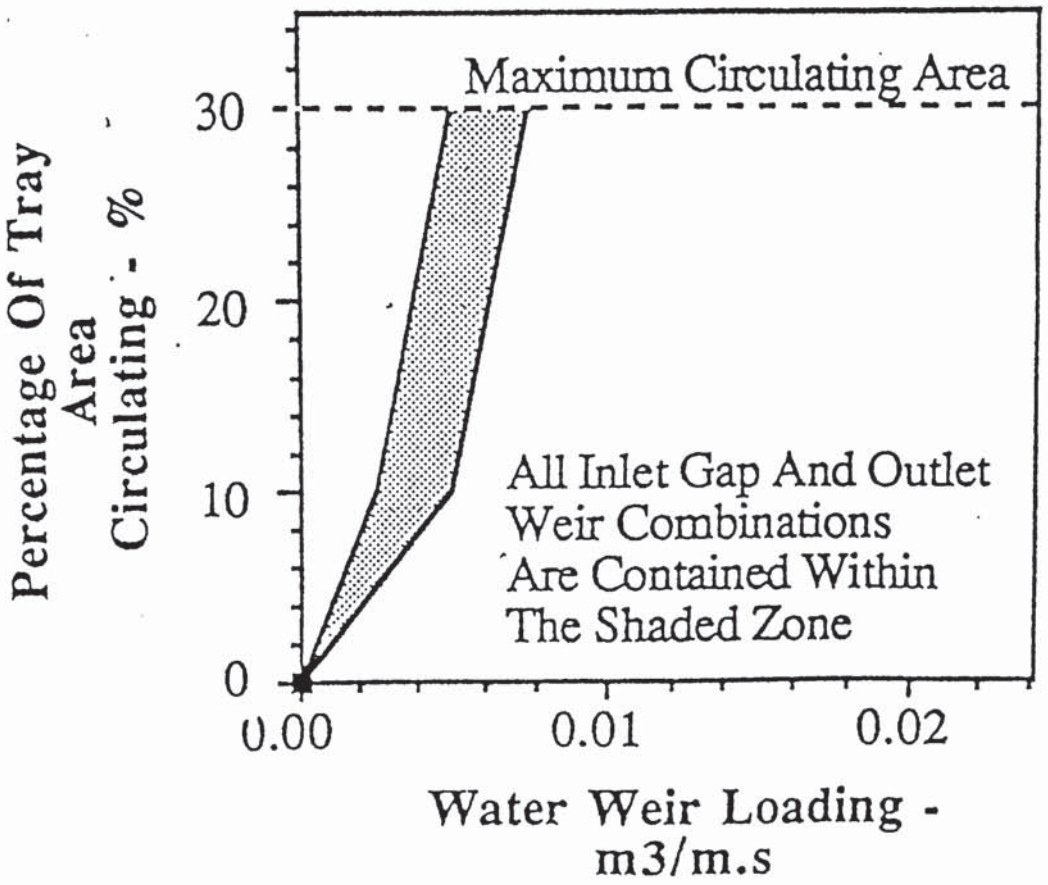

Figure 7.5 Summary of the experiments with water-only. (Reprint of Figure 6.1)

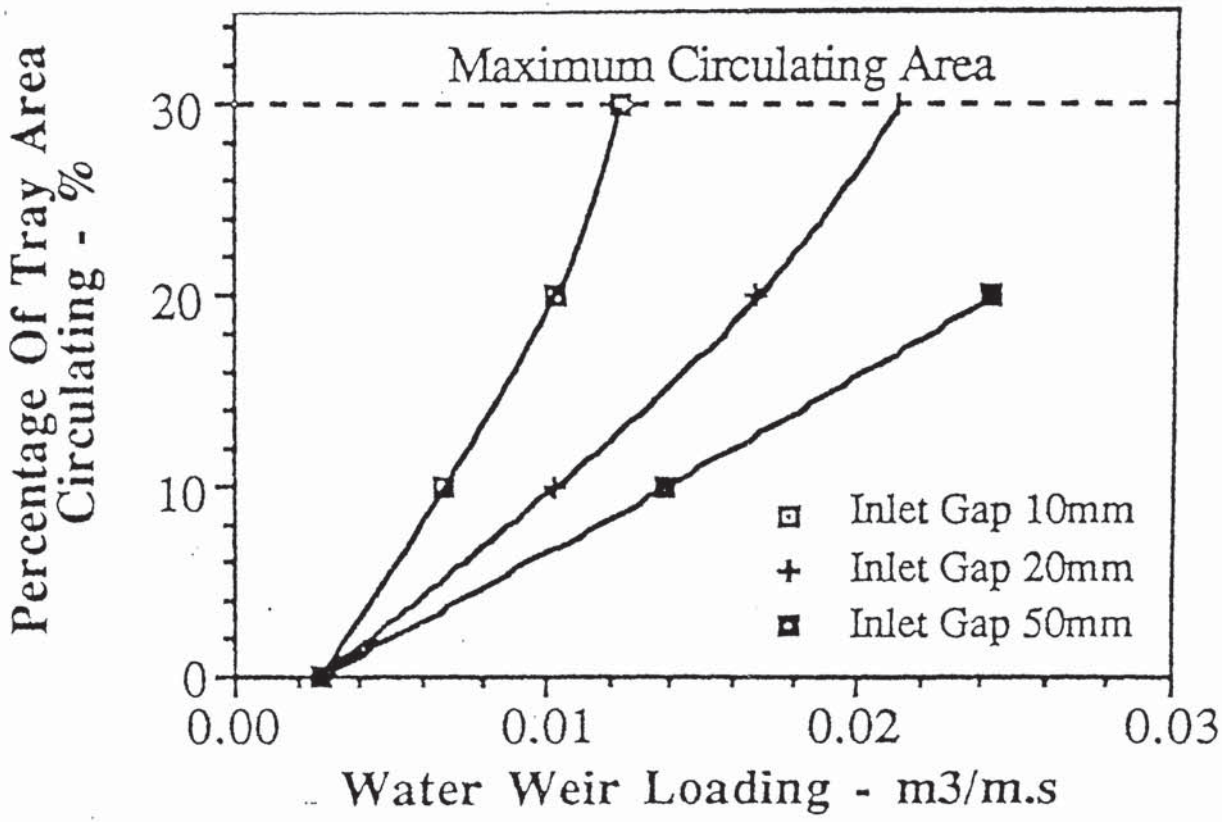

Figure 7.6 Summary of Hine's (1990) experiments on a 1 mm tray

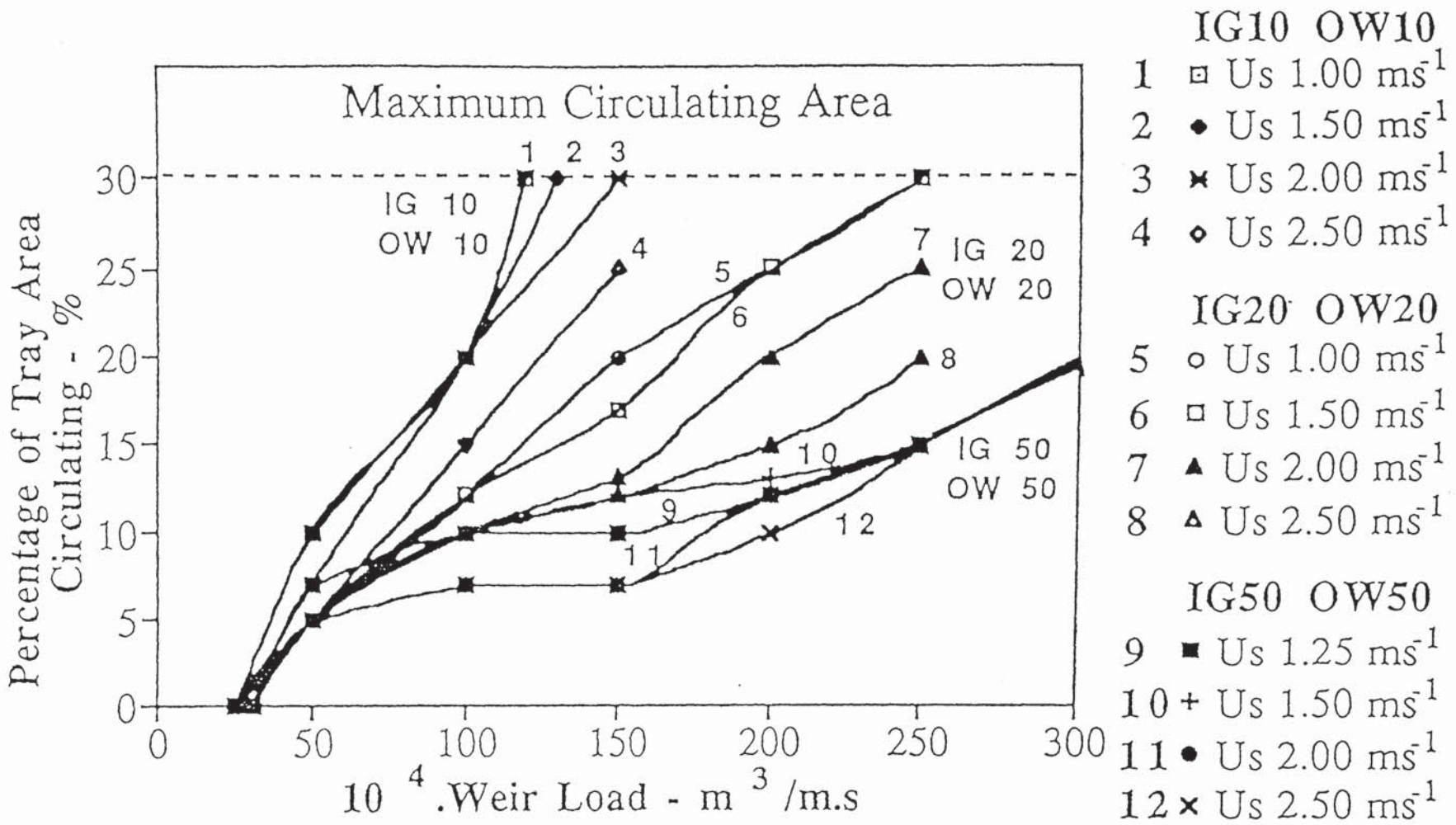

Figure 7.7 Summary of Chambers's (1993) experiments on a 6.35 mm hole tray

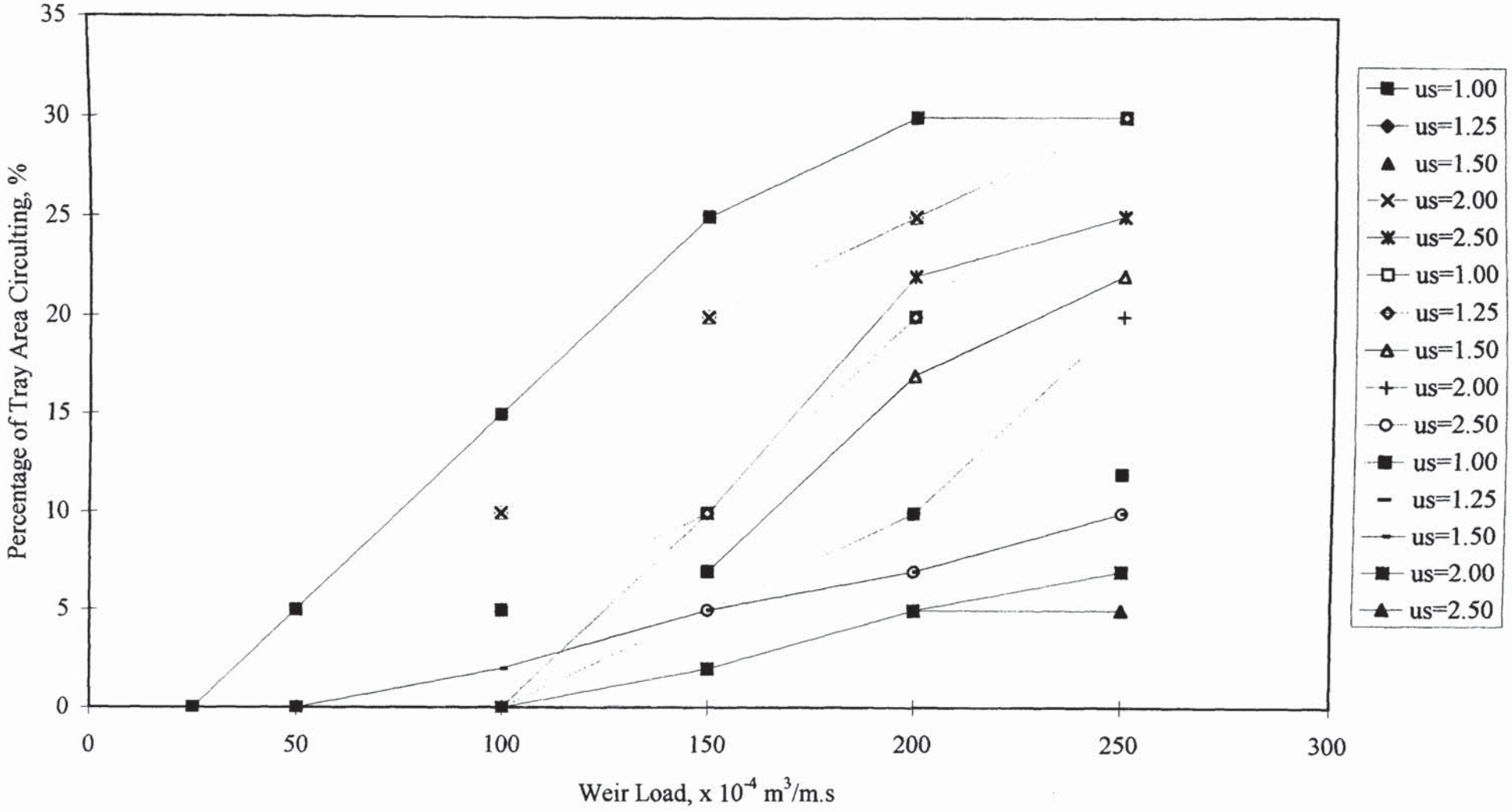

Figure 7.8 Summary of the circulations on a 12.7 mm hole tray. (Some lines coincide)
(Reprint of Figure 6.5)

fixed weir load. The rate of increase of the circulating area was greatest for the 10 mm gap, but interestingly, less than that of the 1 mm diameter hole tray.

Figure 7.8 summarises the results from a tray with 12.7 mm diameter holes. The circulation on this tray also begins at a weir load of 50 x 10^{-4} m^3/m.s, but once again the rate of increase of the circulating area is less than that of the trays with a smaller hole diameter. The inlet gap of 10 mm produces the greatest circulation for a fixed weir load, followed by the 20 mm and then the 50 mm gaps. The maximum circulation encountered is 30% of the tray area.

7.4.2 Discussion and Conclusions

From a comparison of the direct observation experiments carried out on trays with different hole sizes, a number of points become clear, the most marked of which is that the area of circulation at a given weir load is reduced by the increase in hole diameter. This can be seen clearly from a comparison of figures 7.5 to 7.8. The 12.7 mm diameter holes produce the smallest degree of circulation until the maximum of 30% is reached. Another aspect of this is that a higher weir load is required to produce the maximum circulation.

A possible explanation of this characteristic is the momentum contained in each individual jet. As the free area of the holed trays is identical, then the hole velocity of the gas is identical, for a fixed gas velocity. However, with the larger holes, a greater total mass of the gas flows through each hole. This means that the total gas jet emerging from the hole has a greater momentum for the larger holes. As the mass in each jet varies as the square of the hole diameter and the surface across which the liquid / vapour interaction occurs varies with the diameter, then the liquid immediately around the jet must proportionately lose more momentum in its attempt to deflect the vapour jet. However, this does not adequately explain why the effect across the whole tray should vary with the hole size as the total momentum transferred should be the

same e.g. the same mass of gas passes through each tray with the same hole velocity. Further work will need to be undertaken to identify the mechanism at work here.

It has been seen that the entrance velocity plays a big part in the degree of circulation, with the greatest circulations occurring with the greatest entrance velocity. Obviously if the liquid is losing momentum from deflecting the gas, this will be seen as a loss in velocity or a change in head. Either of these factors have been shown to reduce the degree of circulation.

Another point to arise from the comparison of the trays is that the maximum circulating area does not change. This is essentially set by the tray geometry. The trays are of similar geometry and their physical segmental area is approximately 30% of the whole tray. It is expected that the maximum area of circulation will not change until the weir length is changed to produce a tray with a different segmental area.

For all the trays it can be seen that increasing the froth height or the gas-liquid contact time reduces, the degree of circulation produced. Again this could be explained by the magnitude of the momentum transferred. A more likely cause is the increase in the inlet gap which reduces the entrance velocity. The effect of the above aspects on the height of clear liquid on the tray and the mass transfer are discussed in the next sections.

7.5 The Effect on the Height of Clear Liquid

Height of clear liquid data have been collected from all the trays tested. However, only a limited amount is available from the 1 mm hole diameter tray, namely at an inlet gap and an outlet weir of 10 mm. Data from the other hole diameters are more comprehensive and cover a wide range of water and air flow rates. This section covers the comparison of the height of clear liquid data in numerical form and as far as possible draws rough comparisons from the three-dimensional plots of the clear liquid surface.

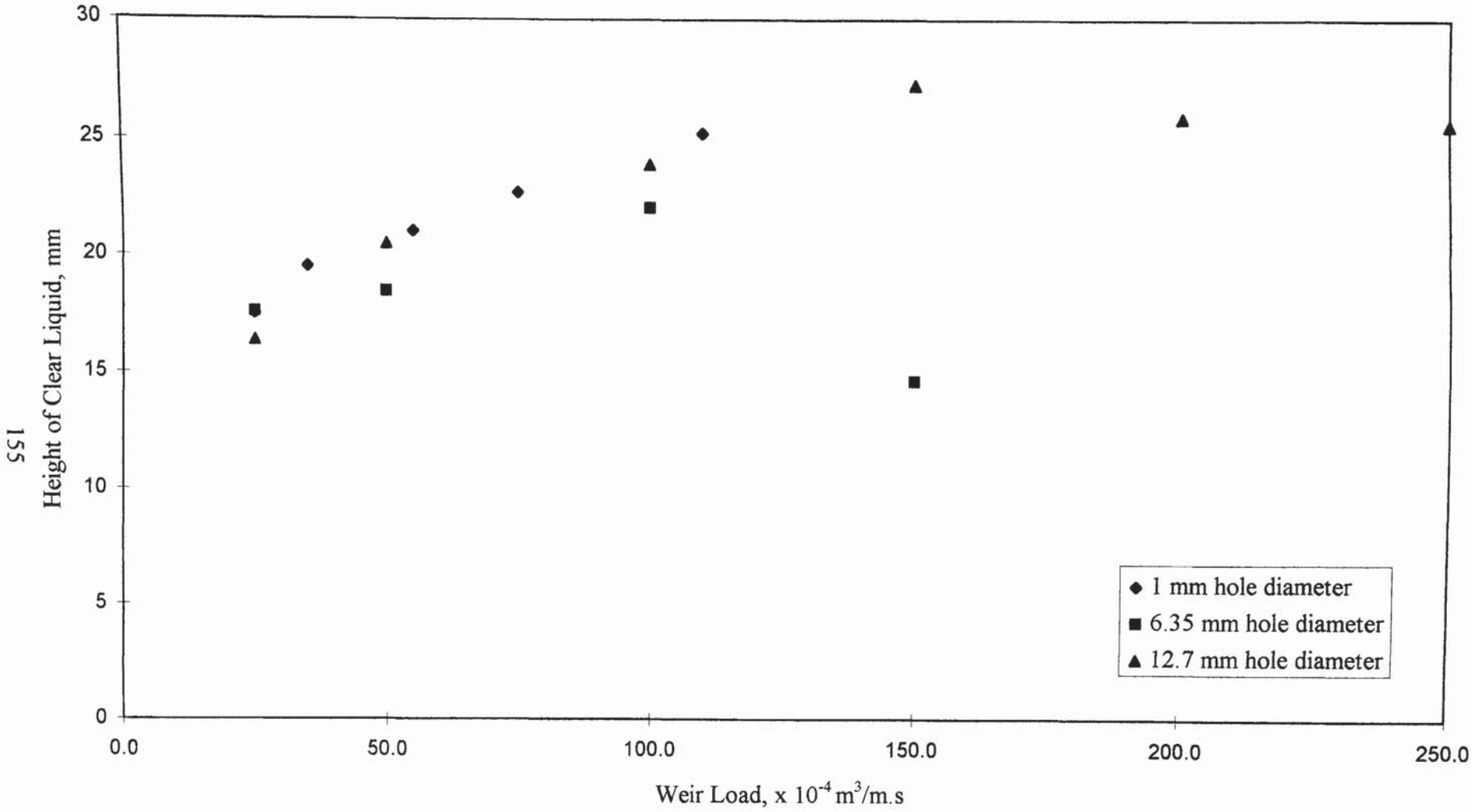

Figure 7.9 Average Height of Clear Liquid for an Inlet Gap of 10mm and an Outlet Weir of 10 mm.

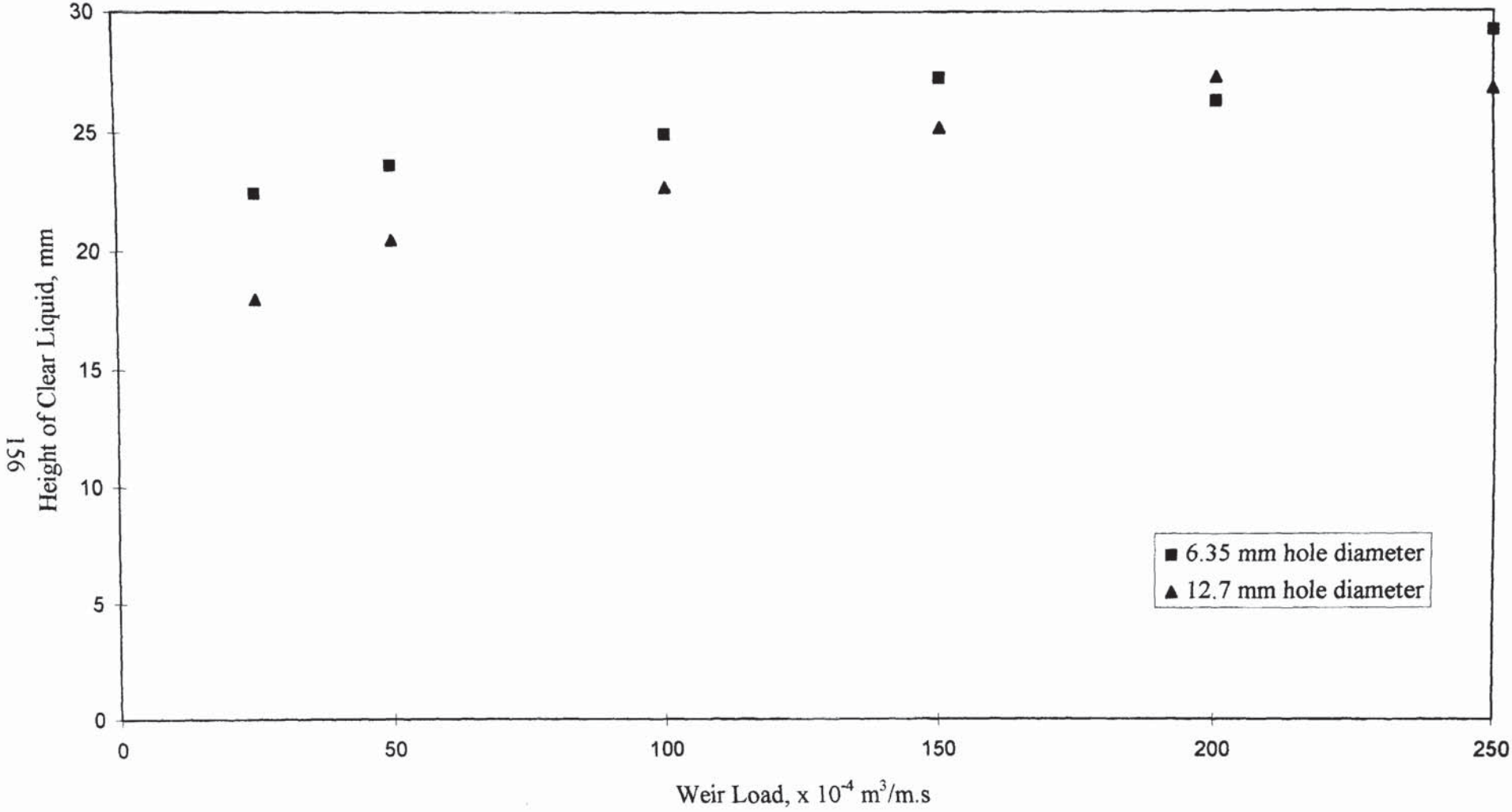

Figure 7.10 Average Height of Clear Liquid for an Inlet Gap of 20 mm and an Outlet Weir of 20 mm.

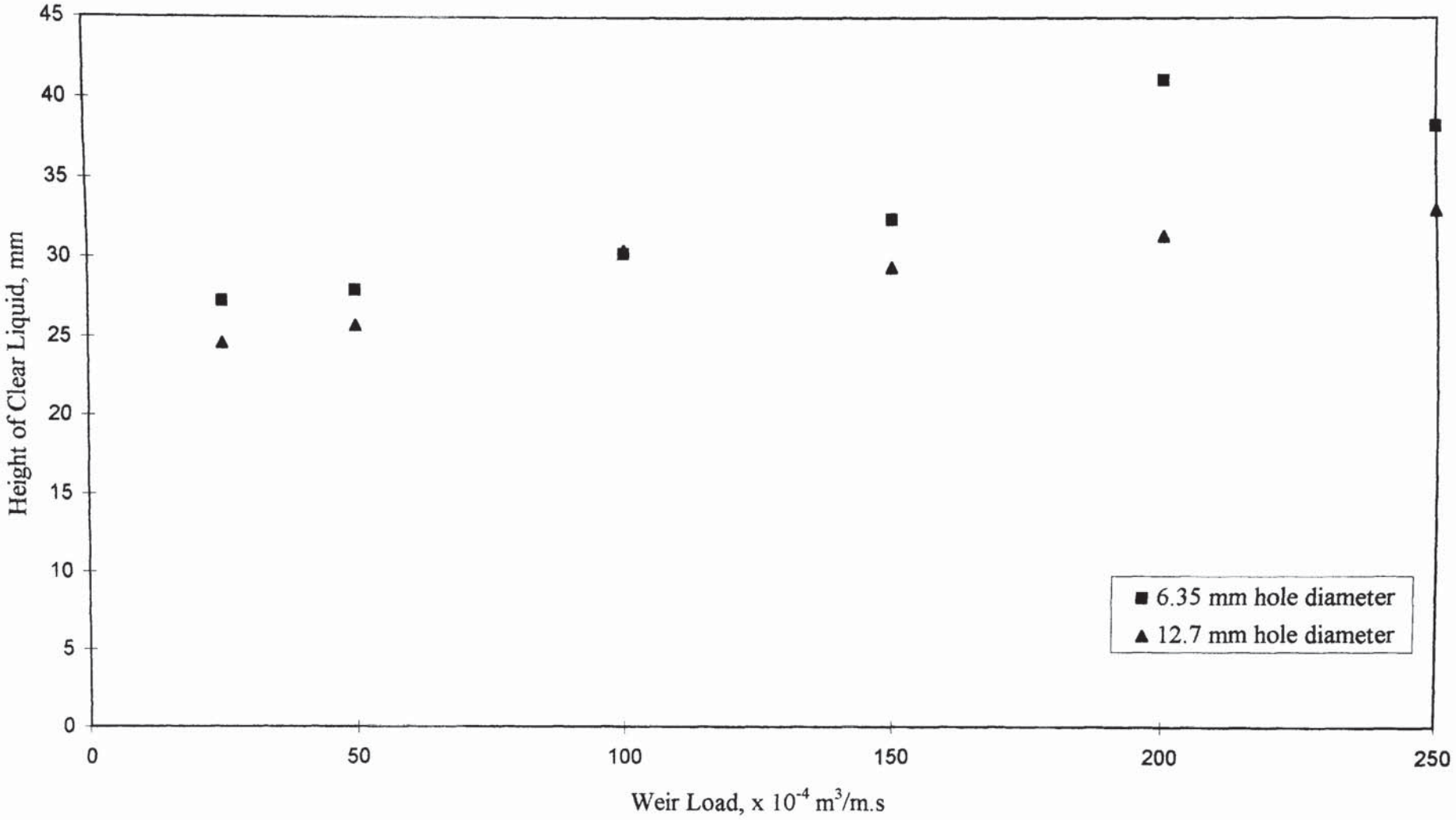

Figure 7.11 Average Height of Clear Liquid for an Inlet Gap of 50 mm and an Outlet Weir of 50 mm.

7.5.1 Numerical Analysis of the Results

The best point to start an analysis of the data is by plotting the relevant points. This is carried out in figures 7.9 to 7.11. The data have been averaged for each air velocity so that the height of clear liquid can be plotted against the water weir load. The variation with the air velocity is small compared with that for the weir load and justifies this approach.

Figure 7.9 contains the data for an inlet gap and outlet weir combination of 10 mm. It can be seen that there is little variation in the height of clear liquid for the different hole sizes. That produced by the 12.7 mm and the 1 mm hole diameter trays are almost identical. The only slight variation is that the 6.35 mm data is slightly below that of the other two. At high entrance velocities there may be a hydraulic jump in front of the inlet downcomer. This would explain the tailing off of the average data at the higher weir loads.

Moving on to figure 7.10, the data collected from the 6.35 mm hole tray is consistently greater than that of the 12.7 mm hole tray. At the widest point, however, the gap is only 4 mm. Therefore it is fair to say that there is little variation shown. The tailing off witnessed on the previous figure is not as significant here as the entrance velocities are reduced due to the higher inlet gap.

The last figure shows the data collected at an inlet gap and outlet weir of 50 mm. Once again the data from the 12.7 mm hole tray lie slightly below that of the 6.35 mm hole tray for the whole of the weir load range. The gap is very small for most of the data points and it can be said that once again there is little variation. The data do not tail off at this combination due to an increase in the height of the inlet gap and the reduction in the inlet jetting this entails.

7.5.2 Qualitative Assessment of the Three-Dimensional Plots

Due to the shear amount of data produced from the height of clear liquid experiments it will only be possible to do a qualitative analysis of the three-dimensional surface plots. It is difficult to assess them in a scientific fashion due to the differences discussed above, mainly, that the gradient across the tray may be different and that there are different degrees of circulation on the various trays. On the whole, the liquid height tends to build up in circulating regions and the gradient across the tray is from inlet to outlet. A significant deviation from this is the case of a hydraulic jump. The liquid at the inlet is lower than at points downstream where the clear liquid height increases as it slows down.

From the experiments carried out by Hine on a 1 mm hole tray four air velocities and five weir loads are used to generate the surface profiles. The data are limited to the set-up with a 10 mm inlet gap and an outlet weir of 10 mm also. Generally the clear liquid hold-up decreases with distance from the inlet gap, with the exception being at the highest weir loading of 110×10^{-4} $m^3/m.s$. At this flow rate the liquid tends to jet onto the tray under the small inlet gap. Also at the lower air velocities of 0.7 and 0.9 m/s the clear liquid height is much greater in the side segments and this is associated with sporadic bubbling. At the higher air velocities the bubbling is more even with the whole tray being 'active'.

At the higher weir loads it was expected that there would be a build up of liquid in the side regions due to significant circulations. It can be seen from the surface profiles of Hine, at the higher gas velocities of 1.2 and 1.5 m/s, that this does not occur. The profiles are very flat in the transverse direction and Hine's conclusion is that the technique is not sensitive enough to pick up on the small deviation that would occur at the higher gas velocities.

The height of clear liquid surface profiles produced by Chambers on a 6.35 mm hole diameter tray represent a more comprehensive coverage than those of the 1 mm tray. The experiments covered four different air velocities and six different weir loads. The

air velocity ranged from 1.00 to 2.00 m/s and the weir load from 25.0 x 10^{-4} to 250.0 x 10^{-4} m^3/m.s. The combinations of equal inlet gap and outlet weir of 10 mm, 20 mm and 50 mm were employed.

The surface profiles for the 6.35 mm hole diameter tray indicate that flat or horizontal profiles were produced at low weir loads and that this is consistent with the direct observation experiments showing forward-only flow, i.e. no circulation or separation. On increasing the weir load, once again the jetting of the liquid on the tray was observed. This was more severe for the lower inlet gaps, as expected. Also, from the direct observation experiments, as the weir load was increased, circulation occurred and increased up to the maximum. There is some evidence that the clear liquid height increased on the segments under these conditions but it is very slight. This could be as a result of the insensitivity of the technique, as mentioned above. It was noted that as the air velocity was increased, the unevenness of the height of clear liquid surface also increased.

The profiles produced from the height of clear liquid data for the 12.7 mm hole diameter tray covers a similar range to that of the 6.35 mm data. Flat surface profiles were produced at low weir loads due to there being no separation of the flow and no jetting from below the inlet gap. The jetting occurred at a weir load of 150 x 10^{-4} m^3/m.s for all inlet gaps, but the distance that the jetting reached was greater for the lower inlet gaps. At the higher air velocities the surface of the dispersion is disrupted by gas jets busting through the surface and carrying liquid with them. From the clear liquid profiles it is impossible to tell what regime the tray is operating in. This is because the profiles plot the clear liquid and give no detail of the fraction at each level above the tray. For example, the majority of the liquid is close to the tray for a froth but it is spread more evenly in the vertical direction for the gas dominated spray. At the sides of some of the profiles there is, once again, a very small increase in the clear liquid height and it is proposed that this is created by separation of the liquid.

7.5.3 Discussion and Conclusions

By comparing the data from the three trays a number of observations can be made. The first point arises from the numerical comparison and it suggests that there is little difference between the trays when it comes to average clear liquid height, i.e. that it is independent of hole size. This is plausible if the residence time of the liquid, and hence the hold-up, is controlled by the liquid flow rate, that is to say that the amount of liquid on the tray is controlled by the weir load and weir height. The only difference between these trays is the way in which the gas enters the tray. For the 1 mm hole diameter the gas enters in small 'packets' and the size of the 'packet' increases for the larger hole diameters. However, we must bear in mind that the numbers compared in the numerical analysis are average figures and do not tell us about any gradient or irregularities that may exist. This gradient will be analysed further by using a rectangular tray, which will cut out any uncertainties caused by the diverging/converging nature of the circular tray.

The second point is that the actual surface of the height of clear liquid is affected by the size of the holes. With the larger hole sizes the surface is more disturbed than for the smaller holes. This is entirely predictable due to the size of the jets or bubbles that are forced through the dispersion. The larger these are, the more liquid that they carry with them. As they break through the dispersion they cause fluctuations in the pressure drop that is measured by the manometers. The more the surface is disrupted, the more the pressure drop fluctuates and this makes the value of the clear liquid recorded less certain. This is born out by the variation in the surface plots.

The jetting that occurs from the inlet gap is reduced with larger holes. This can be seen by comparing the relevant surface plots with the same air and water flow rates and combinations. As an example of this we can compare the 1 mm hole surface profile of the combination of 0.9 m/s gas velocity and the weir load of 110×10^{-4} $m^3/m.s$ with the 6.35 mm and 12.7 mm hole surface profiles using a gas velocity of 1 m/s and 100×10^{-4} $m^3/m.s$. These experiments were carried out with an inlet gap and outlet weir of 10 mm. It can be seen that the greatest jetting is with the 1 mm tray and

the least with the 12.7 mm tray. This trend is repeated for all the profiles that are comparable.

It is impossible to say whether the hole size has any effect on the gradient across the tray. The analysis of the gradient is complicated by the circular nature of the tray. As mentioned above, this particular effect of hole size will be dealt with in the next chapter by using a rectangular tray to eliminate the converging/diverging nature of the tray.

7.6 Water-Cooling Experiments

In this section it is not proposed to offer any explanations for the trends in the data such as why the tray efficiency peaks at low weir loads. This has already been discussed in Chapter 6 and the relevant chapters of the theses by Hine (1990) and Chambers (1993). Trends between the different hole sizes will be tackled in this section. Firstly a numerical analysis of the efficiencies calculated from the water-cooling experiments is undertaken. A qualitative assessment of the two-dimensional temperature profiles is then given. As mentioned above, the emphasis will be on the differences between the trays rather than the trends in any single set of data.

7.6.1 Numerical Analysis of Efficiencies

The data collected from the three trays were processed in an identical manner to produce point and tray efficiencies. These are presented in figures 7.12 and 7.13 plotted against weir load. The enhancement ratio, E_{MV}/E_{OG}, is also presented in figure 7.14.

The point efficiencies for the three trays are shown in figure 7.12 and they all show roughly the same trend, i.e. a rapid increase at lower flow rates and then a levelling off. At low heights of clear liquid, e.g. with a low weir, it appears that the 6.35 mm hole

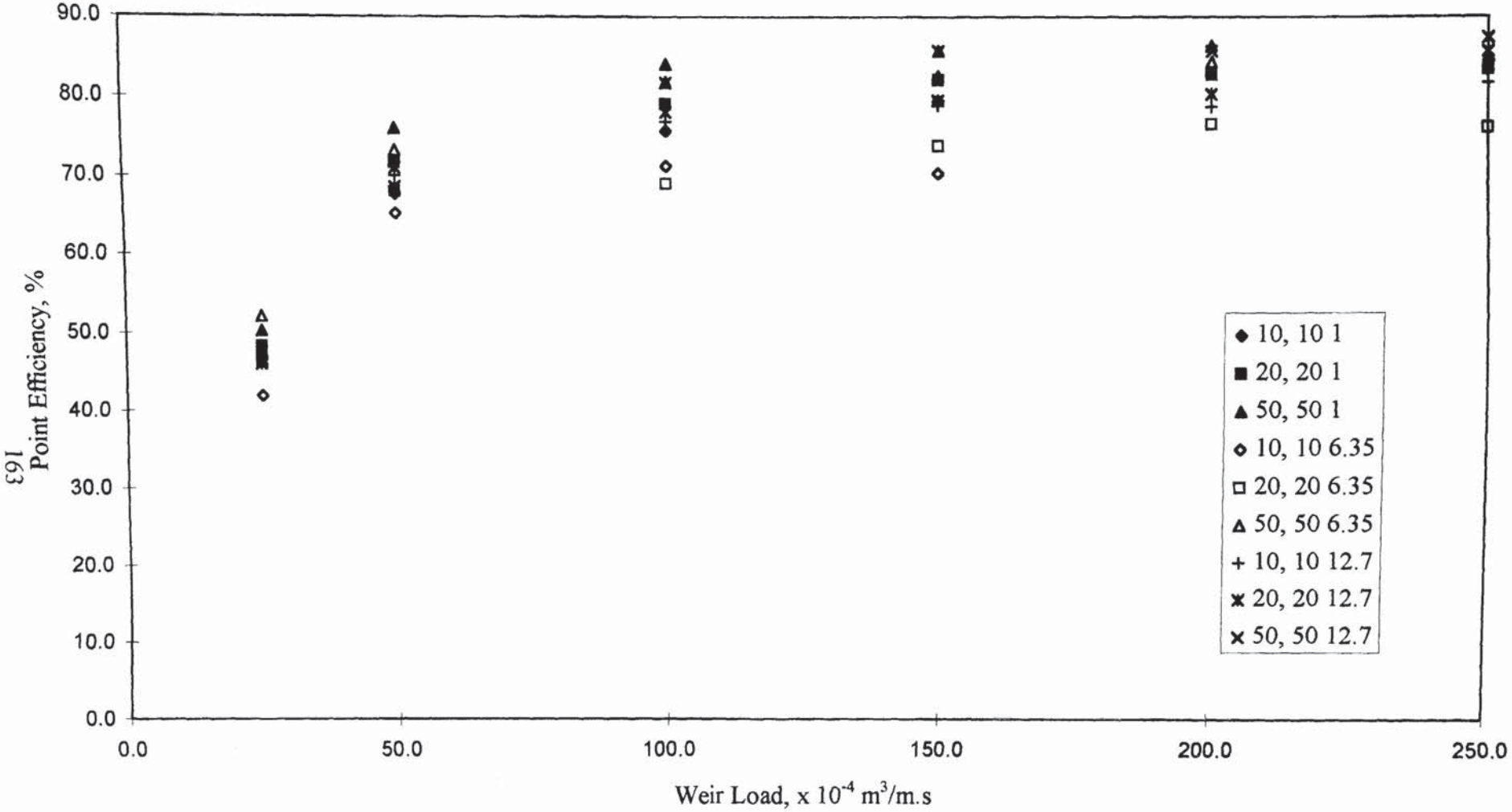

Figure 7.12 Graph of point efficiency versus weir load for three different hole sizes.

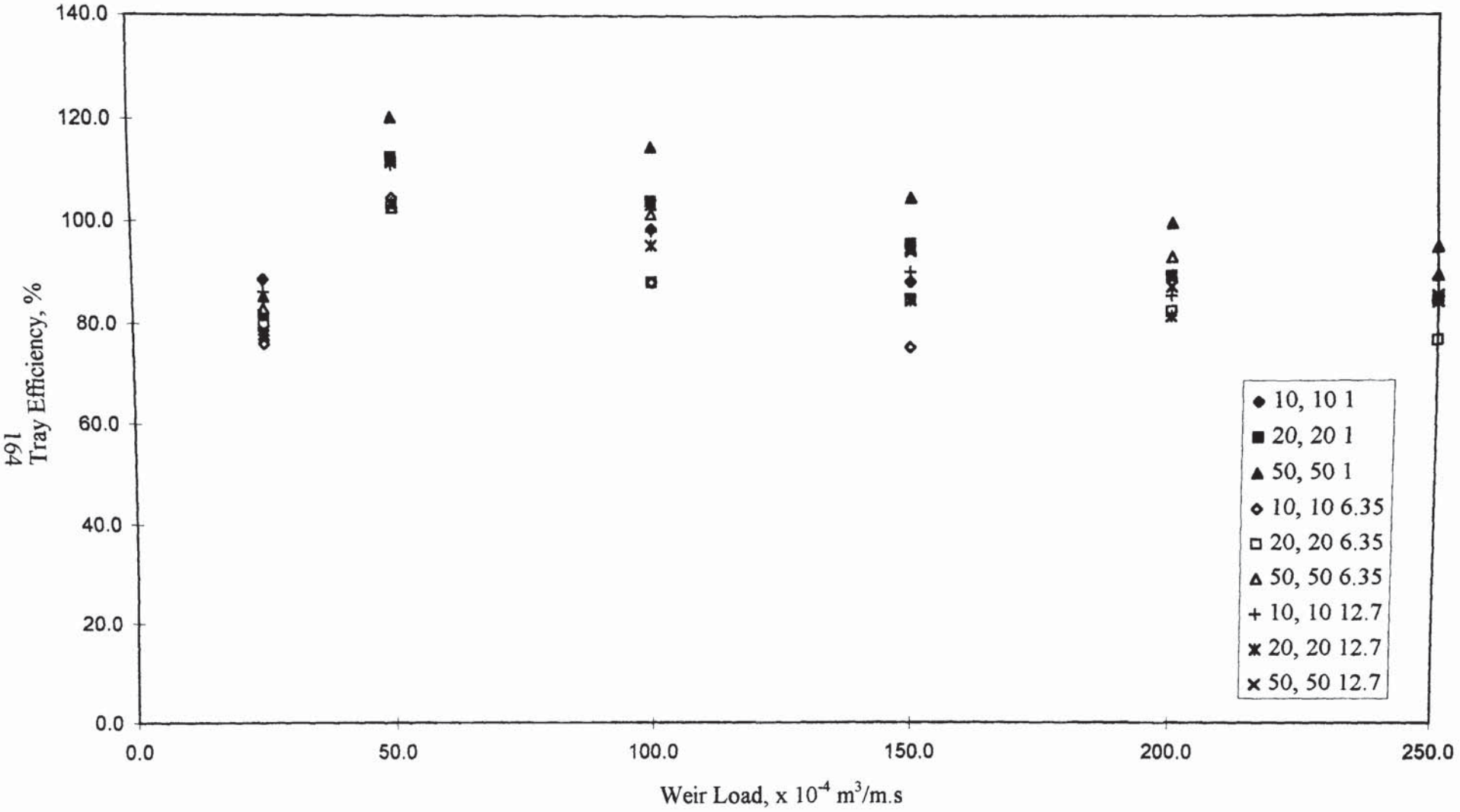

Figure7.13 Graph of tray efficiency versus weir load for three different hole sizes.

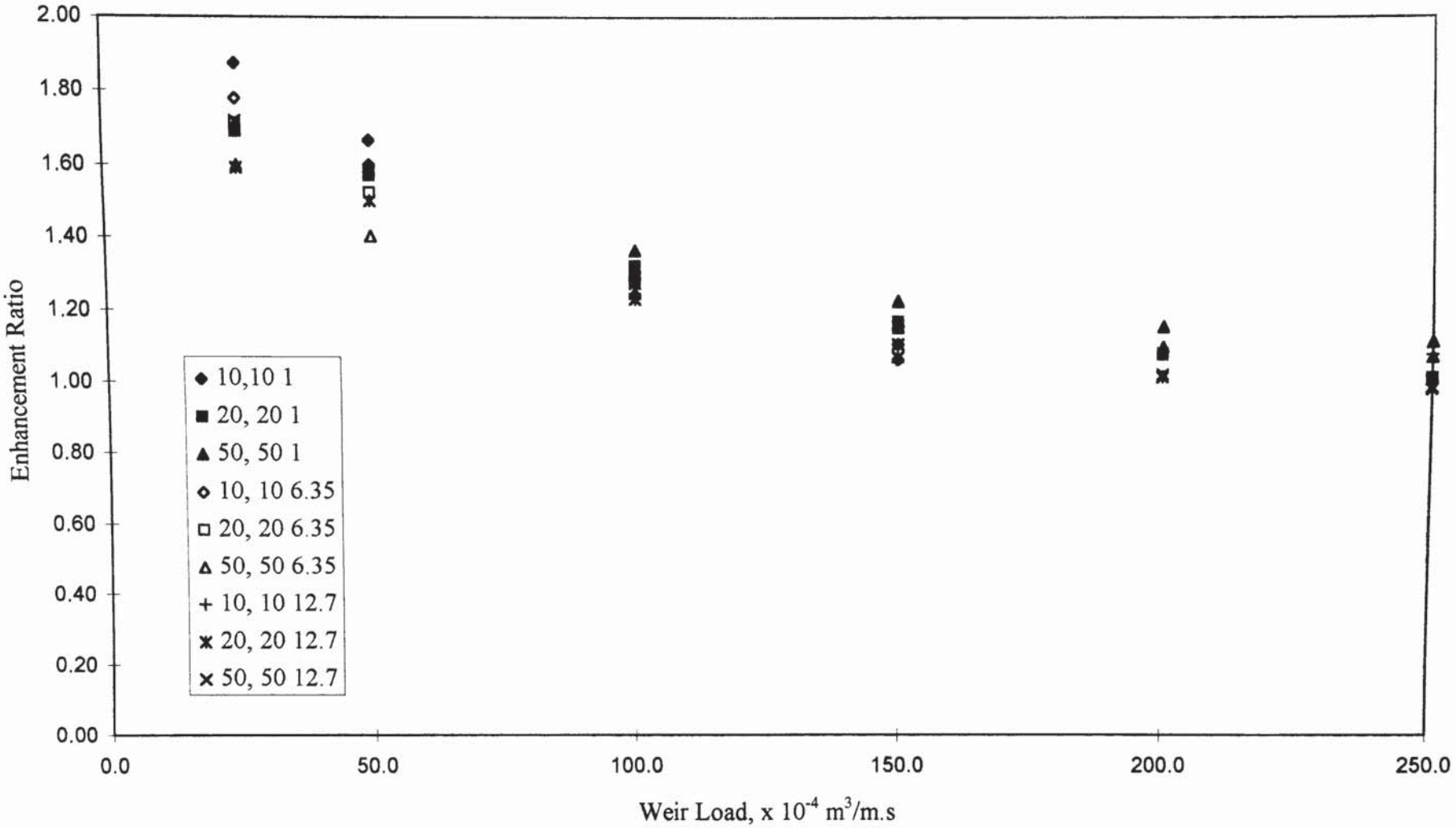

Figure 7.14 Graph of enhancement ratio versus weir load for three different hole sizes.

tray gives the lowest point efficiencies. At the higher clear liquid heights the trend is less obvious. The 1 mm hole tray consistently appears to have the highest point efficiency. In most cases there is less than five percentage points between the three trays at any weir load. The point efficiency is calculated independently of the flow pattern at any point but as it is the average it is affected by any areas of low efficiency.

The tray efficiency is shown in figure 7.13 and once again all three trays show the same trends. Tray efficiency should show any differences caused by the separation of the liquid i.e. any reduction in tray efficiency caused by areas of circulation. We can see that for the most part the 1 mm tray gives the greatest tray efficiency for any given weir load. For the low outlet weir and inlet gap combinations, the 12.7 mm tray gives a greater tray efficiency than the 6.35 mm tray. At the higher combination of inlet gap and outlet weir the trend is not as clear cut. The 1 mm tray gives the highest tray efficiency, but the 12.7 mm and 6.35 mm trays vie for the second highest tray efficiency.

The enhancement ratio is shown in figure 7.14. As the ratio is a combination of the tray and point efficiency, then it is obviously dependent on the trends or fluctuations in these quantities. The enhancement ratios are very close in all cases with a widening of the range at the highest inlet gap and outlet weir combination.

7.6.2 Qualitative Analysis of the Two-Dimensional Temperature Profiles

It is difficult to obtain any insight into the effect of hole size from viewing the temperature profiles, other than what has already been found by other methods. The profiles back up the theory of circulation put forward in the above section on the direct observation experiments, that is to say that the profiles for the 1 mm tray show a large number of U-shaped profiles with isolines joining the ends of the inlet and outlet downcomers. This is the accepted profile for circulation in the segments of the tray. The incidence of this type of profile lessened with an increase in hole size, once again

suggesting that an increase in the hole size decreases the size of circulations for a given weir load.

There is little evidence that the hole size has any significant effect on the residence time of the liquid on the tray. From comparing the outlet reduced temperature of the corresponding profiles, it can be seen that there is little difference between the trays. This method may give an indication of the residence time but it is not exact. The outlet reduced temperature is also dependent on the contact between the phases on the tray and so this can only be an indication of the liquid residence time.

The flow rate combinations that are in the spray regime produce profiles that are parallel to the downcomers. These are most prevalent with the 12.7 mm hole diameter tray as more of the flow rate combinations tested are in this regime. Parallel profiles are also found with the 1 mm tray and are not necessarily indicative of the spray regime, but of un-separated flow.

7.6.3 Discussion and Conclusions

The main point to come out of the analysis of the efficiency data is that the 1 mm tray gives the best tray efficiency for nearly all weir loads and combinations of inlet gap and outlet weir tested. The picture at higher hole diameters is less clear. The reasoning behind this could be due to the presence of circulations on the tray. As we have discovered, the larger hole sizes have the effect of lessening the amount of circulation at a given combination of flow rates and set-up. Balancing the reducing effect circulation has on the tray efficiency is the greater mixing caused by the smaller holes. The small holes produce smaller bubbles than large holes. These are less likely to cause jets that break the surface and cause the tray to enter the spray regime. The small bubbles have a greater surface area per volume than the larger bubbles or jets. In short, more of the gas is in contact with the liquid with smaller bubbles than with the larger ones. Obviously these two effects are opposite. It is proposed that the effect of the greater mixing of the two phases on the 1 mm tray out-weighs the detrimental

effect of the increase in the incidence of circulations. At the hole size of 6.35 mm the effect of the increase in the circulations overtakes the mixing effect. As a result the hole size that gives the smallest incidence of circulations, gives the greatest efficiency. This explains why the 12.7 mm tray gives a greater efficiency than the 6.35 mm tray. At combinations where there is little circulation we can see that the 6.35 mm tray is indeed above the 12.7 mm tray caused by the greater mixing of the smaller holes/bubbles. This would explain why at the higher combination of a 50 mm inlet gap and outlet weir, where the circulations are smaller, the 6.35 mm tray has a higher efficiency.

Little can be gleaned from a comparison of the temperature profiles other than to back up the presence of the circulations and the effect that the hole size has on them. The hole size also seems to have little effect on the residence time. This can be put down to the fact that the major factors in the residence time are the weir load and the weir height. This is not changed between the trays and any effect that the hole size has on this via an increased resistance to flow is dwarfed by these factors. A more detailed assessment of this will be included in the next chapter.

7.7 Conclusions

The main conclusions of this chapter are laid out below:

- The hole diameter has an effect on the regime that the tray operates under. This has been verified by a number of workers. In this case the majority of the experimental data points are in the froth regime. The only exceptions to this are with the 12.7 mm hole diameter at high gas velocities and low liquid heights.

- The hole diameter affects the circulation that is produced on a tray. Larger hole sizes delay the onset of separation and reduce the rate of increase of the area of circulation. For a given weir load, after separation has occurred, the 12.7 mm tray gives the least area of circulation and the 1 mm tray the highest.

- The maximum area that can be covered by circulations on a tray with a weir length of 0.6 times the diameter is approximately 30%. This is physically set by the area of the side segments of such a tray and is not affected by the hole size.

- The hole size has little effect on the average height of clear liquid produced on a circular tray. This is set by the weir load and the outlet weir and any effect due to the hole size is small in comparison.

- The larger the hole size the more uneven the surface of the dispersion. Obviously talking of surfaces is only relevant in the liquid dominant regime, but a steady increase in the turbulence on the surface of the dispersion is noted as hole size increases. The worst case would be increasing the hole size at a high gas velocity. The dispersion changes from froth to spray which can be classified as an increase in the unevenness of the surface.

- The extend of jetting onto the tray is reduced by an increase in the hole size. Jetting occurs where the entrance velocity is high and is usually accompanied by a hydraulic jump. This occurs where the liquid is slowed sufficiently. The larger hole size slows the liquid more effectively so that the hydraulic jump occurs earlier on the tray.

- The hole size seems to have very little effect on the point efficiency. There is less than 5% difference between the trays at the majority of combinations. The 1 mm tray seems to give the greatest point efficiency, which is accounted for by the greater mixing of the two phases associated with the smaller bubbles.

- The hole size effects the tray efficiency in two ways. First the greater mixing on smaller hole trays gives them a higher tray efficiency over larger hole trays. This is due to the greater contact of small bubbles with the liquid. This is offset by the detrimental effect of circulation on the tray efficiency. This can overcome the positive effects of the former mechanism, with the result that the larger hole tray can have a greater tray efficiency.

CHAPTER 8

FLOW PRODUCED ON LARGE RECTANGULAR SIEVE TRAYS

8.1 Introduction

On a circular sieve tray the underlying picture of what is happening is obscured by the shape of the tray. The main body of liquid can channel across the section between the downcomers at high liquid flow rates. In the majority of cases the liquid in this area is moving faster than that at the sides. This leads to differences in the clear liquid height between the two areas and can also lead to areas with reduced mass transfer driving forces. In the extreme case of liquid circulation on the side segments of the tray, the liquid can reach equilibrium with the gas passing through it. The gas will then pass through the tray unchanged and in effect the tray, in this area, is not doing the job it is designed for. This leads to a severe reduction in the tray efficiency.

To gain a scientific insight into the operation of the tray, it is best to use a simplified approach. Operation of a rectangular tray would cut out any changes due to the side segments. It should be possible to gain some knowledge of how the tray operates under certain conditions. The effect of the inlet gap, outlet weir, hole size, weir load and the air velocity can all be assessed without the picture being complicated by what is occurring on the sides of the tray. Further, many efficiency models are based on theoretical rectangular trays and the predicted data are then applied to the circular tray.

A look at the way that the liquid enters the tray and the possible effect hole size has on this is contained in this chapter. Also, it is intended to look at how the hole size effects

the clear liquid height and any gradient that is set up on the tray due to the resistance to the flow of the liquid. The point and tray efficiencies are also calculated and comparison is made with the Chan and Fair (1984) model for the calculation of point efficiencies.

8.2 The Rectangular Tray

The design of the rectangular tray is described elsewhere in this thesis and this section is intended to give a summary of this. The rectangular section is made from the existing circular test facility by blocking off the side sections of the tray. This is done by using aluminium baffles both above and below the tray. The surface of the test tray and the distribution plate are also blocked off. This ensures that the air enters the tray evenly and in the vertical direction. The inlet downcomer is altered to provide an even flow of liquid on to the tray. This is achieved by isolating the small part of the downcomer outside the width of the rectangular section.

The modifications to the test facility produce a rectangular tray of 1.925 m flow path length and a weir length of 1.26 m. As the weir length and the area of the tray are different to those used on the set of circular trays, the various volumetric air and water flows needed to be altered to produce the required water weir loads and air velocities.

8.3 Experimental Procedure

Three sieve trays with different hole sizes were used for the experiments. The sizes were 1, 6.35 and 12.7 mm diameter holes. A range of flow rates and inlet gap and outlet weir combinations were used. These are summarised in table 8.1.

Direct observation experiments were carried out on the three trays, with varying combinations of flow rates, inlet gap and outlet weir. In every case the flow pointers lined up parallel to the walls in the direction from inlet gap to outlet weir. At very low

weir loads there was some small variation of the flag position which was mainly caused by the passage of the gas around the support beams. As the weir load was increased the flags lined up straight down the tray and did not deviate for any combination. This result was as expected but served to show that the water was travelling straight from downcomer to downcomer. No further conclusions could be made from these experiments.

Two other types of experiment were carried out. The height of clear liquid was measured using the manometer method that is detailed elsewhere. The water-cooling method was also used to create isothermal plots and calculate thermal efficiencies. Details of the results of these experiments are given in the following sections.

Weir Load x 10^{-4} m^3/m.s	Air Velocity m/s	Hole Diameter mm	Inlet Gap mm	Outlet Weir mm
50.0	1.00	1.00	10	10
100.0	1.50	6.35	20	20
150.0	2.00	12.7	50	50
200.0	2.50			
250.0				

Table 8.1 Summary of the flow rates, hole sizes, inlet gaps and outlet weirs used in the experiments on a rectangular tray.

8.4 Experiments Involving the Height of Clear Liquid

The experiments to determine the height of clear liquid were carried out using the manometer method described elsewhere. The position of the manometer tappings on the tray floor were altered to give an even coverage of the rectangular tray. Thirty-six tappings were positioned in rows of six along the length of the tray and they are shown in figure 8.1. The height of the liquid in the downcomer was also taken by measurements of six manometers situated in the inlet downcomer. The total pressure drop across the tray was also measured.

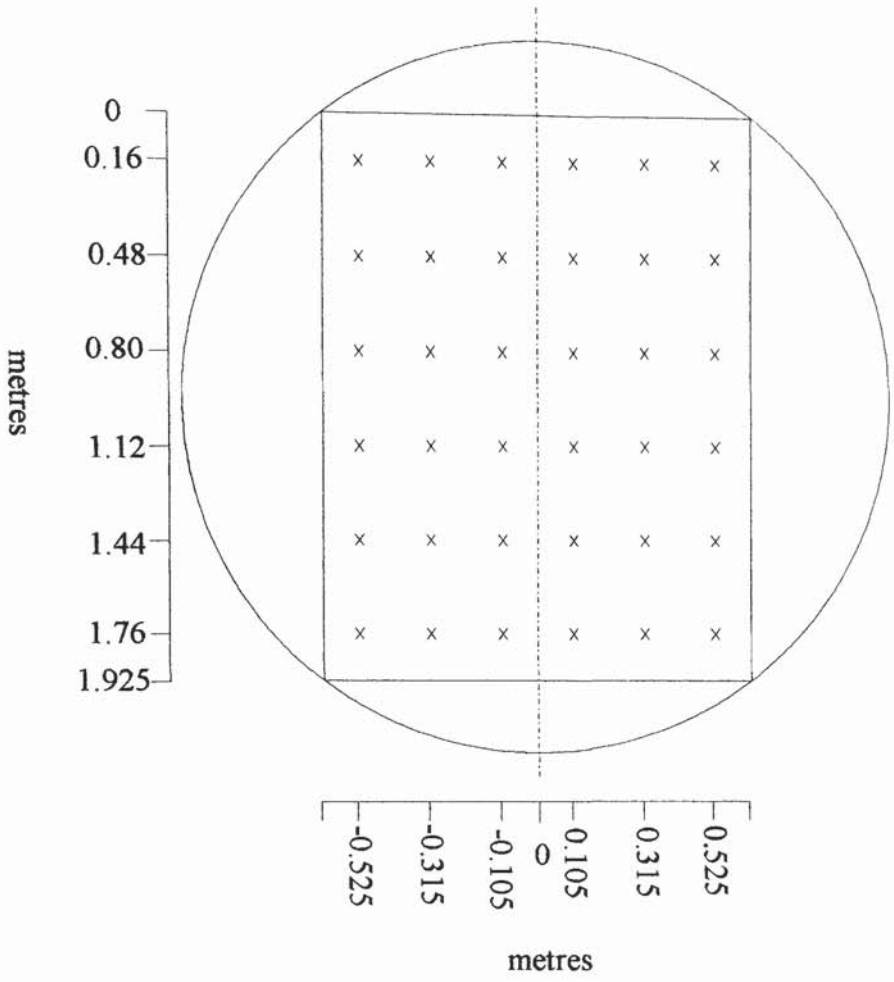

Figure 8.1 Positions of the manometers on the rectangular tray.

The results from the experiments that were carried out are presented in two ways. Firstly, a numerical analysis of the height of clear liquid is given and this is followed by an analysis of the three-dimensional head profiles produced from these data.

8.4.1 Numerical Analysis of the Height of Clear Liquid

Due to entrance effects caused by the liquid jetting onto the tray, analysis was undertaken on data collected over the second half of the tray. Analysis in this way eliminates the 'artificial' lowering of the average height of clear liquid caused by jetting at low inlet gaps and high weir loads. The average height of clear liquid is presented against the weir load in figures 8.2 to 8.4 and the gradient across the second half of the tray is presented, again against weir load, in figures 8.5 to 8.7.

Figure 8.2 shows the variation of the height of clear liquid for the second half of the tray for an inlet gap and outlet weir of 10 mm. Figure 8.3 and 8.4 show the same variations but for an inlet gap and outlet weir of 20 mm and 50 mm respectively. From these three graphs it can be seen that the 12.7 mm hole diameter tray produces the highest clear liquid for all the flow rate combinations except the highest weir load of 200×10^{-4} $m^3/m.s$ with a 10 mm inlet gap and outlet weir. With the smaller hole diameters the picture is less clear cut, but for the majority of the flow rates tested the 6.35 mm hole diameter shows a higher clear liquid height than the 1 mm hole diameter. No comment is made on the actual height of clear liquid values as this has been covered in other chapters. The errors and standard deviations are similar to those produced using this method on a circular tray.

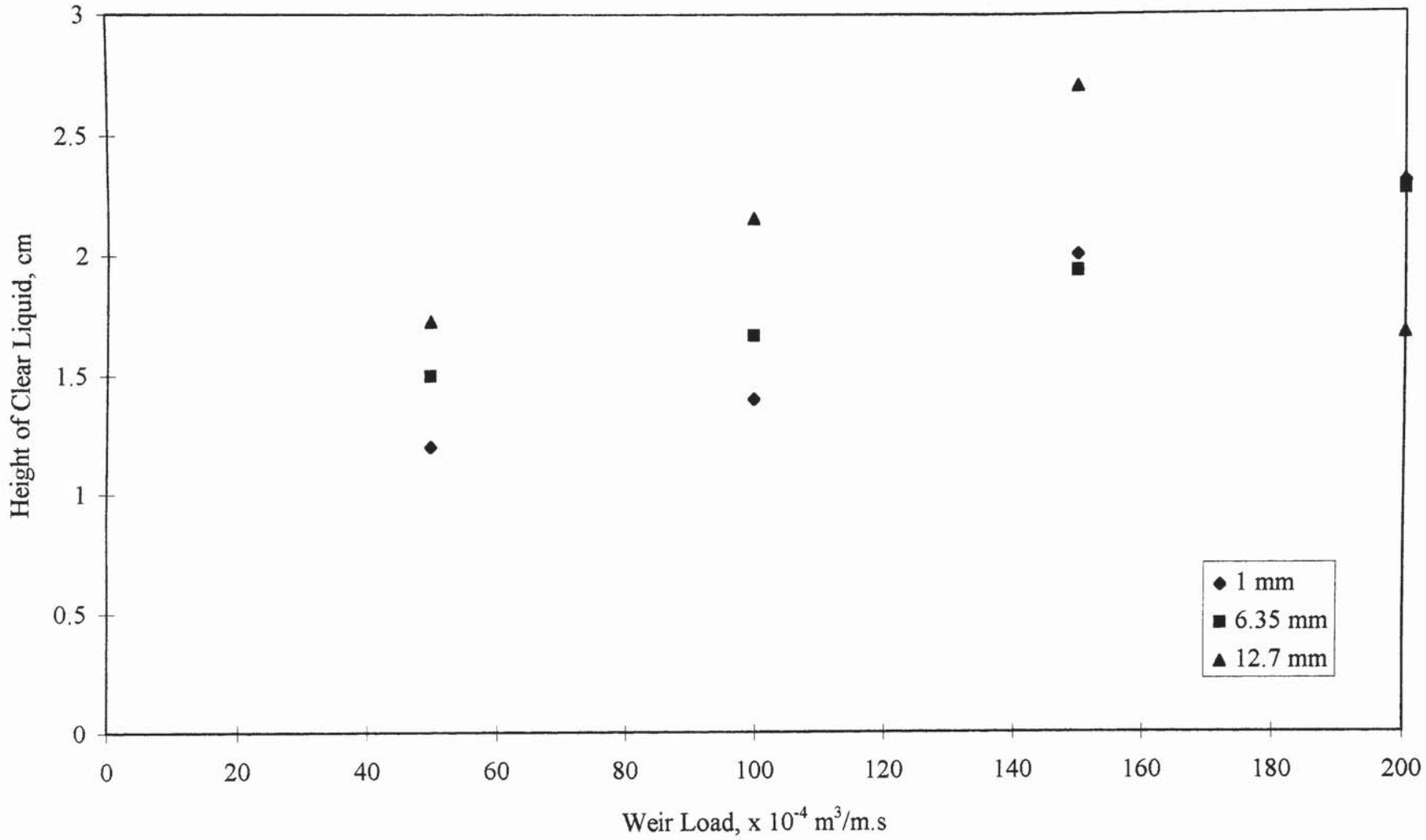

Figure 8.2 The variation in the height of clear liquid for a rectangular column. Inlet gap and outlet weir are both 10 mm.

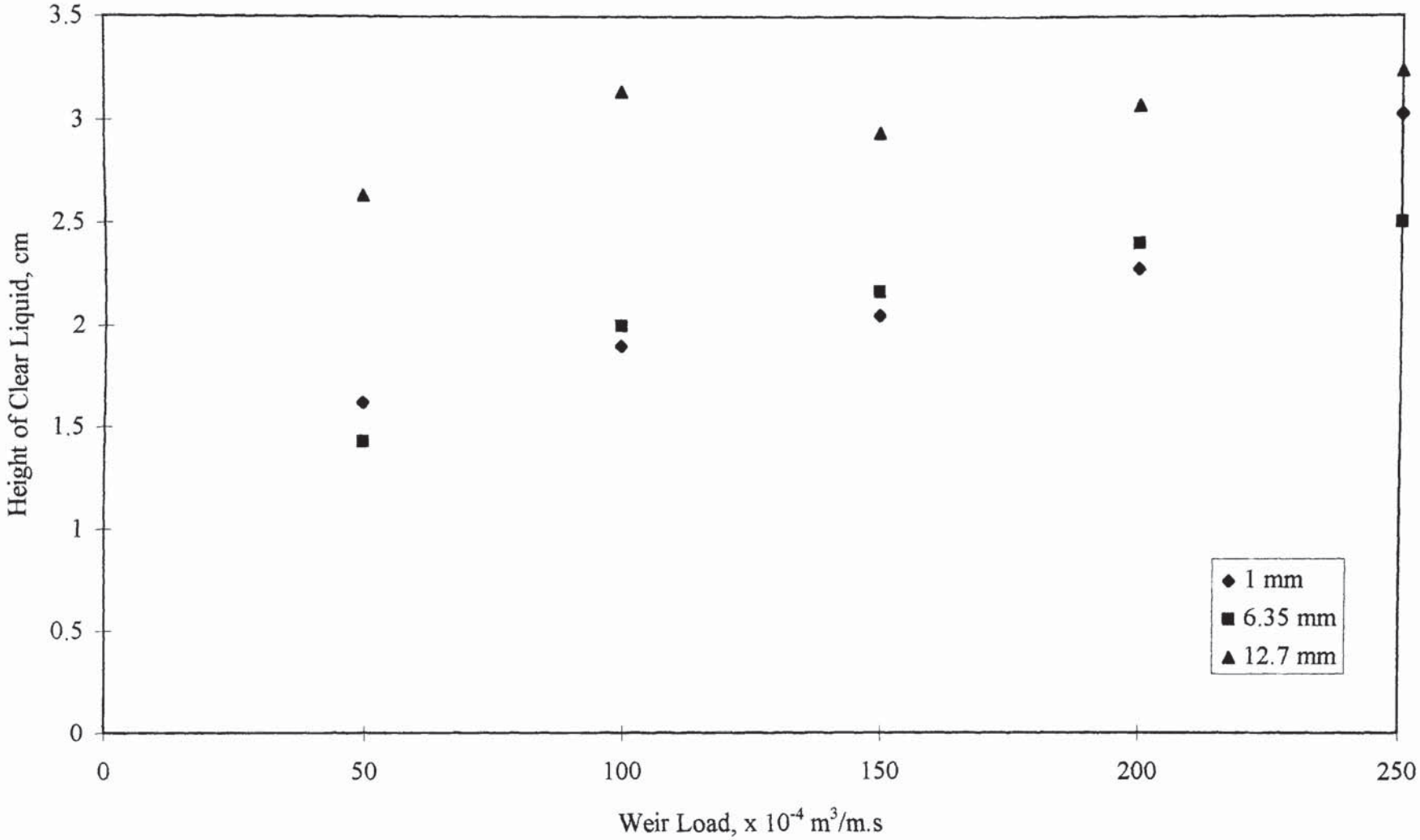

Figure8.3 The variation in the height of clear liquid for a rectangular column. Inlet gap and outlet weir are both 20 mm.

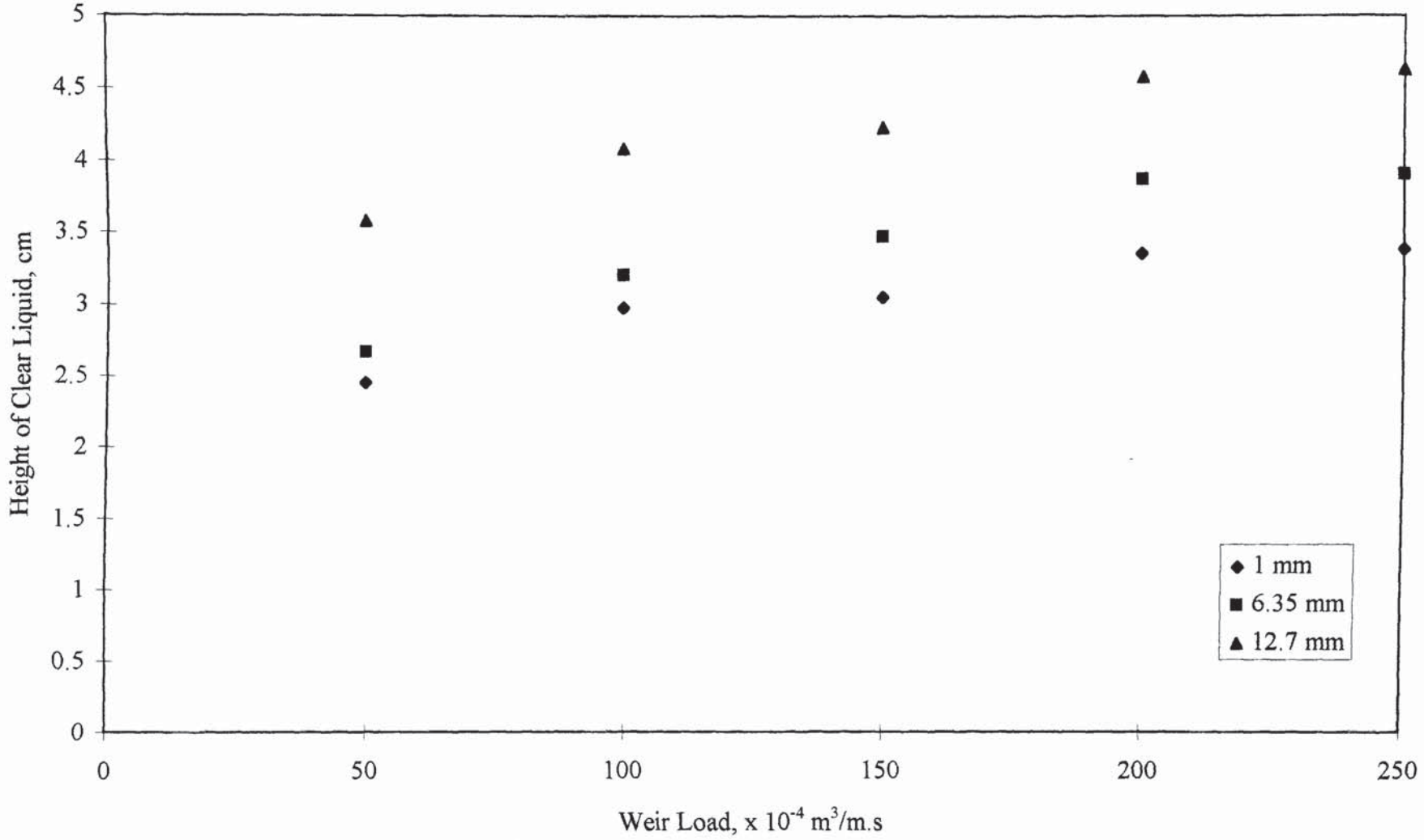

Figure 8.4 The variation in the height of clear liquid for a rectangular column. Inlet gap and outlet weir are both 50 mm.

Figures 8.5 to 8.7 show the gradient measured across the outlet half of the tray. The greatest gradient at the inlet gap and outlet weir combination of 10 mm is shown by the 1 mm tray and generally the smaller the hole the greater the gradient. The picture is less clear cut at the higher inlet gaps and outlet weirs of 20 mm and 50 mm. The gradient at these combinations alternates with every hole size having the greatest gradient for at least one weir load. The most obvious conclusion from these graphs is that the gradient is progressively smaller as the clear liquid height increases. This would explain why the smaller hole size gives a higher gradient, because it produces a lower height of clear liquid. It must be stressed that the gradient is very small for all flow rates and configurations. It is very rarely over one centimetre per metre and therefore the maximum gradient over the whole tray is less than two centimetres over the whole tray.

8.4.2 Analysis of the Three-Dimensional Surface Profiles

From the surface plots the main point that can be obtained is that there is no transverse variation in the clear liquid height on a rectangular tray. Some examples of the plots are contained in figures 8.8 to 8.10, a-d and are representative of the surface plots obtained from the experiments. Jetting is observed at low inlet gaps and under certain circumstances the liquid can jet into the second half of the tray. Fortunately this is very rare and therefore it has little effect on the numerical results. In fact it only occurs with an inlet gap of 10 mm and a weir load of 250 x 10^{-4} $m^3/m.s$ and these results have been eliminated from the average values quoted in the above section. As with the circular tray, the jetting appears to extend slightly further onto the tray with the 1 mm tray than with the higher hole trays, but it is impossible to assess this analytically due to the uncertainty involved in the positioning of the hydraulic jump. This could be overcome with a greater number of measurement points. This would allow a more accurate pinpointing of the position of the hydraulic jump.

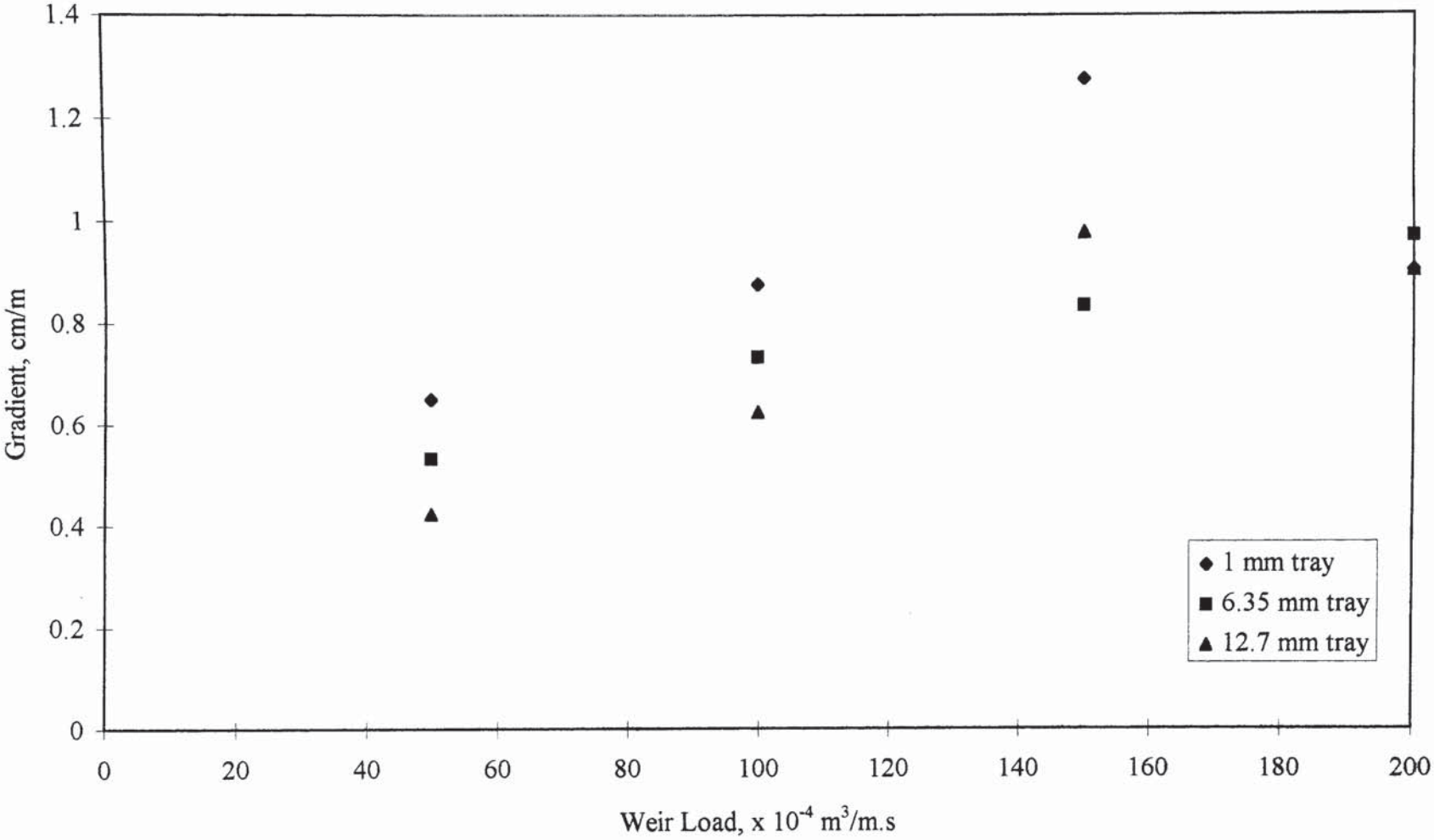

Figure 8.5 Variation in the hydraulic gradient on the outlet half of a rectangular tray. Inlet gap and outlet weir are both 10 mm.

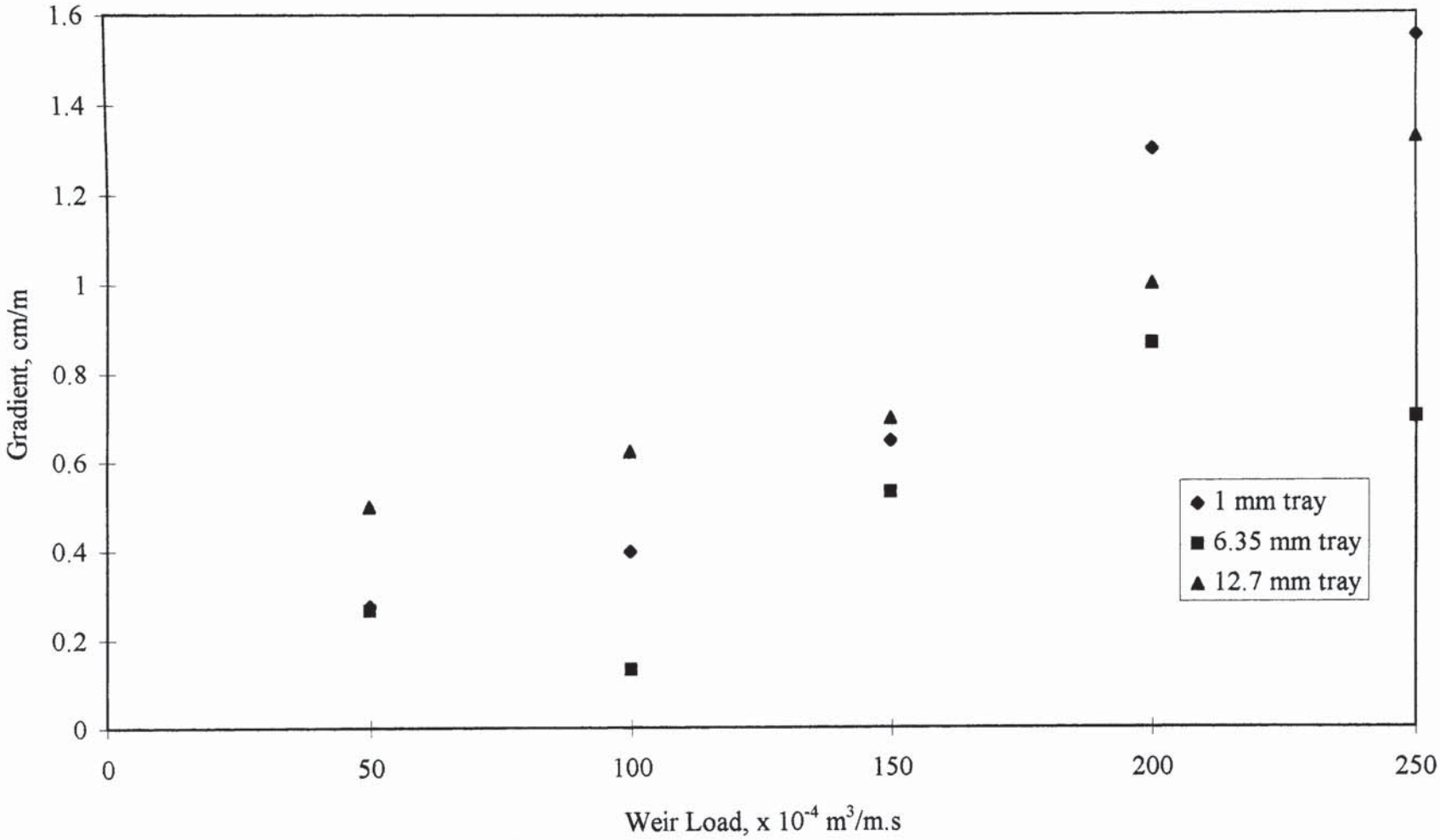

Figure 8.6 Variation in the hydraulic gradient on the outlet half of a rectangular tray. Inlet gap and outlet weir are both 20 mm.

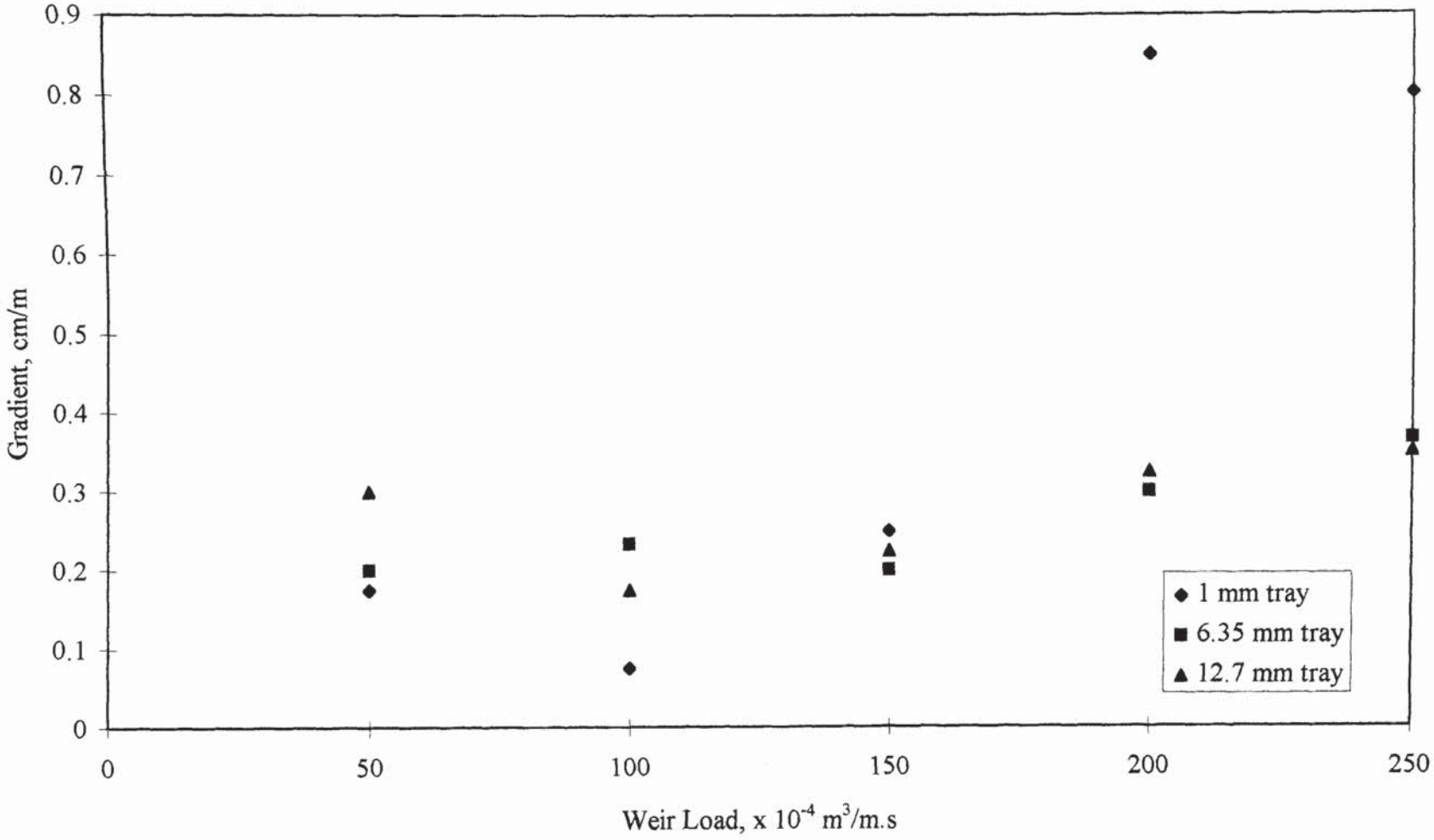

Figure8.7 Variation in the hydraulic gradient on the outlet half of a rectangular tray. Inlet gap and outlet weir are both 50 mm.

8.4.3 Discussion and Conclusions

The result that the height of clear liquid on a rectangular tray is greater for higher hole diameters is interesting. Practically, it means that the amount of liquid held-up on the tray is greater, the larger the hole diameter. This could be explained by more liquid being recycled by the gas. As the gas breaks through the surface of the dispersion, liquid is taken into the space above the bulk liquid. If the gas left the surface vertically then this spray would be dispersed equally in all directions. But the momentum of the liquid may deflect the gas and cause an uneven distribution of this spray. To explain the greater hold-up on the larger hole tray, relatively more liquid must be sprayed against the flow of the bulk liquid than on the lower hole diameters. This would be consistent with less deflection of the gas from the vertical for the higher hole diameters. Many models assume that the eddy diffusivity is equal in all directions. This appears not to be the case and it is affected by hole size. Also the greater momentum of the gas passing from the larger holes may slow the liquid down more and contribute to the greater hold-up.

The gradient experiments show that the reduction in the height of clear liquid is very small. In fact it puts into doubt whether the manometer method is accurate enough to measure the gradient. More work into this area, with a more accurate measurement technique, needs to be undertaken to clarify the situation and to give confidence to the findings of this work.

The surface profiles confirm the presence of jetting at the tray inlet and justify the use of the second half of the tray for the assessment of the height of clear liquid. The position of the hydraulic jump is questionable on these surface plots. It is therefore difficult to gain any firm evidence to back the assertion that the effect of jetting is lessened with an increase in the hole size.

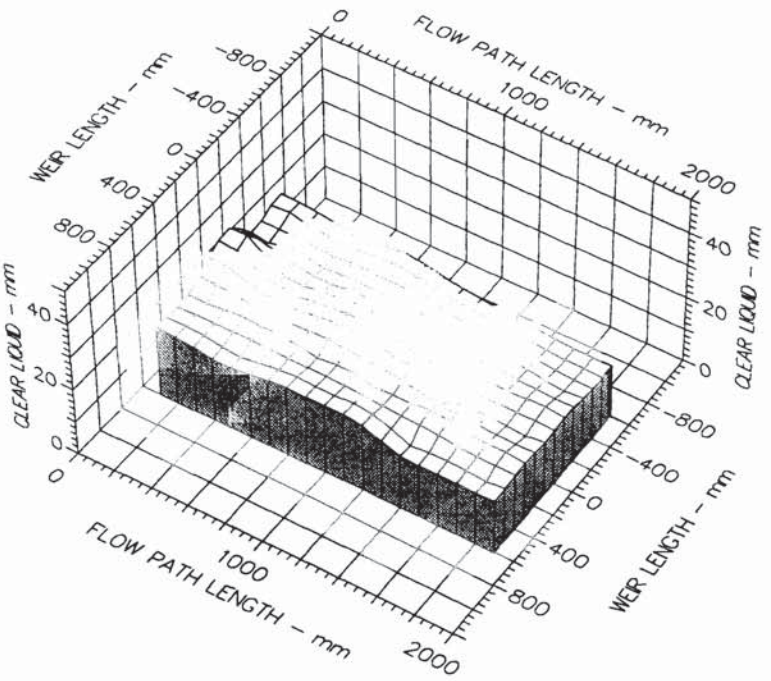

Figure 8.8a Three-dimensional surface profiles of the height of clear liquid on a rectangular tray.

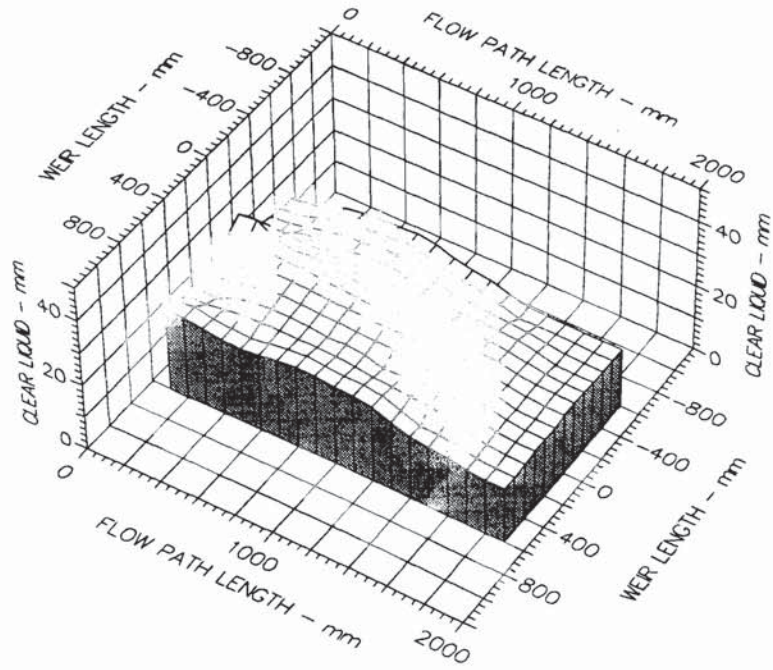

Figure 8.8b Three-dimensional surface profiles of the height of clear liquid on a rectangular tray.

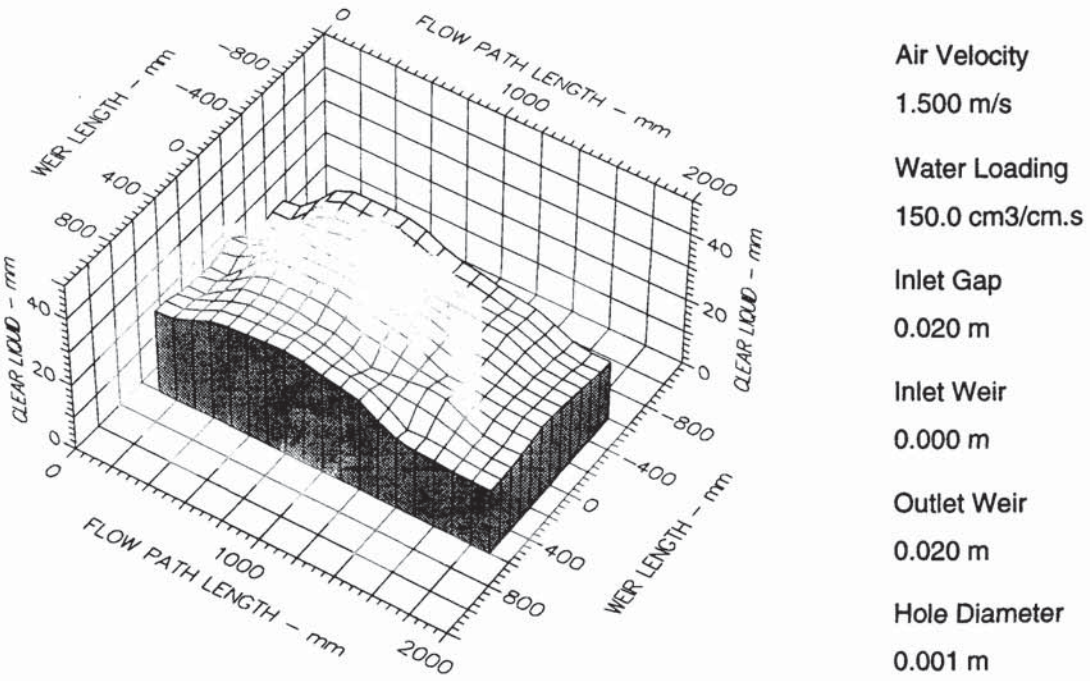

Figure 8.8c Three-dimensional surface profiles of the height of clear liquid on a rectangular tray.

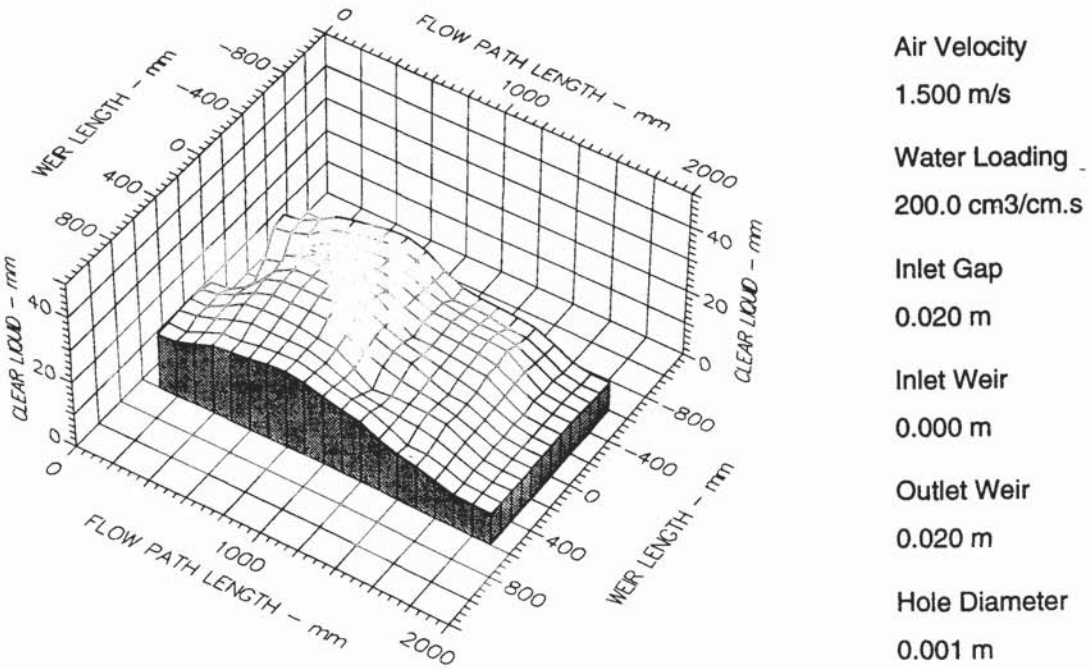

Figure 8.8d Three-dimensional surface profiles of the height of clear liquid on a rectangular tray.

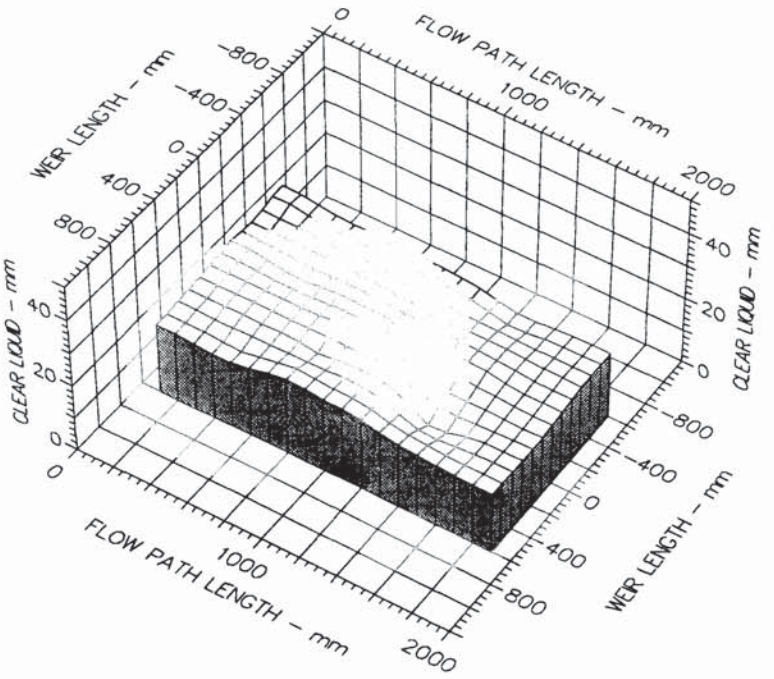

Figure 8.9a Three-dimensional surface profiles of the height of clear liquid on a rectangular tray.

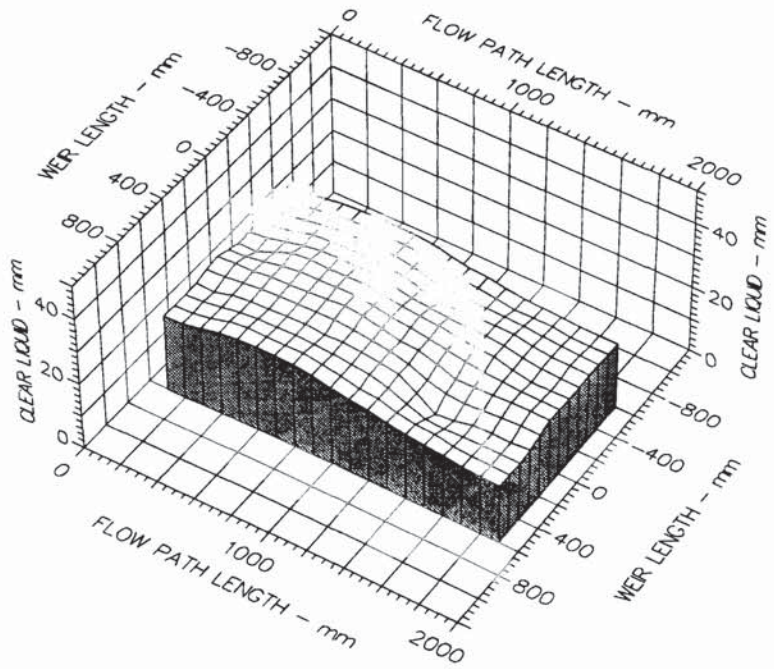

Figure 8.9b Three-dimensional surface profiles of the height of clear liquid on a rectangular tray.

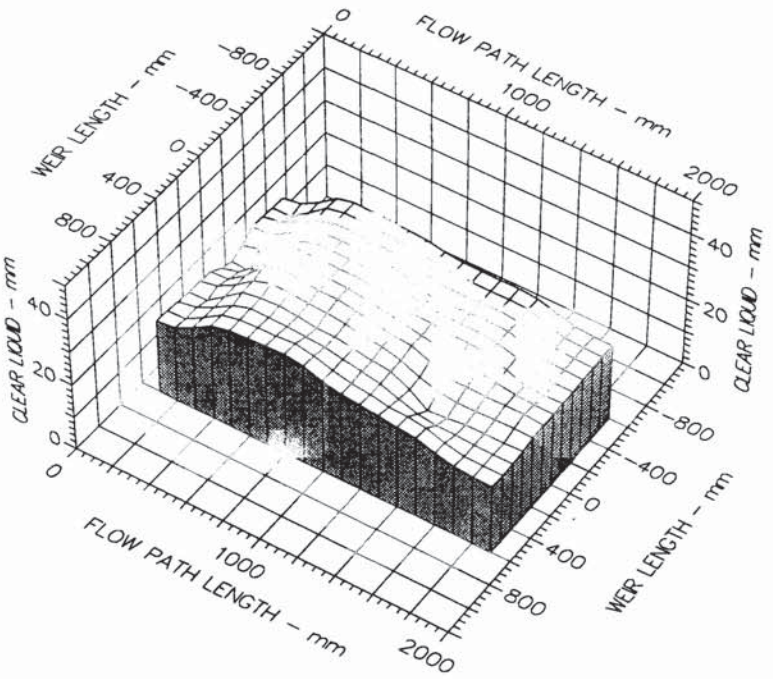

Figure 8.9c Three-dimensional surface profiles of the height of clear liquid on a rectangular tray.

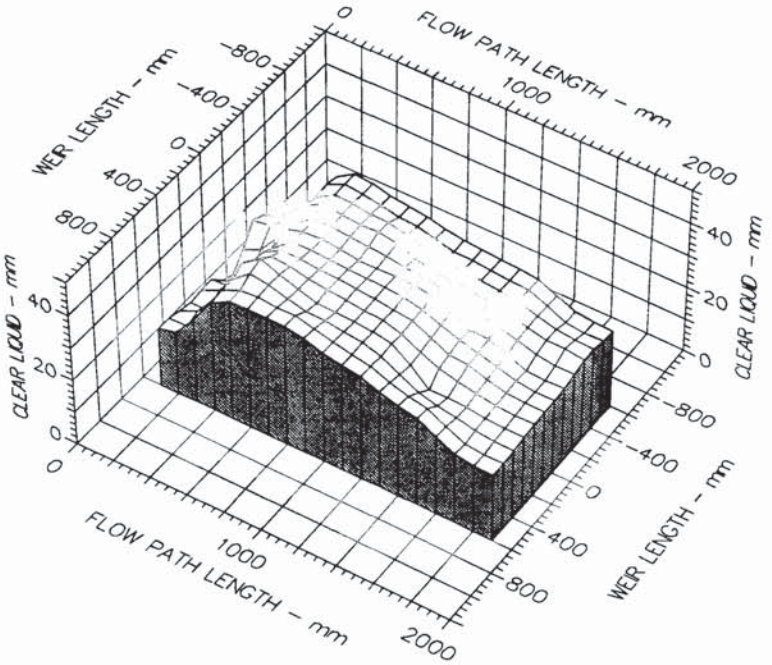

Figure 8.9d Three-dimensional surface profiles of the height of clear liquid on a rectangular tray.

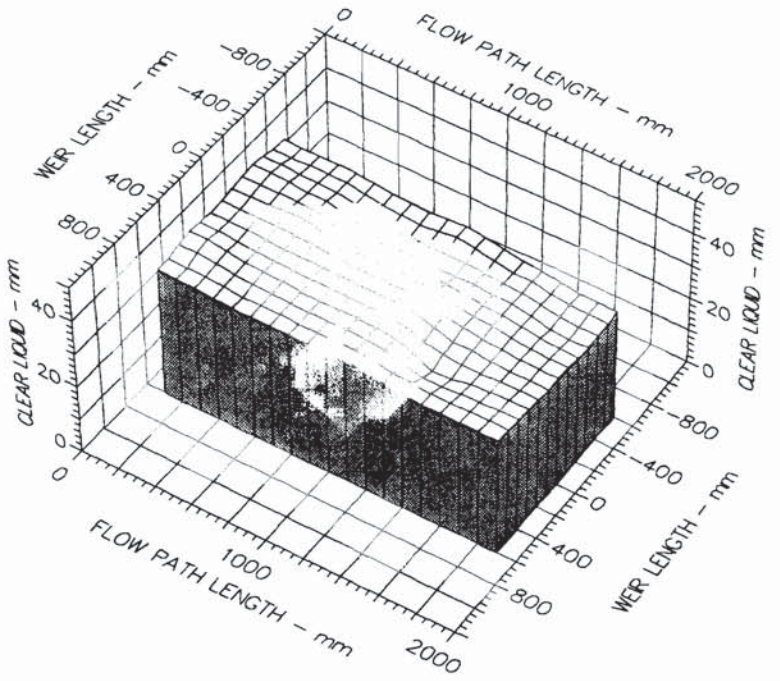

Air Velocity
1.500 m/s

Water Loading
50.0 cm3/cm.s

Inlet Gap
0.020 m

Inlet Weir
0.000 m

Outlet Weir
0.020 m

Hole Diameter
0.013 m

Figure 8.10a Three-dimensional surface profiles of the height of clear liquid on a rectangular tray.

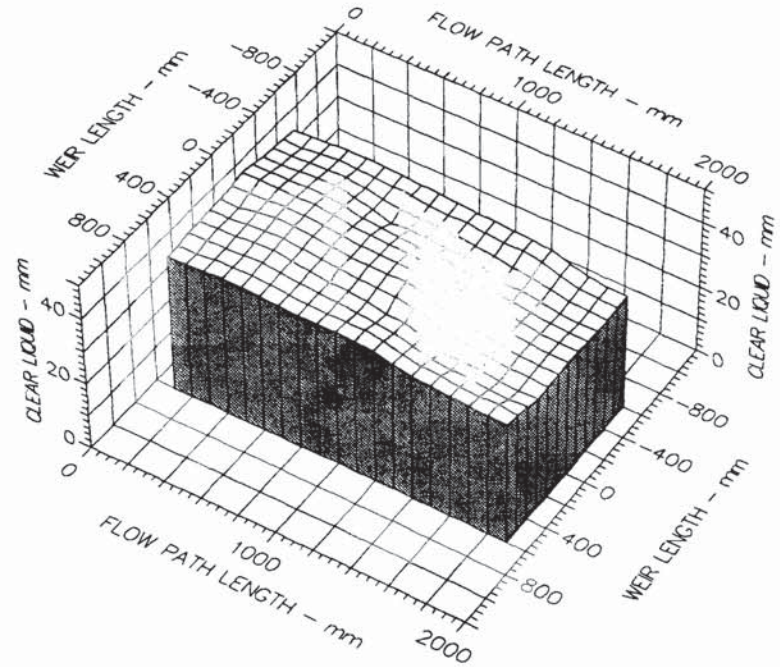

Air Velocity
1.5 m/s

Water Loading
100.0 cm3/cm.s

Inlet Gap
0.020 m

Inlet Weir
0.000 m

Outlet Weir
0.020 m

Hole Diameter
0.013 m

Figure 8.10b Three-dimensional surface profiles of the height of clear liquid on a rectangular tray.

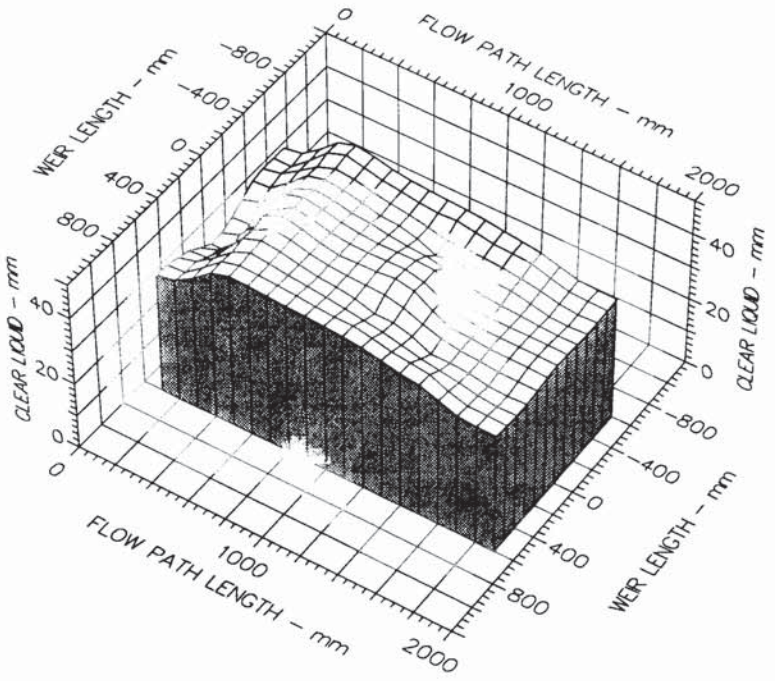

Air Velocity
1.500 m/s

Water Loading
150.0 cm3/cm.s

Inlet Gap
0.020 m

Inlet Weir
0.000 m

Outlet Weir
0.020 m

Hole Diameter
0.013 m

Figure 8.10c Three-dimensional surface profiles of the height of clear liquid on a rectangular tray.

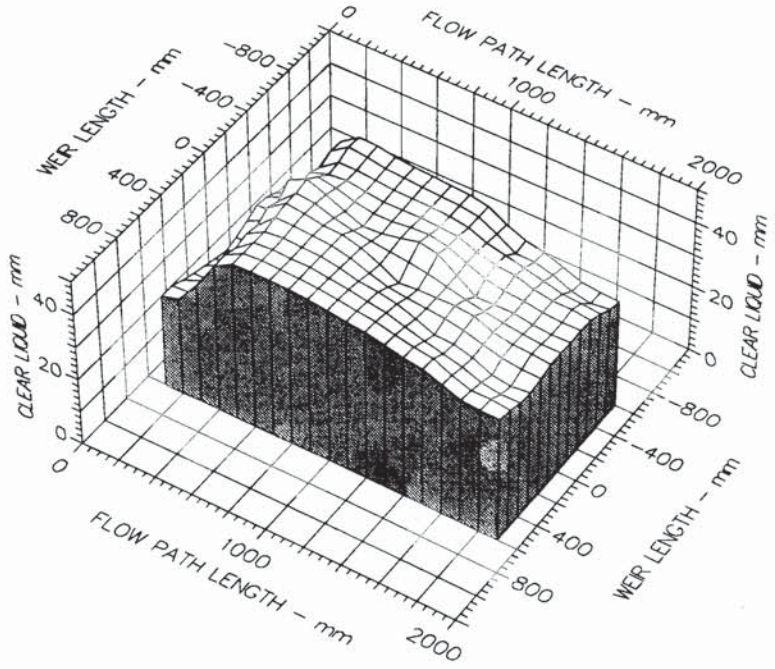

Air Velocity
1.5 m/s

Water Loading
200.0 cm3/cm.s

Inlet Gap
0.020 m

Inlet Weir
0.000 m

Outlet Weir
0.020 m

Hole Diameter
0.013 m

Figure 8.10d Three-dimensional surface profiles of the height of clear liquid on a rectangular tray.

8.5 Water-Cooling Experiments

The water-cooling experiments were carried out using hot water flowing across the rectangular section and being cooled by cool unsaturated air. The temperature of the water and the air is measured by seventy platinum resistance thermometers spread evenly over the tray. These temperature readings were used to calculate thermal efficiencies and to plot cooling diagrams showing isolines, which are analogous to the concentration lines produced on an operating tray.

8.5.1 Two-Dimensional Temperature Profiles

The temperature profiles were plotted for all three trays. Due to the vast number of these plots only a select few are presented in this thesis to illustrate points that are made. The profiles showed similar trends to the centre section of the circular tray. The main difference between these two geometries was that parallel profiles were achieved during the rectangular experiments, whereas with the circular tray the isolines in the centre section tended to be more U-shaped due to the effect of the flow in the side segments.

The other main point that can be obtained from the profiles is that on the whole the water coming off the larger hole tray is cooler than that coming off the smaller hole tray. This implies that the liquid on the larger hole tray has a greater residence time than that of the smaller tray. This is borne out by results of the height of clear liquid on the trays. The other explanation of this is that the larger hole tray is more efficient than the smaller hole tray. This can be seen not to be the case in the following section, as well as through results on the circular tray.

Finally, the temperature profiles do not show any significant tailing off at the wall. This implies that any wall effects are small. This is unsurprising as the level of turbulence caused by the gas would be large enough to break down any boundary layer

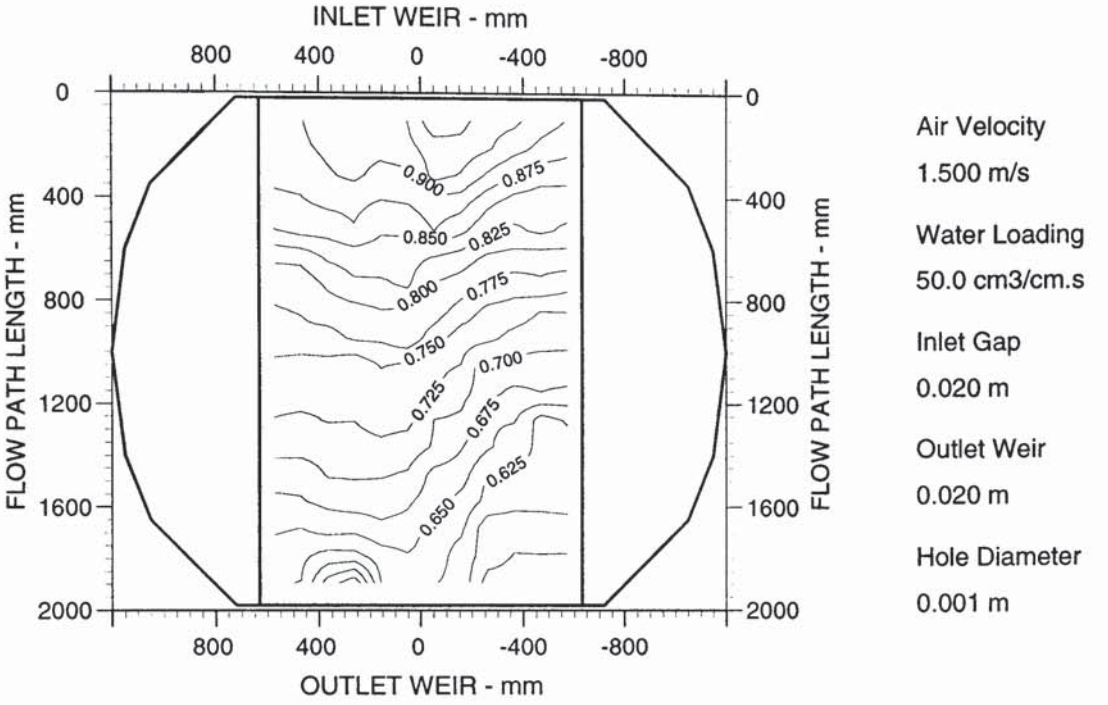

8.11a Two-dimensional temperature profiles for a rectangular tray

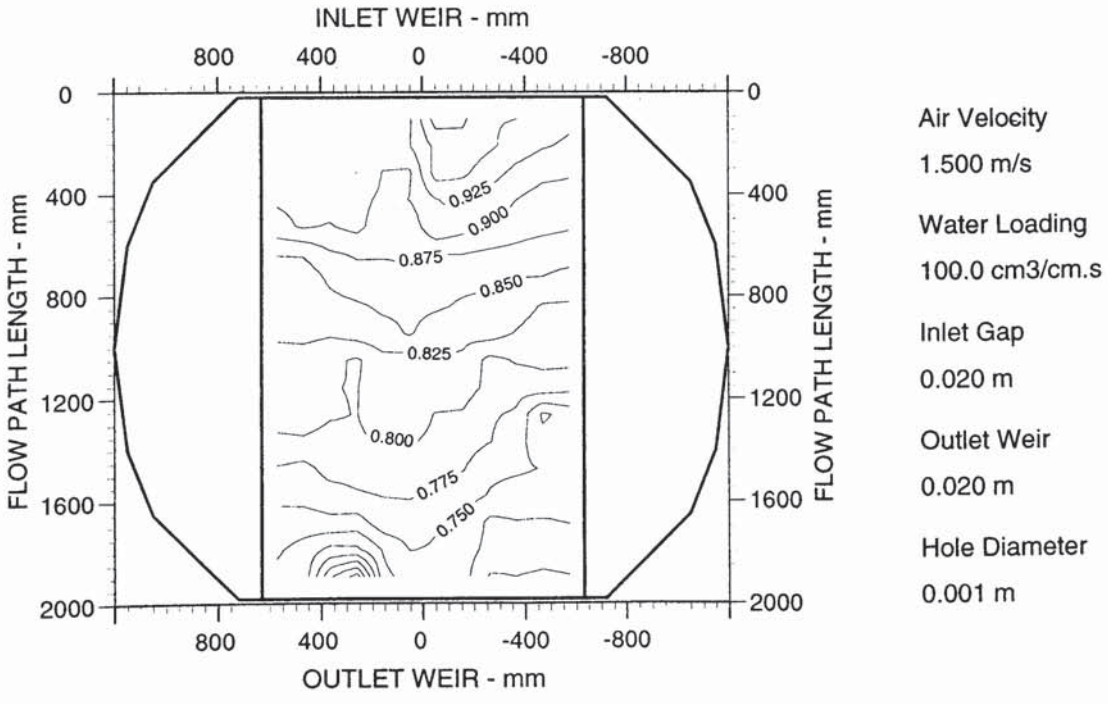

8.11b Two-dimensional temperature profiles for a rectangular tray

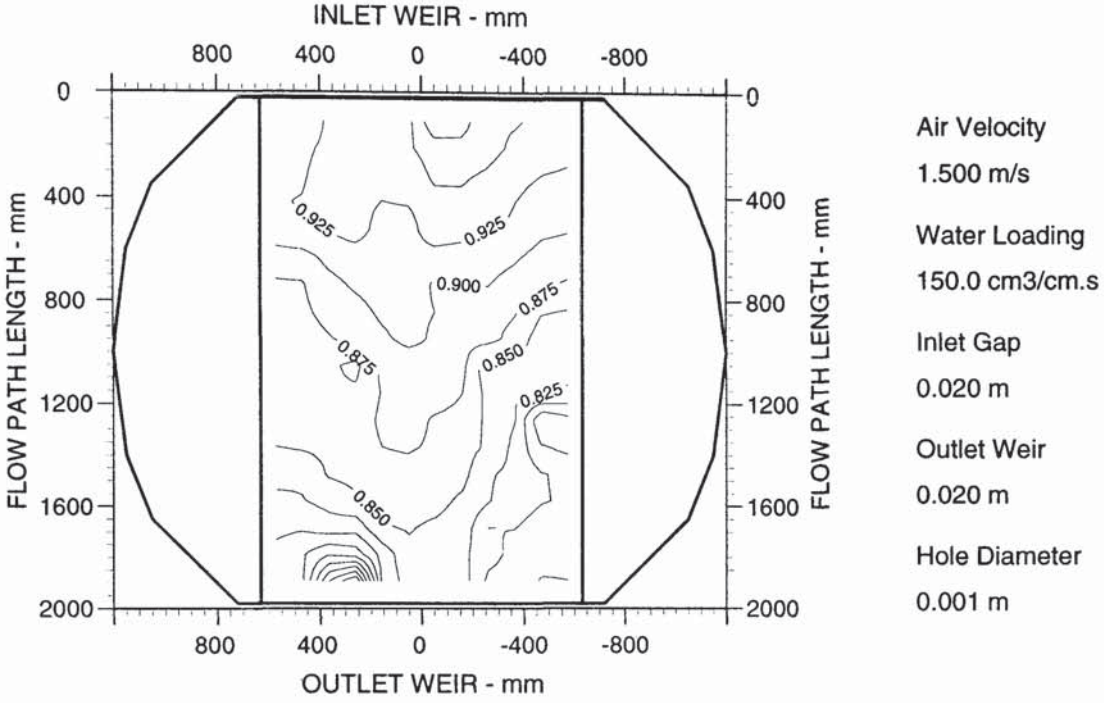

8.11c Two-dimensional temperature profiles for a rectangular tray

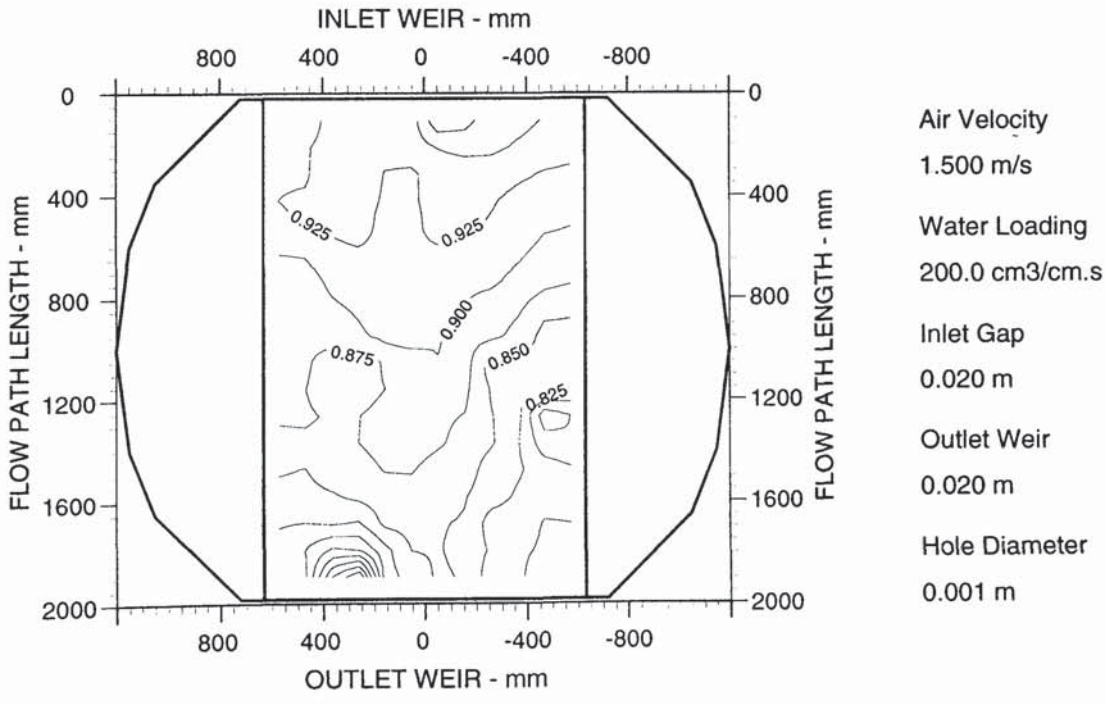

8.11d Two-dimensional temperature profiles for a rectangular tray

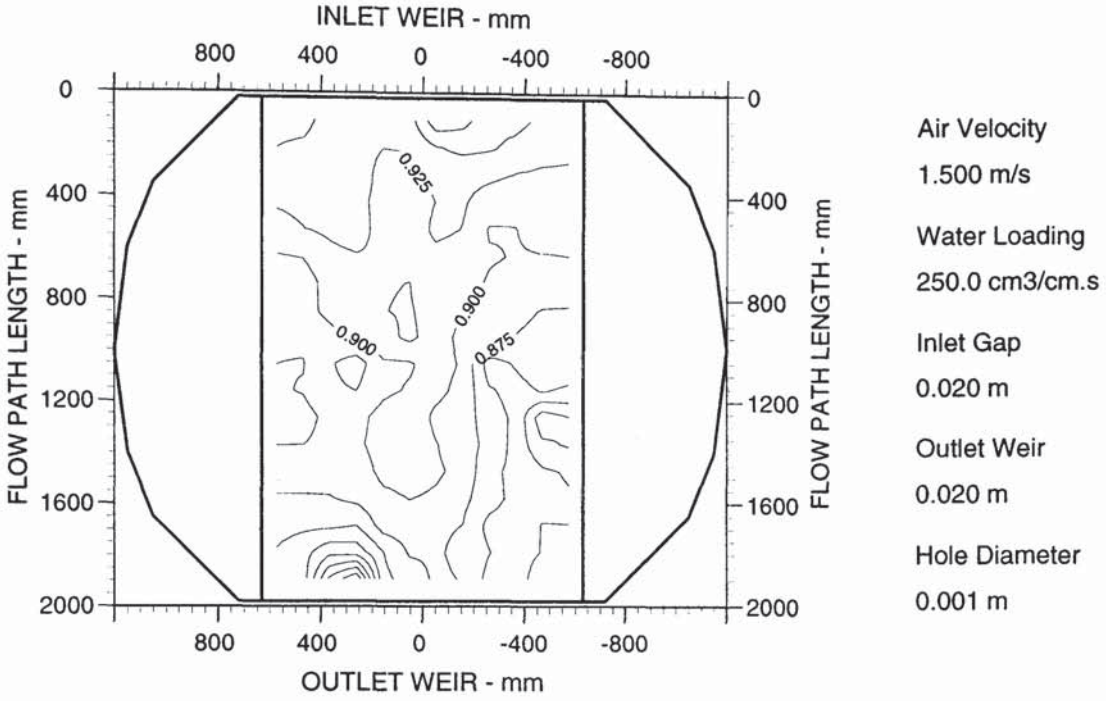

8.11e Two-dimensional temperature profiles for a rectangular tray

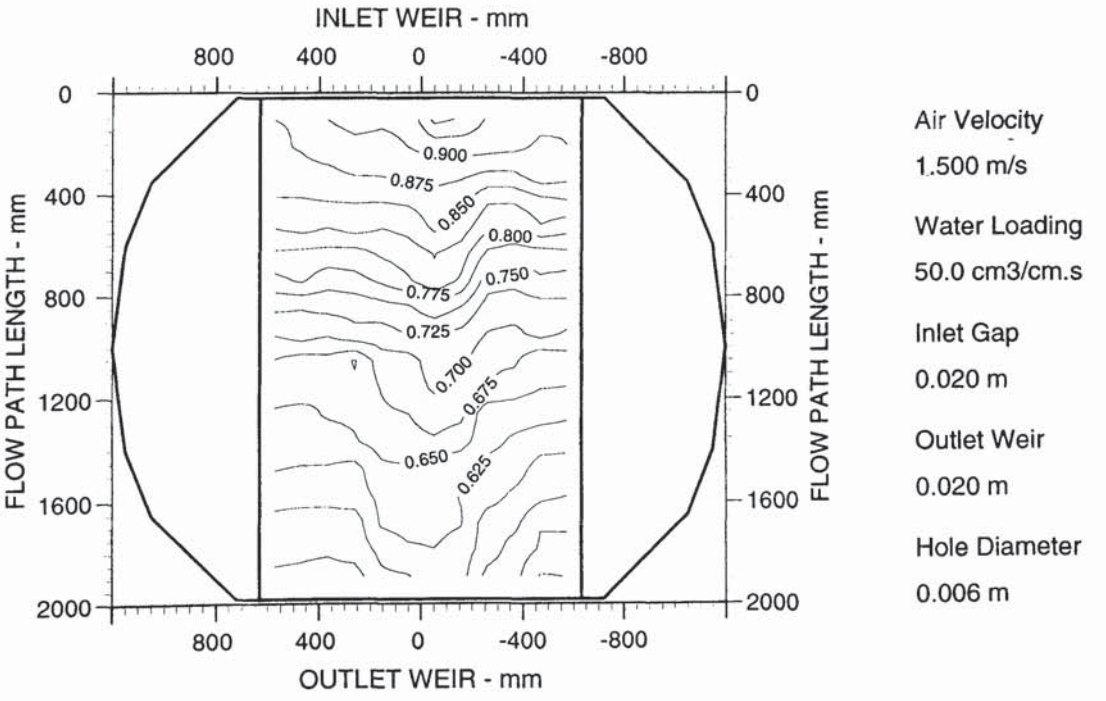

8.12a Two-dimensional temperature profiles for a rectangular tray

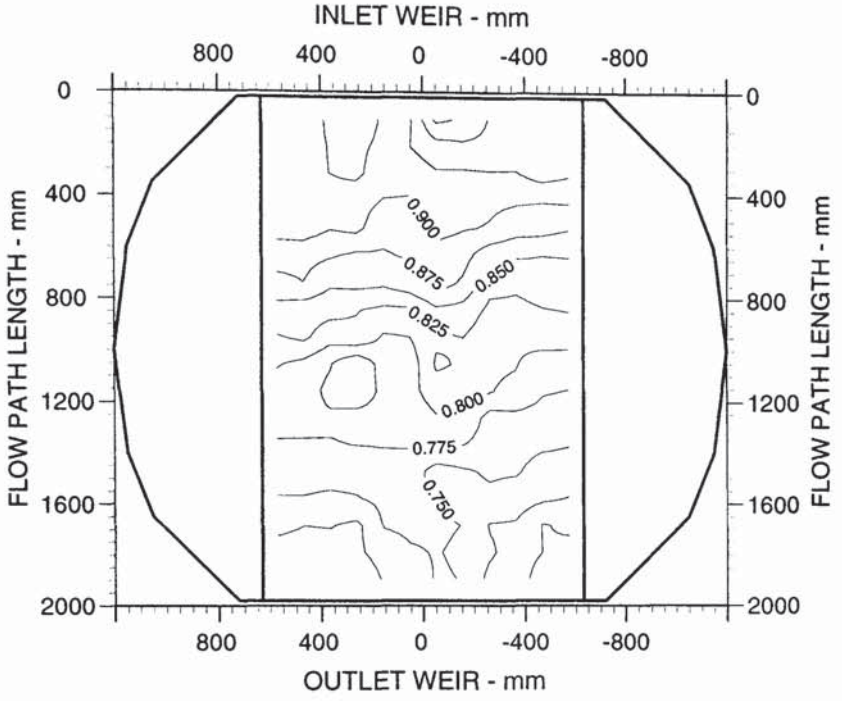

8.12b Two-dimensional temperature profiles for a rectangular tray

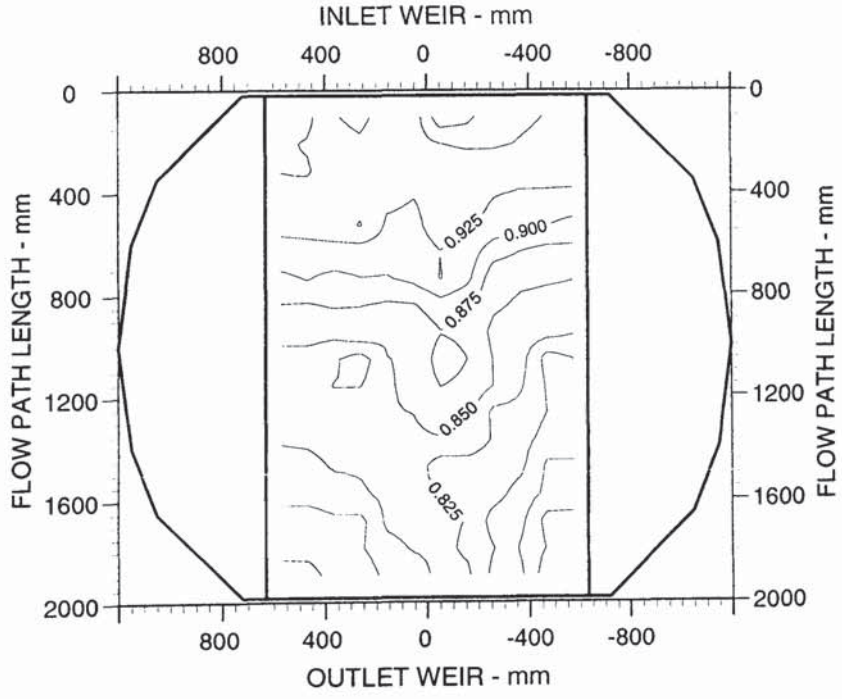

8.12c Two-dimensional temperature profiles for a rectangular tray

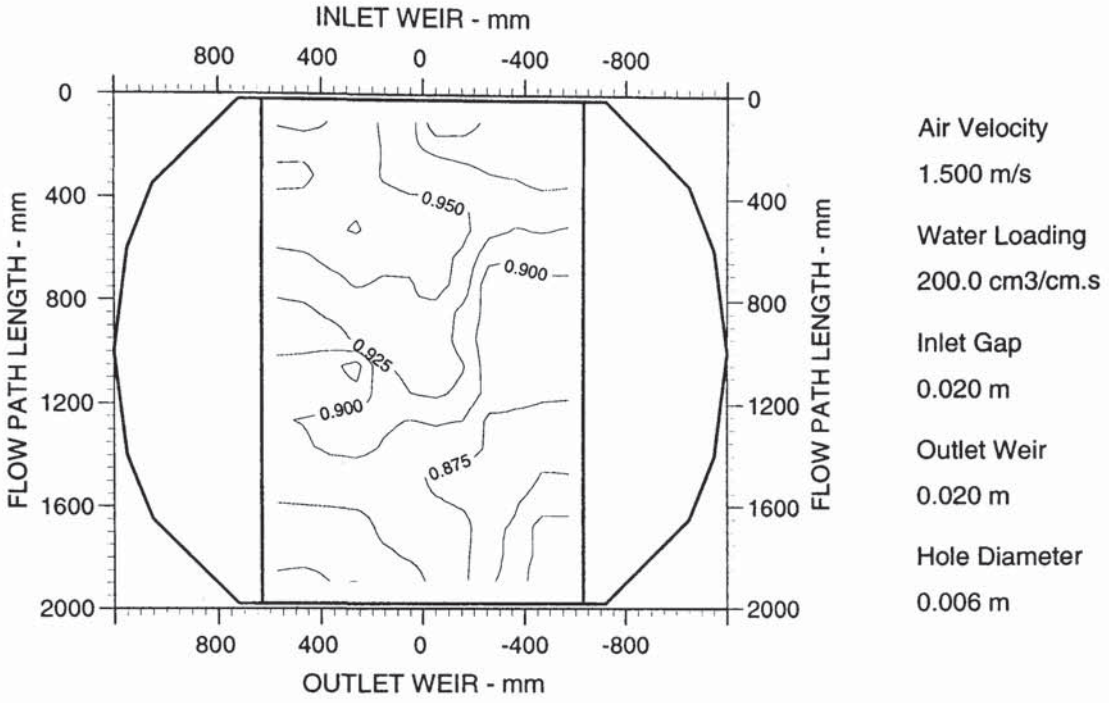

8.12d Two-dimensional temperature profiles for a rectangular tray

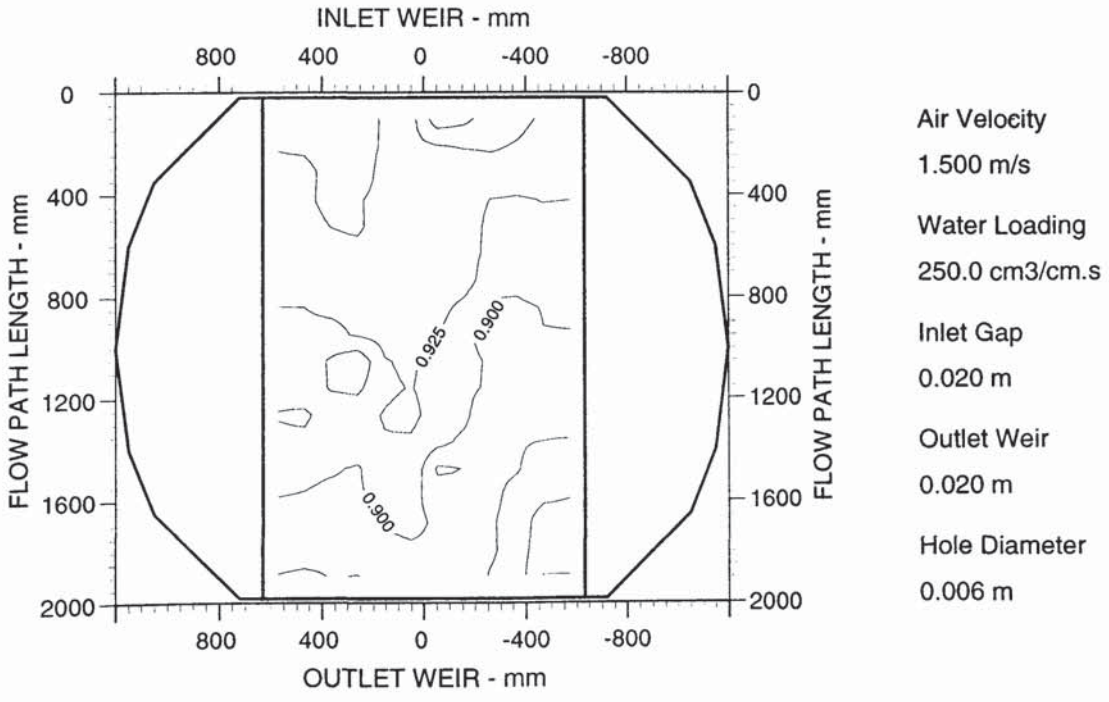

8.12e Two-dimensional temperature profiles for a rectangular tray

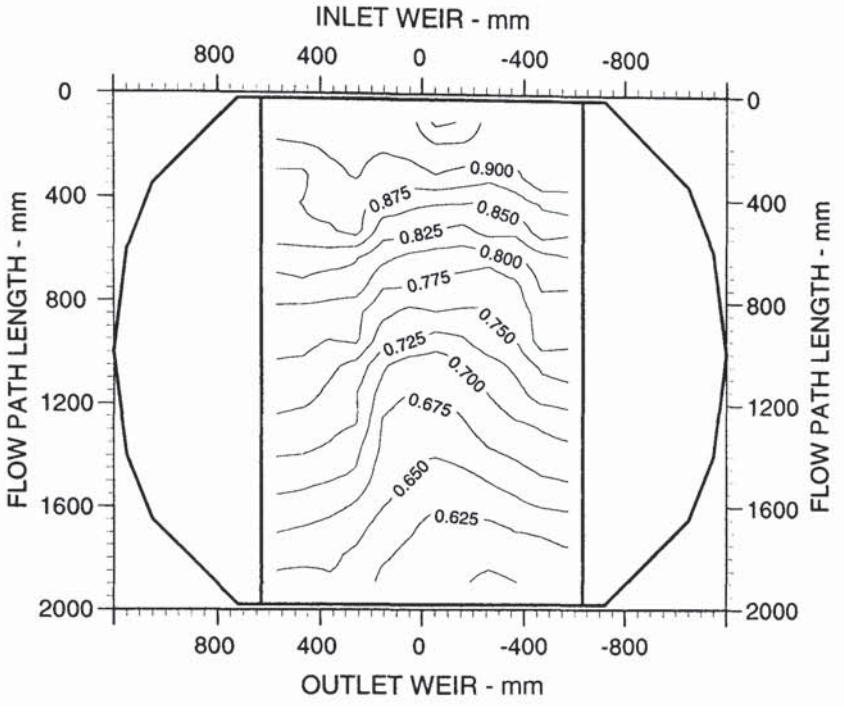

8.13a Two-dimensional temperature profiles for a rectangular tray

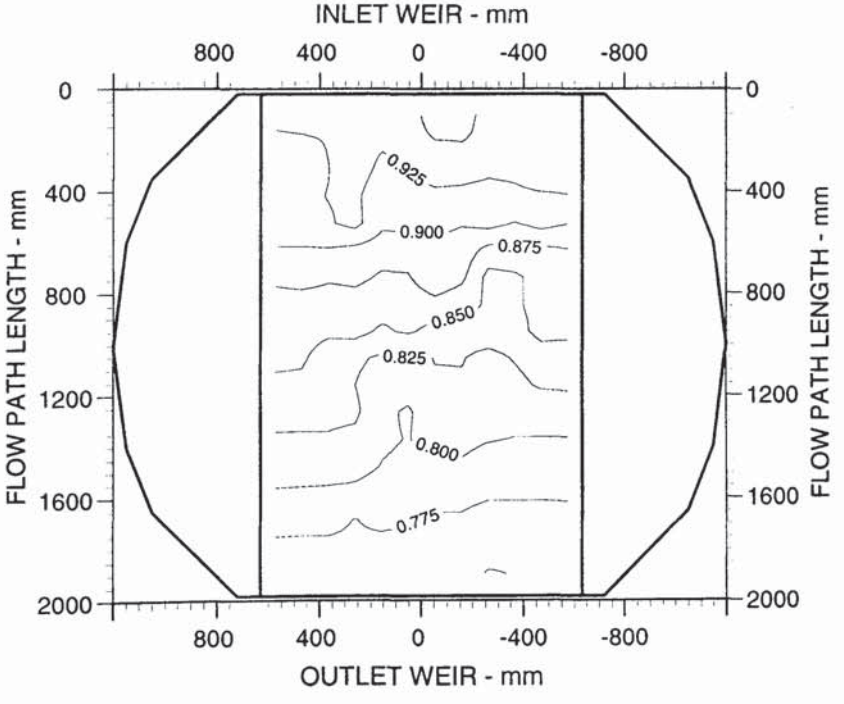

8.13b Two-dimensional temperature profiles for a rectangular tray

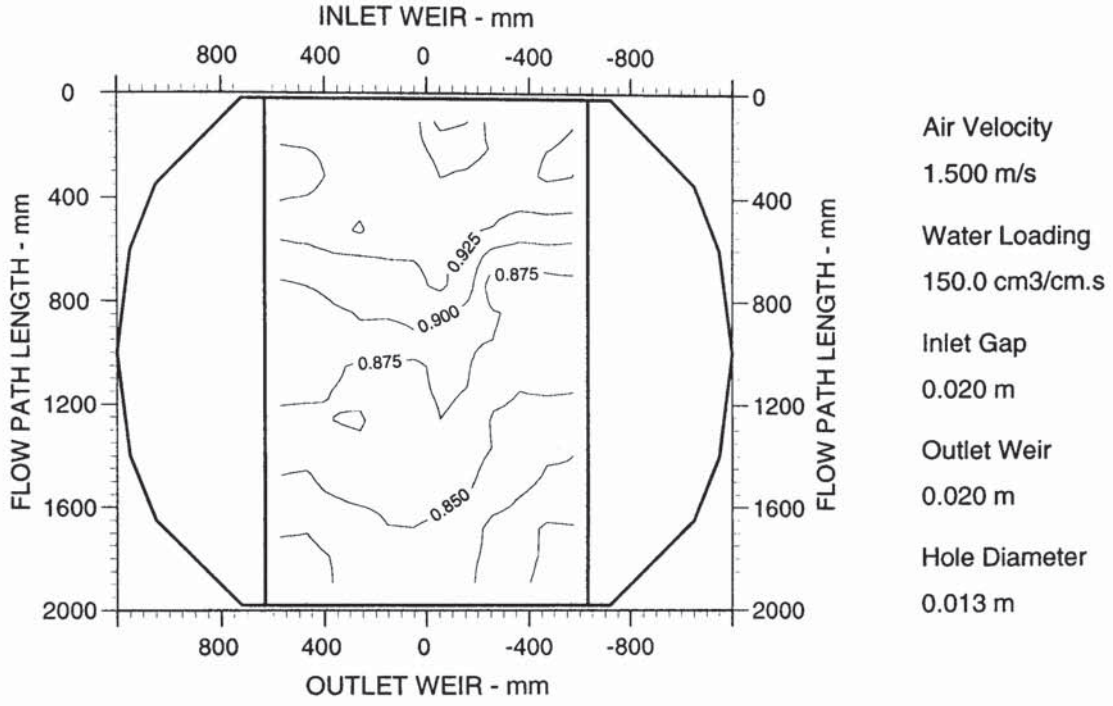

8.13c Two-dimensional temperature profiles for a rectangular tray

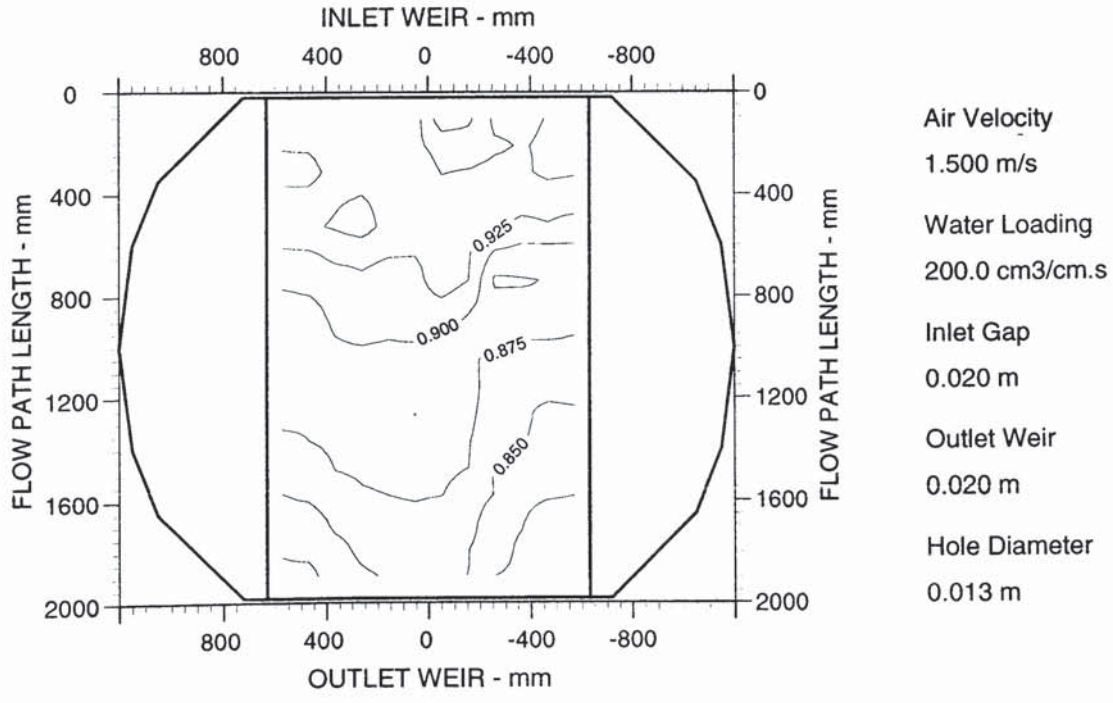

8.13d Two-dimensional temperature profiles for a rectangular tray

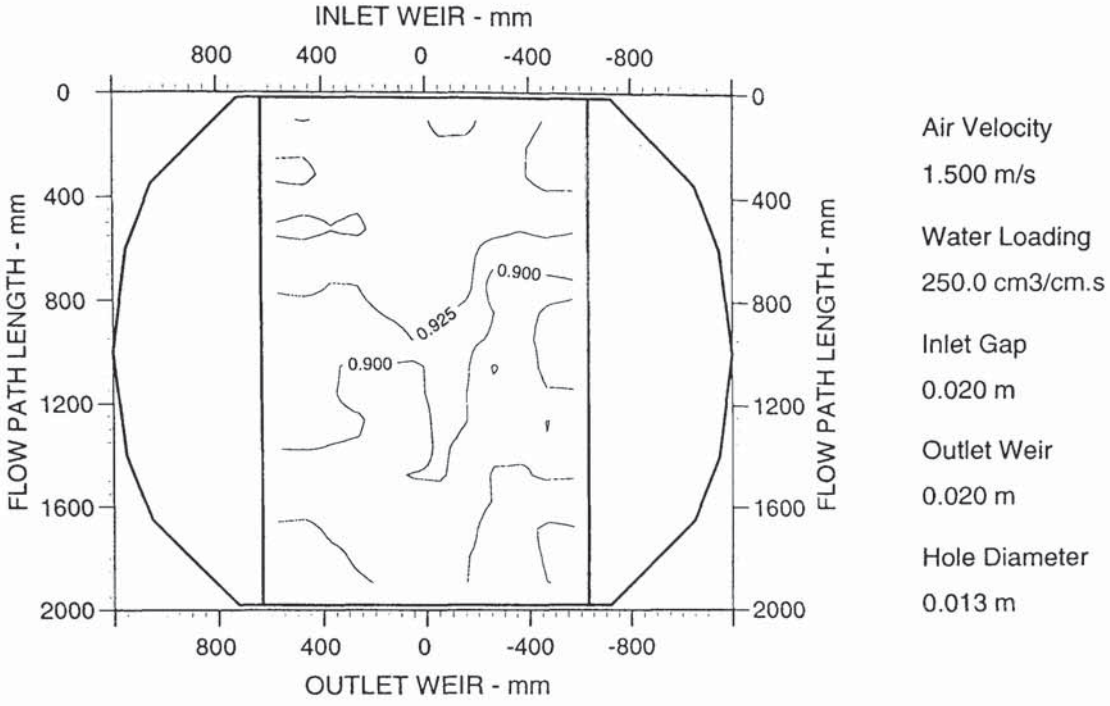

8.13e Two-dimensional temperature profiles for a rectangular tray

created. Also mixing caused by the gas will be taking place over the whole of the tray and liquid from the main body will be 'splashed' into any boundary layer area causing concentration/temperature changes.

Figures 8.11 to 8.13, a-e show typical temperature profiles obtained.

8.5.2 Thermal Efficiencies

The thermal efficiencies for the three trays are presented in tables 8.2 to 8.10. These values are shown graphically in figures 8.14 to 8.16. As with the circular tray there is very little deviation in the efficiencies caused by the hole size. What little there is tends to suggest that the larger hole tray gives the lowest point and tray efficiencies. Another aspect of the efficiency results is that they are considerably less than those on the circular tray.

The trends in the point and tray efficiencies are similar to those with a circular tray. What must be remembered when viewing these graphs is that no readings were taken at the low weir load of 25×10^{-4} $m^3/m.s$. This gives the impression that with a rectangular tray there is no low value of efficiency at low weir loads. If we remember this then the tray efficiency for both circular and rectangular trays drops from a peak at 50×10^{-4} $m^3/m.s$ and the point efficiency generally rises gently from this weir load.

The graph of enhancement ratio also follows the trend of the circular tray and is a more reliable comparison between trays. If we assume point and tray efficiencies are affected to the same degree by the change in geometry, then the ratio between them should be the same. The values for the rectangular enhancement ratio are very similar to those on the circular tray. This would be expected if the above assumption is valid.

I.G., O.W. -mm	10, 10							
Superficial Air Velocity - ms^{-1}	1.00		1.50		2.00		2.50	
Weir Load x 10^4 - $m^3/m.s$	Efficiency - %		Efficiency - %		Efficiency - %		Efficiency - %	
50.0	E_{OG}	57	E_{OG}	63	E_{OG}	49	E_{OG}	45
	E_{MV}	96	E_{MV}	105	E_{MV}	87	E_{MV}	76
	E_{MV}/E_{OG}	1.68	E_{MV}/E_{OG}	1.67	E_{MV}/E_{OG}	1.78	E_{MV}/E_{OG}	1.70
100.0	E_{OG}	55	E_{OG}	54	E_{OG}	49	E_{OG}	47
	E_{MV}	68	E_{MV}	67	E_{MV}	64	E_{MV}	63
	E_{MV}/E_{OG}	1.24	E_{MV}/E_{OG}	1.23	E_{MV}/E_{OG}	1.30	E_{MV}/E_{OG}	1.34
150.0	E_{OG}	63	E_{OG}	58	E_{OG}	53	E_{OG}	47
	E_{MV}	72	E_{MV}	69	E_{MV}	64	E_{MV}	59
	E_{MV}/E_{OG}	1.14	E_{MV}/E_{OG}	1.18	E_{MV}/E_{OG}	1.21	E_{MV}/E_{OG}	1.25
200.0	E_{OG}	61	E_{OG}	50	E_{OG}	51	E_{OG}	45
	E_{MV}	65	E_{MV}	54	E_{MV}	61	E_{MV}	50
	E_{MV}/E_{OG}	1.07	E_{MV}/E_{OG}	1.08	E_{MV}/E_{OG}	1.20	E_{MV}/E_{OG}	1.11
250.0	E_{OG}	64	E_{OG}	55	E_{OG}	45	E_{OG}	39
	E_{MV}	69	E_{MV}	61	E_{MV}	52	E_{MV}	45
	E_{MV}/E_{OG}	1.08	E_{MV}/E_{OG}	1.12	E_{MV}/E_{OG}	1.15	E_{MV}/E_{OG}	1.15

Table 8.2 Efficiencies for a rectangular tray with a 1 mm hole diameter. Inlet gap and outlet weir are both 10 mm.

I.G., O.W. -mm	20, 20							
Superficial Air Velocity - ms^{-1}	1.00		1.50		2.00		2.50	
Weir Load x 10^4 - $m^3/m.s$	Efficiency - %		Efficiency - %		Efficiency - %		Efficiency - %	
50.0	E_{OG}	57	E_{OG}	55	E_{OG}	51	E_{OG}	47
	E_{MV}	88	E_{MV}	93	E_{MV}	82	E_{MV}	74
	E_{MV}/E_{OG}	1.53	E_{MV}/E_{OG}	1.67	E_{MV}/E_{OG}	1.61	E_{MV}/E_{OG}	1.59
100.0	E_{OG}	53	E_{OG}	57	E_{OG}	54	E_{OG}	50
	E_{MV}	66	E_{MV}	78	E_{MV}	75	E_{MV}	66
	E_{MV}/E_{OG}	1.25	E_{MV}/E_{OG}	1.38	E_{MV}/E_{OG}	1.39	E_{MV}/E_{OG}	1.31
150.0	E_{OG}	66	E_{OG}	60	E_{OG}	56	E_{OG}	49
	E_{MV}	75	E_{MV}	71	E_{MV}	70	E_{MV}	60
	E_{MV}/E_{OG}	1.14	E_{MV}/E_{OG}	1.19	E_{MV}/E_{OG}	1.24	E_{MV}/E_{OG}	1.24
200.0	E_{OG}	66	E_{OG}	60	E_{OG}	51	E_{OG}	48
	E_{MV}	71	E_{MV}	70	E_{MV}	61	E_{MV}	56
	E_{MV}/E_{OG}	1.08	E_{MV}/E_{OG}	1.18	E_{MV}/E_{OG}	1.19	E_{MV}/E_{OG}	1.16
250.0	E_{OG}	64	E_{OG}	58	E_{OG}	51	E_{OG}	50
	E_{MV}	67	E_{MV}	64	E_{MV}	56	E_{MV}	55
	E_{MV}/E_{OG}	1.05	E_{MV}/E_{OG}	1.10	E_{MV}/E_{OG}	1.10	E_{MV}/E_{OG}	1.11

Table 8.3 Efficiencies for a rectangular tray with a 1 mm hole diameter. Inlet gap and outlet weir are both 20 mm.

I.G., O.W. -mm	50, 50							
Superficial Air Velocity - ms^{-1}	1.00		1.50		2.00		2.50	
Weir Load x 10^4 - $m^3/m.s$	Efficiency - %		Efficiency - %		Efficiency - %		Efficiency - %	
50.0	E_{OG}	60	E_{OG}	59	E_{OG}	52	E_{OG}	47
	E_{MV}	85	E_{MV}	97	E_{MV}	79	E_{MV}	76
	E_{MV}/E_{OG}	1.43	E_{MV}/E_{OG}	1.64	E_{MV}/E_{OG}	1.52	E_{MV}/E_{OG}	1.59
100.0	E_{OG}	58	E_{OG}	64	E_{OG}	59	E_{OG}	52
	E_{MV}	75	E_{MV}	83	E_{MV}	76	E_{MV}	70
	E_{MV}/E_{OG}	1.28	E_{MV}/E_{OG}	1.29	E_{MV}/E_{OG}	1.29	E_{MV}/E_{OG}	1.34
150.0	E_{OG}	66	E_{OG}	69	E_{OG}	64	E_{OG}	55
	E_{MV}	81	E_{MV}	83	E_{MV}	82	E_{MV}	72
	E_{MV}/E_{OG}	1.22	E_{MV}/E_{OG}	1.20	E_{MV}/E_{OG}	1.28	E_{MV}/E_{OG}	1.31
200.0	E_{OG}	65	E_{OG}	67	E_{OG}	62	E_{OG}	55
	E_{MV}	77	E_{MV}	84	E_{MV}	75	E_{MV}	66
	E_{MV}/E_{OG}	1.18	E_{MV}/E_{OG}	1.24	E_{MV}/E_{OG}	1.21	E_{MV}/E_{OG}	1.21
250.0	E_{OG}	65	E_{OG}	67	E_{OG}	62	E_{OG}	56
	E_{MV}	76	E_{MV}	80	E_{MV}	71	E_{MV}	65
	E_{MV}/E_{OG}	1.16	E_{MV}/E_{OG}	1.19	E_{MV}/E_{OG}	1.16	E_{MV}/E_{OG}	1.17

Table 8.4 Efficiencies for a rectangular tray with a 1 mm hole diameter. Inlet gap and outlet weir are both 50 mm.

I.G., O.W. -mm	10, 10							
Superficial Air Velocity - ms^{-1}	1.00		1.50		2.00		2.50	
Weir Load x 10^4 - $m^3/m.s$	Efficiency - %		Efficiency - %		Efficiency - %		Efficiency - %	
50.0	E_{OG}	-	E_{OG}	49	E_{OG}	48	E_{OG}	46
	E_{MV}	-	E_{MV}	68	E_{MV}	72	E_{MV}	79
	E_{MV}/E_{OG}	-	E_{MV}/E_{OG}	1.39	E_{MV}/E_{OG}	1.49	E_{MV}/E_{OG}	1.71
100.0	E_{OG}	-	E_{OG}	54	E_{OG}	49	E_{OG}	51
	E_{MV}	-	E_{MV}	68	E_{MV}	64	E_{MV}	65
	E_{MV}/E_{OG}	-	E_{MV}/E_{OG}	1.26	E_{MV}/E_{OG}	1.31	E_{MV}/E_{OG}	1.28
150.0	E_{OG}	-	E_{OG}	59	E_{OG}	57	E_{OG}	50
	E_{MV}	-	E_{MV}	72	E_{MV}	71	E_{MV}	62
	E_{MV}/E_{OG}	-	E_{MV}/E_{OG}	1.22	E_{MV}/E_{OG}	1.24	E_{MV}/E_{OG}	1.25
200.0	E_{OG}	-	E_{OG}	57	E_{OG}	51	E_{OG}	52
	E_{MV}	-	E_{MV}	65	E_{MV}	62	E_{MV}	61
	E_{MV}/E_{OG}	-	E_{MV}/E_{OG}	1.13	E_{MV}/E_{OG}	1.21	E_{MV}/E_{OG}	1.17
250.0	E_{OG}	-	E_{OG}	54	E_{OG}	52	E_{OG}	46
	E_{MV}	-	E_{MV}	61	E_{MV}	59	E_{MV}	50
	E_{MV}/E_{OG}	-	E_{MV}/E_{OG}	1.13	E_{MV}/E_{OG}	1.14	E_{MV}/E_{OG}	1.10

Table 8.5 Efficiencies for a rectangular tray with a 6.35 mm hole diameter. Inlet gap and outlet weir are both 10 mm.

I.G., O.W. -mm	20, 20							
Superficial Air Velocity - ms^{-1}	1.00		1.50		2.00		2.50	
Weir Load x 10^4 - $m^3/m.s$	Efficiency - %		Efficiency - %		Efficiency - %		Efficiency - %	
50.0	E_{OG}	-	E_{OG}	50	E_{OG}	52	E_{OG}	49
	E_{MV}	-	E_{MV}	78	E_{MV}	83	E_{MV}	85
	E_{MV}/E_{OG}	-	E_{MV}/E_{OG}	1.55	E_{MV}/E_{OG}	1.61	E_{MV}/E_{OG}	1.74
100.0	E_{OG}	-	E_{OG}	56	E_{OG}	55	E_{OG}	51
	E_{MV}	-	E_{MV}	74	E_{MV}	69	E_{MV}	69
	E_{MV}/E_{OG}	-	E_{MV}/E_{OG}	1.31	E_{MV}/E_{OG}	1.27	E_{MV}/E_{OG}	1.36
150.0	E_{OG}	-	E_{OG}	61	E_{OG}	60	E_{OG}	50
	E_{MV}	-	E_{MV}	73	E_{MV}	70	E_{MV}	61
	E_{MV}/E_{OG}	-	E_{MV}/E_{OG}	1.20	E_{MV}/E_{OG}	1.16	E_{MV}/E_{OG}	1.21
200.0	E_{OG}	-	E_{OG}	52	E_{OG}	57	E_{OG}	51
	E_{MV}	-	E_{MV}	60	E_{MV}	66	E_{MV}	60
	E_{MV}/E_{OG}	-	E_{MV}/E_{OG}	1.15	E_{MV}/E_{OG}	1.15	E_{MV}/E_{OG}	1.15
250.0	E_{OG}	-	E_{OG}	46	E_{OG}	59	E_{OG}	51
	E_{MV}	-	E_{MV}	51	E_{MV}	65	E_{MV}	57
	E_{MV}/E_{OG}	-	E_{MV}/E_{OG}	1.09	E_{MV}/E_{OG}	1.09	E_{MV}/E_{OG}	1.11

Table 8.6 Efficiencies for a rectangular tray with a 6.35 mm hole diameter. Inlet gap and outlet weir are both 20 mm.

I.G., O.W. -mm	50, 50							
Superficial Air Velocity - ms^{-1}	1.00		1.50		2.00		2.50	
Weir Load x 10^4 - $m^3/m.s$	Efficiency - %		Efficiency - %		Efficiency - %		Efficiency - %	
50.0	E_{OG}	-	E_{OG}	56	E_{OG}	54	E_{OG}	51
	E_{MV}	-	E_{MV}	83	E_{MV}	81	E_{MV}	81
	E_{MV}/E_{OG}	-	E_{MV}/E_{OG}	1.48	E_{MV}/E_{OG}	1.51	E_{MV}/E_{OG}	1.60
100.0	E_{OG}	-	E_{OG}	63	E_{OG}	57	E_{OG}	55
	E_{MV}	-	E_{MV}	82	E_{MV}	74	E_{MV}	73
	E_{MV}/E_{OG}	-	E_{MV}/E_{OG}	1.29	E_{MV}/E_{OG}	1.29	E_{MV}/E_{OG}	1.32
150.0	E_{OG}	-	E_{OG}	65	E_{OG}	60	E_{OG}	57
	E_{MV}	-	E_{MV}	79	E_{MV}	70	E_{MV}	66
	E_{MV}/E_{OG}	-	E_{MV}/E_{OG}	1.22	E_{MV}/E_{OG}	1.18	E_{MV}/E_{OG}	1.17
200.0	E_{OG}	-	E_{OG}	73	E_{OG}	60	E_{OG}	57
	E_{MV}	-	E_{MV}	81	E_{MV}	66	E_{MV}	62
	E_{MV}/E_{OG}	-	E_{MV}/E_{OG}	1.12	E_{MV}/E_{OG}	1.10	E_{MV}/E_{OG}	1.10
250.0	E_{OG}	-	E_{OG}	72	E_{OG}	63	E_{OG}	57
	E_{MV}	-	E_{MV}	79	E_{MV}	66	E_{MV}	61
	E_{MV}/E_{OG}	-	E_{MV}/E_{OG}	1.08	E_{MV}/E_{OG}	1.05	E_{MV}/E_{OG}	1.07

Table 8.7 Efficiencies for a rectangular tray with a 6.35 mm hole diameter. Inlet gap and outlet weir are both 50 mm.

I.G., O.W. -mm	10, 10							
Superficial Air Velocity - ms^{-1}	1.00		1.50		2.00		2.50	
Weir Load x 10^4 - $m^3/m.s$	Efficiency - %		Efficiency - %		Efficiency - %		Efficiency - %	
50.0	E_{OG}	48	E_{OG}	46	E_{OG}	46	E_{OG}	45
	E_{MV}	65	E_{MV}	69	E_{MV}	75	E_{MV}	73
	E_{MV}/E_{OG}	1.35	E_{MV}/E_{OG}	1.49	E_{MV}/E_{OG}	1.62	E_{MV}/E_{OG}	1.63
100.0	E_{OG}	56	E_{OG}	51	E_{OG}	49	E_{OG}	45
	E_{MV}	68	E_{MV}	64	E_{MV}	63	E_{MV}	60
	E_{MV}/E_{OG}	1.22	E_{MV}/E_{OG}	1.24	E_{MV}/E_{OG}	1.29	E_{MV}/E_{OG}	1.34
150.0	E_{OG}	55	E_{OG}	50	E_{OG}	49	E_{OG}	46
	E_{MV}	63	E_{MV}	58	E_{MV}	57	E_{MV}	54
	E_{MV}/E_{OG}	1.13	E_{MV}/E_{OG}	1.14	E_{MV}/E_{OG}	1.16	E_{MV}/E_{OG}	1.18
200.0	E_{OG}	51	E_{OG}	47	E_{OG}	52	E_{OG}	45
	E_{MV}	55	E_{MV}	52	E_{MV}	58	E_{MV}	51
	E_{MV}/E_{OG}	1.08	E_{MV}/E_{OG}	1.12	E_{MV}/E_{OG}	1.12	E_{MV}/E_{OG}	1.12
250.0	E_{OG}	45	E_{OG}	45	E_{OG}	53	E_{OG}	51
	E_{MV}	47	E_{MV}	48	E_{MV}	57	E_{MV}	56
	E_{MV}/E_{OG}	1.04	E_{MV}/E_{OG}	1.06	E_{MV}/E_{OG}	1.08	E_{MV}/E_{OG}	1.10

Table 8.8 Efficiencies for a rectangular tray with a 12.7 mm hole diameter. Inlet gap and outlet weir are both 10 mm.

I.G., O.W. -mm	20, 20							
Superficial Air Velocity - ms^{-1}	1.00		1.50		2.00		2.50	
Weir Load x 10^4 - $m^3/m.s$	Efficiency - %		Efficiency - %		Efficiency - %		Efficiency - %	
50.0	E_{OG}	56	E_{OG}	49	E_{OG}	47	E_{OG}	40
	E_{MV}	79	E_{MV}	77	E_{MV}	73	E_{MV}	71
	E_{MV}/E_{OG}	1.41	E_{MV}/E_{OG}	1.56	E_{MV}/E_{OG}	1.56	E_{MV}/E_{OG}	1.79
100.0	E_{OG}	56	E_{OG}	53	E_{OG}	51	E_{OG}	45
	E_{MV}	70	E_{MV}	67	E_{MV}	67	E_{MV}	63
	E_{MV}/E_{OG}	1.25	E_{MV}/E_{OG}	1.28	E_{MV}/E_{OG}	1.32	E_{MV}/E_{OG}	1.41
150.0	E_{OG}	58	E_{OG}	55	E_{OG}	54	E_{OG}	48
	E_{MV}	69	E_{MV}	65	E_{MV}	67	E_{MV}	62
	E_{MV}/E_{OG}	1.20	E_{MV}/E_{OG}	1.18	E_{MV}/E_{OG}	1.23	E_{MV}/E_{OG}	1.31
200.0	E_{OG}	57	E_{OG}	55	E_{OG}	54	E_{OG}	52
	E_{MV}	66	E_{MV}	63	E_{MV}	62	E_{MV}	62
	E_{MV}/E_{OG}	1.16	E_{MV}/E_{OG}	1.15	E_{MV}/E_{OG}	1.14	E_{MV}/E_{OG}	1.20
250.0	E_{OG}	57	E_{OG}	56	E_{OG}	56	E_{OG}	56
	E_{MV}	60	E_{MV}	61	E_{MV}	62	E_{MV}	63
	E_{MV}/E_{OG}	1.05	E_{MV}/E_{OG}	1.08	E_{MV}/E_{OG}	1.11	E_{MV}/E_{OG}	1.12

Table 8.9 Efficiencies for a rectangular tray with a 12.7 mm hole diameter. Inlet gap and outlet weir are both 20 mm.

I.G., O.W. -mm	50, 50							
Superficial Air Velocity - ms^{-1}	1.00		1.50		2.00		2.50	
Weir Load x 10^4 - $m^3/m.s$	Efficiency - %		Efficiency - %		Efficiency - %		Efficiency - %	
50.0	E_{OG}	58	E_{OG}	47	E_{OG}	49	E_{OG}	46
	E_{MV}	86	E_{MV}	66	E_{MV}	75	E_{MV}	78
	E_{MV}/E_{OG}	1.48	E_{MV}/E_{OG}	1.41	E_{MV}/E_{OG}	1.53	E_{MV}/E_{OG}	1.71
100.0	E_{OG}	67	E_{OG}	58	E_{OG}	51	E_{OG}	50
	E_{MV}	86	E_{MV}	77	E_{MV}	71	E_{MV}	70
	E_{MV}/E_{OG}	1.29	E_{MV}/E_{OG}	1.33	E_{MV}/E_{OG}	1.38	E_{MV}/E_{OG}	1.40
150.0	E_{OG}	71	E_{OG}	63	E_{OG}	54	E_{OG}	52
	E_{MV}	86	E_{MV}	78	E_{MV}	67	E_{MV}	67
	E_{MV}/E_{OG}	1.21	E_{MV}/E_{OG}	1.23	E_{MV}/E_{OG}	1.24	E_{MV}/E_{OG}	1.27
200.0	E_{OG}	64	E_{OG}	62	E_{OG}	55	E_{OG}	50
	E_{MV}	75	E_{MV}	70	E_{MV}	65	E_{MV}	59
	E_{MV}/E_{OG}	1.18	E_{MV}/E_{OG}	1.14	E_{MV}/E_{OG}	1.19	E_{MV}/E_{OG}	1.18
250.0	E_{OG}	66	E_{OG}	61	E_{OG}	55	E_{OG}	52
	E_{MV}	77	E_{MV}	69	E_{MV}	64	E_{MV}	59
	E_{MV}/E_{OG}	1.16	E_{MV}/E_{OG}	1.13	E_{MV}/E_{OG}	1.15	E_{MV}/E_{OG}	1.14

Table 8.10 Efficiencies for a rectangular tray with a 12.7 mm hole diameter. Inlet gap and outlet weir are both 50 mm.

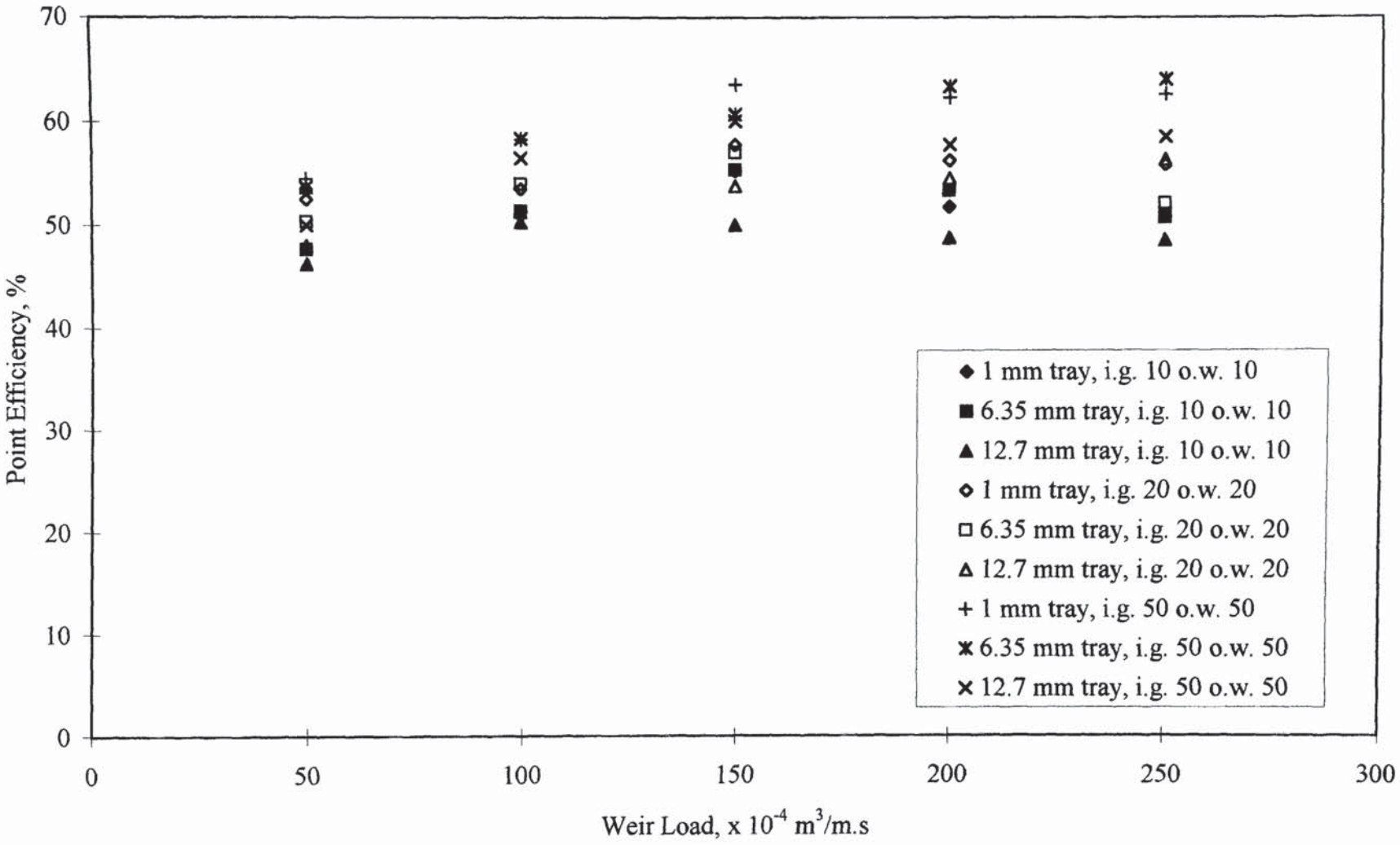

Figure 8.14 Variation of the point efficiency on a rectangular tray. Three different hole sizes are shown.

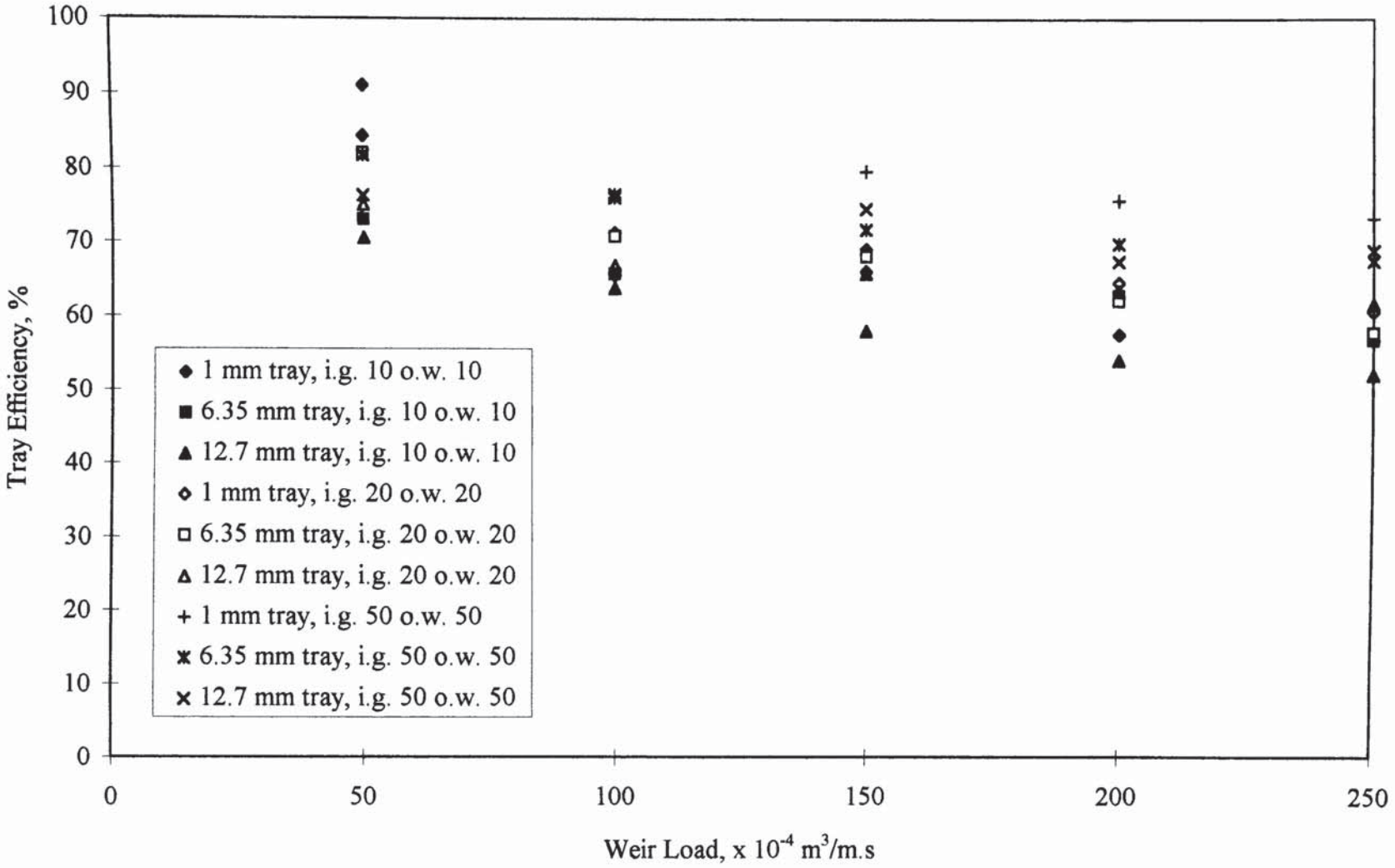

Figure 8.15 Variation of the tray efficiency on a rectangular tray. Three different hole sizes are shown.

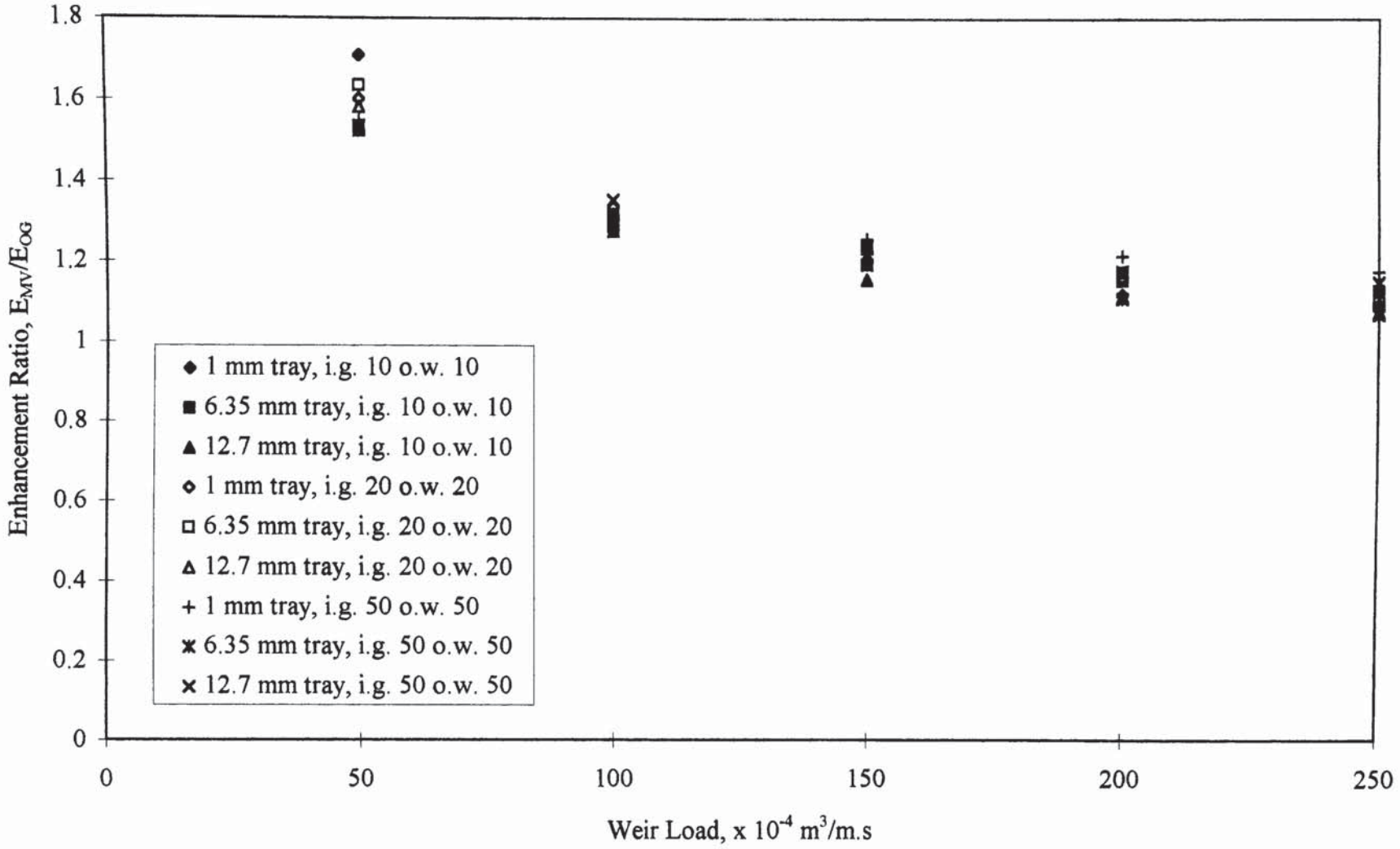

Figure 8.16 Variation of the enhancement ratio on a rectangular tray. Three different hole sizes are shown.

The variation for hole size in the enhancement ratio is very small with several concurrent points. There is no dominant hole size that gives the best enhancement and the picture is confused. The enhancement ratio never drops below unity for any weir load.

8.5.3 The Chan and Fair Model

The Chan and Fair (1984) model is based on a large data bank collected on large scale columns. It is a hybrid of the correlations used by Zuiderweg (1982) and the AIChE (1958) method. The plug flow correlation is used to calculate N_{OG} and the AIChE correlation was used to calculate values of N_L . These were used to calculate N_G values. The distillation data are used to obtain values of E_{OG}. The final correlation is:

$$N_L = 1.97x10^4 (D_L)^{0.5}(0.40F_s + 0.17)t_L \tag{8.1}$$

$$t_L = \frac{h_{cl}ZW}{Q_L} \tag{8.2}$$

$$N_G = \frac{1000(D_G)^{0.5}(10.3(FF) - 8.67(FF)^2 t_G}{h_{cl}^{0.5}} \tag{8.3}$$

$$t_G = \frac{(1-\alpha_e)h_{cl}}{(\alpha_e u_s)} \tag{8.4}$$

A much fuller description of the model is given in Chapter 2. As a rectangular tray is used in the derivation of this model it would be informative to compare the rectangular values with the model values.

The point efficiencies predicted by the model are shown in tables 8.11 to 8.13. The model makes no distinction between different inlet gaps and therefore only the outlet weir height is important. Three figures, 8.17 to 8.19, show the values calculated from the rectangular tray for the point efficiency compared with those predicated by the

model. Also included are the point efficiencies produced from the circular trays. It can be seen from the graphs that the model over-predicts the efficiency for nearly all the weir loads. The rectangular tray efficiencies are very much lower than those predicted and those from the circular tray, which has been mentioned above. The model does predict the circular efficiency fairly well at the lower weir loads. This tails off at the higher weir loads. The model over predicts the efficiency more at low inlet gaps than at the high inlet gaps. This suggests that the circulation on the tray lowers the measured average point efficiency away from that predicted by the model. The maximum deviation is by approximately twenty percentage points and this occurs at the lower inlet gap and outlet weir combinations.

The model also predicts the same trends as the measured data. The predicted point efficiency increases sharply at the low weir loads and then levels off. Also the higher point efficiencies are caused by the higher weir load. These trends are also shown by both the rectangular and circular point efficiencies.

Outlet Weir - mm	10	
Weir Load x 10^{-4} - m^3/m.s	Superficial Air Velocity – m/s	Point Efficiency - %
25.0	1.00	66.2
	1.50	59.9
	2.00	52.0
	2.50	42.4
50.0	1.00	74.5
	1.50	70.6
	2.00	65.4
	2.50	59.0
100.0	1.00	84.2
	1.50	82.9
	2.00	80.8
	2.50	77.9
150.0	1.00	89.2
	1.50	89.1
	2.00	88.4
	2.50	87.2
200.0	1.00	92.1
	1.50	92.6
	2.00	92.6
	2.50	92.2
250.0	1.00	93.9
	1.50	94.7
	2.00	95.0
	2.50	94.9

Table 8.11 Predicted point efficiencies from the Chan and Fair model, for an oulet weir of 10 mm.

Outlet Weir - mm	20	
Weir Load x 10^{-4} - m^3/m.s	Superficial Air Velocity – m/s	Point Efficiency - %
25.0	1.00	68.5
	1.50	62.5
	2.00	55.0
	2.50	45.9
50.0	1.00	76.5
	1.50	72.6
	2.00	67.6
	2.50	61.4
100.0	1.00	85.7
	1.50	84.2
	2.00	82.0
	2.50	79.1
150.0	1.00	90.4
	1.50	90.1
	2.00	89.2
	2.50	87.9
200.0	1.00	93.1
	1.50	93.3
	2.00	93.1
	2.50	92.6
250.0	1.00	94.7
	1.50	95.2
	2.00	95.3
	2.50	95.2

Table 8.12 Predicted point efficiencies from the Chan and Fair model, for an oulet weir of 20 mm.

Outlet Weir - mm	50	
Weir Load x 10^{-4} - m^3/m.s	Superficial Air Velocity – m/s	Point Efficiency - %
25.0	1.00	74.2
	1.50	69.1
	2.00	62.8
	2.50	55.1
50.0	1.00	81.1
	1.50	77.6
	2.00	73.2
	2.50	67.7
100.0	1.00	88.9
	1.50	87.4
	2.00	85.2
	2.50	82.4
150.0	1.00	92.8
	1.50	92.2
	2.00	91.2
	2.50	89.7
200.0	1.00	95.0
	1.50	94.9
	2.00	94.4
	2.50	93.6
250.0	1.00	96.3
	1.50	96.4
	2.00	96.2
	2.50	95.8

Table 8.13 Predicted point efficiencies from the Chan and Fair model, for an oulet weir of 50 mm.

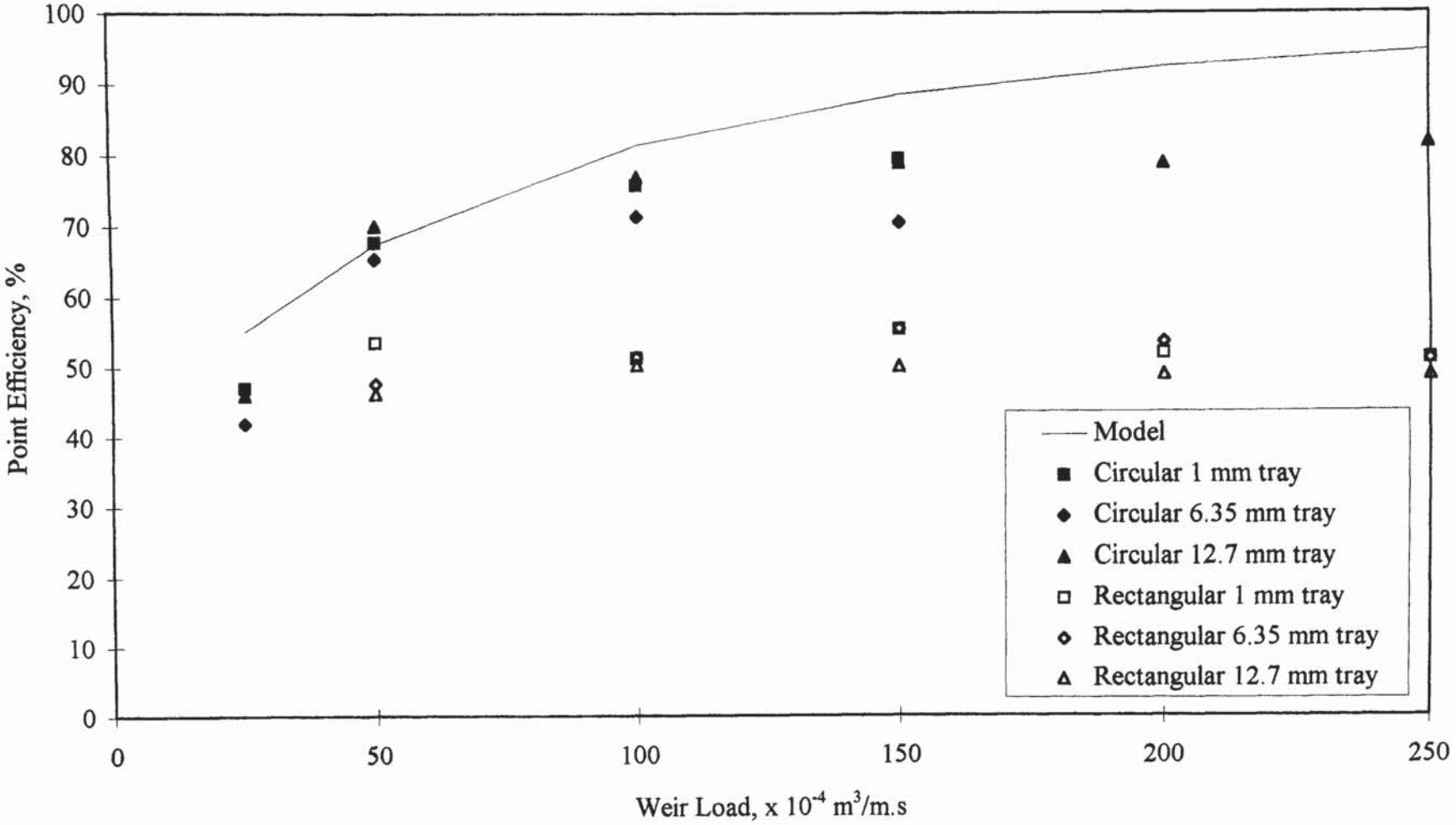

Figure 8.17 Comparison of the point efficiencies for a circular and rectangular tray with the Chan and Fair model. Inlet gap and outlet weir are both 10 mm.

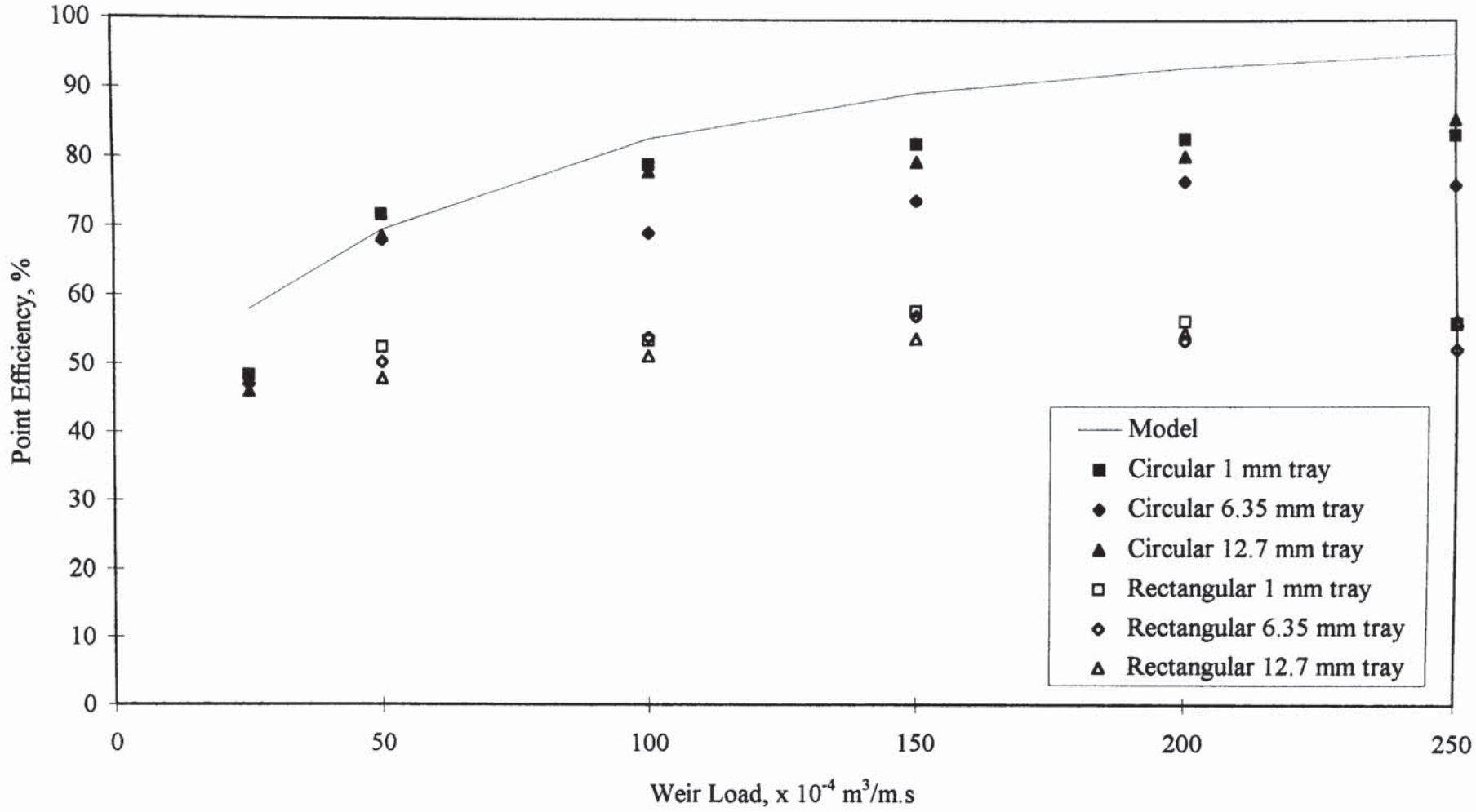

Figure 8.18 Comparison of the point efficiencies for a circular and rectangular tray with the Chan and Fair model. Inlet gap and outlet weir are both 20 mm.

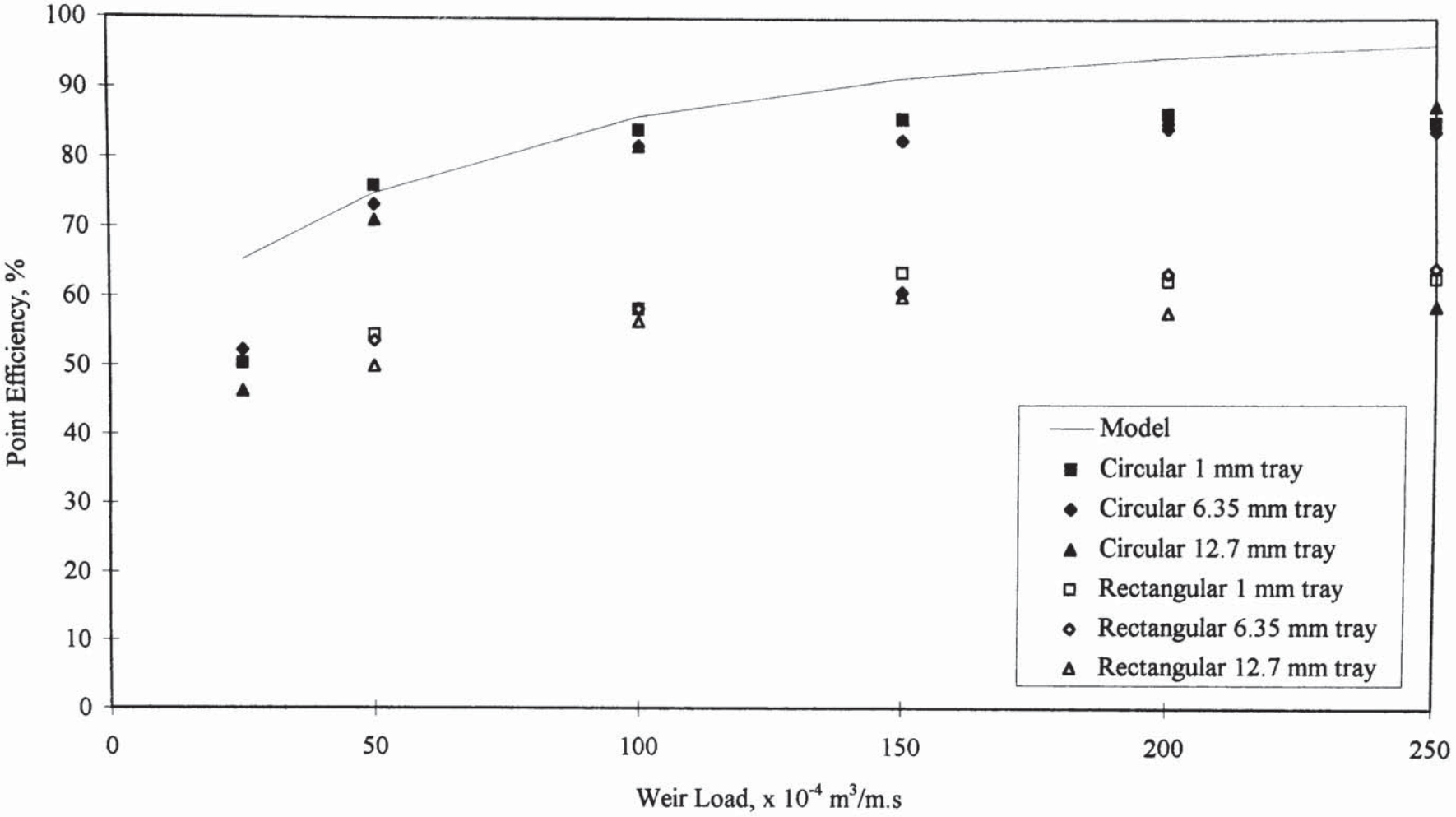

Figure 8.19 Comparison of the point efficiencies for a circular and rectangular tray with the Chan and Fair model. Inlet gap and outlet weir are both 50 mm.

8.5.4 Discussion and Conclusions

The two-dimensional profiles show that the liquid flowed across the tray in almost plug flow. This is associated by some backmixing caused by the gas mixing. Essentially there was no change in the liquid temperature in the transverse direction.

The numerical results of the efficiencies showed that the larger hole trays gave lower efficiencies. This can be explained by the amount of gas that by-passes the liquid. With larger holes the bubbles or jets tend to be larger and as explained with the circular tray the surface area per volume is lower. This means that more of the gas passes through the liquid without being changed. This leads to the lowering of the efficiencies.

The efficiencies are also considerably lower than on the circular tray. This could be caused by the velocity of the liquid on the tray. With circular trays the velocity is reduced by the liquid spreading out over the diverging section. Energy is lost and the inlet velocity is not regained by flowing over the converging, outlet section. The water on the rectangular tray does not expand in the manner of the circular tray and therefore does not slow down to the same extent. This reduces the liquid residence time and hence the contact time with the gas, leading to less temperature change. This effect may mask any comparisons made between circular and rectangular trays and should be taken into account when viewing data collected on different geometries. The rectangular tray is close to the situation which occurs on a circular tray when severe circulation occurs. The bulk of the liquid is confined to the centre of the tray by the circulating zones. This will have the effect of speeding up the liquid in this central section, compared to a case with the same weir load where the liquid can spread out to cover the whole tray. This could be a contributory factor in the reduction of the efficiency caused by circulation.

The enhancement ratio of the trays is similar for all hole sizes which suggested that no hole size is dominant. The enhancement ratio never drops below unity as by definition

the air temperature above the outlet liquid must be lower than the average air temperature and thus leads to lower average point efficiencies than tray efficiencies.

The Chan and Fair model predicts the circular point efficiency fairly well, but it does not follow the reduction in the efficiency caused by the circulation on the tray. The model does not predict the results found on the rectangular tray at all accurately. It does however predict the trend in the point efficiency.

The model does tend to over-predict the efficiency and this could be down to the underestimation of the liquid-phase resistance. This is also the same criticism that is aimed at the AIChE model and is not unsurprising as both models use the same correlation for liquid-phase resistance. It has been well known that the AIChE method over-predicts efficiency and the same could be true of Chan and Fair's correlation. However, the redeeming feature of the correlation is that it is based on actual data.

8.6 Overall Discussion

When the results of the height of clear liquid experiments are taken in context with the water-cooling experiments an interesting point comes forward. The water coming off the higher hole diameter tray tends to be cooler than that coming off lower hole diameter trays. When it is taken into account that the height of clear liquid on the higher hole diameter tray is the largest, and thus more liquid is held-up, it is reasonable to assume that the residence time of the liquid is greater for the higher hole diameters. If, as has been found, there is little change in the efficiency of the tray for the different hole sizes, then the increased hold-up must account for the cooler exit temperature.

The mechanism that may explain this is that the liquid is randomised by the gas flow and some is thrown out of the bulk liquid flow. The extreme case of this is the spray regime. The higher hole diameter throws more liquid in a backwards, against the flow, direction than smaller hole sizes. If we assume that the path of the gas is bent by the liquid flow, then more liquid is thrown forward than backwards, for a given hole size.

The more resistance to bending the gas has, the more liquid will be thrown backwards. Relative to the other trays, with the same flow rates and tray configuration, the tray with the 12.7 mm hole diameter throws more liquid backwards than the other two trays. This would explain the higher hold-up and it suggests that the eddy diffusivity is not the same in all directions, as is assumed by a large number of predictive models. The lower temperature can be explained by the liquid contacting the gas for more time.

The slight reduction in the point efficiency could also be explained by this phenomena due to the reduced driving force. The temperature of the liquid up-stream of the weir will be reduced by mixing with cooler liquid that has been 'splashed' from further downstream. Taking this mechanism and the gas by-passing on higher hole trays, a reduction in the point efficiency as the hole size increases is likely.

The Chan and Fair (1984) correlation of the point efficiency does not predict the efficiency on the rectangular tray very well, but it does predict the trend of the data. The model is a much better prediction of the efficiency of the circular tray. It is surprising that the rectangular efficiencies are not predicted better as the tray is operating in plug flow and the model is based on a rectangular section. But, as mentioned above, the model may be prone to the same overprediction as that associated with the AIChemE model as they share the liquid phase resistance term. However, the problem may indeed arise from the fine tuning of the model that was carried out to match circular tray data.

8.7 Conclusions

- The direct observation of the dispersion showed that all the liquid flowed in the direction from inlet downcomer to outlet downcomer. There was no circulation and the tray appeared to be acting in plug flow.

- The height of clear liquid on the rectangular tray is affected by the hole diameter. Larger hole diameters produce higher heights of clear liquid. Practically this means that more liquid is held-up on these trays with all the adverse and beneficial factors that this brings.

- The gradient produced on a rectangular tray is very small. Further measurements, with perhaps a more sensitive technique, are needed to draw any further conclusions.

- Higher hole trays give a lower efficiency due to an increase in the gas by-passing from the larger holes. This is due to the lower surface area per volume of the larger bubbles or jets produced with larger holes.

- The enhancement ratio for the rectangular tray is similar to that produced on a circular tray, the major difference being that the ratio for the rectangular tray never drops below unity for any combination of flow rates.

- The Chan and Fair (1984) model to predict efficiencies over-predicts in the vast majority of cases. It cannot predict the reduction in efficiency caused by the presence of circulations on a circular tray. It vastly over-predicts the measured point efficiency of the rectangular tray.

- The temperature of the liquid leaving trays with larger hole diameters is slightly lower than that leaving a tray with a lower hole size. This is possibly due to the greater hold-up of liquid on these trays and a subsequent increase in contact time on the tray.

- Work on the height of clear liquid on the tray suggests that the eddy diffusivity is not equal in all directions. It is affected by hole size and the gas and liquid momentum.

CHAPTER 9

DISCUSSION

9.1 Introduction

This chapter brings together all the work reported elsewhere in this thesis. As such it is only intended as a summary and reference to the relevant chapter should be made for fuller details of the experiments and results. Two different tray geometries and three different hole size trays have been tested by a number of different techniques. The work is brought together below to try to give an overall view of the points made throughout the thesis.

9.2 The Circular Tray

It has been found that the passage of the air through the water has a significant effect on the flow pattern that is produced on a tray. Separation occurred at a very low weir load with water-only studies. When air was introduced to the water on the tray the onset of separation was at a much higher weir load. The added resistance of the air obviously affected the flow on the tray in such a way as to make circulation of the bi-phase more unlikely than if the air was not present. Indeed, with some combinations of flow rates, hole size, inlet gap and outlet weir the maximum area of circulation was not reached.

There was a direct relationship between the inlet velocity and the area of the tray covered by circulations. The experiments carried out with an inlet gap of 10 mm

showed a greater area of circulation for a given weir load than those carried out with higher inlet gaps. The rate of increase in the size of the circulations was also reduced with a higher inlet gap. The effect of a higher froth height on the tray and therefore a greater contact time between the two phases, would also help the reduction in the area of circulation.

The height of the inlet gap also has an effect on the height of clear liquid on the tray. With low inlet gaps the water can jet onto the tray at high weir loads. This causes the height of clear liquid to be low in front of the downcomer and then undergo a hydraulic jump once the liquid has slowed down sufficiently. Separation also causes an effect on the height of clear liquid. The hold-up in the side segments of the tray is increased due to either circulation or slower moving bi-phase in these areas. This leads to a higher residence time of the liquid in these areas, which in turn affects the efficiencies in these areas. It has been shown that the increase in air velocity decreases the height of clear liquid. This is consistent with the liquid being preferentially thrown forward by the gas. If the gas were to pass through the liquid in a vertical direction then any mixing would be equal in all directions. If, as has been proposed, the gas is deflected by the liquid then there will be more liquid 'sprayed' in the direction the gas is bent. The increase in gas velocity will throw more liquid out of the main bulk. If the gas is deflected then this would mean more liquid thrown in the direction of the bulk liquid. If the majority of the liquid is flowing in the forward direction then this would reduce the hold-up on the tray and is shown in the decrease in the height of clear liquid. This finding seems to suggest that the eddy diffusivity, which has been assumed to be the same in all directions in a large number of models, is in fact altered by the hole size. The magnitude of the eddy diffusivity in a given direction is dependent on the momentum of the gas jets or bubbles and the amount that they are deflected by the liquid momentum.

The efficiency of the tray was affected by the circulations on the tray and by the liquid hold-up. An increase in the liquid hold-up increased the contact time between the phases and increased the change in the temperature. The extreme case of this is where liquid was circulating in the segments of the tray. This liquid would rapidly

approach the wet bulb temperature of the air and thereafter no further change would occur. This would have a detrimental effect on the point efficiency in these areas and also cause a decrease in the overall tray efficiency. Indeed if circulation was occurring, then the water in the segments could be colder than that crossing the outlet weir. This could lead to a enhancement ratio of less than unity due to the average temperature being lower than the outlet temperature. This can be seen from the efficiencies collected from the water-cooling experiments. Where separation occurs, a reduction in the tray efficiency is noted and this corresponds to the reduction in the temperature in the side segments of the tray.

9.2.1 The Effect of Hole Size

The effect of hole size was assessed by comparing the experimental data collected from the 12.7 mm hole diameter tray with data collected by Hine (1990) and Chambers (1993) on trays with 1 mm and 6.35 mm hole diameters. The data were first classified to find the regime that each combination of flow rates operated under. This was undertaken by using the measured height of clear liquid and comparing them with a correlation for the transition between spray and froth. This showed that the majority of data points were in the froth regime with only a small number of points on the 12.7 mm hole tray being in the spray regime.

The onset of separation was found to be affected by the hole size. At the larger hole sizes it took a greater weir load for circulation to occur. The rate at which the circulation increased was also reduced by the increase in hole size. This could be put down to an increase in resistance to liquid flow on the larger hole trays. It has been noted that the velocity of the liquid affects the degree of circulation and therefore if the liquid is slowed more by higher hole sizes, then it is less likely to circulate. Also any circulations produced are expected to be smaller.

This mechanism also has an effect on the extent of jetting onto the tray. The jetting associated with the larger hole size is less than that occurring with a lower hole size.

This can be explained by the liquid being slowed quicker by the gas from the large holes and therefore undergoing the hydraulic jump earlier.

Hole size does not appear to have any effect on the maximum circulating area or the average clear liquid height on the circular tray. Instead these are set by the physical dimensions of the tray and the outlet weir respectively. Also the hole size appears to have very little effect on the efficiencies produced on the trays. Any differences can be attributed to the size of the bubbles or jets produced by the holes. The smaller holes produce smaller bubbles or jets and therefore more of the gas is contacted by the liquid. This slightly increases the efficiency, but the greater circulation on the smaller hole trays has a detrimental effect which can undermine this increase.

9.3 The Rectangular Tray

To help clarify the underlying mechanisms in the two-phase flow on a sieve tray, a simpler geometry was tested. The rectangular tray takes out the uncertainties caused by the side segments of the tray. This allows us to see what effects are caused by the hole size, inlet gap, outlet weir, flow rates etc. and what has been caused by the circular nature of the tray.

The liquid on the circular tray is generally flowing slower than that on the rectangular tray. This is caused by the liquid spreading out into the side sections. Where this is untrue is the case where the circulation is at a maximum. The liquid will then channel through the area between the downcomers.

The main discussion point to arise from the rectangular tray is that the higher the hole diameter, the higher the clear liquid height. This can be explained by a greater recycling of the liquid by the larger bubbles or jets caused by the larger holes. More liquid is 'sprayed' backwards by the larger holes due to the gas being deflected less. This explains the balance between liquid thrown forward and liquid thrown

backwards being greater in the backwards direction, compared with that produced by the smaller holes, for the larger hole size.

The hold-up of the liquid can also be explained by the increase in the resistance noted for the higher hole size. The gas from the larger holes is more resistant to the liquid flow than that produced by the smaller holes. This increase slows the liquid more, hence the greater residence time and the greater hold-up.

CHAPTER 10

CONCLUSIONS

- Forcing the gas through the liquid on a sieve tray delays the onset of separation of the liquid. Higher weir loads than those on a tray with water-only are required to cause the separation of the liquid and to achieve the maximum circulation of 30% of the tray area. The entrance velocity is the crucial factor in determining the circulation on a tray. A larger area of circulation is encountered when the inlet velocity is increased.

- When separation occurs on a tray it has a significant effect on the height of clear liquid on the tray. The liquid in the side segments of the tray is either moving slower than the bulk flow due to an adverse pressure gradient, has a longer flow path length or is circulating. All these factors give rise to a greater hold-up of liquid on these side sections. This greater hold-up allows the liquid to approach the wet bulb temperature of the air. The effect this has is to reduce the point efficiency in these sections and this in turn reduces the tray efficiency. From these findings it has been shown that the flow pattern has a significant effect on the efficiency of a tray.

- The diameter of the holes on the tray has a number of effects on the operation of the tray. The regime that the tray operates under is greatly influenced by the hole size. Most correlations of the transition rely on the height of clear liquid divided by the hole diameter. From this it can be predicted that the spray regime only occurs with low clear liquid heights, high gas velocities or large hole diameters. The data that has been collected in this experimental work bear this out.

- The circulation on the tray is another factor that is affected by the hole diameter. As with the earlier work on a 1.2 m diameter tray (Porter et al., 1987) the area of circulation at a given weir load is reduced by the increase in hole size. In this work, the 12.7 mm diameter holes give the least circulation for any weir load where circulation is occurring and is below the maximum limit.

- The maximum area that can be covered by circulations on a tray with a weir length of 0.6 times the diameter is approximately 30 %. This corresponds to the area of the side segments of the tray and is a physical property set by the tray design. It is envisaged that the area of circulation on trays with different geometries will differ, but the maximum area of circulation will still correspond to the area of the side segments.

- Jetting onto the tray is a problem at low inlet gaps and high weir loads. The hole size seems to affect this by reducing the distance the jet travels onto the tray with an increase in the hole diameter. This can be attributed to the liquid being slowed quicker by the greater momentum of the bubbles or jets emanating from the larger holes. The liquid therefore undergoes a hydraulic jump earlier.

- The hole size affects the tray efficiency in two ways. Smaller holes give rise to bubbles or jets with a larger surface area to volume ratio. This effectively means that more of the gas is contacting the liquid. With higher hole diameters more of the gas is by-passing the liquid. The second effect is due to the circulation produced. As the smaller hole tray gives rise to a greater degree of circulation, this can have a detrimental effect on the tray efficiency by allowing a large proportion of the gas to pass the liquid relatively unchanged. The liquid in the circulating regions approaches equilibrium with the gas passing through it and is not replenished. There is then little change to either the gas or the liquid and this results in a decrease in the tray efficiency. This effect can overcome the positive effects of the smaller hole size and result in the larger hole size having a greater tray efficiency.

- With a rectangular tray the bi-phase is travelling in plug flow. For this situation it can be seen that the hole diameter affects the height of clear liquid on the tray, the larger the hole size, the larger the clear liquid height. This means that practically there is more liquid held-up on a tray with large holes compared to one with smaller holes. The gradient produced on the outlet half of the rectangular tray is very small and generally in the positive direction, with the highest liquid nearest the inlet. The only exception to this is when the jet from the inlet encroaches into the outlet section.

- The larger hole diameters give a lower point efficiency due to the increase in the gas by-passing as explained above. With the rectangular tray there are no circulating areas and therefore the detrimental effect this can have on the efficiency does not occur.

- Liquid leaving a tray with large holes is generally colder than that leaving a tray with smaller holes. This is down to the increased residence time of the liquid on the larger hole tray due to the greater liquid hold-up.

- The effect that hole size has on the flow across the tray appears to be caused by the resistance offered by the gas. The momentum of the gas from a large hole tray is greater per hole than for the smaller hole and appears to offer a greater resistance to the liquid flow. This leads to the liquid slowing down faster and evidence of this is the position of the hydraulic jump. The hydraulic jump is closer to the inlet for the larger hole trays. The jump occurs when the liquid has slowed sufficiently and therefore this shows that the liquid on the larger hole trays is slowed quicker due to the increased resistance.

- The eddy diffusivity on a sieve tray appears to be related to the hole size by the resistance of the gas to the liquid flow. Larger holes appear to produce gas jets or bubbles with a higher resistance to the liquid flow. This leads to more liquid being 'splashed' in the direction opposite to the bulk flow than for a smaller hole. It appears that the eddy diffusivity is not equal in all directions as has been thought.

10.1 Future Work

The main area for future research is into improving the understanding of the subject of open channel two-phase flow. Two-phase flow in a closed pipeline is fairly well understood and has been modelled successfully using a number of approaches. Less is understood about the flow of a two-phase mixture through an open channel. Experiments need to be designed and undertaken to determine the underlying principles of this branch of fluid mechanics.

The development of models that work from first principles is necessary to achieve a leap forward in the design of sieve trays. This would allow the identification of the flow pattern and regime from simple data on the flow rates and geometry of the tray. This would be an invaluable aid to the tray designer and would help to predict the flow pattern on the tray. In turn this type of model would allow designers to avoid 'bad' designs and if necessary, produce better ways of correcting uneven flow distribution.

Until such models are created and used freely a major area of experimental work that can be exploited is the testing and designing of flow straighteners. These are invariably corrective measures but they may allow the tray to operate efficiently over a wider range of flow rates. Due to the complexity of the mechanisms that are occurring with straightening devices, they are usually empirical in design and may only 'straighten' the flow for a certain combination of flows. Even with this restriction the short term future of efficient distillation may be in the application of flow correction either by way of a straightening device or a flow control tray.

NOMENCLATURE

A_b	Bubbling area of tray	[m^2]
A_D	Area of downcomer	[m^2]
b	Constant in equilibrium lines	[-]
C	Constant in eqn. 2.29	[-]
C_d	Discharge coefficient	[-]
CF	Capacity Factor	[m/s]
D	Tray diameter	[m]
D_e	Eddy diffusivity	[m^2/s]
D_G	Diffusivity of gas	[m^2/s]
D_L	Diffusivity of liquid	[m^2/s]
D_V	Diffusivity of vapour	[m^2/s]
d_h	Hole diameter	[m]
E_{ML}	Murphree tray efficiency, based on liquid phase	[-]
E_{MV}	Murphree tray efficiency, based on vapour phase	[-]
E_{OG}	Murphree point efficiency, based on vapour	[-]
F	Flooding factor in tray design	[-]
FF	Fractional approach to flooding	[-]
F_S	Superficial F factor	[$kg^{0.5}/m^{0.5}s$]
F_V	Column 'F' factor = $u_a\rho_V^{0.5}$	[$kg^{0.5}/m^{0.5}s$]
g	Acceleration due to gravity	[m/s^2]
G	Total vapour mass flow rate	[kg/s]
G'	Vapour mass flow rate	[kg/s]
h_{cl}	Height of clear liquid	[m of H_2O]
h_{DT}	Dry pressure drop of tray	[m of H_2O]
h_f	Height of froth	[m]
H_n	Enthalpy of air above tray n	[kJ/kmol]
h_{ow}	Height of outlet weir	[m]
h_R	Residual pressure drop of tray	[m of H_2O]

H_{Tout}	Enthalpy of saturated air in equilibrium with water	[kJ/kmol]
h_W	Height of outlet weir	[m]
h_{WT}	Wet tray pressure drop	[m of H_2O]
k	Constant in eqn. 6.3	[-]
L	Total liquid mass flow rate	[kg/s]
L'	Liquid mass flow rate	[kg/s]
L_P	Volumetric flow rate across plate divided by average plate width	[m^3/m.s]
M_G	Gas mass flow rate	[kg/s]
M_L	Liquid mass flow rate	[kg/s]
m	Gradient of equilibrium line in mass transfer	[-]
m	Gradient of saturation enthalpy line in heat transfer	[-]
N_G	Number of gas-film transfer units	[-]
N_L	Number of liquid-film transfer units	[-]
N_{OG}	Number of overall gas-phase transfer units	[-]
p	Pressure	[N/m^2]
Q_G	Volumetric flow rate of gas	[m^3/s]
Q_L	Volumetric flow rate of liquid	[m^3/s]
T.S.	Tray spacing	[m]
t_G	Gas contact time	[s]
t_L	Liquid contact time	[s]
U_{DF}	Downcomer velocity	[m/s]
u_a	Vapour velocity based on active area	[m/s]
u_b	Bubble rise velocity	[m/s]
u_G	Mean vapour velocity through dispersion	[m/s]
u_h	Vapour hole velocity	[m/s]
u_S	Superficial vapour velocity based on bubbling area	[m/s]
V	Liquid mass flow rate	[kg/s]
V	Volumetric vapour flow rate (used in total flows chart)	[m^3/s]
W	Weir length	[m]
W_L	Total liquid mass flow rate	[kg/s]
x_n	Average composition of liquid leaving stage n	[kmol/kg]
x_{n+1}	Average composition of liquid leaving stage n+1	[kmol/kg]

x^*_n	Composition of liquid in equilibrium with vapour composition y_n	[kmol/kg]
y_n	Composition of vapour leaving stage n	[kmol/kg]
y_{n-1}	Composition of vapour leaving stage n-1	[kmol/kg]
y^*_n	Composition of vapour in equilibrium with liquid composition x_n	[kmol/kg]
Z	Lquid flow path length	[m]
Z_C	Liquid hold-up	[m]
Z_L	Length of liquid path	[m]

α_e	Effective liquid volume fraction	[-]
α	Relative volatility of a binary mixture	[-]
ε	Volume of gas per unit volume of two-phase dispersion (gas hold-up fraction)	[-]
ε_w	Value of ε in froth flowing over weir	[-]
λ	Ratio of gradient of equilibrium line to operating line	[-]
μ_V	Vapour viscosity	[kg/m.s]
ρ_F	Froth density	[kg/m^3]
ρ_L	Liquid density	[kg/m^3]
ρ_L'	Liquid density	[kmol/m^3]
ρ_V	Vapour density	[kg/m^3]
σ	Surface tension	[N/m]

REFERENCES

AIChE., 1958, Bubble Tray Design Manual, "Prediction of fractionation efficiency", AIChE J., New York.

Aleksandrov, A. and Vybronov, V.G., 1971, "Investigation of the hydrodynamic pattern of liquid flow on cross-flow trays", Teor. Osnovy. Kim. Tekh., **5**, (2), 339.

Ali, Q.H., 1984, "Gas Distribution in Shallow Large Diameter Packed Beds", Ph.D. Thesis, University of Aston in Birmingham, Birmingham, England.

Ani, C.C., 1988, "Flow Patterns, Performance and Scale-up of Distillation Trays", Ph.D. Thesis, University of Aston in Birmingham, Birmingham, England.

Ashley, M.J. and Haselden, G.G., 1970, "The calculation of plate efficiency under conditions of finite mixing in both phases in multiplate columns, and the potential advantage of parallel flow", Chem. Engng. Sci., **25**, 1665.

Bell, R.L., 1972a, "Experimental determination of residence time distributions on commercial scale distillation trays using a fibre optic technique", AIChE J., **18**, (3), 491.

Bell, R.L., 1972b, "Residence time and fluid mixing on commercial scale sieve trays", AIChE J., **18**, (3), 498.

Bell, R.L. and Solari, R.B., 1974, "Effect of non-uniform velocity fields and retrograde flow on distillation plate efficiency", AIChE J., **20**, (4), 688.

Bennett, D.L., Agrawal, R. and Cook, P.J., 1983, "New pressure drop correlation for sieve tray distillation columns", AIChE J., **29**, (3), 434.

Biddulph, M.W., 1975, "Multicomponent distillation simulation-distillation of air", AIChE J., **21**, (2), 327.

Biddulph, M.W. and Bultitude, D.P., 1990, "Flow characteristics of a small-hole sieve tray", AIChE J., **36**, (12), 1913.

Bradshaw, P., 1965, "A compact, null-reading, tilting U-tube micromanometer with a rigid liquid container", J. Sci. Instrum., **42**, 677.

Bruin, S. and Freije, A.D., 1974, "A simple liquid mixing model for distillation plates with stagnant zones", Trans. IChemE., **52**, 75.

Chambers, S., 1993, "Flow Patterns on Sieve Trays", Ph.D. Thesis, University of Aston in Birmingham, Birmingham, England.

Chan, H. and Fair, J.R., 1984, "Prediction of point efficiencies on sieve trays", Ind. Eng. Chem. Proc. Des. Dev., **23**, 814.

Colwell, C.J., 1979, "Clear liquid height and froth density on sieve trays", Ind. Eng. Chem. Proc. Des. Dev., **20**, (2), 298.

Danckwerts, P.V., 1953, "Continuous flow systems. Distribution of residence times", Chem. Engng Sci., **2**, 1.

De Goederen, C.W.J., 1965, "Distillation tray efficiency and interfacial area", Chem. Engng. Sci., **20**, 1115.

Enjugu, B.A., 1986, "Flow Patterns and Performance of Distillation Trays", Ph.D. Thesis, University of Aston in Birmingham, Birmingham, England.

Fair, J.R., 1961, "How to predict sieve tray performance and flooding", Petro. Chem. Engineer, **33**, (10), 45.

Fane, A.G. and Sawistowski, H., 1969 "Plate efficiencies in the foam and spray regimes of sieve-plate distillation", Inst. Chem. Engrs Symp. Series **No. 32**, p. 1:8.

Francis, J.B., 1883, "Lowell Hydraulic Experiments", 4th Edition, Van Nostrand Company, New York.

Gautreaux, M.F. and O'Connell, H.E., 1955, "Effect of length of liquid path on plate efficiency", Chem. Engng Prog., **51**, (5), 232.

Gerster, J.A., Hill, A.B., Hochgraf, N.N. and Robinson, D.G., 1958, "Tray efficiencies in distillation columns", Final Report, University of Delaware, AIChE., New York.

Gerster, J.A., Mizushina, T., Marks, T.N. and Catanach, A.W., 1955, "Plant performance of a 13 ft – diameter extractive distillation column", AIChE J., **1**, (4), 536.

Hausen, H., 1953, "A definition of exchange efficiency of rectifying plates for binary and ternary mixtures", Chem. Ing. Tech., **25**, 595.

Hine, C.J., 1990, "Effect of Liquid Flow Patterns on Distillation Trays", Ph.D. Thesis, University of Aston in Birmingham, Birmingham, England.

Ho, G.E., Muller, R.L. and Prince, R.G.H., 1969, "Characterisation of two-phase flow patterns in plate columns", IChemE. Symp. Series, **No. 32**, 2:10.

Hofhuis, P.A.M. and Zuiderweg, F.J., 1979, "Sieve plates: Dispersion density and flow regimes", Inst. Chem. Engrs Symp. Series **No. 56**, p. 2.2/1.

Holland, C.D., 1963, "Multicomponent Distillation", Prentice Hall, New York.

Jeronimo, M.A.da S. and Sawistowski, H., 1973, "Phase inversion correlation for sieve trays", Trans. IChemE., **51**, 265.

Kafarov, V.V., Shestopalov, V.V. and Komissarov, Y.A., 1979, "Vapour-liquid flow structure on bubbler plates", IChemE. Symp. Series, **No. 56**, 2.3/79.

Kirschbaum, E., 1934, "Efficiency of rectification and appropriate path for liquid flow", Forsch. Gebiete Ingenieur, **5**, 245.

Kirschbaum, E., 1948, "Distillation and Rectification:, Chemical Publishing Co., New York, 276.

Kouri, R.J. and Sohlo, J.J., 1985, "Effect of developing liquid flow patterns on distillation plate efficiency", Chem. Engng Res. Des., **63**, (2), 117.

Legg, R., 1986, "Energy Management Focus", Dec., (9), 2.

Lewis, W.K., 1936, "Rectification of binary mixtures", Ind. Engng Chem., **28**, (1), 399.

Lim, C.T., Porter, K.E. and Lockett, M.J., 1974, "The effect of liquid channelling on two pass distillation plate efficiency", Trans. IChemE., **52**, 193.

Lockett, M.J., 1986, "Distillation Tray Fundamentals", Cambridge University Press, Cambidge, England.

Lockett, M.J., 1981, "The froth to spray transition on sieve trays", Trans. Inst. Chem. Engrs, **59**, 26.

Lockett, M.J., Lim, C.T. and Porter, K.E., 1973, "The effect of liquid channelling on distillation column efficiency in the absence of vapour mixing", Trans. Inst. Chem. Engrs, **51**, 61.

Lockett, M.J., Porter, K.E. and Bassoon, K.S., 1975, "The effect of vapour mixing on distillation plate efficiency when liquid channelling occurs", Trans. IChemE., **53**, 125.

Lockett, M.J. and Safekourdi, A., 1976, "The effect of the liquid flow pattern on distillation plate efficiency", Chem. Engng J., **11**, 111.

Lockett, M.J., Spiller, G.T. and Porter, K.E., 1976, "The effect of the operating regime on entrainment from sieve trays", Trans. IChemE., **54**, 202.

Loon, R.E., Pinczewski, W.V. and Fell, C.J.D., 1973, "Dependence of the froth to spray transition on sieve tray design parameters", Trans. IChemE., **51**, 374.

Muller, R.L. and Prince, R.G.H., 1972, "Regimes of bubbling and jetting from submerged orifices", Chem. Engng Sci., **27**, 1583.

Murphree, E.V., 1925, "Rectifying column calculations", Ind. Engng. Chem., **17**, (7), 747.

Payne, G.J. and Prince, R.G.H., 1975, "The transition from jetting to bubbling at a submerged orifice", Trans. IChemE., **53**, 209.

Payne, G.J. and Prince, R.G.H., 1977, "The relationship between the froth and spray regimes, and the orifice processes occurring on perforated distillation plates", Trans. Inst. Chem. Engrs, **55**, 266.

Pinczewski, W.V. and Fell, C.J.D., 1972, "The transition from froth-to-spray regime on commercially loaded sieve trays", Trans. Inst. Chem. Engrs, **52**, 194.

Pinczewski, W.V. and Fell, C.J.D., 1977, "Droplet sizes on sieve plates operating in the spray regime", Trans. IChemE., **55**, 46.

Pinczewski, W.V., Yeo, H.K. and Fell, C.J.D., 1973, "Transition behaviour at submerged orifices", Chem. Engng Sci., **28**, 2261.

Porter, K.E., Davies, B., Enjugu, B.A. and Ani, C.C., 1987, "Investigating the effect of the liquid flow pattern on sieve tray performance by means of the water-cooling technique", IChemE. Symp. Series **No. 104**, 569.

Porter, K.E., Fletcher, J.P. and Walton, A.G., 1995, "A fluid mechanical model of the liquid flow pattern for predicting tray efficiency". In preparation.

Porter, K.E. and Jenkins, J.D., 1979, "The interrelationship between industrial practice and academic research in distillation and absorption", IChemE. Symp. Series, **No. 56**, 5.1/1.

Porter, K.E., Lockett, M.J. and Lim, C.T., 1972, "The effect of liquid channelling on distillation plate efficiency", Trans. IChemE., **50**, 91.

Porter, K.E., O'Donnell, K.A. and Latifipour, M., 1982, "The use of water-cooling to investigate flow pattern effects on tray efficiency", IChemE. Jubilee Symp. Series, **No. 73**, L33.

Porter, K.E., Safekourdi, A., and Lockett, M.J., 1977, "Plate efficiency in the spray regime", Trans. IChemE., **55**, 190.

Porter, K.E. and Wong, P.F.Y., 1969, "Transition from spray to bubbling on sieve plates", IChemE. Symp. Series **No. 32**, p. 2:22.

Porter, K.E., Yu, K.T., Chambers, S. and Zhang, M.Q., 1992, "Flow patterns and temperature profiles on a 2.44 m diameter sieve tray", IChemE. Symp. Series, **No. 128**, A257.

Prince, R.G.H., Jones, A.P. and Panic, R.J., 1979, "The froth spray transition", IChemE. Symp. Series, **No. 56**, p. 2.2/27.

Raper, J.A., Hai, N.T., Pinczewski, W.V. and Fell, C.J.D., 1979, "Mass transfer efficiency on simulated industrial sieve trays operating in the spray regime", IChemE. Symp. Series, **No. 56**, 4.1/1.

Raper, J.A., Hai, N.T., Pinczewski, W.V. and Fell, C.J.D., 1984, "Liquid passage on sieve trays operating in the spray regime", Chem. Engng Res. Des., **62**, (2), 111.

Rush, F.E.Jr., 1979, "Energy saving alternatives to conventional distillation", IChemE. Symp. Series, **No. 56**, 4.1/1.

Sakata, M. and Yanagi, T., 1979, "Performance of a commercial sieve tray", IChemE. Symp. Series **No. 56**, p. 3.2/21.

Smith, B.D., 1963, "Design of equilibrium stage processes", McGraw-Hill.

Sohlo, J.J., and Kinnunen, S., 1977, "Dispersion and flow phenomena on a sieve plate", Chem. Engng Sci., **55**, (2), 71.

Sohlo, J. and Kouri, R.J., 1982, "An analysis of enhanced transverse dispersion on distillation plates", Chem. Engng Sci., **37**, (2), 193.

Solari, R.B. and Bell, R.L., 1986, "Fluid flow patterns and velocity distribution on commercial scale sieve trays", AIChE. J., **32**, (4), 640.

Solari, R.B., Saez, E., D'Apollo, I. and Bellet, A., 1982, "Velocity distribution and liquid flow patterns on industrial sieve trays", Chem. Engng Comm. **13**, 369.

Standart, G., 1965, "Studies on distillation - V", Chem. Engng Sci., **20**, 611.

Stichlmair, J., 1978, "Bodenkolonne", Verlag Chemie.

Stichlmair, J. and Ulbrich, S., 1987, "Liquid channelling on trays and its effect on plate efficiency", IChemE. Symp. Series, **No. 104**, 555.

Stichlmair, J. and Weisshuhn, E., 1973, "Untersuchungen zum Bodenwirkungsgrad unter besonderer Berücksichtigung der Flüssigkeitsvermischung", Chem. Ing. Tech., **45**, (5), 242.

Stichlmair, J. and Ulbrich, S., 1985, "Effect of maldistribution on separation efficiency of large column plates", Chem. Ing. Tech., **57**, (5), 468.

Walton, A.G., 1995, "Computer Simulation of Liquid Flow Patterns on Distillation Trays", Ph.D. Thesis, University of Aston in Birmingham, Birmingham, England.

Wehner, J.F. and Wilhelm, R.H., 1956, "Boundary conditions of flow reactor", Chem. Engng Sci., **6**, 89.

Weiler, D.W., Bonnet, F.W. and Leavitt, F.W., 1971, "Slotted sieve trays", Chem. Engng Prog., **67**, (9), 86.

Weiler, D.W., Delnicki, W.V. and England, B.L., 1973, "Flow hydraulics of large diameter trays", Chem. Engng Prog., **69**, (10), 67.

Wong, P.F.Y., 1967, "Dispersion Regimes on Sieve Plates", Ph.D. Thesis, University of Birmingham, Birmingham, England.

Yu, K.T., Huang, J. and Gu, F., 1983, "Simulation and efficiency of large trays. Part I. Eddy diffusion model with non-uniform liquid velocity field", Selected Papers of J. Chem. Ind. and Engng (China), **2**, June, 12.

Yu, K.T., Huang, J. and Gu, F., 1983, "Simulation and efficiency of large trays. Part II. Two-dimensional fixed number mixing pool model", Selected Papers of J. Chem. Ind. and Engng (China), **2**, June, 21.

Yu, K.T., Huang, J., Li, J.L. and Song, H.H., 1990, "Two-dimensional flow and eddy diffusion on a sieve tray", Chem. Engng Sci., **45**, (9), 2901.

Yu, K.T., Huang, J. and Zhang, Z.T., 1982, "The residence time distributions and efficiencies of large trays", Proceedings of Joint Meeting of Chemical Engineering, Beijing, China, **2**, 425.

Yu, K.T., Huang, J. and Zhang, Z.T., 1986, "Residence time profile and plate efficiency for a large tray with single-pass or two-pass liquid flow", J. Chem. Ind. Engng (China), **2**, 151.

Yu, K.T., Li, J.L. and Huang, J., c. 1991, "Theoretical computation of liquid flow distribution on a sieve tray", Private communications.

Yu, K.T., Song, H.H. and Huang, J., 1991, "A three-dimensional non-equilibrium pool model for the simulation of a tray column", J. Chem. Ind. Engng (China), **42**, 653.

Zuiderweg, F.J., 1973, "Distillation-science and business", The Chem. Eng., (Sept.), 404.

Zuiderweg, F.J., 1982, "Sieve trays - a view on the state of the art", Chem. Engng Sci., 37, (10), 1441.

Zuiderweg, F.J., Hofhuis, P.A.M., and Kuzniar, J., 1984, "Flow regimes on sieve trays: the significance of the emulsion flow regime", Chem. Engng Res. Dev., **62**, 40.

APPENDIX 1

Source Code for the Collection of Temperature Data

This program is used for the collection of temperature data from the experimental rig. It is written in the FORTRAN 77 programming language and accesses a data-logger to collect the temperature values. The data are output to the screen and to data files. The files are used to produce the efficiency results along with the 2 and 3D plots.

```
      PROGRAM TEMPERATURE
C
C*****************************************************************
C     ASSIGNING VARIABLES AND DATA
C*****************************************************************
C
      LOGICAL*2  OPENGP,SENDCO,CLOSEG
      INTEGER*2  READDA,WRITED
      INTEGER*2  SIFC,UNL,UNT,LAD,TAD,SAD
C
      LOGICAL*2  NUM
      INTEGER*2  WRGE,RRGE,RGE,RTD8H,COMBUF,K
      INTEGER*2  J,I,IMON,MON,BUF(240),BUM,SECADD
      INTEGER*2  CHAN,BUFF(240),PRTINT(120),COUNT
      REAL  RES(120),TEMP(120),AVT(5),AVTE(5,120),SUM,HOLED
      REAL  A,B,C,AIRV,WEIRL,DEW,DIA,WEIR,HOW,GAP,FREE
      REAL  CTEMP(20,120),ACTEMP(120)
      CHARACTER*2  ALPHA,ANS
C
      DATA  SIFC,UNL,UNT / 128,63,95 /
      DATA  LAD,TAD,SAD / 32,64,96 /
      DATA  WRGE,RRGE / 0,4 /
C
      RTD8H=15
      RGE=RRGE
      IMON=1
      DO 10 J=1,25
        WRITE (*,100)
  100   FORMAT (4X,' ')
   10 CONTINUE
```

```
C
C*********************************************************************
C    OPENING OUTPUT FILES
C*********************************************************************
C
     OPEN (UNIT=15,FILE='TEMP.DAT',STATUS='UNKNOWN')
     OPEN (UNIT=16,FILE='CTEMP.DAT',STATUS='UNKNOWN')
C
C*********************************************************************
C    READING IN PRT CALIBRATION DATA
C*********************************************************************
C
     OPEN (UNIT=13,FILE='CAL.DAT',STATUS='UNKNOWN')
     DO 11 I=1,5
       READ (13,101) AVT(I)
  101   FORMAT(26X,F6.2)
       READ (13,102) ALPHA
  102   FORMAT(4X,A2)
       DO 12 J=1,120,8
         READ (13,103) (AVTE(I,K),K=J,(J+7))
  103     FORMAT(13X,8(2X,F6.2))
  12    CONTINUE
  11  CONTINUE
     CLOSE (UNIT=13)
C
C*********************************************************************
C    OPENING CONNECTION WITH DRIVERS
C*********************************************************************
C
     IF (.NOT.OPENGP()) THEN
       WRITE(*,200)
  200   FORMAT(10X,'OPENING ERROR')
       STOP
     END IF
C
C*********************************************************************
C    RESETTING ALL DEVICES CONNECTED TO BUS
C*********************************************************************
C
     COMBUF=SIFC
     NUM=SENDCO(COMBUF)
     IF (.NOT.NUM) THEN
       WRITE(*,201)
  201   FORMAT(10X,'SIGNAL INTERFACE CLEAR ERROR')
       STOP
     END IF
```

```
C
C*************************************************************************
C    DISENGAGING THE HSC
C*************************************************************************
C
     COMBUF=LAD+7
     NUM=SENDCO(COMBUF)
     IF (.NOT.NUM) THEN
       WRITE(*,202)
 202   FORMAT(10X,'LISTEN ADDRESS ERROR -- DISENGAGE')
       STOP
     END IF
     COMBUF=SAD+0
     NUM=SENDCO(COMBUF)
     IF (.NOT.NUM) THEN
       WRITE(*,203)
 203   FORMAT(10X,'LISTEN ADDRESS ERROR -- DISENGAGE')
       STOP
     END IF
     BUF(1)=0
     BUF(2)=0
     CALL INT2BY (BUF(1),2)
     BUM=WRITED(BUF(1),2)
     IF (BUM.NE.2) THEN
       WRITE(*,204)
 204   FORMAT(10X,'DATA TRANSFER ERROR -- DISENGAGE')
       STOP
     END IF
     COMBUF=UNL
     NUM=SENDCO(COMBUF)
     IF (.NOT.NUM) THEN
       WRITE(*,205)
 205   FORMAT(10X,'UNLISTEN ERROR -- DISENGAGE')
       STOP
     END IF
C
C*************************************************************************
C    SETTING THE RANGES OF ALL CHANNELS PLUS
C    RETURNING FLAG AT THE LAST CHANNEL
C*************************************************************************
C
     DO 13 SECADD=1,RTD8H
       DO 14 CHAN=0,7
         COMBUF=LAD+7
         NUM=SENDCO(COMBUF)
         IF (.NOT.NUM) THEN
           WRITE(*,206)
 206         FORMAT(10X,'LISTEN ADDRESS ERROR -- RANGES')
           STOP
```

```
        END IF
        COMBUF=SAD+SECADD
        NUM=SENDCO(COMBUF)
        IF (.NOT.NUM) THEN
          WRITE(*,207)
 207        FORMAT(10X,'LISTEN ADDRESS ERROR -- RANGES')
          STOP
        END IF
        BUF(1)=4*CHAN
        IF ((SECADD.EQ.RTD8H).AND.(CHAN.EQ.7)) THEN
          BUF(1)=BUF(1)+2
        END IF
        BUF(2)=RGE
        CALL INT2BY (BUF(1),2)
        BUM=WRITED(BUF(1),2)
        IF (BUM.NE.2) THEN
          WRITE(*,208)
 208        FORMAT(10X,'DATA TRANSFER ERROR -- RANGES')
          STOP
        END IF
        COMBUF=UNL
        NUM=SENDCO(COMBUF)
        IF (.NOT.NUM) THEN
          WRITE(*,209)
 209        FORMAT(10X,'UNLISTEN ERROR -- RANGES')
          STOP
        END IF
  14    CONTINUE
  13  CONTINUE
C
C*********************************************************************
C    SETTING BASIC UNITS OF THE HSC AND GIVING THE
C    NUMBER OF UNIT BETWEEN EACH CHANNEL
C*********************************************************************
C
    COMBUF=LAD+7
    NUM=SENDCO(COMBUF)
    IF (.NOT.NUM) THEN
      WRITE(*,210)
 210    FORMAT(10X,'LISTEN ADDRESS ERROR -- SETHSC')
      STOP
    END IF
    COMBUF=SAD+0
    NUM=SENDCO(COMBUF)
    IF (.NOT.NUM) THEN
      WRITE(*,211)
 211    FORMAT(10X,'LISTEN ADDRESS ERROR -- SETHSC')
      STOP
    END IF
```

```
      BUF(1)=4+8
      BUF(2)=1
      CALL INT2BY (BUF(1),2)
      BUM=WRITED(BUF(1),2)
      IF (BUM.NE.2) THEN
        WRITE(*,212)
 212    FORMAT(10X,'DATA TRANSFER ERROR -- SETHSC')
        STOP
      END IF
      COMBUF=UNL
      NUM=SENDCO(COMBUF)
      IF (.NOT.NUM) THEN
        WRITE(*,213)
 213    FORMAT(10X,'UNLISTEN ERROR -- SETHSC')
        STOP
      END IF
C
C*********************************************************************
C     SETTING TALK ADDRESS TO THE FIRST RTD8H
C*********************************************************************
C
 99   COMBUF=TAD+7
      NUM=SENDCO(COMBUF)
      IF (.NOT.NUM) THEN
        WRITE(*,214)
 214    FORMAT(10X,'LISTEN ADDRESS ERROR -- FIRSTRTD8H')
        STOP
      END IF
      COMBUF=SAD+1
      NUM=SENDCO(COMBUF)
      IF (.NOT.NUM) THEN
        WRITE(*,215)
 215    FORMAT(10X,'LISTEN ADDRESS ERROR -- FIRSTRTD8H')
        STOP
      END IF
C
C*********************************************************************
C     ENABLING THE GET COMMAND
C*********************************************************************
C
      COMBUF=8
      NUM=SENDCO(COMBUF)
      IF (.NOT.NUM) THEN
        WRITE(*,216)
 216    FORMAT(10X,'LISTEN ADDRESS ERROR -- ENABLE')
        STOP
      END IF
```

```
C
C*********************************************************************
C    READING IN TWO TIMES THE NUMBER OF CHANNELS OF DATA
C    BYTES, CONVERTING ALL DATA BYTES TO INTEGERS AND
C    REARRANGING DATA DUE TO THE HSC READING FROM CHANNEL
C    7 TO 0
C*********************************************************************
C
     BUM=READDA(BUF(1),(RTD8H*8*2))
     IF (BUM.NE.(RTD8H*8*2)) THEN
       WRITE(*,217)
 217   FORMAT(10X,'DATA TRANSFER ERROR -- READ DATA')
       STOP
     END IF
     COMBUF=UNT
     NUM=SENDCO(COMBUF)
     IF (.NOT.NUM) THEN
       WRITE(*,218)
 218   FORMAT(10X,'UNTALK ADDRESS ERROR -- READ DATA')
       STOP
     END IF
     CALL BYT2IN (BUF(1),(RTD8H*8*2))
     DO 15 I=1,(RTD8H*8*2),16
       DO 16 J=0,14,2
         BUFF(I+J)=BUF(I+14-J)
         BUFF(I+J+1)=BUF(I+14-J+1)
 16    CONTINUE
 15  CONTINUE
C
C*********************************************************************
C    CALCULATING RESISTANCES AND TEMPERATURES
C*********************************************************************
C
     DO 17 I=1,((RTD8H*8*2)-1),2
       COUNT=(I+1)/2
       PRTINT(COUNT)=((BUFF(I)*256)+BUFF(I+1))
       RES(COUNT)=((PRTINT(COUNT)*0.00625)+96.0)
       TEMP(COUNT)=((RES(COUNT)-100.0)*60.0/(119.40-96.09))
 17  CONTINUE
C
C*********************************************************************
C    HIGH AND LOW ERROR DETECTION AND TEMPERATURE
C    CONVERSION USING CALIBRATION DATA
C*********************************************************************
C
     DO 18 I=1,(RTD8H*8)
       IF (I.EQ.29) THEN
         CTEMP(IMON,I)=99.99
         GO TO 18
```

```
      ELSE IF (I.EQ.66) THEN
        CTEMP(IMON,I)=99.99
        GO TO 18
      ELSE IF (I.EQ.120) THEN
        CTEMP(IMON,I)=99.99
        GO TO 18
      END IF
      IF (TEMP(I).LT.-10.0) THEN
        CTEMP(IMON,I)=99.99
        GO TO 18
      ELSE IF (TEMP(I).GE.55.0) THEN
        CTEMP(IMON,I)=99.99
        GO TO 18
      ELSE IF (AVTE(1,I).EQ.99.99) THEN
        CTEMP(IMON,I)=99.99
        GO TO 18
      END IF
      IF (TEMP(I).GT.AVT(2)) THEN
        A=AVT(1)-AVT(2)
        B=AVTE(1,I)-AVTE(2,I)
        C=TEMP(I)-AVTE(2,I)
        CTEMP(IMON,I)=AVT(2)+(C*A/B)
      ELSE IF (TEMP(I).GT.AVT(3)) THEN
        A=AVT(2)-AVT(3)
        B=AVTE(2,I)-AVTE(3,I)
        C=TEMP(I)-AVTE(3,I)
        CTEMP(IMON,I)=AVT(3)+(C*A/B)
      ELSE IF (TEMP(I).GT.AVT(4)) THEN
        A=AVT(3)-AVT(4)
        B=AVTE(3,I)-AVTE(4,I)
        C=TEMP(I)-AVTE(4,I)
        CTEMP(IMON,I)=AVT(4)+(C*A/B)
      ELSE IF (TEMP(I).LE.AVT(4)) THEN
        A=AVT(4)-AVT(5)
        B=AVTE(4,I)-AVTE(5,I)
        C=TEMP(I)-AVTE(5,I)
        CTEMP(IMON,I)=AVT(5)+(C*A/B)
      END IF
   18 CONTINUE
C
C*****************************************************************
C     SUBROUTINE TO RETURN THE CURSOR TO
C     THE TOP LEFT OF THE SCREEN
C*****************************************************************
C
      CALL HOME
```

```
C
C*****************************************************************
C    OUTPUT TO RAW TEMPERATURE FILE - TEMP.DAT
C*****************************************************************
C
     WRITE(15,300) TEMP(21),TEMP(19),TEMP(18),TEMP(22),
    >TEMP(113)
     WRITE(15,301) TEMP(1),TEMP(29),TEMP(51),TEMP(50),
    >TEMP(116),TEMP(115),TEMP(114),TEMP(9)
     WRITE(15,302) TEMP(5),TEMP(2),TEMP(30),TEMP(52),
    >TEMP(49),TEMP(117),TEMP(120),TEMP(88),TEMP(10),
    >TEMP(14)
     WRITE(15,303) TEMP(8),TEMP(6),TEMP(3),TEMP(31),
    >TEMP(53),TEMP(24),TEMP(118),TEMP(87),TEMP(86),
    >TEMP(11),TEMP(15),TEMP(42)
     WRITE(15,303) TEMP(25),TEMP(7),TEMP(4),TEMP(32),
    >TEMP(55),TEMP(23),TEMP(119),TEMP(85),TEMP(84),
    >TEMP(12),TEMP(16),TEMP(43)
     WRITE(15,303) (TEMP(I),I=26,28),TEMP(97),TEMP(56),
    >TEMP(109),TEMP(89),TEMP(82),TEMP(83),TEMP(13),
    >TEMP(41),TEMP(44)
     WRITE(15,303) TEMP(59),TEMP(58),TEMP(57),TEMP(98),
    >TEMP(73),TEMP(54),TEMP(112),TEMP(81),
    >(TEMP(I),I=48,45,-1)
     WRITE(15,303) TEMP(37),TEMP(61),TEMP(36),TEMP(99),
    >TEMP(76),TEMP(75),TEMP(111),TEMP(66),TEMP(96),
    >TEMP(70),TEMP(90),TEMP(91)
     WRITE(15,303) TEMP(104),TEMP(64),TEMP(102),TEMP(74),
    >TEMP(77),TEMP(78),TEMP(65),TEMP(67),TEMP(69),
    >TEMP(94),TEMP(93),TEMP(92)
     WRITE(15,302) TEMP(95),TEMP(101),TEMP(33),TEMP(80),
    >TEMP(63),TEMP(71),TEMP(72),TEMP(106),TEMP(105),
    >TEMP(107)
     WRITE(15,301) TEMP(103),TEMP(100),TEMP(34),TEMP(35),
    >TEMP(39),TEMP(40),TEMP(110),TEMP(108)
     WRITE(15,304) TEMP(38)
     WRITE(15,305) TEMP(17),TEMP(20),TEMP(68),TEMP(79)
 300 FORMAT(43X,5(F6.2,4X))
 301 FORMAT(28X,8(F6.2,4X))
 302 FORMAT(18X,10(F6.2,4X))
 303 FORMAT(8X,12(F6.2,4X))
 304 FORMAT(63X,F6.2)
 305 FORMAT(19X,4(F6.2,4X))
C
C*****************************************************************
C    OUTPUT TO CALIBRATED TEMPERATURE FILE - CTEMP.DAT
C*****************************************************************
C
     WRITE(16,300) CTEMP(IMON,21),CTEMP(IMON,19),
```

```
>CTEMP(IMON,18),CTEMP(IMON,22),CTEMP(IMON,113)
 WRITE(16,301) CTEMP(IMON,1),CTEMP(IMON,29),
>CTEMP(IMON,51),CTEMP(IMON,50),CTEMP(IMON,116),
>CTEMP(IMON,115),CTEMP(IMON,114),CTEMP(IMON,9)
 WRITE(16,302) CTEMP(IMON,5),CTEMP(IMON,2),
>CTEMP(IMON,30),CTEMP(IMON,52),CTEMP(IMON,49),
>CTEMP(IMON,117),CTEMP(IMON,120),CTEMP(IMON,88),
>CTEMP(IMON,10),CTEMP(IMON,14)
 WRITE(16,303) CTEMP(IMON,8),CTEMP(IMON,6),
>CTEMP(IMON,3),CTEMP(IMON,31),CTEMP(IMON,53),
>CTEMP(IMON,24),CTEMP(IMON,118),CTEMP(IMON,87),
>CTEMP(IMON,86),CTEMP(IMON,11),CTEMP(IMON,15),
>CTEMP(IMON,42)
 WRITE(16,303) CTEMP(IMON,25),CTEMP(IMON,7),
>CTEMP(IMON,4),CTEMP(IMON,32),CTEMP(IMON,55),
>CTEMP(IMON,23),CTEMP(IMON,119),CTEMP(IMON,85),
>CTEMP(IMON,84),CTEMP(IMON,12),CTEMP(IMON,16),
>CTEMP(IMON,43)
 WRITE(16,303) (CTEMP(IMON,I),I=26,28),CTEMP(IMON,97),
>CTEMP(IMON,56),CTEMP(IMON,109),CTEMP(IMON,89),
>CTEMP(IMON,82),CTEMP(IMON,83),CTEMP(IMON,13),
>CTEMP(IMON,41),CTEMP(IMON,44)
 WRITE(16,303) CTEMP(IMON,59),CTEMP(IMON,58),
>CTEMP(IMON,57),CTEMP(IMON,98),CTEMP(IMON,73),
>CTEMP(IMON,54),CTEMP(IMON,112),CTEMP(IMON,81),
>(CTEMP(IMON,I),I=48,45,-1)
 WRITE(16,303) CTEMP(IMON,37),CTEMP(IMON,61),
>CTEMP(IMON,36),CTEMP(IMON,99),CTEMP(IMON,76),
>CTEMP(IMON,75),CTEMP(IMON,111),CTEMP(IMON,66),
>CTEMP(IMON,96),CTEMP(IMON,70),CTEMP(IMON,90),
>CTEMP(IMON,91)
 WRITE(16,303) CTEMP(IMON,104),CTEMP(IMON,64),
>CTEMP(IMON,102),CTEMP(IMON,74),CTEMP(IMON,77),
>CTEMP(IMON,78),CTEMP(IMON,65),CTEMP(IMON,67),
>CTEMP(IMON,69),CTEMP(IMON,94),CTEMP(IMON,93),
>CTEMP(IMON,92)
 WRITE(16,302) CTEMP(IMON,95),CTEMP(IMON,101),
>CTEMP(IMON,33),CTEMP(IMON,80),CTEMP(IMON,63),
>CTEMP(IMON,71),CTEMP(IMON,72),CTEMP(IMON,106),
>CTEMP(IMON,105),CTEMP(IMON,107)
 WRITE(16,301) CTEMP(IMON,103),CTEMP(IMON,100),
>CTEMP(IMON,34),CTEMP(IMON,35),CTEMP(IMON,39),
>CTEMP(IMON,40),CTEMP(IMON,110),CTEMP(IMON,108)
 WRITE(16,304) CTEMP(IMON,38)
 WRITE(16,305) CTEMP(IMON,17),CTEMP(IMON,20),CTEMP(IMON,68),
>CTEMP(IMON,79)
```

```
C
C*********************************************************************
C    OUTPUT TO SCREEN
C*********************************************************************
C
     WRITE(*,501) CTEMP(IMON,21),CTEMP(IMON,19),
    >CTEMP(IMON,18),CTEMP(IMON,22),CTEMP(IMON,113)
     WRITE(*,502) CTEMP(IMON,1),CTEMP(IMON,51),
    >CTEMP(IMON,115),CTEMP(IMON,9)
     WRITE(*,503) CTEMP(IMON,25),CTEMP(IMON,4),
    >CTEMP(IMON,55),CTEMP(IMON,85),CTEMP(IMON,12),
    >CTEMP(IMON,43)
     WRITE(*,503) CTEMP(IMON,59),CTEMP(IMON,57),
    >CTEMP(IMON,73),CTEMP(IMON,81),CTEMP(IMON,47),
    >CTEMP(IMON,45)
     WRITE(*,503) CTEMP(IMON,104),CTEMP(IMON,102),
    >CTEMP(IMON,77),CTEMP(IMON,67),CTEMP(IMON,94),
    >CTEMP(IMON,92)
     WRITE(*,502) CTEMP(IMON,103),CTEMP(IMON,34),
    >CTEMP(IMON,40),CTEMP(IMON,108)
     WRITE(*,504) CTEMP(IMON,38)
     WRITE(*,505) CTEMP(IMON,20)
  501 FORMAT (16X,5(F6.2,6X))
  502 FORMAT (22X,4(F6.2,6X))
  503 FORMAT (10X,6(F6.2,6X))
  504 FORMAT (40X,F6.2)
  505 FORMAT (19X,F6.2)
C
C*********************************************************************
C    NUMBER OF SCANS
C*********************************************************************
C
     MON=20
     IF (IMON.LT.MON) THEN
       IMON=IMON+1
       GO TO 99
     END IF
C
C*********************************************************************
C    AVERAGING OF THE 20 SETS OF DATA
C*********************************************************************
C
     DO 19 I=1,120
       SUM=0.0
       COUNT=0
       ACTEMP(I)=99.99
       DO 20 J=1,20
         IF (CTEMP(J,I).NE.99.99) THEN
           COUNT=COUNT+1
```

```
          SUM=SUM+CTEMP(J,I)
        END IF
 20    CONTINUE
       IF (COUNT.NE.0) THEN
         ACTEMP(I)=SUM/COUNT
       END IF
 19  CONTINUE
C
C*********************************************************************
C    SAVE RUN AND OPERATING PARAMETERS ?
C*********************************************************************
C
     WRITE (*,600)
  600 FORMAT (4X,' ')
     WRITE (*,601)
  601 FORMAT (4X,'DO YOU WISH TO RECORD THE RUN ? (Y OR N)')
     READ (*,602) ANS
  602 FORMAT (A1)
     IF ((ANS.EQ.'Y').OR.(ANS.EQ.'y')) THEN
C
C*********************************************************************
C    ENTERING DATA TO IDENTIFY RUN
C*********************************************************************
C
       WRITE (*,603)
  603   FORMAT (4X,'INPUT AIR VELOCITY ? (m/s)')
       READ(*,*) AIRV
       WRITE(*,604)
  604   FORMAT(4X,'INPUT WEIR LOAD ? (cm3/cm.s)')
       READ(*,*) WEIRL
       WRITE(*,605)
  605   FORMAT(10X,'INPUT DEW POINT ? (deg c)')
       READ(*,*) DEW
C
         WRITE(*,700)
  700   FORMAT(4X,'INPUT OUTLET WEIR HEIGHT ? (m)')
         READ(*,*) HOW
         WRITE(*,701)
  701   FORMAT(4X,'INPUT INLET GAP ? (m)')
         READ( *,*) GAP
       WRITE(*,702)
  702   FORMAT(4X,'INPUT HOLE DIAMETER ? (m)')
         READ(*,*) HOLED

       DIA=2.440
       WEIR=1.50
       FREE=10.0
C
       WRITE (*,600)
```

```
      WRITE (*,600)
      WRITE (*,600)
      WRITE (*,606) AIRV
      WRITE (*,607) WEIRL
      WRITE (*,608) DEW
      WRITE (*,600)
      WRITE (*,609) DIA
      WRITE (*,610) WEIR
      WRITE (*,611) FREE
      WRITE (*,612) HOW
      WRITE (*,613) GAP
      WRITE (*,614) HOLED
C
      WRITE (15,600)
      WRITE (15,600)
      WRITE (15,600)
      WRITE (15,606) AIRV
      WRITE (15,607) WEIRL
      WRITE (15,608) DEW
      WRITE (15,600)
      WRITE (15,609) DIA
      WRITE (15,610) WEIR
      WRITE (15,611) FREE
      WRITE (15,612) HOW
      WRITE (15,613) GAP
      WRITE (15,614) HOLED
C
      WRITE (16,600)
      WRITE (16,600)
      WRITE (16,600)
      WRITE (16,606) AIRV
      WRITE (16,607) WEIRL
      WRITE (16,608) DEW
      WRITE (16,600)
      WRITE (16,609) DIA
      WRITE (16,610) WEIR
      WRITE (16,611) FREE
      WRITE (16,612) HOW
      WRITE (16,613) GAP
      WRITE (16,614) HOLED
C
C*********************************************************************
C     OPENING, AND OUTPUTING, TO DATA FILE
C*********************************************************************
C
      OPEN (UNIT=17,FILE='ACTEMP.DAT',STATUS='UNKNOWN')
C
      WRITE (17,606) AIRV
      WRITE (17,607) WEIRL
```

```
      WRITE (17,608) DEW
      WRITE (17,600)
      WRITE (17,609) DIA
      WRITE (17,610) WEIR
      WRITE (17,611) FREE
      WRITE (17,612) HOW
      WRITE (17,613) GAP
      WRITE (17,614) HOLED
      WRITE (17,600)
      WRITE (17,600)
      WRITE(17,300)ACTEMP(21),ACTEMP(19),
     >ACTEMP(18),ACTEMP(22),ACTEMP(113)
      WRITE(17,301) ACTEMP(1),ACTEMP(29),
     >ACTEMP(51),ACTEMP(50),ACTEMP(116),
     >ACTEMP(115),ACTEMP(114),ACTEMP(9)
      WRITE(17,302) ACTEMP(5),ACTEMP(2),
     >ACTEMP(30),ACTEMP(52),ACTEMP(49),
     >ACTEMP(117),ACTEMP(120),ACTEMP(88),
     >ACTEMP(10),ACTEMP(14)
      WRITE(17,303) ACTEMP(8),ACTEMP(6),
     >ACTEMP(3),ACTEMP(31),ACTEMP(53),
     >ACTEMP(24),ACTEMP(118),ACTEMP(87),
     >ACTEMP(86),ACTEMP(11),ACTEMP(15),
     >ACTEMP(42)
      WRITE(17,303) ACTEMP(25),ACTEMP(7),
     >ACTEMP(4),ACTEMP(32),ACTEMP(55),
     >ACTEMP(23),ACTEMP(119),ACTEMP(85),
     >ACTEMP(84),ACTEMP(12),ACTEMP(16),
     >ACTEMP(43)
      WRITE(17,303) (ACTEMP(I),I=26,28),ACTEMP(97),
     >ACTEMP(56),ACTEMP(109),ACTEMP(89),
     >ACTEMP(82),ACTEMP(83),ACTEMP(13),
     >ACTEMP(41),ACTEMP(44)
      WRITE(17,303) ACTEMP(59),ACTEMP(58),
     >ACTEMP(57),ACTEMP(98),ACTEMP(73),
     >ACTEMP(54),ACTEMP(112),ACTEMP(81),
     >(ACTEMP(I),I=48,45,-1)
      WRITE(17,303) ACTEMP(37),ACTEMP(61),
     >ACTEMP(36),ACTEMP(99),ACTEMP(76),
     >ACTEMP(75),ACTEMP(111),ACTEMP(66),
     >ACTEMP(96),ACTEMP(70),ACTEMP(90),
     >ACTEMP(91)
      WRITE(17,303) ACTEMP(104),ACTEMP(64),
     >ACTEMP(102),ACTEMP(74),ACTEMP(77),
     >ACTEMP(78),ACTEMP(65),ACTEMP(67),
     >ACTEMP(69),ACTEMP(94),ACTEMP(93),ACTEMP(92)
      WRITE(17,302) ACTEMP(95),ACTEMP(101),
     >ACTEMP(33),ACTEMP(80),ACTEMP(63),
     >ACTEMP(71),ACTEMP(72),ACTEMP(106),
```

```
     >ACTEMP(105),ACTEMP(107)
       WRITE(17,301) ACTEMP(103),ACTEMP(100),
     >ACTEMP(34),ACTEMP(35),ACTEMP(39),
     >ACTEMP(40),ACTEMP(110),ACTEMP(108)
       WRITE(17,304) ACTEMP(38)
       WRITE(17,305) ACTEMP(17),ACTEMP(20),
     >ACTEMP(68),ACTEMP(79)
  606 FORMAT (4X,'AIR VELOCITY (m/s)    ',F5.3)
  607 FORMAT (4X,'WEIR LOAD (cm3/cm.s)  ',F5.1)
  608 FORMAT (4X,'DEW POINT (deg c)     ',F4.1)
  609 FORMAT (4X,'COLUMN DIAMETER (m)   ',F5.3)
  610 FORMAT (4X,'WEIR LENGTH (m)       ',F5.3)
  611 FORMAT (4X,'FREE AREA (%)         ',F4.1)
  612 FORMAT (4X,'OUTLET WEIR HEIGHT (m) ',F5.3)
  613 FORMAT (4X,'INLET GAP (m)         ',F5.3)
  614 FORMAT (4X,'HOLE DIAMETER (m)     ',F5.3)
     END IF
     CLOSE (UNIT=15)
     CLOSE (UNIT=16)
     CLOSE (UNIT=17)
C
C*********************************************************************
C    CLOSING CONNECTION WITH DRIVERS
C*********************************************************************
C
     IF (.NOT.CLOSEG()) THEN
       WRITE(*,219)
  219   FORMAT(10X,'CLOSING ERROR')
       STOP
     END IF
C
C*********************************************************************
C    STOP AND END
C*********************************************************************
C
     STOP
     END
C
C*********************************************************************
C    SUBROUTINE USED TO RETURN THE CURSOR
C    TO THE TOP LEFT OF THE SCREEN
C*********************************************************************
C
     SUBROUTINE HOME
     CHARACTER*4  STRING
     STRING='\x1B[;H'C
     PRINT*,STRING
     RETURN
     END
```

APPENDIX 2

Source Code for the Plotting of Temperature Profiles and the Co-ordinates of the PRTs on the Tray

The program listed below is written in FORTRAN 77 and is used to generate the two-dimensional temperature contour diagrams. Use is made of the UNIRAS suite of subroutines to plot the diagrams. The program reads the position of the platinum resistance thermometers (PRTs) contained in a separate file. A positional representation of the file is shown after the listing.

```
      PROGRAM TEMPERATURE
C
C   NOTE :   THIS VERSION OF THE PROGRAM REQUIRES A SEPARATE
C            FILE FOR THE PRT POSITIONS AND THE DATA OUTPUT FILE
C            FROM COLTEMP.FOR
C              REQUIRES i) PRTCOORD.DAT
C                       ii) DATA FILE WITH NAME OF USER'S CHOICE
C
C    2D PLOT
C*****************************************************************
C   ASSIGNING VARIABLES AND PLOTTING DATA
C*****************************************************************
C
      INTEGER  I,J,K,NUM,LENY(6),LENX(7),IPLANE(3),LENGTH(6)
      REAL  AIRV,WEIRL,DEW,DIA,WEIR,HOW,GAP,FREE,TDOWN,HOLED
      REAL  TEMPIN(5),TEMP(108),AIR(4),X(108),Y(108)
      REAL  XPOS(108),YPOS(108),TPOS(108),TR(108),ZCL(39)
      REAL  ZEST(24,20),XEDGE(44),YEDGE(44)
      CHARACTER*2  ALPHA
      CHARACTER*4  LABY(6),LABX(7)
      CHARACTER*21  TEXT(6)
      CHARACTER*15 FILEIN
C
      PARAMETER(JMEMFX=10000,JMEMSZ=JMEMFX+400)
      COMMON /UNIMEM/ IDUM1,MEMMAX,IDUM2,ITEM(JMEMSZ)
      MEMMAX=JMEMFX
C
      DATA  ZCL / 0.025,0.050,0.075,0.100,0.125,0.150,0.175
```

```
   $,0.200,0.225,0.250,0.275,0.300,0.325,0.350,0.375,0.400
   $,0.425,0.450,0.475,0.500,0.525,0.550,0.575,0.600,0.625
   $,0.650,0.675,0.700,0.725,0.750,0.775,0.800,0.825,0.850
   $,0.875,0.900,0.925,0.950,0.975 /
    DATA  LENY /6*-1/
    DATA  LENX /7*-1/
    DATA  LABY /'2000','1600','1200','800','400','0'/
    DATA  LABX /' ','800','400',' 0','-400','-800',' '/
    DATA  IPLANE /1,1,1/,LENGTH /0,16,0,21,0,16/
    DATA  TEXT /' ','WEIR LENGTH - mm',' '
   #,'FLOW PATH LENGTH - mm',' ','REDUCED TEMP'/
C
C*********************************************************************
C    ENTER DATA FILE NAME
C*********************************************************************
C
    WRITE (*,*) 'INPUT FILE NAME FOR DATA INPUT'
    READ (*,'(A15)') FILEIN
C
C*********************************************************************
C    COLUMN WALL DATA
C*********************************************************************
C
    RAD=1200
    HS=1925/20

    DO 1000 I=1,11
          YEDGE(I)=(1-I)*HS
          YEDGE(23-I)=YEDGE(I)
1000  CONTINUE
    DO 1100 I=1,10
          YEDGE(22+I)=I*HS
          YEDGE(43-I)=YEDGE(22+I)
1100  CONTINUE
    YEDGE(43)=YEDGE(1)
    YEDGE(44)=999.999
C
    DO 1200 I=1,11
          XEDGE(I)=-SQRT(RAD**2-YEDGE(I)**2)
          XEDGE(23-I)=-XEDGE(I)
1200  CONTINUE
    DO 1300 I=1,10
          XEDGE(I+22)=SQRT(RAD**2-YEDGE(I+22)**2)
          XEDGE(43-I)=-XEDGE(I+22)
1300  CONTINUE
    XEDGE(43)=XEDGE(1)
    XEDGE(44)=999.999
```

```
C
C*********************************************************************
C    PRT POSITIONS ON TRAY AND INLET DOWNCOMER
C*********************************************************************
C
     OPEN (UNIT=15,FILE='PRTCOORD.DAT',STATUS='OLD')
     DO 42 I=1,108
           READ (15,*) X(I),Y(I)
  42 CONTINUE
     CLOSE (UNIT=15)
C
C*********************************************************************
C    READING IN TEMPERATURE DATA
C*********************************************************************
C
     OPEN (UNIT=14,FILE=FILEIN,STATUS='OLD')
     READ (14,300) AIRV
     READ (14,301) WEIRL
     READ (14,301) DEW
     READ (14,302) ALPHA
     READ (14,300) DIA
     READ (14,300) WEIR
     READ (14,301) FREE
     READ (14,300) HOW
     READ (14,300) GAP
     READ (14,300) HOLED
     READ (14,302) ALPHA
     READ (14,302) ALPHA
     READ (14,303) (TEMPIN(I),I=1,5)
     READ (14,304) (TEMP(I),I=1,8)
     READ (14,305) (TEMP(I),I=9,18)
     READ (14,306) (TEMP(I),I=19,30)
     READ (14,306) (TEMP(I),I=31,42)
     READ (14,306) (TEMP(I),I=43,54)
     READ (14,306) (TEMP(I),I=55,66)
     READ (14,306) (TEMP(I),I=67,78)
     READ (14,306) (TEMP(I),I=79,90)
     READ (14,305) (TEMP(I),I=91,100)
     READ (14,304) (TEMP(I),I=101,108)
     READ (14,307) TDOWN
     READ (14,308) (AIR(I),I=1,4)
     CLOSE (UNIT=14)
C
 300 FORMAT (27X,F5.3)
 301 FORMAT (27X,F4.1)
 302 FORMAT (4X,A2)
 303 FORMAT (43X,5(F6.2,4X))
 304 FORMAT (28X,8(F6.2,4X))
 305 FORMAT (18X,10(F6.2,4X))
```

```
 306 FORMAT (8X,12(F6.2,4X))
 307 FORMAT (63X,F6.2)
 308 FORMAT (19X,4(F6.2,4X))
C
C*********************************************************************
C    SETTING UP IRREGULAR ARRAYS
C*********************************************************************
C
     NUM=0
     DO 12 I=1,108
        IF (TEMP(I).NE.99.99) THEN
          NUM=NUM+1
          XPOS(NUM)=X(I)
          YPOS(NUM)=Y(I)
          TPOS(NUM)=TEMP(I)
        END IF
 12  CONTINUE
C
C*********************************************************************
C    AVERAGING INLET WATER TEMPERATURE
C*********************************************************************
C
     WINT=DEW
     DO 13 I=1,5
        IF (TEMPIN(I).NE.99.99) THEN
          IF (TEMPIN(I).GT.WINT) THEN
            WINT=TEMPIN(I)
          END IF
        END IF
 13  CONTINUE
C
C*********************************************************************
C    WET BULB TEMPERATURE
C*********************************************************************
C
    TWB=DEW
C
C*********************************************************************
C    SETTING UP REDUCED TEMPERATURES
C*********************************************************************
C
    DO 14 I=1,NUM
       TR(I)=(TPOS(I)-TWB)/(WINT-TWB)
 14  CONTINUE
```

```
C
C*********************************************************************
C   ROUTINES TO COMMENCE PLOTTING
C*********************************************************************
C
      CALL GROUTE ('S HPOSTA4;E ')
      CALL GOPEN
      CALL RORIEN (2)
      CALL GLIMIT (-1200.0,1200.0,-1000.0,1000.0,0.0,1.0)
      CALL RUNDEF (999.999,9999)
      CALL GFAULT (XEDGE,YEDGE,44,0)
      CALL GINTPF (XPOS,YPOS,TR,NUM,ZEST,24,20)
      HFAC=118.0
      CALL GVPORT (50.0,(42.0+HFAC),80.0,80.0)
      CALL GWBOX (1.2,1.0,0.0)
      CALL RCLASS (ZCL,39,0)
      CALL GSMTH (-1)
      CALL GCONAA (-60,60)
      CALL GCONA (1.7,3,30.0,3)
      CALL GCNR2V (ZEST,24,20)
      CALL GSCALE
      CALL GWICOL  (0.4,1)
      CALL GVECT (XEDGE,YEDGE,44)
      CALL GSCAMM
      CALL RTXJUS (0,6)
      CALL RTXHEI (2.5)
      CALL RTX (-1,'Air Velocity',155.0,(105.0+HFAC))
      CALL RTXN (AIRV,3,155.0,(99.0+HFAC))
      CALL RTXC (-1,' m/s')
      CALL RTX (-1,'Weir Load',155.0,(91.0+HFAC))
      CALL RTX (-1,'Inlet Gap',155.0,(77.0+HFAC))
      CALL RTXN (GAP,3,155.0,(71.0+HFAC))
      CALL RTXC (-1,' m')
      CALL RTX (-1,'Outlet Weir',155.0,(63.0+HFAC))
      CALL RTXN (HOW,3,155.0,(57.0+HFAC))
      CALL RTXC (-1,' m')
      CALL RTX (-1,'Hole Diameter',155.0,(49.0+HFAC))
      CALL RTXN (HOLED,3,155.0,(43.0+HFAC))
      CALL RTXC (-1,' m')
      CALL RTXNBO (8,'T')
      CALL RTXN (WEIRL,3,155.0,(85.0+HFAC))
      CALL RTXC (-1,' cm3/cm.s')
C
      CALL GSCALE
      CALL RUXLOP (1)
      CALL RUXSTI (7)
      CALL RUXDIS (1,1,9999)
      CALL RUXDIS (2,1,9999)
      CALL RUXDIS (3,1,9999)
```

```
      CALL RUXDIS (4,1,9999)
      CALL RUXDIS (6,1,9999)
      CALL RUXDIS (7,0,9999)
      CALL RUXDIS (8,0,9999)
      CALL RUXTEX (6,-1,'FLOW PATH LENGTH - mm'
     #,999.999,999.999,2.4)
      CALL RUXIS (2,-1200.0,2.3,1,LENY,LABY,6)
      CALL RUXTEA (4,9999,9999,999.999,9999,9999,-90.0)
      CALL RUXTEX (6,-1,'FLOW PATH LENGTH - mm'
     #,999.999,999.999,2.4)
      CALL RUXIS (2,1200.0,2.3,2,LENY,LABY,6)
      CALL RUXTEA (4,9999,9999,999.999,9999,9999,0.0)
      CALL RUXTEX (6,-1,'OUTLET WEIR - mm'
     #,999.999,999.999,2.5)
      CALL RUXIS (1,-1000.0,2.3,1,LENX,LABX,7)
      CALL RUXTEX (6,-1,'INLET DOWNCOMER - mm'
     #,999.999,999.999,2.5)
      CALL RUXIS (1,1000.0,2.3,2,LENX,LABX,7)
C
C*********************************************************************
C     SECOND 2D PLOT
C*********************************************************************
C     COLUMN WALL DATA
C*********************************************************************
C
      RAD=1200
      HS=1925/20

      DO 1098 I=1,11
            YEDGE(I)=(1-I)*HS
            YEDGE(23-I)=YEDGE(I)
1098  CONTINUE
      DO 1198 I=1,10
            YEDGE(22+I)=I*HS
            YEDGE(43-I)=YEDGE(22+I)
1198  CONTINUE
      YEDGE(43)=YEDGE(1)
      YEDGE(44)=999.999
C
      DO 1298 I=1,11
            XEDGE(I)=-SQRT(RAD**2-YEDGE(I)**2)
            XEDGE(23-I)=-XEDGE(I)
1298  CONTINUE
      DO 1398 I=1,10
            XEDGE(I+22)=SQRT(RAD**2-YEDGE(I+22)**2)
            XEDGE(43-I)=-XEDGE(I+22)
1398  CONTINUE
      XEDGE(43)=XEDGE(1)
      XEDGE(44)=999.999
```

```
C
C*********************************************************************
C    PRT POSITIONS ON TRAY AND INLET DOWNCOMER
C*********************************************************************
C
     OPEN (UNIT=15,FILE='PRTCOORD.DAT',STATUS='OLD')
     DO 62 I=1,108
          READ (15,*) X(I),Y(I)
  62 CONTINUE
     CLOSE (UNIT=15)
C
C*********************************************************************
C    READING IN TEMPERATURE DATA
C*********************************************************************
C
     WRITE(*,*)'INPUT FILENAME FOR SECOND PLOT'
     READ(*,'(A15)')FILEIN
     OPEN (UNIT=14,FILE=FILEIN,STATUS='OLD')
     READ (14,300) AIRV
     READ (14,301) WEIRL
     READ (14,301) DEW
     READ (14,302) ALPHA
     READ (14,300) DIA
     READ (14,300) WEIR
     READ (14,301) FREE
     READ (14,300) HOW
     READ (14,300) GAP
     READ (14,300) HOLED
     READ (14,302) ALPHA
     READ (14,302) ALPHA
     READ (14,303) (TEMPIN(I),I=1,5)
     READ (14,304) (TEMP(I),I=1,8)
     READ (14,305) (TEMP(I),I=9,18)
     READ (14,306) (TEMP(I),I=19,30)
     READ (14,306) (TEMP(I),I=31,42)
     READ (14,306) (TEMP(I),I=43,54)
     READ (14,306) (TEMP(I),I=55,66)
     READ (14,306) (TEMP(I),I=67,78)
     READ (14,306) (TEMP(I),I=79,90)
     READ (14,305) (TEMP(I),I=91,100)
     READ (14,304) (TEMP(I),I=101,108)
     READ (14,307) TDOWN
     READ (14,308) (AIR(I),I=1,4)
     CLOSE (UNIT=14)
```

```
C
C*********************************************************************
C    SETTING UP IRREGULAR ARRAYS
C*********************************************************************
C
     NUM=0
     DO 20 I=1,108
          IF (TEMP(I).NE.99.99) THEN
            NUM=NUM+1
            XPOS(NUM)=X(I)
            YPOS(NUM)=Y(I)
            TPOS(NUM)=TEMP(I)
          END IF
 20  CONTINUE
C
C*********************************************************************
C    AVERAGING INLET WATER TEMPERATURE
C*********************************************************************
C
     WINT=DEW
     DO 21 I=1,5
          IF (TEMPIN(I).NE.99.99) THEN
            IF (TEMPIN(I).GT.WINT) THEN
              WINT=TEMPIN(I)
            END IF
          END IF
 21  CONTINUE
C
C*********************************************************************
C    WET BULB TEMPERATURE
C*********************************************************************
C
     TWB=DEW
C
C*********************************************************************
C    SETTING UP REDUCED TEMPERATURES
C*********************************************************************
C
     DO 22 I=1,NUM
          TR(I)=(TPOS(I)-TWB)/(WINT-TWB)
 22  CONTINUE
C
C*********************************************************************
C    ROUTINES TO COMMENCE PLOTTING
C*********************************************************************
C
     CALL GRESET
     CALL RORIEN (2)
     CALL GLIMIT (-1200.0,1200.0,-1000.0,1000.0,0.0,1.0)
```

```
      CALL RUNDEF (999.999,9999)
      CALL GFAULT (XEDGE,YEDGE,44,0)
      CALL GINTPF (XPOS,YPOS,TR,NUM,ZEST,24,20)
      HFAC=0.0
      CALL GVPORT (50.0,(42.0+HFAC),80.0,80.0)
      CALL GWBOX (1.2,1.0,0.0)
      CALL RCLASS (ZCL,39,0)
      CALL GSMTH (-1)
      CALL GCONAA (-60,60)
      CALL GCONA (1.7,3,30.0,3)
      CALL GCNR2V (ZEST,24,20)
      CALL GSCALE
      CALL GWICOL  (0.4,1)
      CALL GVECT (XEDGE,YEDGE,44)
      CALL GSCAMM
      CALL RTXJUS (0,6)
      CALL RTXHEI (2.5)
      CALL RTX (-1,'Air Velocity',155.0,(105.0+HFAC))
      CALL RTXN (AIRV,3,155.0,(99.0+HFAC))
      CALL RTXC (-1,' m/s')
      CALL RTX (-1,'Weir Load',155.0,(91.0+HFAC))
      CALL RTX (-1,'Inlet Gap',155.0,(77.0+HFAC))
      CALL RTXN (GAP,3,155.0,(71.0+HFAC))
      CALL RTXC (-1,' m')
      CALL RTX (-1,'Outlet Weir',155.0,(63.0+HFAC))
      CALL RTXN (HOW,3,155.0,(57.0+HFAC))
      CALL RTXC (-1,' m')
      CALL RTX (-1,'Hole Diameter',155.0,(49.0+HFAC))
      CALL RTXN (HOLED,3,155.0,(43.0+HFAC))
      CALL RTXC (-1,' m')
      CALL RTXNBO (8,'T')
      CALL RTXN (WEIRL,3,155.0,(85.0+HFAC))
      CALL RTXC (-1,' cm3/cm.s')
C
      CALL GSCALE
      CALL RUXLOP (1)
      CALL RUXSTI (7)
      CALL RUXDIS (1,1,9999)
      CALL RUXDIS (2,1,9999)
      CALL RUXDIS (3,1,9999)
      CALL RUXDIS (4,1,9999)
      CALL RUXDIS (6,1,9999)
      CALL RUXDIS (7,0,9999)
      CALL RUXDIS (8,0,9999)
      CALL RUXTEX (6,-1,'FLOW PATH LENGTH - mm'
     #,999.999,999.999,2.4)
      CALL RUXIS (2,-1200.0,2.3,1,LENY,LABY,6)
      CALL RUXTEA (4,9999,9999,999.999,9999,9999,-90.0)
      CALL RUXTEX (6,-1,'FLOW PATH LENGTH - mm'
```


```
#,999.999,999.999,2.4)
 CALL RUXIS (2,1200.0,2.3,2,LENY,LABY,6)
 CALL RUXTEA (4,9999,9999,999.999,9999,9999,0.0)
 CALL RUXTEX (6,-1,'OUTLET WEIR - mm'
#,999.999,999.999,2.5)
 CALL RUXIS (1,-1000.0,2.3,1,LENX,LABX,7)
 CALL RUXTEX (6,-1,'INLET DOWNCOMER - mm'
#,999.999,999.999,2.5)
 CALL RUXIS (1,1000.0,2.3,2,LENX,LABX,7)
 CALL GCLOSE
 END
```

Co-ordinates of the PRTs on the Tray

One-hundred and eight platinum resistance thermometers (PRTs) are employed to measure the temperature across the tray. The co-ordinates of their positions on the tray are given below in a schematic set-up. The centre of the tray is designated (0,0) for the purposes of the plotting programme listed above.

Tray Inlet

		(-700,900)	(-500,900)	(-300,900)	(-100,900)	(100,900)	(300,900)	(500,900)	(700,900)		
	(-900,700)	(-700,700)	(-500,700)	(-300,700)	(-100,700)	(100,700)	(300,700)	(500,700)	(700,700)	(900,700)	
(-1000,500)	(-900,500)	(-700,500)	(-500,500)	(-300,500)	(-100,500)	(100,500)	(300,500)	(500,500)	(700,500)	(900,500)	(1000,500)
(-1100,300)	(-900,300)	(-700,300)	(-500,300)	(-300,300)	(-100,300)	(100,300)	(300,300)	(500,300)	(700,300)	(900,300)	(1100,300)
(-1150,100)	(-900,100)	(-700,100)	(-500,100)	(-300,100)	(-100,100)	(100,100)	(300,100)	(500,100)	(700,100)	(900,100)	(1150,100)
(-1150,-100)	(-900,-100)	(-700,-100)	(-500,-100)	(-300,-100)	(-100,-100)	(100,-100)	(300,-100)	(500,-100)	(700,-100)	(900,-100)	(1150,-100)
(-1100,-300)	(-900,-300)	(-700,-300)	(-500,-300)	(-300,-300)	(-100,-300)	(100,-300)	(300,-300)	(500,-300)	(700,-300)	(900,-300)	(1100,-300)
(-1000,-500)	(-900,-500)	(-700,-500)	(-500,-500)	(-300,-500)	(-100,-500)	(100,-500)	(300,-500)	(500,-500)	(700,-500)	(900,-500)	(1000,-500)
	(-900,-700)	(-700,-700)	(-500,-700)	(-300,-700)	(-100,-700)	(100,-700)	(300,-700)	(500,-700)	(700,-700)	(900,-700)	
		(-700,-900)	(-500,-900)	(-300,-900)	(-100,-900)	(100,-900)	(300,-900)	(500,-900)	(700,-900)		

Tray Outlet

APPENDIX 3

Source Code for the Calculation of Efficiencies

This section contains the program used for the calculation of the point and tray efficiencies. The language used is FORTRAN 77. The program requires the temperature data file from the experimental run.

```
PROGRAM EFFICIENCY
C
C*********************************************************************
C   ASSIGNING VARIABLES
C*********************************************************************
C
    INTEGER*2  I,J,K,NUM
    REAL  PAIR,PWATER,PI,CP,AIRV,WEIRL,DEW,DIA,WEIR,HOLED
    REAL  FREE,HOW,GAP,TEMPIN(5),TEMP(108),AIR(4),TDOWN
    REAL  T(108),SUM,TIN,TOUT,DRY,MG,ML,HUMIN,HIN,HOUT,HLOSS
    REAL  HUMEQ,HOUTEQ,EMV,HUM(108),H(108),EOG,RATIO,CF
    REAL  EOG1(108),SUMH2,H2(108)
    CHARACTER*2  ALPHA
C
    PAIR=1.22
    PWATER=1000.0
    PI=3.141593
    CP=4.18
C
C*********************************************************************
C   OPENING THE DATA OUTPUT FILE
C*********************************************************************
C
    OPEN (UNIT=15,FILE='EFF.DAT',STATUS='NEW')
C
C*********************************************************************
C   READING IN TEMPERATURE DATA
C*********************************************************************
C
      OPEN (UNIT=14,FILE='FOR014.DAT',STATUS='OLD')
      READ (14,300) AIRV
      READ (14,301) WEIRL
      READ (14,302) DEW
```

```
      READ (14,303) ALPHA
      READ (14,304) DIA
      READ (14,305) WEIR
      READ (14,306) FREE
      READ (14,307) HOW
      READ (14,308) GAP
      READ (14,300) HOLED
      READ (14,303) ALPHA
      READ (14,303) ALPHA
      READ (14,309) (TEMPIN(I),I=1,5)
      READ (14,310) (TEMP(I),I=1,8)
      READ (14,311) (TEMP(I),I=9,18)
      READ (14,312) (TEMP(I),I=19,30)
      READ (14,312) (TEMP(I),I=31,42)
      READ (14,312) (TEMP(I),I=43,54)
      READ (14,312) (TEMP(I),I=55,66)
      READ (14,312) (TEMP(I),I=67,78)
      READ (14,312) (TEMP(I),I=79,90)
      READ (14,311) (TEMP(I),I=91,100)
      READ (14,310) (TEMP(I),I=101,108)
      READ (14,313) TDOWN
      READ (14,314) (AIR(I),I=1,3)
      CLOSE (UNIT=14)
C
 300   FORMAT (27X,F3.1)
 301   FORMAT (27X,F4.0)
 302   FORMAT (27X,F4.1)
 303   FORMAT (4X,A2)
 304   FORMAT (27X,F5.3)
 305   FORMAT (27X,F5.3)
 306   FORMAT (27X,F4.1)
 307   FORMAT (27X,F5.3)
 308   FORMAT (27X,F5.3)
 309   FORMAT (43X,5(F6.2,4X))
 310   FORMAT (28X,8(F6.2,4X))
 311   FORMAT (18X,10(F6.2,4X))
 312   FORMAT (8X,12(F6.2,4X))
 313   FORMAT (63X,F6.2)
 314   FORMAT (10X,3(F6.2,4X))
C
C*********************************************************************
C    SCREENING OUT NULL TEMPERATURE VALUES
C*********************************************************************
C
    NUM=0
    DO 10 I=1,108
      IF (TEMP(I).NE.99.99) THEN
        NUM=NUM+1
        T(NUM)=TEMP(I)
```

```
      END IF
 10  CONTINUE
C
C*********************************************************************
C    AVERAGING INLET AND OUTLET MEASURED TEMPERATURES - °C
C*********************************************************************
C
     J=0
     SUM=0.0
     DO 11 I=1,5
       IF (TEMPIN(I).NE.99.99) THEN
         J=J+1
         SUM=SUM+TEMPIN(I)
         END IF
 11  CONTINUE
     TIN=SUM/J
     WRITE(15,400) TIN
C
     J=0
     SUM=0.0
     DO 12 I=101,108
       IF (TEMP(I).NE.99.99) THEN
         J=J+1
         SUM=SUM+TEMP(I)
       END IF
 12  CONTINUE
     TOUT=SUM/J
     WRITE(15,401) TOUT
     WRITE(15,402) TDOWN
     IF (TDOWN.NE.99.99) THEN
       IF (TDOWN.GT.TOUT) THEN
         TOUT=TDOWN
       END IF
     END IF
C
     J=0
     SUM=0.0
     DO 13 I=1,3
       IF (AIR(I).NE.99.99) THEN
         J=J+1
         SUM=SUM+AIR(I)
       END IF
 13  CONTINUE
     DRY=SUM/J
     WRITE(15,403) DRY
     WRITE(15,404) DEW

 400 FORMAT (4X,'TIN = ',F9.5)
 401 FORMAT (4X,'TOUT =',F9.5)
```

```
 402 FORMAT (4X,'TDOWN =',F9.5)
 403 FORMAT (4X,'DRY =',F9.5)
 404 FORMAT (4X,'DEW =',F9.5)
C
C*********************************************************************
C    CALCULATING MASS FLOWRATES - KG/S
C*********************************************************************
C
    MG=PAIR*AIRV*PI*(DIA**2)/4
    WRITE(15,405) MG
    ML=PWATER*WEIRL*WEIR/10000.0
    WRITE(15,406) ML

 405 FORMAT (4X,'MG =',F10.6)
 406 FORMAT (4X,'ML =',F10.6)
C
C*********************************************************************
C    CALCULATING INLET AIR HUMIDITY AND ENTHALPY
C    VIA SUBROUTINE
C*********************************************************************
C
    CALL PSYCHRO (DRY,DEW,HUMIN,HIN)
    WRITE(15,407) HUMIN
    WRITE(15,408) HIN
 407 FORMAT (4X,'HUMIN = ',E13.7)
 408 FORMAT (4X,'HIN = ',F9.5)
C
C*********************************************************************
C    OVERALL HEAT BALANCE TO GIVE HOUT
C*********************************************************************
C
    HOUT=((ML*CP/MG)*(TIN-TOUT))+HIN
    HLOSS =(ML*CP*(TIN-TOUT))

    WRITE(15,409) HLOSS
    WRITE(15,410) HOUT

 409 FORMAT (4X,'HEAT LOST FROM WATER = ',F9.4)
 410 FORMAT (4X,'HOUTAV = ',F9.5)
C
C*********************************************************************
C    CALCULATING TRAY EFFICIENCY VIA SUBROUTINE
C*********************************************************************
C
    CALL PSYCHRO (TOUT,TOUT,HUMEQ,HOUTEQ)
    WRITE(15,412) HUMEQ
    WRITE(15,413) HOUTEQ
    EMV=(HOUT-HIN)/(HOUTEQ-HIN)
    WRITE(15,414) EMV
```

```
 412 FORMAT (4X,'HUMEQ = ',E13.7)
 413 FORMAT (4X,'HOUTEQ = ',F9.4)
 414 FORMAT (4X,'EMV = ',F9.7)
C
C**********************************************************************
C    CALCULATING POINT EFFICIENCY VIA SUBROUTINE
C**********************************************************************
C
    SUM=0.0
    DO 14 I=1,NUM
      CALL PSYCHRO (T(I),T(I),HUM(I),H(I))
      WRITE(15,*) T(I),H(I)
      SUM=SUM+H(I)
 14  CONTINUE
    WRITE(15,*) SUM,NUM,SUM/NUM
    EOG=(ML*CP/MG)*(TIN-TOUT)*NUM/(SUM-(NUM*HIN))
    WRITE(15,415) EOG


 415 FORMAT (4X,'EOG = ',F9.7)
    SUMH2=0
    DO 15 I=1,NUM
      H2(I)=EOG*(H(I)-HIN)+HIN
      WRITE(15,*)H2(I)
      SUMH2=SUMH2+H2(I)
 15  CONTINUE
    CF=NUM*HOUT/SUMH2
    WRITE (15,*)SUMH2,SUMH2/NUM,HOUT,CF
    DO 16 I=1,NUM
      H2(I)=H2(I)*CF
      EOG1(I)=(H2(I)-HIN)/(H(I)-HIN)
      WRITE (15,*) H2(I),EOG1(I)
 16  CONTINUE

C
C**********************************************************************
C    CALCULATING EMV/EOG
C**********************************************************************
C
    RATIO=EMV/EOG
    WRITE(15,416) RATIO
 416 FORMAT (4X,'RATIO = ',F9.6)
    END
```

```
C
C*****************************************************************
C    SUBROUTINE TO CALCULATE AIR HUMIDITY AND ENTHALPY
C*****************************************************************
C
      SUBROUTINE PSYCHRO (TDB,TWB,HUM,ENTH)
      REAL  A,B,C,D,E,F,G,Z1,Z2,Z3,Z4,Z5
      REAL  TD1,TD2,M1,M2,C1,C2,C3,Y1,Y2
      REAL  LO,TWB,TDB,P0,PSS,HUM,ENTH
      A=-2948.997118
      B=-2.1836674
      C=-0.000150474
      D=-0.0303738468
      E=0.00042873
      F=4.76955
      G=25.83220018
      TD1=273.15
      TD2=273.16
      P0=101.325
      M1=18.01534
      M2=28.9645
      C1=0.000666
      C2=1.00568
      C3=1.84598
      LO=2500.84
      Z1=A/(TWB+TD1)
      Z2=B*LOG(TWB+TD1)
      Z3=C*(10**(D*(TWB-0.01)))
      Z4=E*(10**(F*(1.0-(TD2/(TWB+TD1)))))
      Z5=G
      PSS=10**(Z1+Z2+Z3+Z4+Z5)
      Y1=P0*C1*(TDB-TWB)
      HUM=(M1/M2)*(PSS-(1000.0*Y1))/((1000.0*P0)-PSS+(1000.0*Y1))
      ENTH=(C2*TDB)+(HUM*(LO+(C3*TDB)))
      RETURN
      END
```

APPENDIX 4

Source Code for the Plotting of Clear Liquid Height Profiles

The program listed below is used to generate three dimensional surface plots of the height of clear liquid. The language used is FORTRAN 77 and the program uses subroutines from the UNIRAS suite. The position of the manometer tappings are read from a data file giving the co-ordinates.

```
      PROGRAM HCLALL
C
C*********************************************************************
C     PROGRAM REQUIRES : CONFIG.DAT
C                        MANOM.DAT
C                        DATUM.DAT
C                        MCOORD.DAT
C     PROGRAM OUTPUT FILE : HCLOUT.DAT
C*********************************************************************
C     ASSIGNING VARIABLES AND DATA
C*********************************************************************
C
      INTEGER  I,J,IPLANE(3),LENGTH(6),NDATA
C
      REAL  XEDGE(17),YEDGE(17),X(32),Y(32),MHCL(12,32)
      REAL  AIRV(12),WEIRL(12),WTDP(12),CORDP(12)
      REAL  DAIRV(12),DWEIRL(12),DWTDP(12),DCORDP(12)
      REAL  DMHCL(12,32),XED(17),YED(17),XPOS(32),YPOS(32)
      REAL  HCL(12,32),CMHCL(12,32),DCMHCL(12,32)
      REAL  ZEST(25,21),HFAC,HEIGHT(32)
      REAL  INGAP,INWEIR,OUTWEIR,HOLEDIA
      CHARACTER*21  TEXT(6)
C
      DATA  IPLANE /1,1,1/,LENGTH /0,16,0,21,0,17/
      DATA  TEXT /' ','WEIR LENGTH - mm',' '
     #,'FLOW PATH LENGTH - mm',' ','CLEAR LIQUID - mm'/
```

```
C
C*********************************************************************
C    COLUMN WALL DATA
C*********************************************************************
C
     XEDGE(1)=999.999
     XEDGE(2)=-1200.0
     XEDGE(3)=-1150.0
     XEDGE(4)=-1050.0
     XEDGE(5)=-720.0
     XEDGE(6)=720.0
     XEDGE(7)=1050.0
     XEDGE(8)=1150.0
     XEDGE(9)=1200.0
     XEDGE(10)=1150.0
     XEDGE(11)=1050.0
     XEDGE(12)=720.0
     XEDGE(13)=-720.0
     XEDGE(14)=-1050.0
     XEDGE(15)=-1150.0
     XEDGE(16)=-1200.0
     XEDGE(17)=999.999
C
     YEDGE(1)=999.999
     YEDGE(2)=1000.0
     YEDGE(3)=600.0
     YEDGE(4)=350.0
     YEDGE(5)=0.0
     YEDGE(6)=0.0
     YEDGE(7)=350.0
     YEDGE(8)=600.0
     YEDGE(9)=1000.0
     YEDGE(10)=1400.0
     YEDGE(11)=1650.0
     YEDGE(12)=2000.0
     YEDGE(13)=2000.0
     YEDGE(14)=1650.0
     YEDGE(15)=1400.0
     YEDGE(16)=1000.0
     YEDGE(17)=999.999
C
C*********************************************************************
C    MANOMETER POSITIONS ON TRAY
C*********************************************************************
C
     OPEN(15,FILE='MCOORD.DAT',STATUS='OLD')
     DO 99 I=1,32
      READ(15,*) X(I),Y(I)
99  CONTINUE
```

```
      CLOSE(15)
C
C*********************************************************************
C     READING IN MEASURED MANOMETER DATA
C*********************************************************************
C
      OPEN(14,FILE='MANOM.DAT',STATUS='OLD')
      DO 11 I=1,100
        READ (14,500,END=999) AIRV(I),WEIRL(I)
 500  FORMAT (1X,F4.1,1X,F5.1)
        READ (14,501,END=999) WTDP(I),CORDP(I)
 501  FORMAT (1X,F4.1,1X,F4.1)
        READ (14,502,END=999) (MHCL(I,J),J=1,16)
 502  FORMAT (1X,16(F4.1,1X))
        READ (14,502,END=999) (MHCL(I,J),J=17,32)
  11 CONTINUE
 999 NDATA=I-1
      CLOSE (14)
C
C*********************************************************************
C     READING IN DATUM TUBE LEVELS
C*********************************************************************
C
      OPEN (UNIT=15,FILE='DATUM.DAT',STATUS='UNKNOWN')
      DO 12 I=1,NDATA
        READ (15,503) DAIRV(I)
 503  FORMAT (1X,F4.1)
        READ (15,501) DWTDP(I),DCORDP(I)
        READ (15,502) (DMHCL(I,J),J=1,16)
        READ (15,502) (DMHCL(I,J),J=17,32)
  12 CONTINUE
     CLOSE (UNIT=15)
C
C*********************************************************************
C  READ INLET GAP & WEIR, OUTLET GAP AND HOLE DIAMETER IN
C  METRES
C*********************************************************************
C
     OPEN (UNIT=15,FILE='CONFIG.DAT',STATUS='UNKNOWN')
     READ (15,*)INGAP,INWEIR,OUTWEIR,HOLEDIA
     CLOSE (15)
C
C*********************************************************************
C     PROCEDURE TO CALCULATE HCL VALUES
C*********************************************************************
C
     DO 19 I=1,NDATA
       DO 20 J=1,32
         CMHCL(I,J)=MHCL(I,J)-CORDP(I)
```

```
        DCMHCL(I,J)=DMHCL(I,J)-DCORDP(I)
        HCL(I,J)=10*(CMHCL(I,J)-DCMHCL(I,J))
 20   CONTINUE
 19  CONTINUE
C
C*********************************************************************
C    OUTPUT OF HCL DATA
C*********************************************************************
C
    OPEN(18,FILE='HCLOUT.DAT',STATUS='NEW')
C
      DO 21 I=1,NDATA
       WRITE (18,200) AIRV(I),WEIRL(I)
 200  FORMAT (15X,'AIRV = ',F3.1,5X,'WEIRL = ',F5.1)
       WRITE (18,201)
 201  FORMAT (2X,' ')
       WRITE (18,201)
       DO 299 J=1,32
        WRITE(18,*) J,HCL(I,J)
 299   CONTINUE

       WRITE (18,201)
       WRITE (18,201)
  21  CONTINUE
    CLOSE(18)
C
C*********************************************************************
C    READING IN DATA TO CONTROL PLOTTING
C*********************************************************************
C
     DO 22 I=1,NDATA,2
       W=WEIRL(I)
       A=AIRV(I)
       DO 23 K=1,17
         XED(K)=XEDGE(K)
         YED(K)=YEDGE(K)
  23   CONTINUE
       DO 24 J=1,32
         HEIGHT(J)=HCL(I,J)
         XPOS(J)=X(J)
         YPOS(J)=Y(J)
  24   CONTINUE
C
C*********************************************************************
C    ROUTINES TO COMMENCE PLOTTING
C*********************************************************************
C
       CALL GROUTE ('S HPOSTA4;E ')
       CALL GOPEN
```

```
CALL RORIEN (2)
CALL GLIMIT (-1200.0,1200.0,0.0,2000.0,0.0,50.0)
CALL RUNDEF (999.999,9999)
HFAC=118.0
CALL GVPORT (40.0,(42.0+HFAC),80.0,80.0)
CALL GWBOX (1.0,1.0,0.5)
CALL GEYE (6.0,4.0,7.0)
CALL GSCALE
CALL GVPROJ(2)
CALL RAXDIS (3,1,9999)
CALL RAXDIS (7,1,9999)
CALL RAXDIS (6,1,9999)
CALL RAXLFO (0,0,1,0)
CALL RAXBTI (9999,999.999,999.999,200.0)
CALL RAXSTI (3)
CALL RAXDIS (4,1,3)
CALL RAXIS3 (1,3.0,IPLANE,LENGTH,TEXT)
CALL RAXDIS (4,1,0)
CALL RAXIS3 (2,3.0,IPLANE,LENGTH,TEXT)
CALL RAXBTI (9999,999.999,999.999,10.0)
CALL RAXSTI (4)
CALL RAXIS3 (3,3.0,IPLANE,LENGTH,TEXT)
CALL GFAULT (XED,YED,17,1)
CALL GINTPF (XPOS,YPOS,HEIGHT,32,ZEST,25,21)
CALL GSMTH (-1)
CALL GCONWI (0.0,1)
CALL GCNR3V (ZEST,25,21)
CALL GRESET
CALL GSCAMM
CALL RTXJUS (0,6)
CALL RTXHEI (2.5)
CALL RTX (-1,'Air Velocity',145.0,(116.0+HFAC))
CALL RTXN (A,3,145.0,(110.0+HFAC))
CALL RTXC (-1,' m/s')
CALL RTX (-1,'Water Loading',145.0,(102.0+HFAC))
CALL RTX (-1,'Inlet Gap',145.0,(88.0+HFAC))
CALL RTXN (INGAP,3,145.0,(82.0+HFAC))
CALL RTXC (-1,' m')
CALL RTX (-1,'Inlet Weir',145.0,(74.0+HFAC))
CALL RTXN (INWEIR,3,145.0,(68.0+HFAC))
CALL RTXC (-1,' m')
CALL RTX (-1,'Outlet Weir',145.0,(60.0+HFAC))
CALL RTXN (OUTWEIR,3,145.0,(54.0+HFAC))
CALL RTXC (-1,' m')
CALL RTX (-1,'Hole Diameter',145.0,(46.0+HFAC))
CALL RTXN (HOLEDIA,3,145.0,(40.0+HFAC))
CALL RTXC (-1,' m')
CALL RTXNBO (8,'T')
CALL RTXN (W,1,145.0,(96.0+HFAC))
```

```
      CALL RTXC (-1,' cm3/cm.s')
C
C*********************************************************************
C    READING VALUES FOR THE SECOND PLOT
C*********************************************************************
C
      IF ((I+1).LE.NDATA) THEN
       W=WEIRL(I+1)
       A=AIRV(I+1)
       DO 25 K=1,17
         XED(K)=XEDGE(K)
         YED(K)=YEDGE(K)
 25    CONTINUE
       DO 26 J=1,32
         XPOS(J)=X(J)
         YPOS(J)=Y(J)
         HEIGHT(J)=HCL((I+1),J)
 26    CONTINUE
C
C*********************************************************************
C    COMMENCING PLOTTING OF SECOND SURFACE
C*********************************************************************
C
       CALL GRESET
       CALL GLIMIT (-1200.0,1200.0,0.0,2000.0,0.0,50.0)
       CALL RUNDEF (999.999,9999)
       HFAC=0.0
       CALL GVPORT (40.0,(42.0+HFAC),80.0,80.0)
       CALL GWBOX (1.0,1.0,0.5)
       CALL GEYE (6.0,4.0,7.0)
       CALL GSCALE
       CALL GVPROJ(2)
       CALL RAXDIS (3,1,9999)
       CALL RAXDIS (7,1,9999)
       CALL RAXDIS (6,1,9999)
       CALL RAXLFO (0,0,1,0)
       CALL RAXBTI (9999,999.999,999.999,200.0)
       CALL RAXSTI (3)
       CALL RAXDIS (4,1,3)
       CALL RAXIS3 (1,3.0,IPLANE,LENGTH,TEXT)
       CALL RAXDIS (4,1,0)
       CALL RAXIS3 (2,3.0,IPLANE,LENGTH,TEXT)
       CALL RAXBTI (9999,999.999,999.999,10.0)
       CALL RAXSTI (4)
       CALL RAXIS3 (3,3.0,IPLANE,LENGTH,TEXT)
       CALL GFAULT (XED,YED,17,1)
       CALL GINTPF (XPOS,YPOS,HEIGHT,32,ZEST,25,21)
       CALL GSMTH (-1)
       CALL GCONWI (0.0,1)
```

```
      CALL GCNR3V (ZEST,25,21)
      CALL GRESET
      CALL GSCAMM
      CALL RTXJUS (0,6)
      CALL RTXHEI (2.5)
      CALL RTX (-1,'Air Velocity',145.0,(116.0+HFAC))
      CALL RTXN (A,3,145.0,(110.0+HFAC))
      CALL RTXC (-1,' m/s')
      CALL RTX (-1,'Water Loading',145.0,(102.0+HFAC))
      CALL RTX (-1,'Inlet Gap',145.0,(88.0+HFAC))
      CALL RTXN (INGAP,3,145.0,(82.0+HFAC))
      CALL RTXC (-1,' m')
      CALL RTX (-1,'Inlet Weir',145.0,(74.0+HFAC))
      CALL RTXN (INWEIR,3,145.0,(68.0+HFAC))
      CALL RTXC (-1,' m')
      CALL RTX (-1,'Outlet Weir',145.0,(60.0+HFAC))
      CALL RTXN (OUTWEIR,3,145.0,(54.0+HFAC))
      CALL RTXC (-1,' m')
      CALL RTX (-1,'Hole Diameter',145.0,(46.0+HFAC))
      CALL RTXN (HOLEDIA,3,145.0,(40.0+HFAC))
      CALL RTXC (-1,' m')
      CALL RTXNBO (8,'T')
      CALL RTXN (W,1,145.0,(96.0+HFAC))
      CALL RTXC (-1,' cm3/cm.s')
     ENDIF
     CALL GCLOSE
22   CONTINUE
      END
```

APPENDIX 5

Two-Dimensional Reduced Temperature Isotherm Diagrams for the Effect of Gas Flow on the Separation of the Liquid Flow

This appendix contains a full set of the two-dimensional isotherm diagrams obtained during the water-cooling experiments. The diagrams are complementary to the water-cooling experiments of Chapter 6. During the experiments the water weir load was varied for a fixed gas velocity to attempt to show the effect of flow separation on mass transfer. The experiments were repeated for the equal inlet gap and outlet weir settings of 10 mm, 20 mm and 50 mm. Repeated below is a summary table of the flow rate information and inlet and outlet settings.

Air Velocity $m.s^{-1}$	Weir Load $x\ 10^4\ m^3/m.s$	Inlet Gap mm	Outlet Weir mm
1.00	25.0		
1.25	50.0	10	10
1.50	100.0	20	20
2.00	150.0	50	50
2.50	200.0		
	250.0		

Table A5.1 Summary of flow rates and inlet and outlet settings used in air-water experiments.

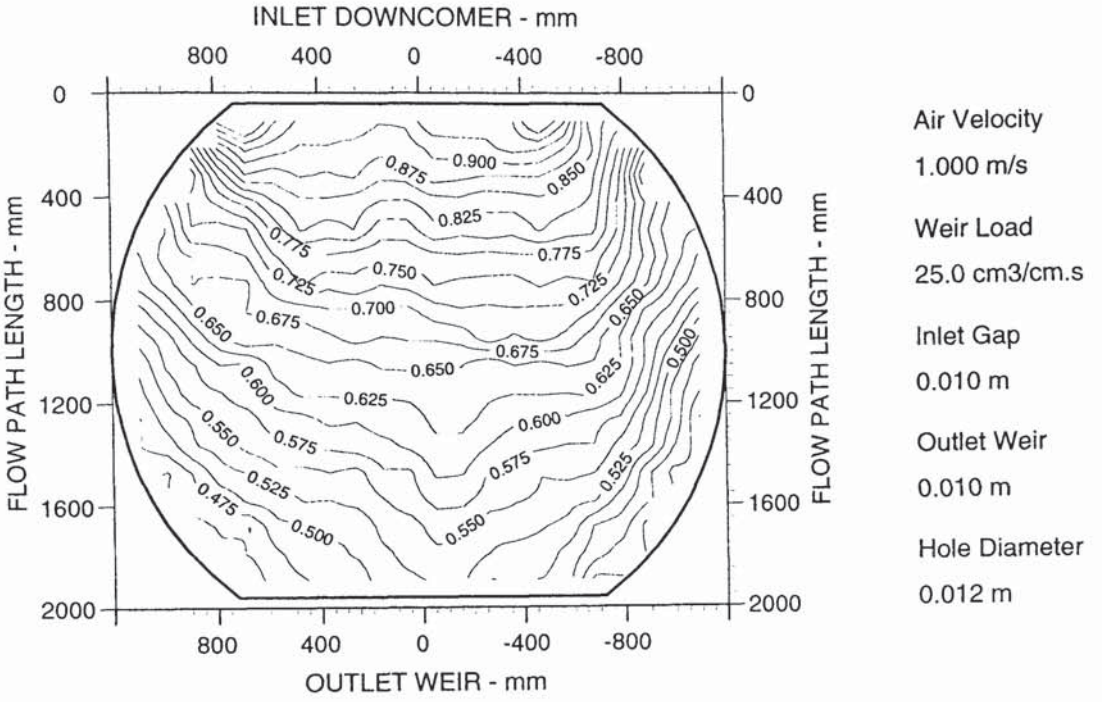

Figure A5.1a Two dimensional reduced temperature profiles.

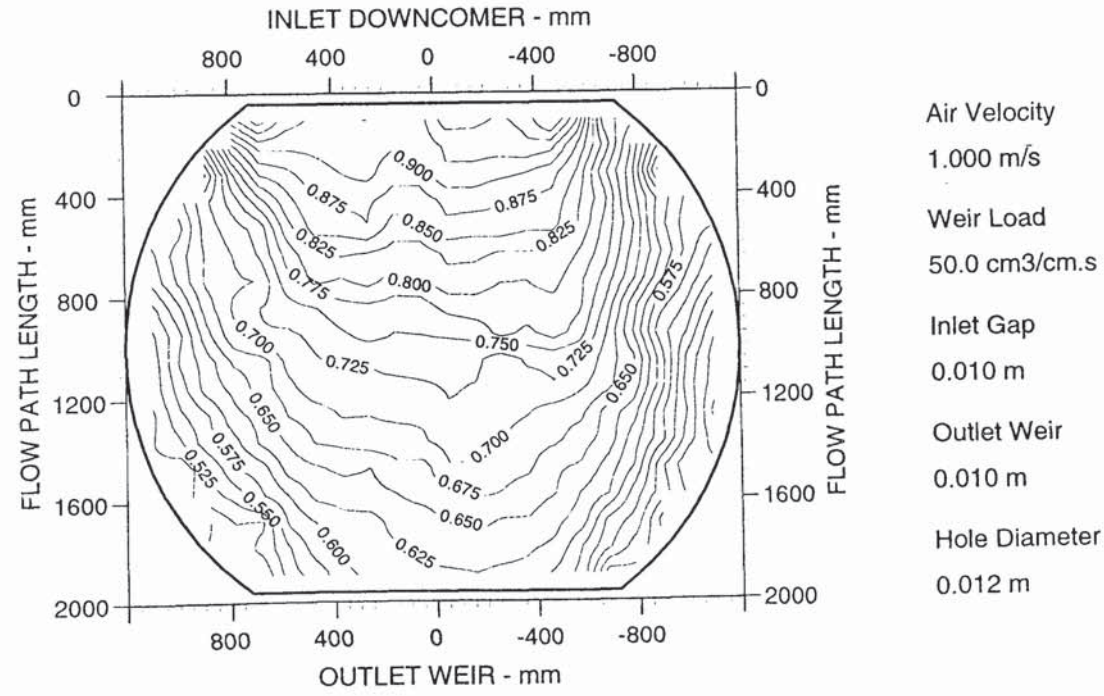

Figure A5.1b Two dimensional reduced temperature profiles.

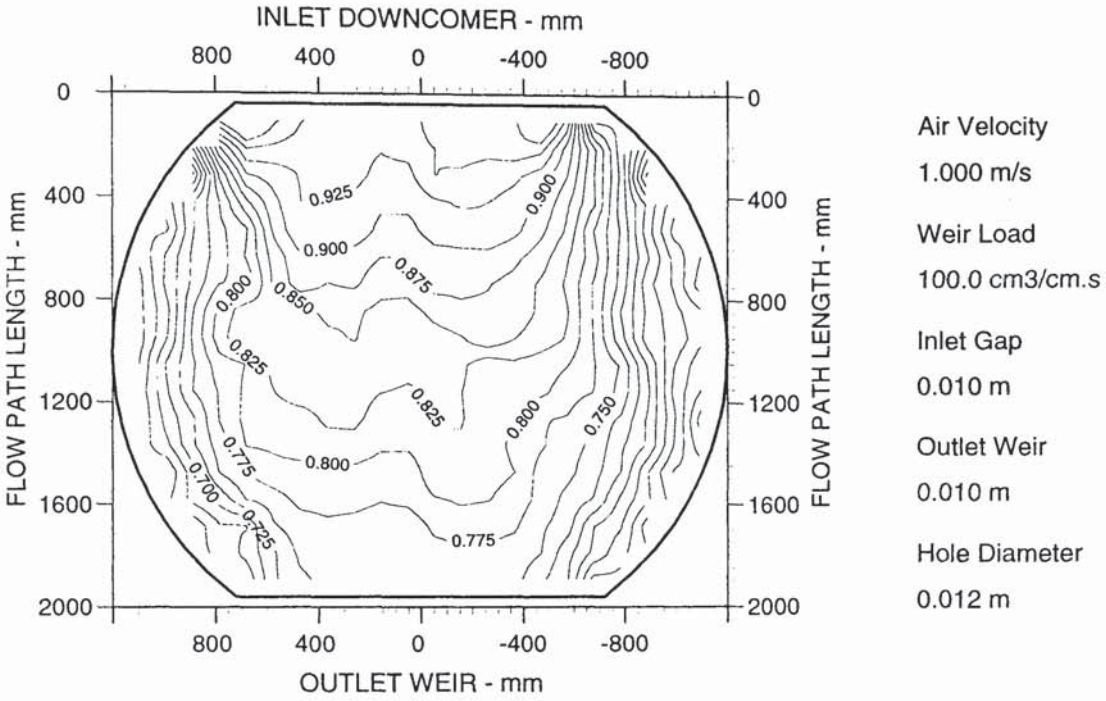

Figure A5.1c Two dimensional reduced temperature profiles.

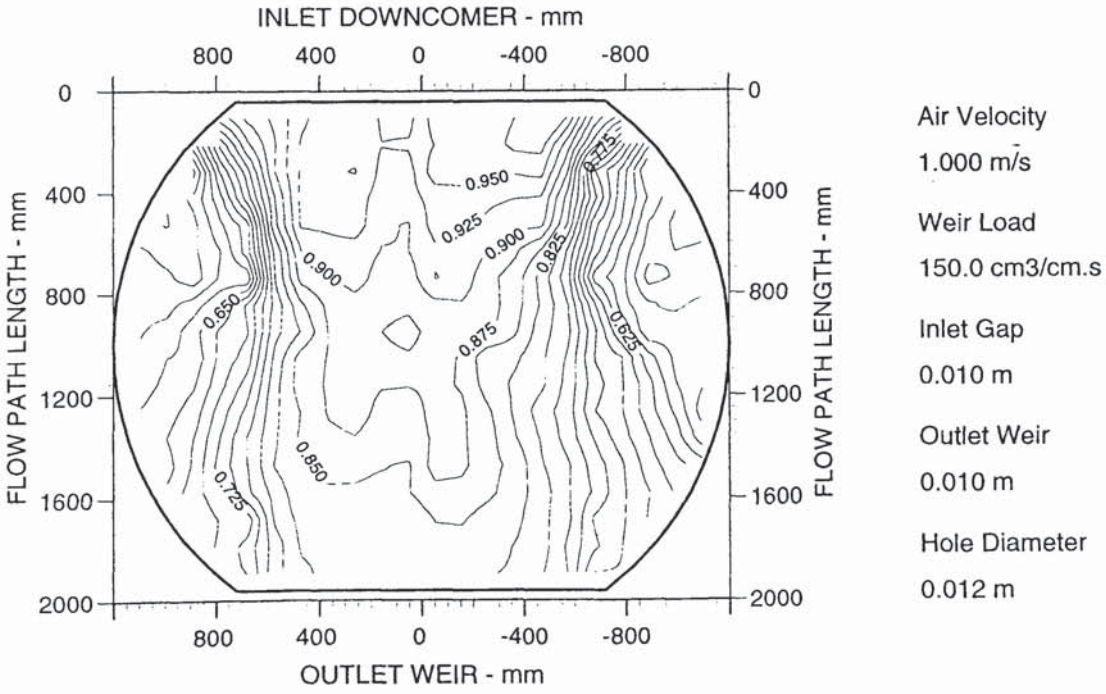

Figure A5.1d Two dimensional reduced temperature profiles.

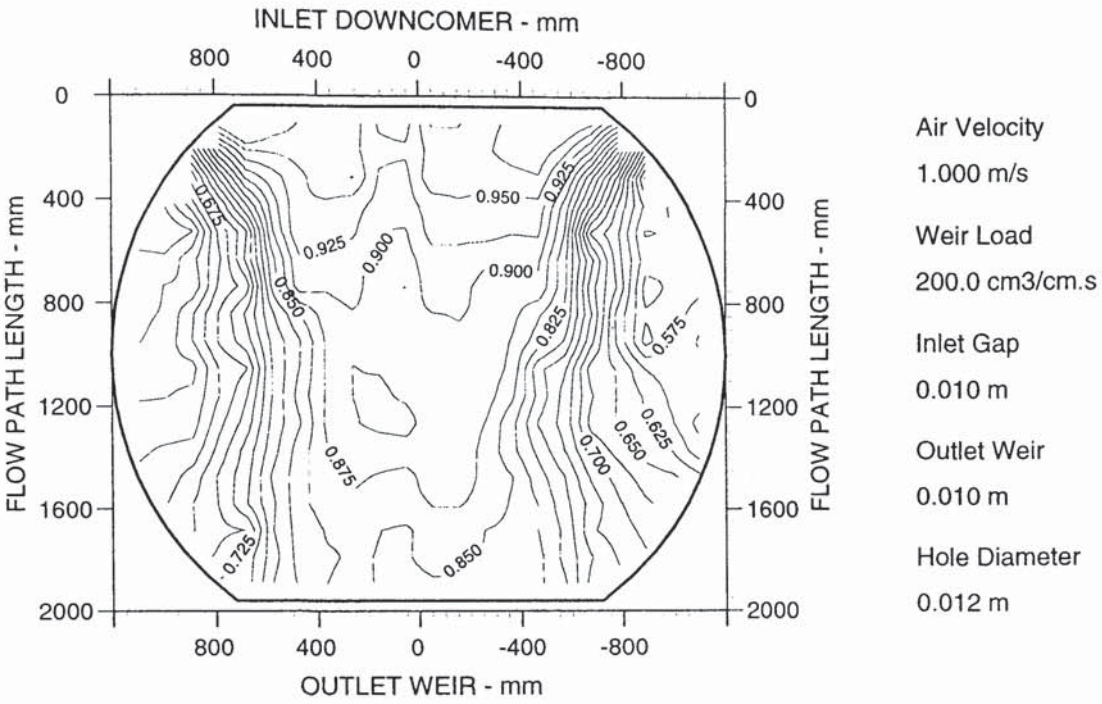

Figure A5.1e Two dimensional reduced temperature profiles.

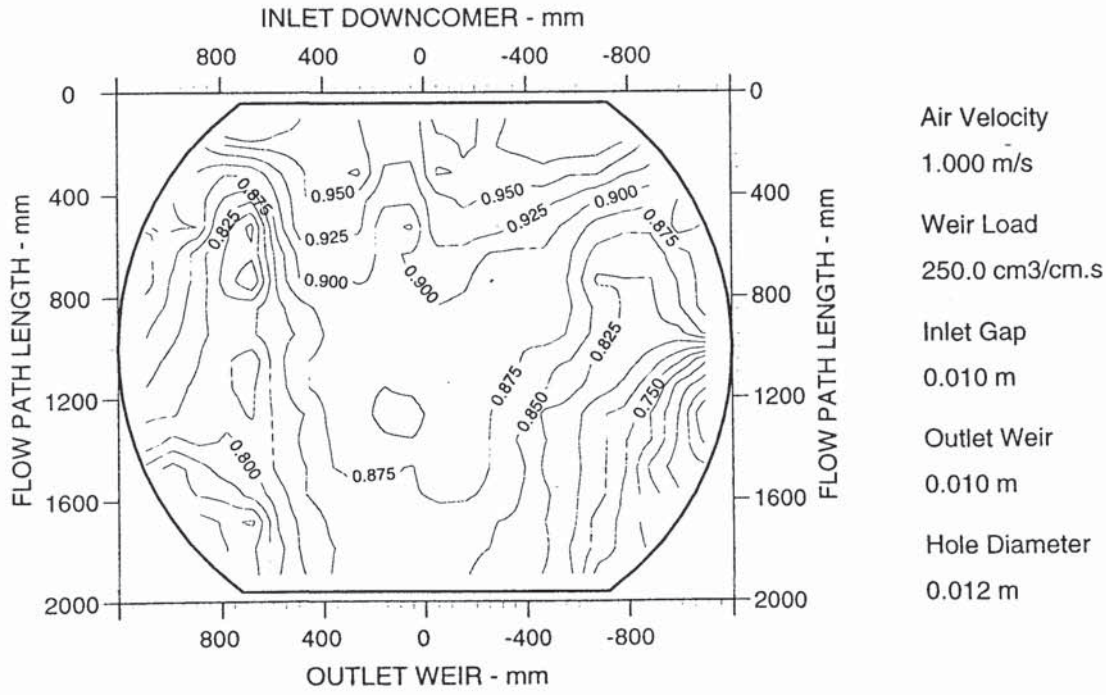

Figure A5.1f Two dimensional reduced temperature profiles.

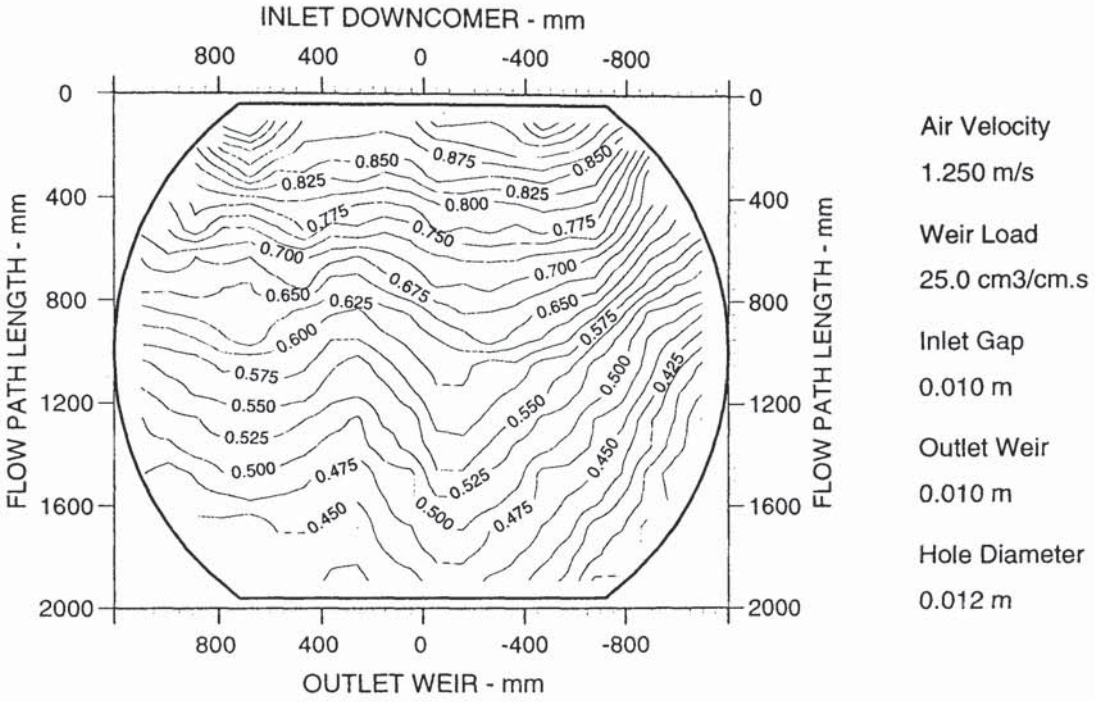

Figure A5.2a Two dimensional reduced temperature profiles.

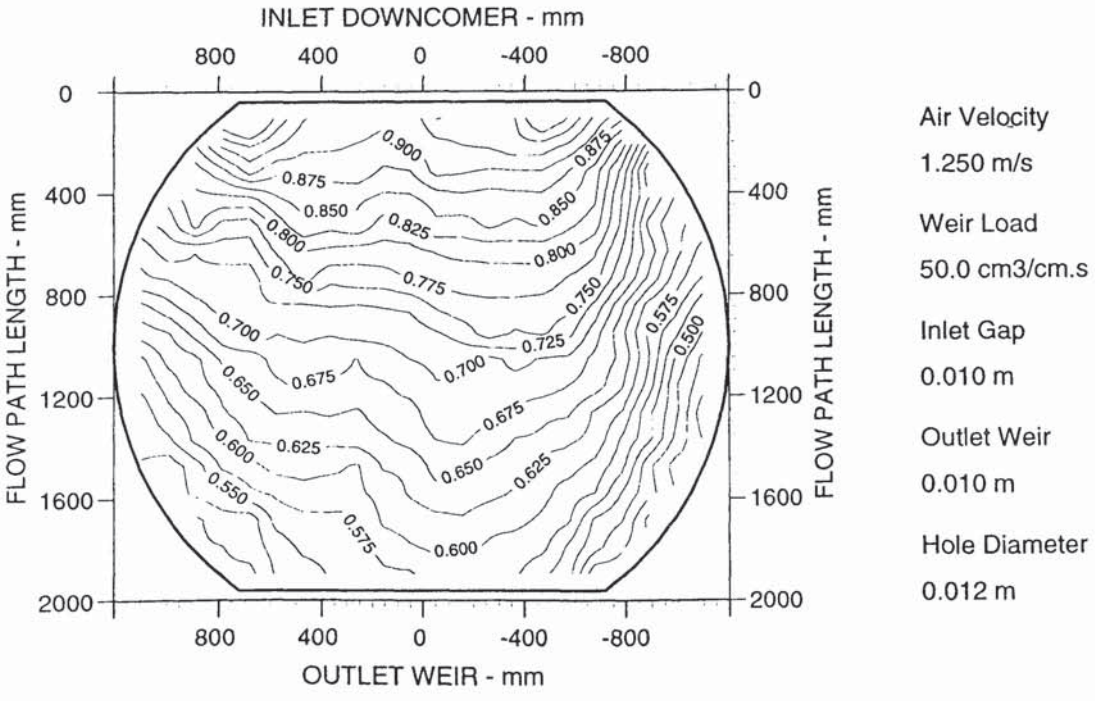

Figure A5.2b Two dimensional reduced temperature profiles.

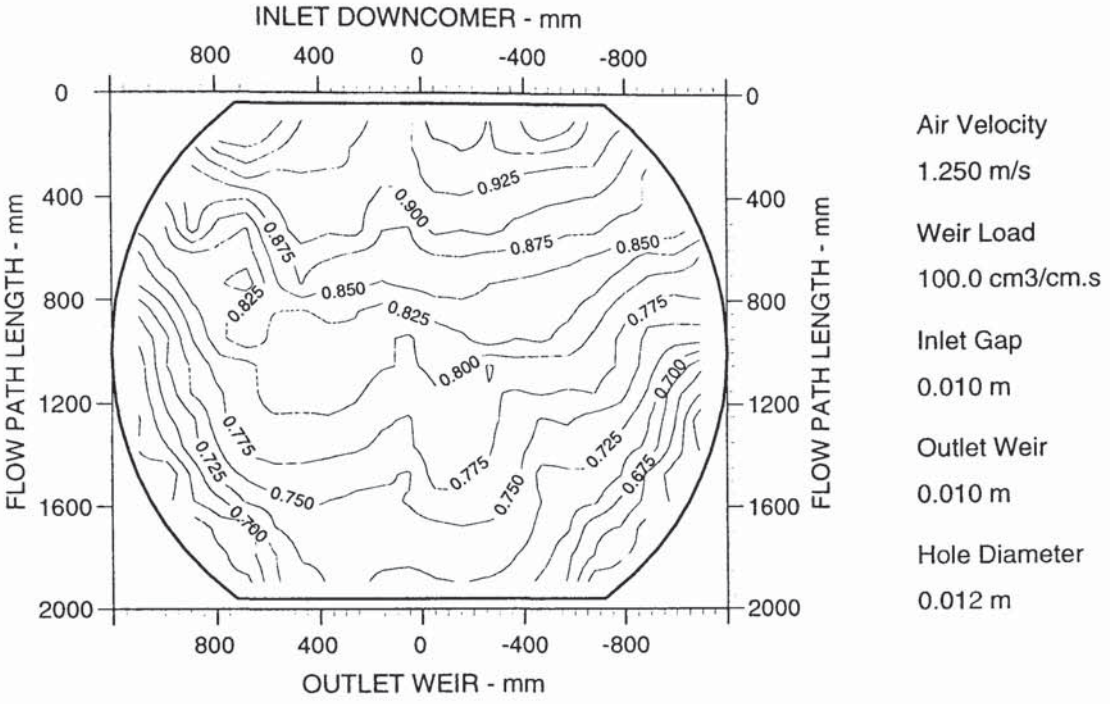

Figure A5.2c Two dimensional reduced temperature profiles.

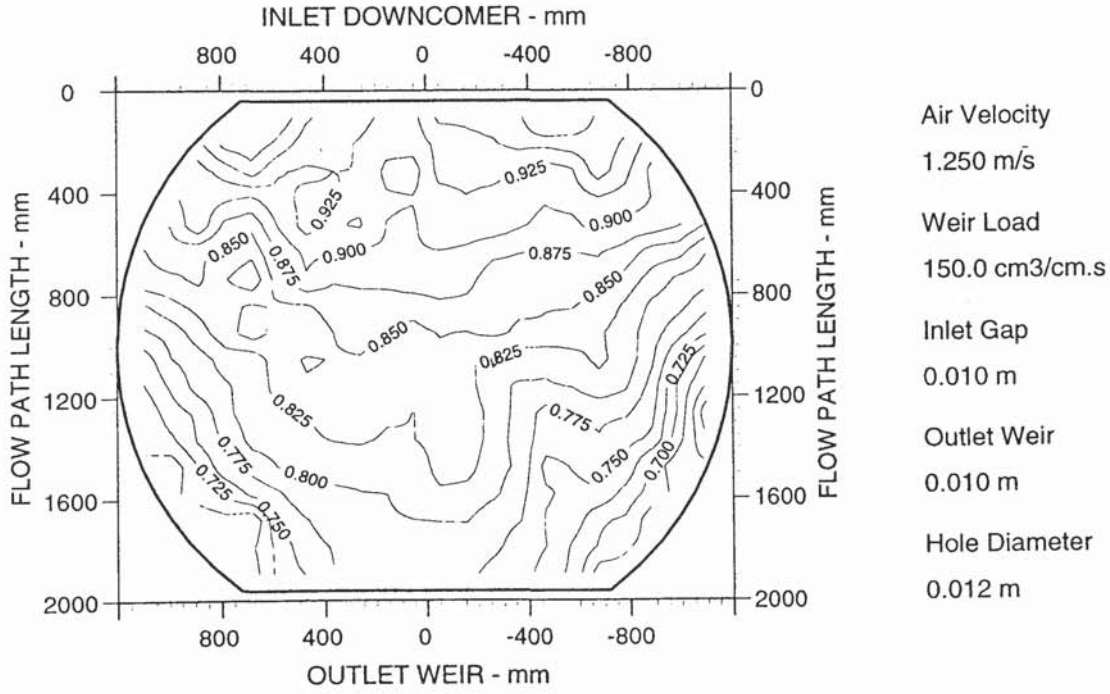

Figure A5.2d Two dimensional reduced temperature profiles.

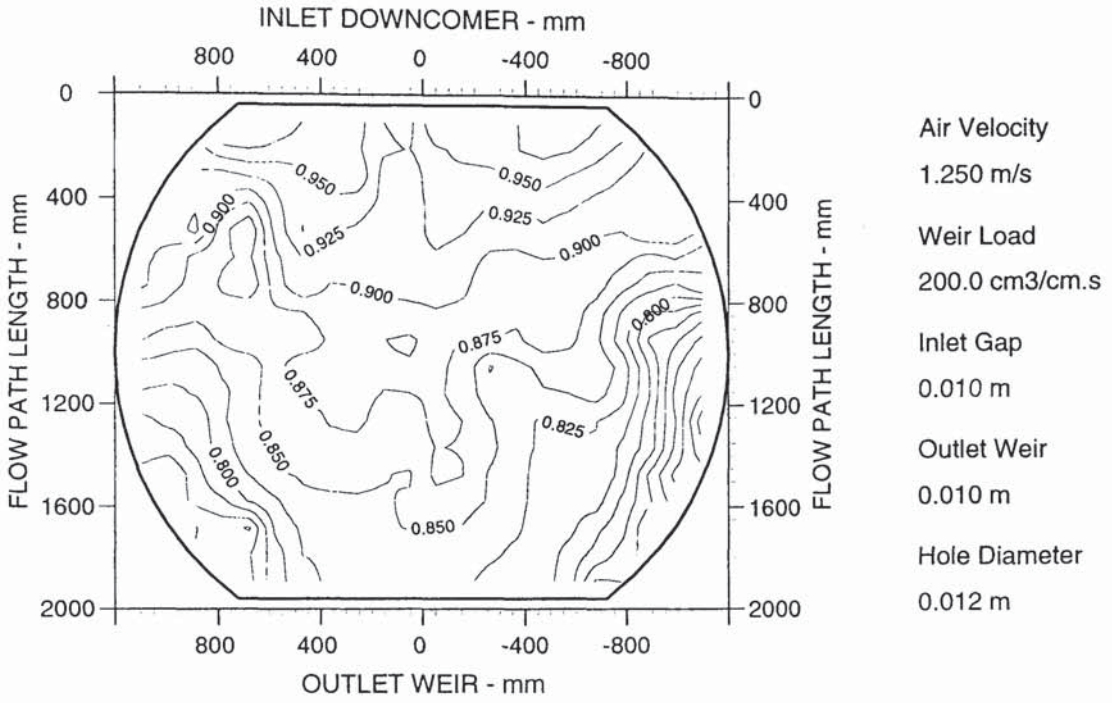

Figure A5.2e Two dimensional reduced temperature profiles.

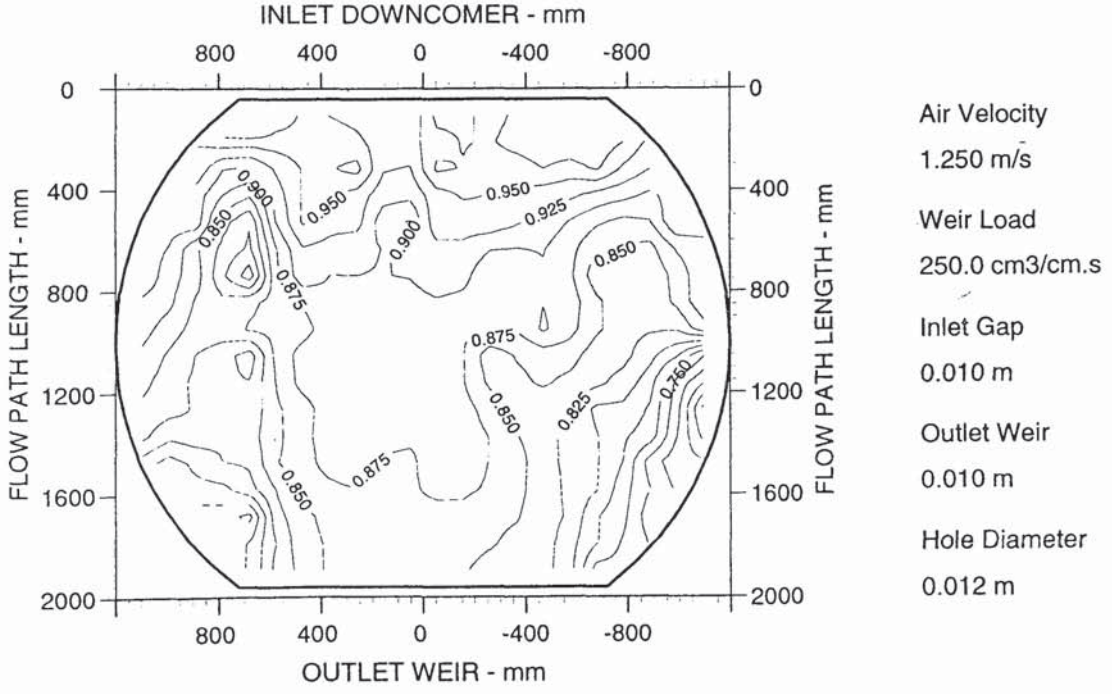

Figure A5.2f Two dimensional reduced temperature profiles.

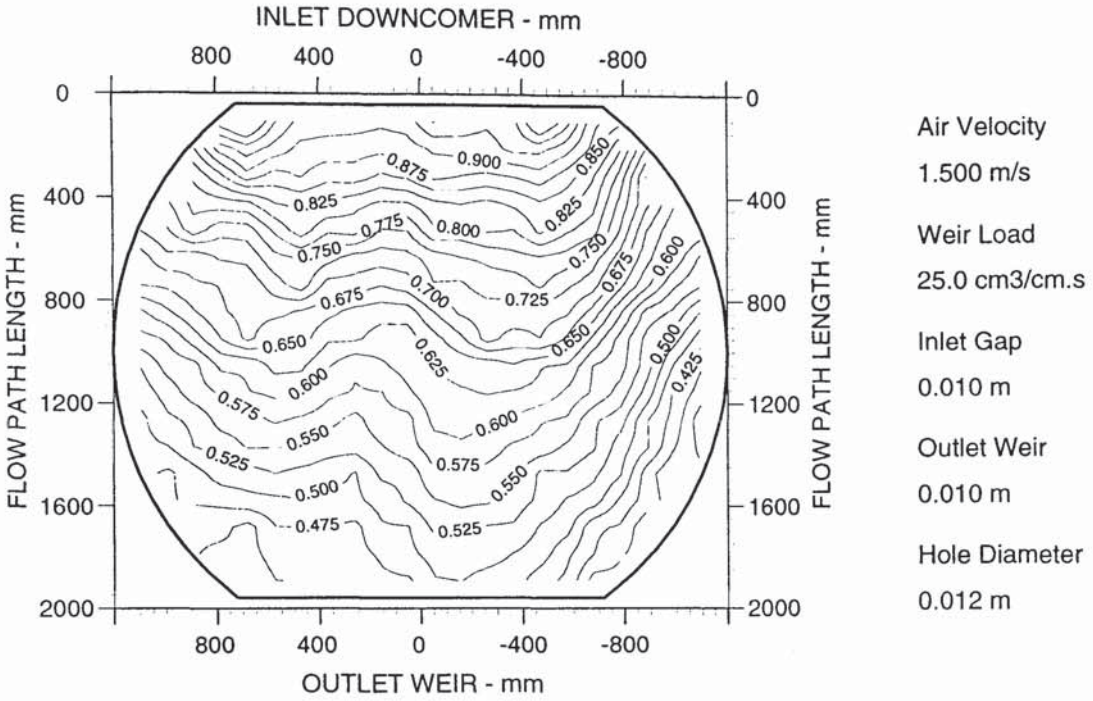

Figure A5.3a Two dimensional reduced temperature profiles.

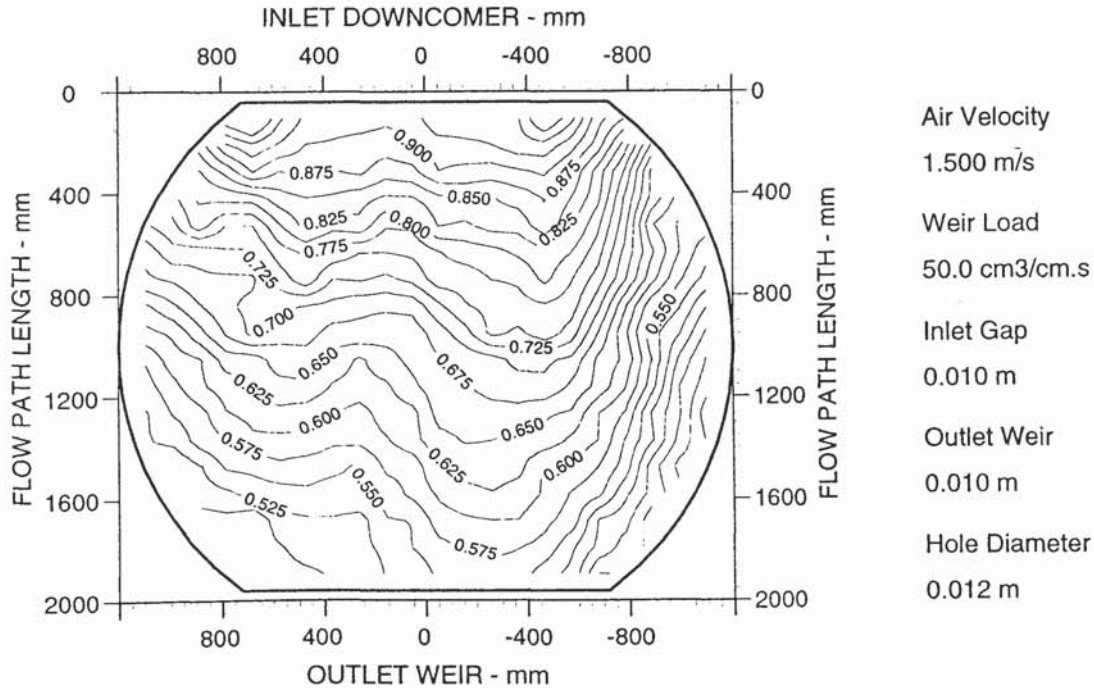

Figure A5.3b Two dimensional reduced temperature profiles.

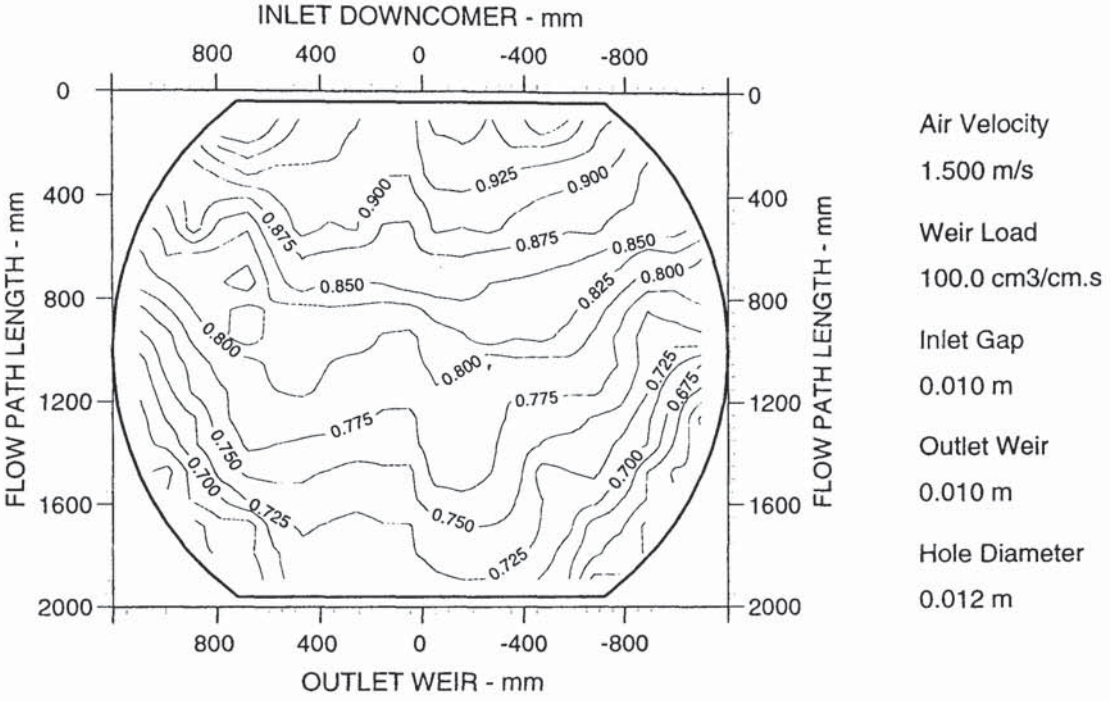

Figure A5.3c Two dimensional reduced temperature profiles.

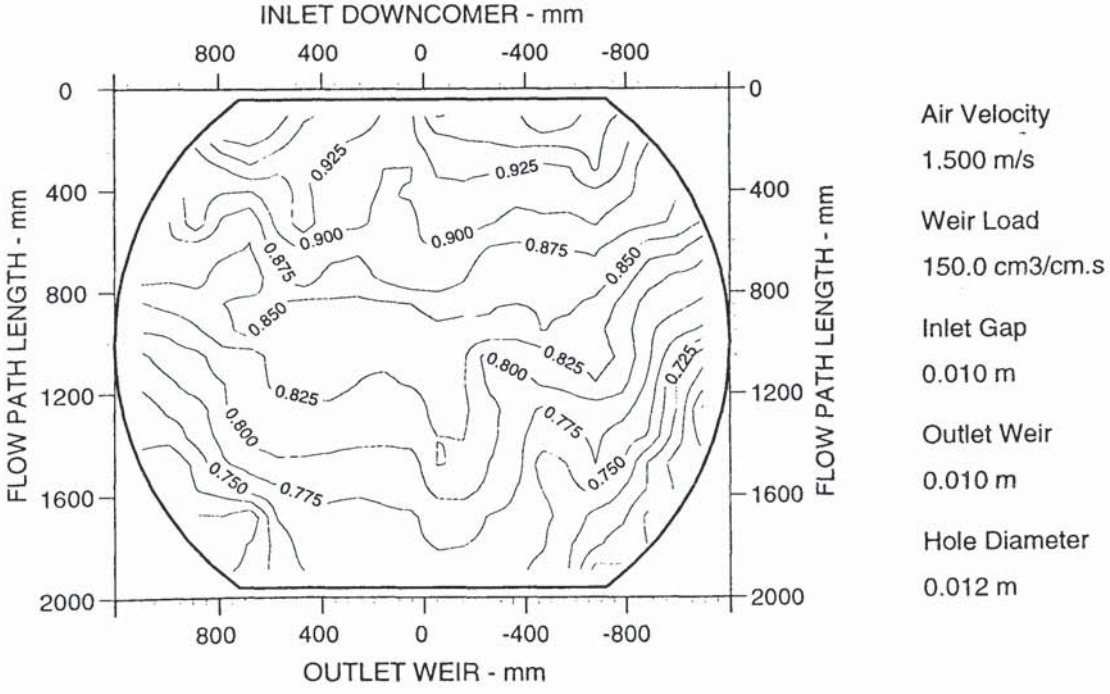

Figure A5.3d Two dimensional reduced temperature profiles.

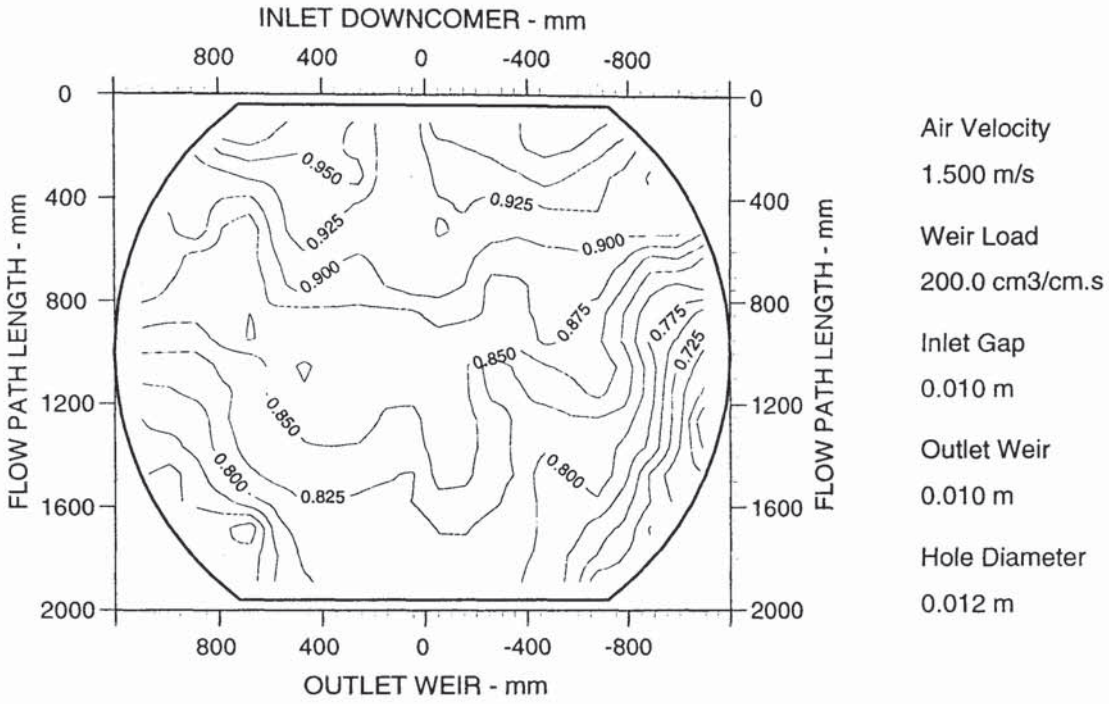

Figure A5.3e Two dimensional reduced temperature profiles.

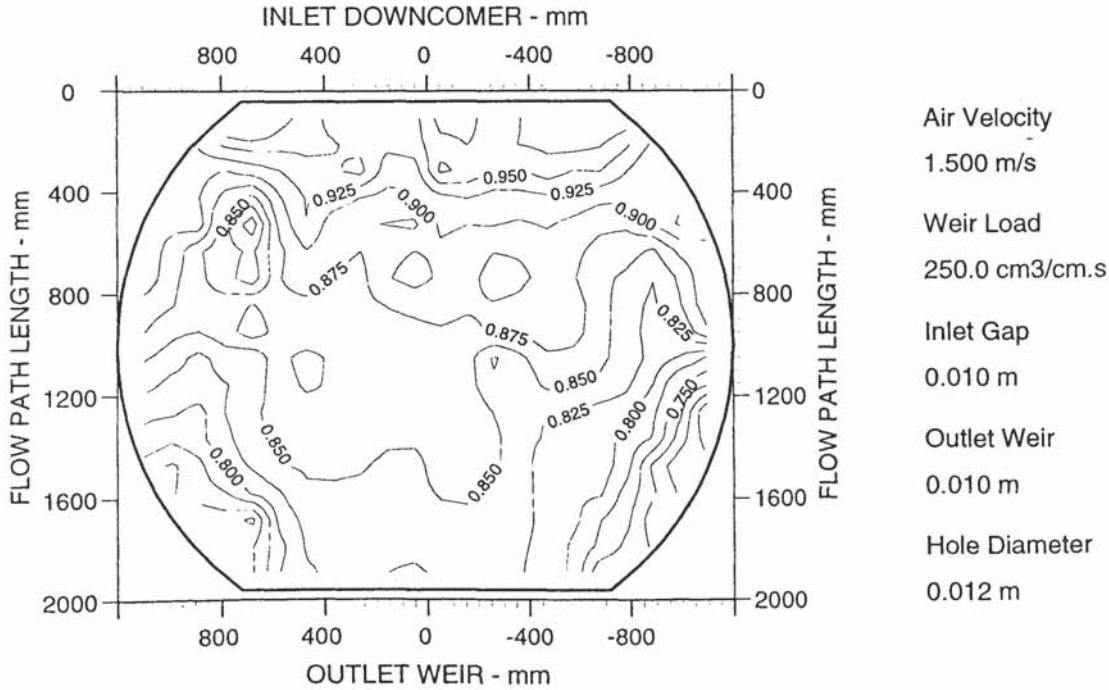

Figure A5.3f Two dimensional reduced temperature profiles.

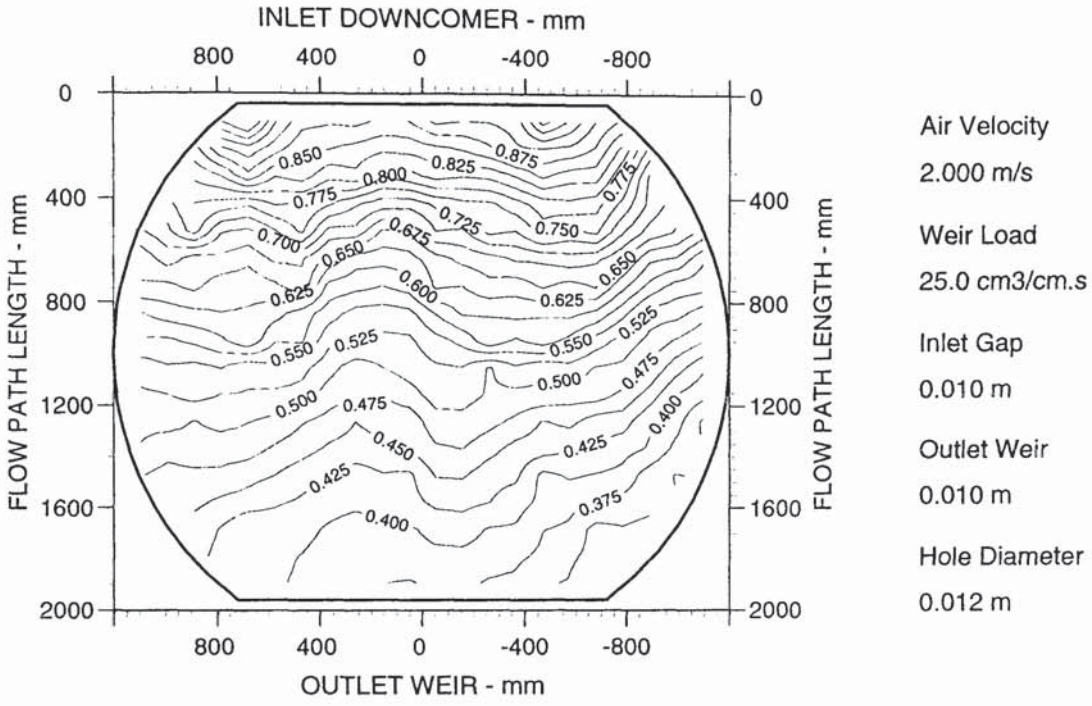

Figure A5.4a Two dimensional reduced temperature profiles.

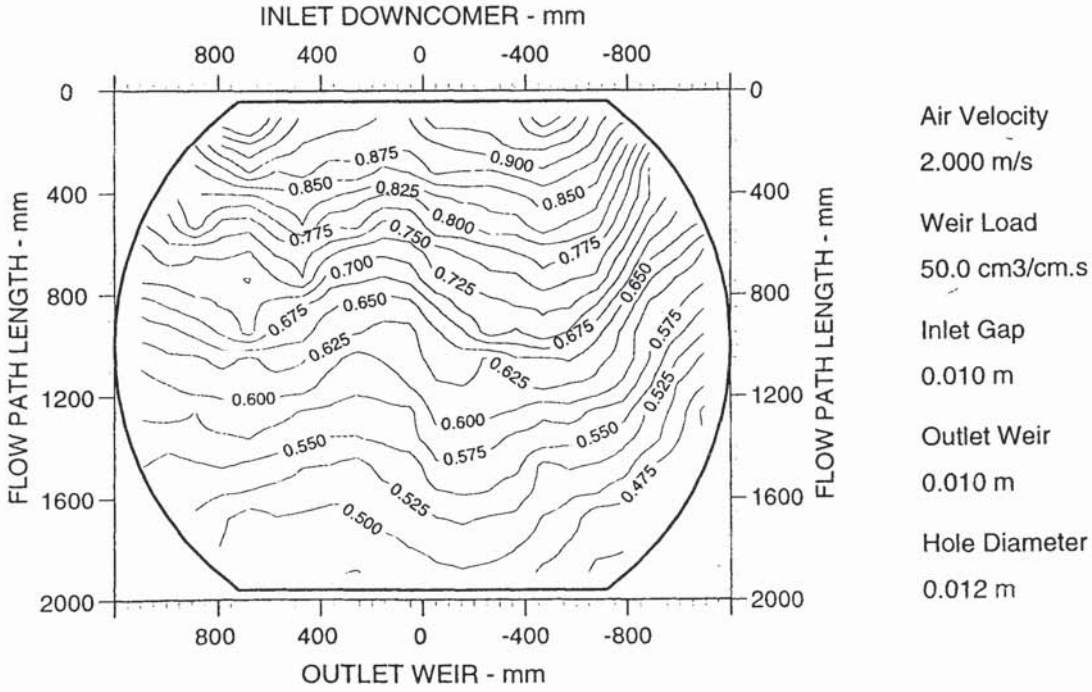

Figure A5.4b Two dimensional reduced temperature profiles.

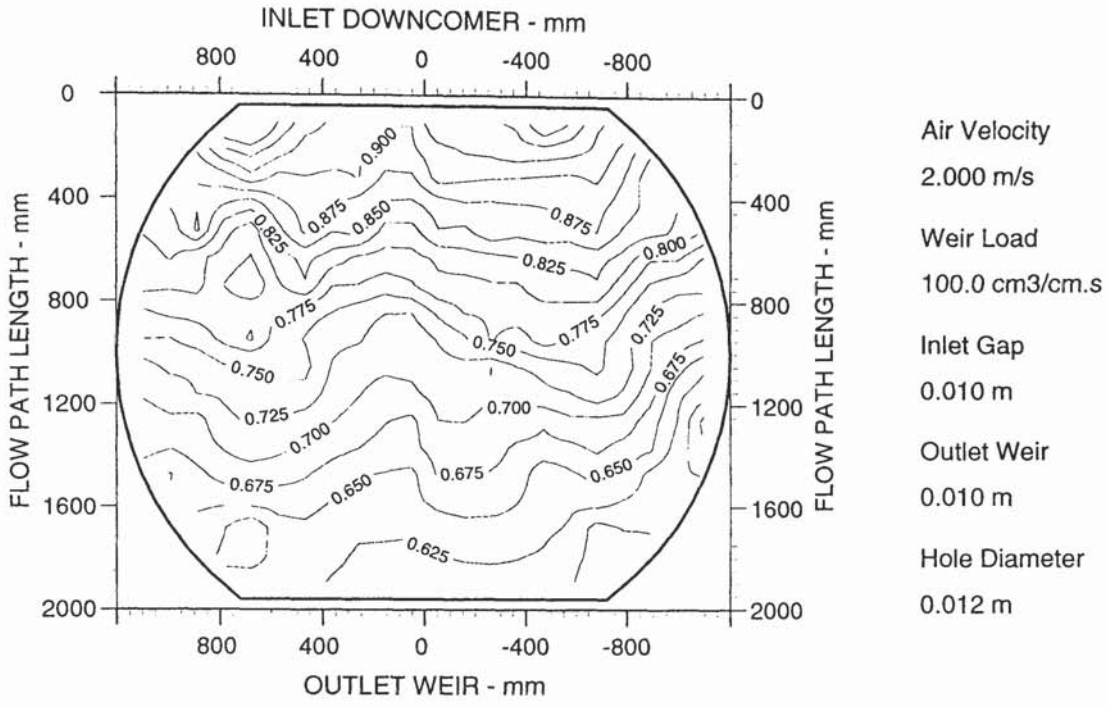

Figure A5.4c Two dimensional reduced temperature profiles.

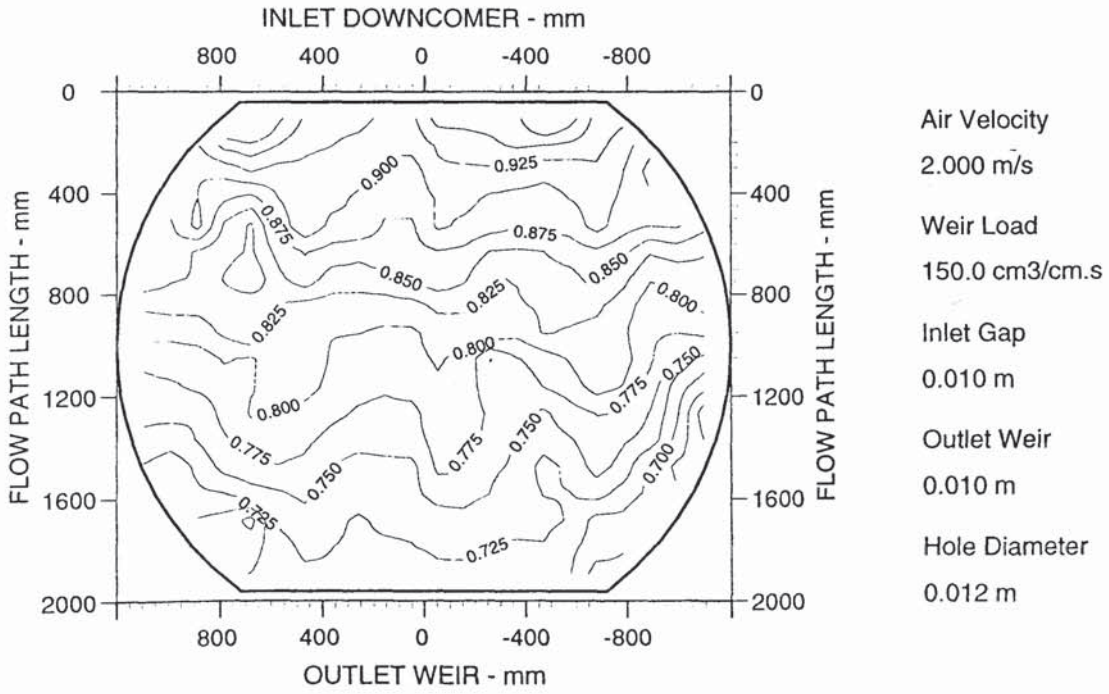

Figure A5.4d Two dimensional reduced temperature profiles.

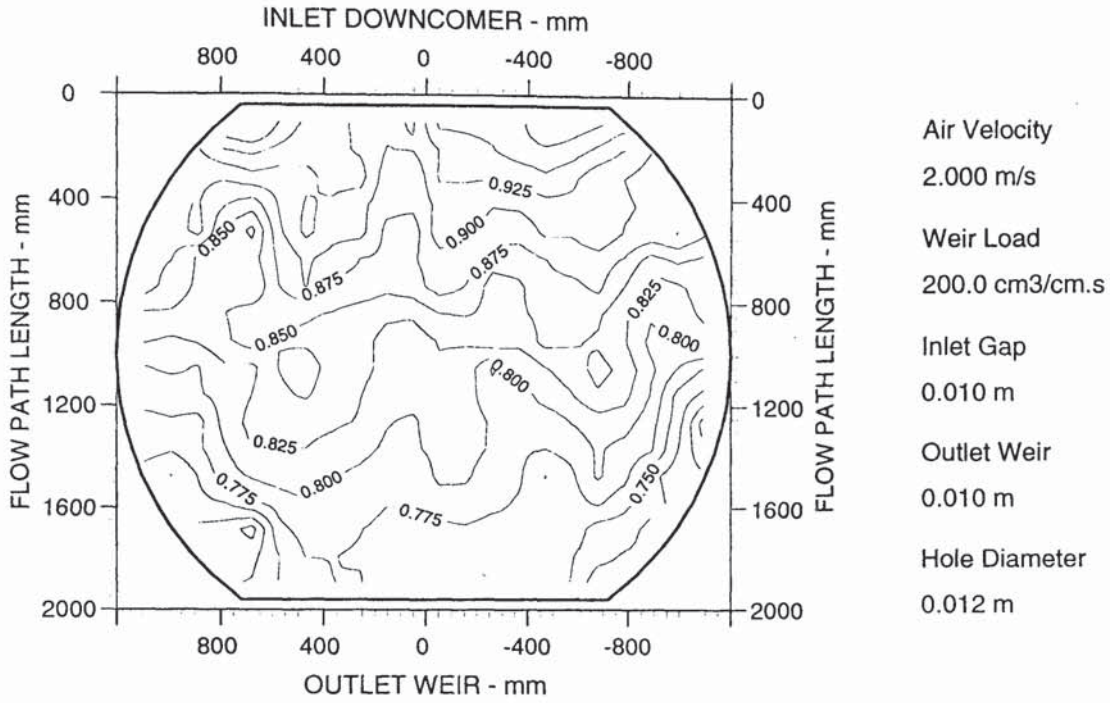

Figure A5.4e Two dimensional reduced temperature profiles.

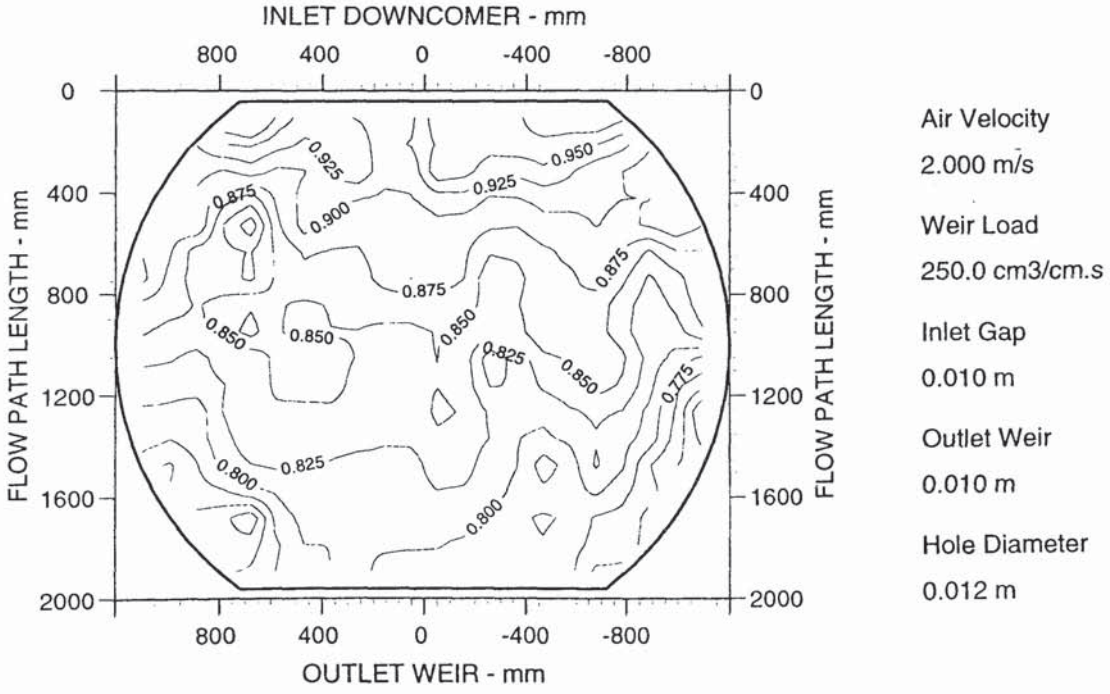

Figure A5.4f Two dimensional reduced temperature profiles.

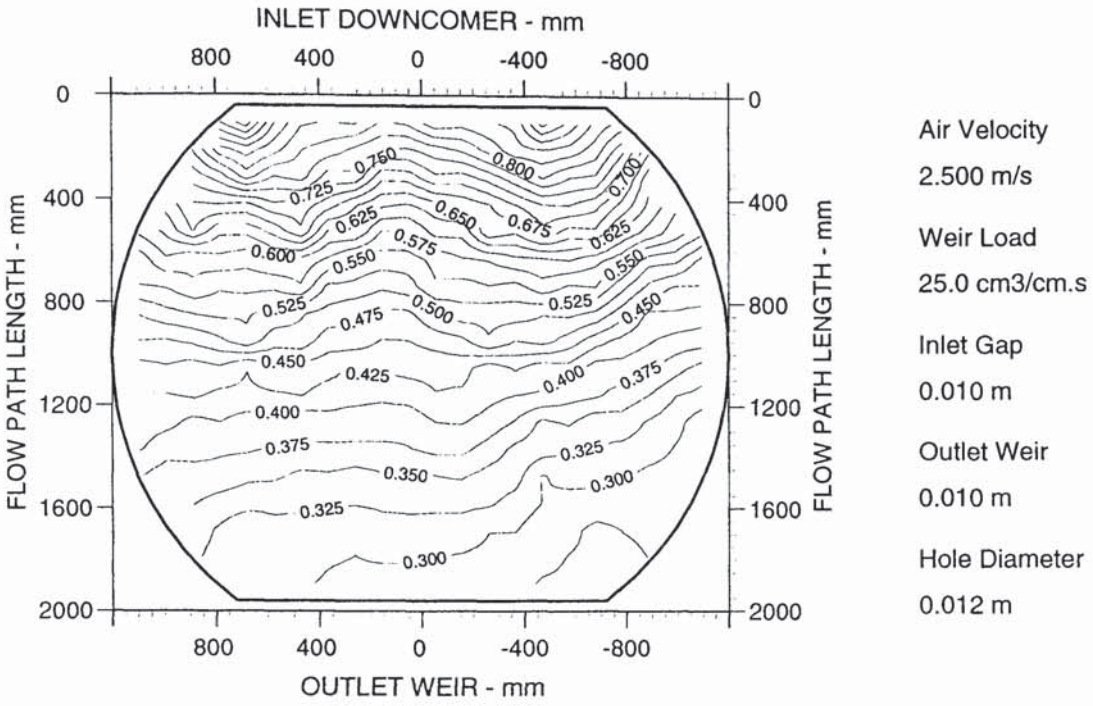

Figure A5.5a Two dimensional reduced temperature profiles.

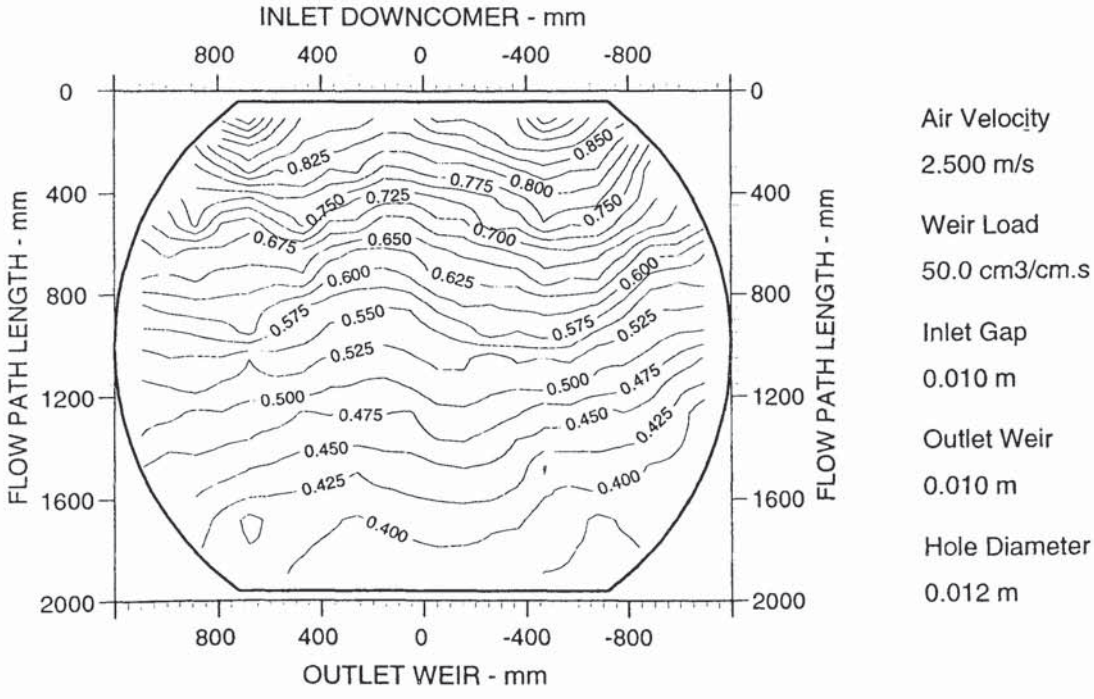

Figure A5.5b Two dimensional reduced temperature profiles.

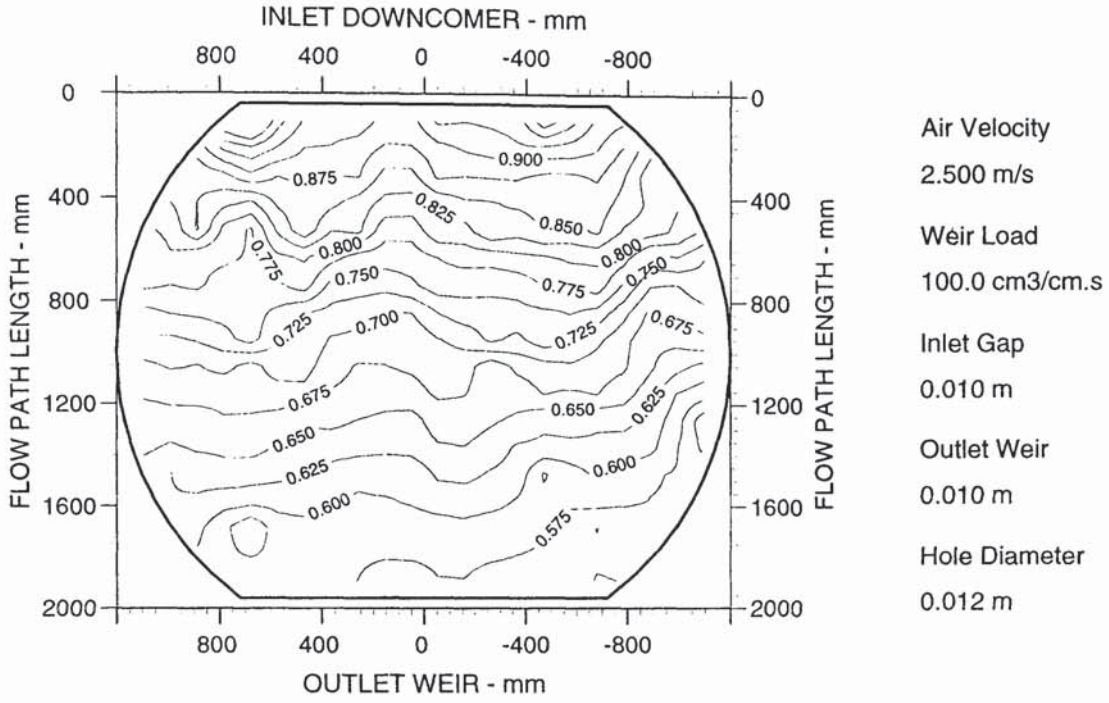

Figure A5.5c Two dimensional reduced temperature profiles.

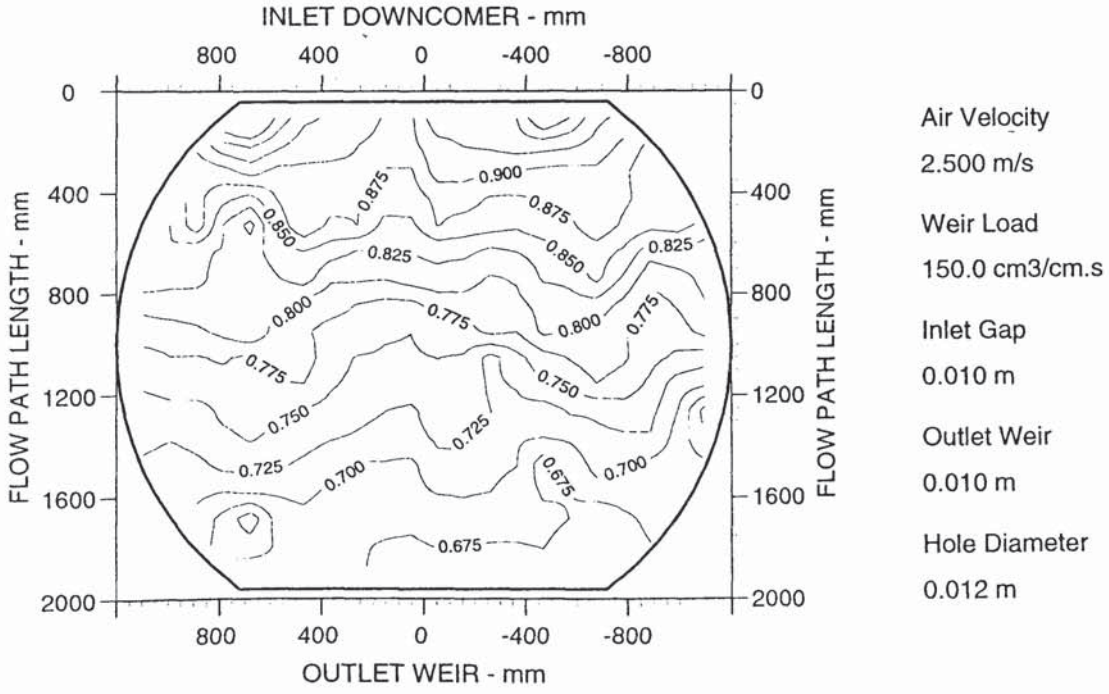

Figure A5.5d Two dimensional reduced temperature profiles.

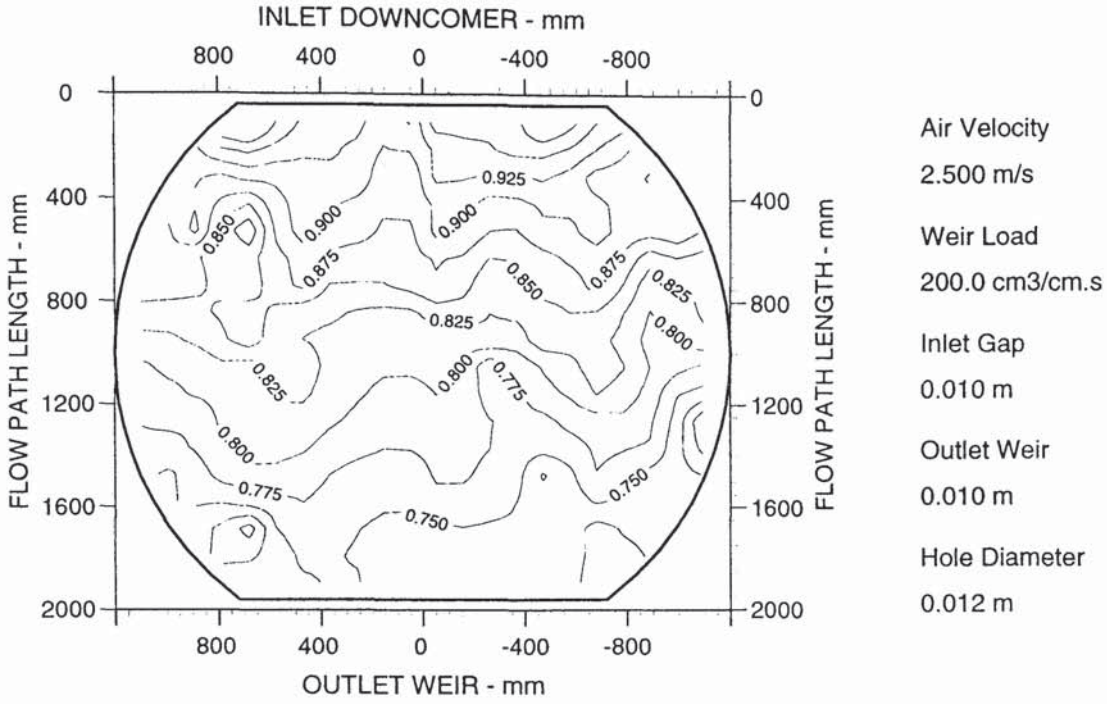

Figure A5.5e Two dimensional reduced temperature profiles.

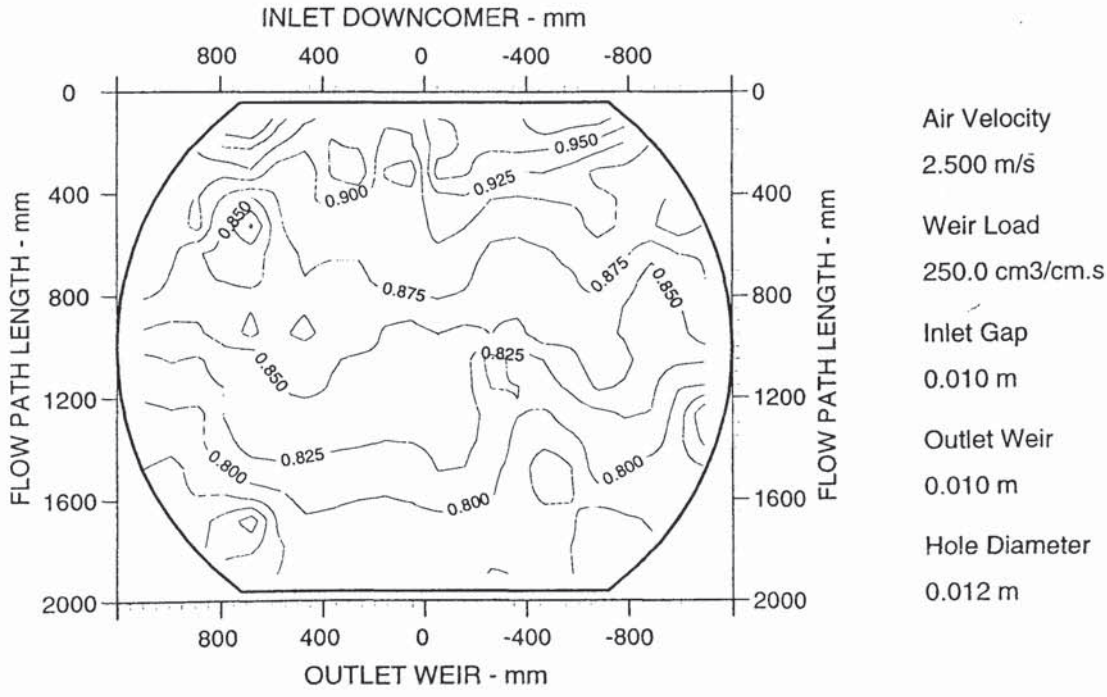

Figure A5.5f Two dimensional reduced temperature profiles.

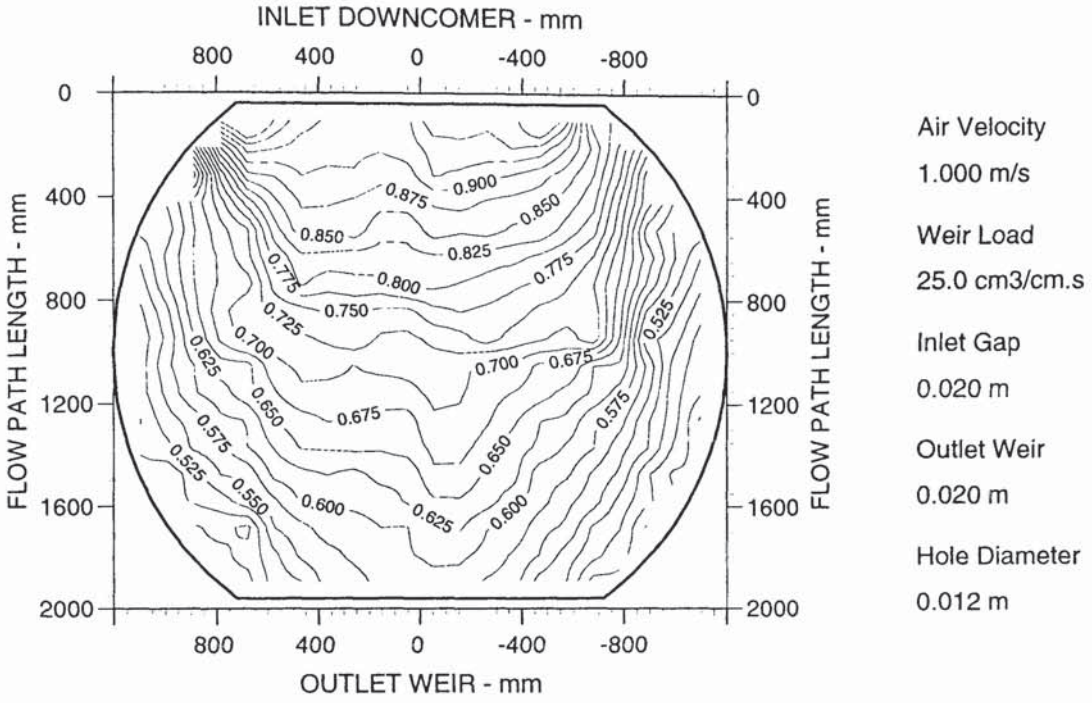

Figure A5.6a Two dimensional reduced temperature profiles.

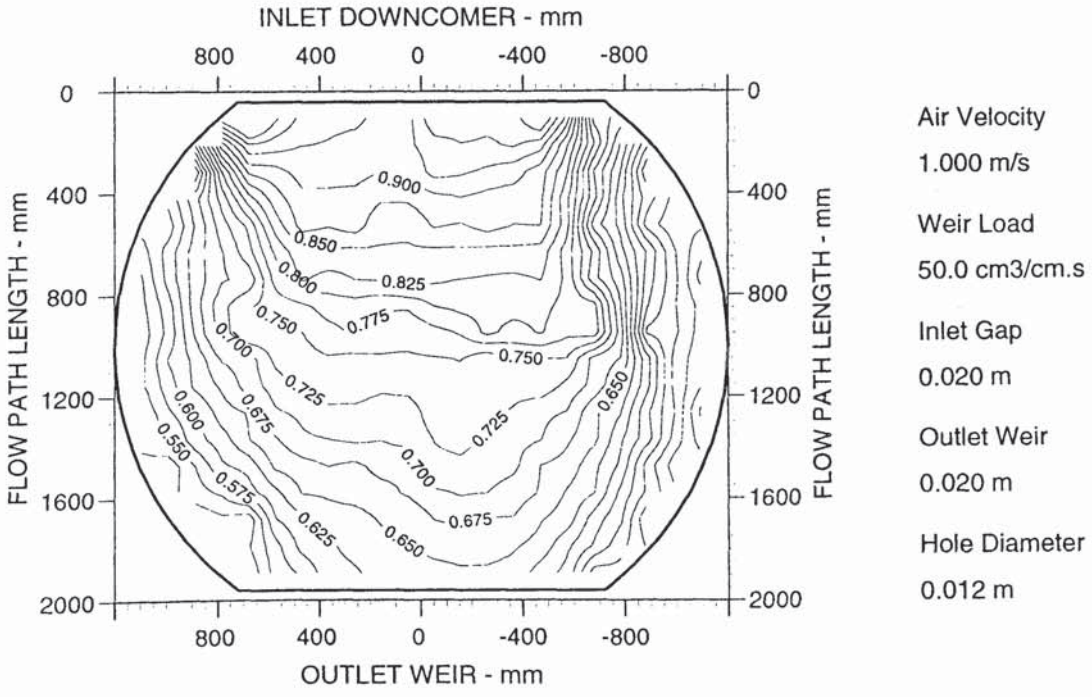

Figure A5.6b Two dimensional reduced temperature profiles.

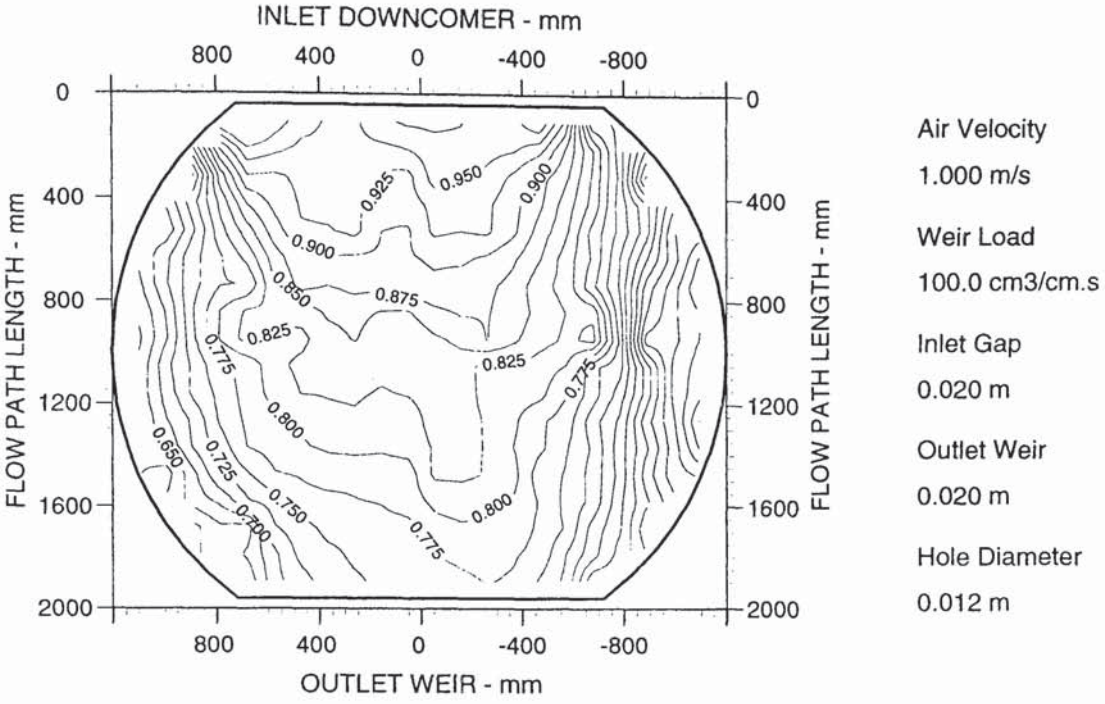

Figure A5.6c Two dimensional reduced temperature profiles.

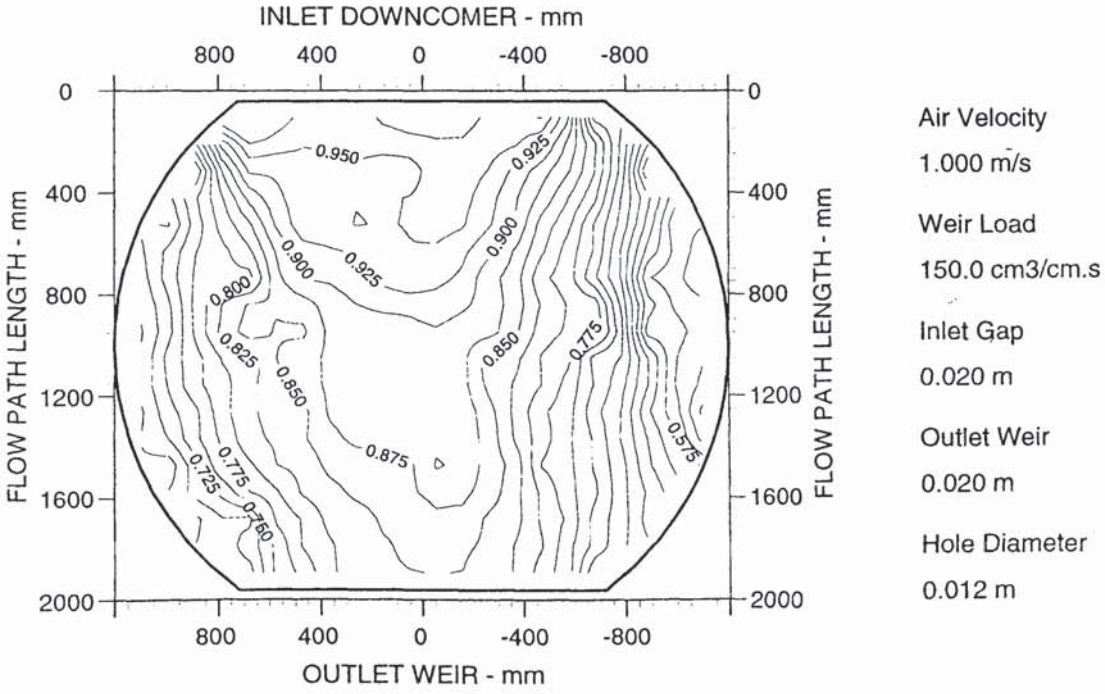

Figure A5.6d Two dimensional reduced temperature profiles.

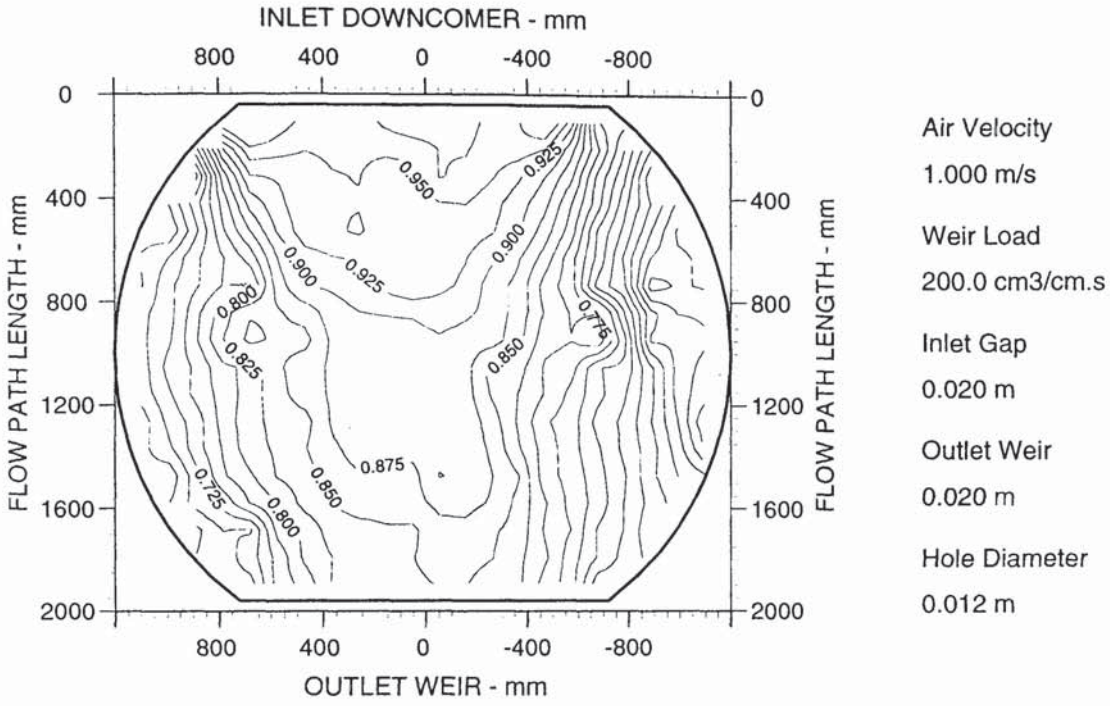

Figure A5.6e Two dimensional reduced temperature profiles.

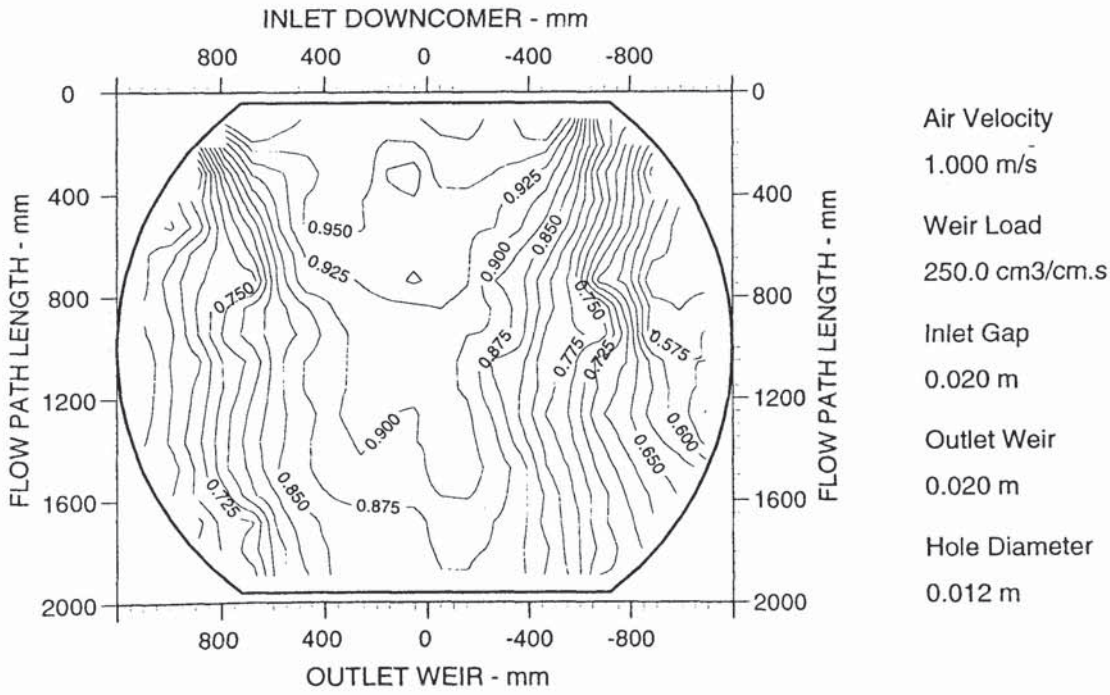

Figure A5.6f Two dimensional reduced temperature profiles.

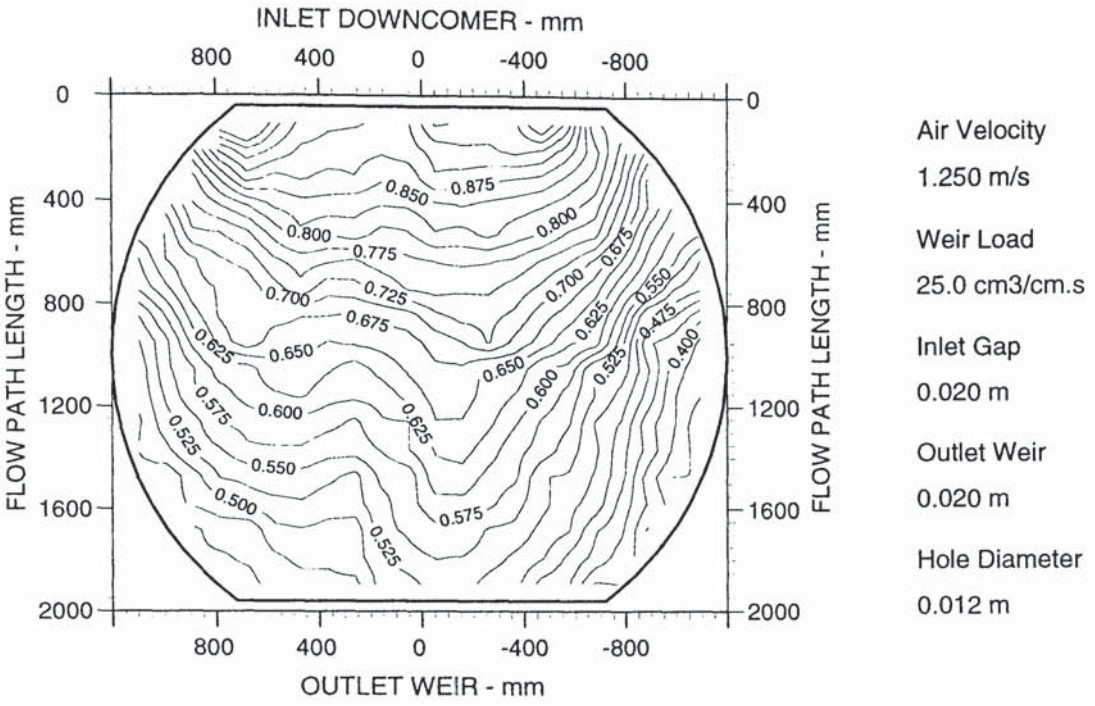

Figure A5.7a Two dimensional reduced temperature profiles.

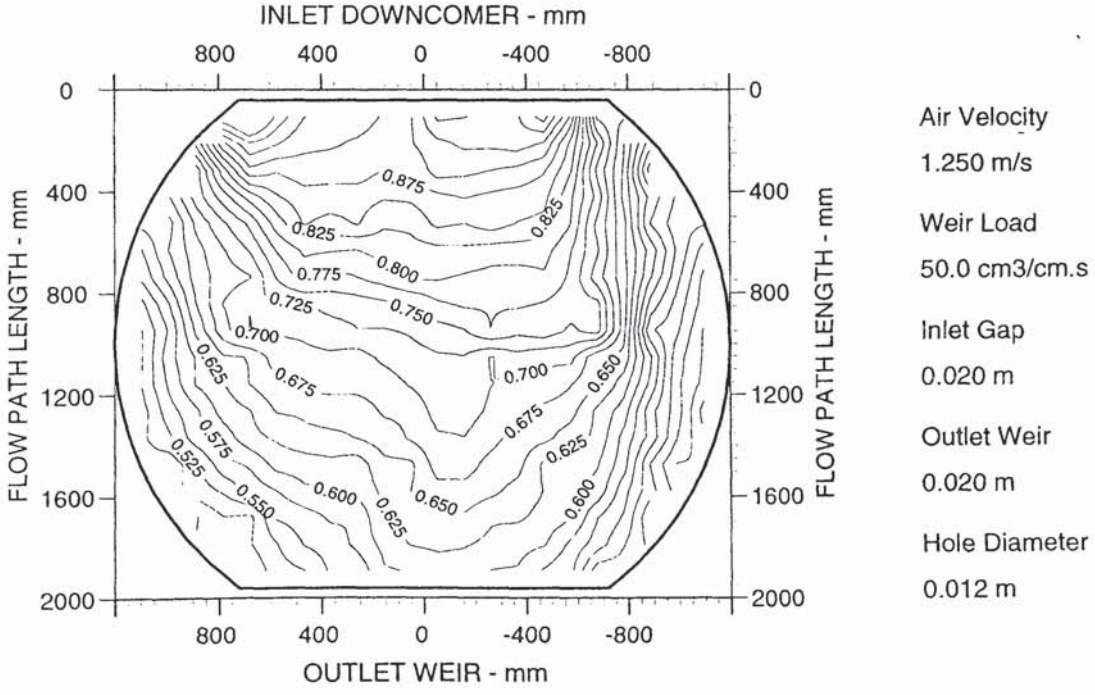

Figure A5.7b Two dimensional reduced temperature profiles.

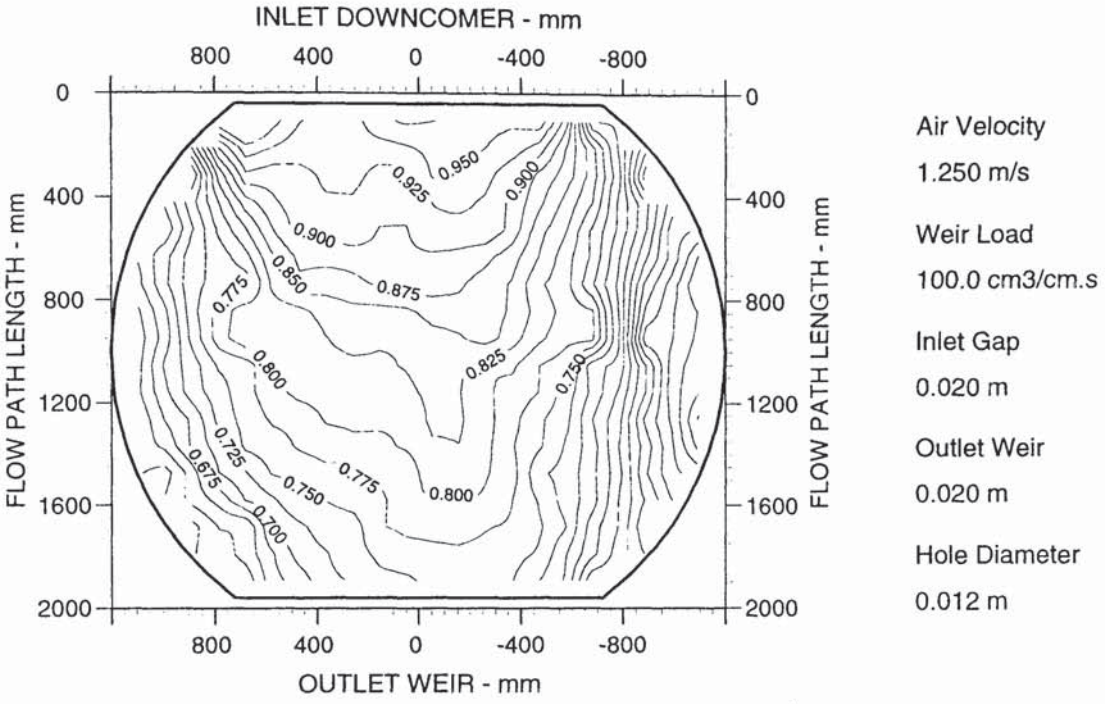

Figure A5.7c Two dimensional reduced temperature profiles.

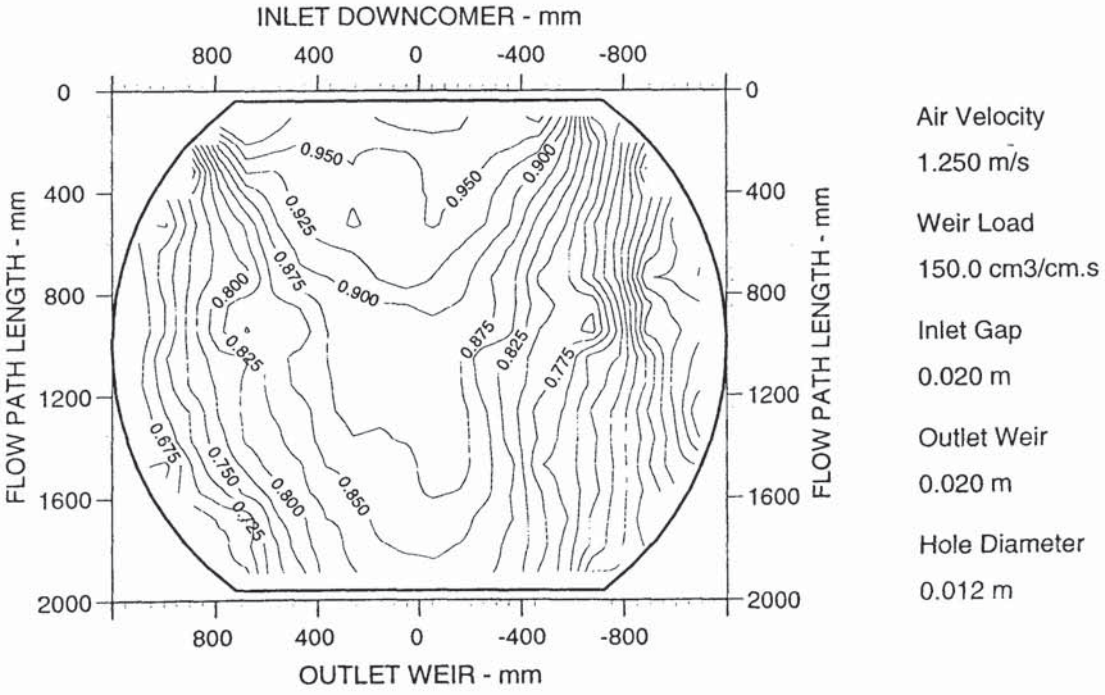

Figure A5.7d Two dimensional reduced temperature profiles.

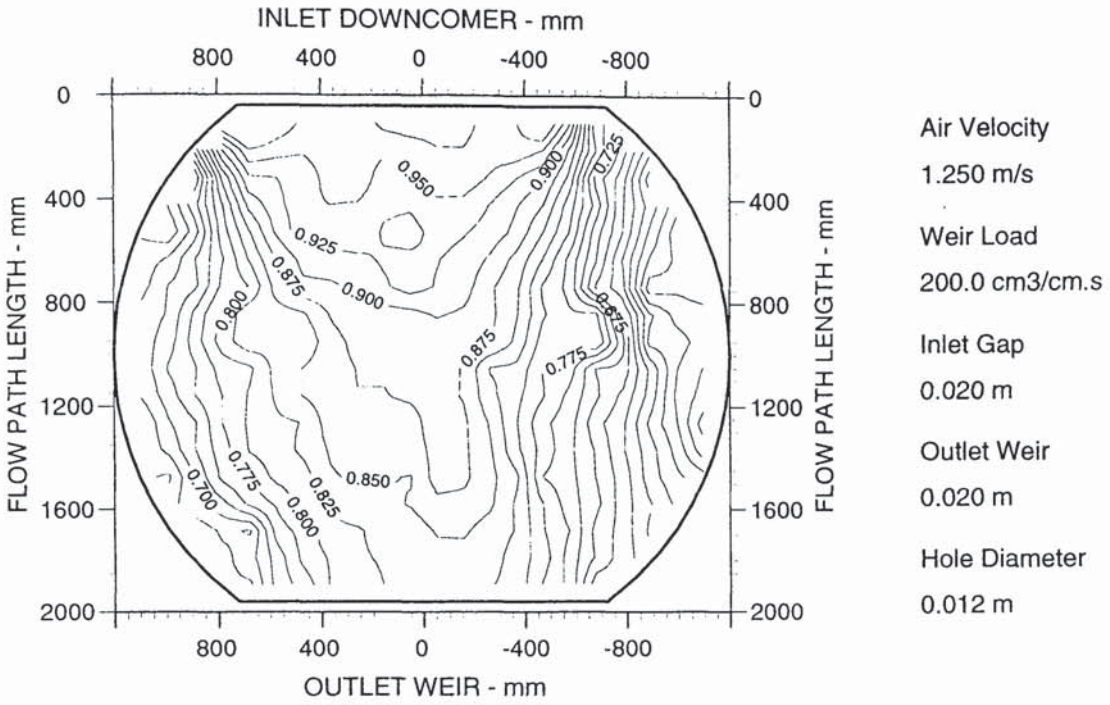

Figure A5.7e Two dimensional reduced temperature profiles.

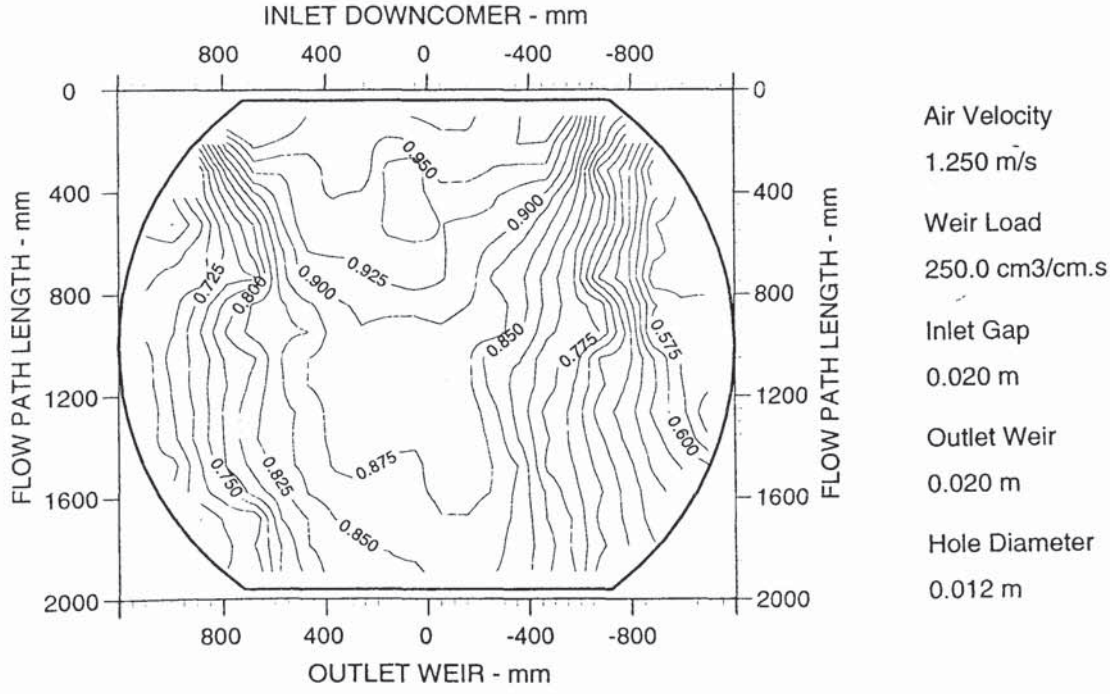

Figure A5.7f Two dimensional reduced temperature profiles.

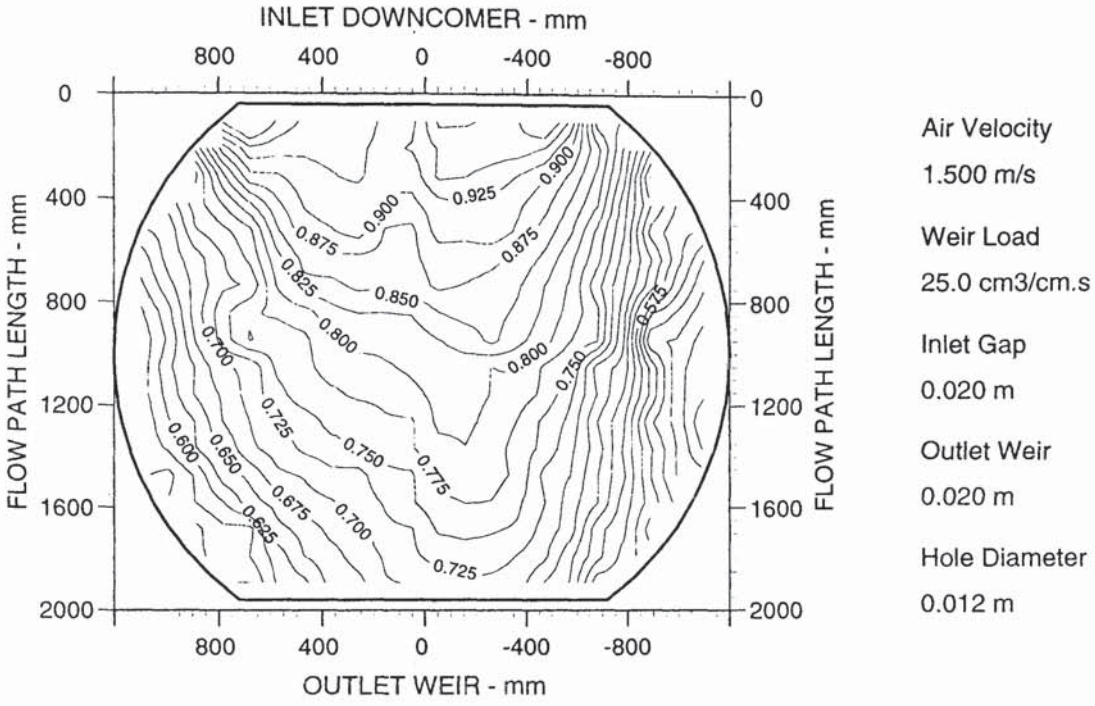

Figure A5.8a Two dimensional reduced temperature profiles.

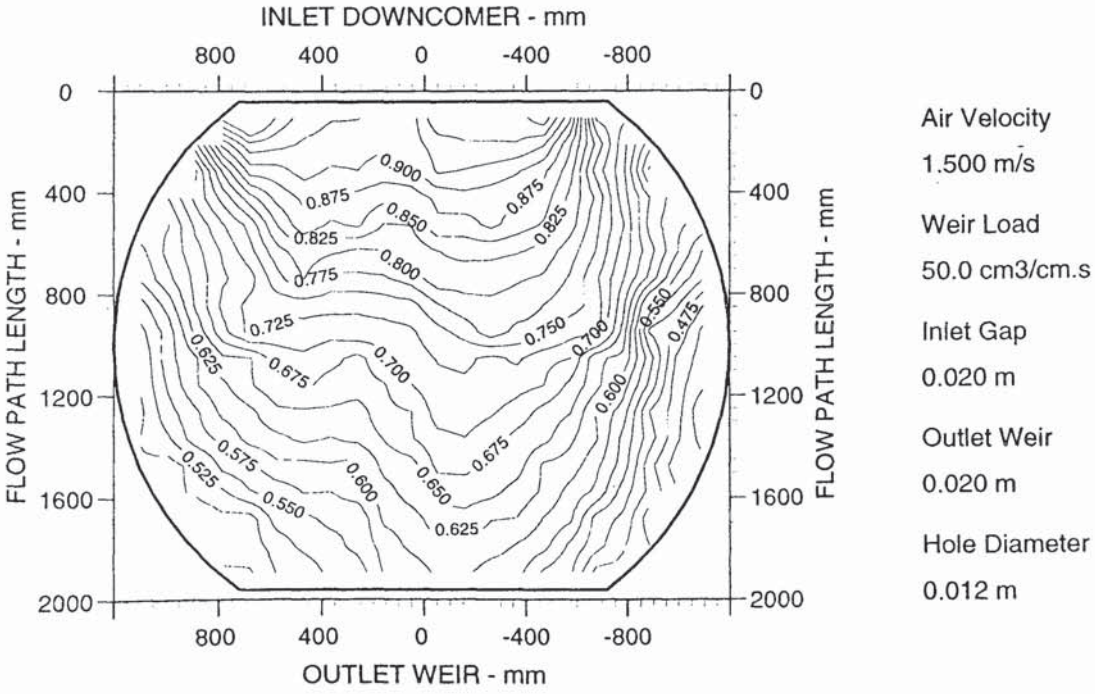

Figure A5.8b Two dimensional reduced temperature profiles.

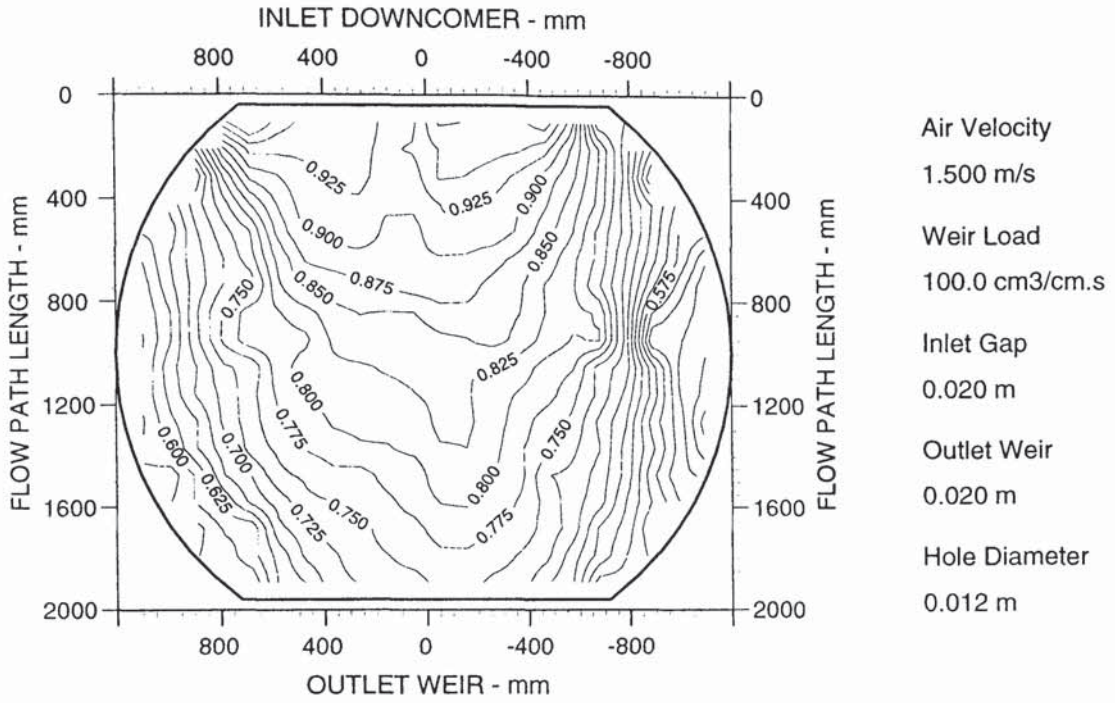

Figure A5.8c Two dimensional reduced temperature profiles.

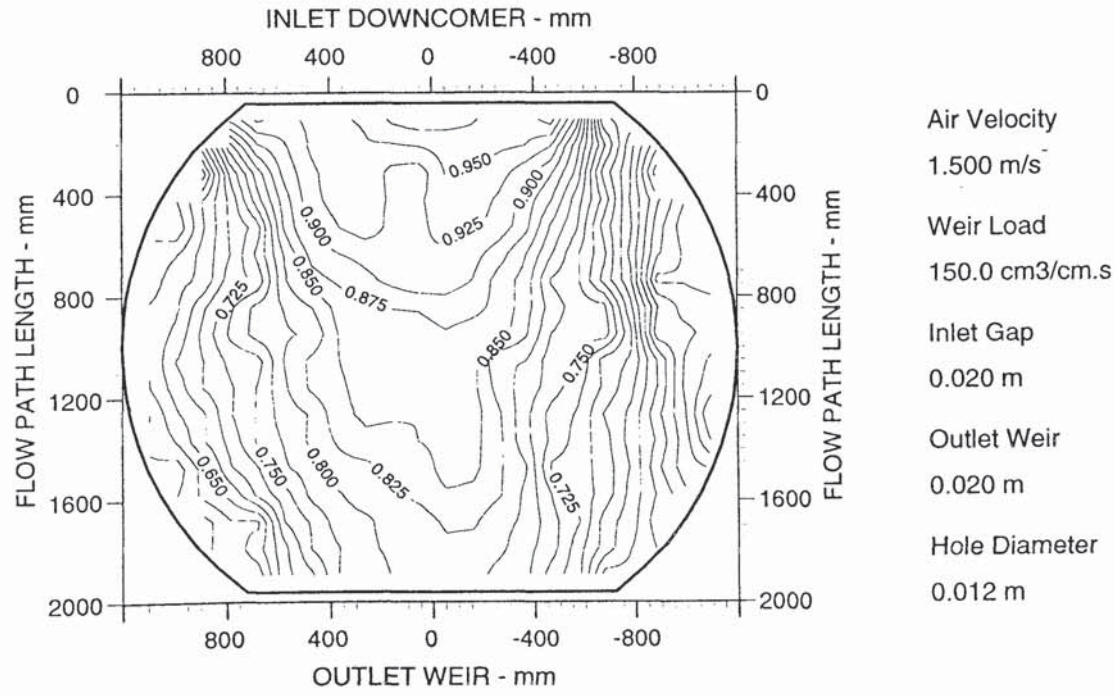

Figure A5.8d Two dimensional reduced temperature profiles.

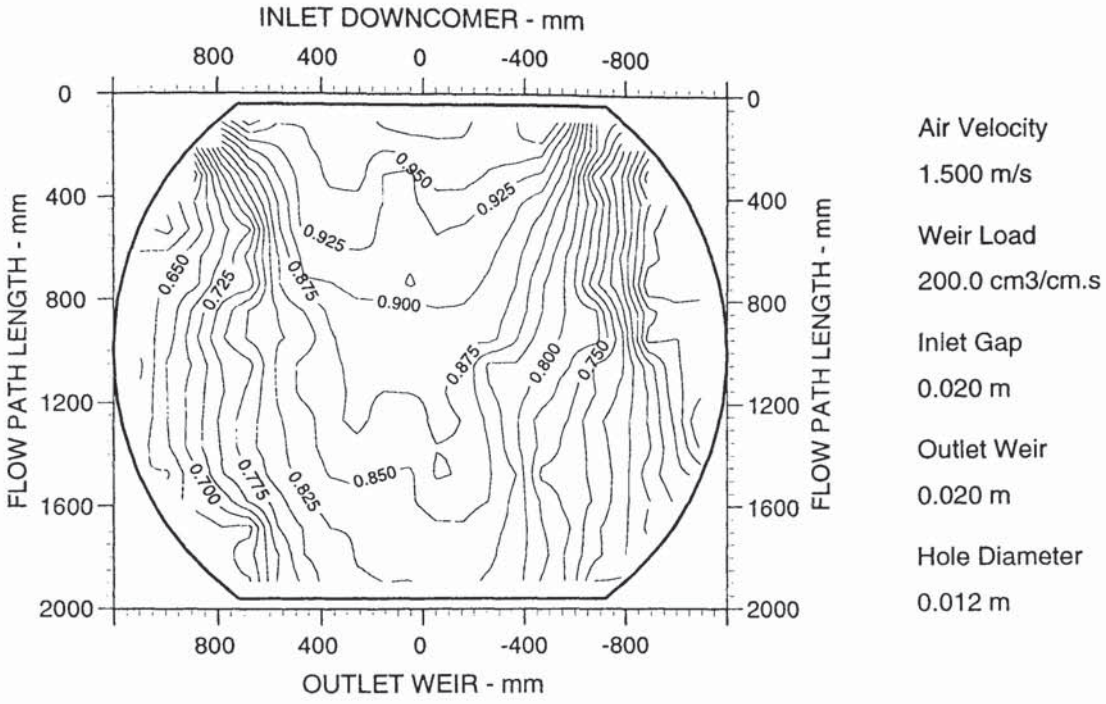

Figure A5.8e Two dimensional reduced temperature profiles.

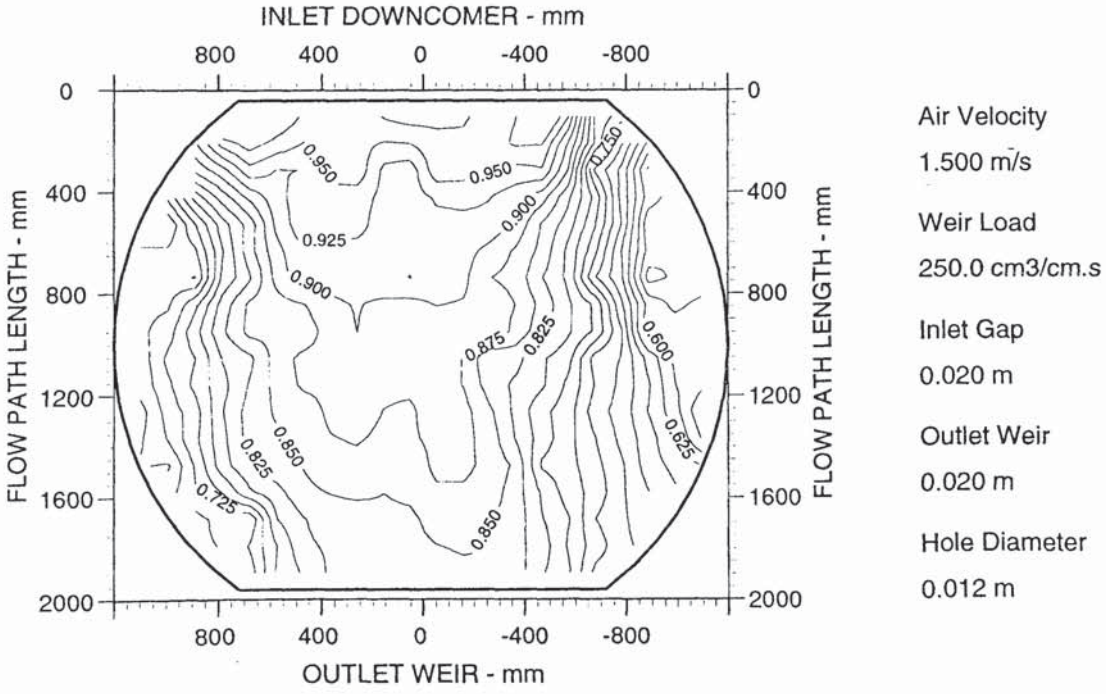

Figure A5.8f Two dimensional reduced temperature profiles.

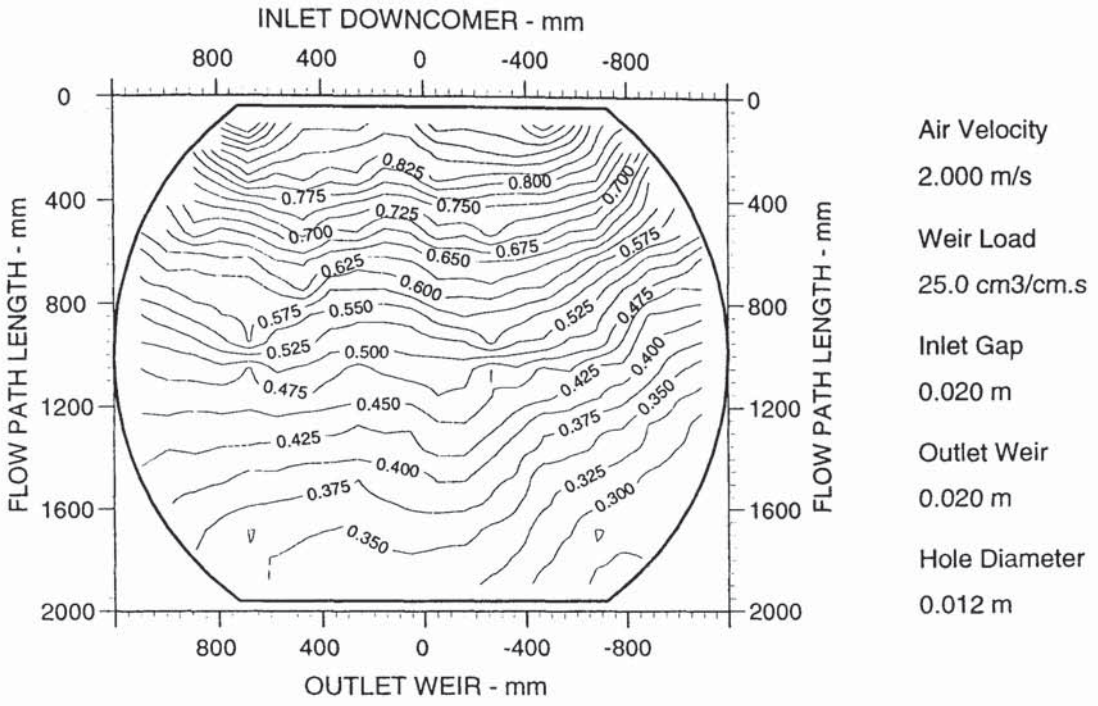

Figure A5.9a Two dimensional reduced temperature profiles.

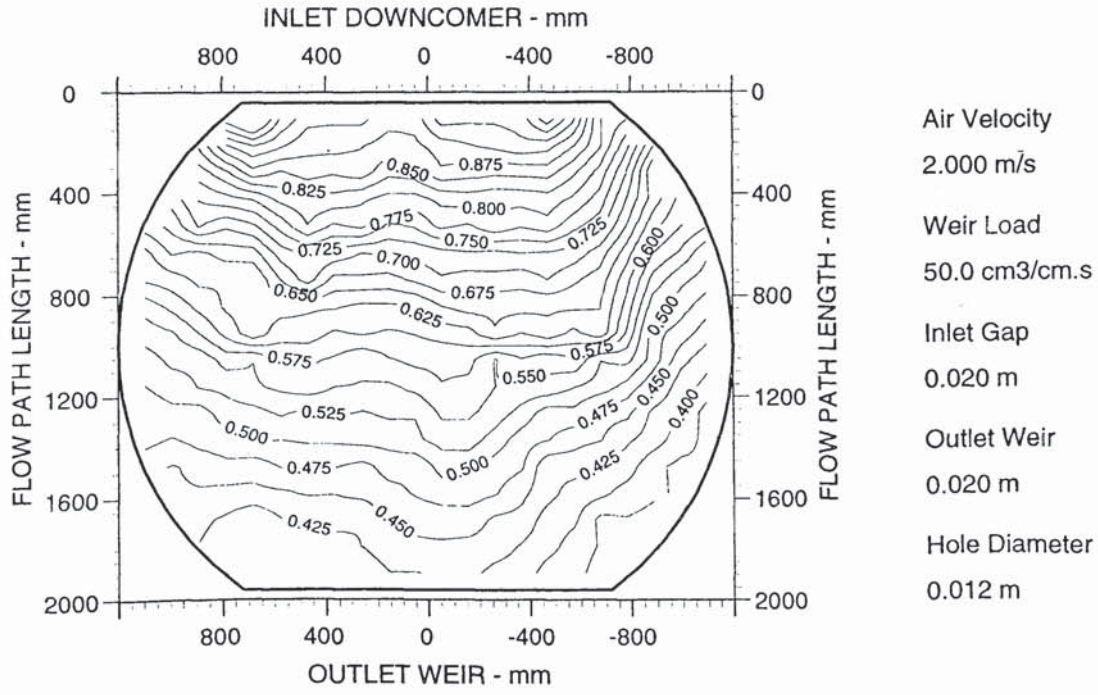

Figure A5.9b Two dimensional reduced temperature profiles.

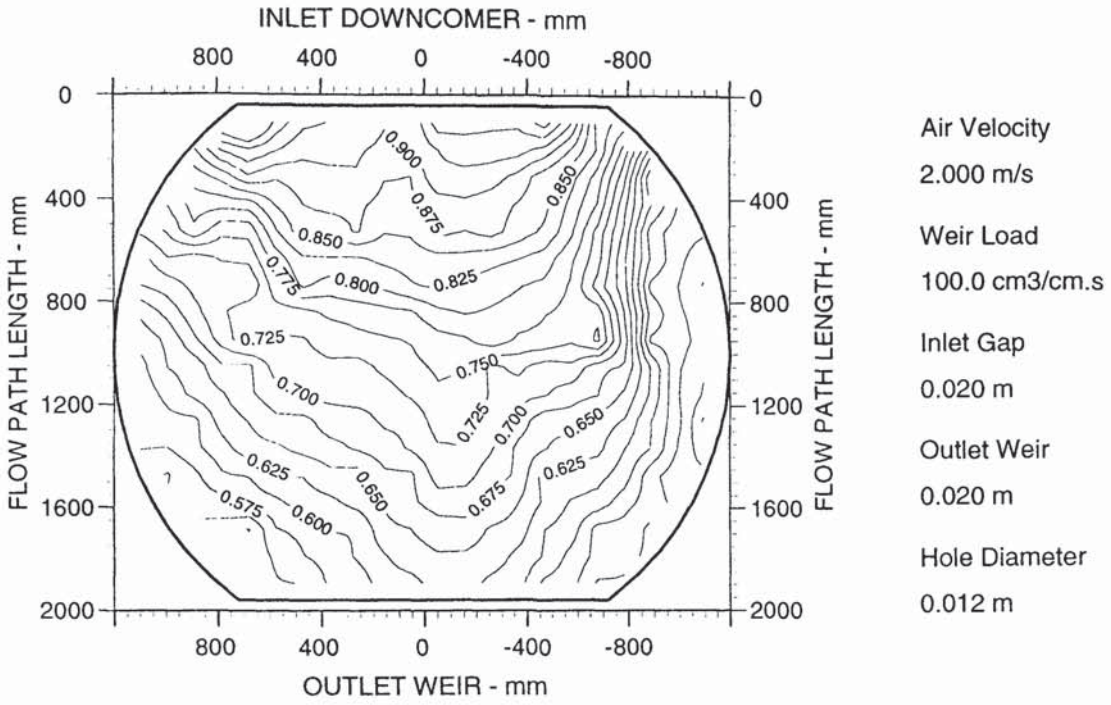

Figure A5.9c Two dimensional reduced temperature profiles.

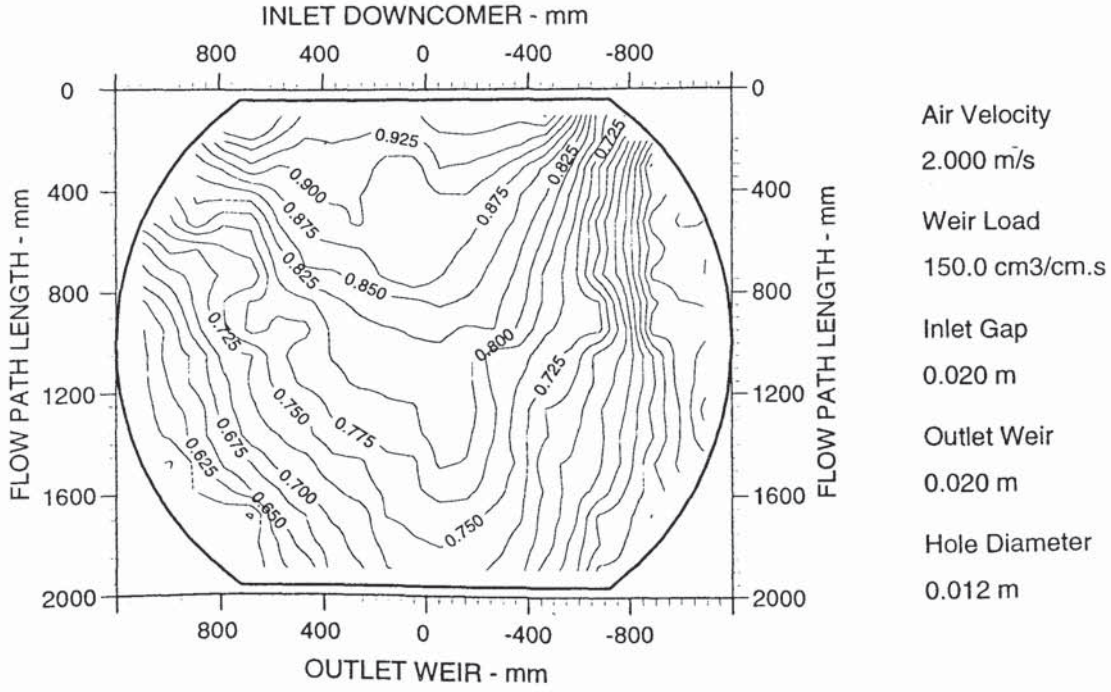

Figure A5.9d Two dimensional reduced temperature profiles.

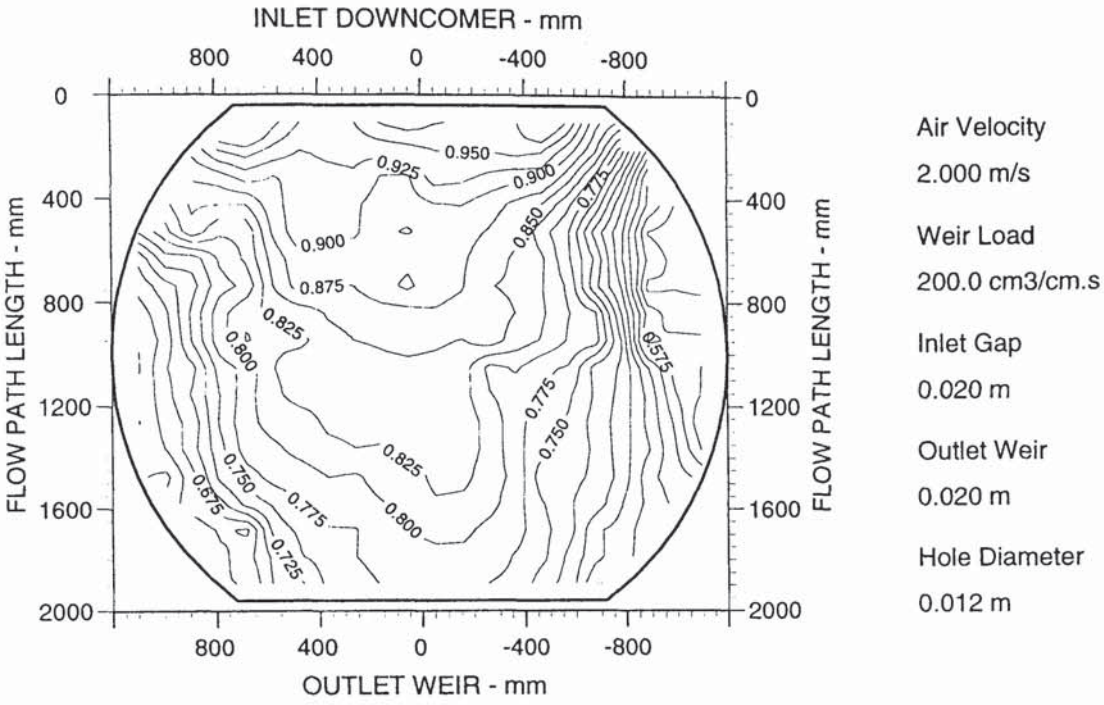

Figure A5.9e Two dimensional reduced temperature profiles.

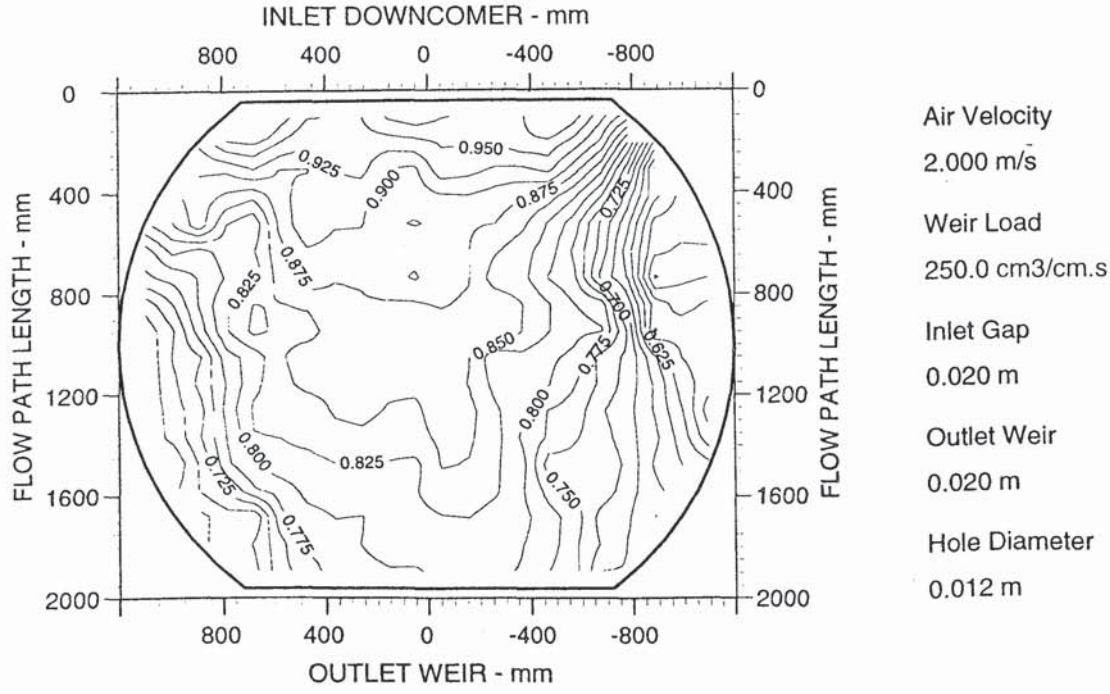

Figure A5.9f Two dimensional reduced temperature profiles.

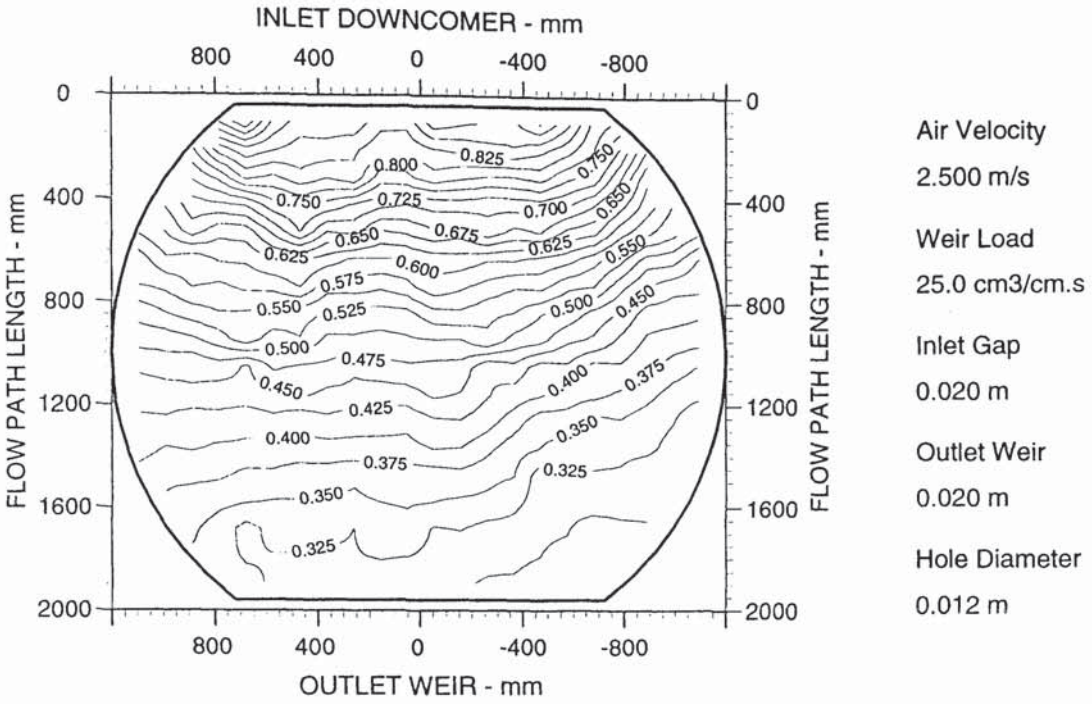

Figure A5.10a Two dimensional reduced temperature profiles.

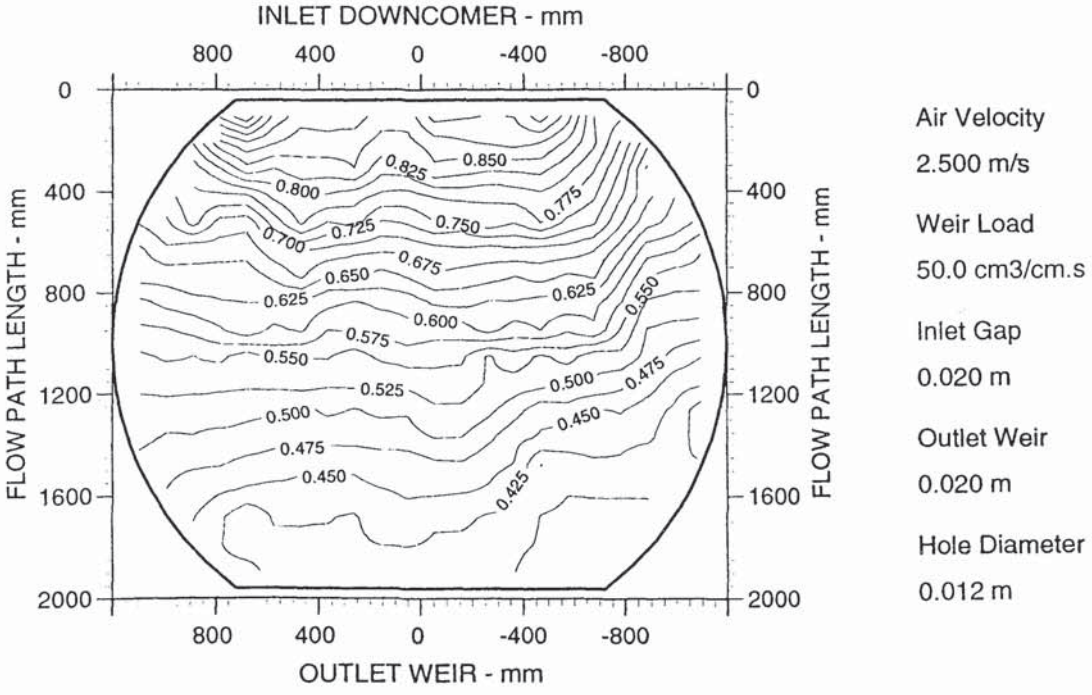

Figure A5.10b Two dimensional reduced temperature profiles.

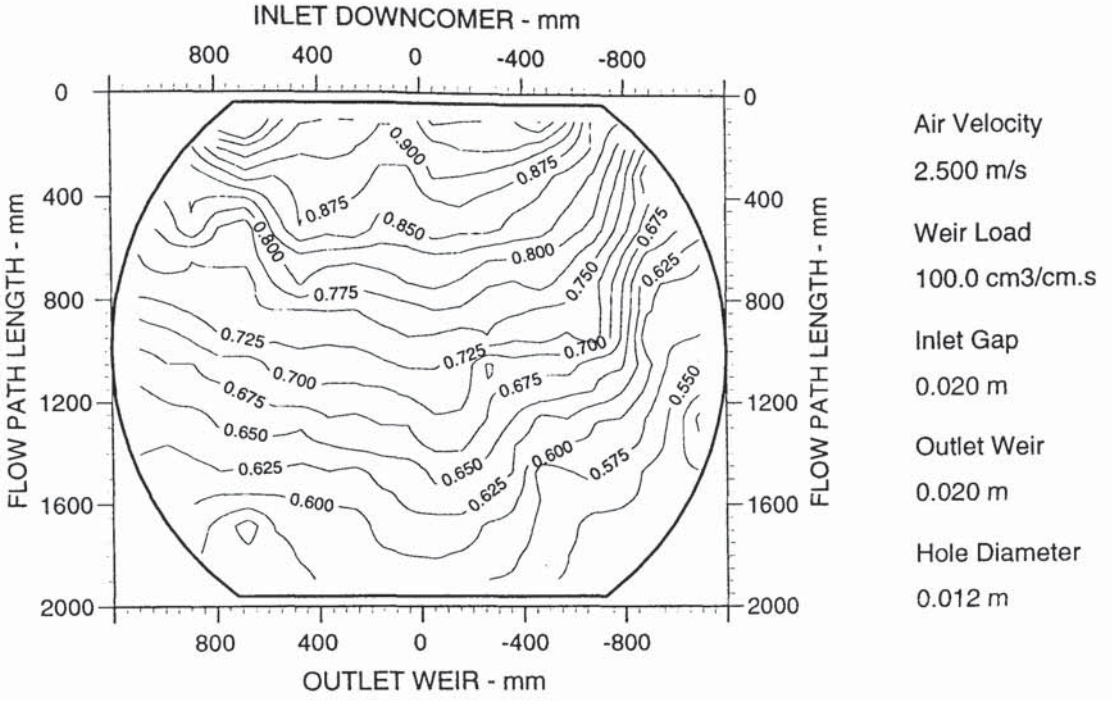

Figure A5.10c Two dimensional reduced temperature profiles.

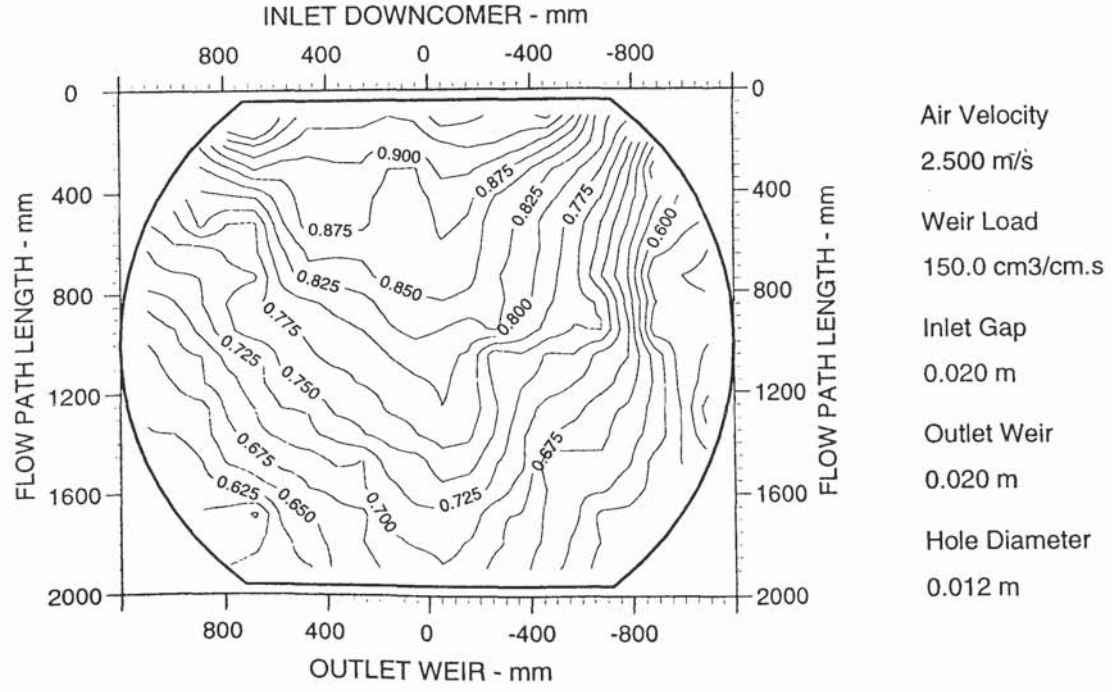

Figure A5.10d Two dimensional reduced temperature profiles.

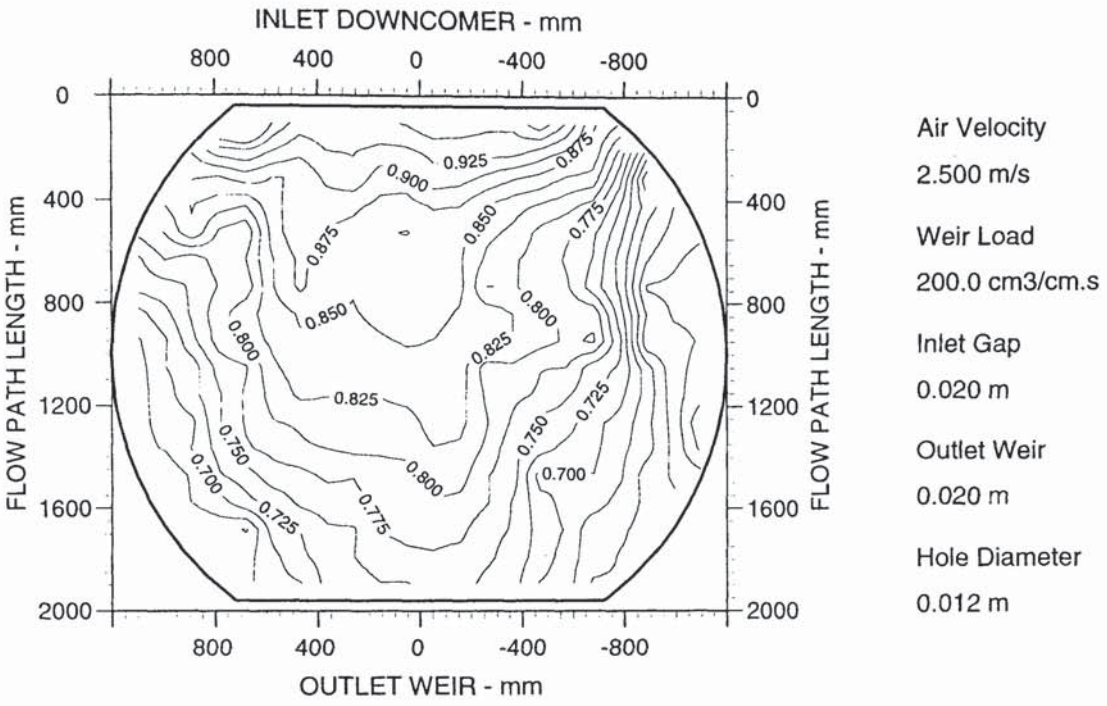

Figure A5.10e Two dimensional reduced temperature profiles.

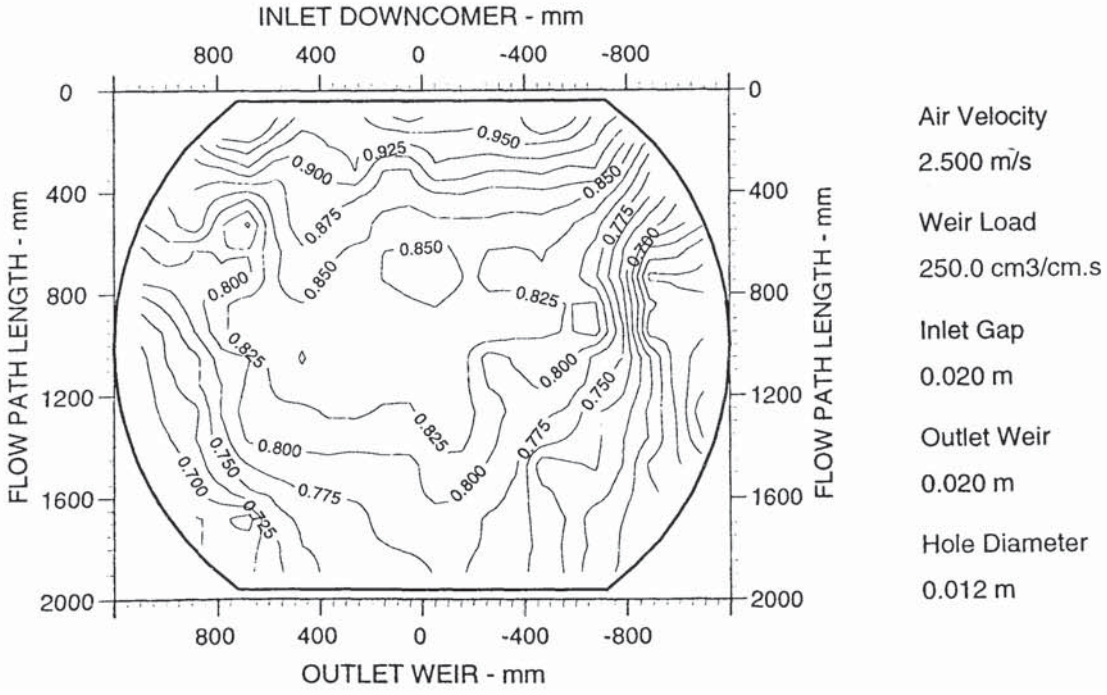

Figure A5.10f Two dimensional reduced temperature profiles.

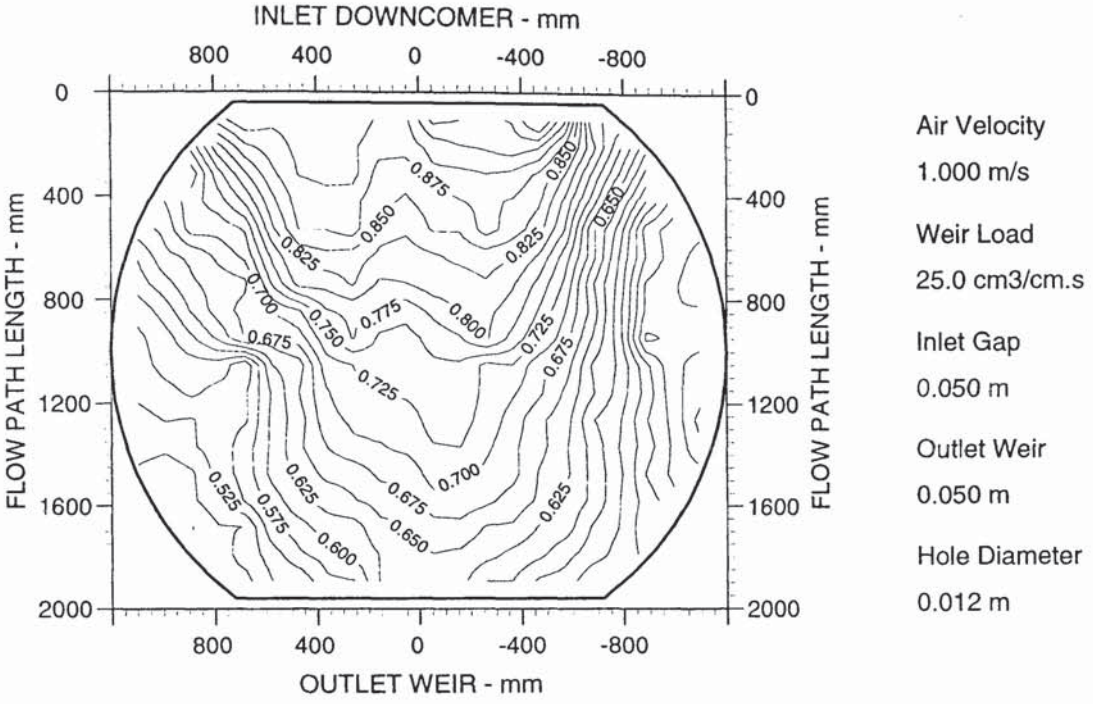

Figure A5.11a Two dimensional reduced temperature profiles.

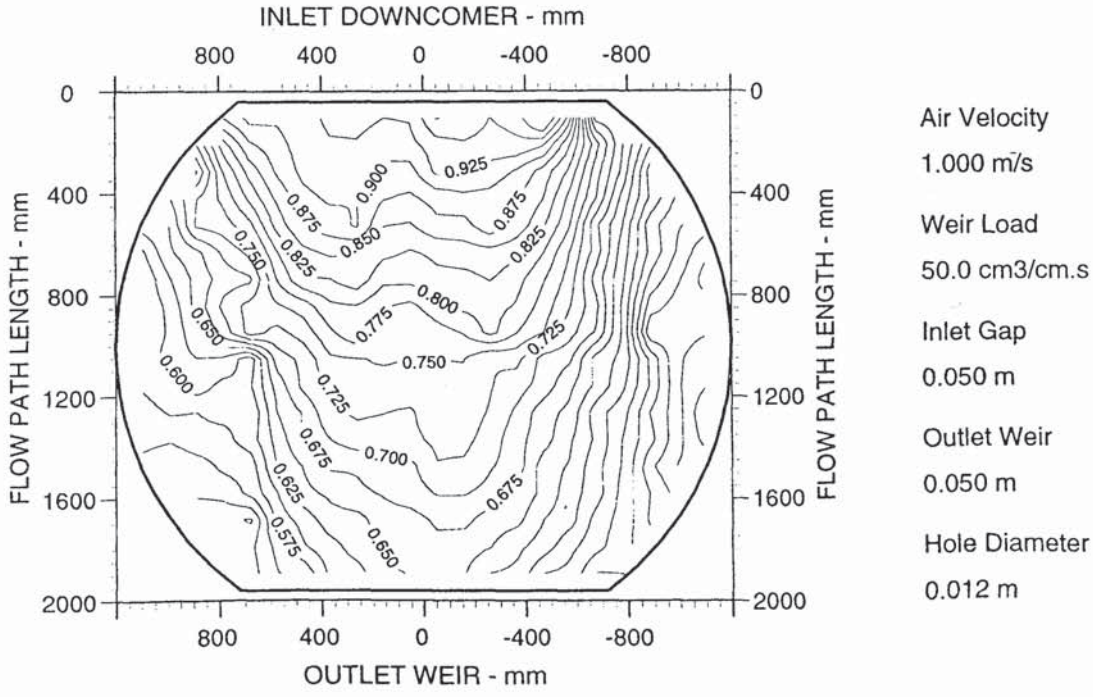

Figure A5.11b Two dimensional reduced temperature profiles.

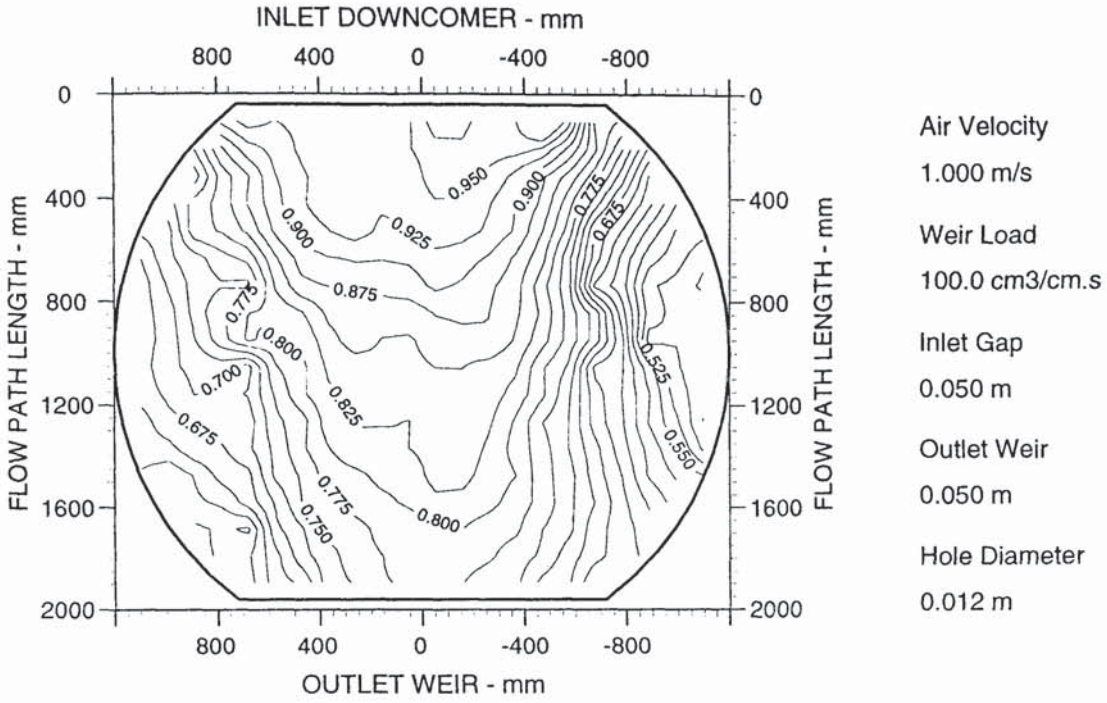

Figure A5.11c Two dimensional reduced temperature profiles.

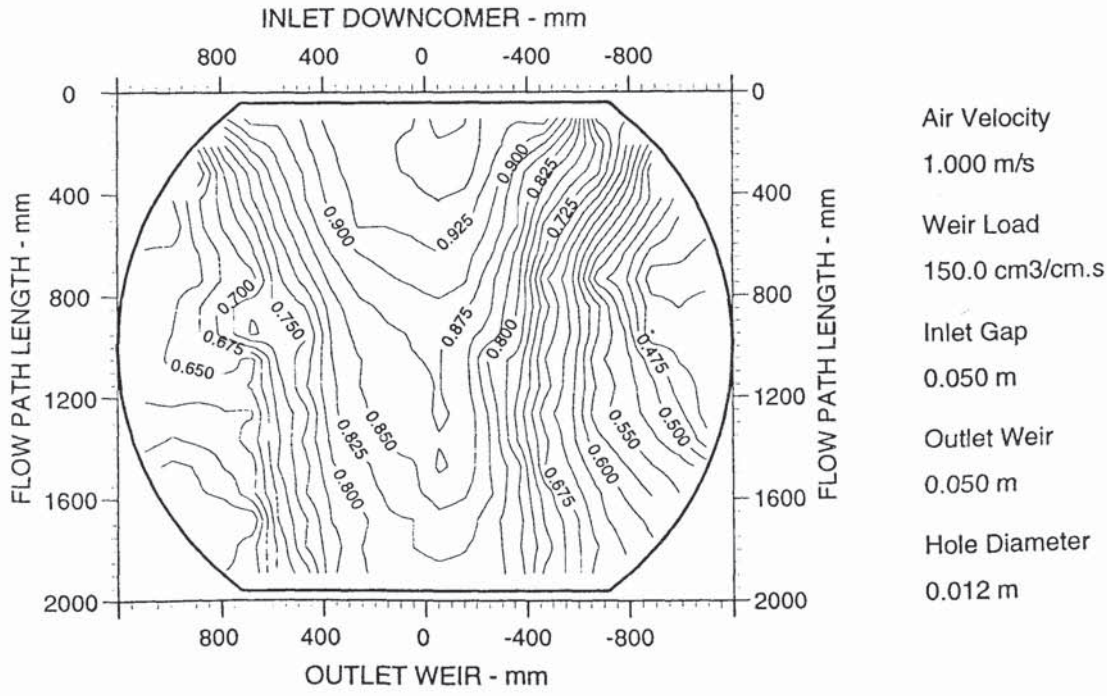

Figure A5.11d Two dimensional reduced temperature profiles.

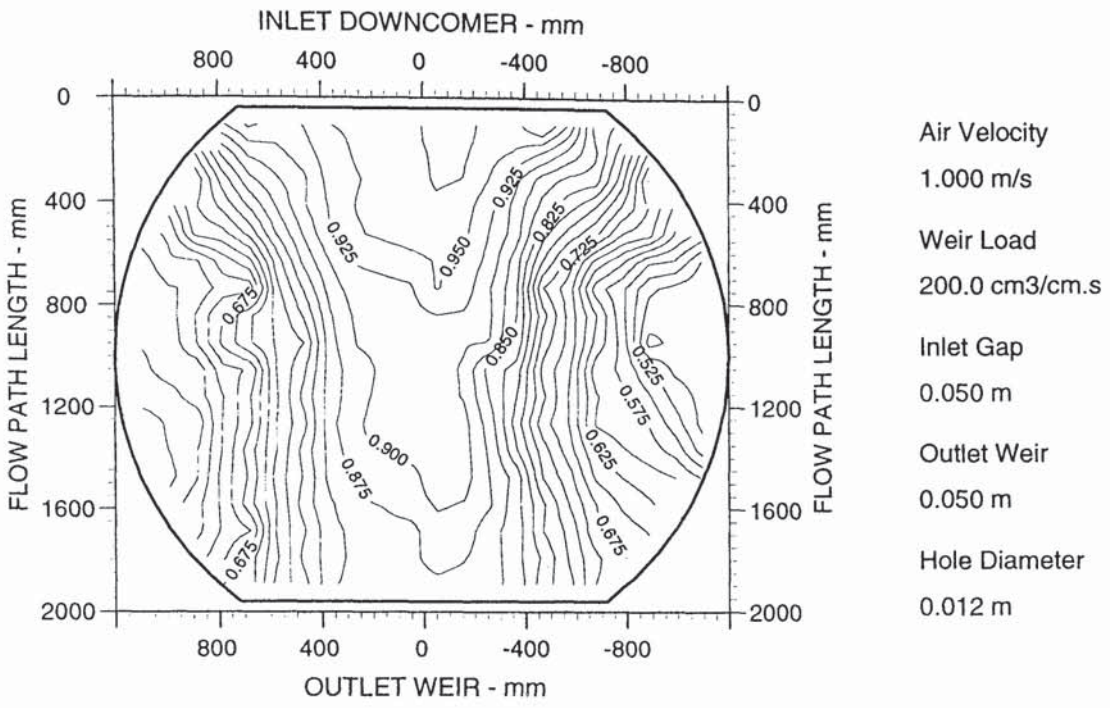

Figure A5.11e Two dimensional reduced temperature profiles.

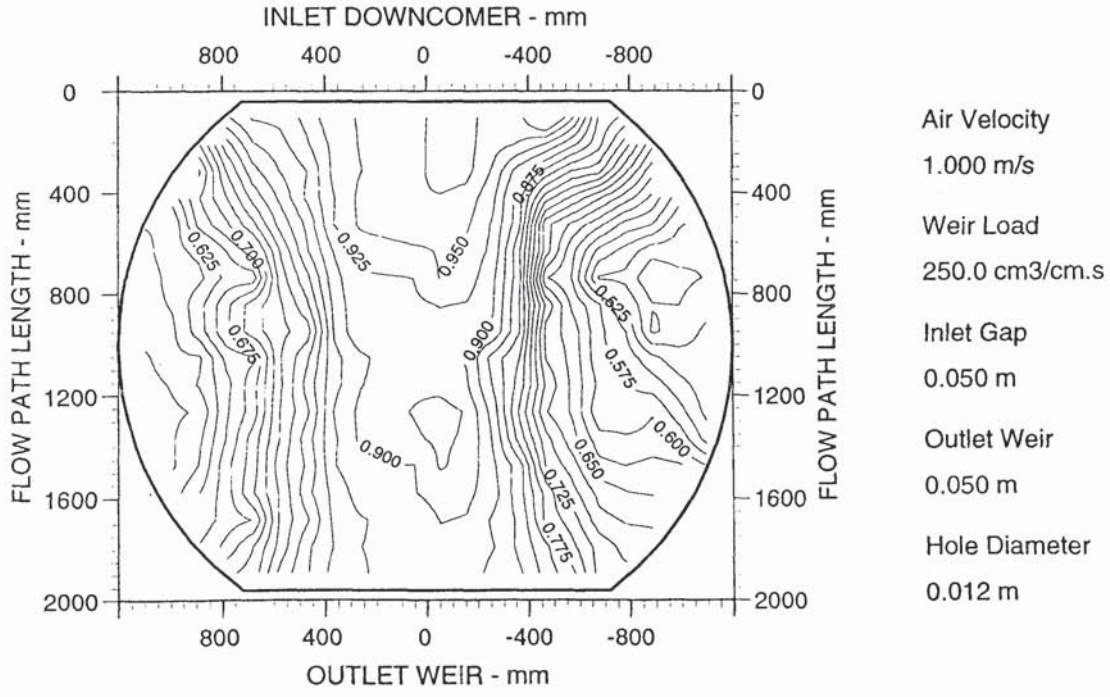

Figure A5.11f Two dimensional reduced temperature profiles.

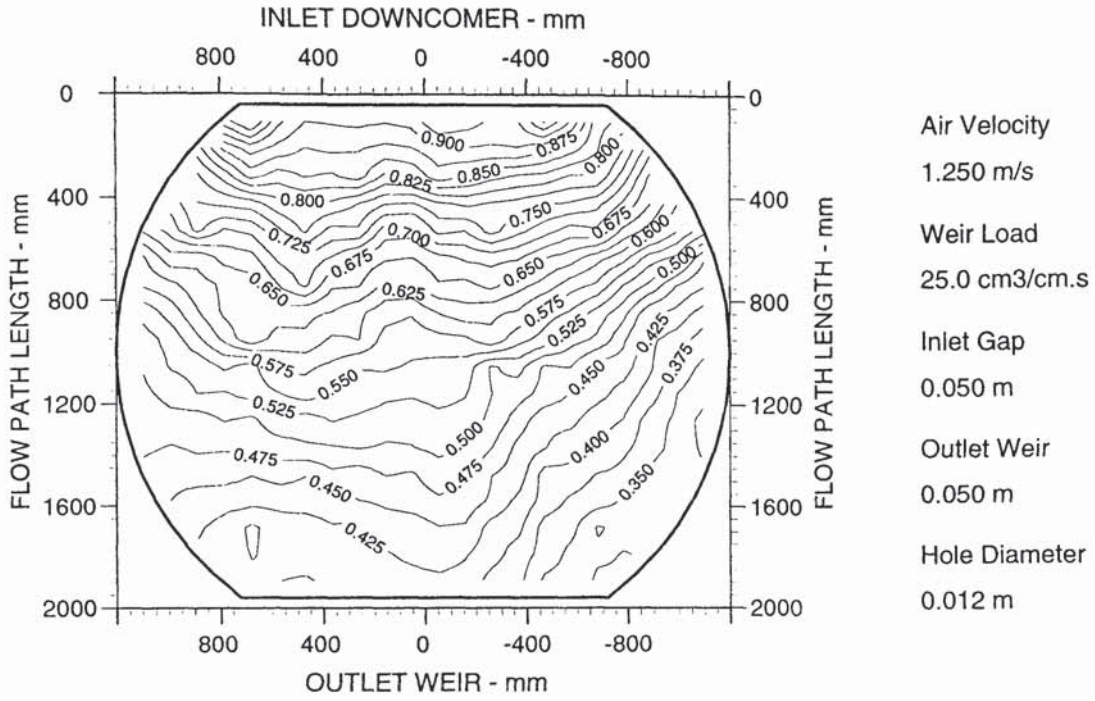

Figure A5.12a Two dimensional reduced temperature profiles.

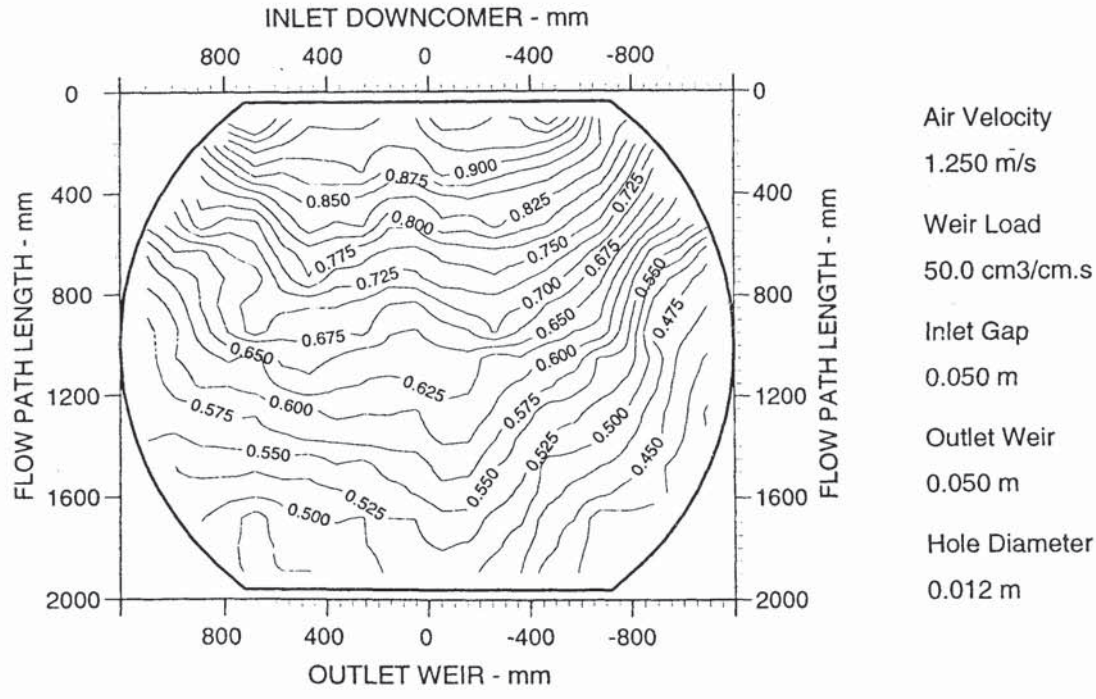

Figure A5.12b Two dimensional reduced temperature profiles.

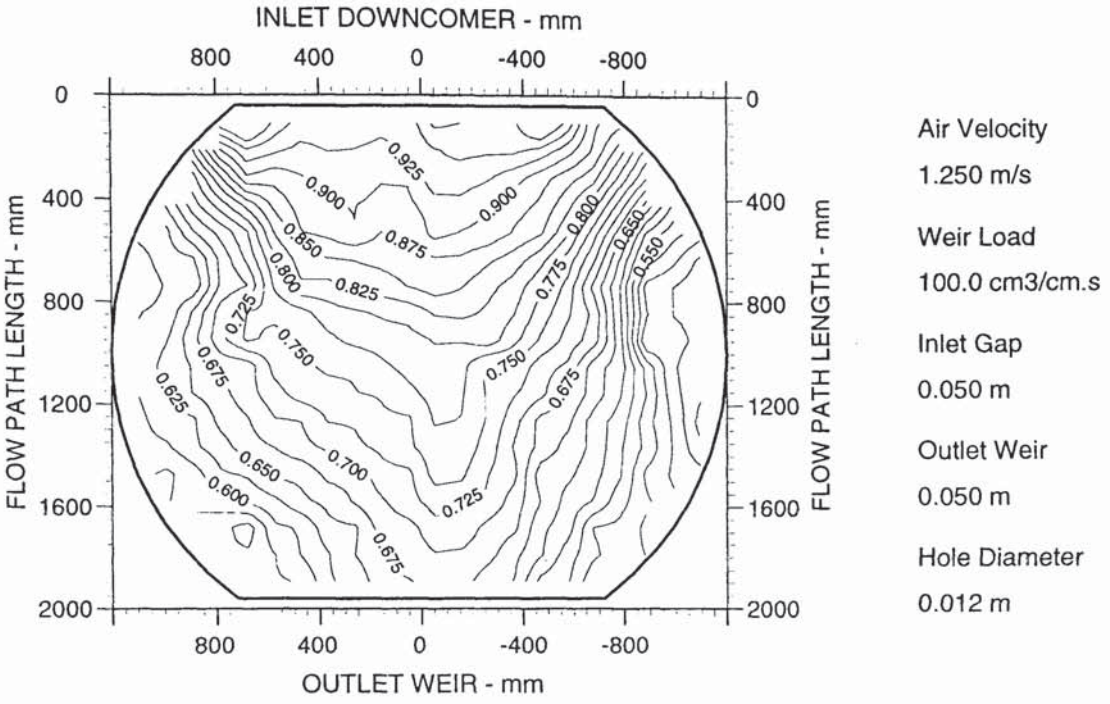

Figure A5.12c Two dimensional reduced temperature profiles.

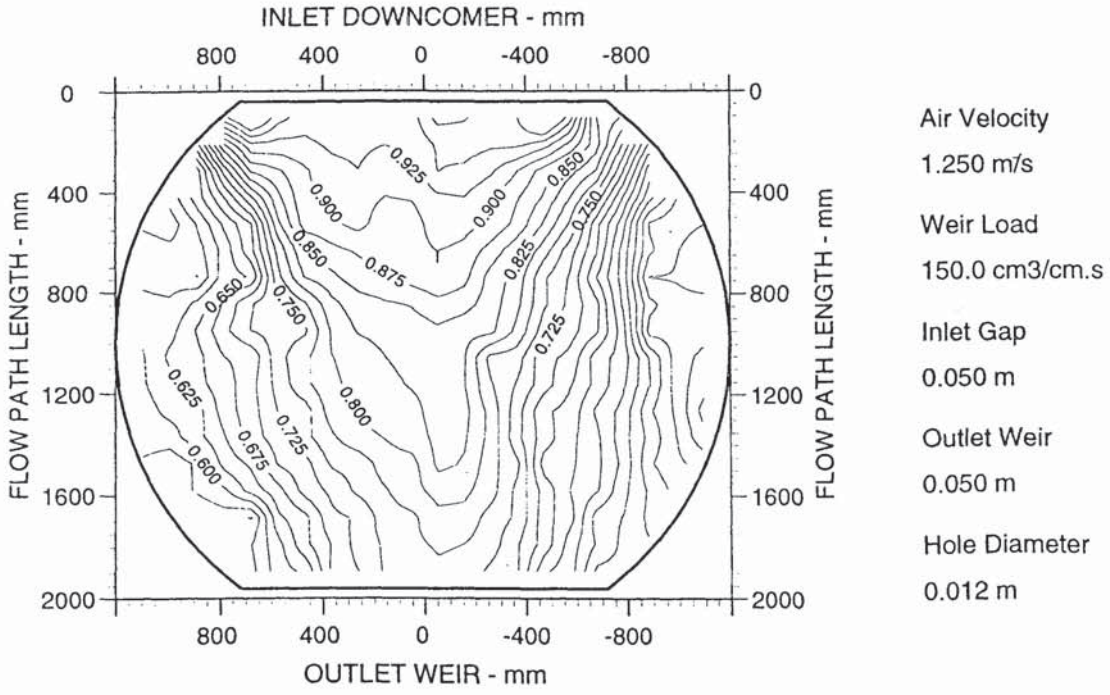

Figure A5.12d Two dimensional reduced temperature profiles.

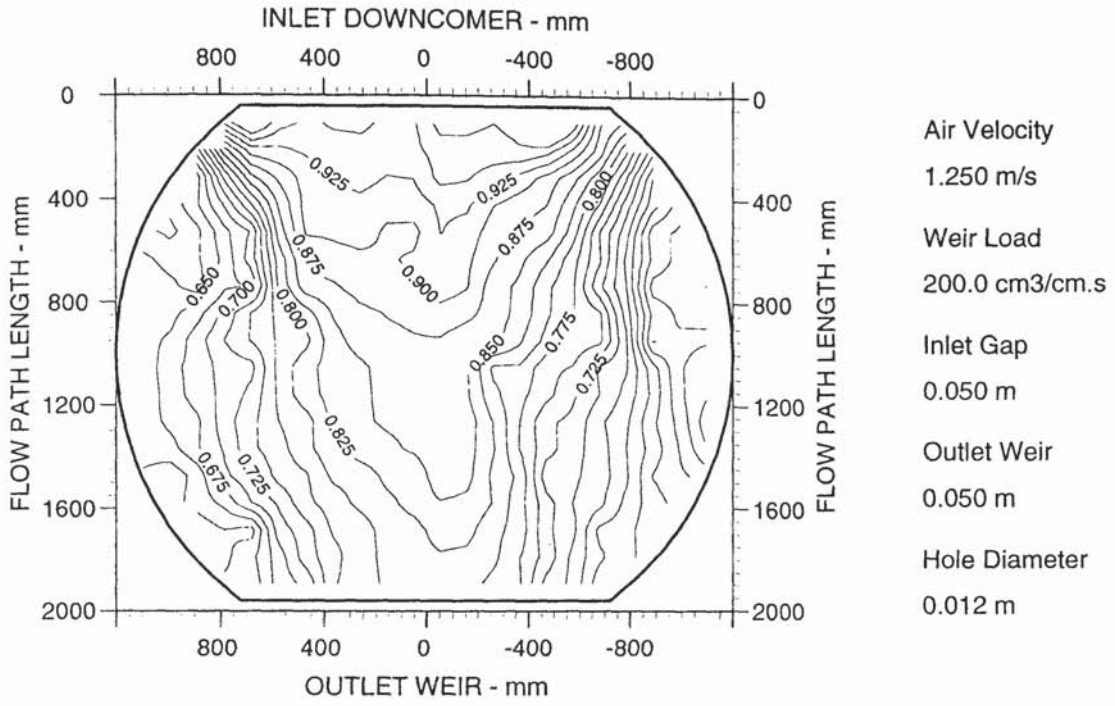

Figure A5.12e Two dimensional reduced temperature profiles.

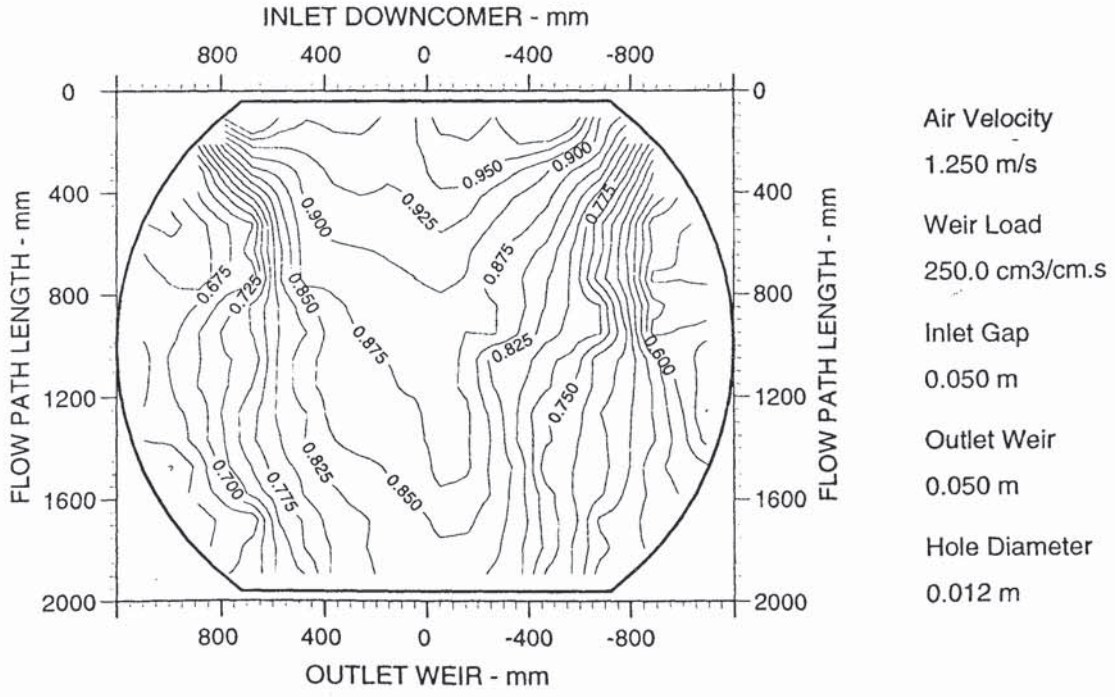

Figure A5.12f Two dimensional reduced temperature profiles.

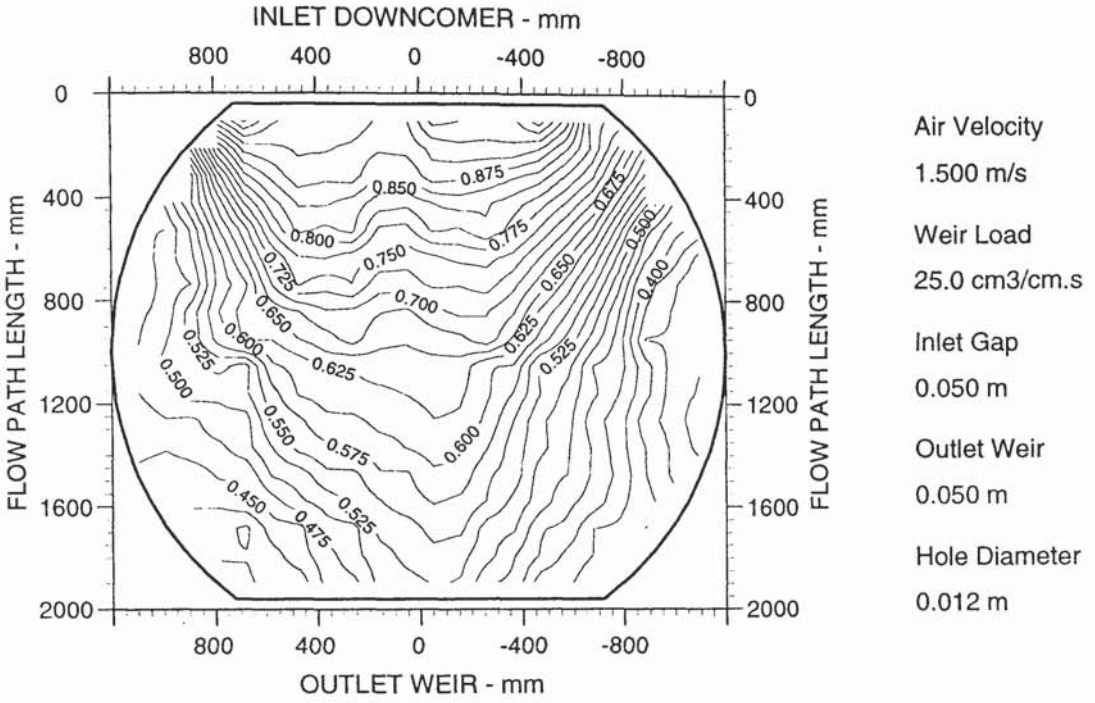

Figure A5.13a Two dimensional reduced temperature profiles.

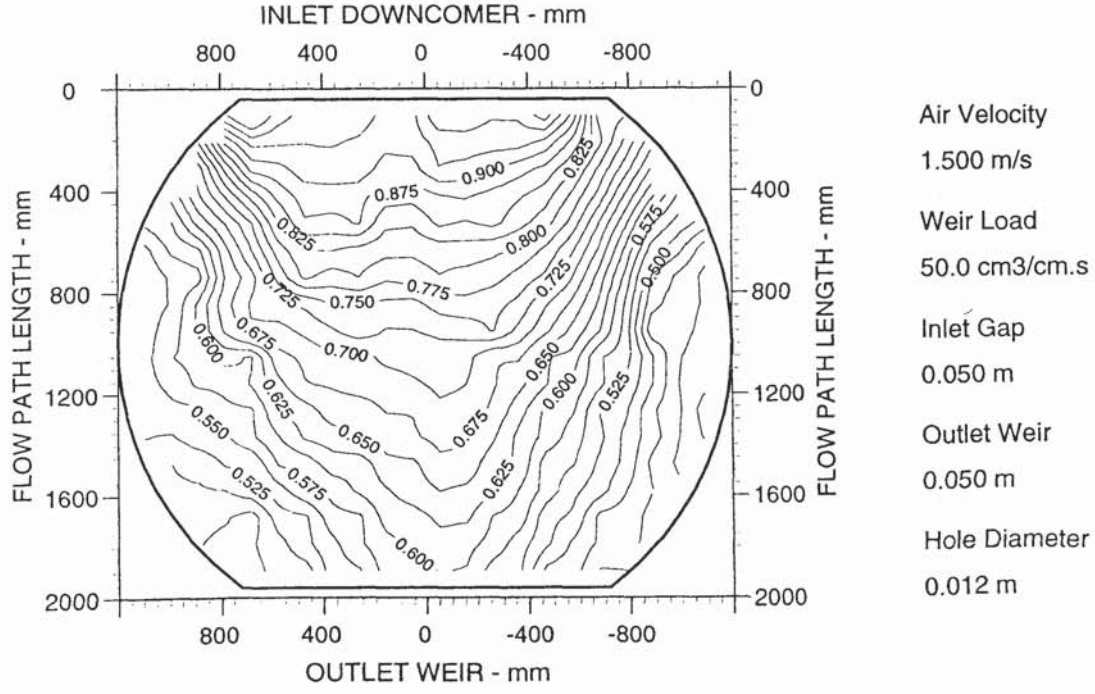

Figure A5.13b Two dimensional reduced temperature profiles.

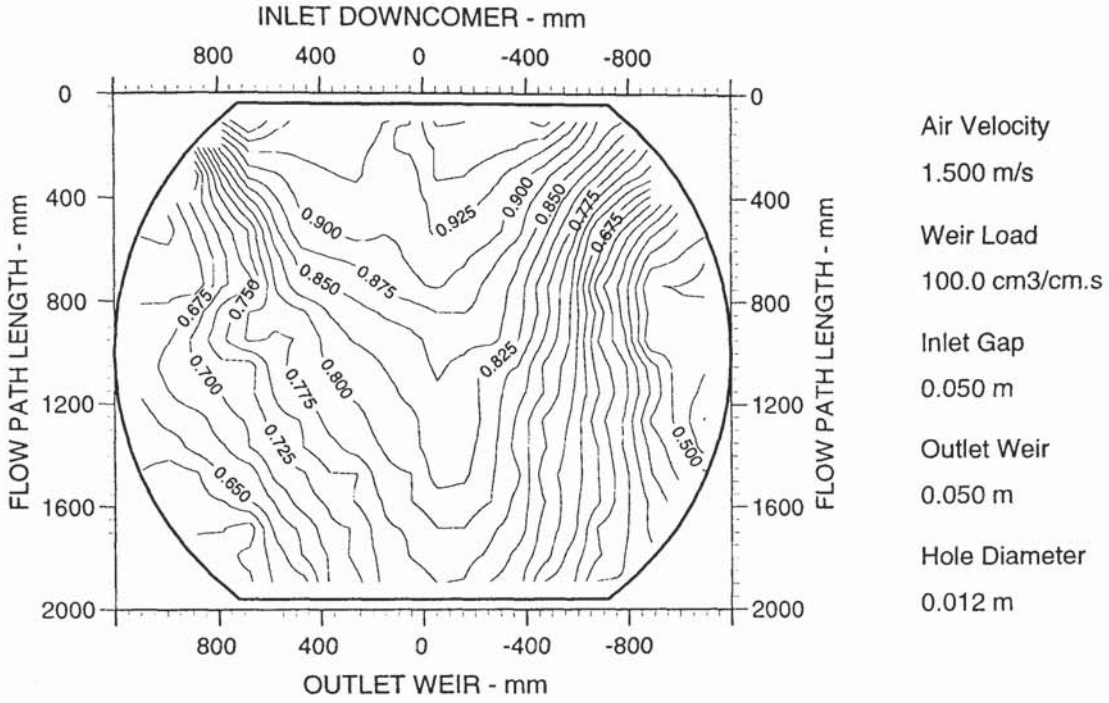

Figure A5.13c Two dimensional reduced temperature profiles.

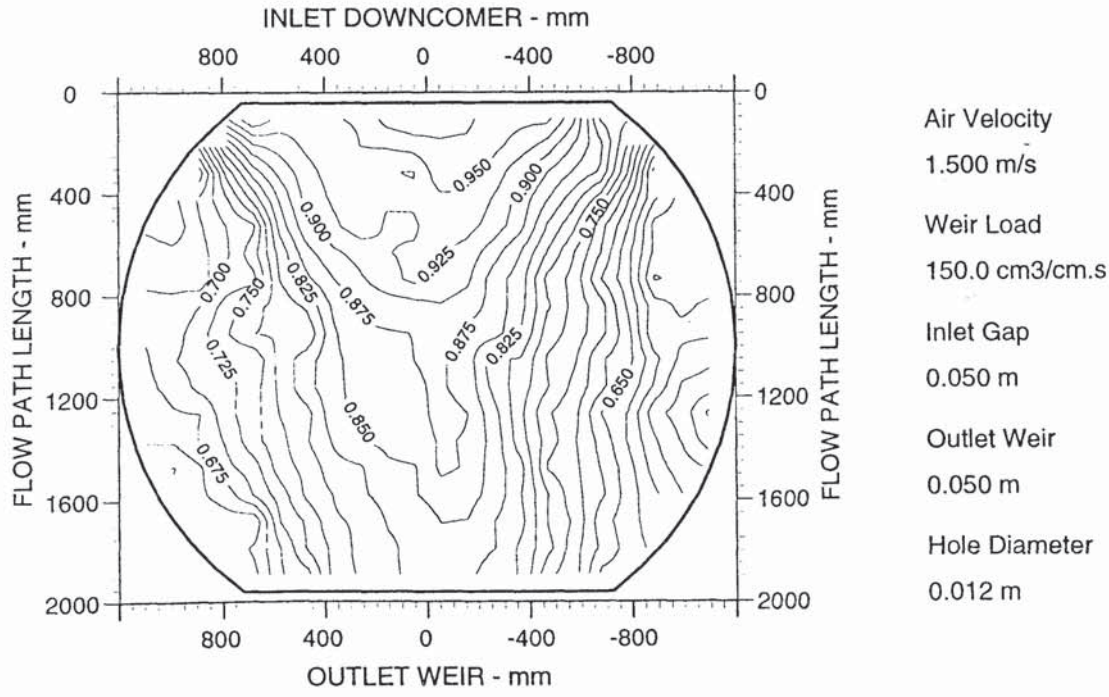

Figure A5.13d Two dimensional reduced temperature profiles.

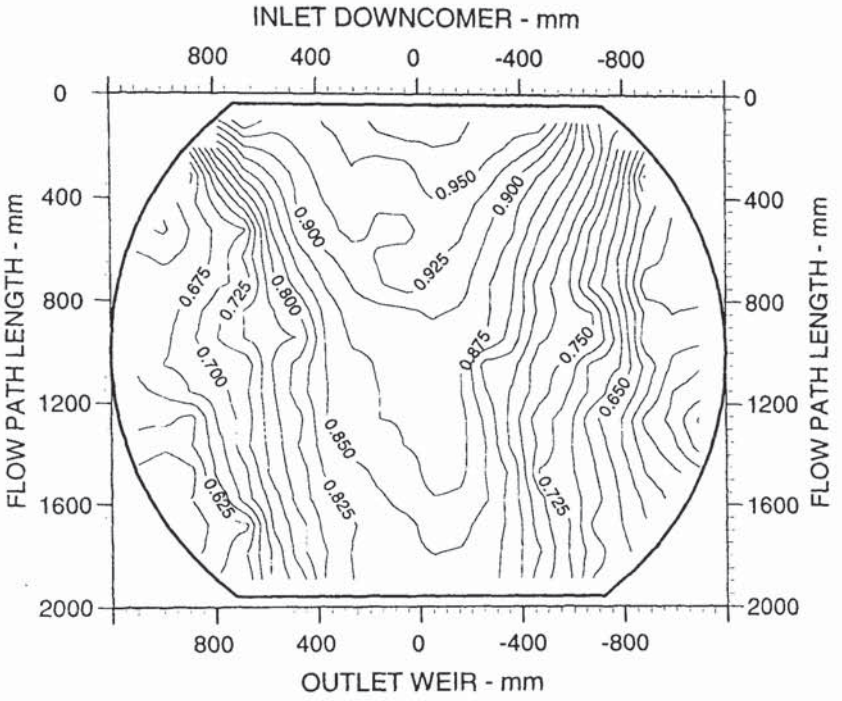

Figure A5.13e Two dimensional reduced temperature profiles.

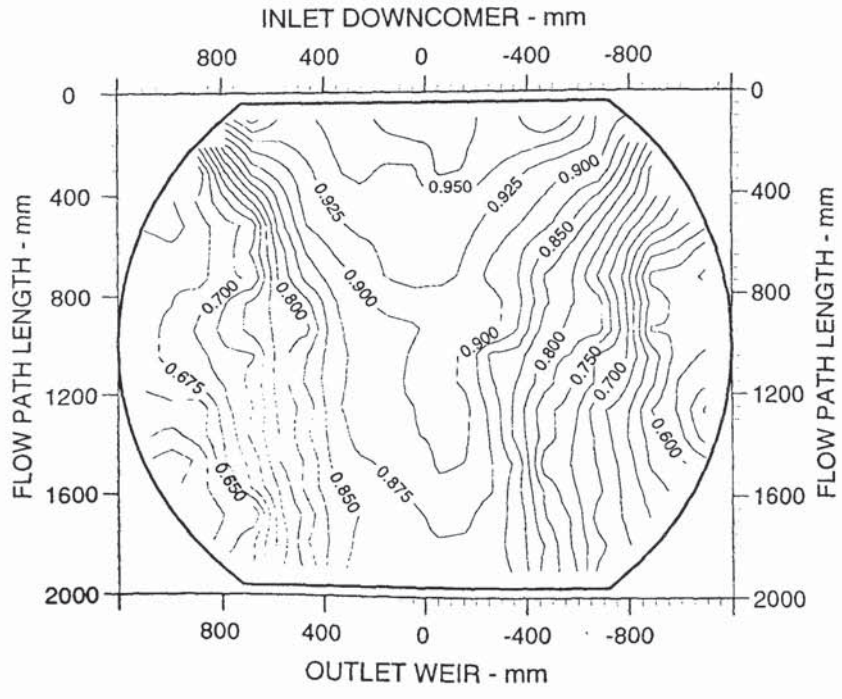

Figure A5.13f Two dimensional reduced temperature profiles.

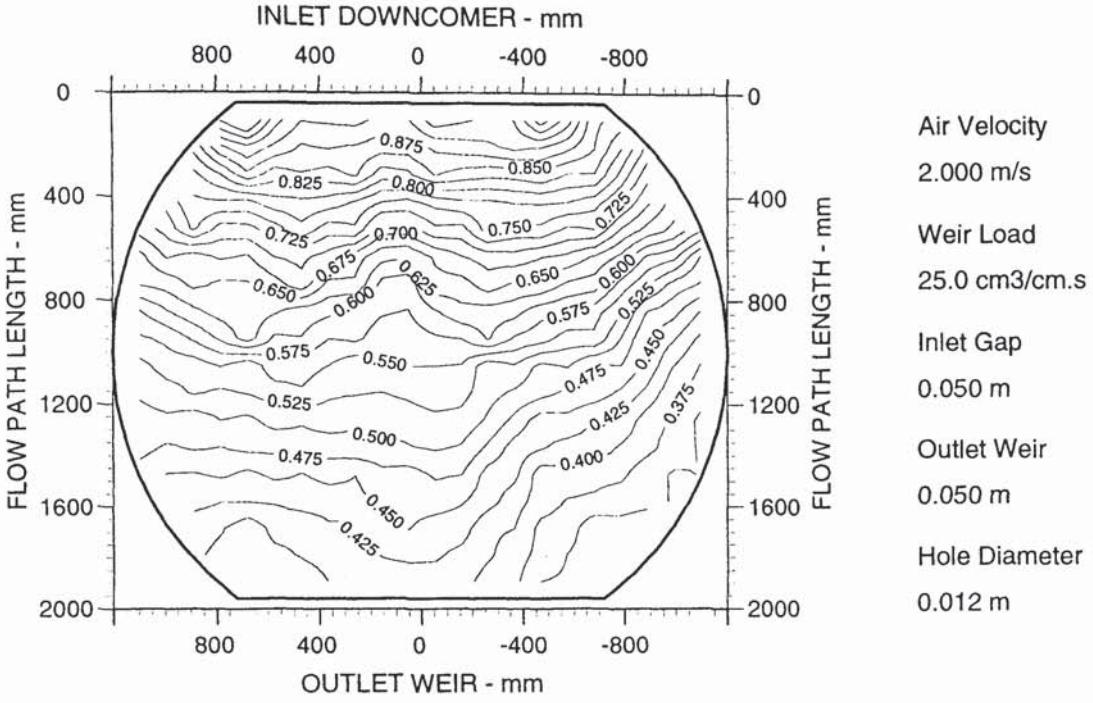

Figure A5.14a Two dimensional reduced temperature profiles.

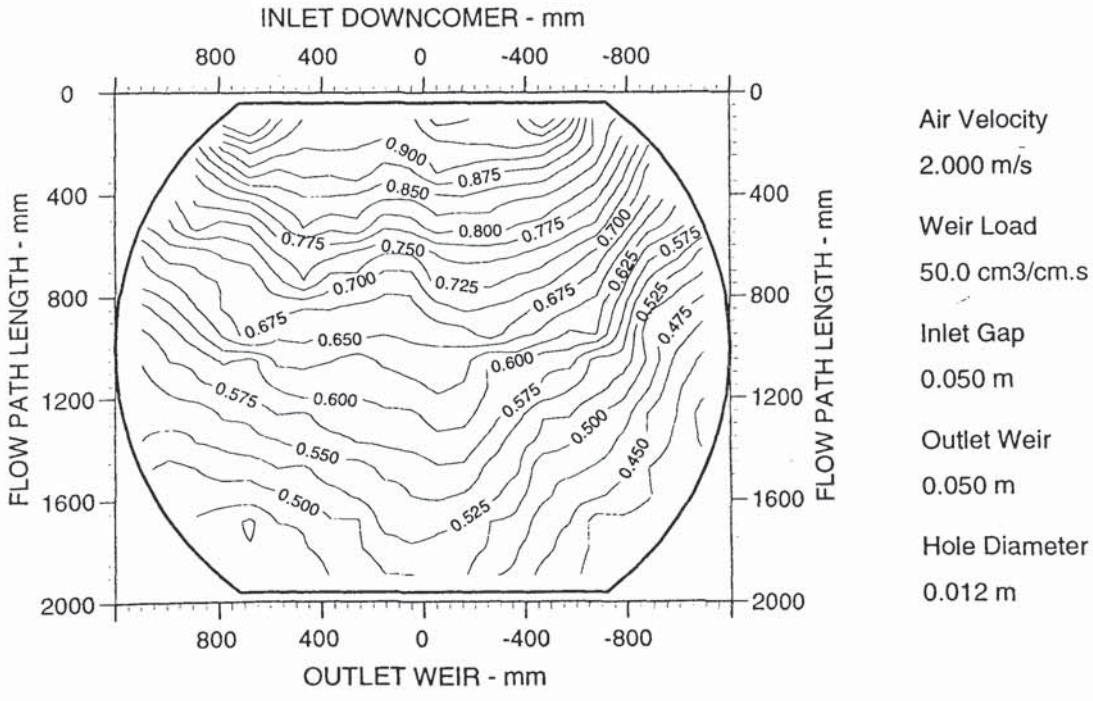

Figure A5.14b Two dimensional reduced temperature profiles.

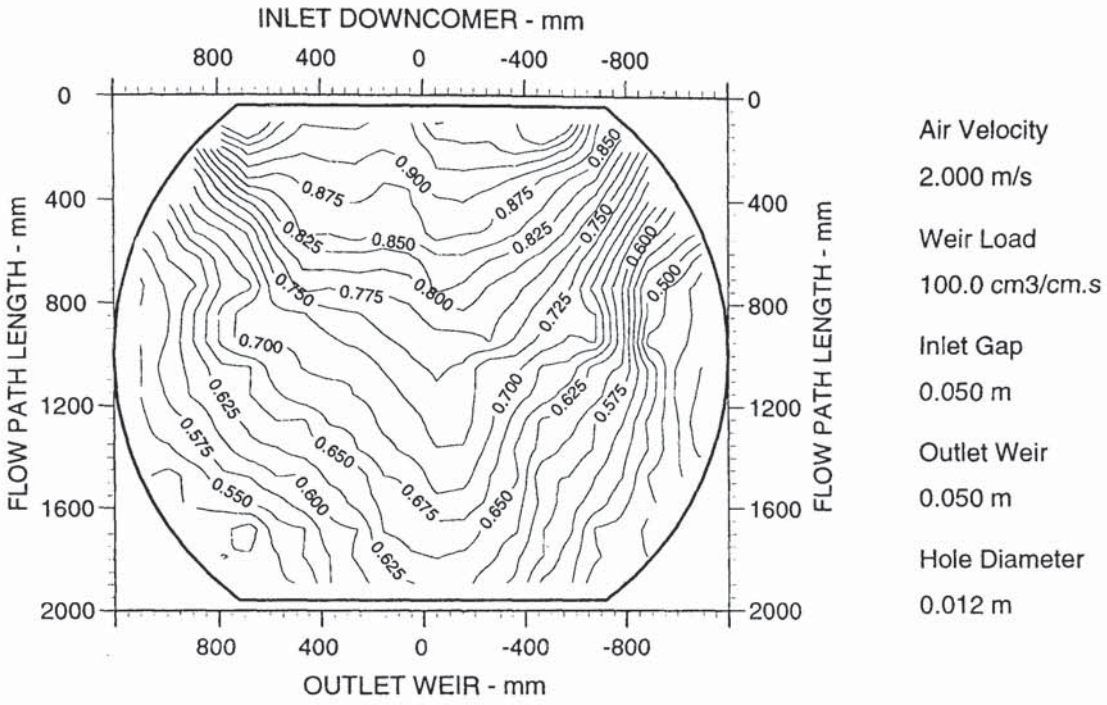

Figure A5.14c Two dimensional reduced temperature profiles.

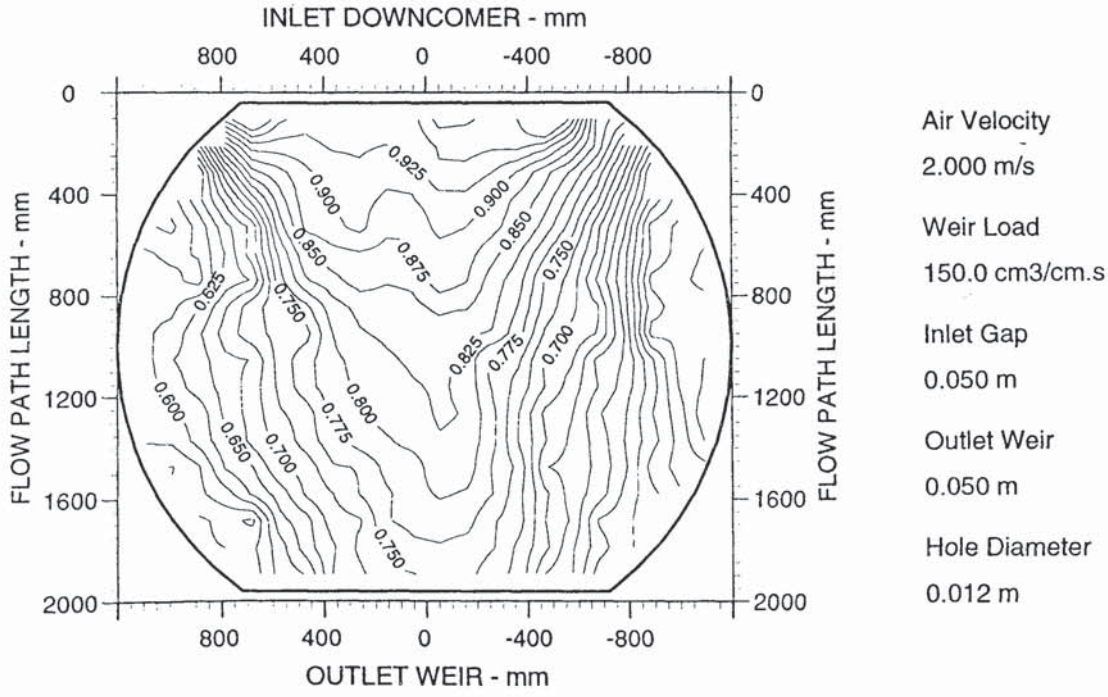

Figure A5.14d Two dimensional reduced temperature profiles.

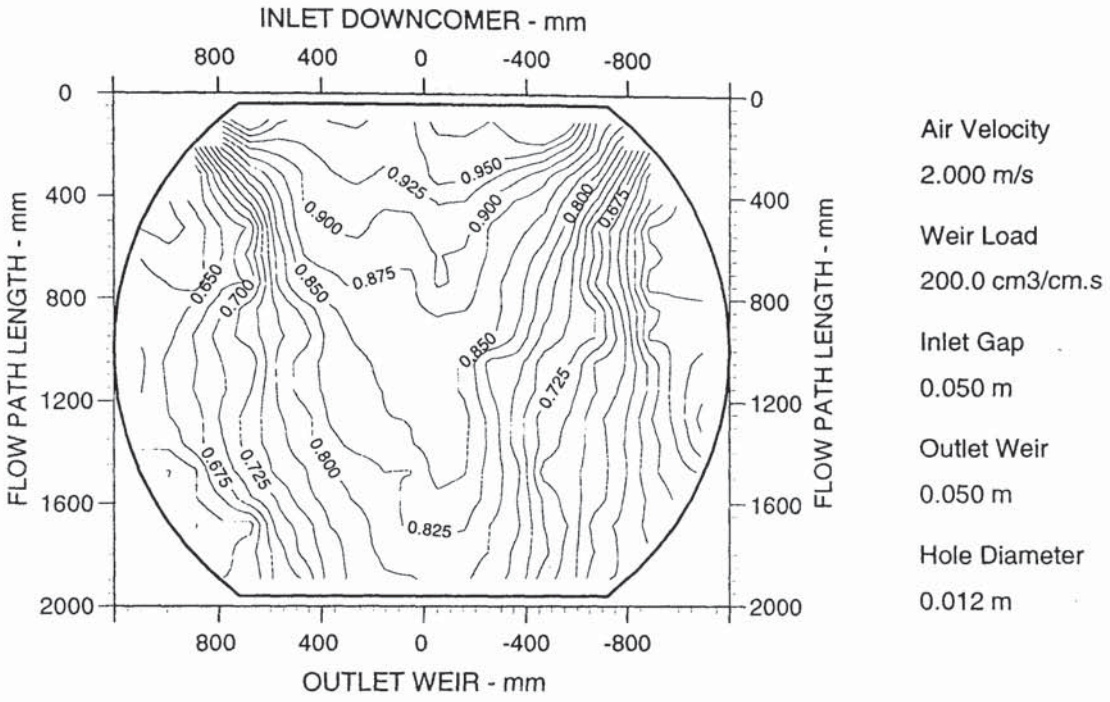

Figure A5.14e Two dimensional reduced temperature profiles.

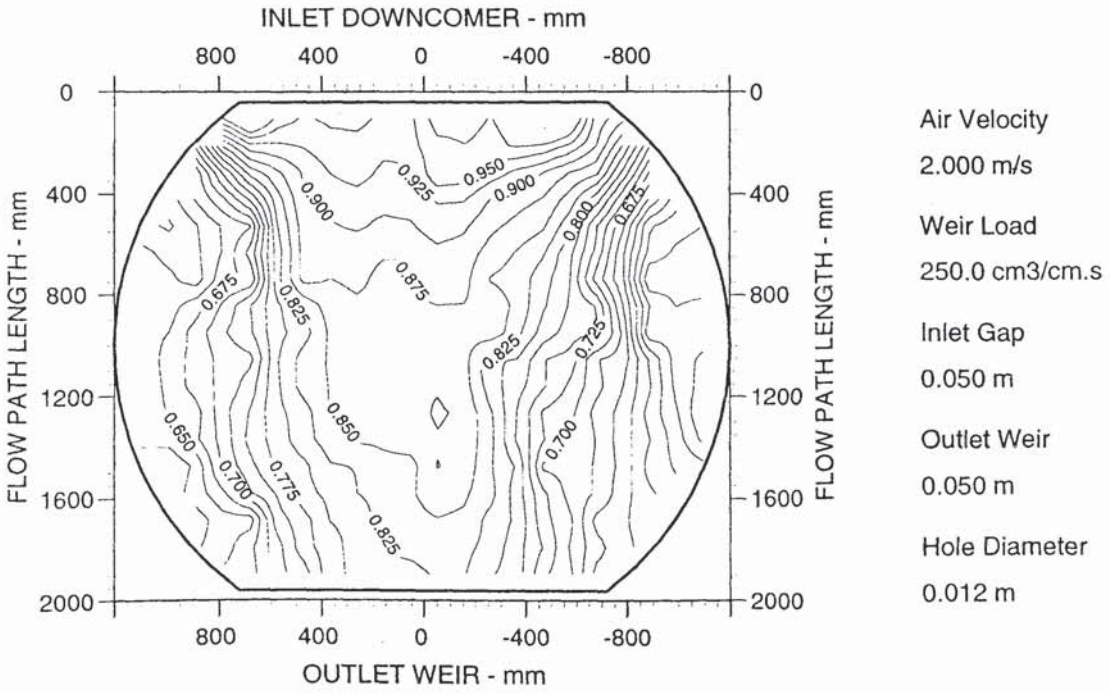

Figure A5.14f Two dimensional reduced temperature profiles.

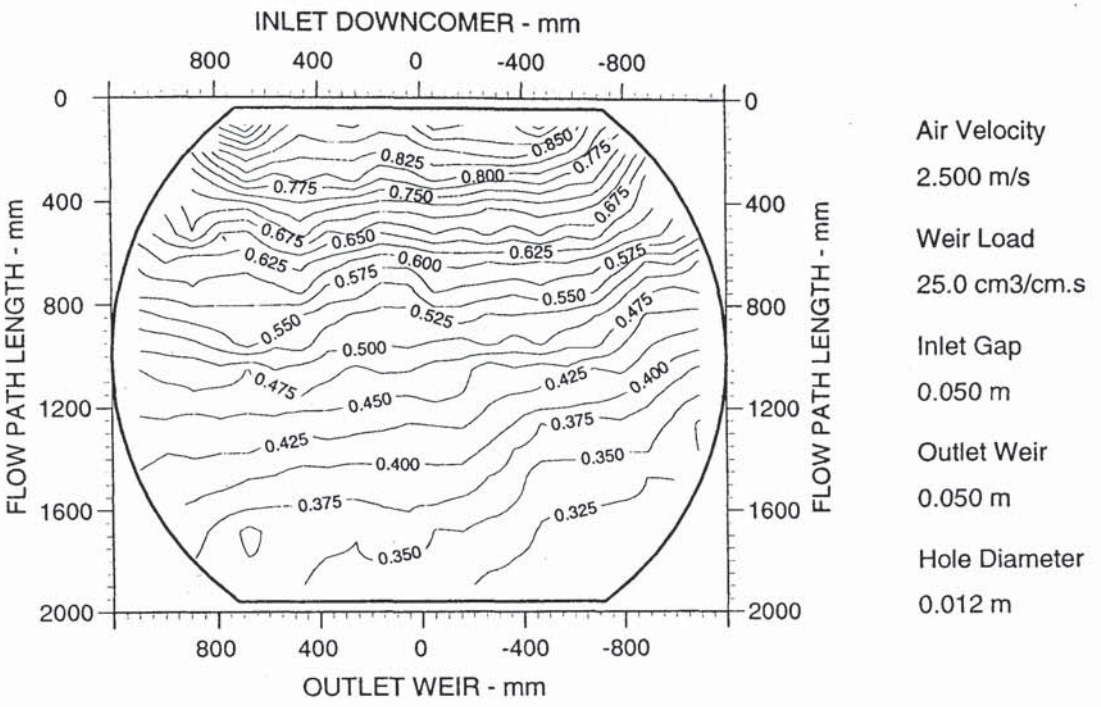

Figure A5.15a Two dimensional reduced temperature profiles.

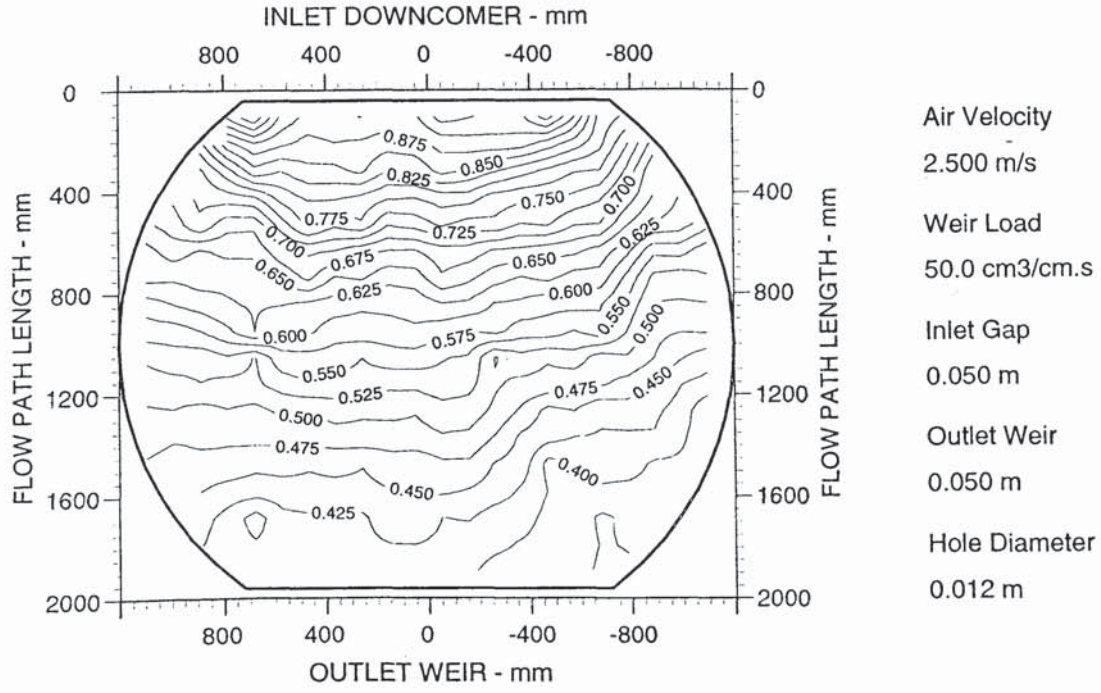

Figure A5.15b Two dimensional reduced temperature profiles.

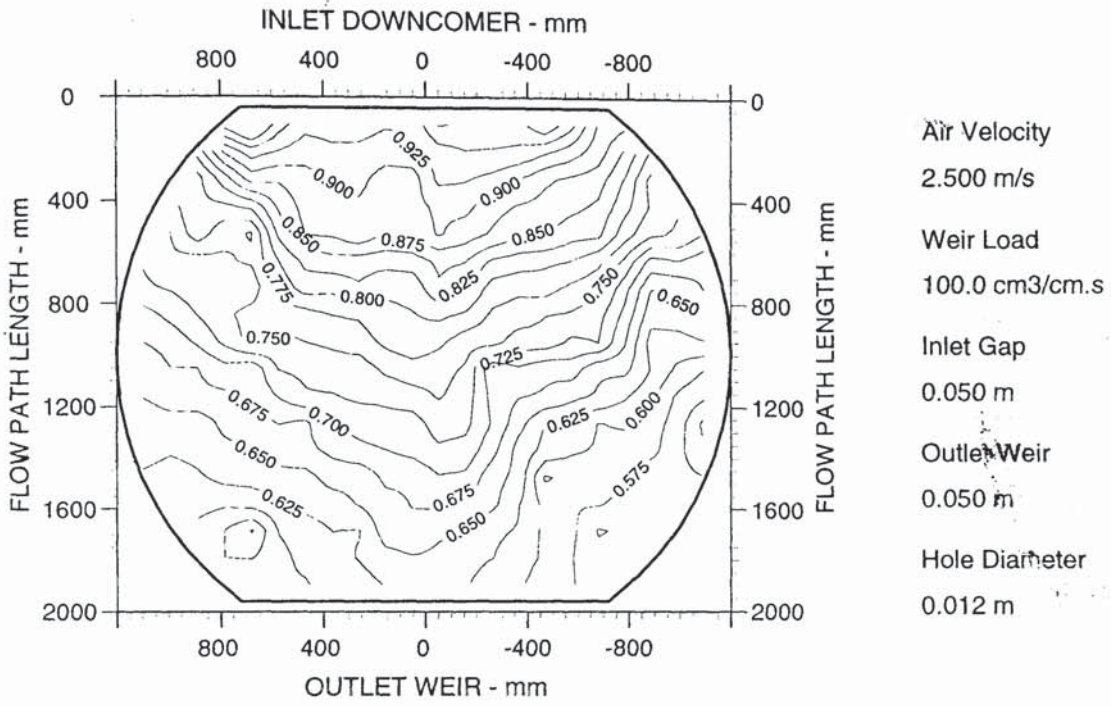

Figure A5.15c Two dimensional reduced temperature profiles.

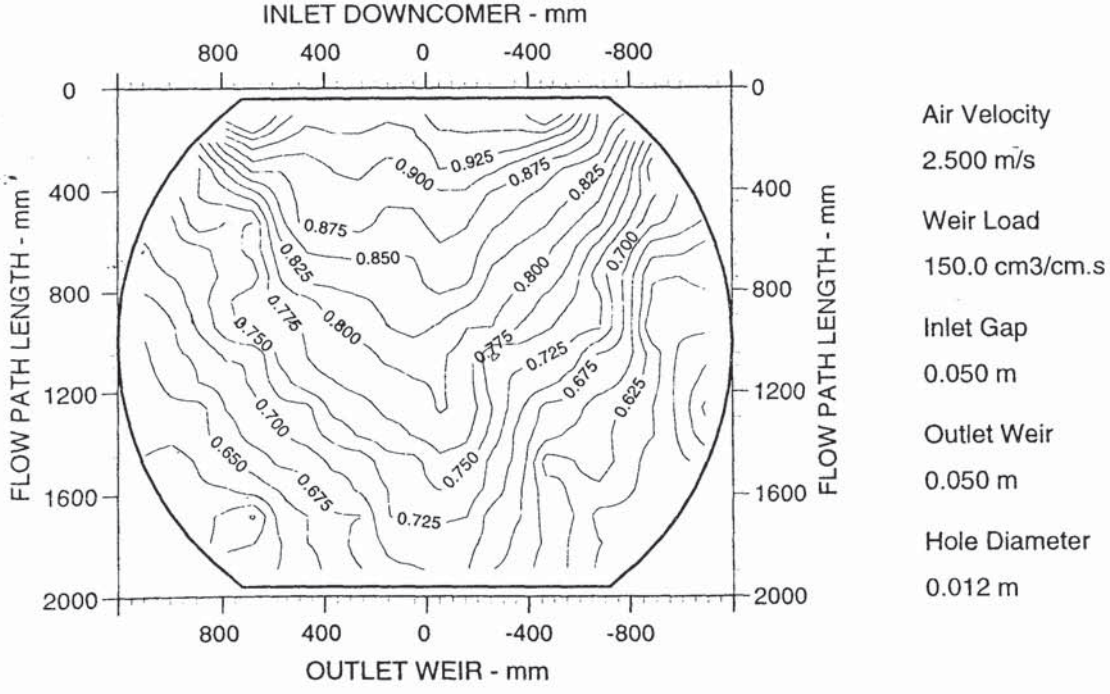

Figure A5.15d Two dimensional reduced temperature profiles.

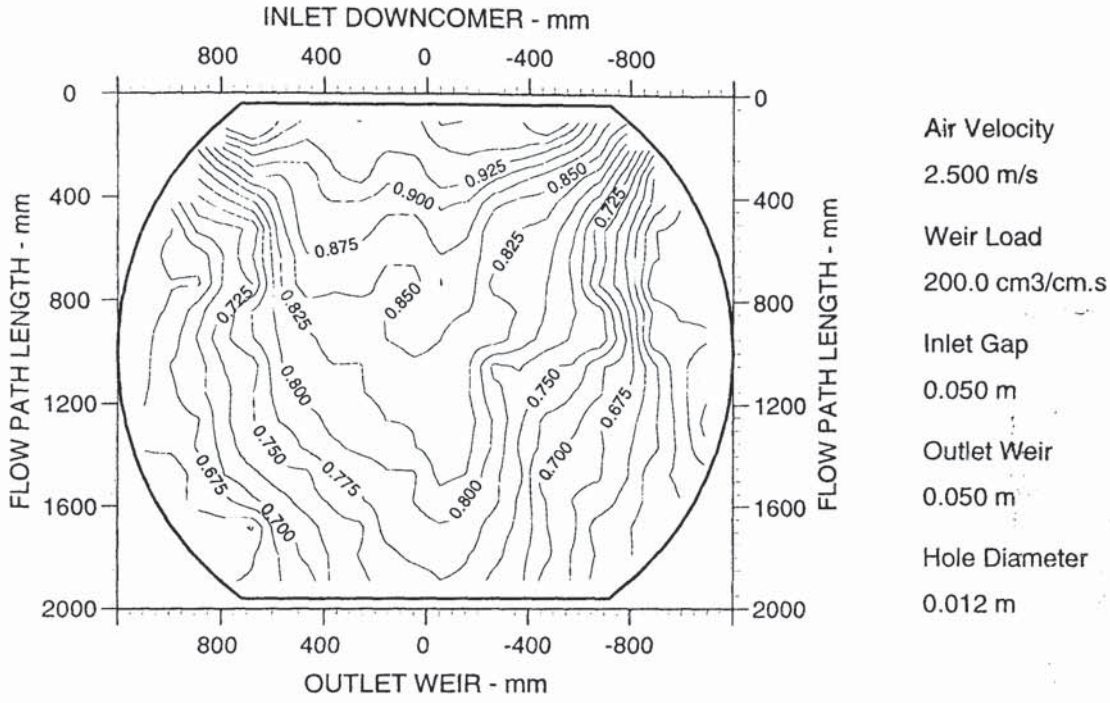

Figure A5.15e Two dimensional reduced temperature profiles.

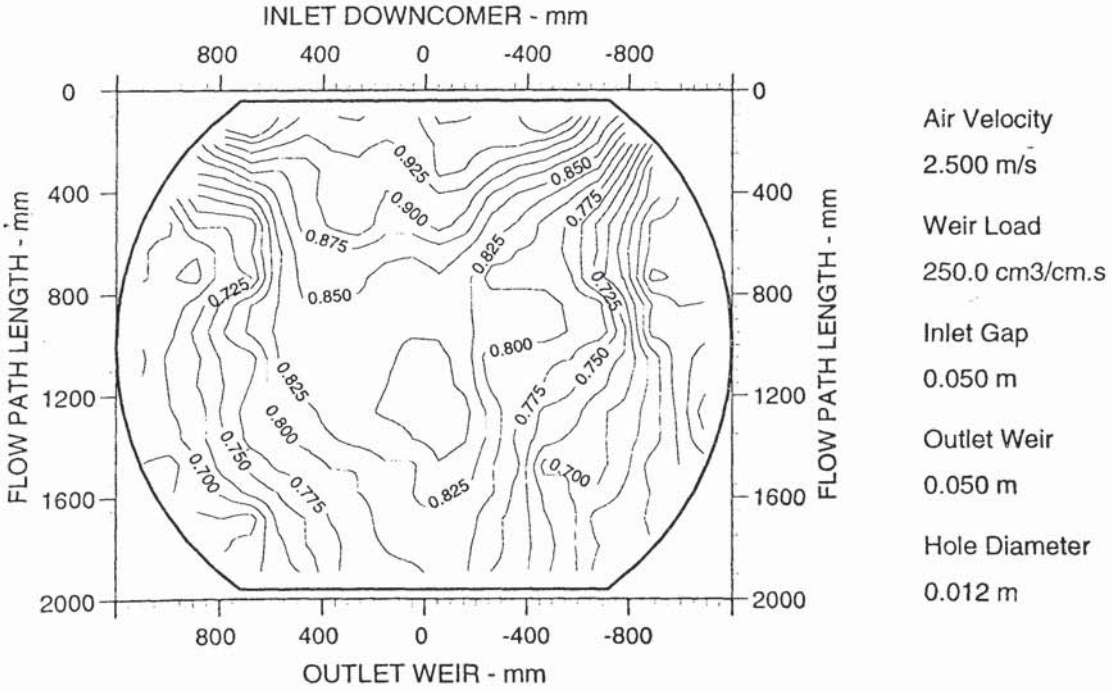

Figure A5.15f Two dimensional reduced temperature profiles.

APPENDIX 6

Three-Dimensional Height of Clear Liquid Surface Diagrams for the Effect of Gas Flow on the Separation of the Liquid Flow

This appendix contains a full set of the three-dimensional surface profile diagrams obtained during the fluid mechanical investigation of the flow. The diagrams are complementary to the experiments presented in Chapter 6. The flow rates used are the same as those for Appendix 6 except for the 2.50 m/s air velocity.

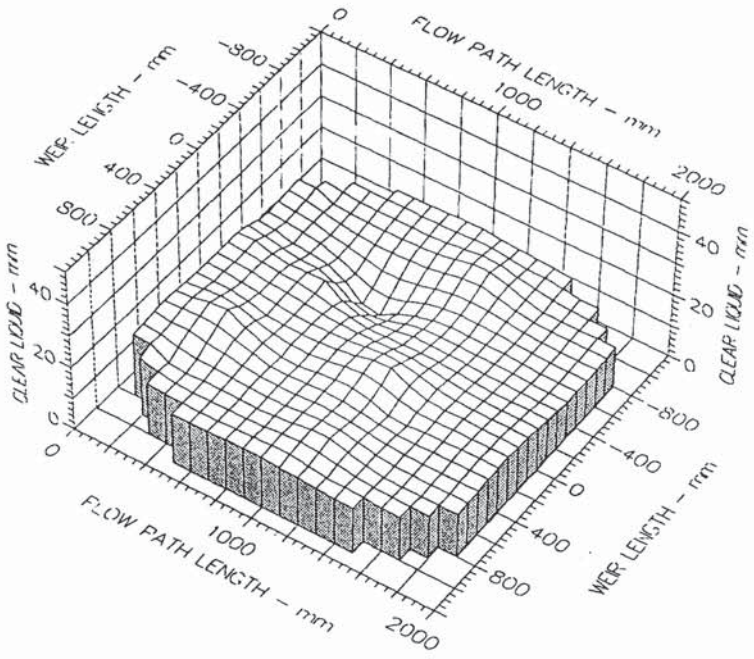

Air Velocity
1.000 m/s

Water Loading
25.0 cm3/cm.s

Inlet Gap
0.010 m

Inlet Weir
0.000 m

Outlet Weir
0.010 m

Hole Diameter
0.013 m

Fig. A6.1a Three-dimensional height of clear liquid surface profiles

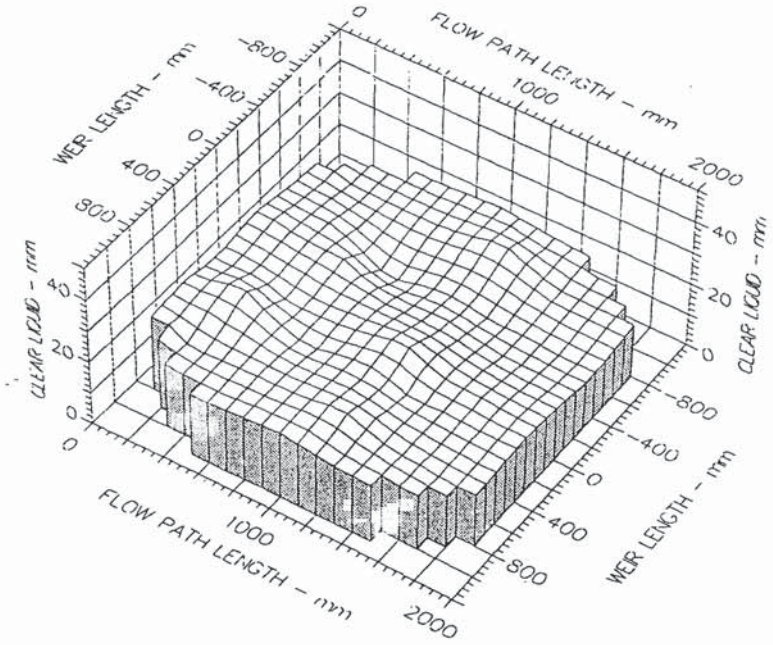

Air Velocity
1.000 m/s

Water Loading
50.0 cm3/cm.s

Inlet Gap
0.010 m

Inlet Weir
0.000 m

Outlet Weir
0.010 m

Hole Diameter
0.013 m

Fig. A6.1b Three-dimensional height of clear liquid surface profiles

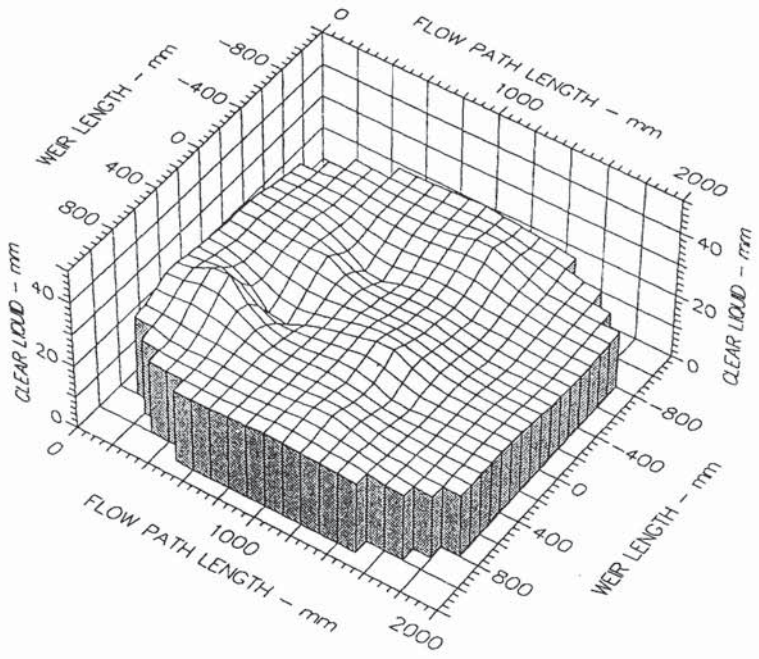

Air Velocity
1.000 m/s

Water Loading
100.0 cm3/cm.s

Inlet Gap
0.010 m

Inlet Weir
0.000 m

Outlet Weir
0.010 m

Hole Diameter
0.013 m

Fig. A6.1c Three-dimensional height of clear liquid surface profiles

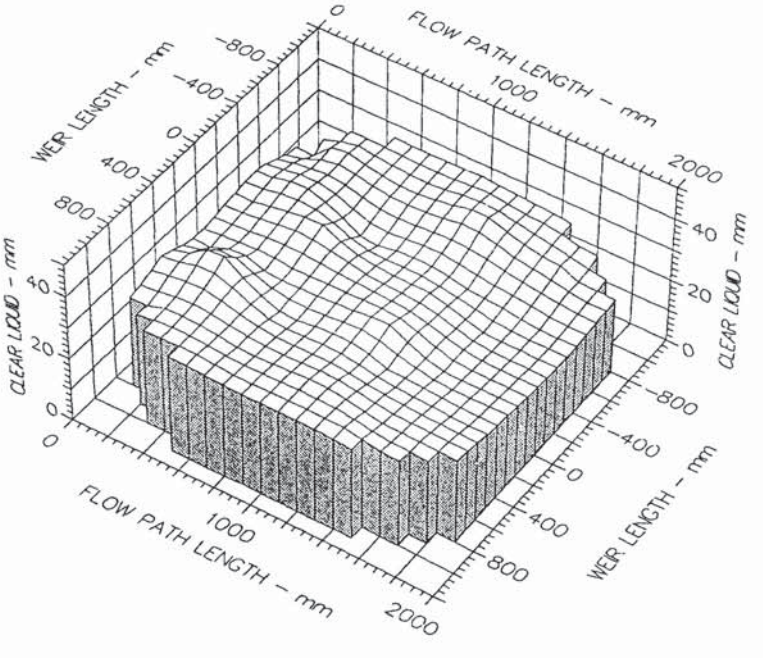

Air Velocity
1.0 m/s

Water Loading
150.0 cm3/cm.s

Inlet Gap
0.010 m

Inlet Weir
0.000 m

Outlet Weir
0.010 m

Hole Diameter
0.013 m

Fig. A6.1d Three-dimensional height of clear liquid surface profiles

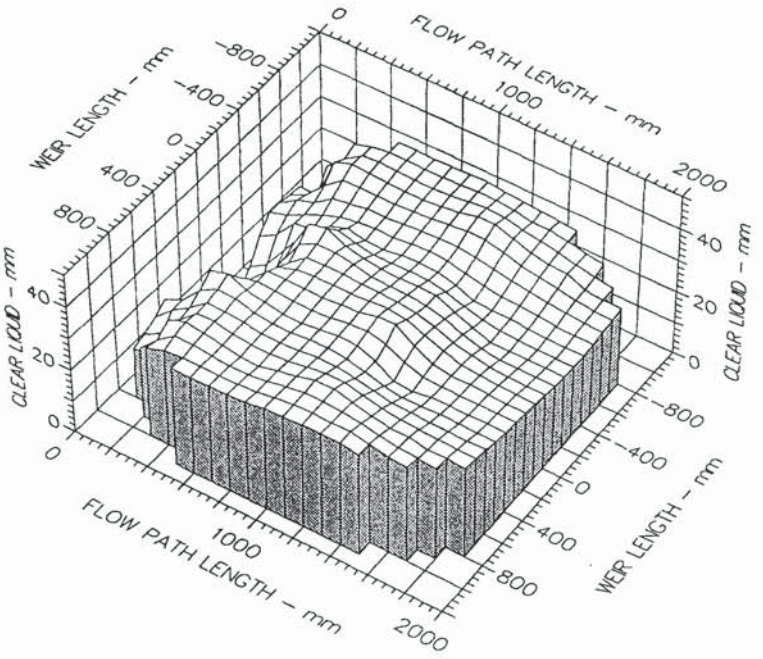

Air Velocity
1.000 m/s

Water Loading
200.0 cm3/cm.s

Inlet Gap
0.010 m

Inlet Weir
0.000 m

Outlet Weir
0.010 m

Hole Diameter
0.013 m

Fig. A6.1e Three-dimensional height of clear liquid surface profiles

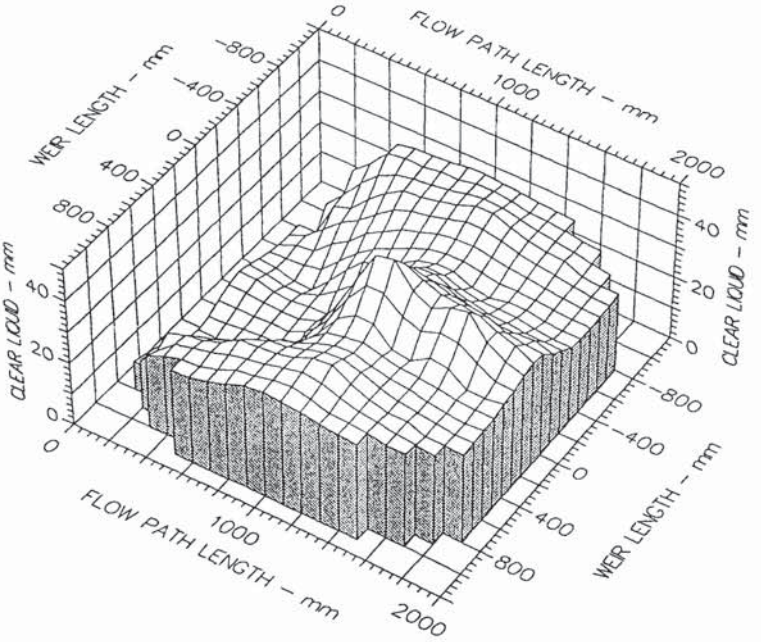

Air Velocity
1.0 m/s

Water Loading -
250.0 cm3/cm.s

Inlet Gap
0.010 m

Inlet Weir
0.000 m

Outlet Weir
0.010 m

Hole Diameter
0.013 m

Fig. A6.1f Three-dimensional height of clear liquid surface profiles

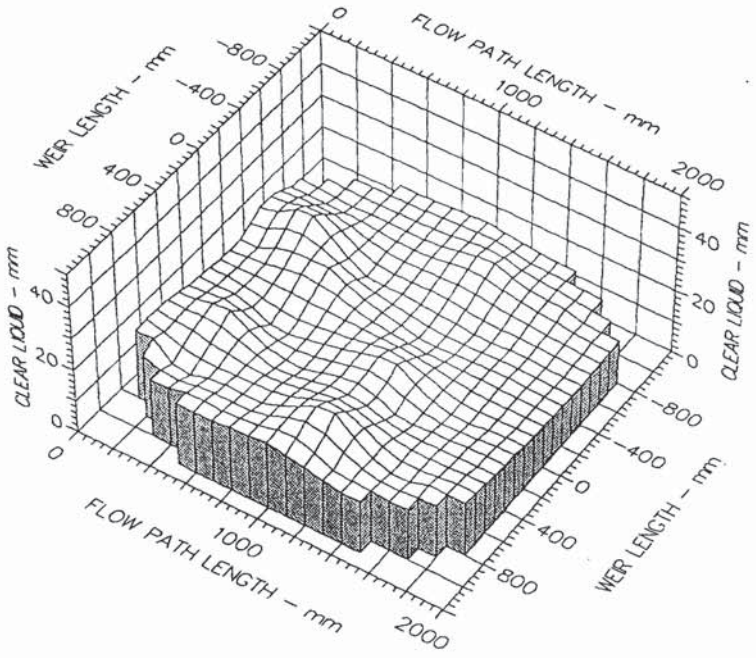

Air Velocity
1.250 m/s

Water Loading
25.0 cm3/cm.s

Inlet Gap
0.010 m

Inlet Weir
0.000 m

Outlet Weir
0.010 m

Hole Diameter
0.013 m

Fig. A6.2a Three-dimensional height of clear liquid surface profiles

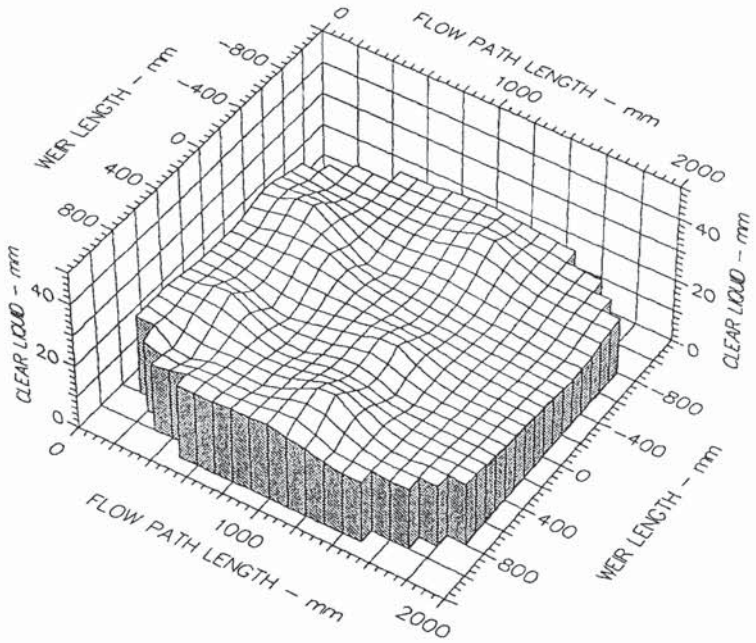

Air Velocity
1.2 m/s

Water Loading
50.0 cm3/cm.s

Inlet Gap
0.010 m

Inlet Weir
0.000 m

Outlet Weir
0.010 m

Hole Diameter
0.013 m

Fig. A6.2b Three-dimensional height of clear liquid surface profiles

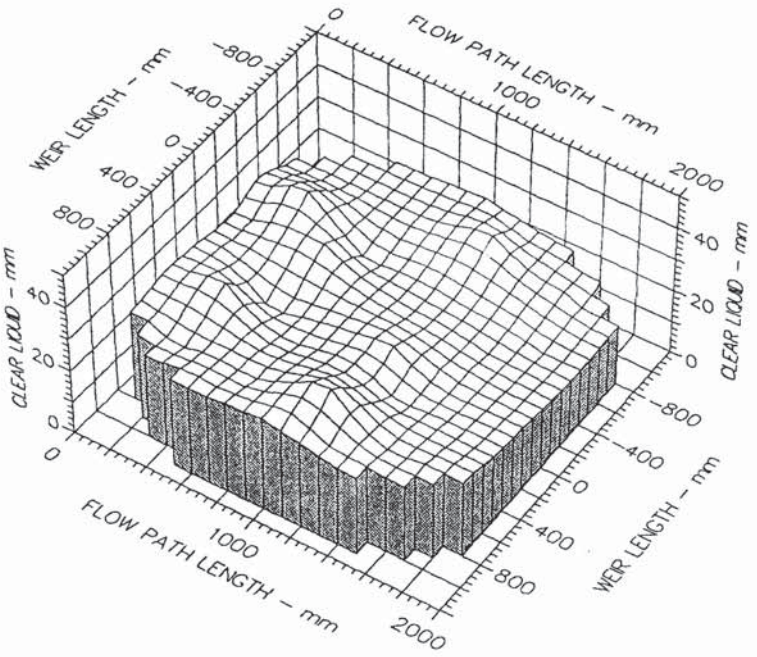

Air Velocity
1.250 m/s

Water Loading
100.0 cm3/cm.s

Inlet Gap
0.010 m

Inlet Weir
0.000 m

Outlet Weir
0.010 m

Hole Diameter
0.013 m

Fig. A6.2c Three-dimensional height of clear liquid surface profiles

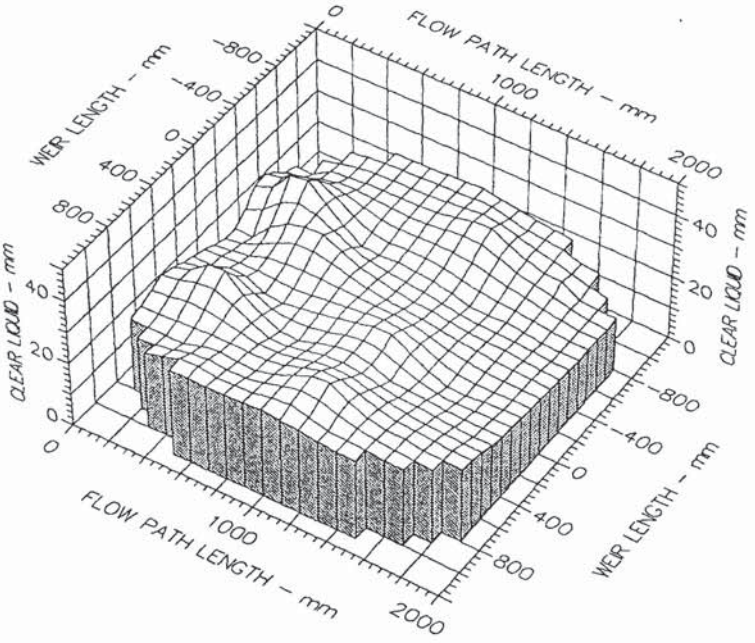

Air Velocity
1.2 m/s

Water Loading
150.0 cm3/cm.s

Inlet Gap
0.010 m

Inlet Weir
0.000 m

Outlet Weir
0.010 m

Hole Diameter
0.013 m

Fig. A6.2d Three-dimensional height of clear liquid surface profiles

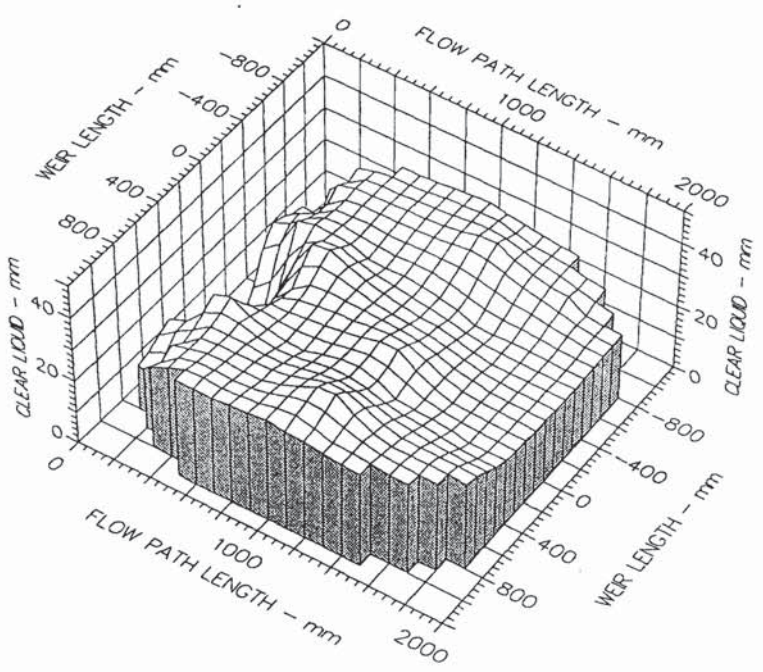

Air Velocity
1.250 m/s

Water Loading
200.0 cm3/cm.s

Inlet Gap
0.010 m

Inlet Weir
0.000 m

Outlet Weir
0.010 m

Hole Diameter
0.013 m

Fig. A6.2e Three-dimensional height of clear liquid surface profiles

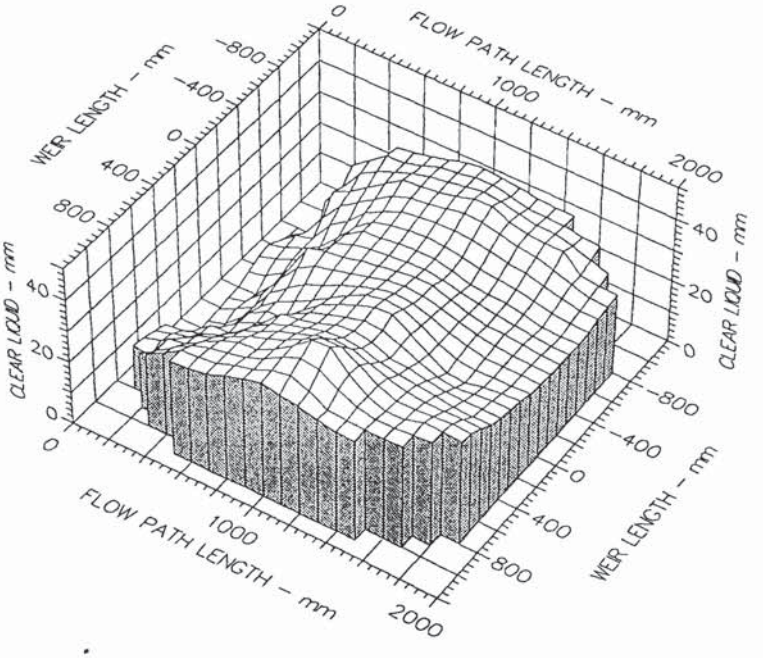

Air Velocity
1.2 m/s

Water Loading
250.0 cm3/cm.s

Inlet Gap
0.010 m

Inlet Weir
0.000 m

Outlet Weir
0.010 m

Hole Diameter
0.013 m

Fig. A6.2f Three-dimensional height of clear liquid surface profiles

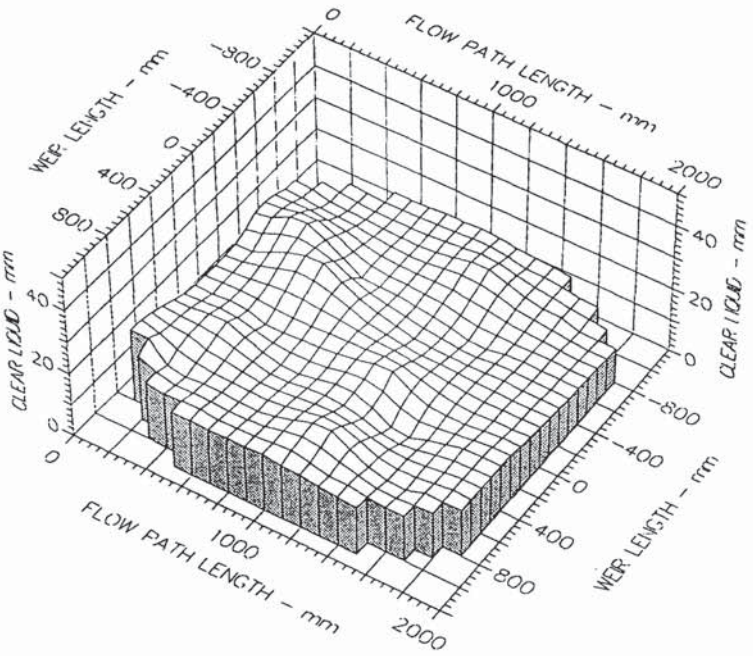

Air Velocity
1.500 m/s

Water Loading
25.0 cm3/cm.s

Inlet Gap
0.010 m

Inlet Weir
0.000 m

Outlet Weir
0.010 m

Hole Diameter
0.013 m

Fig. A6.3a Three-dimensional height of clear liquid surface profiles

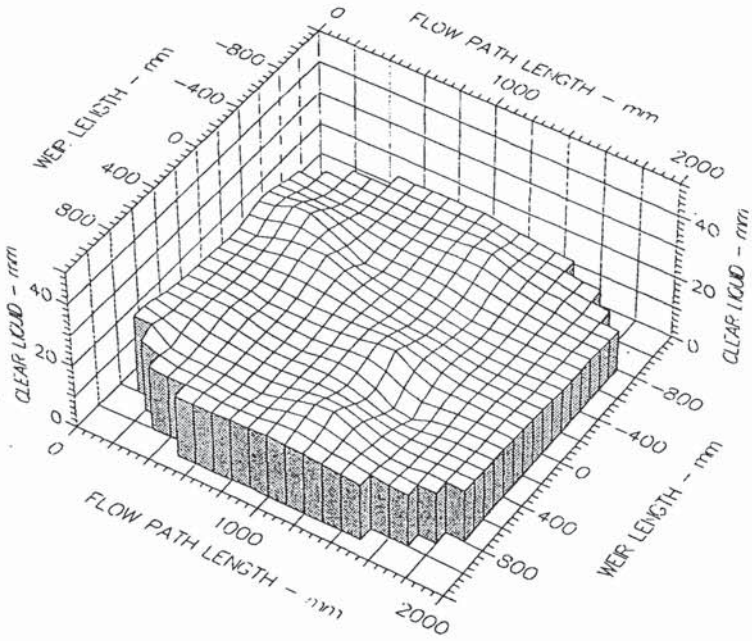

Air Velocity
1.500 m/s

Water Loading
50.0 cm3/cm.s

Inlet Gap
0.010 m

Inlet Weir
0.000 m

Outlet Weir
0.010 m

Hole Diameter
0.013 m

Fig. A6.3b Three-dimensional height of clear liquid surface profiles

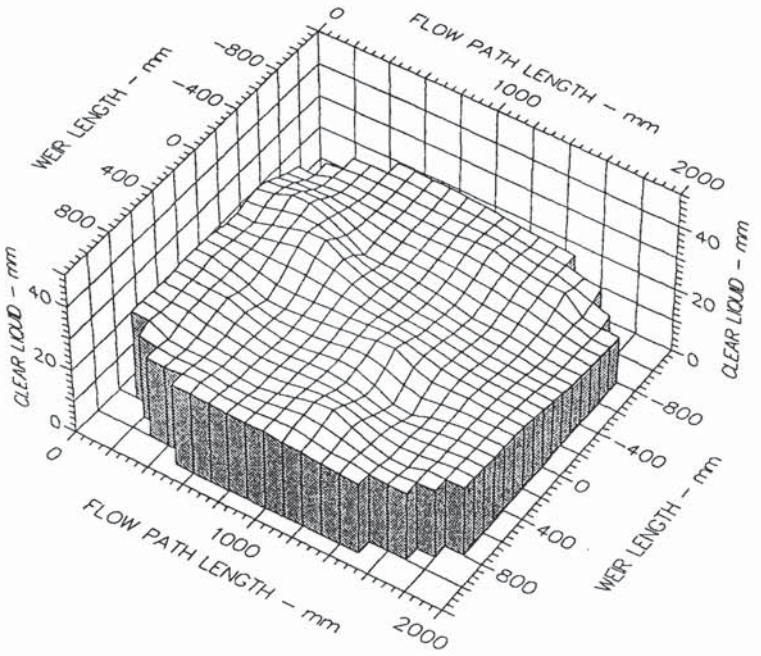

Air Velocity
1.500 m/s

Water Loading
100.0 cm3/cm.s

Inlet Gap
0.010 m

Inlet Weir
0.000 m

Outlet Weir
0.010 m

Hole Diameter
0.013 m

Fig. A6.3c Three-dimensional height of clear liquid surface profiles

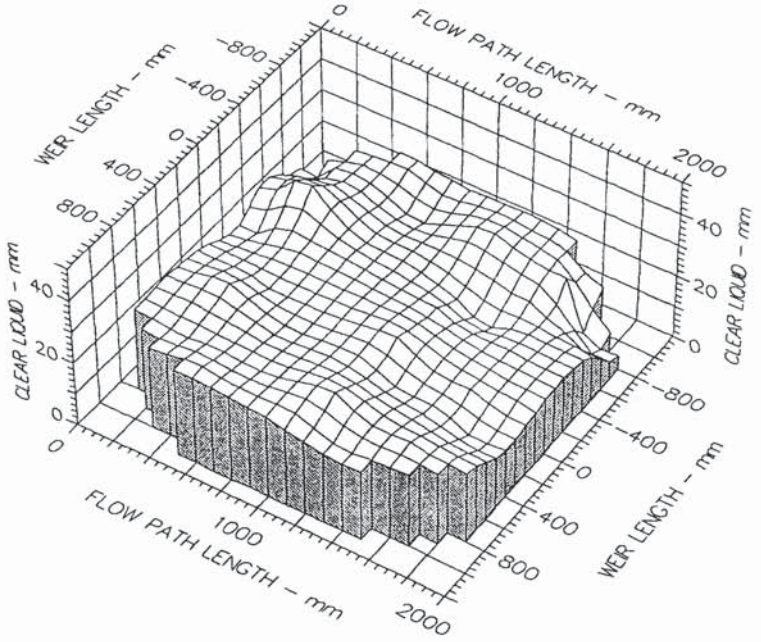

Air Velocity
1.5 m/s

Water Loading
150.0 cm3/cm.s

Inlet Gap
0.010 m

Inlet Weir
0.000 m

Outlet Weir
0.010 m

Hole Diameter
0.013 m

Fig. A6.3d Three-dimensional height of clear liquid surface profiles

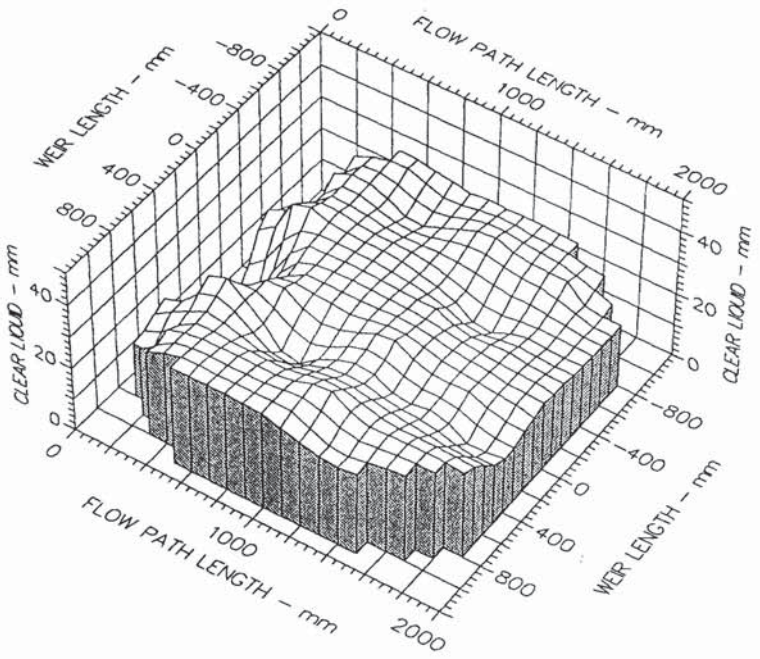

Air Velocity
1.500 m/s

Water Loading
200.0 cm3/cm.s

Inlet Gap
0.010 m

Inlet Weir
0.000 m

Outlet Weir
0.010 m

Hole Diameter
0.013 m

Fig. A6.3e Three-dimensional height of clear liquid surface profiles

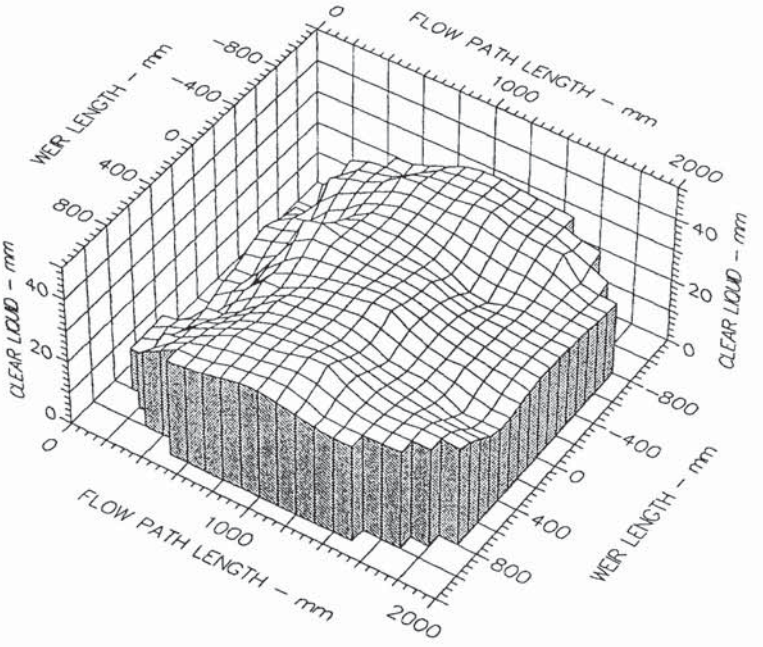

Air Velocity
1.5 m/s

Water Loading
250.0 cm3/cm.s

Inlet Gap
0.010 m

Inlet Weir
0.000 m

Outlet Weir
0.010 m

Hole Diameter
0.013 m

Fig. A6.3f Three-dimensional height of clear liquid surface profiles

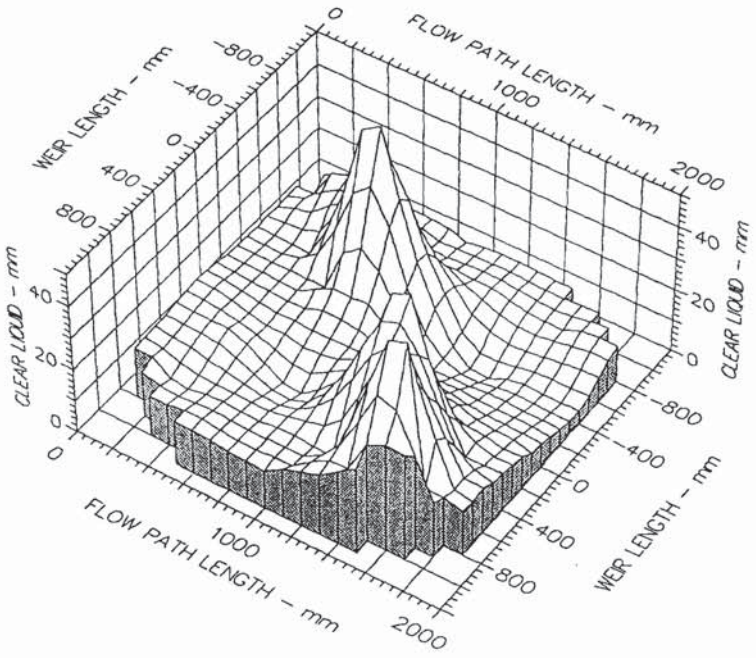

Air Velocity
2.000 m/s

Water Loading
25.0 cm3/cm.s

Inlet Gap
0.010 m

Inlet Weir
0.000 m

Outlet Weir
0.010 m

Hole Diameter
0.013 m

Fig. A6.4a Three-dimensional height of clear liquid surface profiles

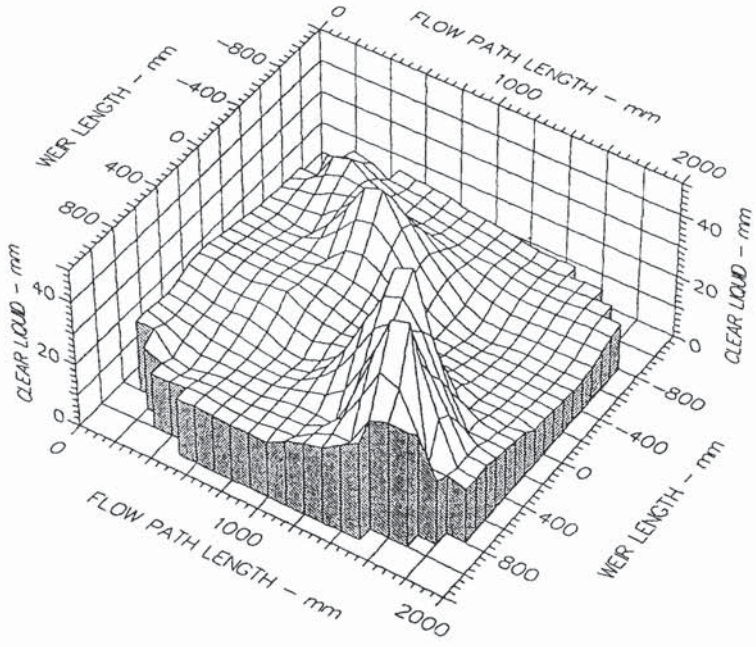

Air Velocity
2.0 m/s

Water Loading
50.0 cm3/cm.s

Inlet Gap
0.010 m

Inlet Weir
0.000 m

Outlet Weir
0.010 m

Hole Diameter
0.013 m

Fig. A6.4b Three-dimensional height of clear liquid surface profiles

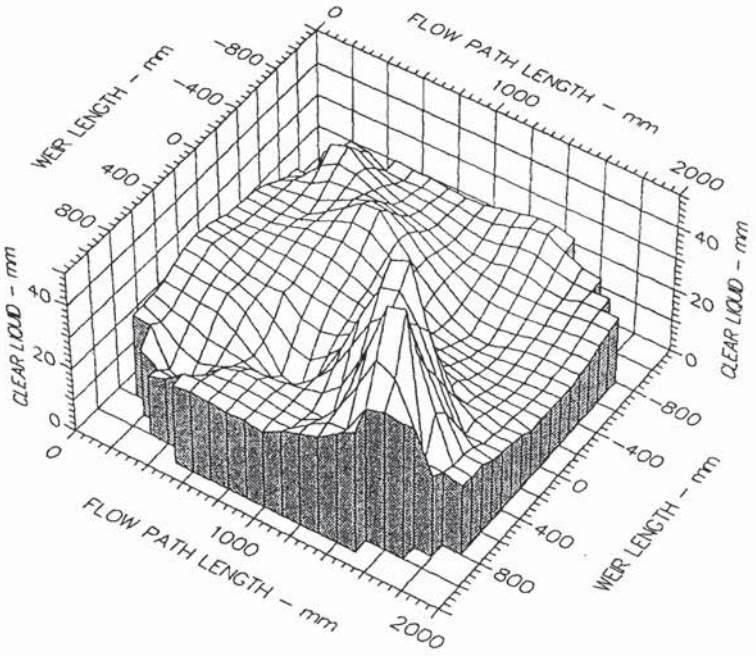

Air Velocity
2.000 m/s

Water Loading
100.0 cm3/cm.s

Inlet Gap
0.010 m

Inlet Weir
0.000 m

Outlet Weir
0.010 m

Hole Diameter
0.013 m

Fig. A6.4c Three-dimensional height of clear liquid surface profiles

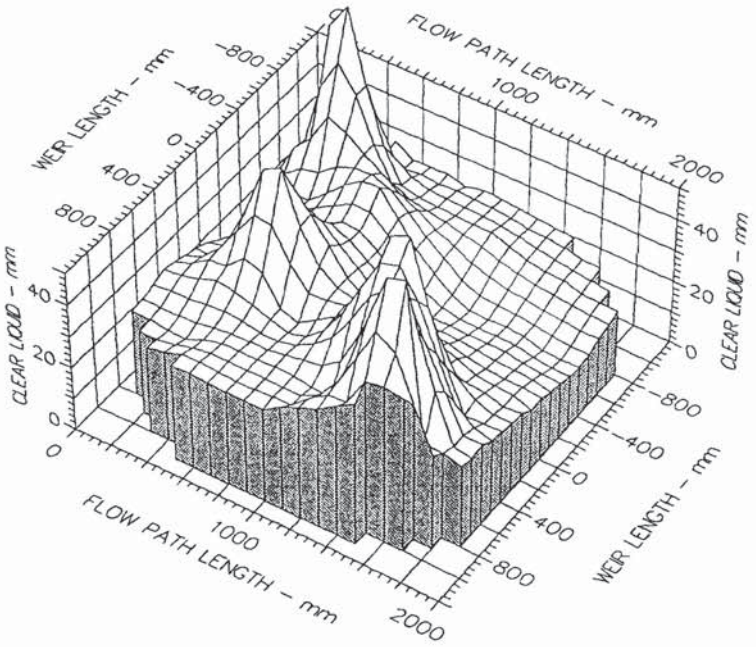

Air Velocity
2.0 m/s

Water Loading
150.0 cm3/cm.s

Inlet Gap
0.010 m

Inlet Weir
0.000 m

Outlet Weir
0.010 m

Hole Diameter
0.013 m

Fig. A6.4d Three-dimensional height of clear liquid surface profiles

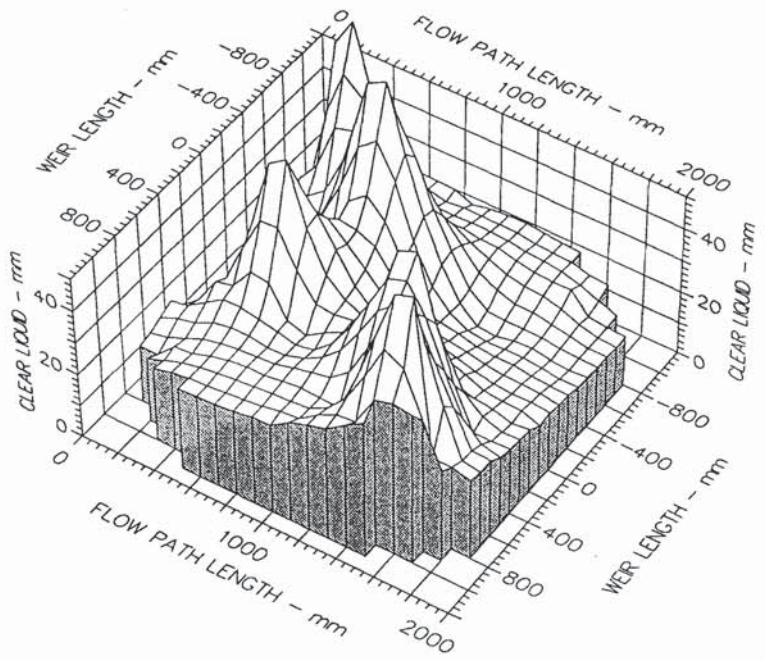

Air Velocity
2.000 m/s

Water Loading
200.0 cm3/cm.s

Inlet Gap
0.010 m

Inlet Weir
0.000 m

Outlet Weir
0.010 m

Hole Diameter
0.013 m

Fig. A6.4e Three-dimensional height of clear liquid surface profiles

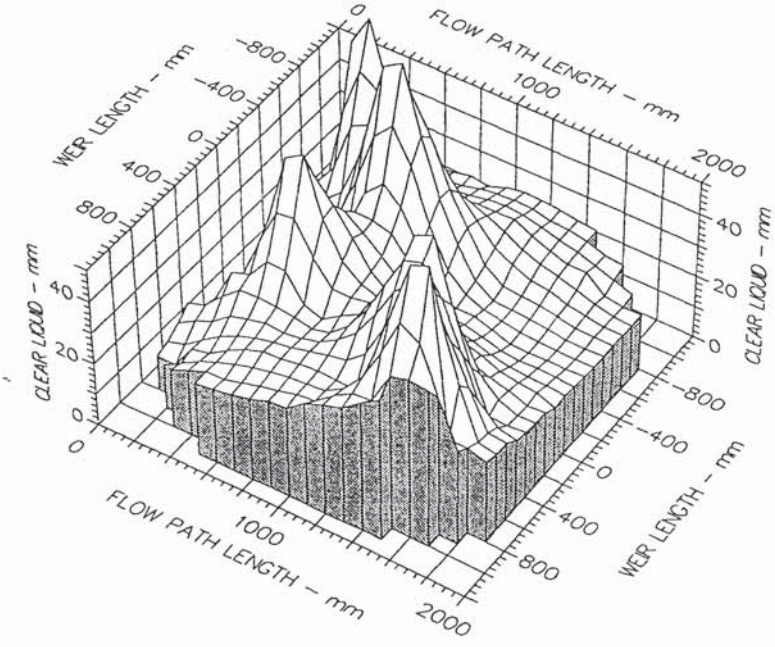

Air Velocity
2.0 m/s

Water Loading
250.0 cm3/cm.s

Inlet Gap
0.010 m

Inlet Weir
0.000 m

Outlet Weir
0.010 m

Hole Diameter
0.013 m

Fig. A6.4f Three-dimensional height of clear liquid surface profiles

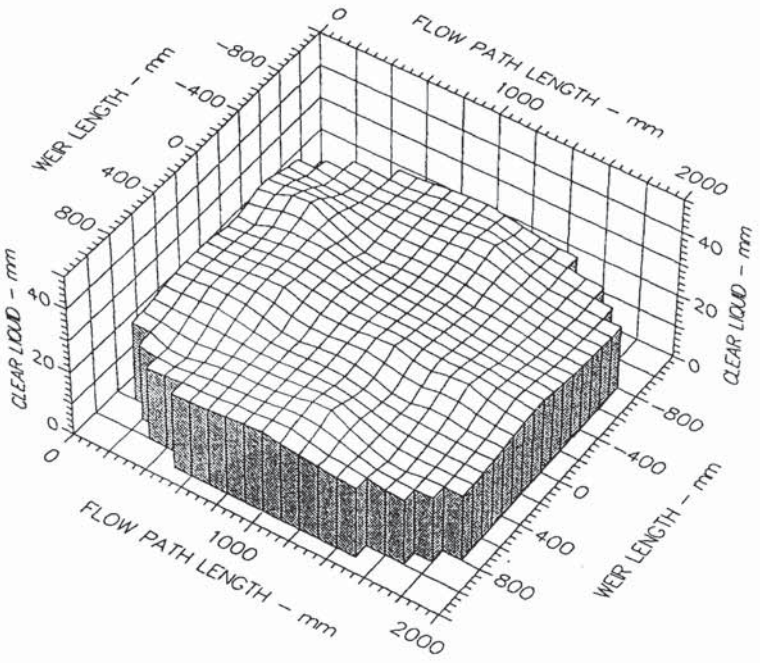

Air Velocity
1.000 m/s

Water Loading
25.0 cm3/cm.s

Inlet Gap
0.020 m

Inlet Weir
0.000 m

Outlet Weir
0.020 m

Hole Diameter
0.013 m

Fig. A6.5a Three-dimensional height of clear liquid surface profiles

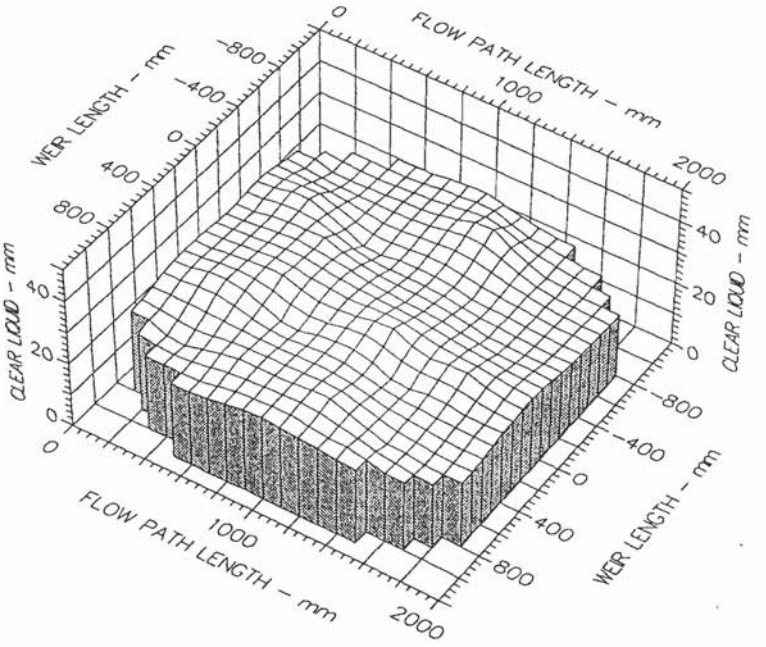

Air Velocity
1.000 m/s

Water Loading -
50.0 cm3/cm.s

Inlet Gap
0.020 m

Inlet Weir
0.000 m

Outlet Weir
0.020 m

Hole Diameter
0.013 m

Fig. A6.5b Three-dimensional height of clear liquid surface profiles

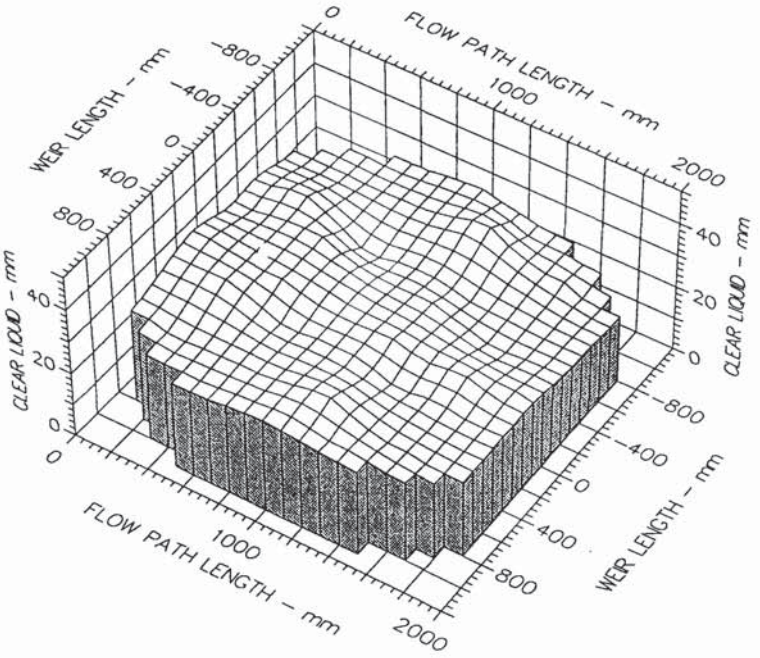

Air Velocity
1.000 m/s

Water Loading
100.0 cm3/cm.s

Inlet Gap
0.020 m

Inlet Weir
0.000 m

Outlet Weir
0.020 m

Hole Diameter
0.013 m

Fig. A6.5c Three-dimensional height of clear liquid surface profiles

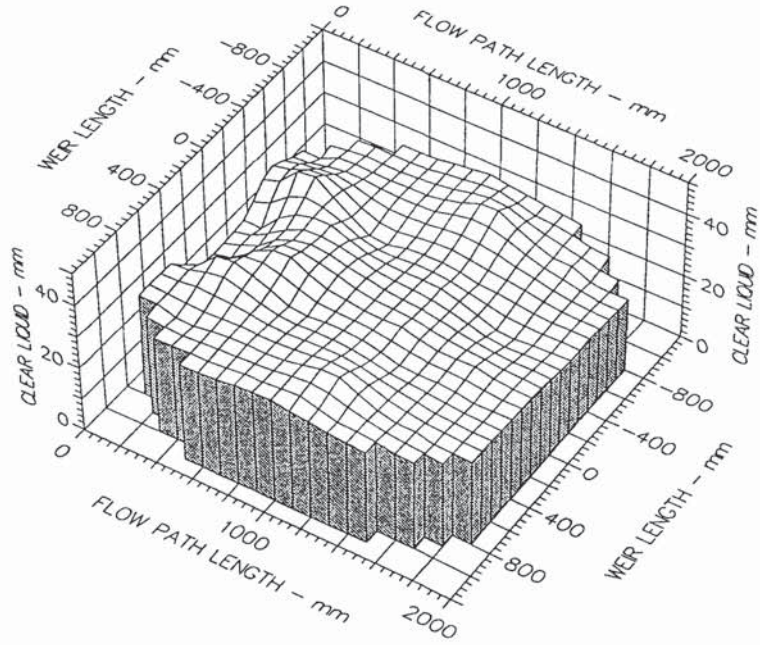

Air Velocity
1.000 m/s

Water Loading
150.0 cm3/cm.s

Inlet Gap
0.020 m

Inlet Weir
0.000 m

Outlet Weir
0.020 m

Hole Diameter
0.013 m

Fig. A6.5d Three-dimensional height of clear liquid surface profiles

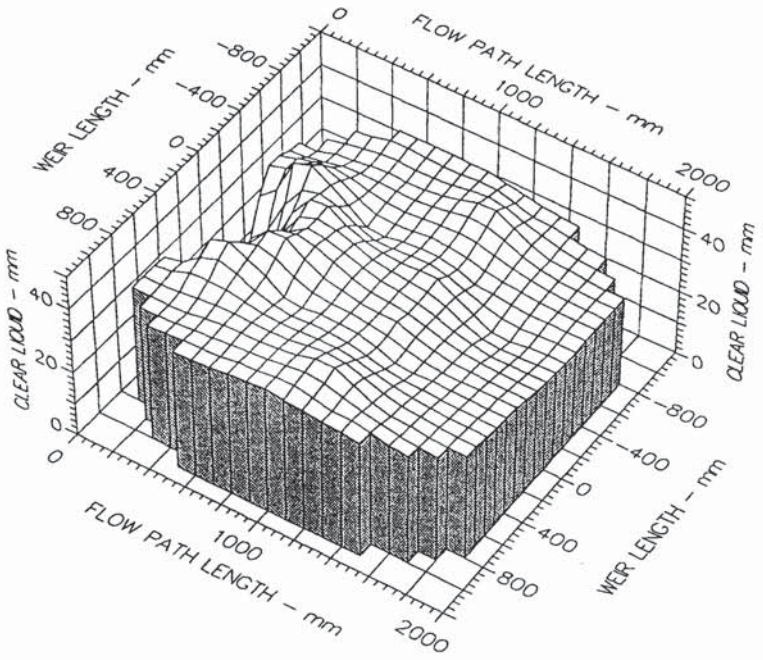

Air Velocity
1.000 m/s

Water Loading
200.0 cm3/cm.s

Inlet Gap
0.020 m

Inlet Weir
0.000 m

Outlet Weir
0.020 m

Hole Diameter
0.013 m

Fig. A6.5e Three-dimensional height of clear liquid surface profiles

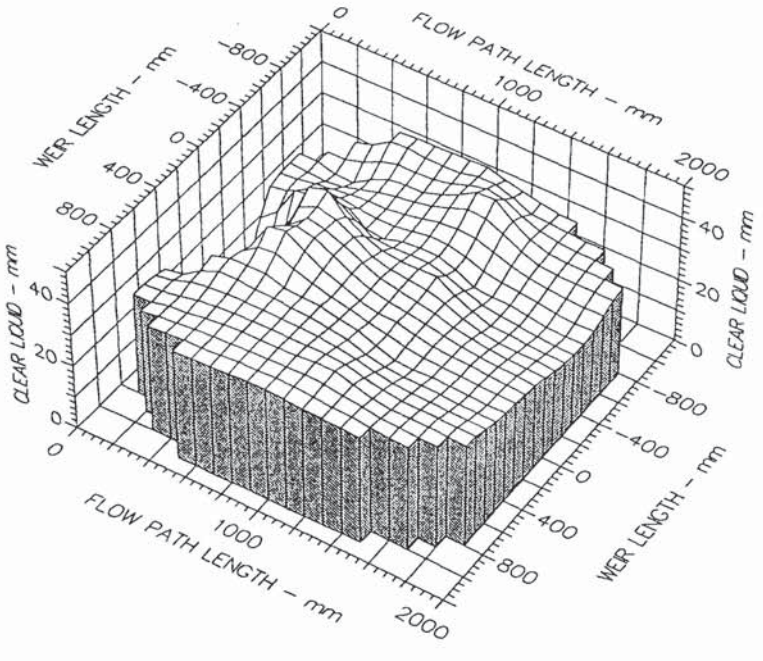

Air Velocity
1.000 m/s

Water Loading
250.0 cm3/cm.s

Inlet Gap
0.020 m

Inlet Weir
0.000 m

Outlet Weir
0.020 m

Hole Diameter
0.013 m

Fig. A6.5f Three-dimensional height of clear liquid surface profiles

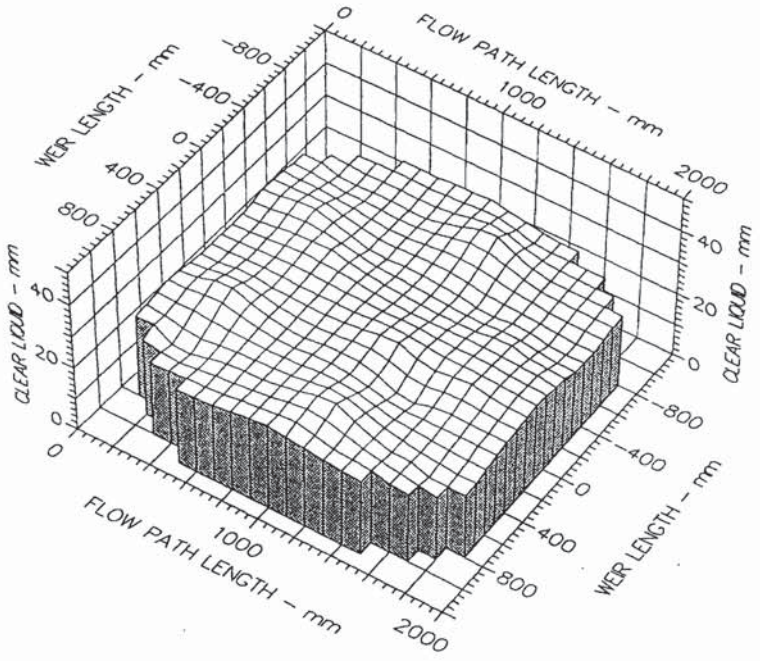

Air Velocity
1.250 m/s

Water Loading
25.0 cm3/cm.s

Inlet Gap
0.020 m

Inlet Weir
0.000 m

Outlet Weir
0.020 m

Hole Diameter
0.013 m

Fig. A6.6a Three-dimensional height of clear liquid surface profiles

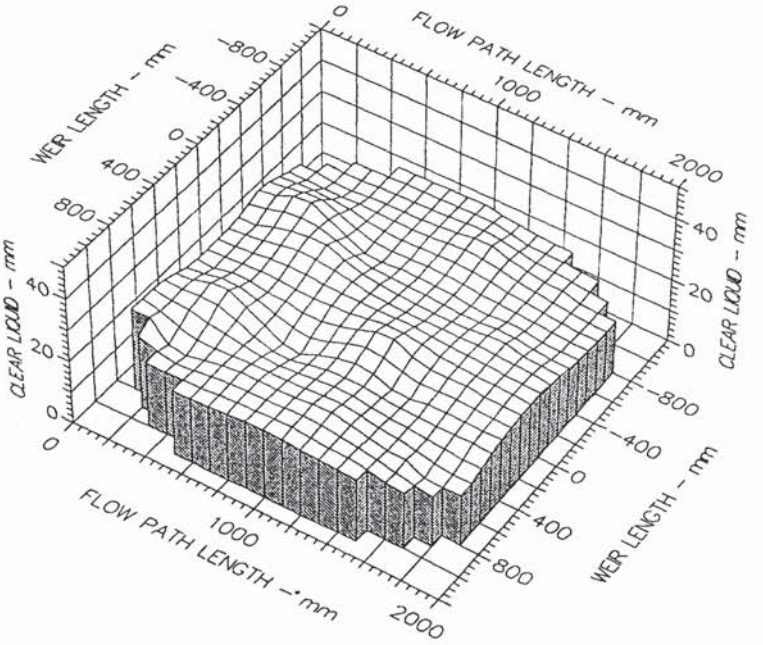

Air Velocity
1.250 m/s

Water Loading
50.0 cm3/cm.s

Inlet Gap
0.020 m

Inlet Weir
0.000 m

Outlet Weir
0.020 m

Hole Diameter
0.013 m

Fig. A6.6b Three-dimensional height of clear liquid surface profiles

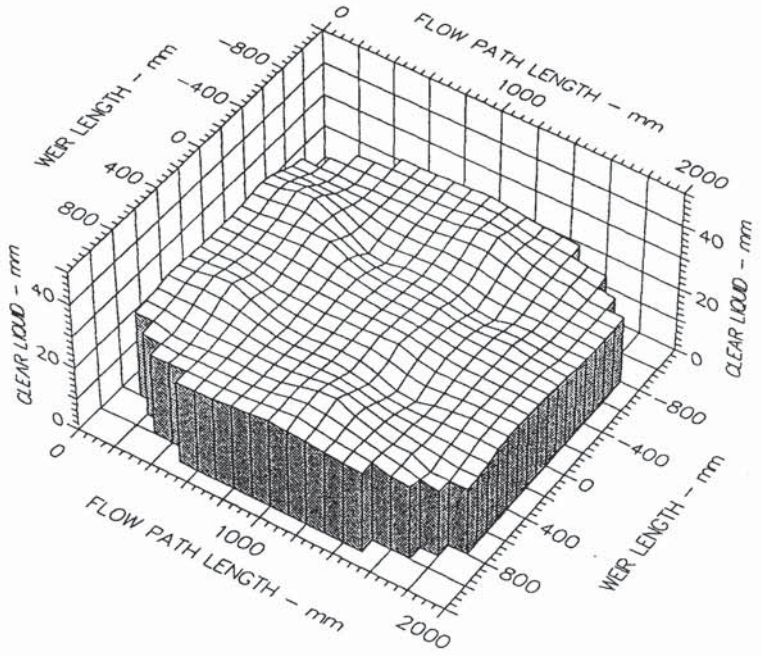

Air Velocity
1.250 m/s

Water Loading
100.0 cm3/cm.s

Inlet Gap
0.020 m

Inlet Weir
0.000 m

Outlet Weir
0.020 m

Hole Diameter.
0.013 m

Fig. A6.6c Three-dimensional height of clear liquid surface profiles

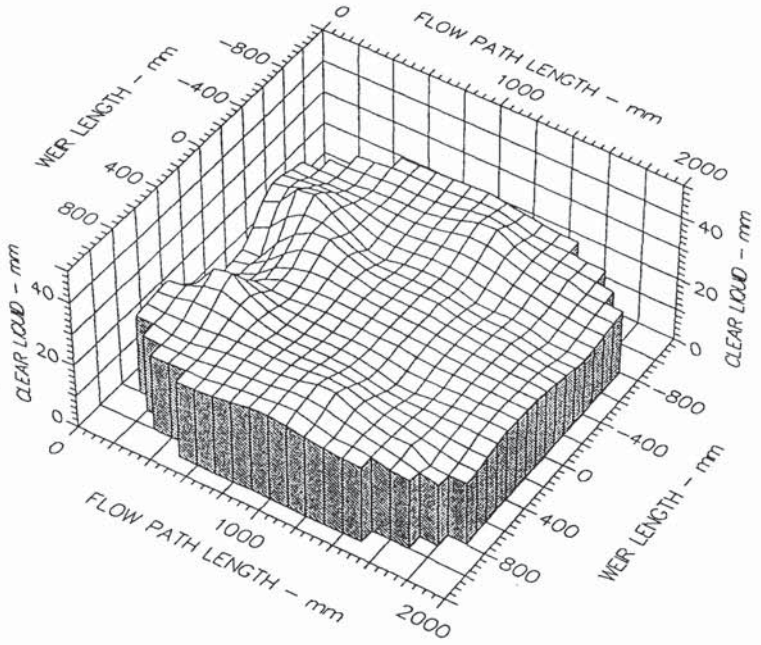

Air Velocity
1.250 m/s

Water Loading
150.0 cm3/cm.s

Inlet Gap
0.020 m

Inlet Weir
0.000 m

Outlet Weir
0.020 m

Hole Diameter
0.013 m

Fig. A6.6d Three-dimensional height of clear liquid surface profiles

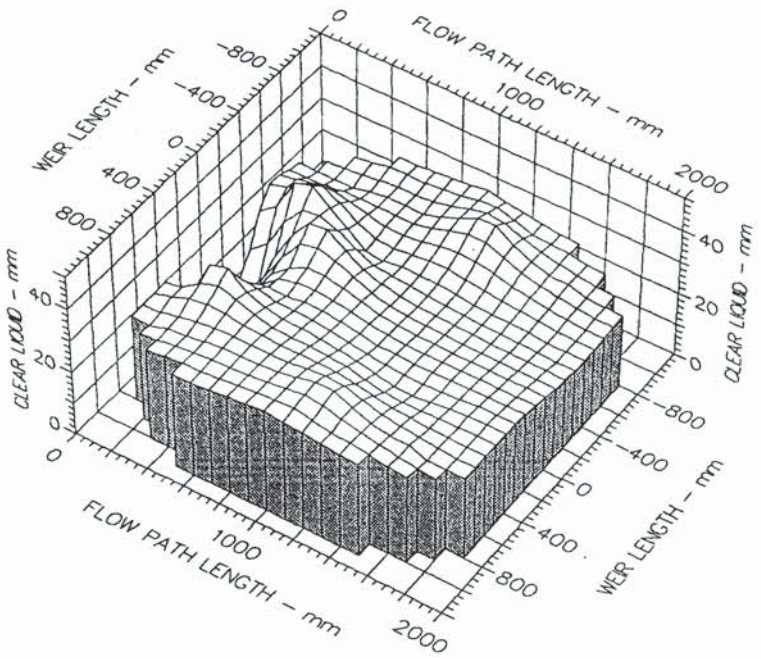

Air Velocity
1.250 m/s

Water Loading
200.0 cm3/cm.s

Inlet Gap
0.020 m

Inlet Weir
0.000 m

Outlet Weir
0.020 m

Hole Diameter
0.013 m

Fig. A6.6e Three-dimensional height of clear liquid surface profiles

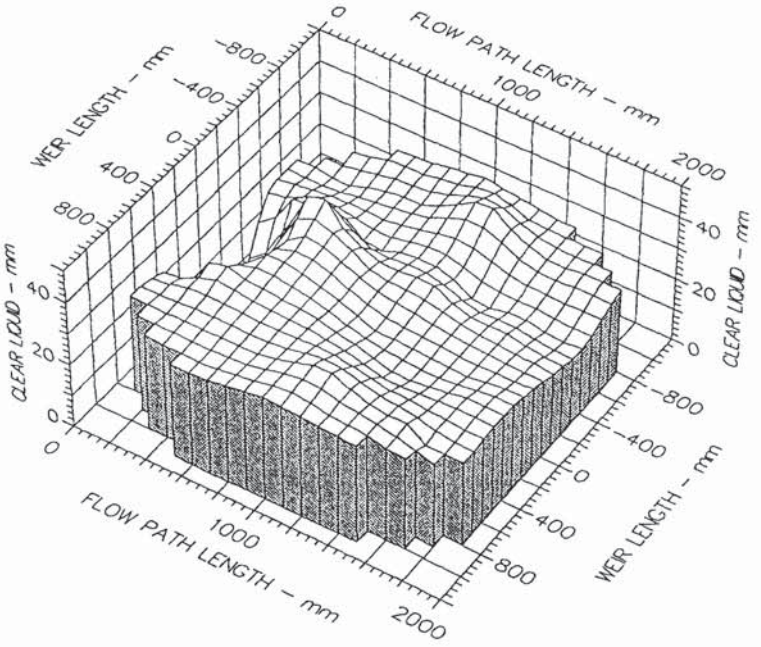

Air Velocity
1.250 m/s

Water Loading
250.0 cm3/cm.s

Inlet Gap
0.020 m

Inlet Weir
0.000 m

Outlet Weir
0.020 m

Hole Diameter
0.013 m

Fig. A6.6f Three-dimensional height of clear liquid surface profiles

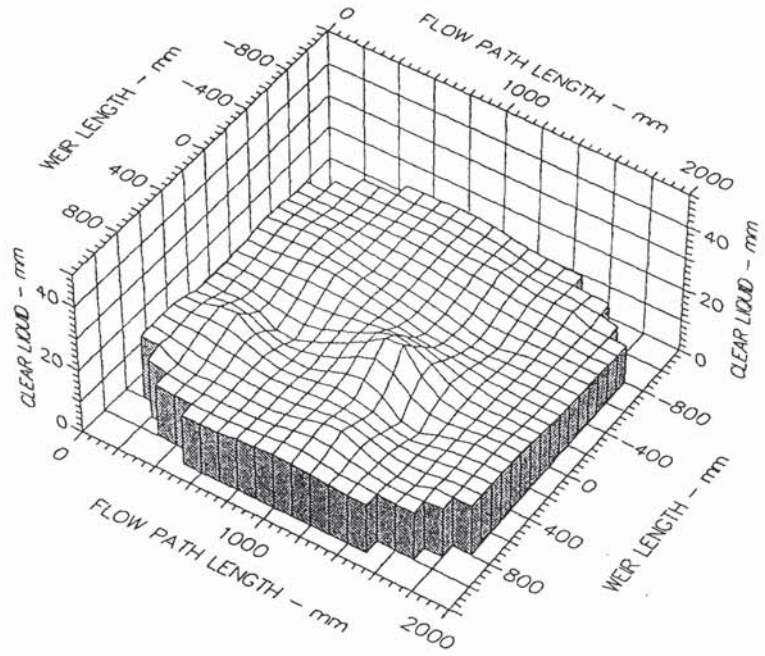

Air Velocity
1.500 m/s

Water Loading
25.0 cm3/cm.s

Inlet Gap
0.020 m

Inlet Weir
0.000 m

Outlet Weir
0.020 m

Hole Diameter
0.013 m

Fig. A6.7a Three-dimensional height of clear liquid surface profiles

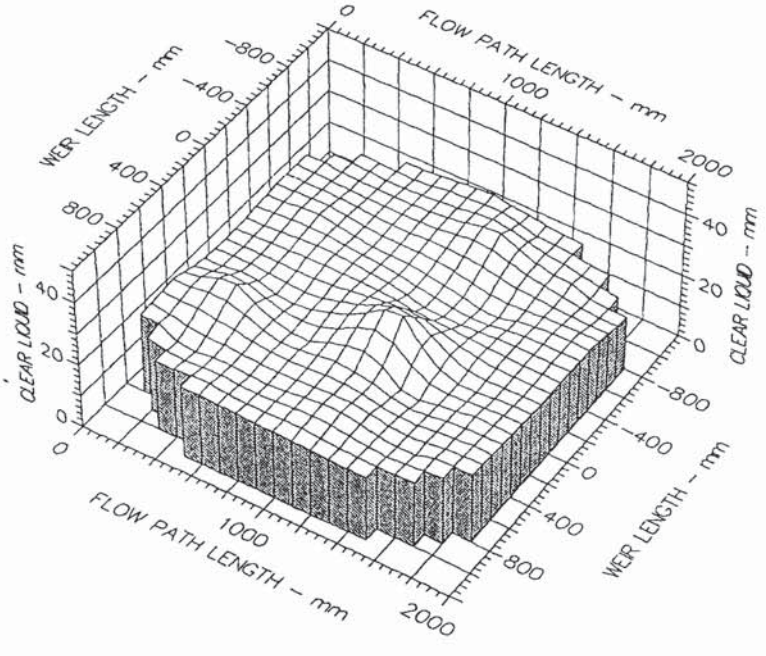

Air Velocity
1.500 m/s

Water Loading
50.0 cm3/cm.s

Inlet Gap
0.020 m

Inlet Weir
0.000 m

Outlet Weir
0.020 m

Hole Diameter
0.013 m

Fig. A6.7b Three-dimensional height of clear liquid surface profiles

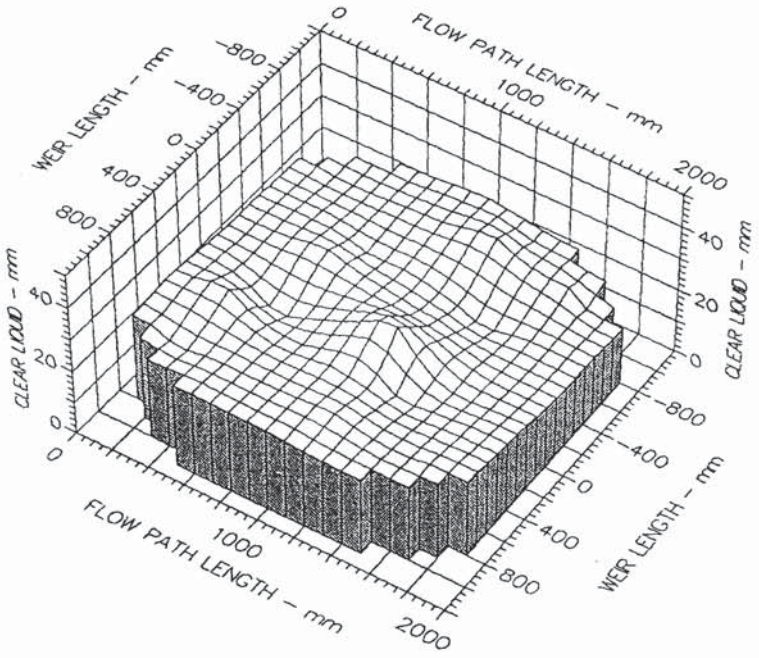

Air Velocity
1.500 m/s

Water Loading
100.0 cm3/cm.s

Inlet Gap
0.020 m

Inlet Weir
0.000 m

Outlet Weir
0.020 m

Hole Diameter
0.013 m

Fig. A6.7c Three-dimensional height of clear liquid surface profiles

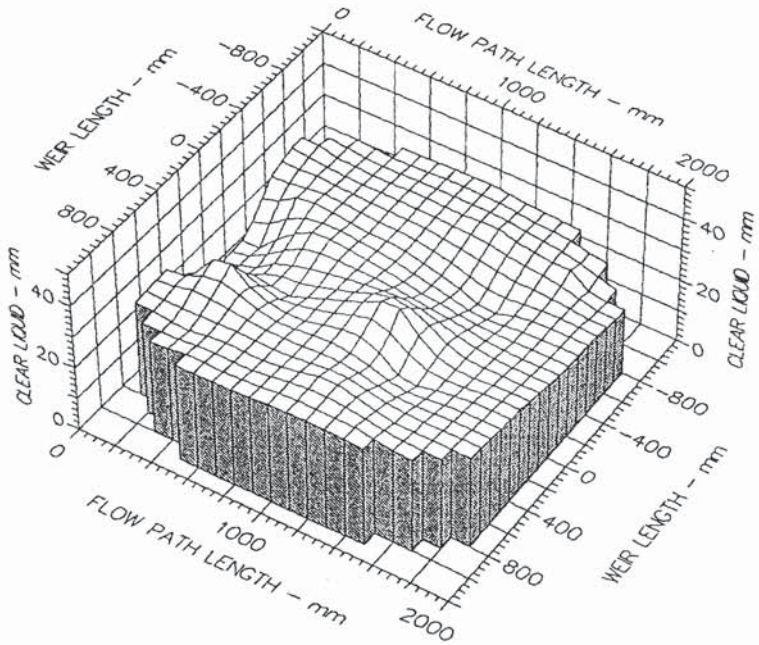

Air Velocity
1.500 m/s

Water Loading
150.0 cm3/cm.s

Inlet Gap
0.020 m

Inlet Weir
0.000 m

Outlet Weir
0.020 m

Hole Diameter
0.013 m

Fig. A6.7d Three-dimensional height of clear liquid surface profiles

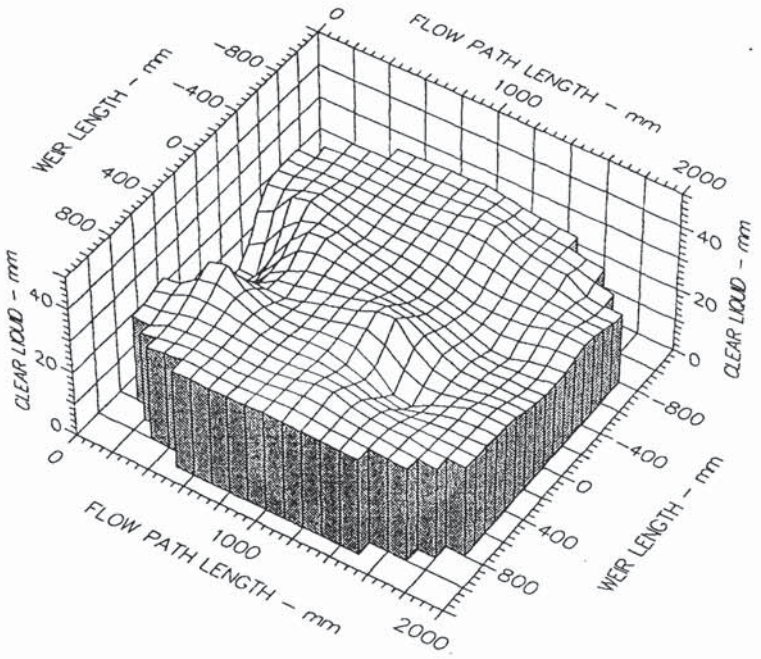

Air Velocity
1.500 m/s

Water Loading
200.0 cm3/cm.s

Inlet Gap
0.020 m

Inlet Weir
0.000 m

Outlet Weir
0.020 m

Hole Diameter
0.013 m

Fig. A6.7e Three-dimensional height of clear liquid surface profiles

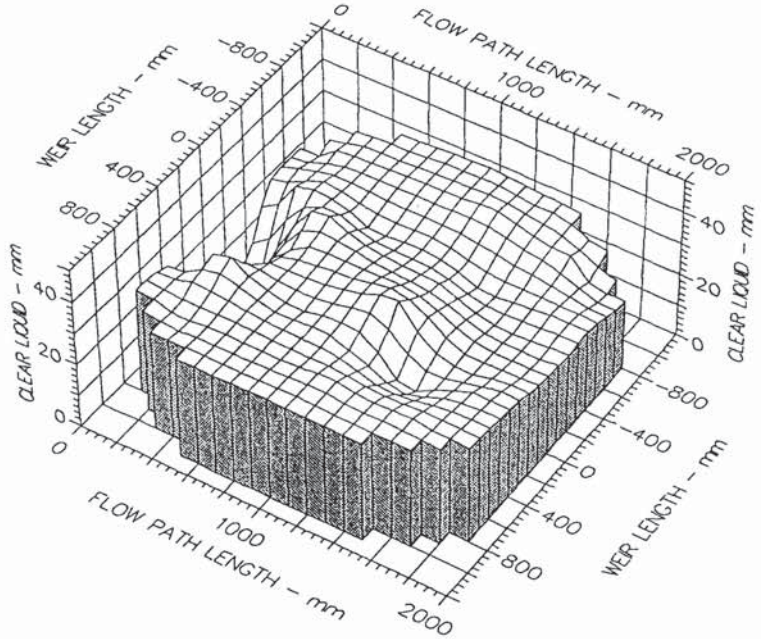

Air Velocity
1.500 m/s

Water Loading
250.0 cm3/cm.s

Inlet Gap
0.020 m

Inlet Weir
0.000 m

Outlet Weir
0.020 m

Hole Diameter
0.013 m

Fig. A6.7f Three-dimensional height of clear liquid surface profiles

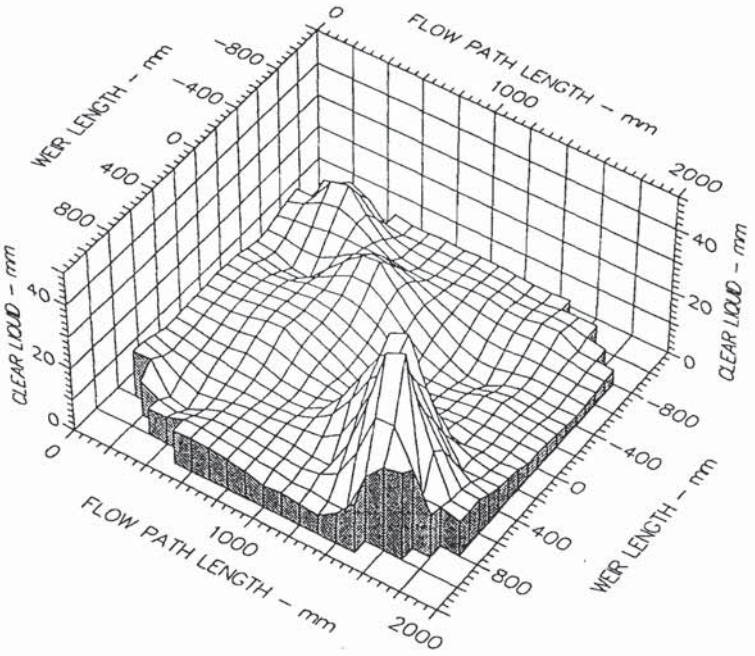

Air Velocity
2.000 m/s

Water Loading
25.0 cm3/cm.s

Inlet Gap
0.020 m

Inlet Weir
0.000 m

Outlet Weir
0.020 m

Hole Diameter
0.013 m

Fig. A6.8a Three-dimensional height of clear liquid surface profiles

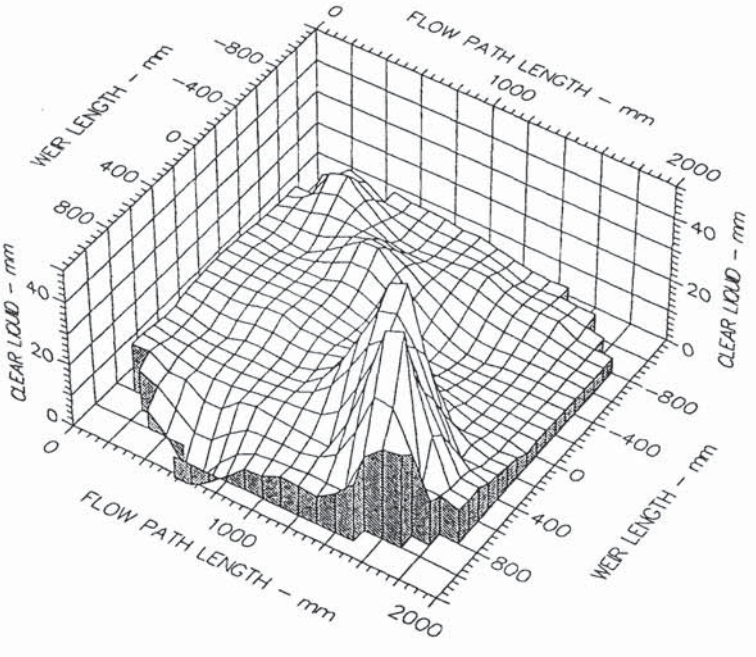

Air Velocity
2.000 m/s

Water Loading
50.0 cm3/cm.s

Inlet Gap
0.020 m

Inlet Weir
0.000 m

Outlet Weir
0.020 m

Hole Diameter
0.013 m

Fig. A6.8b Three-dimensional height of clear liquid surface profiles.

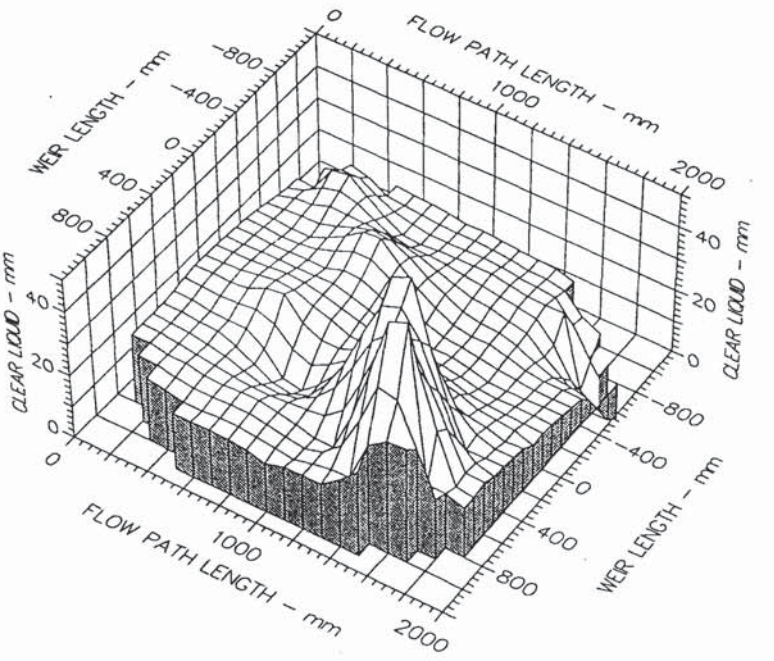

Air Velocity
2.000 m/s

Water Loading
100.0 cm3/cm.s

Inlet Gap
0.020 m

Inlet Weir
0.000 m

Outlet Weir
0.020 m

Hole Diameter
0.013 m

Fig. A6.8c Three-dimensional height of clear liquid surface profiles

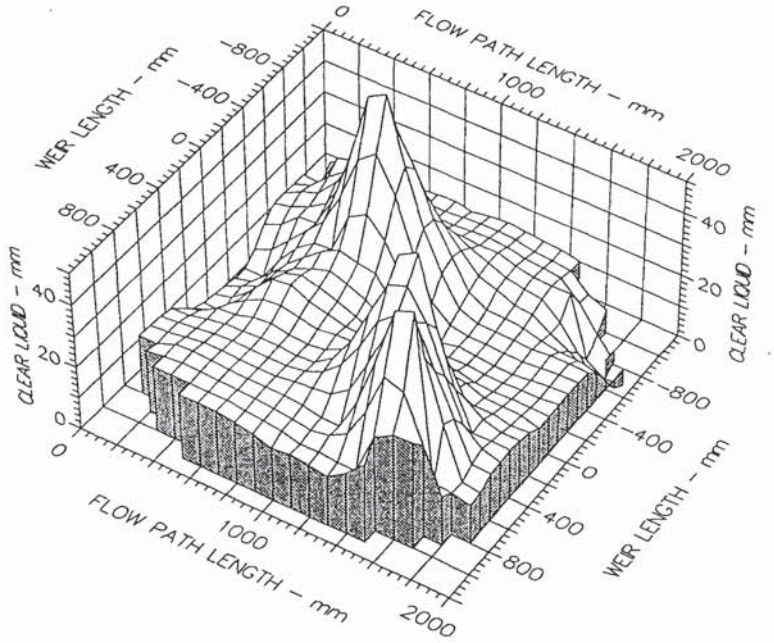

Air Velocity
2.000 m/s

Water Loading
150.0 cm3/cm.s

Inlet Gap
0.020 m

Inlet Weir
0.000 m

Outlet Weir
0.020 m

Hole Diameter
0.013 m

Fig. A6.8d Three-dimensional height of clear liquid surface profiles

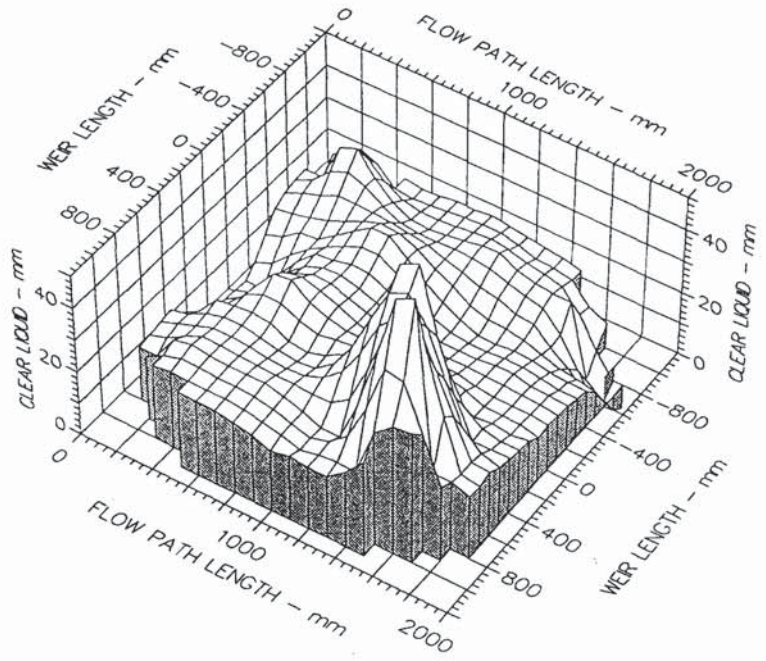

Air Velocity
2.000 m/s

Water Loading
200.0 cm3/cm.s

Inlet Gap
0.020 m

Inlet Weir
0.000 m

Outlet Weir
0.020 m

Hole Diameter
0.013 m

Fig. A6.8e Three-dimensional height of clear liquid surface profiles

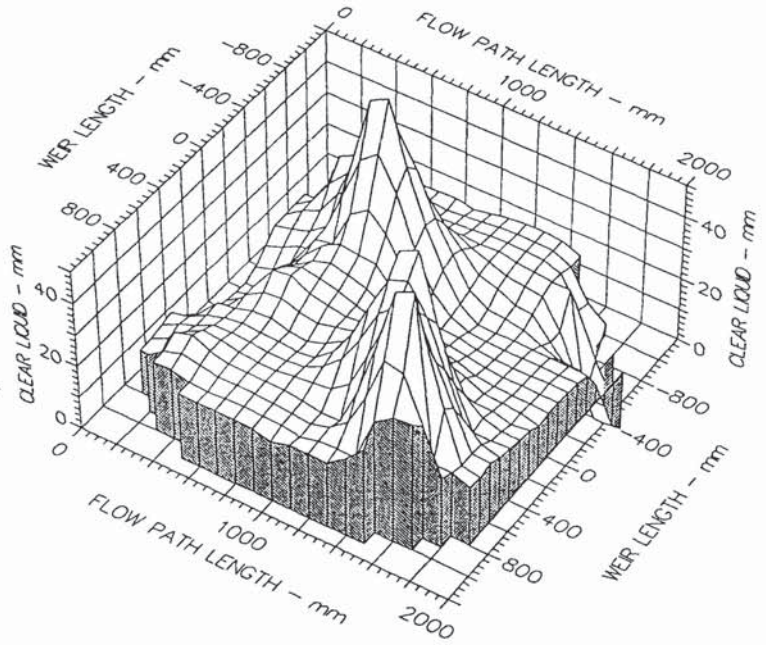

Air Velocity
2.000 m/s

Water Loading
250.0 cm3/cm.s

Inlet Gap
0.020 m

Inlet Weir
0.000 m

Outlet Weir
0.020 m

Hole Diameter
0.013 m

Fig. A6.8f Three-dimensional height of clear liquid surface profiles

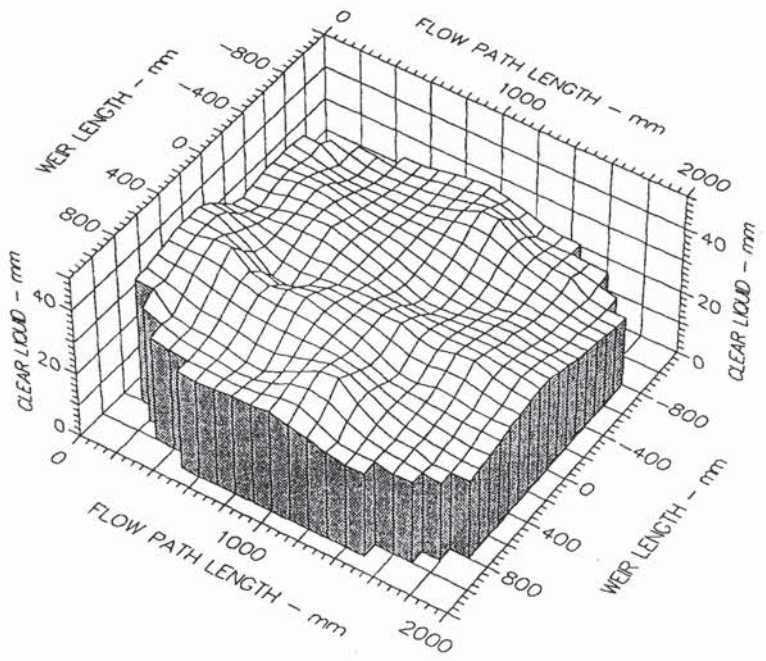

Air Velocity
1.000 m/s

Water Loading
25.0 cm3/cm.s

Inlet Gap
0.050 m

Inlet Weir
0.000 m

Outlet Weir
0.050 m

Hole Diameter
0.013 m

Fig. A6.9a Three-dimensional height of clear liquid surface profiles

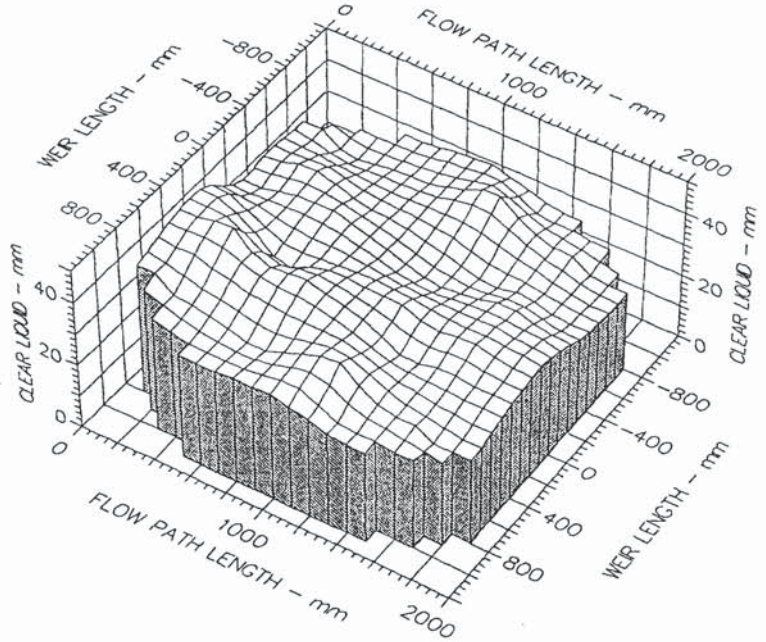

Air Velocity
1.000 m/s

Water Loading
50.0 cm3/cm.s

Inlet Gap
0.050 m

Inlet Weir
0.000 m

Outlet Weir
0.050 m

Hole Diameter
0.013 m

Fig. A6.9b Three-dimensional height of clear liquid surface profiles

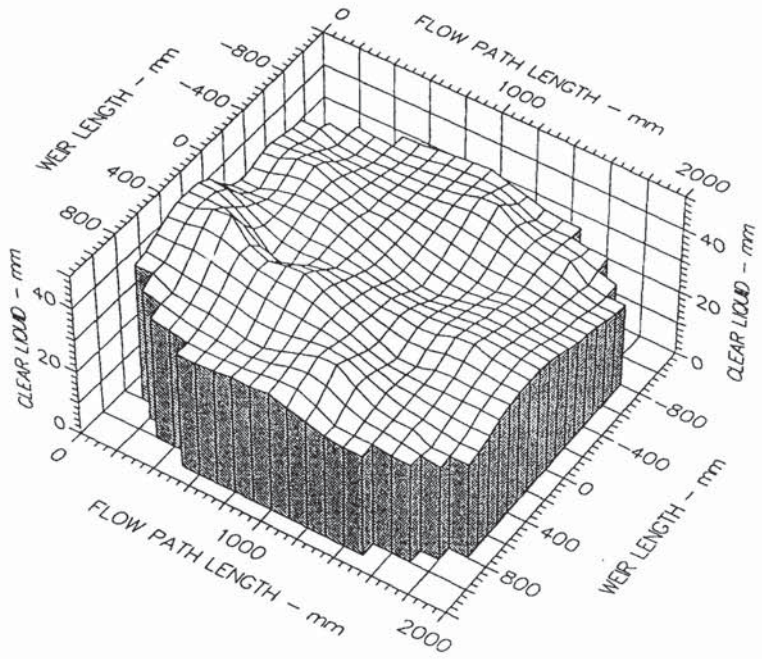

Air Velocity
1.000 m/s

Water Loading
100.0 cm3/cm.s

Inlet Gap
0.050 m

Inlet Weir
0.000 m

Outlet Weir
0.050 m

Hole Diameter
0.013 m

Fig. A6.9c Three-dimensional height of clear liquid surface profiles

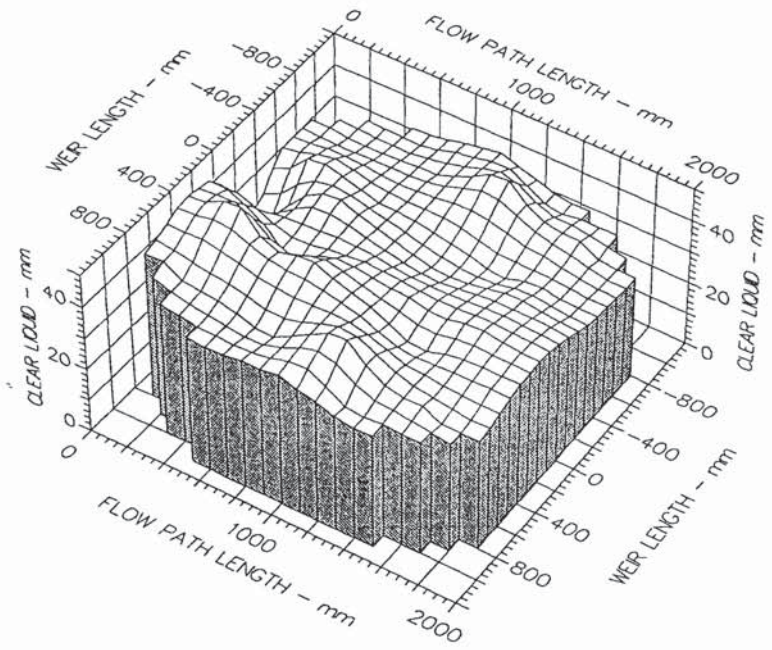

Air Velocity
1.000 m/s

Water Loading
150.0 cm3/cm.s

Inlet Gap
0.050 m

Inlet Weir
0.000 m

Outlet Weir
0.050 m

Hole Diameter
0.013 m

Fig. A6.9d Three-dimensional height of clear liquid surface profiles

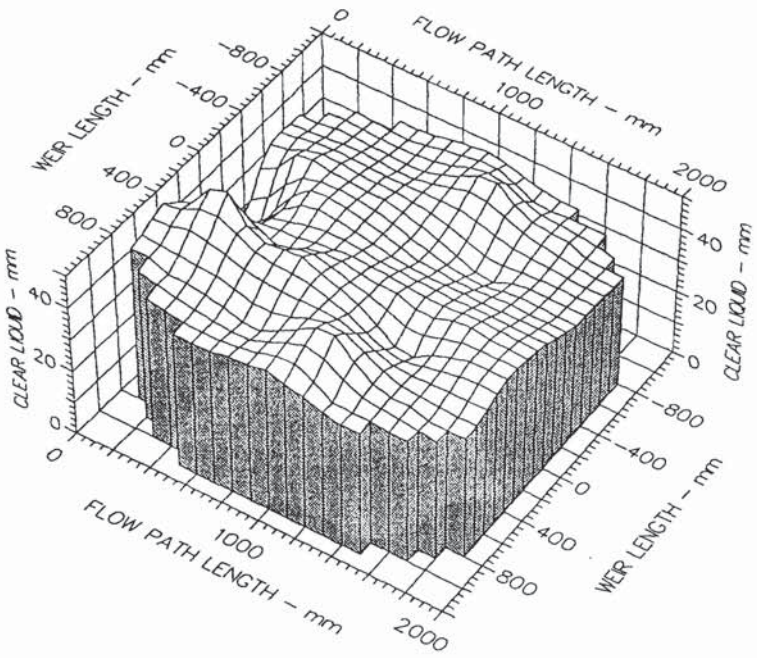

Air Velocity
1.000 m/s

Water Loading
200.0 cm3/cm.s

Inlet Gap
0.050 m

Inlet Weir
0.000 m

Outlet Weir
0.050 m

Hole Diameter
0.013 m

Fig. A6.9e Three-dimensional height of clear liquid surface profiles

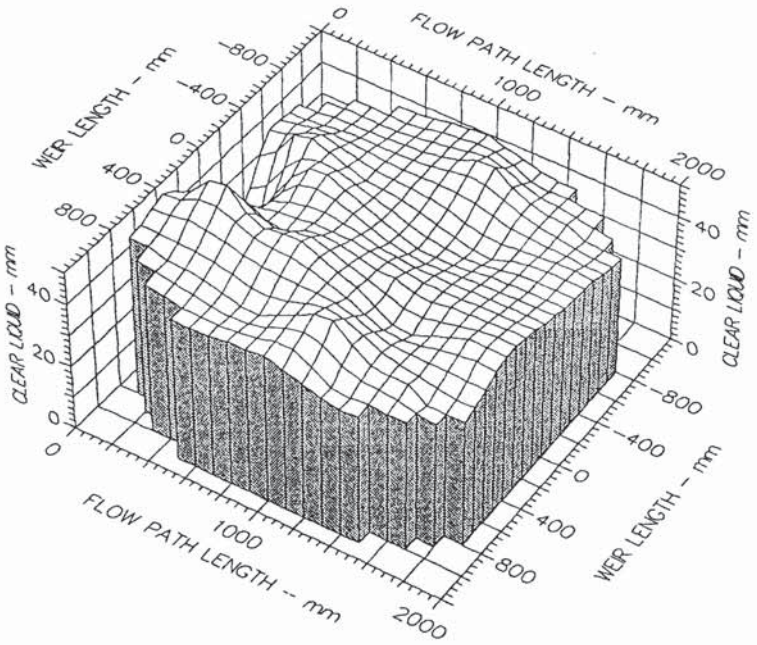

Air Velocity
1.000 m/s

Water Loading
250.0 cm3/cm.s

Inlet Gap
0.050 m

Inlet Weir
0.000 m

Outlet Weir
0.050 m

Hole Diameter
0.013 m

Fig. A6.9f Three-dimensional height of clear liquid surface profiles

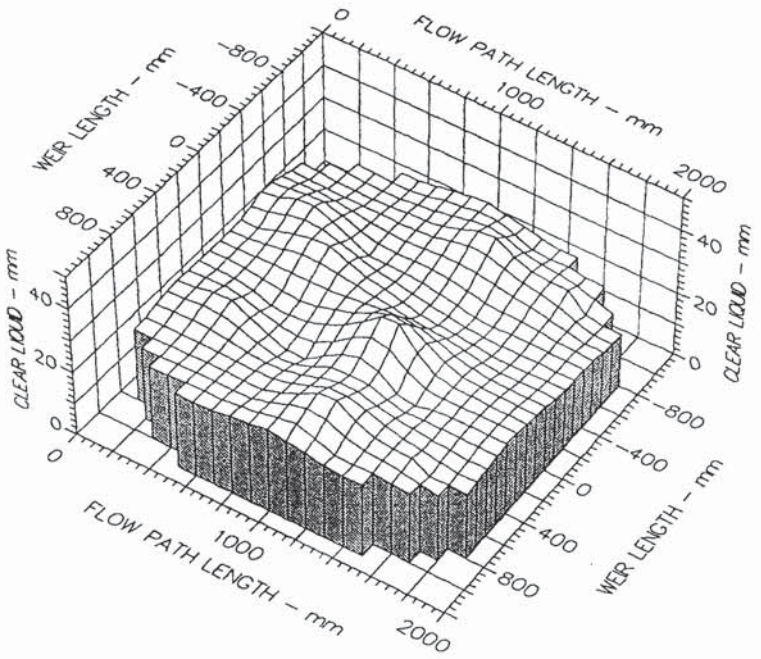

Air Velocity
1.250 m/s

Water Loading
25.0 cm3/cm.s

Inlet Gap
0.050 m

Inlet Weir
0.000 m

Outlet Weir
0.050 m

Hole Diameter
0.013 m

Fig. A6.10a Three-dimensional height of clear liquid surface profiles

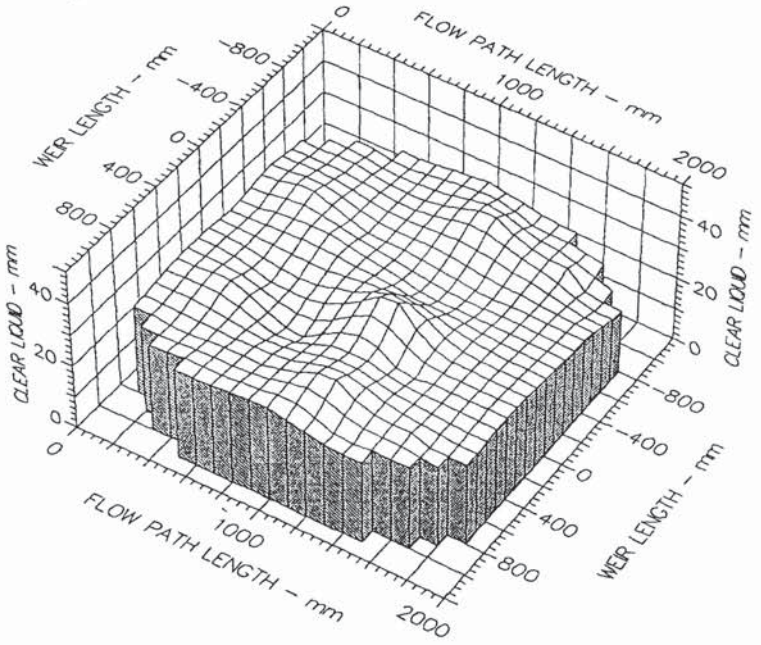

Air Velocity
1.250 m/s

Water Loading
50.0 cm3/cm.s

Inlet Gap
0.050 m

Inlet Weir
0.000 m

Outlet Weir
0.050 m

Hole Diameter
0.013 m

Fig. A6.10b Three-dimensional height of clear liquid surface profiles

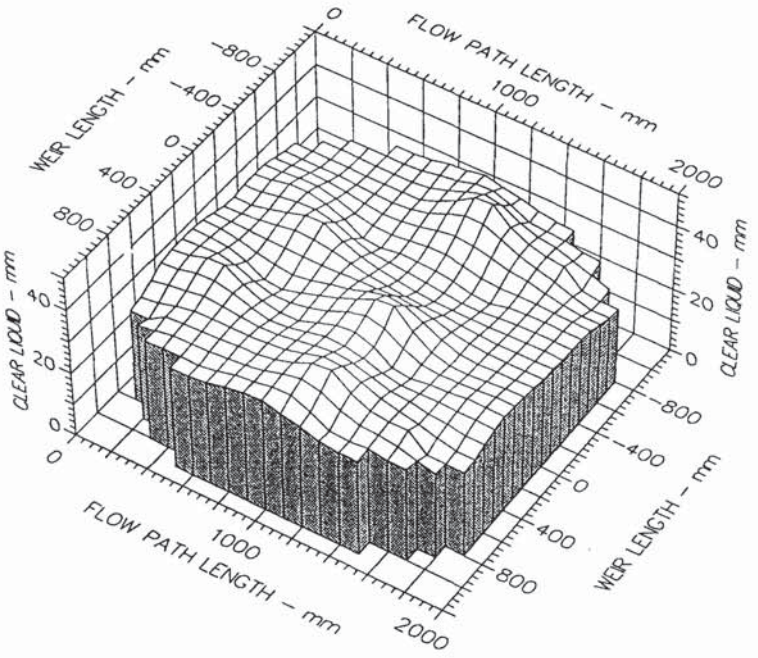

Air Velocity
1.250 m/s

Water Loading
100.0 cm3/cm.s

Inlet Gap
0.050 m

Inlet Weir
0.000 m

Outlet Weir
0.050 m

Hole Diameter
0.013 m

Fig. A6.10c Three-dimensional height of clear liquid surface profiles

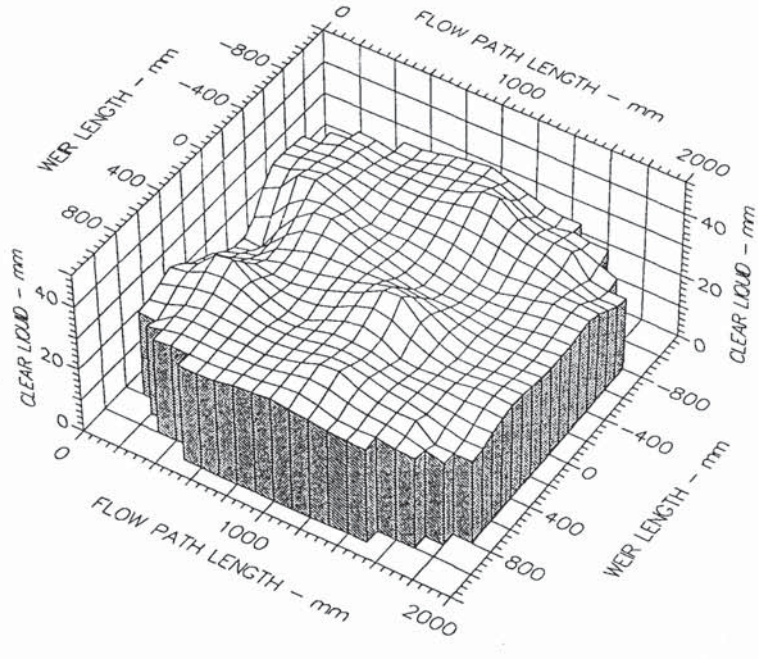

Air Velocity
1.250 m/s

Water Loading
150.0 cm3/cm.s

Inlet Gap
0.050 m

Inlet Weir
0.000 m

Outlet Weir
0.050 m

Hole Diameter
0.013 m

Fig. A6.10d Three-dimensional height of clear liquid surface profiles

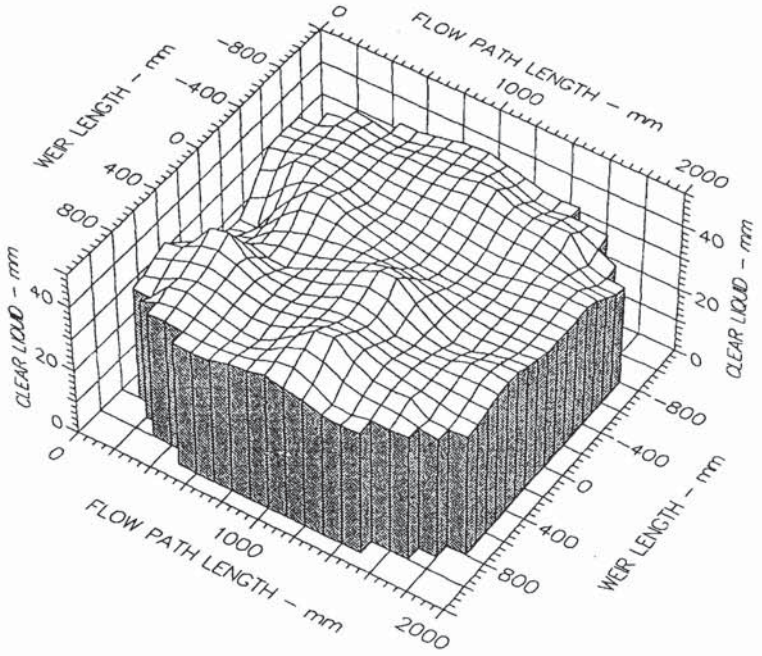

Air Velocity
1.250 m/s

Water Loading
200.0 cm3/cm.s

Inlet Gap
0.050 m

Inlet Weir
0.000 m

Outlet Weir
0.050 m

Hole Diameter
0.013 m

Fig. A6.10e Three-dimensional height of clear liquid surface profiles

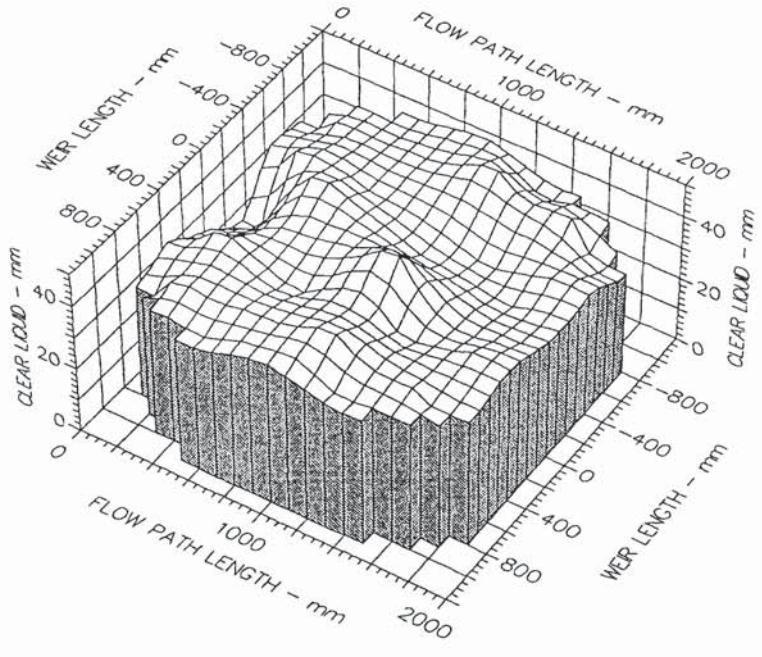

Air Velocity
1.250 m/s

Water Loading
250.0 cm3/cm.s

Inlet Gap
0.050 m

Inlet Weir
0.000 m

Outlet Weir
0.050 m

Hole Diameter
0.013 m

Fig. A6.10f Three-dimensional height of clear liquid surface profiles

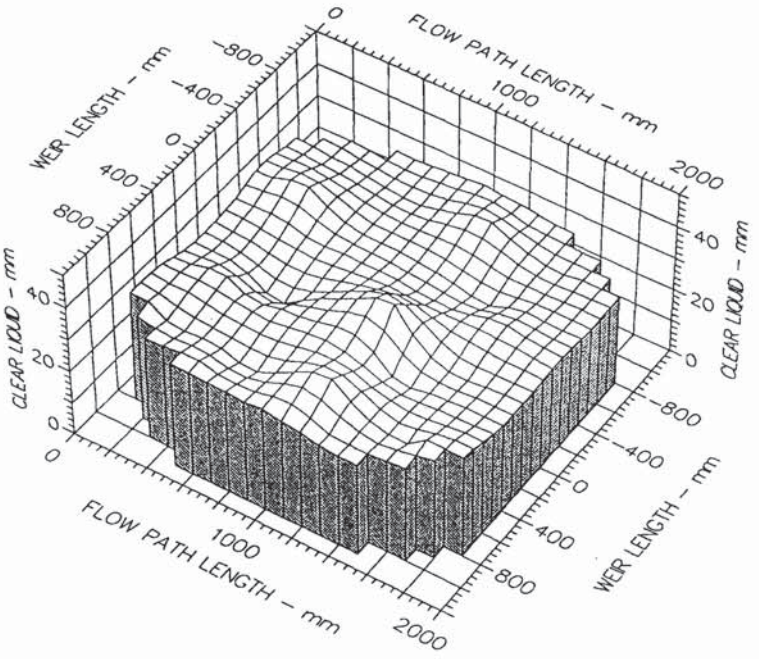

Air Velocity
1.500 m/s

Water Loading
25.0 cm3/cm.s

Inlet Gap
0.050 m

Inlet Weir
0.000 m

Outlet Weir
0.050 m

Hole Diameter
0.013 m

Fig. A6.11a Three-dimensional height of clear liquid surface profiles

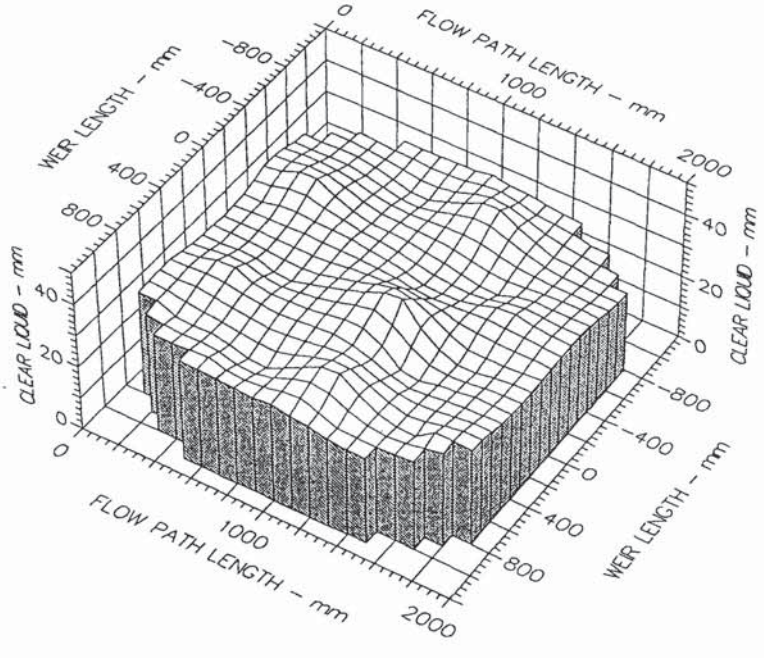

Air Velocity
1.500 m/s

Water Loading
50.0 cm3/cm.s

Inlet Gap
0.050 m

Inlet Weir
0.000 m

Outlet Weir
0.050 m

Hole Diameter
0.013 m

Fig. A6.11b Three-dimensional height of clear liquid surface profiles

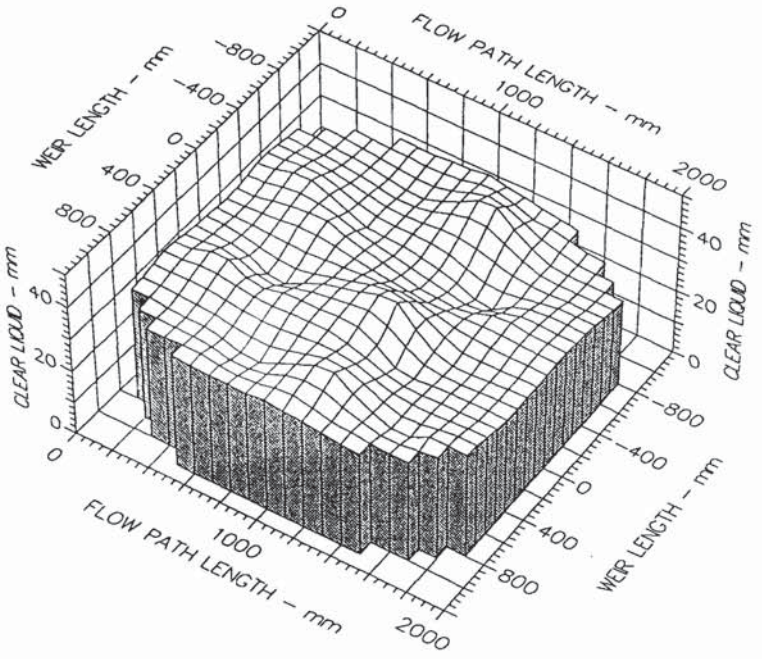

Air Velocity
1.500 m/s

Water Loading
100.0 cm3/cm.s

Inlet Gap
0.050 m

Inlet Weir
0.000 m

Outlet Weir
0.050 m

Hole Diameter
0.013 m

Fig. A6.11c Three-dimensional height of clear liquid surface profiles

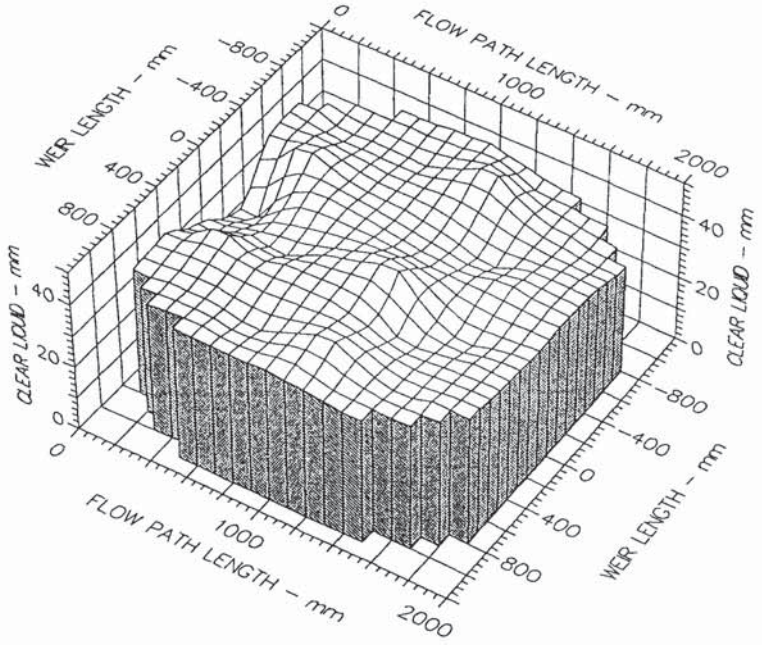

Air Velocity
1.500 m/s

Water Loading
150.0 cm3/cm.s

Inlet Gap
0.050 m

Inlet Weir
0.000 m

Outlet Weir
0.050 m

Hole Diameter
0.013 m

Fig. A6.11d Three-dimensional height of clear liquid surface profiles

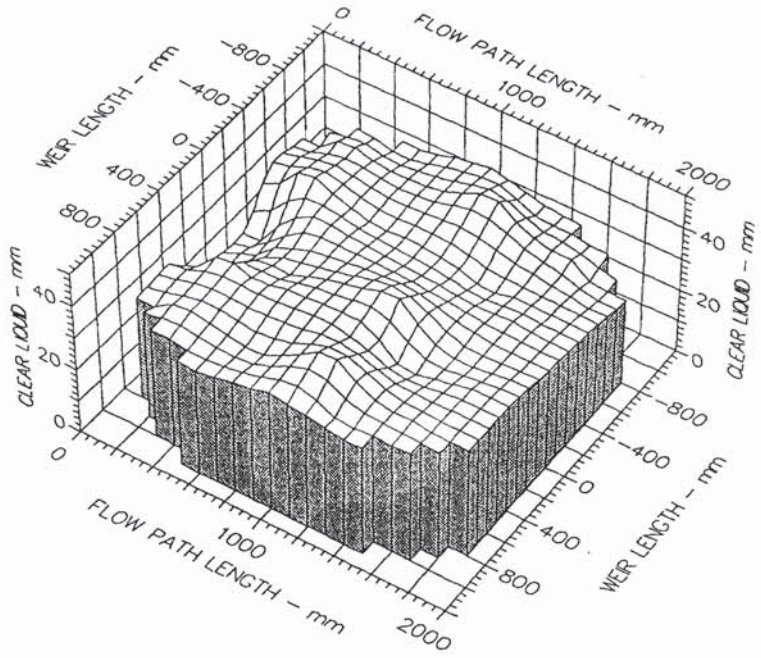

Air Velocity
1.500 m/s

Water Loading
200.0 cm3/cm.s

Inlet Gap
0.050 m

Inlet Weir
0.000 m

Outlet Weir
0.050 m

Hole Diameter
0.013 m

Fig. A6.11e Three-dimensional height of clear liquid surface profiles

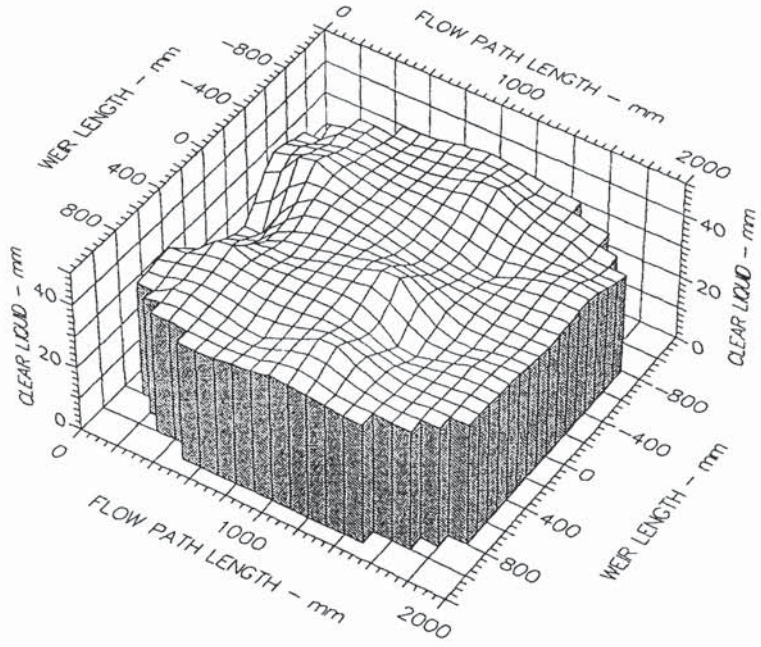

Air Velocity
1.500 m/s

Water Loading
250.0 cm3/cm.s

Inlet Gap
0.050 m

Inlet Weir
0.000 m

Outlet Weir
0.050 m

Hole Diameter
0.013 m

Fig. A6.11f Three-dimensional height of clear liquid surface profiles

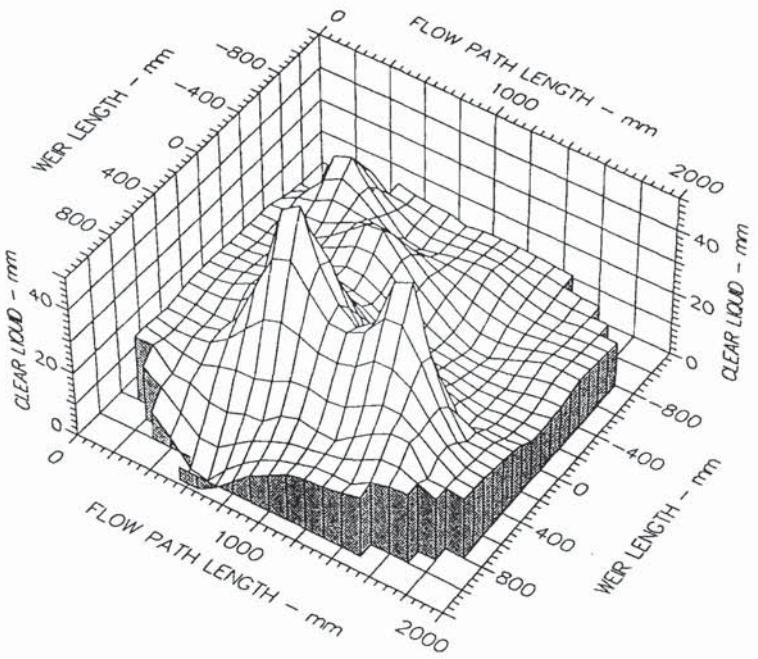

Air Velocity
2.000 m/s

Water Loading
25.0 cm3/cm.s

Inlet Gap
0.050 m

Inlet Weir
0.000 m

Outlet Weir
0.050 m

Hole Diameter
0.013 m

Fig. A6.12a Three-dimensional height of clear liquid surface profiles

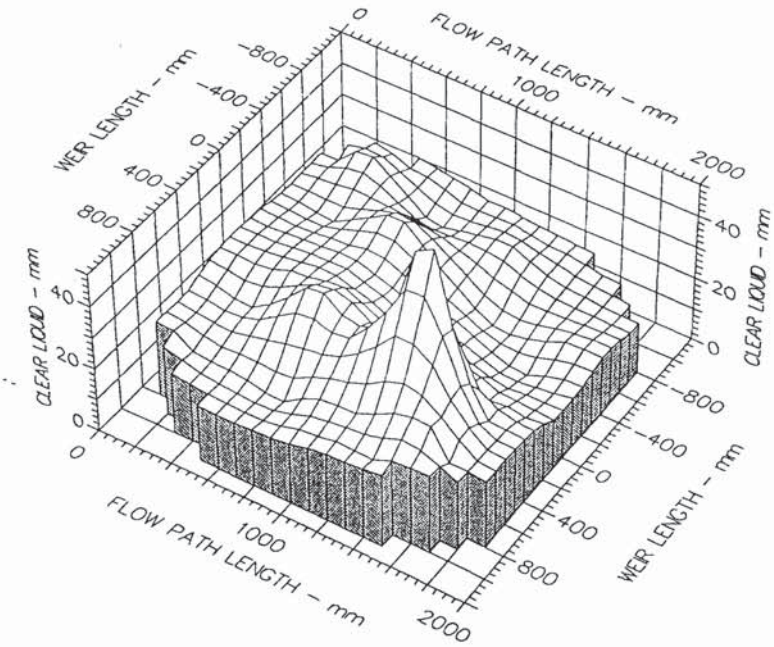

Air Velocity
2.000 m/s

Water Loading
50.0 cm3/cm.s

Inlet Gap
0.050 m

Inlet Weir
0.000 m

Outlet Weir
0.050 m

Hole Diameter
0.013 m

Fig. A6.12b Three-dimensional height of clear liquid surface profiles

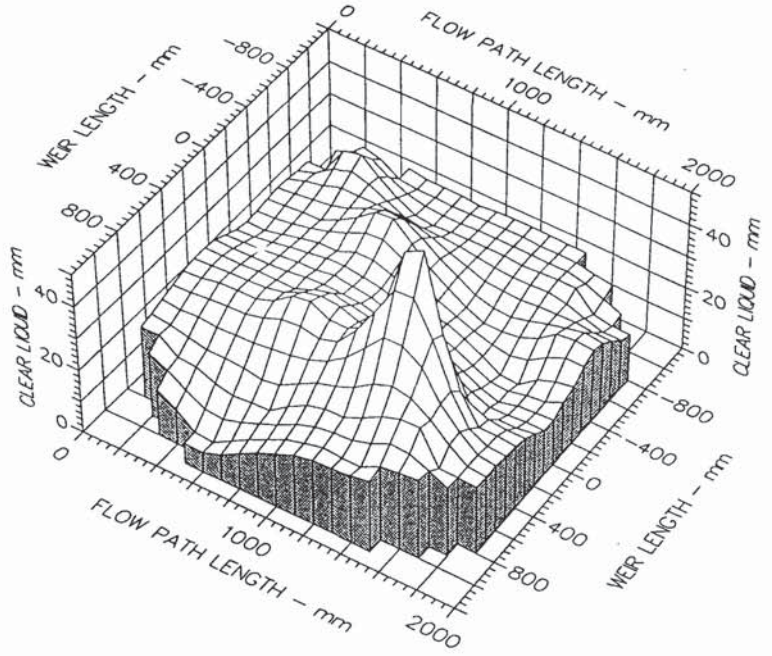

Air Velocity
2.000 m/s

Water Loading
100.0 cm3/cm.s

Inlet Gap
0.050 m

Inlet Weir
0.000 m

Outlet Weir
0.050 m

Hole Diameter
0.013 m

Fig. A6.12c Three-dimensional height of clear liquid surface profiles

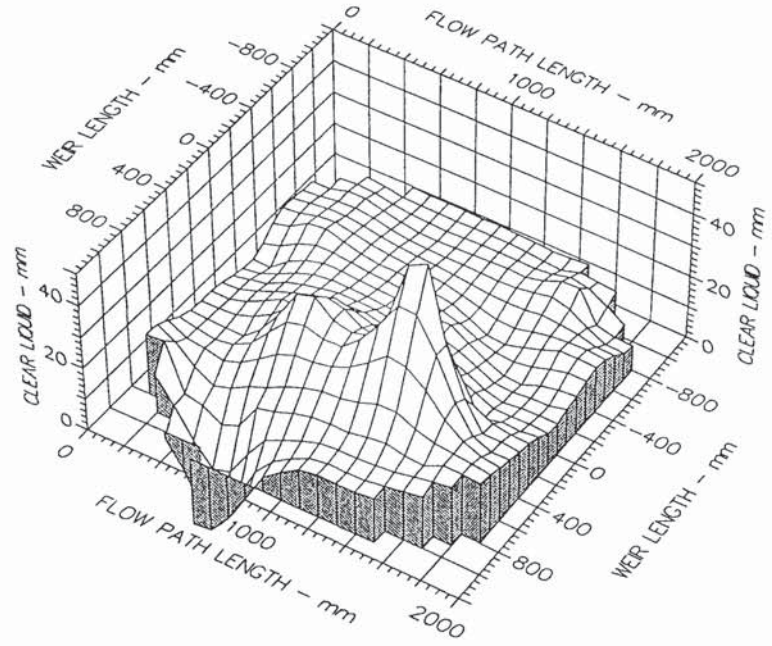

Air Velocity
2.000 m/s

Water Loading
150.0 cm3/cm.s

Inlet Gap
0.050 m

Inlet Weir
0.000 m

Outlet Weir
0.050 m

Hole Diameter
0.013 m

Fig. A6.12d Three-dimensional height of clear liquid surface profiles

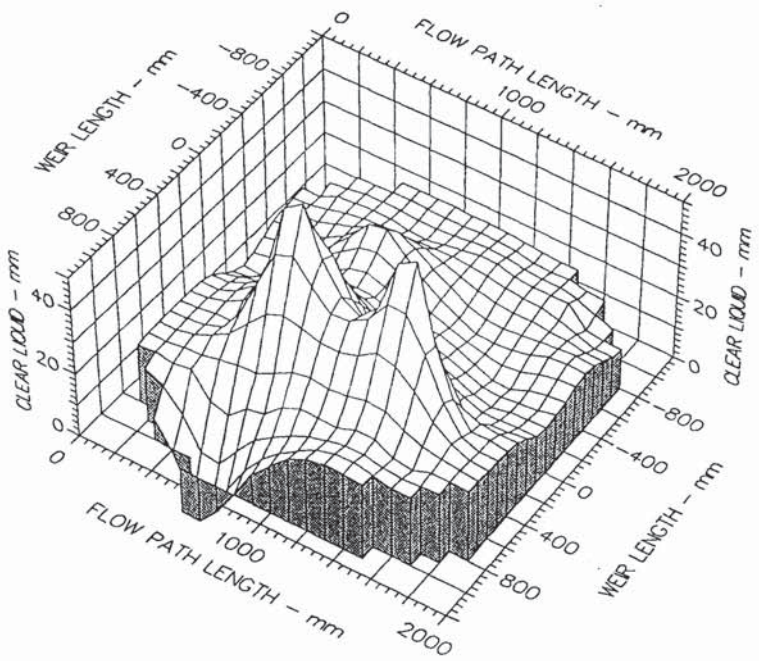

Air Velocity
2.000 m/s

Water Loading
200.0 cm3/cm.s

Inlet Gap
0.050 m

Inlet Weir
0.000 m

Outlet Weir
0.050 m

Hole Diameter
0.013 m

Fig. A6.12e Three-dimensional height of clear liquid surface profiles

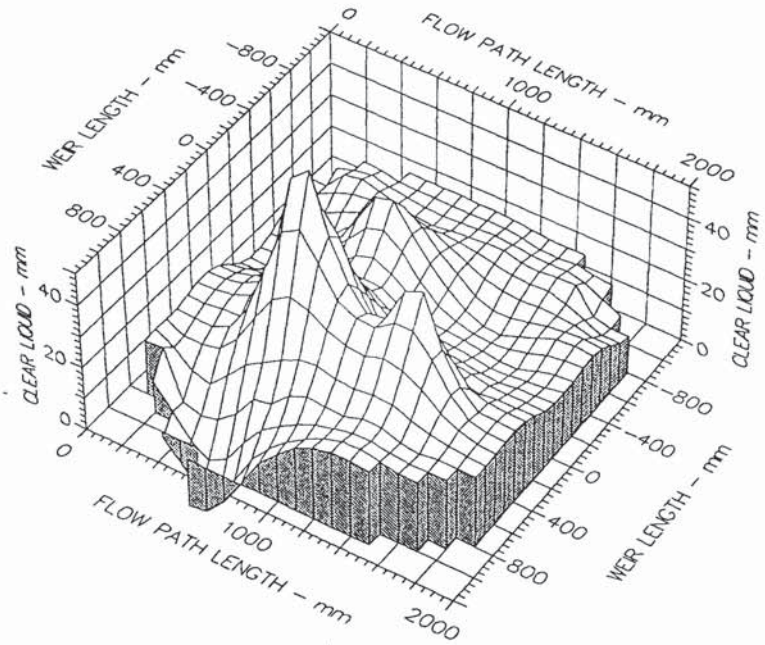

Air Velocity
2.000 m/s

Water Loading
250.0 cm3/cm.s

Inlet Gap
0.050 m

Inlet Weir
0.000 m

Outlet Weir
0.050 m

Hole Diameter
0.013 m

Fig. A6.12f Three-dimensional height of clear liquid surface profiles